Coordination Chemistry of Main Group Cyclopentadienyl Compounds

Dissertation

zur Erlangung des Grades

des Doktors der Naturwissenschaften

der Naturwissenschaftlich-Technischen Fakultät

der Universität des Saarlandes

von

Dipl.-Chem. Carsten Müller

Saarbrücken

2021

Tag des Kolloquiums:	13.05.2022
Dekan:	Prof. Dr. Jörn Walter
Berichterstatter:	Dr. André Schäfer
	Prof. Dr. Guido Kickelbick
	Prof. Dr. Ulrich Siemeling
Vorsitz:	Prof. Dr. Gregor Jung
Akademischer Mitarbeiter:	Dr. Andreas Rammo

The present dissertation was prepared in the time between September 2017 and July 2021 at the Department of Chemistry of the Faculty of Natural Sciences and Technology at Saarland University under the supervision of Dr. André Schäfer.

Die vorliegende Dissertation wurde in der Zeit zwischen September 2017 und Juli 2021 am Fachbereich Chemie der Naturwissenschaftlich-Technischen Fakultät an der Universität des Saarlandes unter der Aufsicht von Dr. André Schäfer erstellt.

Abstract

The first part of this thesis deals with complexes of *N*-heterocyclic carbenes with group 14 metallocenes as well as with complexes of a cyclic (alkyl)(amino)carbene with related tin(II) halfsandwich complexes. The bonding nature in these complexes was examined using DFT calculations, which revealed that attractive dispersion force interactions play a substantial role. These complexes are the first of their kind representing an important contribution to the class of carbene complexes of tetrylene-type compounds.

In the second part of this thesis, phosphanyl substituted metallocenes and derived coordination compounds of magnesium, antimony and the group 14 elements, germanium, tin and lead, were investigated. These compounds exhibit Lewis amphiphilic character due to the Lewis acidic central atoms and the Lewis basic phosphorus atoms. The phosphanyl substituted magnesocenes, which are the first donor-functionalized magnesocenes, could be used both to activate small molecules and as ligands for transition metal fragments. The coordination chemistry of the corresponding group 14 metallocenes, which were obtained by transmetalation of the magnesocenes, was studied extensively towards main group and transition metal fragments, whereby significant structural differences to the related phosphanyl substituted ferrocenes were found.

Zusammenfassung

Der erste Teil dieser Arbeit beschäftigt sich mit Komplexen von *N*-heterozyklischen Carbene mit Gruppe 14 Metallocenen sowie Komplexen eines zyklischen Alkylaminocarbens mit verwandten Zinn(II) Halbsandwich. Die Bindungssituation in diesen Komplexen wurde mittels DFT-Rechnungen untersucht, wobei sich zeigte, dass attraktive Dispersionswechselwirkungen von großer Bedeutung sind. Diese Komplexe sind die ersten ihrer Art, was einen wichtigen Beitrag zur Klasse der Carbenkomplexe tetrylenartiger Verbindungen darstellt.

Im zweiten Teil der Arbeit wurden phosphanylsubstituierte Metallocene und abgeleitete Koordinationsverbindungen des Magnesiums, Antimons und der Gruppe 14 Elemente, Germanium, Zinn und Blei, untersucht. Diese Verbindungen zeigen, aufgrund der Lewis aciden Zentralatome und der Lewis basischen Phosphoratome, Lewis amphiphilen Charakter. Die phosphanylsubstituierten Magnesocene konnten zur Aktivierung kleiner Moleküle und als Liganden für Übergangsmetallfragmente genutzt werden. Die Koordinationschemie der Gruppe 14 Metallocene, welche durch Transmetallierung der Magnesocene erhalten werden konnten, wurde intensiv untersucht wobei signifikante strukturelle Unterschiede zu den verwandten, phosphanylsubstituierten Ferrocenen gefunden wurden.

List of publications

As part of this cumulative thesis:

Carsten Müller, Angelika Stahlich, Lisa Wirtz, Claude Gretsch, Volker Huch, André Schäfer, Carbene Complexes of Stannocenes.

Inorg. Chem. **2018**, *57*, 8050-8053.

https://doi.org/10.1021/acs.inorgchem.8b01432

Carsten Müller, Diego M. Andrada, Inga-Alexandra Bischoff, Michael Zimmer, Volker Huch, Nils Steinbrück, André Schäfer, Synthesis, Structure and Bonding Analysis of Tin(II) Dihalide and Cyclopentadienyl Tin(II) Halide (Alkyl)(amino)carbene Complexes.

Organometallics **2019**, *38*, 1052-1061.

https://doi.org/10.1021/acs.organomet.8b00861

Sergi Danés[§], Carsten Müller[§], Lisa Wirtz[§], Volker Huch, Theresa Block, Rainer Pöttgen, André Schäfer, Diego M. Andrada, On the Bonding Situation in Stannocene and Plumbocene *N*-Heterocyclic Carbene Complexes.

[§]These authors contributed equally

Organometallics **2020**, *39*, 516-527.

https://doi.org/10.1021/acs.organomet.9b00667

Carsten Müller, Joshua Warken, Volker Huch, Bernd Morgenstern, Inga-Alexandra Bischoff, Michael Zimmer, André Schäfer, Diphosphanylmetallocenes of Main-Group Elements.

Chem. Eur. J. **2021**, *27*, 6500-6510.

https://doi.org/10.1002/chem.202005198

Other publications during doctorate:

Inga-Alexandra Bischoff, Carsten Müller, Volker Huch, Michael Zimmer, André Schäfer, Imidazolium Cyclopentadienide Salts and Their Use as Cp-transfer Reagents.

Eur. J. Inorg. Chem. **2019**, 1941–1944.

https://doi.org/10.1002/ejic.201900047

Sergej Lauk, Michael Zimmer, Bernd Morgenstern, Volker Huch, Carsten Müller, Helmut Sitzmann, André Schäfer, Tetra- and Pentaisopropylcyclopentadienyl Complexes of Group 15 Elements.

Organometallics **2021**, *40*, 618–626.

https://doi.org/10.1021/acs.organomet.1c00008

Other publications before doctorate:

Oliver A. Groß, Sergej Lauk, Carsten Müller, Wjatscheslaw Gidt, Yu Sun, Serhiy Demeshko, Franc Meyer, Helmut Sitzmann. Iron(II) High-Spin and Low-Spin Complexes from Pentaisopropylcyclopentadienyliron(II) Bis(Trimethylsilyl)Amide.

Eur. *J*. *Inorg*. *Chem*. **2017**, *2017*, 3635–3643.

https://doi.org/10.1002/ejic.201700236

Lukas Burkhardt, Carsten Müller, Oliver A. Groß, Yu Sun, Helmut Sitzmann, Matthias Bauer, The Bonding Situation in the Dinuclear Tetra-Hydrido Complex [{^{5}CpFe}$_2$(μ-H)$_4$] Revisited by Hard X-Ray Spectroscopy.

Inorg. Chem. **2019**, *58*, 6609–6618.

https://doi.org/10.1021/acs.inorgchem.8b03032

Acknowledgment

Ich möchte mich besonders bei **Dr. André Schäfer** für die Vergabe des interessanten sowie anspruchsvollen Themas bedanken. Nach meinem Wechsel von der TU Kaiserslautern in seinen Arbeitskreis konnte ich viele neue Dinge lernen sowie mich, durch seine große Unterstützung, mit DFT-Rechnungen auseinandersetzen. Ich schätze seine ehrliche wissenschaftliche Einschätzung meiner Arbeit sowie das in mich gesetzte Vertrauen und bereue keinen Tag meinen Wechsel nach Saarbrücken. Ebenfalls bedanken möchte ich mich bei **Prof. Dr. Guido Kickelbick**, welcher meinen Werdegang als wissenschaftlicher Begleiter sowie Zweitgutachter seit Jahren verfolgt und dabei immer hilfreiche Hinweise einfließen lies sowie aufrichtiges Interesse an meiner Arbeit zeigte.

Susanne Limbach danke ich sehr für die Unterstützung in organisatorischen Fragen. Ein großes Dankeschön geht an **Dr. Volker Huch** sowie **Dr. Bernd Morgenstern** für die Durchführung der Kristallstrukturanalysen welche natürlich außerordentlich wichtig sind in unserem Bereich und an **Dr. Michael Zimmer** für seine Unterstützung bei den NMR-Experimenten und stetige Diskussionsbereitschaft bei Problemstellungen. **Susanne Harling** danke ich für die Durchführung von Elementaranalysen sowie ihre immer freundliche und aufgeschlossene Art. Dem Arbeitskreis Kickelbick danke ich für das angenehme Miteinander und die gute Arbeitsatmosphäre.

Ein ganz großes Dankeschön geht an den Arbeitskreis Schäfer, hier vor allem an **Wasim Haider**, welcher mir bereits als Studienkollege in Kaiserslautern ans Herz gewachsen war, und **Inga Bischoff**, welche ich ein ganzes Stück ihres Studiums begleiten durfte und welche als HiWi in unserem Arbeitskreis hervorragende Arbeit geleistet hat. Ebenfalls danke ich **Lisa Wirtz**, **Sergej Lauk**, **Claude Gretsch** sowie **Angelika Stahlich**, welche alle für ein schönes Arbeitsklima sowie viele lustige Momente sorgten. Auch bedanken möchte ich mich bei meinen ehemaligen Bachelor-Studenten und Vertiefern **Joshua Warken**, **Justin Schu**, **Liane Staub**, **Marces-Devonne Calvin-Brown** und **Muniba Bhatti**.

An dieser Stelle möchte ich mich bei einigen Personen aus meiner Studienzeit in Kaiserslautern bedanken. Allen voran ist dies **Prof. Dr. Helmut Sitzmann**, bei welchem ich während meiner Diplomarbeit viel über Cyclopentadienylverbindungen lernen durfte, was mir auch in meiner Zeit in Saarbrücken sehr geholfen hat. Bei **Dr. Wjatscheslaw Gidt** und **Dr. Igor Smytschkow** danke ich für die Unterstützung im Labor, viele hilfreiche Hinweise,

die ich auch heute noch nutzen kann, sowie die familiäre und lockere Atmosphäre im Arbeitskreis Sitzmann.

Ich möchte meinen Eltern **Elke** und **Michael Müller** sowie meinem Bruder **Sebastian Müller** meine Dankbarkeit ausdrücken für die Unterstützung die sie mir zukommen liesen. Besonders meine Mutter hat mich im Laufe meines Studiums immer sehr unterstützt, wofür ich ihr danke.

Zuletzt danke ich **Angie Huszti** für die große Unterstützung während meines Studiums sowie während meiner Promotion und dass sie mir immer ein großer Rückhalt war. Danke für Alles!

Content

List of Abbreviations 1
List of Figures 4
List of Schemes 7
List of Tables 14
1. Introduction 15
1.1 Metallocenes: History and Bonding Characteristics 15
1.2 Beryllocenes 18
1.3 Magnesocenes 23
1.4 Calcocenes 33
1.5 Strontocenes 48
1.6 Barocenes 57
1.7 Lewis Base Adducts of Magnesocenes 72
1.8 Group 14 Metallocenes 80
1.9 Group 14 Halfsandwich Compounds 135
2. Motivation 189
3. Results and Discussion 191
3.1 Carbene Complexes of Stannocenes 191
3.2 Synthesis, Structure, and Bonding Analysis of Tin(II) Dihalide and Cyclopentadienyltin(II) Halide (Alkyl)(amino)carbene Complexes 196
3.3 Bonding Situation in Stannocene and Plumbocene N-Heterocyclic Carbene Complexes 208
3.4 Diphosphanylmetallocenes of Main-Group Elements 221
4. Conclusion 233
5. References 238
6. Supporting Information 244
6.1 Carbene Complexes of Stannocenes 244
6.2 Synthesis, Structure, and Bonding Analysis of Tin(II) Dihalide and Cyclopentadienyltin(II) Halide (Alkyl)(amino)carbene Complexes 286
6.3 Bonding Situation in Stannocene and Plumbocene N-Heterocyclic Carbene Complexes 316
6.4 Diphosphanylmetallocenes of Main-Group Elements 357

List of Abbreviations

Ad	Adamantyl, -$C_{10}H_{15}$
BiPy	2,2'-Bipyridine, $C_{10}H_8N_2$
BDE	Bond dissociation energy
^{tBu}Bcat	5-(*tert*-butyl)-2-benzo[*d*][1,3,2]dioxaborole, $C_{17}H_{16}BO_2$
Bn	Benzyl; -C_7H_7
cAAC	cyclic (alkyl)(amino)carbene, 1-(2,6-di-*iso*propylphenyl)-3,3,5,5-tetramethyl-pyrrolidin-2-ylidene
Cp	Cyclopentadienyl, -C_5H_5
^{Me}Cp	Methylcyclopentadienyl, -$CH_3C_5H_4$
^{Me3}Cp	1,2,4-Trimethylcyclopentadienyl, -$(CH_3)_3C_5H_2$
^{Et}Cp	Ethylcyclopentadienyl, -$(C_2H_5)C_5H_4$
Cp$^{\#}$	1,2,3,4-Tetramethylcyclopentadienyl, -$(CH_3)_4C_5H$
Cp*	Pentamethylcyclopentadienyl, -$(CH_3)_5C_5$
^{TMS}Cp	Trimethylsilylcyclopentadienyl, -$(SiMe_3)C_5H_4$
^{TMS2}Cp	1,3-Bis(trimethylsilyl)cyclopentadienyl, -$(SiMe_3)_2C_5H_3$
^{TMS3}Cp	1,2,4-Tris(trimethylsilyl)cyclopentadienyl, -$(SiMe_3)_3C_5H_2$
^{3}Cp	1,2,4-Tri-*iso*propylcyclopentadienyl, -$^{i}Pr_3C_5H_2$
^{4}Cp	1,2,3,4-Tetra-*iso*propylcyclopentadienyl, -$^{i}Pr_4C_5H$
^{5}Cp	1,2,3,4,5-Penta-*iso*propylcyclopentadienyl, -$^{i}Pr_5C_5$
Cp'	*tert*-Butylcyclopentadienyl, -$^{t}BuC_5H_4$
Cp''	1,3-Di(*tert*-butyl)cyclopentadienyl, -$^{t}Bu_2C_5H_3$
Cp'''	1,2,4-Tri(*tert*-butyl)cyclopentadienyl, -$^{t}Bu_3C_5H_2$
CP/MAS	Cross-polarization/Magic angle spinning
crypt	[2.2.2]cryptand, $C_{18}H_{36}N_2O_6$
CVD	Chemical vapor deposition
Cy	Cyclohexyl, -C_6H_{11}
DFT	Density functional theory
diglyme	Bis(2-methoxyethyl)ether
Dip	2,6-Di-*iso*propylphenyl, -2,6-$^{i}Pr_2C_6H_3$

dme	Dimethoxyethane
dmf	Dimethylformamide
dmso	Dimethylsulfoxide
depe	(Ethane-1,2-diyl)bis(diethylphosphane)
dppe	(Ethane-1,2-diyl)bis(diphenylphosphane)
eq.	equivalents
Et	Ethyl, -C_2H_5
et al.	et alii
Fc	Ferrocene/Ferrocenyl
g	Gram
h	Hour
HMB	Hexamethylbenzene, 1,2,3,4,5,6-$(CH_3)_6C_6$
HOMO	Highest occupied molecular orbital
Hz	Hertz
ipmpa	1-*Iso*propyl-2-methylpropylamine, -$H_2NCH(^iPr)_2$
^{i}Pr	*Iso*propyl, -C_3H_7
^{i}Pr$_2$Me$_2$NHC	1,3-Di-*iso*propyl-4,5-dimethylimidazolin-2-ylidene
IR	Infrared
J	Coupling constant
K	Kelvin
L	Liter
LUMO	Lowest unoccupied molecular orbital
m	Meter
Me	Methyl, -CH_3
Me$_2$bipy	4,4'-Dimethyl-2,2'-bipyridine, $C_{12}H_{12}N_2$
Me$_4$NHC	1,3,4,5-Tetramethylimidazolin-2-ylidene
Mes	Mesityl (2,4,6-trimethyphenyl), -$(CH_3)_3C_6H_2$
MesNHC	1,3-Dimesitylimidazolin-2-ylidene
*n*Bu	*n*-Butyl, -C_4H_9
Naphthyr	1,8-Naphthyridine, $C_8H_6N_2$
NHC	*N*-Heterocyclic Carbene

NHSi	*N*-Heterocyclic Silylene
NIPr	(1,3-Bis(2,6-di-*iso*propylphenyl)imidazolin-2-iminato)
NMR	Nuclear magnetic resonance
Ph	Phenyl, -C_6H_5
pmdta	Methylbis(2-dimethylaminoethyl)amin, $MeN(C_2H_4NMe_2)_2$
ppm	Parts per million
ptfb	Perfluoro-*tert*-butoxide, -$OC(CF_3)_3$
Py	Pyridine/Pyridinyl
Pyraz	Pyrazine, 1,4-Diazabenzene, $C_4H_4N_2$
r.t.	Room temperature
^{t}Bu	*tert*-Butyl, -C_4H_9
OTf	Triflate, -SO_3CF_3
thf	Tetrahydrofuran
tmeda	*N*,*N*,*N*′,*N*′-Tetramethylethane-1,2-diamine, $C_6H_{16}N_2$
^{t}Bu$_2$NHSi	1,3-Di-*tert*-butyl-1,3,2-diazasilol-2-ylidene
TMP	2,2,6,6-Tetramethylpiperidine, $C_9H_{19}N$
TMS	Trimethylsilyl, -$Si(CH_3)_3$
Trip	2,4,6-Tri-*iso*propylphenyl, -^{i}Pr$_3$C$_6$H$_2$
Tp^{Me}	κ^3-*N*,*N*′,*N*″-hydridotris(3,5-dimethyl-1-pyrazolyl)borate
VSEPR	Valence shell electron pair repulsion

List of Figures

Figure 1: Depiction of different hapticities of the cyclopentadienyl ligand. 16
Figure 2: Angle δ. 17
Figure 3: Left: structural proposal by Almenningen *et al*. based on gas phase electron diffraction[23]; right: molecular structure in the solid state revealed by Wong and coworkers.[24] 19
Figure 4: Molecular structure of beryllocene (2a) in the crystal[26] (hydrogen atoms omitted for clarity, ball-and-stick representation). 19
Figure 5: Molecular structure of a) $Cp^{\#}_2Be$ (2c) and b) Cp^*_2Be (2d) in the crystal[32] (hydrogen atoms omitted for clarity, thermal ellipsoids at 50% probability level). 21
Figure 6: Molecular structure of magnesocene (3a) in the crystal[37] (hydrogen atoms omitted for clarity, ball-and-stick representation). 24
Figure 7: Hexakis(trimethylsilyl)magnesocene (3d). 25
Figure 8: Di-*tert*-butylmagnesocene (3i). 26
Figure 9: Octamethyldi-*tert*-butylmagnesocene (3l). 27
Figure 10: Decamethylmagnesocene (3m). 28
Figure 11: Molecular structure of calcocene (4a)[61] in the crystal (hydrogen atoms omitted for clarity, ball-and-stick representation). 34
Figure 12: Left: molecular structure of Cp^*_2Mg (3m)[54] in the crystal (hydrogen atoms omitted for clarity, thermal ellipsoids at 50% probability level; right: molecular structure of Cp^*_2Ca (4b)[63] in the crystal (thermal ellipsoids at 50% probability level). 36
Figure 13: Definition of “inner” and “outer” sphere methyl groups in 4g. 39
Figure 14: Molecular structure of hexa-*tert*-butylcalcocene (4i) in the crystal[48] (hydrogen atoms omitted for clarity, ball-and-stick representation). 40
Figure 15: Molecular structure of $^{H2C=CHC2H4}Cp^{\#}_2Ca$ (4v) in the crystal[59] (hydrogen atoms omitted for clarity, thermal ellipsoids at 50% probability level). 45
Figure 16: Molecular structure of $^{(p\text{-}n\text{BuPh})5}Cp_2Sr$ (5i) in the crystal[80] for clarification of the out-of-plane bending (hydrogen atoms omitted and only *ipso* carbon atoms of (*para*-*n*-butyl)phenyl groups depicted for clarity, remaining aryl groups depicted as wireframe, thermal ellipsoids at 50% probability level). 53
Figure 17: Molecular structure of decamethylbarocene (6b) in the crystal[63] (ball-and-stick representation). 59
Figure 18: Molecular structure of hexakis(trimethylsilyl)barocene[66] (6d) in the crystal (thermal ellipsoids at 50% probability level). 60
Figure 19: Molecular structure of hexa-*tert*-butylbarocene (6i)[79] in the crystal (thermal ellipsoids at 50% probability level). 64
Figure 20: Molecular structure of $(Cp_3Ba)^-$ (6j)[83] in the crystal (counterion omitted for clarity, ball-and-stick representation). 64
Figure 21: Molecular structure of $(C_5Me_4CH_2C_5Me_5)BaCp^*$ (6x)[86] in the crystal (hydrogen atoms omitted for clarity, thermal ellipsoids at 50% probability level). 70
Figure 22: Overview of Lewis base adducts of magnesocenes (hapticity of η^5/η^5 chosen for schematic depiction). 72
Figure 23: Lewis base adducts of magnesocene with: left: acetonitrile (3a·MeCN); right: 1,2-dimethoxyethane (3a·dme).[60] 73
Figure 24: Lewis base adduct of magnesocene with diglyme (3a·diglyme).[60] 73
Figure 25: Lewis base adduct of magnesocene with tmeda (3a·tmeda).[60] 74
Figure 26: Lewis base adduct of magnesocene with two thf molecules $(3a\cdot(thf)_2)$.[29] 74
Figure 27: Lewis base adduct of magnesocene with one thf molecule (3a·thf).[88] 74
Figure 28: Lewis base adduct of magnesocene with one thf molecule and one *tert*-butylamine molecule $(3a\cdot(^t BuNH_2)(thf))$.[89] 75

Figure 29: Lewis base adduct of magnesocene with 1-*iso*propyl-2-methylpropylamine (3a·ipmpa).[90] 75
Figure 30: Interaction of N-H with cyclopentadienyl ligand in magnesocene amine adduct.[90] 76
Figure 31: Lewis base adduct of magnesocene with *iso*propylbenzylamine (3a·HN^{i}PrBn).[91] 76
Figure 32: Lewis base adduct of decamethylmagnesocene (3m) with Me_4NHC (3m·Me_4NHC).[92] 77
Figure 33: Lewis base adduct of: left: octamethylmagnesocene with $^{i}Pr_2Me_2$NHC (3n·$^{i}Pr_2Me_2$NHC); right: 1-trimethylsily-3-*tert*-butylmagnesocene with $^{i}Pr_2Me_2$NHC (3t·$^{i}Pr_2Me_2$NHC).[49] 77
Figure 34: Depiction of the frontier orbitals for a singlet tetrylene (left) and a tetrelocene (right). 80
Figure 35: NMR chemical shifts of selected silylenes, stannylenes, plumbylenes and group 14 cyclopentadienyl compounds.[101–109] 81
Figure 36: Qualitative molecular orbital diagram for tetrelocenes. 82
Figure 37: Section of the qualitative molecular orbital diagram of tetrelocenes comparing the interactions of the s and p_x orbital with total symmetric orbitals of the cyclopentadienyl ligand for coplanar and bent structures. 83
Figure 38: Molecular structures of the a) coplanar and b) bent conformers of decamethylsilicocene (7a)[114] in the crystal (hydrogen atoms omitted for clarity, ball-and-stick representation) 85
Figure 39: Structurally characterized products of oxidative addition reactions between Cp^*_2Si and (from left to right): benzaldehyde, methyl thiocyanate, dimethyl cyanamide and trimethylsilyl cyanide.[123,124] 90
Figure 40: Molecular structure of Cp_2Sn·tmeda (9a·tmeda)[98] in the crystal (hydrogen atoms omitted for clarity, thermal ellipsoids at 50% probability level). 97
Figure 41: Molecular structure (polymeric zig zag) of plumbocene (10a)[15] in the crystal (hydrogen atoms omitted for clarity, ball-and-stick representation). 99
Figure 42: Molecular structures of a) 10a·tmeda and b) 10a·Me_2bipy[99] in the crystal (hydrogen atoms omitted for clarity, ball-and-strick representation). 100
Figure 43: Molecular structure of $^{5}Cp_2Sn$ (9k)[165] in the crystal (hydrogen atoms omitted for clarity, ball-and-stick representation). 108
Figure 44: Molecular structure of (0.5μ-PhCp*^{Me2}Cp)Ge (8p)[181] in the crystal (hydrogen atoms omitted for clarity, ball-and-stick representation). 120
Figure 45: Cationic tin tripledecker compound. 127
Figure 46: Molecular structure of $[Cp_4Sn_3]^{2+}$[98] in the crystal (hydrogen atoms and counter ions omitted for clarity, thermal ellipsoids at 50% probability level). 128
Figure 47: Cationic germanium cyclopentadienyl compound. 129
Figure 48: Anionic lead multidecker compound. 129
Figure 49: Depiction of frontier orbitals in a tetryliumylidene. 135
Figure 50: Molecular structures of penta-*iso*propylcyclopentadienylsilicon cation (7i)[117] in the crystal (hydrogen atoms and tetra(perfluoroalkoxy)aluminate omitted for clarity, thermal ellipsoids at 50% probability level). 137
Figure 51: Molecular structure of pentamethylcyclopentadienylgermanium chloride (8u)[228] in the crystal (hydrogen atoms omitted for clarity, ball-and-stick representation) 147
Figure 52: Molecular structure of (dimehtylaminoethyl)tetramethylcyclopentadienylgermanium chloride (8ah)[232] in the crystal (hydrogen atoms omitted for clarity, ball-and-stick representation). 149
Figure 53: Molecular structure of Cp'''$Ge^{+}GeCl_3^{-}$ (8ajGeCl_3^{-})[234] in the crystal (hydrogen atoms omitted for clarity, thermal ellipsoids at 50% probability level). 153

Figure 54: Molecular structure of Cp*GeCl·$W(CO)_5$ (8u·$W(CO)_5$)[236] in the crystal (hydrogen atoms omitted for clarity, ball-and-stick representation).....155
Figure 55: Molecular structure of CpGeDip (8bc)[243] in the crystal (hydrogen atoms omitted for clarity, thermal ellipsoids at 50% probability level).....158
Figure 56: Molecular structure of 8bd$GeCl_3^-$[171] in the crystal (hydrogen atoms and counter ion omitted for clarity, ball-and-stick representation). 159
Figure 57: Molecular structure of cyclopentadienyltin chloride (9ai)[230] in the crystal (hydrogen atoms omitted for clarity, ball-and-stick representation).....163
Figure 58: Molecular structure of [$^{(t}$BuMe2Si)$Cp^{\#}_6Sn_9Cl_{12}$] (9ay)[247] in the crystal (hydrogen atoms omitted for clarity, cyclopentadienyl ligand depicted as wireframe, thermal ellipsoids at 50% probability level).....165
Figure 59: Molecular structure of Cp*$Sn^+BPh_4^-$ (9aoBPh_4^-)[250] in the crystal displaying Sn-Ph contacts (hydrogen atoms omitted for clarity, thermal ellipsoids at 50% probability level). 170
Figure 60: Molecular structure of CpSn(μ-O^{t}Bu)$_2$Ge(O^{t}Bu) (9bf)[253] in the crystal (hydrogen atoms omitted for clarity, ball-and-stick representation).....174
Figure 61: Molecular structure of Cp*$Pb^+BF_4^-$ (10awBF_4^-)[105] in the crystal (hydrogen atoms omitted for clarity, ball-and-stick representation). 184
Figure 62: From left to right: Cp_2Sn·tmeda (9a·tmeda), Cp_2Pb·tmeda (10a·tmeda) and Cp_2Pb·Me_2bipy (10a·Me_2BiPy) adducts as reported by *Wright et al*.[98,99].....189
Figure 63: Lewis adducts of stannocenes and plumbocene with *N*-heterocyclic carbenes. 233
Figure 64: Complexes of tin(II) compounds with cAAC.....234
Figure 65: Equilibrium between heteroleptic and homoleptic species as well as free cAAC. 235
Figure 66: Synthesis of phosphanyl substituted magnesocenes, tetrelocenes and related complexes as well as a chlorostibonocene and related stibonocenium cation.....236

List of Schemes

Scheme 1: Synthesis of ferrocene (1) as conducted by Pauson and Kealy.[2] 15
Scheme 2: Overview of synthetic procedures for beryllocenes (hapticity of cyclopentadienyl ligands of formed beryllocenes not reflected). 18
Scheme 3: First synthesis of beryllocene (2a) as conducted by Fischer *et al*.[6] 18
Scheme 4: Synthesis of heteroleptic CpBeCp* (2b) as conducted by Pratten *et al*.[31] 20
Scheme 5: Synthesis of $Cp^{\#}{}_2Be$ (2c) and $Cp^*{}_2Be$ (2d) as conducted by Carmona and coworkers.[32] 20
Scheme 6: Synthesis of $Cp^{\#}BeCp^*$ (2e) as conducted by Conejo *et al*.[34].....21
Scheme 7: Overview of possible synthetic routes for magnesocenes. 23
Scheme 8: Synthesis of magnesocene (3a) as conducted by Fischer *et al*.[8] 24
Scheme 9: Synthesis of bis(trimethylsilyl)magnesocene (3b) and tetrakis(trimethylsilyl)magnesocene (3c) as conducted by Duff *et al*.[38] 25
Scheme 10: Synthetic route to hexa-*iso*propylmagnesocene (3h) as conducted by Burkey *et al*.[42] 26
Scheme 11: Synthesis of tetra-*tert*-butylmagnesocene (3j) and hexa-*tert*-butylmagnesocene (3k).[45,46] 27
Scheme 12: Synthesis of $^{(C3H5)2HC}Cp_2Mg$ (3o) and $^{(1\text{-}EtPh)}Cp_2Mg$ (3p) as carried out by Westerhausen and coworkers.[56] 29
Scheme 13: Synthesis of $^{Ph4}Cp_2Mg$ (3q) as carried out by Deacon *et al*.[57] 29
Scheme 14: Synthesis of deca(*p-tert*-butylphenyl)magnesocene (3r) as conducted by Schulte and coworkers.[58].....30
Scheme 15: Synthesis of butenyl substituted magnesocene (3s) as conducted by Schumann *et al*.[59] 30
Scheme 16: Overview of possible synthetic routes for calcocenes.....33
Scheme 17: First synthesis of calcocene (4a) as carried out by Ziegler and coworkers.[9] 34
Scheme 18: Synthesis of decamethylcalcocene (4b) as conducted by Andersen and coworkers.[62] 35
Scheme 19: Metal vapour synthesis of $^{TMS2}Cp_2Ca$ (4c) as conducted by Engelhardt *et al*.[65] 36
Scheme 20: Synthesis of $^{TMS3}Cp_2Ca$ (4d) as carried out by Harvey *et al*.[66].....37
Scheme 21: Synthesis of hexa-*iso*propylcalcocene (4e) as carried by Burkey *et al*.[69] 37
Scheme 22: Synthesis of octa-*iso*propylcalcocene (4f) as conducted by Williams *et al*.[67]38
Scheme 23: Synthesis of deca-*iso*propylcalcocene (4g) as conducted by Sitzmann *et al*.[68] 38
Scheme 24: Metal vapour synthesis of Cp'_2Ca (4h) as conducted by Gardiner *et al*.[44] 39
Scheme 25: Synthesis of hexa-*tert*-butylcalcocene (4i) as conducted by Weber *et al*.[48] ..39
Scheme 26: Synthesis of $4j\cdot(thf)_6$ as carried out by Deacon *et al*.[70] 40
Scheme 27: Synthesis of deca(*para-n*-butylphenyl)calcocene (4k) as reported by Ruspic *et al*.[71] 41
Scheme 28: Synthesis of deca(*para-tert*-butylphenyl)calcocene (4l) as conducted by Schulte *et al*.[58] 42
Scheme 29: Synthesis of $^{Me2NC2H4}Cp^{\#}{}_2Ca$ (4m) as carried out by Jutzi *et al*.[74] 42
Scheme 30: Synthesis of ester functionalized calcocenes (4n, 4o) as carried out by Li *et al*.[72] 43
Scheme 31: Syntheses of methoxy- and amino substituted calcocenes (4p-4s) as conducted by Molander *et al*.[75] 43
Scheme 32: Syntheses of methoxy- and pyridinyl substituted calcocenes (4t, 4u) as carried out by Hays *et al*.[76] 44

Scheme 33: Synthesis of butenyl substituted calcocene (4v) as reported by Schumann *et al*.[59] 45
Scheme 34: Overview of possible synthetic routes for strontocenes. 48
Scheme 35: Synthesis of strontocene (5a) as conducted by Fischer and Stölzle.[10] 49
Scheme 36: Synthesis of $Cp^*_2Sr{\cdot}OEt_2$ (5b·OEt_2) carried out by Burns and coworkers.[77] 49
Scheme 37: Synthesis of $^{TMS2}Cp_2Sr$ (5c) as carried out by Engelhardt *et al*.[65] 49
Scheme 38: Synthesis of $^{TMS3}Cp_2Sr$ (5d) as conducted by Harvey *et al*.[66] 50
Scheme 39: Synthesis of hexa-*iso*propylstrontocene (5e) as conducted by Burkey *et al*.[69] 50
Scheme 40: Synthesis of deca-*iso*propylstrontocene (5f) as carried out by Sitzmann *et al*.[68] 51
Scheme 41: Synthesis of di-*tert*-butylstrontocene (5g) as conducted by Gardiner *et al*.[44] 51
Scheme 42: Synthesis of $Cp'''_2Sr{\cdot}(thf)_x$ (5h·$(thf)_x$) as carried out by Hatanpää *et al*.[79] 52
Scheme 43: Synthesis of deca(*para*-*n*-butylphenyl)strontocene (5i) as conducted by Orzechowski *et al*.[80] 52
Scheme 44: Synthesis of deca(*para*-*tert*-butylphenyl)strontocene (5j) as carried out by Schulte *et al*.[58] 53
Scheme 45: Syntheses of methoxy- and pyridinyl substituted strontocenes (5k, 5l) as conducted by Hays *et al*.[76] 54
Scheme 46: Syntheses of ester functionalized strontocenes (5m, 5n) as carried out by Li *et al*.[72] 54
Scheme 47: Synthesis of butenyl substituted strontocene (5o) as conducted by Schumann *et al*.[59] 55
Scheme 48: Overview of possible synthetic routes for barocenes. 57
Scheme 49: Synthesis of barocene (6a) as conducted by Fischer and Stölzle.[10] 58
Scheme 50: Synthesis of decamethylbarocene thf adduct (6b·thf) as carried out by Andersen *et al*.[78] 58
Scheme 51: Synthesis of $^{TMS2}Cp_2Ba$ (6c) as conducted by Engelhardt *et al*.[65] 59
Scheme 52: Synthesis of hexakis(trimethylsilyl)barocene (6d) as carried out by Harvey *et al*.[66] 60
Scheme 53: Synthesis of hexa-*iso*propylbarocene thf adduct (6e·$(thf)_x$) as carried out by Burkey *et al*.[69] 61
Scheme 54: Synthesis of octa-*iso*propylbarocene (6f) as conducted by Williams *et al*.[67] 61
Scheme 55: Synthesis of deca-*iso*propylbarocene (6g) as carried out by Sitzmann *et al*.[68] 62
Scheme 56: Metal vapor synthesis of di-*tert*-butylbarocene (6h) as conducted by Gardiner *et al*.[44] 62
Scheme 57: Synthesis of hexa-*tert*-butylbarocene (6i) as carried out by Hatanpää *et al*.[79] 63
Scheme 58: Synthesis of octaphenylbarocene thf adduct (6k·thf) as conducted by Tanner *et al*.[84] 65
Scheme 59: Synthesis of decaphenylbarocene thf adduct (6l·$(thf)_x$) as carried out by Deacon *et al*.[70] 65
Scheme 60: Synthesis of deca(*para*-*n*-butylphenyl)barocene (6m) using dibenzylbarium as conducted by Orzechowski *et al*.[80] 66
Scheme 61: Synthesis for deca(*para*-*tert*-butylphenyl)barocene (6n) carried out by Schulte and coworkers.[58] 66
Scheme 62: Synthesis of methoxy- and pyridinyl substituted barocenes (6r, 6s) as carried out by Hays *et al*.[76] 67
Scheme 63: Synthesis of $^{Me2NC2H4}Cp^{\#}_2Ba$ (6p) and $^{EtOC2H4}Cp^{\#}_2Ba$ (6q) as conducted by Hatanpää *et al*.[85] 67

Scheme 64: Synthesis of ester substituted barocenes (6t, 6u) as carried out by Li *et al*.[72] 68
Scheme 65: Synthesis of another ester substituted barocene (6v, 6w) as carried out by Li *et al*.[72] 68
Scheme 66: Synthesis of butenyl substituted barocene (6o) reported by Schumann *et al*.[59] 69
Scheme 67: Synthesis of Cp* based barocene olefin (6x) complex as conducted by Wiecko *et al*.[86] 69
Scheme 68: Overview of synthetic pathways to silicocenes. 84
Scheme 69: Synthesis of decamethylsilicocene as conducted by Ghana *et al*.[115] 85
Scheme 70: Synthesis of Cp*SiCp (7c) as carried out by Jutzi and coworkers.[117] 86
Scheme 71: Synthesis of Cp*Si^{TMS2}Cp (7d) as conducted by Jutzi and coworkers.[117] 86
Scheme 72: Reaction of Cp*Si$^+$ with 1,2,4-trimethylcyclopentadienyllithium as conducted by Jutzi *et al*.[117] 87
Scheme 73: Synthesis of Cp*$_2$SiH$^+$ (7aH$^+$) as reported by Jutzi and Bunte.[118] 87
Scheme 74: Reaction of Cp*$_2$Si (7a) with AuCl(PPh$_3$).[120] 88
Scheme 75: Reaction of Cp*$_2$Si (7a) with CpNiCl(PPh$_3$).[120] 89
Scheme 76: Reaction of Cp*$_2$Si (7a) with Hg$_2$Cl$_2$.[122] 89
Scheme 77: Transmetalation reactions for syntheses of homoleptic, alkyl and silyl substituted tetrelocenes. 92
Scheme 78: Synthesis of germanocene (8a) as conducted by Scibelli *et al*.[13] 93
Scheme 79: Synthesis of germanocene (8a) as carried out by Grenz *et al*.[128] 93
Scheme 80: Synthesis of stannocene (9a) as conducted by Fischer and Grubert.[11] 94
Scheme 81: Reaction of stannocene (9a) with trifluoroborane as carried out by Harrison and Zuckerman.[131] 95
Scheme 82: Synthesis of [Cp$_2$Sn(μ-Fe(CO)$_4$)]$_2$ as conducted by Harrison *et al*.[133,134] 95
Scheme 83: Syntheses of bimetallic complexes as conducted by Cornwell *et al*.[134] 96
Scheme 84: Synthesis of Cp$_2$Sn·tmeda (9a·tmeda) as carried out by Beswick *et al*.[98] 97
Scheme 85: Synthesis of the mixed stannocene CpSnCp* (9d) as conducted by de Lima *et al*.[139] 97
Scheme 86: Synthesis of plumbocene (10a) as carried out by Fischer and Grubert.[12] 98
Scheme 87: Synthesis of 10a·tmeda and 10a·Me$_2$bipy as carried out by Beswick *et al*.[99] 99
Scheme 88: Synthesis of dimethylgermanocene (8b) as conducted by Bonny *et al*.[142] ..101
Scheme 89: Synthesis of dimethylstannocene (9b) as carried out by Dave *et al*.[14] 101
Scheme 90: Synthesis of dimethylplumbocene (10b) as carried out by Dave *et al*.[14] 101
Scheme 91: Synthesis of decamethylgermanocene (8c) and decamethylstannocene (9c) as conducted by Jutzi *et al*.[144] 102
Scheme 92: Synthesis of decamethylplumbocene (10c) as carried out by Atwood and coworkers.[16] 103
Scheme 93: Synthesis of diethyl(octamethyl)plumbocene (10e) as carried out by Evans *et al*.[152] 103
Scheme 94: Synthesis of polyalkylated plumbocenes (10f-h) as conducted by Evans *et al*.[153] 104
Scheme 95: Synthesis of bis(dimethyl-*tert*-butylsilyl)octamethyltetrelocenes (8d, 9e, 10i) as conducted by Constantine *et al*.[154–156] 104
Scheme 96: Synthesis of ^{TMS}Cp$_2$Ge, ^{TMS2}Cp$_2$Ge and ^{TMS3}Cp$_2$Ge (8e-g) as conducted by Jutzi *et al*.[157] 105
Scheme 97: Synthesis of ^{TMS}Cp$_2$Sn, ^{TMS2}Cp$_2$Sn and ^{TMS3}Cp$_2$Sn (9f-h) as conducted by Cowley *et al*.[158,159] 105
Scheme 98: Synthesis of ^{TMS}Cp$_2$Pb, ^{TMS2}Cp$_2$Pb and ^{TMS3}Cp$_2$Pb (10d,j,k) as conducted by Jutzi *et al*.[160] 106

Scheme 99: Synthesis of hexa(*iso*propyl)- and octa(*iso*propyl)stannocene (9i; 9j) as conducted by Burkey and Hanusa.[164] 107
Scheme 100: Synthesis of deca(*iso*propyl)stannocene (9k) as conducted by Sitzmann *et al*.[165] 108
Scheme 101: Synthesis of hexa(*iso*propyl)plumbocene (10l) as carried out by Burkey *et al*.[166,167] 109
Scheme 102: Synthesis of octa(*iso*propyl)- and deca(*iso*propyl)plumbocene (10m; 10n) as conducted by Sitzmann *et al*.[168] 109
Scheme 103: Synthesis of di-*tert*-butylstannocene (9l) as conducted by Hani and Geanangel.[169] 110
Scheme 104: Synthesis of tetra-*tert*-butyltetrelocenes (8h, 9m, 10o) as carried out by Jutzi and coworkers.[170] 111
Scheme 105: Synthesis of hexa-*tert*-butylplumbocene (10p) as carried out by Sitzmann *et al*.[168] 111
Scheme 106: Synthesis of $[Me_2Si[1](\eta^5\text{-}Cp^{\#})(Cp^{\#}H)]_2E$ (8i, 9n, 10q) as conducted by Jutzi *et al*.[171] 112
Scheme 107: Overview of syntheses of homoleptic, aryl substituted tetrelocenes. 114
Scheme 108: Synthesis of octaphenyltetrelocenes (8j, 9o, 10r) as conducted by Schumann *et al*.[172,173] 114
Scheme 109: Synthesis of phenyl substituted tetrelocenes (8l, 9q, 10t) as carried out by Schumann *et al*.[172,173] 115
Scheme 110: Synthesis of decaphenyltetrelocenes (8k, 9p, 10s) as conducted by Heeg and coworkers.[174,175] 115
Scheme 111: Synthesis of decabenzyltetrelocenes (8m, 9r, 10u) as conducted by Schumann *et al*.[176,177] 116
Scheme 112: Synthesis of deca(para-*iso*propylbenzyl)germanocene (8n) as conducted by Naglav *et al*.[178] 117
Scheme 113: Synthesis of deca(*para*-*n*-butylphenyl)stannocene (9s) as carried out by Harder *et al*.[147] 117
Scheme 114: Synthesis of deca(*para*-*tert*-butylphenyl)tetrelocenes (8o, 9t, 10v) as conducted by Schulte *et al*.[58] 118
Scheme 115: Synthesis of oxygen containing aryl substituted tetrelocenes (9u, 10w, 10x) as conducted by Lowack *et al*.[179] 119
Scheme 116: Synthesis of bis(germanocenes) and bis(stannocenes) as conducted by Rouzaud *et al*.[180,181] 120
Scheme 117: Synthesis of mono- and bis(ferrocenyl) substituted tetrelocenes (8v, 8w, 9z, 9aa) as conducted by Joudat *et al*.[182] 121
Scheme 118: Synthesis of di(bis[di*iso*propylamino]phosphanyl)stannocene (9ab) as carried out by Cowley *et al*.[158] 122
Scheme 119: Synthesis of bis(*iso*propyldimethylphosphine)octamethylstannocene (9ac) and -plumbocene (10y) as conducted by Bellabarba *et al*.[183] 122
Scheme 120: Synthesis of bis(trimethylstannyl)stannocene (9ad) as carried out by Bulten and Budding.[184] 123
Scheme 121: Synthesis of heteroleptic germanocenes (8x-z) as conducted by Jutzi *et al*.[185] 124
Scheme 122: Synthesis of 9ae and 10z as carried out by Cowley *et al*.[186] 124
Scheme 123: Synthesis of heteroleptic, acetyl and ester functionalized stannocenes (9af-ah) as conducted by Dory *et al*.[187] 125
Scheme 124: Synthesis of pentaphenylstannocene (9aj) as carried out by Heeg *et al*.[175] 125
Scheme 125: Overview of heterotetrelocenes obtained by transmetalation. 126

Scheme 126: Synthesis of silyliumylidene Cp*Si^{+}B(C$_6$F$_5$)$_4^-$ (7bB(C$_6$F$_5$)$_4^-$) as conducted by Jutzi *et al*.[102] 136
Scheme 127: Synthesis of ^{5}CpSi^{+}Al(ptfb)$_4^-$ (7iAl(ptfb)$_4^-$) as carried out by Jutzi *et al*.[117] 137
Scheme 128: Synthesis of pentamethylcyclopentadienylsilicon(2,6-(Trip)$_2$C$_6$H$_3$) (7j) as carried out by Jutzi *et al*.[215] 138
Scheme 129: Synthesis of Cp*SiFeCp*(CO)$_2$ (7bFeCp*(CO)$_2$) as carried out by Jutzi *et al*.[216] 138
Scheme 130: Degradation of ethers catalyzed by 7bB(C$_6$F$_5$)$_4^-$ on the example of the degradation of dme as conducted by Jutzi *et al*.[218] 139
Scheme 131: Synthesis of Cp*Si(NIPr) (7k) as carried out by Inoue and Leszczyńska.[220] 140
Scheme 132: Synthesis of Cp*Si(NIPr)[B(C$_6$F$_5$)$_3$] (7l) as conducted by Inoue and Leszczyńska.[220] 140
Scheme 133: Synthesis of molybdenum silylidyne complex (7bMoTp^{Me}(CO)$_2$) as carried out by Ghana *et al*.[115] 141
Scheme 134: Synthesis of Cp*SiSi(TMS)$_3$ (7m) as conducted by Leszczyńska *et al*.[223] 142
Scheme 135: Synthesis of Cp*Si(Me$_4$NHC)Si(TMS)$_3$ (7m·Me$_4$NHC) as conducted by Leszczyńska *et al*.[223] 142
Scheme 136: Reaction between 7m and ^{t}Bu$_2$NHSi as carried out by Leszczyńska *et al*.[223] 143
Scheme 137: Synthesis of Lewis adducts of Cp*(N[TMS]$_2$)Si (7h) with aluminum(III) halides and oxidative addition of diphenylchlorophospine at silicon center of Cp*(N[TMS]$_2$)Si (7h) as conducted by Sen *et al*.[224] 143
Scheme 138: Synthesis of pentamethylcyclopentadienylgermanium chloride (8u) as carried out by Jutzi *et al*.[226] 146
Scheme 139: Synthesis of (Cp*GeBr)$_2$ (8af)$_2$ as conducted by Winter *et al*.[228] 147
Scheme 140: Synthesis of (Cp*GeI)$_\infty$ (8ag) as conducted by Filippou *et al*.[231] 148
Scheme 141: Synthesis of (dimehtylaminoethyl)tetramethylcyclopentadienylgermanium chloride (8ah) as carried out by Jutzi *et al*.[232] 148
Scheme 142: Synthesis of CpGe^{+}(μ-F{Al(ptfb)$_3$}$_2$)$^-$ (8ae(μ-F{Al(ptfb)$_3$}$_2$)$^-$) as carried out by Schorpp *et al*.[196] 149
Scheme 143: Synthesis of Cp*Ge^{+}BF$_4^-$ (8aaBF$_4^-$) as conducted by Jutzi and coworkers.[144] 150
Scheme 144: Syntheses of pentamethylcyclopentadienyl substituted germyliumylidenes by halide abstraction. 151
Scheme 145: Synthesis of Cp*Ge^{+}AlCl$_4^-$ (8aaAlCl$_4^-$)as conducted by Sen *et al*.[224] 151
Scheme 146: Synthesis of Cp*Ge$^{+(COOMe)5}$Cp$^-$ (8aa$^{(COOMe)5}$Cp$^-$) as conducted by Jutzi *et al*.[188] 152
Scheme 147: Synthesis of Cp*Ge^{+}OTf$^-$ (8aaOTf$^-$) as carried out by Jutzi *et al*.[233] 152
Scheme 148: Synthesis of Cp''Ge^{+}BF$_4^-$ (8aiBF$_4^-$) as conducted by Jutzi *et al*.[170] 153
Scheme 149: Synthesis of Cp'''Ge^{+}GeCl$_3^-$ (8ajGeCl$_3^-$) as conducted by Ding *et al*.[234] ..153
Scheme 150: Syntheses of heteroleptic germylenes as conducted by Jutzi *et al*.[185,235] .154
Scheme 151: Syntheses of chromium- and tungstenpentacarbonyl complexes of CpGeCl and Cp*GeCl (8u) as conducted by Jutzi *et al*.[236] 155
Scheme 152: Syntheses of various substituted tungstenpentacarbonyl germylene complexes as carried out by Jutzi *et al*.[238] 156
Scheme 153: Syntheses of germylene substituted group 6 metal complexes as conducted by Filippou *et al*.[231,239–241] 157
Scheme 154: Syntheses of Lewis base adducts of Cp*Ge^{+}OTf$^-$ (8aaOTf$^-$) as carried out by Jutzi *et al*.[242] 157
Scheme 155: Synthesis of the heteroleptic germylene CpGeDip (8bc) as conducted by Summerscales *et al*.[243] 158

Scheme 156: Syntheses of olefin complexes of germyliumylidenes as conducted by Jutzi *et al*.[171] 159
Scheme 157: Syntheses of cyclopentadienyltin halides (9ai, 9av) as conducted by Bos *et al*.[245] 162
Scheme 158: Synthesis of cyclopentadienyltin iodide (9au) as carried out by Bos *et al*.[136] 162
Scheme 159: Synthesis of Cp*SnCl (9y) as conducted by Constantine *et al*.[109] 164
Scheme 160: Synthesis of $^{(t\text{BuMe2Si})}$Cp$^{\#}$SnCl (9ax) as carried out by Constantine *et al*.[109] 164
Scheme 161: Synthesis of catecholborane substituted tin halfsandwich complex (9az) as conducted by Cassani *et al*.[248] 166
Scheme 162: Homoleptic/heteroleptic equilibrium as suggested by *Cassani et al*.[248] 166
Scheme 163: Redistribution reaction between tri-*iso*propyl- and tetra-*iso*propylcyclopentadienyltin halfsandwich and corresponding sandwich compounds.[164] 167
Scheme 164: Synthesis of Cp*Sn$^{+(\text{COOMe})5}$Cp^{-} (9a$^{(\text{COOMe})5}$Cp^{-}) as carried out by Jutzi *et al*.[188] 167
Scheme 165: Synthesis of pentamethylcyclopentadienylstannyliumylidene tetrafluoroborate (9aoBF$_4^-$) as conducted by Jutzi *et al*.[144,249] 168
Scheme 166: Syntheses of cyclopentadienyl stannyliumylidenes as carried out by Jutzi *et al*.[51] 168
Scheme 167: Synthesis of Cp*Sn$^+$B(C$_6$F$_5$)$_4^-$ (9aoB(C$_6$F$_5$)$_4^-$) as conducted by Rhodes *et al*.[104] 169
Scheme 168: Synthesis of Cp*Sn$^+$BPh$_4^-$ (9aoBPh$_4^-$) as carried out by Beckmann *et al*.[250] 169
Scheme 169: Syntheses of 9bbBF$_4^-$ and 9bbOTf$^-$ as conducted by de Lima *et al*.[251,252] 170
Scheme 170: Synthesis of Cp'Sn$^+$BF$_4^-$ (9bcBF$_4^-$) as carried out by Hani and Geanangel.[169] 171
Scheme 171: Synthesis of 9bdBF$_4^-$ as conducted by Jutzi and Dickbreder.[170] 171
Scheme 172: Synthesis of Cp'''Sn$^+$SnCl$_3^-$ (9beSnCl$_3^-$) as conducted by Ding *et al*.[234] 172
Scheme 173: Cyclopentadienyl substituted stannyliumylidenes obtained by Schleep *et al*.[195] 172
Scheme 174: Synthesis of CpSn$^+$Al(ptfb)$_4^-$·HMB (9aqAl(ptfb)$_4^-$·HMB) as conducted by Schorpp *et al*.[196] 173
Scheme 175: Syntheses of homo- and heterobimetallic complexes as conducted by Veith *et al*.[253,254] 174
Scheme 176: Synthesis of (^{t}BuO)$_2$ClZr[μ-Cl(CpSn)](μ-O^{t}Bu)$_2$ZrCl(O^{t}Bu)$_2$ (9bl) as conducted by Njua *et al*.[257] 175
Scheme 177: Synthesis of Lewis acid base adducts of 9aoOTf$^-$ and 9aoBF$_4^-$ as conducted by Kohl *et al*.[242] 176
Scheme 178: Synthesis of cyclopentadienyltin (bis(dimethylamino)methylene)amide (9bm) as conducted by Paver *et al*.[258] 176
Scheme 179: Synthesis of cyclopentadienyltin imino complex (9bk) as conducted by Ochiai and Inoue.[255] 177
Scheme 180: Synthesis of transition metal complexes of Cp*SnCl (9y) as conducted by Jutzi *et al*.[236] 178
Scheme 181: Synthesis of cyclopentadienyltin halide bridged iron tetracarbonyl complexes as conducted by Sriyunyongwat *et al*.[207] 178
Scheme 182: Synthesis of CpSnDip (9bn) as carried out by Summerscales *et al*.[243] 179
Scheme 183: Synthesis of Cp*Sn(2,6-(Trip)$_2$C$_6$H$_3$) (9bo) as conducted by Sindlinger *et al*.[259] 179

Scheme 184: Syntheses of olefin complexes of stannyliumylidenes as conducted by Jutzi *et al*.[171] 180
Scheme 185: Syntheses of lead halfsandwich complexes as carried out by Holliday *et al*.[261,262] 183
Scheme 186: Synthesis of pentamethylcyclopentadienyllead chloride (10av) as conducted by Jutzi *et al*.[105] 183
Scheme 187: Syntheses of plumbyliumylidenes as conducted by Jutzi *et al*.[105] 184
Scheme 188: Synthesis of $Cp^*Pb^+B(C_6F_5)_4^-$ (10awB$(C_6F_5)_4^-$) as conducted by Jones *et al*.[194] 185
Scheme 189: Synthesis of $Cp''Pb^+BF_4^-$ (10axBF_4^-) as carried out by Jutzi and Dickbreder.[170] 185
Scheme 190: Synthesis of Lewis base adducts of cyclopentadienyl substituted plumbyliumylidenes as conducted by Jutzi *et al*.[105] 186
Scheme 191: Synthesis of $CpPb(\mu\text{-}O^tBu)_2Sn(O^tBu)$ (10ay) as conducted by Veith *et al*.[254] 186
Scheme 192: Syntheses of olefin complexes of plumbyliumylidenes as conducted by Jutzi *et al*.[171] 187
Scheme 193: Reaction of cyclopentadienyltin and -lead compounds with *N*-heterocyclic carbenes. 189
Scheme 194: Reaction of diphosphanylmetallocenes with small molecules and main group and transition metal fragments. 190
Scheme 195: Equilibrium between carbene complexes and uncoordinated stannocene and NHC. 234

List of Tables

Table 1: Selected structural parameters and references of beryllocenes. 22
Table 2: Selected structural parameters and references of magnesocenes. 32
Table 3: Selected structural parameters and references of calcocenes. 47
Table 4: Selected structural parameters and references of strontocenes. 56
Table 5: Selected structural parameters and references of barocenes. 71
Table 6: Selected structural parameters and references of Lewis base adducts of magnesocenes. 79
Table 7: ^{29}Si NMR shifts, selected structural parameters and references for silicocenes. .91
Table 8: Heteronuclear NMR shifts, selected structural parameters and references for heavier group 14 metallocenes and related Lewis base adducts. 130
Table 9: ^{29}Si NMR shifts, selected structural parameters and references of cyclopentadienylsilicon halfsandwich compounds. 144
Table 10: Selected structural parameters and references of cyclopentadienylgermanium halfsandwich compounds. 160
Table 11: ^{119}Sn NMR shifts, selected structural parameters and references of cyclopentadienyltin halfsandwich compounds. 181
Table 12: ^{207}Pb NMR shifts, selected structural parameters and references of cyclopentadienyllead halfsandwich compounds. 188

1. Introduction

1.1 Metallocenes: History and Bonding Characteristics

The first metallocene to be reported was ferrocene (**1**), which was discovered accidentally in the 1950s by the groups of Pauson and Miller independently.[1,2] Pauson and Kealy obtained ferrocene by the reaction of cyclopentadienylmagnesium bromide with iron(III)chloride (Scheme 1).

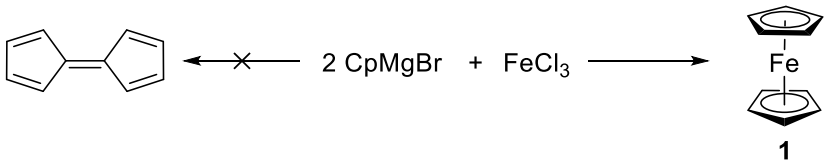

1

Scheme 1: Synthesis of ferrocene (**1**) as conducted by Pauson and Kealy.[2]

The initial aim of the authors was to prepare a fulvalene, but after workup of the reaction mixture yellow crystals were obtained which did not decompose when exposed to air or even to strong acids. On the basis of the analytical data of this yellow compound, the authors concluded that bis(cyclopentadienyl)iron had formed.[2] Miller *et al*. investigated the synthesis of amines by reaction of hydrocarbons with nitrogen for which reason they reacted cyclopentadiene under nitrogen atmosphere with reduced iron. To their surprise, the authors isolated a yellow solid which sublimed readily and came to the conclusion that this compound was an iron complex; ferrocene (**1**). The first proposal of the structure of ferrocene by Pauson and Kealy contained of an iron atom σ bonded to the two cyclopentadienyl ligands, but they already recognized the aromaticity of the cyclopentadienyl ligand to be important for the stability of ferrocene.[2] In 1956, Dunitz *et al*. reported the structure of ferrocene in the crystal: Two π complexed cyclopentadienyl ligands are attached to the central iron atom in an η^5 fashion.[3] This result was in line with the observation of a single stretching band for C-H in the infrared spectrum of ferrocene and that the dipole moment was zero as well as the fact that the compound was diamagnetic.[4] Already in 1952, Fischer and Pfab suggested that ferrocene exhibits noble gas configuration due to the 12 electrons from the cyclopentadienyl ligands and 6 electrons from the central iron(II)atom leading to 18 valence

electrons for this π complex.[5] Closely linked to the remarkable history of ferrocene is the history of the unsubstituted main group metallocenes, many of which were discovered in the 1950s and at the beginning of the 1960s.[6–13] The first main group metallocene, magnesocene (**3a**), was discovered in 1954 by the groups of Wilkinson and Fischer.[7,8] This compound was obtained as a colorless, crystalline solid by heating cyclopentadienylmagnesium bromide.[8] In 1956, stannocene (**9a**) and plumbocene (**10a**) were discovered by Fischer and Grubert, who observed that both compounds exhibit dipole moments which shows that these metallocenes cannot possess a coplanar structure as it was observed for ferrocene (**1**). On basis of these dipole moment measurements, the authors concluded that in both complexes the central atom is σ bonded to the cyclopentadienyl ligands. However, in 1959 already, Dave *et al*. could provide evidence for π complexation of the cyclopentadienyl ligands in stannocene (**9a**) and plumbocene (**10a**) by IR spectroscopy.[11,12,14] The final proofs for the bent sandwich structures of both group 14 metallocenes were the reports of the structures in the solid state in 1966 (**10a**) and 1981 (**9a**).[15,16] In contrast to ferrocene chemistry, where various substitution patterns have been introduced to the cyclopentadienyl ligands,[17] main group metallocenes mostly possess alkyl, silyl, aryl or benzyl substituents, ,while functional groups are extreme rare, as will be discussed in the chapters 1.2 to 1.8.

The cyclopentadienyl ligands in transition metal compounds most often exhibit a hapticity of η^5, whereas in cyclopentadienyl compounds of main group elements σ/η^1 bonded and η^3 bonded Cp groups are quite common, in addition to the η^5 coordination motif.[17–20]

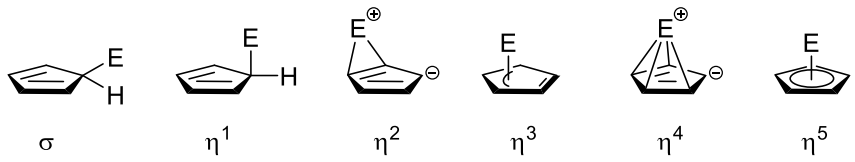

Figure 1: Depiction of different hapticities of the cyclopentadienyl ligand.

The hapticities will be drawn as shown in Figure 1 in this thesis, though other representations exist in literature.[21] It is worth mentioning that the bonding of cyclopentadienyl ligands *via* only one carbon atom to a central atom is sometimes referred to as η^1, which can differ from classical σ bonding. The differences between the coordination modes of σ and η^1 are a tetrahedral coordination environment at the *ipso* carbon atom as well as unequal C-C bond

lengths refering to single and double bonds, along with an E-Cp^{plane} angle which is significantly larger than 90° in case of σ bonded cyclopentadienyl ligands. One the other hand, a bonding may be refered to as η^1, when relatively equal C-C bond lengths, depicting a high degree of aromaticity, along with an E-Cp^{plane} angle close to 90° are observed. Classically σ bonded cyclopentadienyl ligands are often observed for E-Cp bonds exhibiting an increased covalent character, as is the case in many p block cyclopentadienyl compounds, while for cyclopentadienyl compounds of s block elements, which exhibit a more ionic bonding character, the η^1 coordination mode is sometimes observed in the solid state. It must be noted however that in many cases a clear distinction between these two bonding modes is difficult.

Another important structural characteristic of metallocenes is the angle δ, which can be used to describe the degree of the bending in a metallocene moiety (Figure 2).

Figure 2: Angle δ.

Many metallocenes of main group elements exhibit bent structures, the reason for which will be discussed in detail later. Bulky substituents at the cyclopentadienyl ligand can influence the degree of bending in main group metallocenes, but in most cases no unequivocal predictions can be done on basis of the substitution pattern of the cyclopentadienyl ligand.

In the next chapters, the group 2 metallocenes will be presented and their synthesis, structural features and reactivities will be discussed. Following this, group 14 metallocenes will be discussed, which all exhibit a hapticity of η^5/η^5 and an elevated covalent bonding character in comparison to group 2 metallocenes. The last chapter of the introduction deals with the group 14 halfsandwich compounds, which are closely related to their metallocene analogues.

1.2 Beryllocenes

All beryllocenes known were obtained by transmetalation of beryllium(II)chloride or cyclopentadienylberyllium chloride with alkali metal cyclopentadienides (Scheme 2).

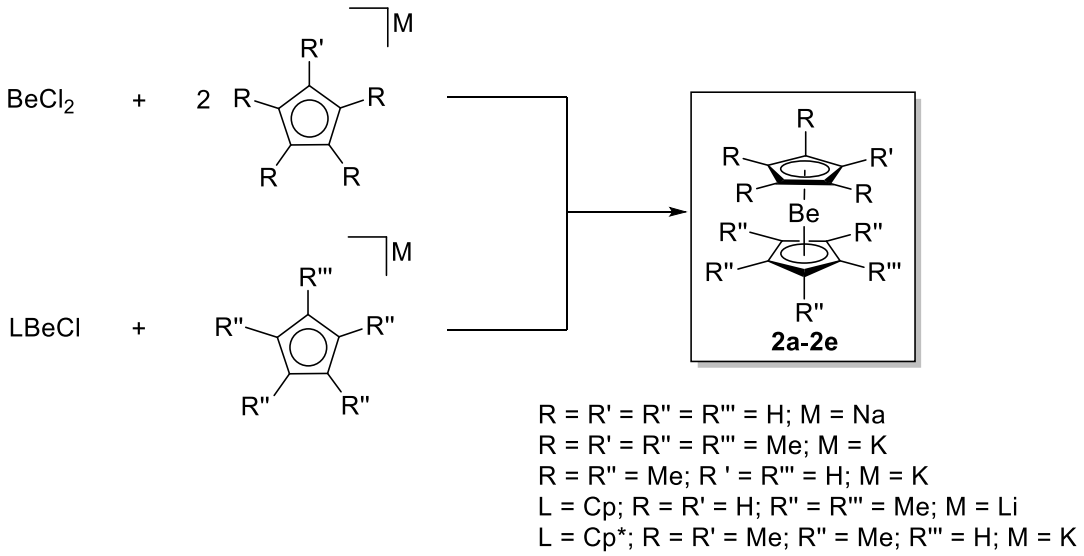

Scheme 2: Overview of synthetic procedures for beryllocenes (hapticity of cyclopentadienyl ligands of formed beryllocenes not reflected).

The history of the lightest alkaline earth metallocenes started with beryllocene (**2a**), which was first synthesized in 1959 by Fischer *et al*.[6] by the reaction of cyclopentadienylsodium with beryllium(II)chloride and described as an highly air sensitive, colorless compound (Scheme 3).

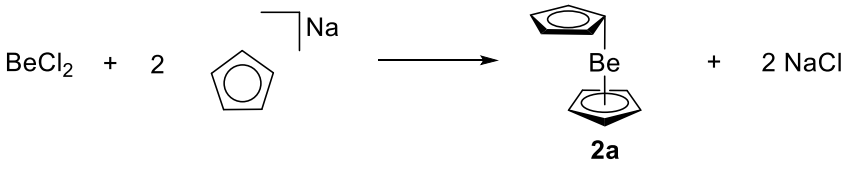

Scheme 3: First synthesis of beryllocene (**2a**) as conducted by Fischer *et al*.[6]

In contrast to magnesocene, **3a**, which was discovered 1954 independently from the groups of Wilkinson and Fischer,[7,8] beryllocene exhibited a dipole moment in solution. Fischer and

coworkers concluded on the basis of these dipole moment measurements and infrared spectroscopy that beryllocene, **2a**, did neither consist of two η^1 nor of two η^5 bound cyclopentadienyl rings, but presumably of one η^1 and one η^5 bound cyclopentadienyl ring.[6] Further infrared spectroscopic studies in the solid state investigated the bonding character in various cyclopentadienyl compounds revealing that the element cyclopentadienyl bonding in beryllocene exhibited a significant degree of ionic character, which was also observed for magnesocene.[22] In 1964, Almenningen *et al*. conducted gas phase electron diffraction (GED) studies on beryllocene concluding that **2a** should possess a C_{5V} symmetry and, by that, a coplanar geometry with both η^5 bound cyclopentadienyl rings (Figure 3).[23]

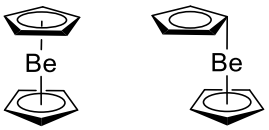

Figure 3: Left: structural proposal by Almenningen *et al*. based on gas phase electron diffraction[23]; right: molecular structure in the solid state revealed by Wong and coworkers.[24]

These results were revised 15 years later by Almenningen and coworkers, who proposed an η^5/η^1 hapticity for beryllocene based on gas phase electron diffraction spectroscopy considering the slipped-sandwich structure which was reported by Wong *et al*. in 1972.[24,25] The final proof for the slipped-sandwich structure of **2a** came with the molecular structures in the solid state in 1972, 1973 and 1984 at different temperatures (Figure 4).[24,26,27]

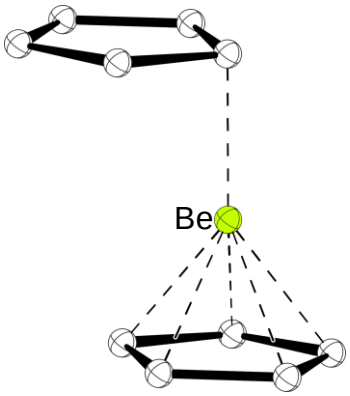

Figure 4: Molecular structure of beryllocene (**2a**) in the crystal[26] (hydrogen atoms omitted for clarity, ball-and-stick representation).

This slipped-sandwich type structure was first observed for **2a**, but is also present in other cyclopentadienyl compounds, for example in decamethylzincocene or Lewis base adducts of magnesocene.[28,29] Though beryllocene possesses an η^1 bound cyclopentadienyl ring, there is no evidence for located single or double bonds in that ring which can be seen in the equidistant C-C bond lengths in both cyclopentadienyl rings for which reason the Be-Cp bond should not be regarded as a σ bond.[30] The hapticity of η^1 can be justified by the small size of the central berrylium atom as well as the highly ionic bonding character in this metallocene. Another example of a beryllocene, CpBeCp* (**2b**), was reported by Pratten *et al*. in 1990. Their synthetic approach for this heteroleptic metallocene in solution failed for which reason they conducted the synthesis by the reaction of CpBeCl and LiCp* in the melt at 333 K (Scheme 4).[31]

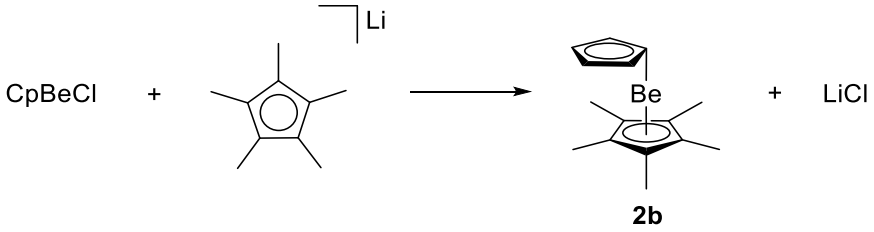

Scheme 4: Synthesis of heteroleptic CpBeCp* (**2b**) as conducted by Pratten *et al*.[31]

However, **2b** was only characterized by NMR and infrared spectroscopy providing evidence for the formation of this compound.[31] In 2000, Carmona *et al*. introduced the tetramethylcyclopentadienyl ligand ($Cp^{\#}$) and pentamethylcyclopentadienyl ligand (Cp*) to beryllium chemistry. Both beryllocenes were obtained by transmetalation reaction of beryllium(II)chloride with the corresponding potassiumcyclopentadienides (Scheme 5).[32]

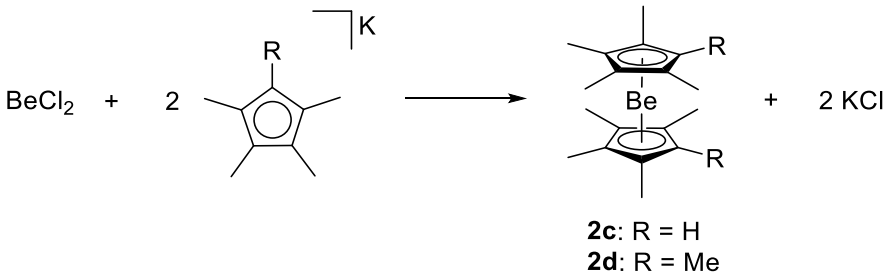

Scheme 5: Synthesis of $Cp^{\#}_2Be$ (**2c**) and Cp^*_2Be (**2d**) as conducted by Carmona and coworkers.[32]

In solution, $Cp^{\#}_2Be$ (**2c**) exhibited a high fluxionality in analogy to Cp_2Be (**2a**), which was not reflected by ^1H NMR spectroscopy but was demonstrated by spin-spin coupling between ^{13}C and ^9Be.[32,33] $Cp^{\#}_2Be$ (**2c**) possesses a similar molecular structure in the solid state compared to Cp_2Be (**2a**), where one cyclopentadienyl ring is η^5 bound and the other one η^1.[32] In contrast to that finding, **2d** exhibits a coplanar arrangement of the cyclopentadienyl ligands in the solid state with a hapticity of η^5/η^5, presumably due to the sterics of the Cp* ligand and packing effects in the crystal.[32] Another reason for the observed sandwich structure of **2d** might also be repulsive van der Waals interactions between the methyl groups of the cyclopentadienyl rings. The Be-Cp^{cent} distances are relatively long compared to those in **2a** and **2c**, presumably due to the elevated steric demand of the Cp* ligand and the presence of an η^5/η^5 coordination mode in **2d** in contrast to an η^1/η^5 coordination mode found in **2a** and **2c**.[32]

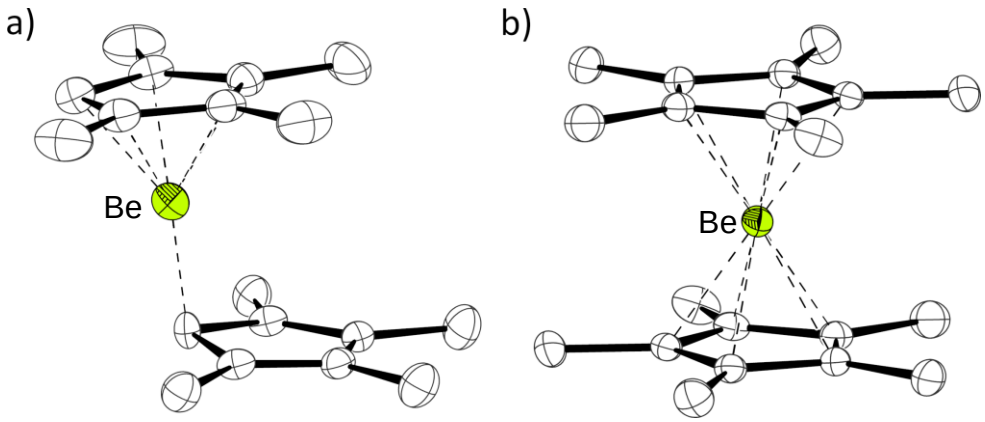

Figure 5: Molecular structure of a) $Cp^{\#}_2Be$ (**2c**) and b) Cp^*_2Be (**2d**) in the crystal[32] (hydrogen atoms omitted for clarity, thermal ellipsoids at 50% probability level).

In 2003, the mixed slipped-sandwich complex nonamethylberyllocene (**2e**) was synthesized by Conejo *et al*. by reaction of Cp*BeCl with $KCp^{\#}$ (Scheme 6).[34]

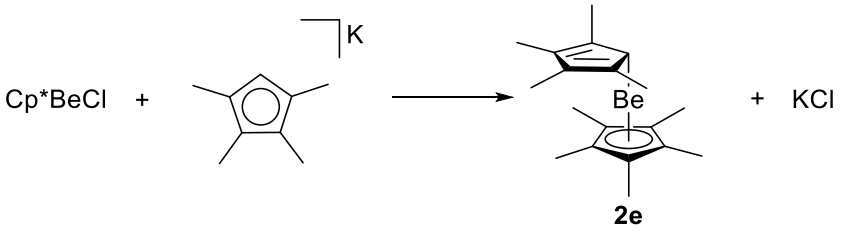

Scheme 6: Synthesis of $Cp^{\#}BeCp^*$ (**2e**) as conducted by Conejo *et al*.[34]

In the solid state structure of this compound, a hapticity of η^1/η^5 with a Be-Cp^{cent} distance of 147.36(25) pm was found similar to the structures of **2a** and **2c**.[34]

In conclusion, it can be stated that an important feature of beryllocene chemistry is the fluxional behavior of the compounds in solution as determined by IR and NMR spectroscopy.[31–33,35] Only five examples of beryllocenes exist of which four are structurally characterized. In the solid state **2a**, **2c** and **2e** exhibit slipped-sandwich structures[24,26,27,32,34] presumably due to the high ionic character of the Be-Cp bonding. In the molecular structure in the solid state of **2d**, both cyclopentadienyl ligands are η^5 bound probably due to the steric demand of the Cp* ligand and packing effects in the crystal, but the difference in energy between the η^5/η^5 and η^1/η^5 coordination modes is very small, as DFT calculations suggest.[32,34]

Table 1: Selected structural parameters and references of beryllocenes.

Compound	Cp^{cent}-Be-Cp^{cent} δ[°][a]	Cp^{cent}-Be [pm][a]	Reference
Cp_2Be (**2a**)	-	150.78(64)[26]	[6,23–27]
CpBeCp* (**2b**)	-	-	[31]
$Cp^{\#}{}_2Be$ (**2c**)	-	147.10(67)	[32]
$Cp^*{}_2Be$ (**2d**)	179.9	165.5	[32]
$Cp^{\#}$BeCp* (**2e**)	-	147.36(25)	[34]

[a]: Only given in the case of η^5 coordination of cyclopentadienyl ligand to beryllium atom.

1.3 Magnesocenes

The deprotonation with dibutylmagnesium is the most common synthetic route for magnesocenes, but also other routes exist from transmetalation of magnesium(II)bromide with tri-*iso*propylcyclopentadienylpotassium to the thermally driven reactions of magnesium with cyclopentadiene or the disproportionation of cyclopentadienylmagnesium bromide or the reaction of the anthracenylmagnesium tris(thf) adduct with penta(*para*-*tert*-butylphenyl)cyclopentadiene radical (Scheme 7).

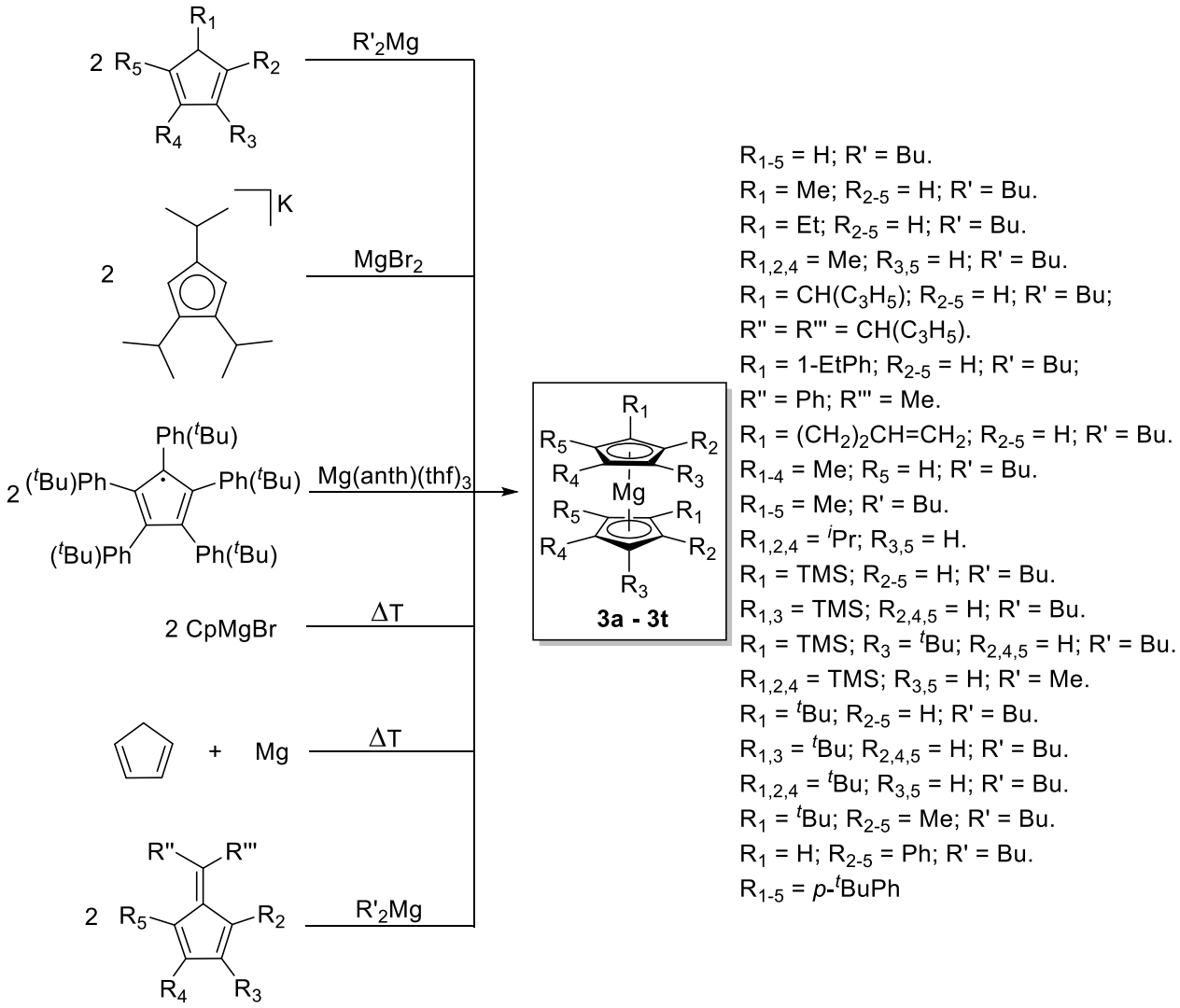

Scheme 7: Overview of possible synthetic routes for magnesocenes.

Only shortly after the groundbreaking discovery of ferrocene, the first main group metallocene, magnesocene (**3a**), was discovered. The first preparation was conducted by heating

cyclopentadienylmagnesium bromide and subliming off the resulting magnesocene (Scheme 8).[8]

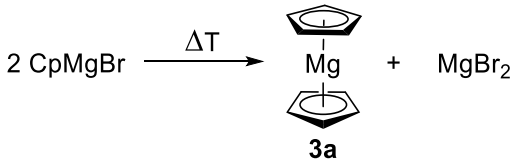

Scheme 8: Synthesis of magnesocene (**3a**) as conducted by Fischer *et al*.[8]

In fact, Fischer and coworkers did not intend to synthesize magnesocene, but observed the formation of this colorless material during the workup of cyclopentadienylvanadiumtetracarbonyl.[8] One year later, the structure of magnesocene in the solid state could be revealed by X-ray crystallography[36] and in 1975, Bünder and Weiss reported a refinement of the structure of **3a**.[37] The two cyclopentadienyl rings exhibit a staggered conformation and are practically coplanar making magnesocene, **3a**, isostructural to ferrocene (Figure 6).

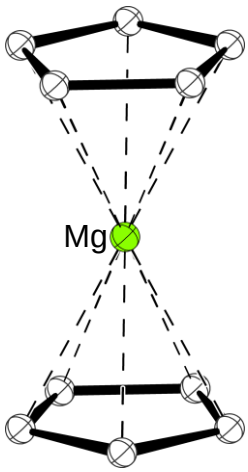

Figure 6: Molecular structure of magnesocene (**3a**) in the crystal[37] (hydrogen atoms omitted for clarity, ball-and-stick representation).

The Mg-Cp^{cent} distance in Cp_2Mg (**3a**) is with 199.11(1) pm significantly elongated in comparison to the Fe-Cp^{cent} distance in Cp_2Fe (**1**) (166.06(11) pm[3]) justified by the stronger covalent character of the Fe-Cp bond in comparison to the more ionic Mg-Cp bond. In 1985, the first report of the usage of dibutylmagnesium as starting material for the synthesis of a

magnesocene together with the synthesis of bis(trimethylsilyl)magnesocene (**3b**) and tetrakis(trimethylsilyl)magnesocene (**3c**) appeared (Scheme 9).[38]

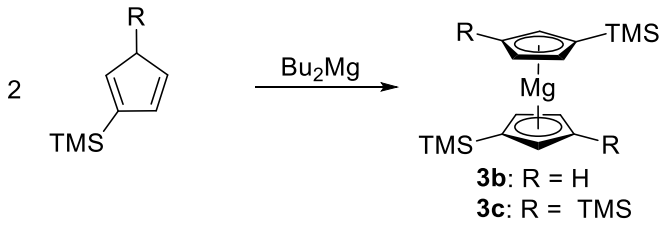

Scheme 9: Synthesis of bis(trimethylsilyl)magnesocene (**3b**) and tetrakis(trimethylsilyl)magnesocene (**3c**) as conducted by Duff *et al*.[38]

Introducing the 1,2,4-tris(trimethylsily)cyclopentadienyl ligand to magnesium, Morley *et al*. were able to obtain a bent magnesocene (δ = 170.4°) in the solid state.[39]

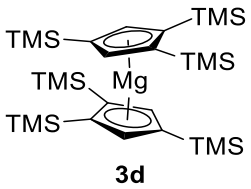

Figure 7: Hexakis(trimethylsilyl)magnesocene (**3d**).

This hexakis(trimethylsilyl)magnesocene (Figure 7), **3d**, was obtained by the reaction of 1,2,4-tris(trimethylsilyl)cyclopentadiene and dimethylmagnesium in the presence of tetramethylethylenediamine (tmeda) conducted in di-*n*-butylether under stirring for five days.[39] If this reaction was carried out in the absence of tmeda, no formation of the corresponding magnesocene was observed.[39] Since dibutylmagnesium is commercially available, it has become the common starting material for magnesocenes and different substitution patterns have been established on magnesocenes since the discovery of the unsubstituted magnesocene, **3a**, in 1954 (see Table 2). Examples of magnesocenes, for which dibutylmagnesium was used as starting material are dimethylmagnesocene (**3e**),[40] hexamethylmagnesocene (**3f**)[40] and diethylmagnesocene (**3g**).[41] Prominent bulky ligand systems are the *iso*-

propyl substituted ligands tri-*iso*propylcyclopentadienyl (^{3}Cp), tetra-*iso*propylcyclopentadienyl (^{4}Cp) and penta-*iso*propylcyclopentadienyl (^{5}Cp). Notably, for magnesium no example of a structurally characterized *iso*propyl substituted base free metallocene is known to date, the only example in literature, which was characterized by NMR spectroscopy and its melting point, is **3h** which was synthesized by Burkey *et al*. in 1994 (Scheme 10).[42]

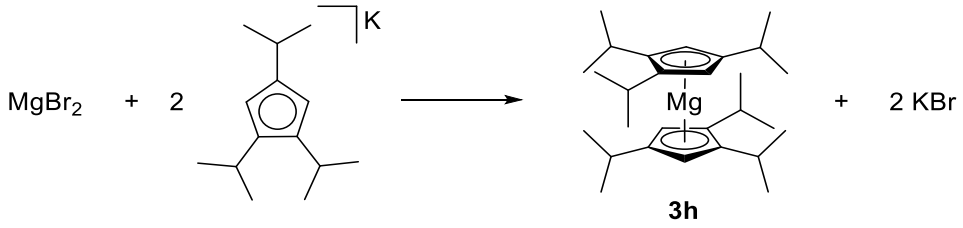

Scheme 10: Synthetic route to hexa-*iso*propylmagnesocene (**3h**) as conducted by Burkey *et al*.[42]

This metallocene, **3h**, was described as a waxy solid with a wide melting point range.[42] Remarkably, only one example of a disubstituted magnesocene is structurally characterized, **3i**, which was first reported by Thiele *et al*.[43] and structurally characterized by Gardiner and coworkers in 1991 (Figure 8).[44]

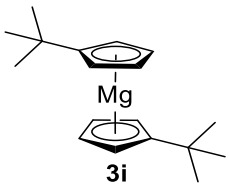

Figure 8: Di-*tert*-butylmagnesocene (**3i**).

The structural features of di-*tert*-butylmagnesocene, **3i**, are comparable to those of unsubstituted magnesocene (see Table 2) owing to the long Mg-Cp bond which is not strongly influenced by the substitution pattern of the cyclopentadienyl ligand. Sofield *et al*. reported the synthesis of Cp''$_2$Mg (Scheme 11), **3j**, in 1995 and used this compound as a Cp transfer reagent for a cerium complex.[45] Another *tert*-butyl substituted ligand, tri-*tert*-butylcyclopentadienyl ligand, usually abbreviated as Cp''', was introduced to magnesium chemistry in 2001. This complex, hexa-*tert*-butylmagnesocene (**3k**), was first reported by Duval *et al*.,[46]

but the improved synthesis of 1,2,4-tri-*tert*-butylcyclopentadiene was known since 1993.[47] In this first report of **3k** (Scheme 11), the authors published NMR data, but no molecular structure.

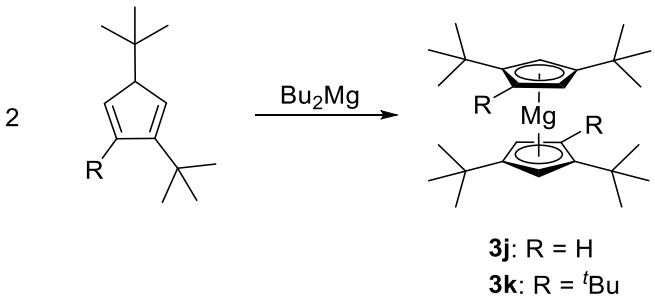

Scheme 11: Synthesis of tetra-*tert*-butylmagnesocene (**3j**) and hexa-*tert*-butylmagnesocene (**3k**).[45,46]

Only one year later, the Sitzmann group published the crystal structure of this encapsulated metallocene **3k**. Interestingly, this metallocene exhibits a bent structure which is surprising in view of the steric demand of the ligand. Weber *et al*. concluded that packing effects in the crystal of hexa-*tert*-butylmagnesocene ensure good crystallizability of this compound.[48] The octamethyldi-*tert*-butylmagnesocene (**3l**), synthesized by the reaction of the free ligand with dibutylmagnesium, is another example where a significant deviation of the angle δ from 180° is observed (169.0°), presumably due to the asymmetry of the ligand incorporated by the *tert*-butyl groups (Figure 8).[49] Another explanation for the bending in this magnesocene can be packing effects in the crystal which exhibit typically only small energy values which fits the high ionic character of the Mg-Cp bond.

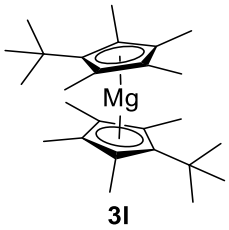

Figure 9: Octamethyldi-*tert*-butylmagnesocene (**3l**).

The Mg-Cp^{cent} distance is not elongated compared to unsubstituted magnesocene which is

indeed surprising when comparing the steric pressure of both cyclopentadienyl ligands. By introducing electron donating groups at the cyclopentadienyl ring, the electron density is increased and results in a stronger and by that shorter element cyclopentadienyl bond which can also be seen in **3l**. A hint that a bend geometry is not a feature of all magnesocenes exhibiting bulky cyclopentadienyl ligands, is shown by decamethylmagnesocene (**3m**) (Figure 10).

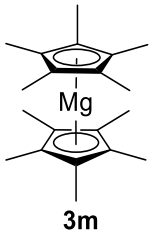

3m

Figure 10: Decamethylmagnesocene (**3m**).

In 2003, the structure in the solid state of this metallocene, **3m**, was revealed[50] though the preparation method was known for a long time.[38,51–53] In the crystal, decamethylmagnesocene, **3m**, exhibits coplanar cyclopentadienyl rings (δ = 179.9°) with marginally shortened Mg-Cp^{cent} distances compared to the unsubstituted magnesocene (see Table 2).[50] This shortening of the Mg-Cp^{cent} distance might be counterintuitive because of the steric demand of the pentamethylcyclopentadienyl ligand, but the increased electron density of this ligand, caused by the inductive effect of the methyl groups, strengthens the Mg-Cp bonding. In 2014, Jaenschke *et al*. reported the molecular structure of **3m** at even lower temperature (153 K), where no disorders were observed in the crystal.[54] In contrast to **3m**, the related metallocene Cp*$_2$Ca (**4b**) is bent in the solid state, the reason for which will be discussed in detail in the next chapter. Replacing one methyl group in the pentamethylcyclopentadienyl ligand by a proton, the tetramethylcyclopentadienyl ligand, Cp$^{\#}$, is attained. The corresponding magnesocene, octamethylmagnesocene, **3n**, was first synthesized by Shapiro *et al*. in 1995[55] but structurally characterized first in 2001 by Schumann and coworkers.[49] The features of this compound in the solid state do not differ significantly from the decamethyl analogue since Cp$^{\#}_2$Mg (**3n**) also exhibits almost coplanar cyclopentadienyl rings and similar Mg-Cp^{cent} distances (see Table 2). By transmetalation of **3n** with aluminum(III)chloride, Shapiro *et al*. obtained Cp$^{\#}_3$Al, revealing the applicability of magnesocenes as Cp transfer reagents.[55] An unusual synthetic pathway was chosen by Westerhausen *et al*. for the two

disubstituted magnesocenes $^{(C3H5)2HC}Cp_2Mg$ (**3o**) and $^{(1\text{-}EtPh)HC}Cp_2Mg$ (**3p**). They conducted the synthesis of both complexes starting from the corresponding fulvenes with dibutylmagnesium as β-hydride transfer reagent (Scheme 12).[56]

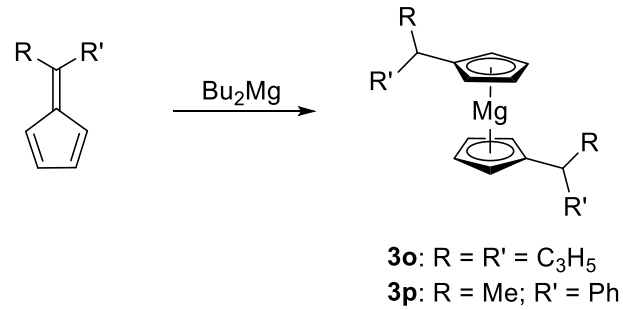

Scheme 12: Synthesis of $^{(C3H5)2HC}Cp_2Mg$ (**3o**) and $^{(1\text{-}EtPh)}Cp_2Mg$ (**3p**) as carried out by Westerhausen and coworkers.[56]

Both magnesocenes were characterized by single crystal X-ray diffraction revealing almost coplanar cyclopentadienyl rings and typical Mg-Cp^{cent} distances.[56] Another common substitution pattern in cyclopentadienyl chemistry are phenyl rings, which influence the electronic structure of the cyclopentadienyl ligand and the solubility of the corresponding metallocenes in hydrocarbon solvents.[57] For magnesium, only two examples of phenyl substituted metallocene derivatives are known which were reported by Deacon *et al*.[57] and Schulte and coworkers.[58] The octaphenylmagnesocene, $^{Ph4}Cp_2Mg$ (**3q**), was synthesized in 2015 by Deacon *et al*. and could be structurally characterized by that group (Scheme 13).

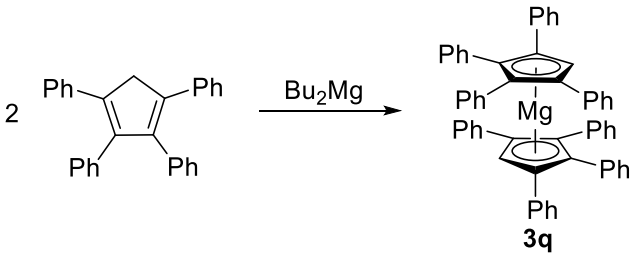

Scheme 13: Synthesis of $^{Ph4}Cp_2Mg$ (**3q**) as carried out by Deacon *et al*.[57]

This metallocene of magnesium, **3q**, also possesses a coplanar structure and the Mg-Cp^{cent}

distance is only marginally elongated compared to Cp_2Mg (**3a**). The authors concluded that the reason for the comparatively short Mg-Cp^{cent} distance lays in π interactions between the two tetraphenylcyclopentadienyl ligands.[57] One strategy to obtain better solubility of metallocenes with decaarylcyclopentadienyl (Cp^{BIG}) ligands in hydrocarbons is substitution with alkyl groups in *para* position at the phenyl rings which was also carried out in the case of deca(*p-tert*-butylphenyl)magnesocene, $^{(p\text{-}t\text{BuPh})5}Cp_2Mg$ (**3r**), by Schulte *et al*. in 2020 (Scheme 14).[58]

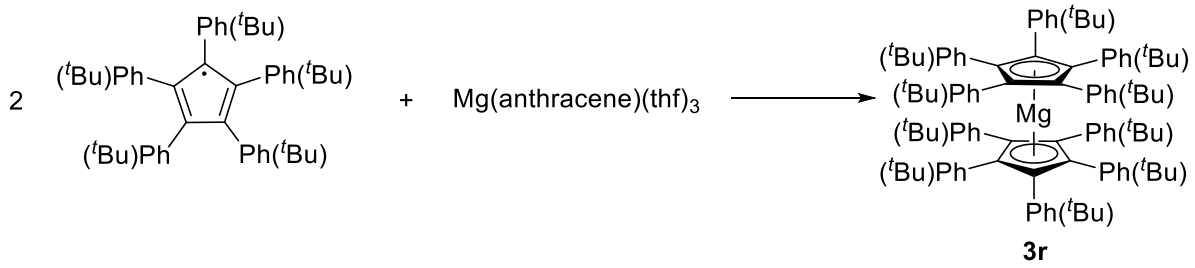

Scheme 14: Synthesis of deca(*p-tert*-butylphenyl)magnesocene (**3r**) as conducted by Schulte and coworkers.[58]

The angle δ in $^{(p\text{-}t\text{BuPh})5}Cp_2Mg$, **3r**, is 179.9° and the Mg-Cp^{cent} distance is elongated in comparison to unsubstituted magnesocene presumably due to steric hindrance caused by the *tert*-butyl groups in *para* position of the phenyl substituents at the cyclopentadienyl ligands.[58] In 2004, Schumann and coworkers reported of a butenyl substituted magnesocene (**3s**) synthesized by deprotonation of the corresponding ligand with dibutylmagnesium (Scheme 15).[59]

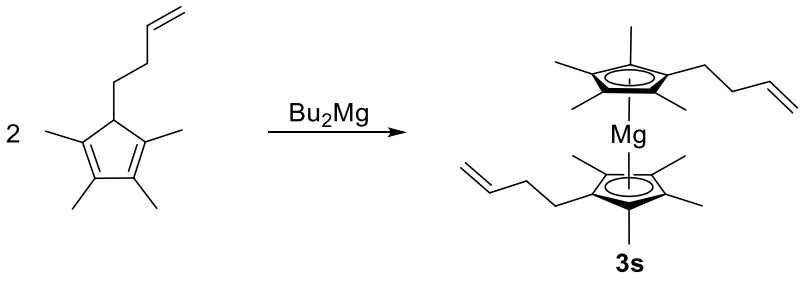

Scheme 15: Synthesis of butenyl substituted magnesocene (**3s**) as conducted by Schumann *et al*.[59]

The crystal structure of this alkenyl substituted magnesocene, **3s**, shows that there is no interaction between the magnesium centre and the butenyl group which is discussed later (*vide infra*). The structural characteristics of this complex exhibit values (Mg-Cp^{cent} distances and angle δ) similar to Cp^*_2Mg (see Table 2).

It is worth mentioning that none of the 12 structurally characterized magnesocenes is heavily bent in the solid state since the most bent magnesocene exhibits a value of only 169.0° for the angle δ (**3l**[49]). In this context it must be stated that steric demand of the cyclopentadienyl ligand does not seem to influence the degree of bending of the magnesocene directly, moreover it seems to be the asymmetry of the ligand, since asymmetrically substituted cyclopentadienyl ligands seem to force the magnesocene to be bent. The three bent magnesocenes are **3d**,[39] **3k**[46,48] and **3l**,[49] which all bear asymmetrically substituted cyclopentadienyl ligands. By comparison of the Mg-Cp^{cent} distances of the different substituted magnesocenes, there is a trend to observe since the magnesocenes with the bulkiest cyclopentadienyl ligands (**3k**[46,48]; **3r**[58]) exhibit the longest Mg-Cp^{cent} distances (see Table 2). The range of the Mg-Cp^{cent} distances in the presented compounds goes from 195.62(1) to 206.28(11) pm which is elongated in comparison to the Fe-Cp^{cent} distance in Cp_2Fe (166.06(11) pm[3]) what can be attributed to the stronger covalent character of the Fe-Cp bond in comparison to the Mg-Cp bond, which is significantly more ionic.

Table 2: Selected structural parameters and references of magnesocenes.

Compound	Cp^{cent}-Mg-Cp^{cent} δ[°][a]	Cp^{cent}-Mg [pm][a]	Reference
Cp_2Mg (**3a**)	179.9[60]	199.11(1)[60]	[7,8,37,60]
$^{TMS}Cp_2Mg$ (**3b**); $^{TMS2}Cp_2Mg$ (**3c**)	-	-	[38]
$^{TMS3}Cp_2Mg$ (**3d**)	170.4	202.32(43); 202.38(44)	[39]
$^{Me}Cp_2Mg$ (**3e**)	-	-	[38,40,43]
$^{Me3}Cp_2Mg$ (**3f**)	-	-	[40]
$^{Et}Cp_2Mg$ (**3g**)	-	-	[41]
$^{3}Cp_2Mg$ (**3h**)	-	-	[42]
Cp'_2Mg (**3i**)	179.9[44]	200.19(5)[44]	[43,44]
Cp''_2Mg (**3j**)	-	-	[45]
Cp'''_2Mg (**3k**)	173.5[48]	205.81(11); 206.28(11)[48]	[46,48]
$^{tBu}Cp^{\#}_2Mg$ (**3l**)	169.0	199.22(7); 199.42(7)	[49]
Cp^*_2Mg (**3m**)	178.7 – 179.9[54]	195.62(1) – 196.35(6)[54]	[38,50–54]
$Cp^{\#}_2Mg$ (**3n**)	179.9	197.02(0)	[49,55]
$^{(C3H5)2HC}Cp_2Mg$ (**3o**)	176.3	199.27(8); 199.96(8)	[56]
$^{(1\text{-}EtPh)}Cp_2Mg$ (**3p**)	179.9	198.06(6)	[56]
$^{Ph4}Cp_2Mg$ (**3q**)	179.9	201.60(4)	[57]
$^{(p\text{-}tBuPh)5}Cp_2Mg$ (**3r**)	179.9	206.26(2)	[58]
$^{H2C=CHC2H4}Cp^{\#}_2Mg$ (**3s**)	179.9	196.35(2)	[59]
$^{TMStBu}Cp_2Mg$ (**3t**)	-	-	[49]

[a]: Only given in the case of η^5 coordination of cyclopentadienyl ligand to magnesium atom.

1.4 Calcocenes

Similar to the afore discussed magnesocenes, there are several different synthetic routes for calcocenes. However, in contrast to the syntheses of magnesocenes, which are mostly synthesized by deprotonation of the corresponding cyclopentadiene with dibutylmagnesium, the predominant synthetic procedure for calcocenes is the transmetalation of sodium- or potassiumcyclopentadienides with calcium(II)iodide. Another common route for the synthesis of calcocenes is the deprotonation of the corresponding cyclopentadiene with calcium bis(trimethylsilylamide) (Scheme 16).

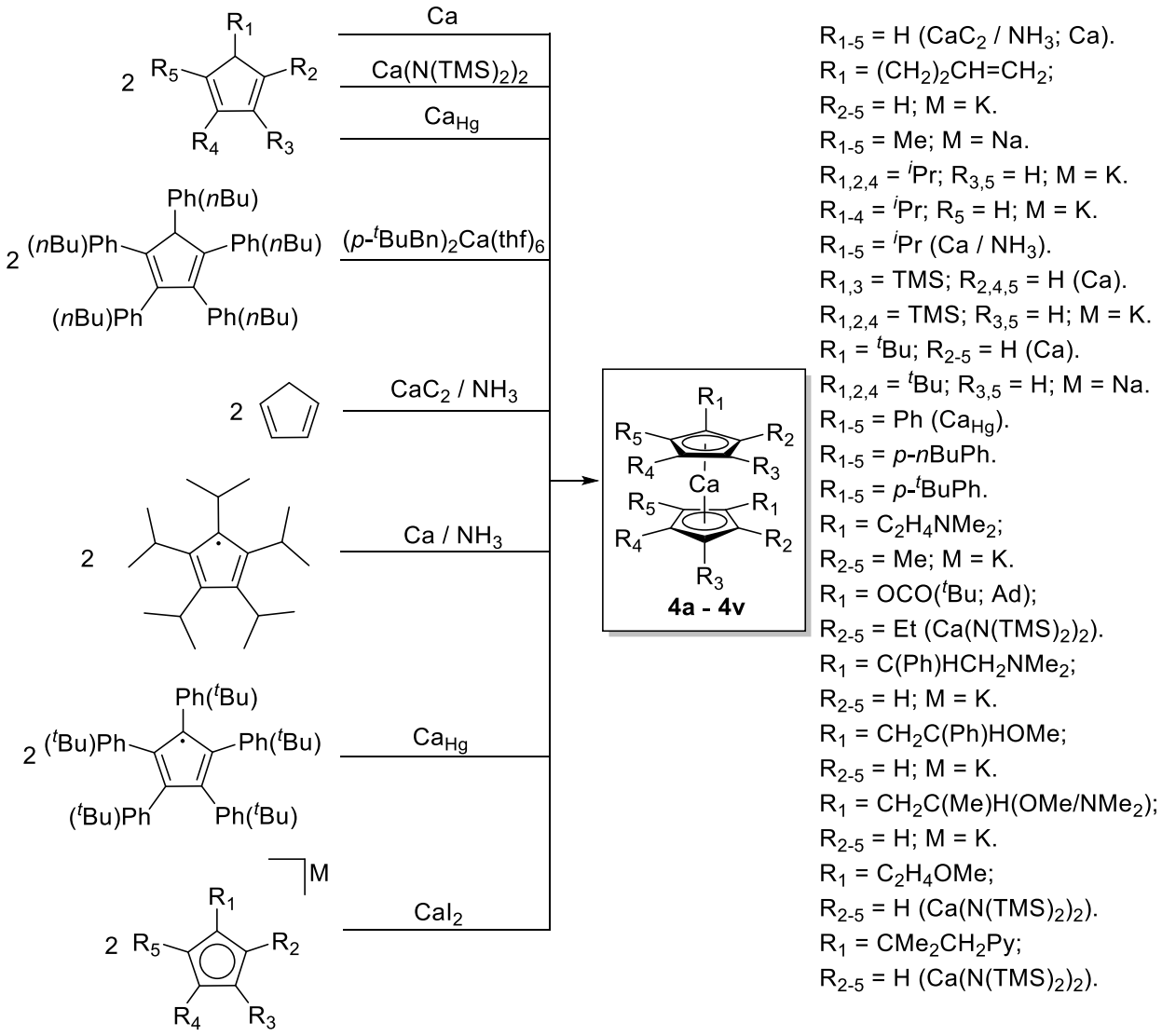

Scheme 16: Overview of possible synthetic routes for calcocenes.

The unsubstituted calcocene Cp_2Ca, **4a**, was first synthesized by Ziegler *et al*. in 1956 by reaction of calcium carbide with cyclopentadiene (Scheme 17).[9]

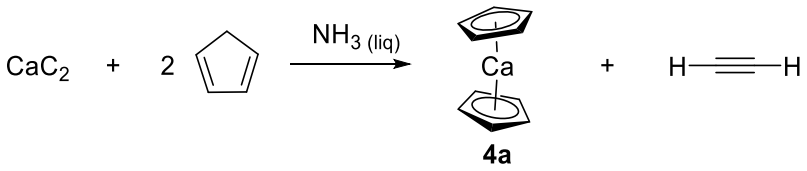

Scheme 17: First synthesis of calcocene (**4a**) as carried out by Ziegler and coworkers.[9]

Five years later, in 1961, Fischer and coworkers reported another synthetic route to **4a**: They reacted calcium metal with cyclopentadiene in tetrahydrofuran to obtain the bis thf adducts, which was dried at 383 K to yield donor solvent free calcocene.[10] In 1974, Zerger and Stucky revealed the structure of **4a**, which is, in contrast to magnesocene, polymeric in the solid state. The authors conducted the synthesis following the method of Fischer[10] and were able to obtain crystals by subliming the dried, crude product at 538 K. In the crystal, one calcium atom is attached to three cyclopentadienyl ligands: two rings are η^5 coordinated and one ring η^1 (Figure 11).[61]

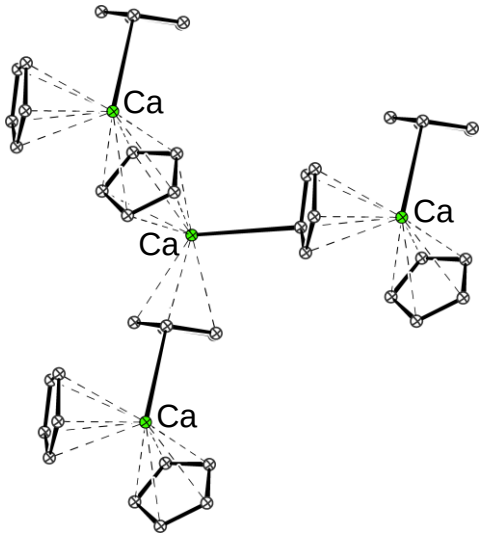

Figure 11: Molecular structure of calcocene (**4a**)[61] in the crystal (hydrogen atoms omitted for clarity, ball-and-stick representation).

In 1986, the first report of decamethylcalcocene, **4b**, appeared by Andersen *et al*. who synthesized this metallocene by salt metathesis reaction between calcium(II)iodide and pentamethylcyclopentadienylsodium (Scheme 18).[62]

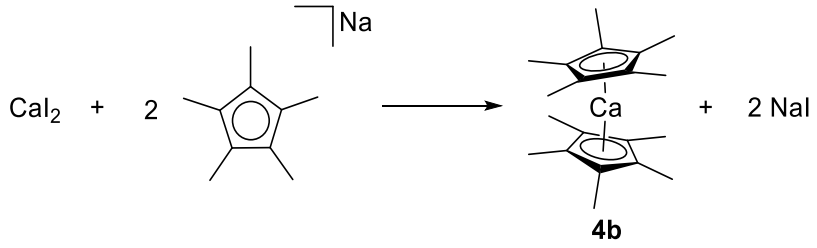

Scheme 18: Synthesis of decamethylcalcocene (**4b**) as conducted by Andersen and coworkers.[62]

The authors investigated the structure in the gas phase by electron diffraction and concluded on the basis of their data that decamethylcalcocene, **4b**, should be a bent metallocene.[62] In 1990, Williams *et al*. were able to get insight in the structural features of **4b** by single crystal X-ray diffraction and found that it is indeed bent.[63] It is worth mentioning that the angle δ in the solid state (147.7°[63]) is different from the one observed in the gas phase (154(3)°[62]), what might also be due to the different methods used to determine these angles. Williams and coworkers already observed Ca···H-CH_2 interactions and came to the conclusion that no distortion of the angle at that methyl group is observable. The authors assumed intermolecular forces in **4b** to be marginal since this compound exhibits high solubility in hydrocarbon solvents and doubted packing effects in the crystal to be crucial for the bent geometry of this compound. They substantiated intermolecular electronic forces as significant driving force for the bent geometry.[63] Pal *et al*. investigated the structural features of Cp^*_2Mg (**3m**) and Cp^*_2Ca (**4b**) with the aim to explore why **3m** is coplanar, while **4b** is bent (Figure 12). By using the DFT framework, the authors calculated different forces and interactions in and between the molecules in the solid state to find out what makes the difference in these complexes. On one side, according to Pal *et al.*, d electrons play a role in the bending in **4b**, but most of the interaction of calcium with Cp^C is limited to electrostatic interaction between the calcium atom and the π surface of the cyclopentadienyl ligand. On the other side, Pal and coworkers detected several Ca···H contacts in the crystal structure of **4b** which, as the authors suggested, might also be the reason for the bending in this compound as well as London H···H dispersion forces (Figure 12). For these Ca···H contacts,

the authors created the term of pseudo-pregostic interaction based on the term of agostic interaction.[64]

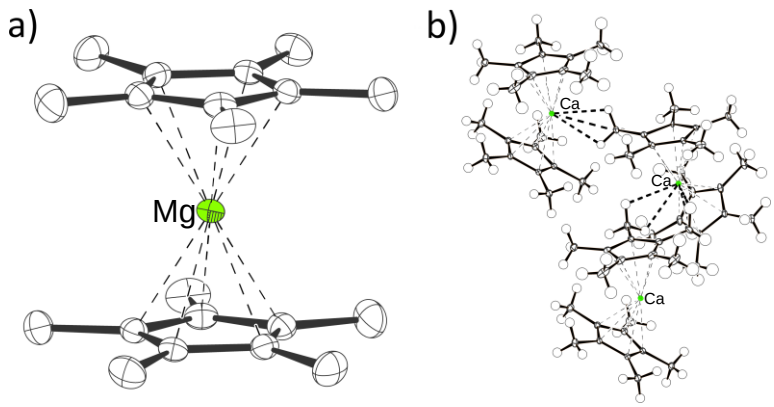

Figure 12: Left: molecular structure of Cp^*_2Mg (**3m**)[54] in the crystal (hydrogen atoms omitted for clarity, thermal ellipsoids at 50% probability level; right: molecular structure of Cp^*_2Ca (**4b**)[63] in the crystal (thermal ellipsoids at 50% probability level).

In 1988, Engelhardt *et al*. synthesized a silyl substituted calcocene, $^{TMS2}Cp_2Ca$ (**4c**), *via* metal vapour technique at 77 K (Scheme 19).[65]

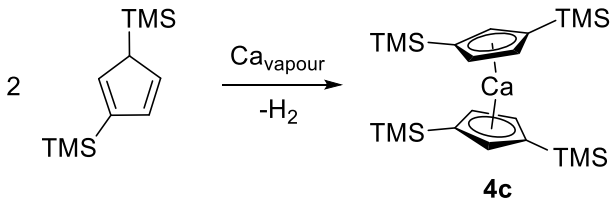

Scheme 19: Metal vapour synthesis of $^{TMS2}Cp_2Ca$ (**4c**) as conducted by Engelhardt *et al*.[65]

They were able to crystallize the corresponding mono thf adducts of **4c**, which loses donor solvent after repeated sublimation at 453 K.[65] The related, more bulky ^{TMS3}Cp was introduced 2003 to calcium chemistry by Harvey *et al*. by reaction of the corresponding potassiumcyclopentadienide with calcium(II)iodide (Scheme 20).[66]

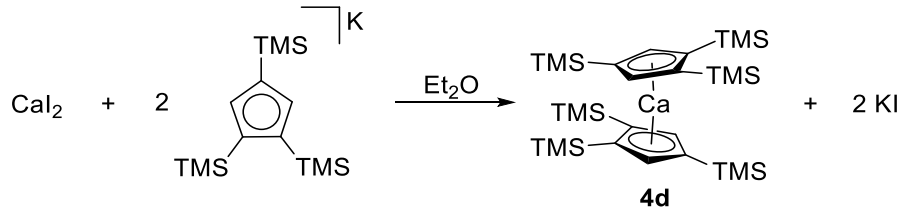

Scheme 20: Synthesis of $^{TMS3}Cp_2Ca$ (**4d**) as carried out by Harvey *et al*.[66]

The authors obtained crystals suitable for X-ray crystallography unravelling a bent geometry in **4d** (δ = 167.3°) with Ca-Cp^{cent} distances similar to those observed in **4b**. This example demonstrates how difficult the determination of correlation between steric demand and degree of bending in group 2 metallocenes is. As discussed above, in **4b** Ca···H contacts exist, which seem to have a significant influence on the geometry in the solid state of this compound. Harvey and coworkers exhorted in their report to take manifold factors into account when discussing bending angles, δ, in group 2 metallocenes.[66] In the division of *iso*propyl substituted metallocenes of calcium, $^{3}Cp_2Ca$ (**4e**)[42] and $^{4}Cp_2Ca$ (**4f**)[67] are structurally characterized while the calcocene with the superbulky penta-*iso*propylcyclopentadienyl ligand, $^{5}Cp_2Ca$ (**4g**), is only characterized by NMR spectroscopy and its melting point.[68] The hexa-*iso*propylcalcocene, **4e**, was reported jointly with hexa-*iso*propylmagnesocene, **4f**, (*vide supra*) in 1993 by Burkey *et al*. and described as an oil which crystallizes when standing for a longer period.[42,69] They conducted the synthesis starting from tri-*iso*propylcyclopentadienylpotassium and calcium(II)iodide (Scheme 21).[69]

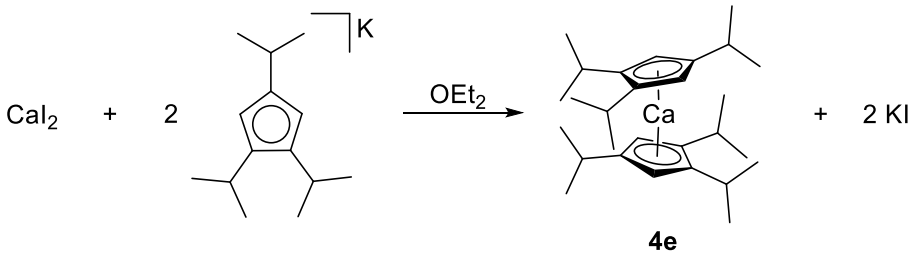

Scheme 21: Synthesis of hexa-*iso*propylcalcocene (**4e**) as carried by Burkey *et al*.[69]

In the solid state, **4e** exhibits a moderately bent geometry (δ = 169.7°[42]), comparable to what is found in **4d**. The synthesis of octa-*iso*propylcalcocene (**4f**) was carried out by Williams *et al*. in the same manner as for **4e** (Scheme 22).[67]

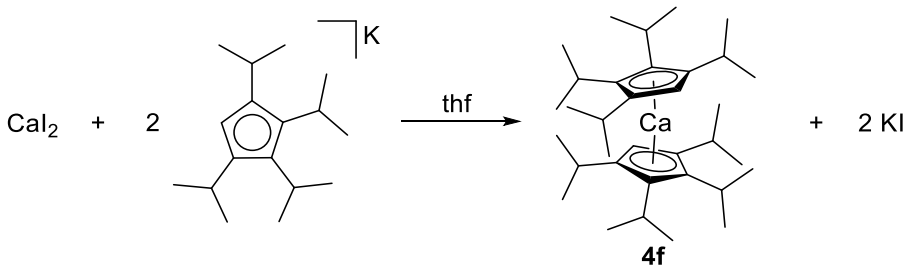

Scheme 22: Synthesis of octa-*iso*propylcalcocene (**4f**) as conducted by Williams *et al*.[67]

Surprisingly, **4f** (162.3°[67]) is more bent than $^{3}Cp_2Ca$, **4e**, which possesses less bulky tri-*iso*propylcyclopentadienyl substituents. Reasons for this difference in the solid state structures might be that the unsubstituted carbon atoms are almost congruent to each other causing a strong repulsion of the remaining *iso*propyl groups. It must be mentioned here again that the Ca-Cp bond exhibits high ionic character making the structures of calcocenes flexible in the solid state and different conformations in the crystal possess only small differences in energy. This metallocene was stable toward air oxidation for minutes owing to the bulkiness of the cyclopentadienyl ligand.[67] The synthesis of $^{5}Cp_2Ca$, **4g**, was carried out in an unique synthetic pathway: Sitzmann *et al*. reacted the penta-*iso*propylcyclopentadienyl radical with calcium in liquid ammonia (Scheme 23).[68]

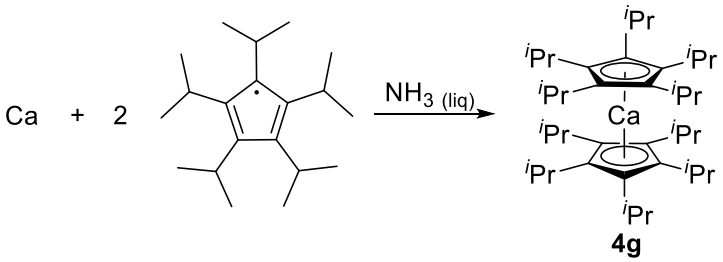

Scheme 23: Synthesis of deca-*iso*propylcalcocene (**4g**) as conducted by Sitzmann *et al*.[68]

The ^{1}H-NMR spectrum of this compound in solution exhibited an interesting feature regarding the splitting of the signals of the methyl groups: at 313 K, one doublet was observed for the “inner” sphere (pointing to the metal center) of each of the two isomers and one doublet for the “outer” sphere (pointing away from the metal center) for both stereoisomers (Figure 13).[68]

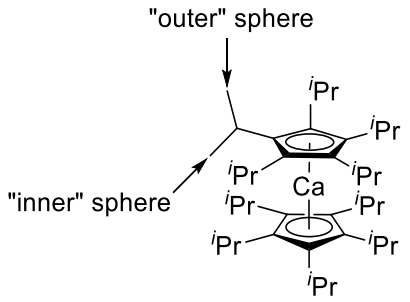

Figure 13: Definition of “inner” and “outer” sphere methyl groups in **4g**.

In the area of *tert*-butyl substituted calcocenes, only the disubstituted Cp’$_2$Ca (**4h**) and the hexasubstituted Cp’’’$_2$Ca (**4i**) are reported to date.[44,48] The di-*tert*-butylcalcocene (**4h**) was synthesized by metal vapour technique by Gardiner *et al*. in 1991 (Scheme 24).[44]

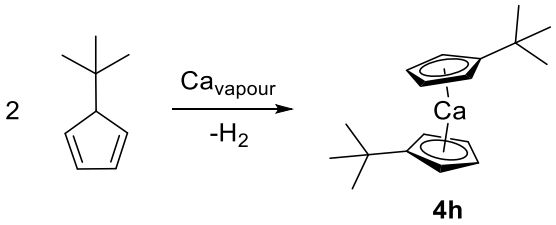

Scheme 24: Metal vapour synthesis of Cp’$_2$Ca (**4h**) as conducted by Gardiner *et al*.[44]

The authors condensed *tert*-butylcyclopentadiene and hexane to calcium metal and obtained the crystalline product, **4h**, by sublimation at 453 K (10^{-4} mbar). No solid state structure was reported for this compound, but for its bis thf adducts. Interestingly, the donor solvent molecule could be removed by heating this complex to 453 K *in vacuo*.[44] Weber *et al*. synthesized **4i** by transmetalation (Scheme 25).[48]

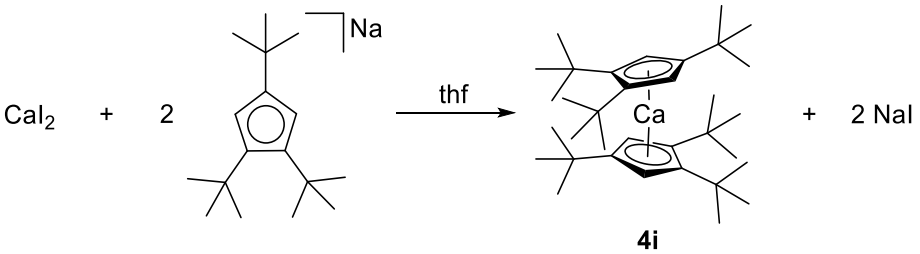

Scheme 25: Synthesis of hexa-*tert*-butylcalcocene (**4i**) as conducted by Weber *et al*.[48]

Though tetrahydrofuran was used as solvent in this reaction, the resulting metallocene was not obtained as a donor solvent adduct, which is a result of the steric demand of the bulky tri-*tert*-butylcyclopentadienyl ligand. Weber and coworkers were successful in crystallizing this complex (Figure 14) revealing a slightly bent geometry (δ = 170.7°) and Ca-Cp^{cent} distances comparable to those found in Cp*$_2$Ca (**4b**).[48]

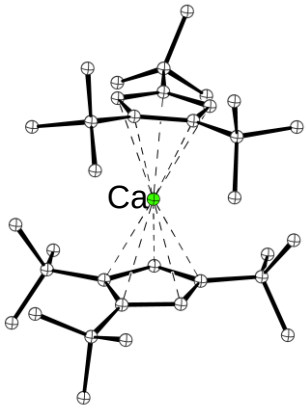

Figure 14: Molecular structure of hexa-*tert*-butylcalcocene (**4i**) in the crystal[48] (hydrogen atoms omitted for clarity, ball-and-stick representation).

The reason for the low degree of bending in Cp'''$_2$Ca (**4i**) stems from the bulkiness of the ligand: taking a closer look in the structure it becomes visible that over every unsubstituted carbon atom a *tert*-butyl group of the other cyclopentadienyl ligand is positioned. By this arrangement an almost spherical molecule is attained by which no efficient packing in the crystal can be reached. Although the calcium(II) cation is efficiently shielded by the Cp''' ligand, the authors reported a high sensitivity of **4i** toward moisture.[48] Though exhibiting bulky substituents, decaphenylmetallocenes possess only low solubilities in aliphatic and aromatic solvents, which is also valid for decaphenylcalcocene. This metallocene was synthesized by Deacon and coworkers in 2008 (Scheme 26).[70]

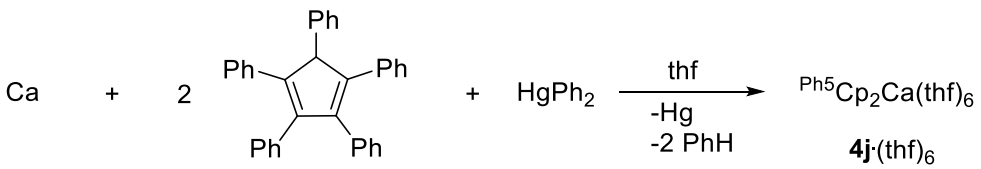

Scheme 26: Synthesis of **4j**·(thf)$_6$ as carried out by Deacon *et al*.[70]

By adding toluene to the solvated metallocene, the base free decaphenylcalcocene, **4j**, was afforded. [70] The only calcocene with almost perfect coplanar arranged cyclopentadienyl ligands is $^{(p\text{-}n\text{BuPh})5}Cp_2Ca$ (**4k**), synthesized by Ruspic *et al*. in 2008 (Scheme 27).[71]

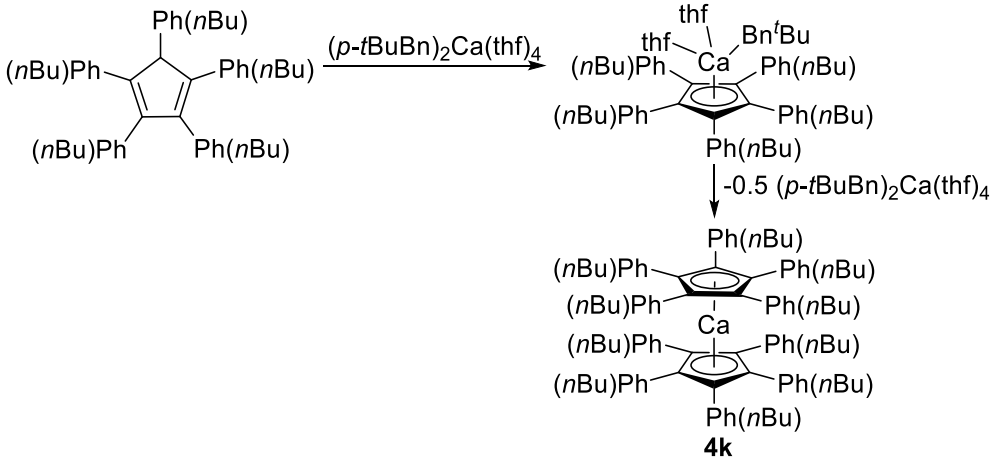

Scheme 27: Synthesis of deca(*para*-*n*-butylphenyl)calcocene (**4k**) as reported by Ruspic *et al*.[71]

In the molecular structure, **4k** exhibits an angle δ of 179.9° and, in view of the steric demand of the ligand interestingly, Ca-Cp^{cent} distances comparable to those found in Cp^*_2Ca (**4b**).[71] The difference in the electronic properties between aryl and alkyl substituted cyclopentadienyl ligands is significant: while in alkyl substituted cyclopentadienyl ligands the electron density is elevated by the +I effect of the alkyl substituents, in aryl substituted cyclopentadienyl ligands the negative charge can be delocalized over the π system of the aryl group (-M-effect).[71] The authors demonstrated the high stability of metallocenes with the penta(*para*-*n*-butylphenyl)cyclopentadienyl ligand by the ease of formation of the corresponding samarocene from its starting material. They suggested a network of C-H···C(π) interactions (somewhat analogous to cation-π interactions) to provide significant contribution to the stability of metallocenes bearing the reported ligand system.[71] A related calcocene, deca(*para*-*tert*-butylphenyl)calcocene, $^{(p\text{-}t\text{BuPh})5}Cp_2Ca$ (**4l**), was reported by Schulte *et al*. in 2020. Their synthetic route to this Cp^{BIG} metallocene of calcium started with calcium amalgam and the penta(*para*-*tert*-butylphenyl)cyclopentadiene radical (Scheme 28).[58]

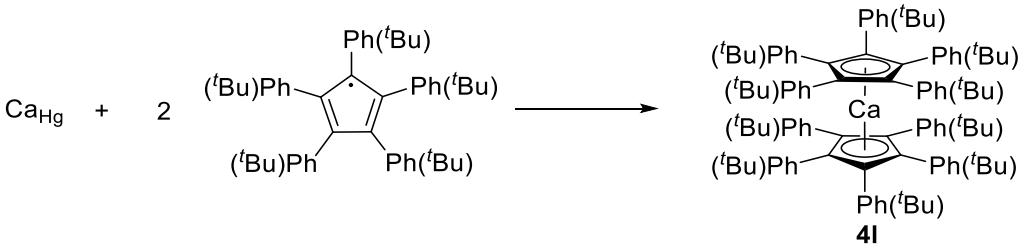

Scheme 28: Synthesis of deca(*para-tert*-butylphenyl)calcocene (**4l**) as conducted by Schulte *et al*.[58]

Unfortunately, the authors reported of crystals of low quality of $^{(p\text{-}t\text{BuPh})5}Cp_2Ca$, **4l**, making a structural characterization of this calcocene impossible. This deca(*para-tert*-butylphenyl)calcocene (**4l**) was soluble in benzene and could be recrystallized from this solvent which depicts again the effect of alkyl substituents present on phenyl groups of derivatives of Cp^{BIG} ligands.[58] In the row of calcocene chemistry, few examples of metallocenes with heteroatom substituted cyclopentadienyl ligands are known and, in part, structurally characterized.[72] In general, calcocenes with heteroatoms attached to the cyclopentadienyl ligand are relatively rare in comparison to substituted ferrocenes.[73] The first representative of this class of calcocenes was synthesized by Jutzi and coworkers in 1993.[74] This calcocene, **4m**, bears two tetramethyl(dimethylaminoethyl)cyclopentadienyl ligands depicting a double donor system. Noteworthy, no complexes exist with this calcocene as bidentate ligand. The synthesis was carried out by starting from calcium(II)iodide and tetramethyl(dimethylaminoethyl)cyclopentadienylpotassium (Scheme 29).[74]

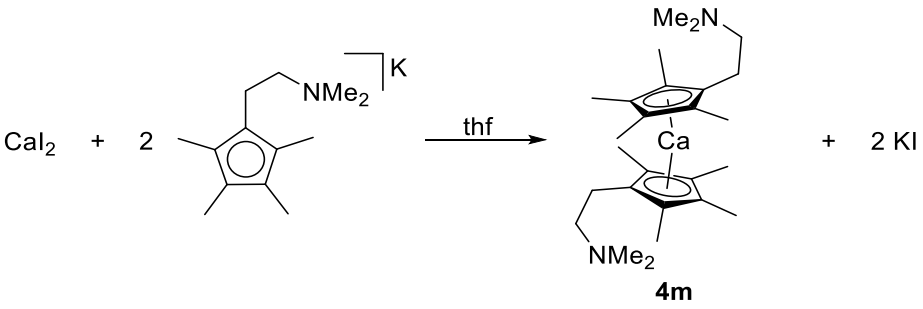

Scheme 29: Synthesis of $^{Me2NC2H4}Cp^{\#}_2Ca$ (**4m**) as carried out by Jutzi *et al*.[74]

Two calcocenes with ester functionalities were synthesized by Li *et al*. in 2013, which represent the first ester functionalized metallocenes of group 2 elements of this type. They

conducted the synthesis with calcium bis(trimethylsilylamide) and the corresponding free ligand (Scheme 30).[72]

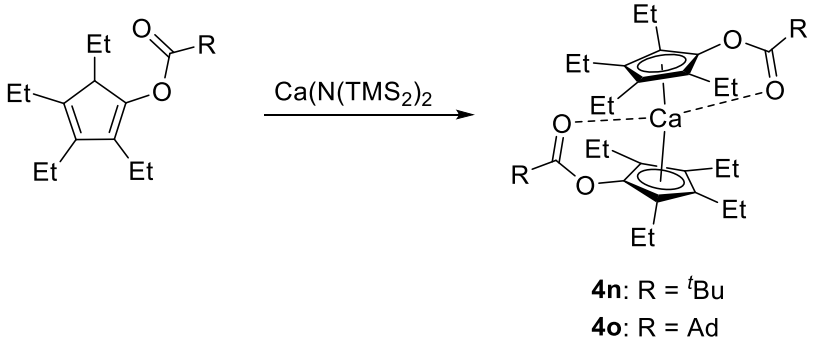

Scheme 30: Synthesis of ester functionalized calcocenes (**4n**, **4o**) as carried out by Li *et al*.[72]

Li and coworkers reported the calcium complexes to be stable in dry air for 12 h, but still moisture sensitive. By recrystallization of the adamantyl substituted calcocene from a hexane / thf mixture, the thf adduct could be crystallized and investigated by single crystal X-ray crystallography revealing two Ca-O=C bonds and one coordinated thf molecule. Notably, the coordinated donor solvent could be easily removed by applying *vacuo*, presumably due to the saturated coordination environment on calcium centre created by the ester groups coordinated to calcium.[72] In 1996, Molander *et al*. reported the syntheses of methoxy and amino substituted calcocenes starting from the corresponding potassiumcyclopentadienide and calcium(II)iodide (Scheme 31).[75]

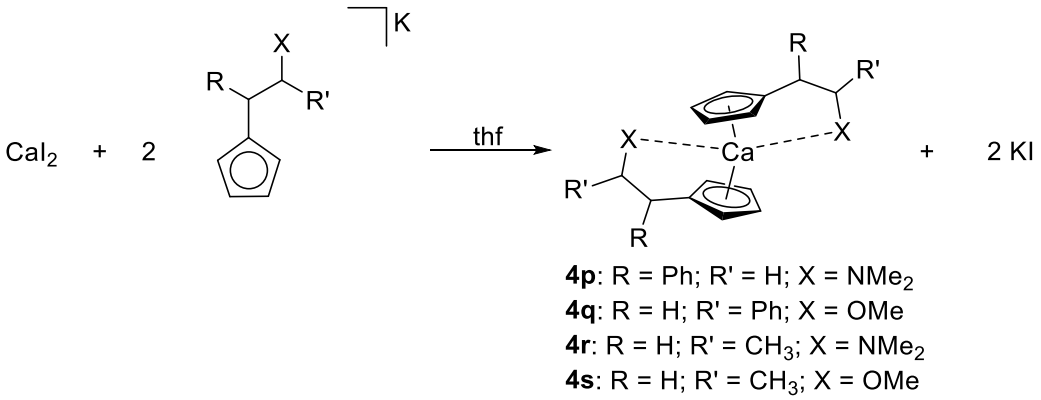

Scheme 31: Syntheses of methoxy- and amino substituted calcocenes (**4p**-**4s**) as conducted by Molander *et al*.[75]

The authors managed to crystallize two of these calcocenes (**4p** and **4q**) possessing two oxygen-calcium or nitrogen-calcium bonds, respectively. Though the reactions were all carried out in thf, no coordinating donor solvent remained in the crystal structure again displaying the concept of the increased chemical inertness of these donor substituted metallocenes. Remarkably, the Ca-Cp^{cent} distances are only marginally elongated in comparison to calcocenes without internal donor function, but the angles δ exhibit significant smaller values (are more bent) compared to what is observed in Cp*$_2$Ca (**4b**).[75] Another example for a structurally characterized methoxy functionalized calcocene stems from Hays *et al*. from 1996, where they started from calcium bis(trimethylsilylamide) and the corresponding cyclopentadiene (Scheme 32).[76]

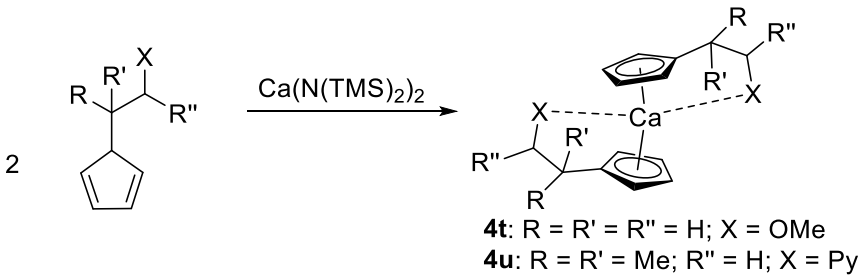

Scheme 32: Syntheses of methoxy- and pyridinyl substituted calcocenes (**4t**, **4u**) as carried out by Hays *et al*.[76]

In the crystal structure, Ca-Cp^{cent} distances and angle δ similar to those observed in calcocenes reported of Molander *et al*. are displayed.[76] It is worth mentioning that the structurally characterized examples of calcocenes reported by Molander and Hays have in common that they possess cyclopentadienyl rings with a small steric demand and though, all of these complexes are monomeric in the solid state due to the donor functionalities embedded in the cyclopentadienyl ligand.[75,76] An alkene substituted calcocene was reported by Schumann *et al*. in 2004, displaying the similarities between group 2 cations and lanthanoids in the oxidation state +II (Scheme 33).[59]

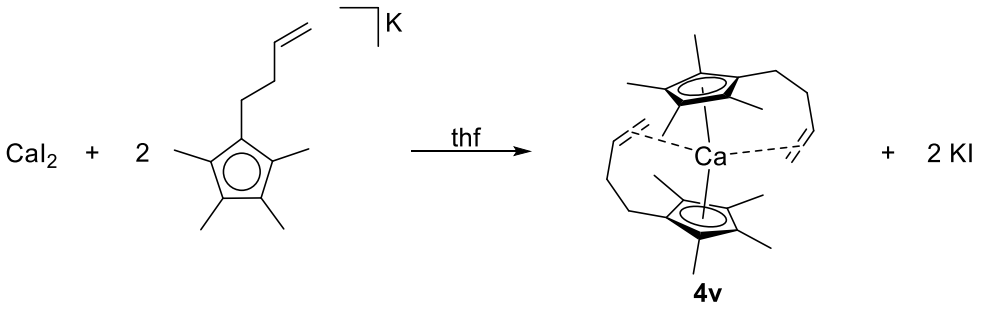

Scheme 33: Synthesis of butenyl substituted calcocene (**4v**) as reported by Schumann *et al*.[59]

In the crystal structure of $^{H2C=CHC2H4}Cp^{\#}_2Ca$, **4v**, the alkene group is inclined toward the calcium centre (Figure 15).

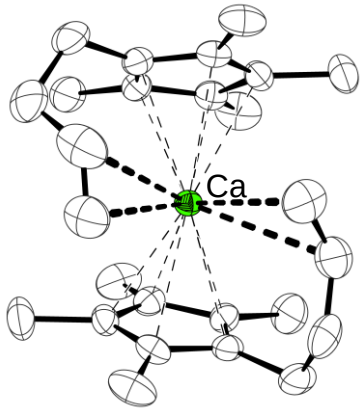

Figure 15: Molecular structure of $^{H2C=CHC2H4}Cp^{\#}_2Ca$ (**4v**) in the crystal[59] (hydrogen atoms omitted for clarity, thermal ellipsoids at 50% probability level).

The authors stated that the interaction of the alkene and the calcium centre cannot be viewed as a classical interaction as the Dewar-Chatt-Duncanson model would explain due to the absence of d orbitals of sufficient energy in group 2 metals.[59] However, the reason for this kind of interaction is presumably electrostatic.[59] Remarkably, only the heavier congeners in the series of group 2 butenyl substituted metallocenes presented by Schumann *et al*. exhibit this alkene-metal attraction since the corresponding magnesium complex does not display this interaction.[59] When comparing the structural characteristics of the donor substituted calcocenes reported by Hays and Molander (*vide supra*) with this butenyl substituted calcocene reported by Schumann *et al*., it can be stated that these characteristics only differ marginally but it should be considered in this comparison that only the butenyl

substituted calcocene exhibits additionally methyl groups at the cyclopentadienyl ring, which increase the electron density of the cyclopentadienyl ligand.[59,75,76]

In summary it should be noted that of the 22 calcocenes described, out of which 10 are structurally characterized, one calcocene exhibits tendencies to interact with methyl groups of the cyclopentadienyl ligands in the solid state which can be seen in **4b**.[63,64] Also the interaction of the central calcium atom with the alkene moiety in **4v** presents a difference in the coordination chemistry between calcocenes and magnesocenes.[59] By comparison of the structural characteristics of calcocenes and magnesocenes, it is obvious that the tendency to stronger bending angles (δ) is evident in calcocenes since only one example of a coplanar calcocene exists. However, the reasons for this observation might be the bigger coordination sphere of calcium in comparison to that of magnesium and pseudo-pregostic interactions (*vide supra*).[64] Another tendency which becomes visible in the comparison between magnesocenes and calcocenes is the ease of removal of coordinated solvent when descending group 2. The Ca-Cp^{cent} distances are relatively uniform for all calcocenes, with the exception of **4a** which is polymeric in the solid state, depicting the incoherence between substitution pattern and Ca-Cp^{cent} distance in calcocene chemistry.

Table 3: Selected structural parameters and references of calcocenes.

Compound	Cp^{cent}-Ca-Cp^{cent} δ[°][a]	Cp^{cent}-Ca [pm][a]	Reference
Cp_2Ca (**4a**)	117.9[61]	247.94(4); 259.28(6)[61]	[9,10,61]
Cp^*_2Ca (**4b**)	147.7[63]	233.31(11); 235.82(10)[63]	[53,62,63]
$^{TMS2}Cp_2Ca$ (**4c**)	-	-	[65]
$^{TMS3}Cp_2Ca$ (**4d**)	167.3	233.32(13); 233.45(13)	[66]
$^{3}Cp_2Ca$ (**4e**)	169.7	233	[42,69]
$^{4}Cp_2Ca$ (**4f**)	162.3	235.28(13); 234.93(13)	[67]
$^{5}Cp_2Ca$ (**4g**)	-	-	[68]
Cp'_2Ca (**4h**)	-	-	[44]
Cp'''_2Ca (**4i**)	170.7	234.03(20); 235.86(20)	[48]
$^{Ph5}Cp_2Ca$ (**4j**)	-	-	[70]
$^{(p\text{-}n\text{BuPh})5}Cp_2Ca$ (**4k**)	179.9	235.62(0)	[71]
$^{(p\text{-}t\text{BuPh})5}Cp_2Ca$ (**4l**)	-	-	[58]
$^{Me2NC2H4}Cp^{\#}_2Ca$ (**4m**)	-	-	[74]
$^{(t\text{Bu})OCO[Et4]}Cp_2Ca$ (**4n**); $^{(Ad)OCO[Et4]}Cp_2Ca$ (**4o**)	-	-	[72]
$^{Me2NCH2CH(Ph)}Cp_2Ca$ (**4p**)	136.7	239.62(18); 240.07(21)	[75]
$^{MeOCH(Ph)CH2}Cp_2Ca$ (**4q**)	139.7	237.97(15); 238.15(14)	[75]
$^{Me2NCH(CH3)CH2}Cp_2Ca$ (**4r**) $^{MeOCH(CH3)CH2}Cp_2Ca$ (**4s**)	-	-	[75]
$^{MeOC2H4}Cp_2Ca$ (**4t**)	136.6	239.42(10); 240.07(8)	[76]
$^{PyCH2CMe2}Cp_2Ca$ (**4u**)	-	-	[76]
$^{H2C=CHC2H4}Cp^{\#}_2Ca$ (**4v**)	141.3	241.23(3); 239.64(3)	[59]

[a]: Only given in the case of η^5 coordination of cyclopentadienyl ligand to calcium atom.

1.5 Strontocenes

Most strontocenes were obtained by transmetalation of sodium- or potassiumcyclopentadienides with strontium(II)bromide and -iodide. Another important synthetic route for strontocenes is the deprotonation of the corresponding cyclopentadiene with strontium bis(trimethylsilylamide) (Scheme 34).

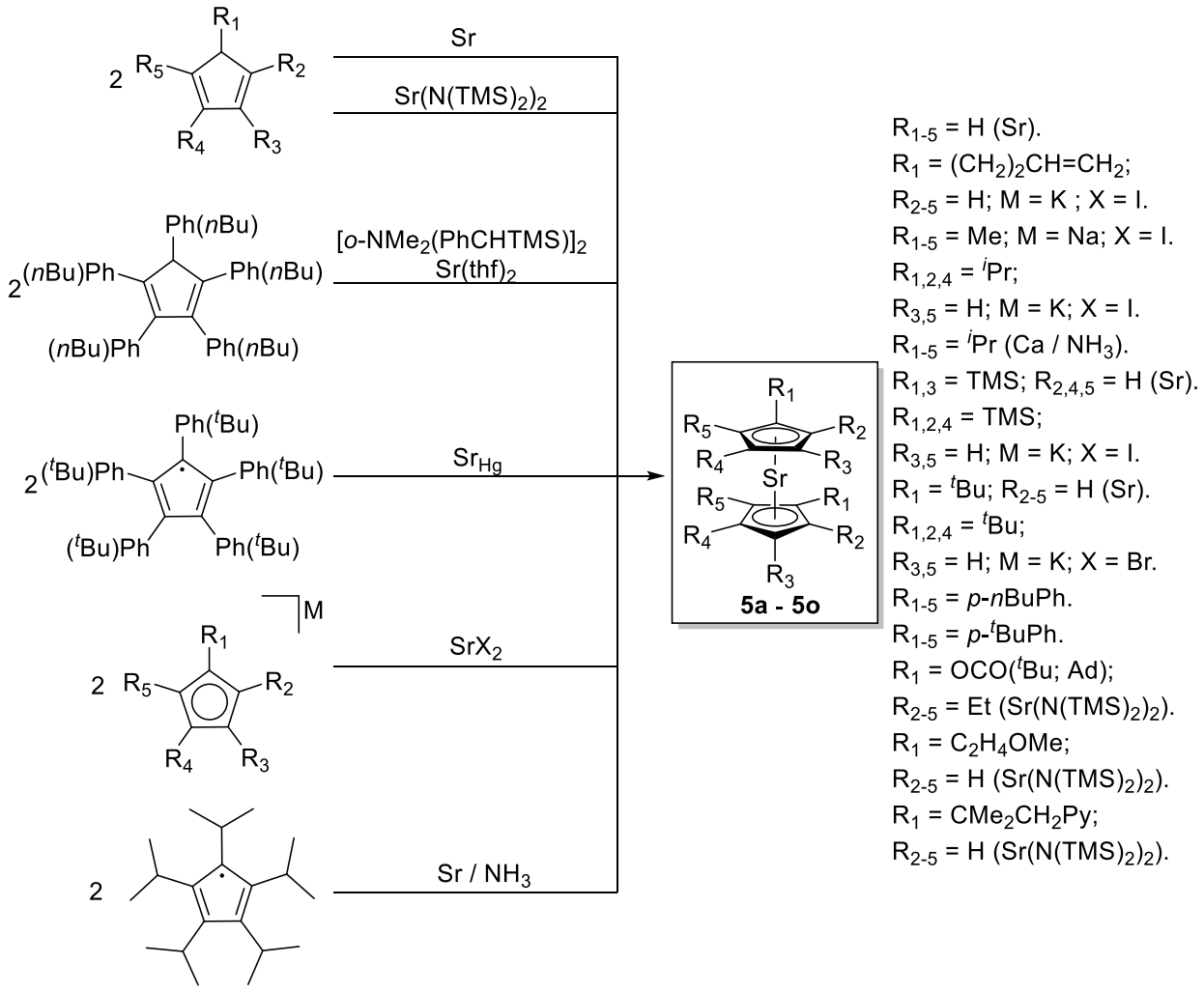

Scheme 34: Overview of possible synthetic routes for strontocenes.

The first report of strontocene (**5a**) dates back to 1961 where Fischer and Stölzle reported the challenging synthesis of this late group 2 metallocene.[10] Attempts of the authors to obtain strontocene, **5a**, by reaction of the finely dispersed metal with cyclopentadiene in various solvents failed, only the synthesis conducted in dimethylformamide was successful (Scheme 35).[10]

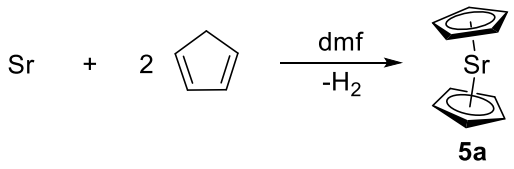

Scheme 35: Synthesis of strontocene (**5a**) as conducted by Fischer and Stölzle.[10]

The crude strontocene, **5a**, could be purified by sublimation at temperatures around 633-713 K affording the complex as a colorless solid.[10] The decamethylstrontocene, **5b**, was discovered in 1987, where Burns *et al*. reported of the syntheses of Cp^*_2Sr and its diethylether adduct (Scheme 36).[77]

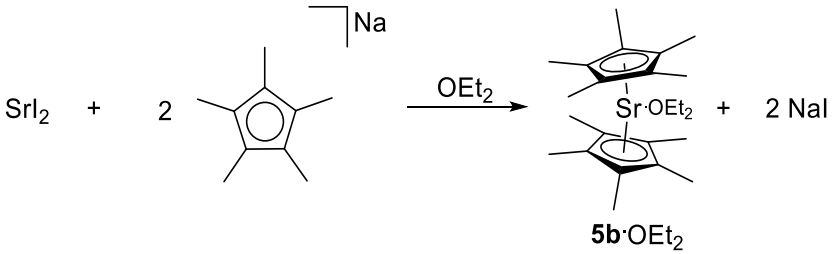

Scheme 36: Synthesis of $Cp^*_2Sr{\cdot}OEt_2$ (**5b**$\cdot OEt_2$) carried out by Burns and coworkers.[77]

By refluxing of the diethylether adduct in toluene, the authors were able to obtain decamethylstrontocene which they investigated by mass spectrometry , IR- and ^{13}C-NMR spectroscopy.[77] In the same year, Andersen *et al*. examined this compound by gas phase electron diffraction and reported structural parameters based on their measurements. Similar to decamethylcalcocene, **4b**, the corresponding strontium compound, **5b**, exhibits a bent geometry (δ = 149(3)°) and a Sr-Cp^{cent} distance of 246.9(6) pm.[78] The first trimethylsilyl substituted strontocene $^{TMS2}Cp_2Sr$ (**5c**) was synthesized by Engelhardt *et al*. in 1988 (Scheme 37).[65]

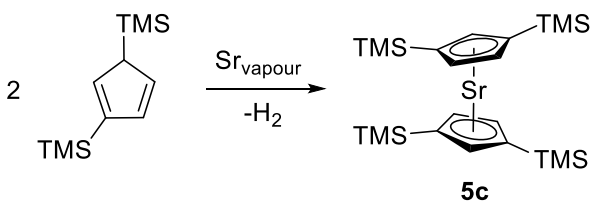

Scheme 37: Synthesis of $^{TMS2}Cp_2Sr$ (**5c**) as carried out by Engelhardt *et al*.[65]

Unfortunately, only structural data for the thf adduct are available.[65] In 2003, Harvey *et al*. reported of the synthesis of the more encapsulated strontocene $^{TMS3}Cp_2Sr$ (**5d**) (Scheme 38).[66]

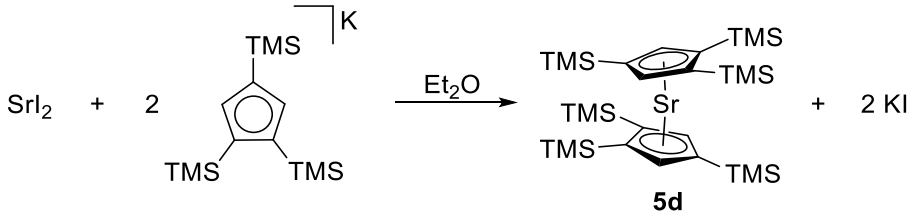

Scheme 38: Synthesis of $^{TMS3}Cp_2Sr$ (**5d**) as conducted by Harvey *et al*.[66]

The authors were able to obtain crystals suitable for single crystal X-ray diffraction revealing a bent geometry (δ = 159.4°) of $^{TMS3}Cp_2Sr$ (**5d**) and Sr-Cp^{cent} distances comparable to what was found for Cp^*_2Sr (notice: Sr-Cp^{cent} distance of **5b** was determined by gas phase electron diffraction).[66,78] In view of the almost similar radii, a comparison of Sr(II) with Sm(II) cyclopentadienyl compounds seems appropriate: The similarly bulky octa-*iso*propylsamarocene ($^4Cp_2Sm$) exhibits comparable E-Cp^C distances displaying the parallels between group 2 and lanthanoid dications.[66] In the row of *iso*propyl substituted strontocenes, no structurally characterized examples exist to date. The only known examples are the hexa-*iso*propylstrontocene, $^3Cp_2Sr$ (**5e**) and deca-*iso*propylstrontocene, $^5Cp_2Sr$ (**5f**). In 1993, the synthesis of $^3Cp_2Sr$, **5e**, was carried out by Burkey *et al*. by reaction of strontium(II)iodide with tri-*iso*propylcyclopentadienylpotassium (Scheme 39).[69]

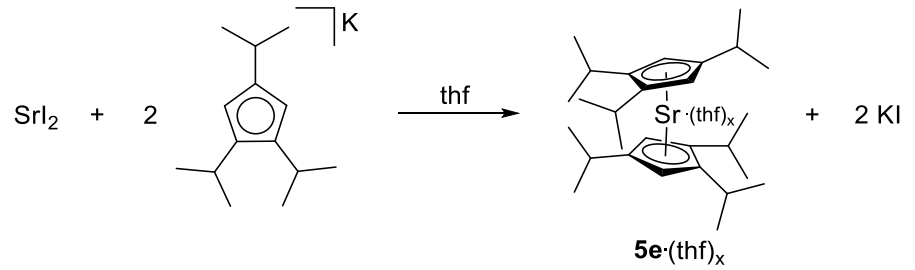

Scheme 39: Synthesis of hexa-*iso*propylstrontocene (**5e**) as conducted by Burkey *et al*.[69]

The authors described the thf adduct of hexa-*iso*propylstrontocene as a white solid which melted at the attempt to sublime the material and became a yellow solid. However, the donor solvent free metallocene could only be obtained by dissolving the compound in toluene and distill off the solvent. After this procedure a yellow viscous oil, which could be distilled, was observed which did not solidify even within standing for months. Burkey *et al*. even attempted the synthesis of $^{3}Cp_2Sr$ (**5e**) in diethylether analogously to the synthesis of $^{3}Cp_2Ca$, **4e**, but only obtained a gray suspension containing the starting materials.[69] In 1998, Sitzmann and coworkers presented the synthesis of $^{5}Cp_2Sr$, **5f**, which can be conducted in the same manner as for $^{5}Cp_2Ca$ (**4g**) (Scheme 40).[68]

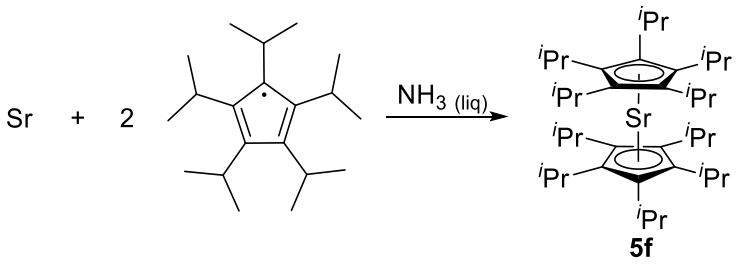

Scheme 40: Synthesis of deca-*iso*propylstrontocene (**5f**) as carried out by Sitzmann *et al*.[68]

The authors stated that the synthesis can alternatively be conducted in a sealed glas tube in an ultrasonic bath. In the case of this strontocene, **5f**, the same splitting of signals for methyl groups was observed as it was the case in the related calcium compound (*vide supra*).[68] When exposed to air, deca-*iso*propylstrontocene (**5f**) is stable for multiple weeks owing to the bulkiness of the ^{5}Cp ligand. The compound is marginally to mediocre soluble in alkanes and crystallizes willingly out of these solvents.[68] Analogously to the synthesis of **4h**, Cp'_2Sr (**5g**), could be obtained by metal vapor technique (Scheme 41).[44]

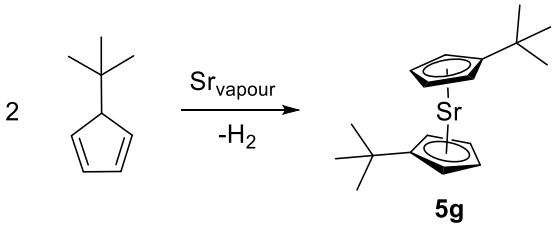

Scheme 41: Synthesis of di-*tert*-butylstrontocene (**5g**) as conducted by Gardiner *et al*.[44]

Gardiner *et al*. did not manage to crystallize the base free di-*tert*-butylstrontocene, **5g**, presumably due to low solubility of the compound in hydrocarbon solvents. By sublimation at 533 K (10^{-4} mbar), this complex could be purified but there was also decomposition observable. The bis(tetrahydrofuran) adduct of Cp'_2Sr (**5g**·$(thf)_2$) exhibits mediocre solubility in thf, is insoluble in benzene and can be sublimated under loss of thf to afford the base free metallocene.[44] The group of Hatanpää reported of hexa-*tert*-butylstrontocene (**5h**) which was obtained by reaction of strontium bromide with tri-*tert*-butylcyclopentadienylpotassium in 2007 (Scheme 42).[79]

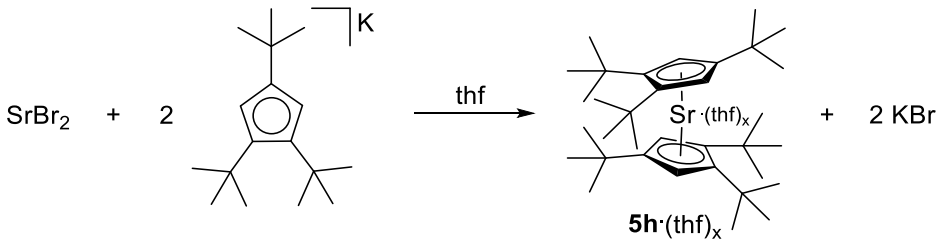

Scheme 42: Synthesis of $Cp'''_2Sr·(thf)_x$ (**5h**·$(thf)_x$) as carried out by Hatanpää *et al*.[79]

Workup of the crude material after the synthesis afforded the thf adduct of hexa-*tert*-butylstrontocene, but by applying *vacuo*, the base free metallocene (**5h**) was obtained.[79] Crystals suitable for single crystal X-ray crystallography were obtained by sublimation of **5h** revealing a bent geometry and Sr-Cp^{cent} distances comparable to those found in the silyl derivative **5d**.[79] In literature, two examples of strontocenes with aryl substituted cyclopentadienyl rings were reported to date, one with *n*-butyl groups in *para* position ($(p\text{-}n\text{BuPh})_5Cp_2Sr$) and the other with *tert*-butyl groups in *para* position ($(p\text{-}t\text{BuPh})_5Cp_2Sr$).[58,80] Orzechowski *et al*. synthesized $(p\text{-}n\text{BuPh})_5Cp_2Sr$ (**5i**) by ligand exchange reaction in 2008 (Scheme 43).[80]

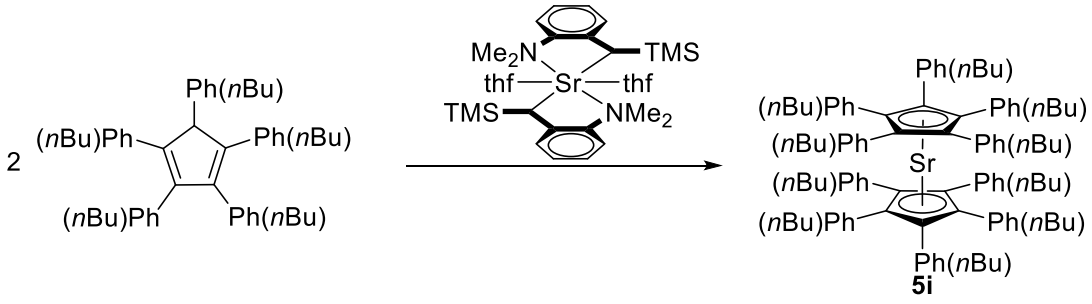

Scheme 43: Synthesis of deca(*para*-*n*-butylphenyl)strontocene (**5i**) as conducted by Orzechowski *et al*.[80]

Crystals suitable for X-ray crystallography of this strontocene were obtained from *n*-pentane displaying the significant effect of alkyl substitution on the solubility of aryl substituted metallocenes. In the crystal structure of **5i** (Figure 16) a coplanar geometry (δ = 179.9°) is revealed together with Sr-Cp^{cent} distance similar to what was found in Cp'''$_2$Sr (**5h**).[80]

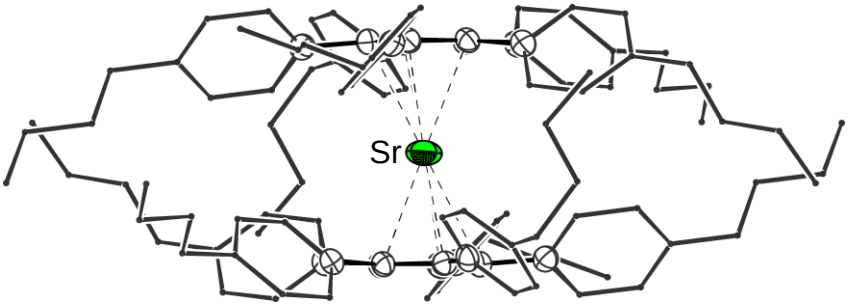

Figure 16: Molecular structure of $^{(p\text{-}n\text{BuPh})5}Cp_2Sr$ (**5i**) in the crystal[80] for clarification of the out-of-plane bending (hydrogen atoms omitted and only *ipso* carbon atoms of (*para*-*n*-butyl)phenyl groups depicted for clarity, remaining aryl groups depicted as wireframe, thermal ellipsoids at 50% probability level).

The attractive forces observed in the **4k** (C-H···C(π) interactions) were also investigated in this analogous strontocene: the authors stated that in the strontocene such an attractive force was prevalent due to the out-of-plane bending angle observed in that structure.[80] By inspection of the crystal structure of **5i** it is obvious that the *ipso* carbon atoms of the (*para*-*n*-butyl)phenyl groups are not in plane with the cyclopentadienyl ring. This is a clear hint in Cp^{BIG} complexes for attractive interactions between the ligands.[80] The other example of aryl substituted strontocene, **5j**, was published in 2020 by Schulte *et al*. Their synthetic pathway included strontium amalgam and the penta(*tert*-butylphenyl)cyclopentadiene radical as starting materials (Scheme 44).[58]

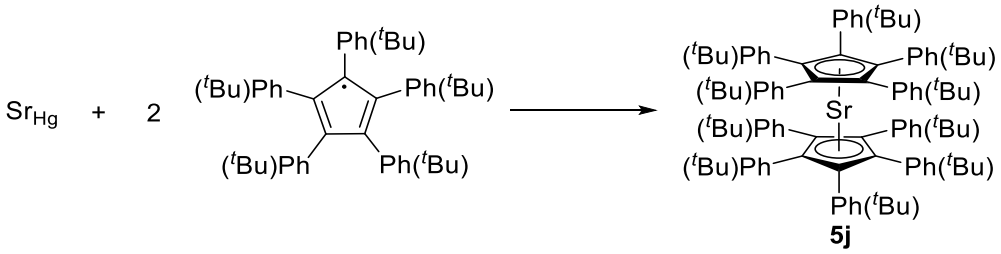

Scheme 44: Synthesis of deca(*para*-*tert*-butylphenyl)strontocene (**5j**) as carried out by Schulte *et al*.[58]

The molecular structure of **5j** in the solid state revealed an almost coplanar geometry (δ = 177.2°) and Sr-Cp^{cent} distances similar to those observed in **5i**.[58,80] Very few examples of heteroatom functionalized strontocenes are known, one of them stems from Hays *et al*. from 1996 (Scheme 45).[76]

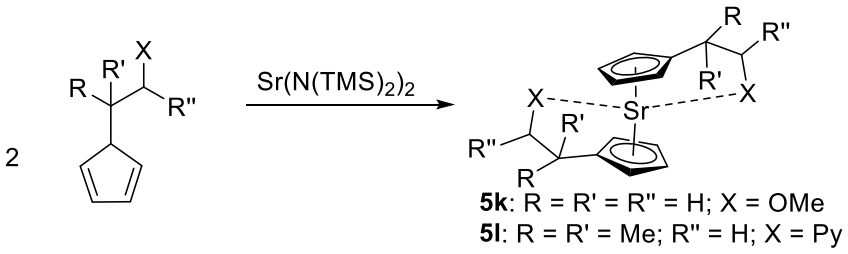

Scheme 45: Syntheses of methoxy- and pyridinyl substituted strontocenes (**5k**, **5l**) as conducted by Hays *et al*.[76]

The authors managed to crystallize the pyridinyl substituted strontocene (**5l**) unravelling a significantly bent structure (δ = 141.2°) with Sr-Cp^{cent} distances similar to what is observed for Cp'$_2$Sr·(thf)$_2$.[76] In 2013, Li and coworkers presented the synthesis of ester functionalized strontocenes which calcium relatives have already been introduced (*vide supra*). The synthesis of these complexes was conducted analogously to the corresponding calcocenes (Scheme 46).[72]

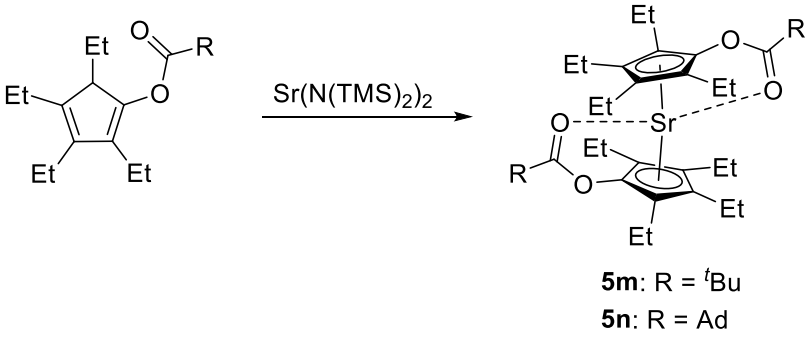

Scheme 46: Syntheses of ester functionalized strontocenes (**5m**, **5n**) as carried out by Li *et al*.[72]

Li *et al*. obtained the crystal structure of the mono thf adduct of the adamantyl substituted derivative, **5n**·thf, but unfortunately not that of the base free metallocene. Alike the calcocene congeners, the strontocenes (**5m**, **5n**) reported by Li and coworkers are stable in dry air for about 12 h, but moisture sensitive.[72] In 2004, Schumann and coworkers reported of the butenyl substituted strontocene **5o**, which was synthesized analogously to the corresponding calcocene (Scheme 47).[59]

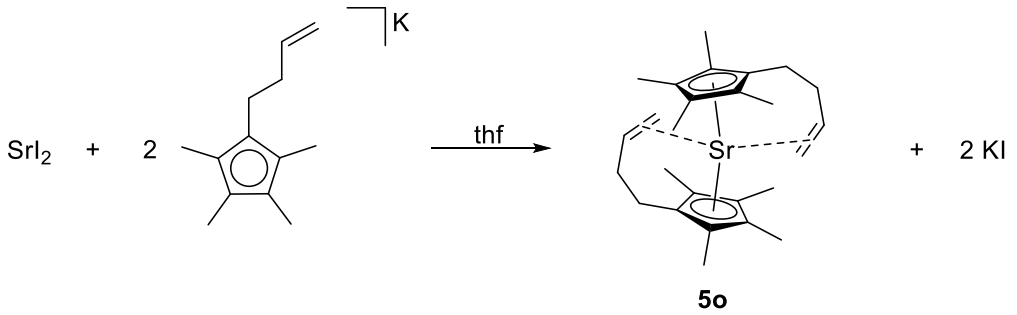

Scheme 47: Synthesis of butenyl substituted strontocene (**5o**) as conducted by Schumann *et al*.[59]

In the molecular structure in the crystal of $^{H2C=CHC2H4}Cp^{\#}_2Sr$, **5o**, interactions of the strontium centre with the alkenyl moieties are visible similar to what was observed in the analogous calcium complex (*vide supra*).

Since there are only seven examples of structurally characterized base free strontocenes, drawing solid conclusions on basis of comparisons between magnesocenes, calcocenes and strontocenes is difficult. Comparison of the bending angle δ between **4d** (167.3°) and **5d** (159.4°) reveals a difference between these two metallocenes exposing the tendency of a stronger bending in the metallocenes when descending group 2. However, this trend should not be overestimated since in the hexa-*tert*-butylmetallocenes of calcium (**4i**) and strontium (**5h**) there is only a difference of 1.4° between the bending angles. The Sr-Cp^{cent} distances in all structurally characterized strontocenes are approximately the same, which shows that only very limited correlation can be drawn between substitution pattern and Sr-Cp^{cent} distance.

Table 4: Selected structural parameters and references of strontocenes.

Compound	Cp^{cent}-Sr-Cp^{cent} δ[°][a]	Cp^{cent}-Sr [pm][a]	Reference
Cp_2Sr (**5a**)	-	-	[10]
Cp^*_2Sr (**5b**)	149(3)[c]	246.9(6)[b]	[77,78]
$^{TMS2}Cp_2Sr$ (**5c**)	-	-	[65]
$^{TMS3}Cp_2Sr$ (**5d**)	159.4	253.96(4)	[66]
$^{3}Cp_2Sr$ (**5e**)	-	-	[69]
$^{5}Cp_2Sr$ (**5f**)	-	-	[68]
Cp'_2Sr (**5g**)	-	-	[44]
Cp'''_2Sr (**5h**)	169.3	252.59(8); 253.27(7)	[79]
$^{(p\text{-}n\text{BuPh})5}Cp_2Sr$ (**5i**)	179.9	251.25(2)	[80]
$^{(p\text{-}t\text{BuPh})5}Cp_2Sr$ (**5j**)	177.2	249.22(5); 249.50(5)	[58]
$^{MeOC2H4}Cp_2Sr$ (**5k**)	-	-	[76]
$^{PyCH2CMe2}Cp_2Sr$ (**5l**)	141.2	257.74(9)	[76]
$^{(t\text{Bu})OCO[Et4]}Cp_2Sr$ (**5m**); $^{(Ad)OCO[Et4]}Cp_2Sr$ (**5n**)	-	-	[72]
$^{H2C=CHC2H4}Cp^{\#}_2Sr$ (**5o**)	139.3	254.58(11)	[59]

[a]: Only given in the case of η^5 coordination of cyclopentadienyl ligand to strontium atom; [b]: Determined by electron diffraction spectroscopy.

1.6 Barocenes

Analogously to strontocenes, the most common synthetic pathway to barocenes is transmetalation of the corresponding potassiumcyclopentadienide with barium(II)iodide (see Scheme 48). Also, the Brønsted acid base reaction of barium bis(trimethylsilylamide) with the corresponding cyclopentadiene is often represented.

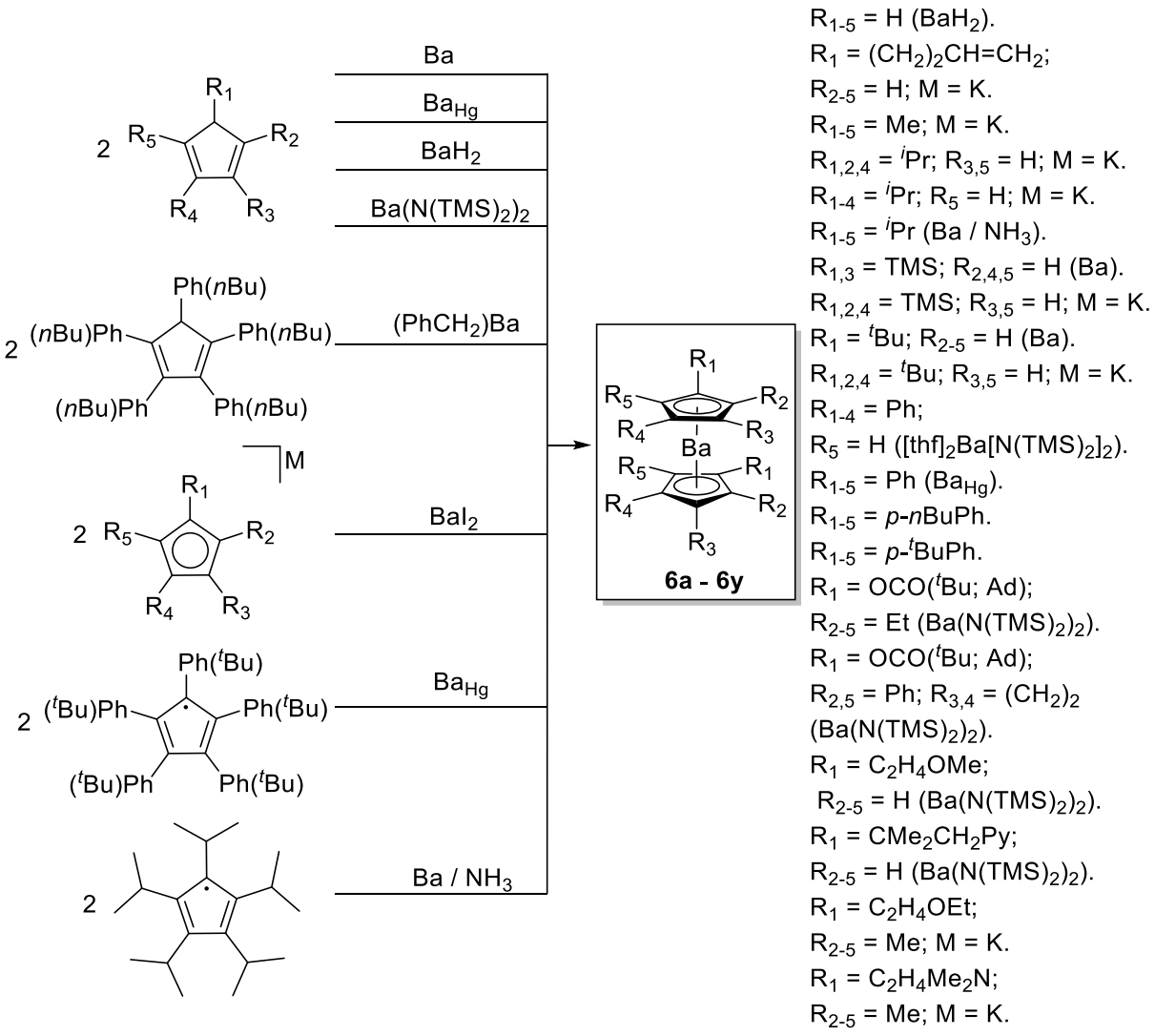

Scheme 48: Overview of possible synthetic routes for barocenes.

Barocene, **6a**, was discovered in 1961 by Fischer and Stölzle. They reported of significant difficulties in the synthesis, for example the seeking for a suitable solvent for the reaction of barium metal with cyclopentadiene. By the reaction of bariumhydride with cyclopentadiene under heating above 673 K, barocene could be obtained in traces (Scheme 49).[10]

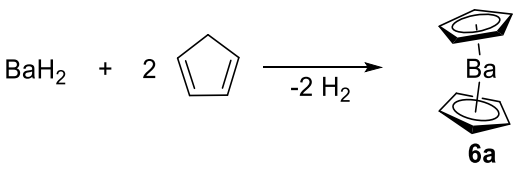

Scheme 49: Synthesis of barocene (**6a**) as conducted by Fischer and Stölzle.[10]

By extraction with dmf and subsequent sublimation at 693 to 733 K, Cp_2Ba (**6a**) could be obtained and characterized by NMR spectroscopy.[10] Dissolution of barocene in dimethyl sulfoxide leads to the formation of a polymeric structure where the barium atom is η^5 coordinated to four cyclopentadienyl ligands and no contacts between the dmso molecules and the barium atoms are observed in the crystal structure as could be shown by Fichtel *et al*. in 2004.[81] In 1987, Andersen and coworkers reported of the structure of Cp^*_2Ba (**6b**) in the gas phase which was investigated by gas phase electron diffraction. They synthesized **6b**·thf by reaction of Cp*K with barium(II)iodide and were able to obtain the base free metallocene by the “toluene-reflux methode” (Scheme 50).[78]

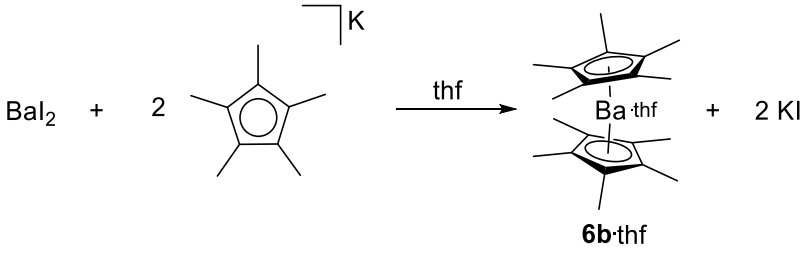

Scheme 50: Synthesis of decamethylbarocene thf adduct (**6b**·thf) as carried out by Andersen *et al*.[78]

The authors determined the Ba-Cp^{cent} distance to 263.1(6) pm and the angle δ to 148(6)°. Only one year later, Williams *et al*. reported of the crystal structure of decamethylbarocene (**6b**), which was synthesized in the same way Andersen and coworkers did one year earlier (Scheme 50).[53,63] Notably, Williams *et al*. reported the removal of coordinated thf from decamethylbarocene (**6b**) to be facile since the bis thf adduct can simply be sublimed at 463 K to obtain the base free metallocene.[63] The structure of Cp^*_2Ba, **6b**, reveals a bent geometry (δ = 131.0°), more bent than determined in the gas phase by gas phase electron diffraction. The authors suggested packing effects in the crystal to provide significant contribution to the stronger bending observed in the solid state compared to the bending in the gas phase.[63]

As seen in Cp^*_2Ca (**4b**) (*vide supra*), the decamethylbarocene, **6b**, also exhibits metal-H···CH_2 contacts (Figure 17), but the authors excluded agostic interactions due to no change observable in the bond angles of the closest methyl group.[63,82] Also the recorded infrared spectra of Cp^*_2Ba did not depict any indications for agostic interactions.[63]

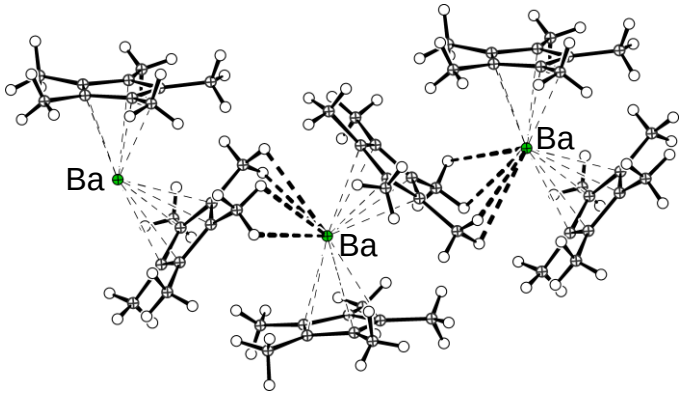

Figure 17: Molecular structure of decamethylbarocene (**6b**) in the crystal[63] (ball-and-stick representation).

The first silyl substituted barocene, $^{TMS2}Cp_2Ba$ (**6c**), was published 1988 by Engelhardt and coworkers who synthesized this compound *via* the metal vapor technique.[65]

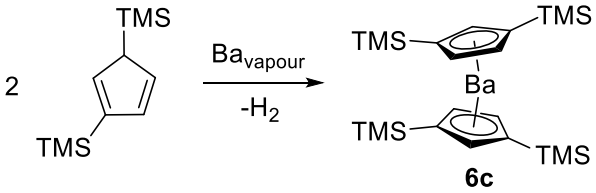

Scheme 51: Synthesis of $^{TMS2}Cp_2Ba$ (**6c**) as conducted by Engelhardt *et al*.[65]

Tetrakis(trimethylsilyl)barocene (**6c**) exhibits a mediocre solubility in benzene, whereas the thf adduct possesses a low solubility in benzene. Interestingly, the solubility of the alkaline earth metal complexes bearing the bis(trimethylsilyl)cyclopentadienyl ligand decreases in the series $^{TMS2}Cp_2Ca$ (**4c**) > $^{TMS2}Cp_2Sr$ (**5c**) > $^{TMS2}Cp_2Ba$ (**6c**).[65] The hexakis(trimethylsilyl)barocene (**6d**) was discovered in 2003 by Harvey *et al*. (Scheme 52).[66]

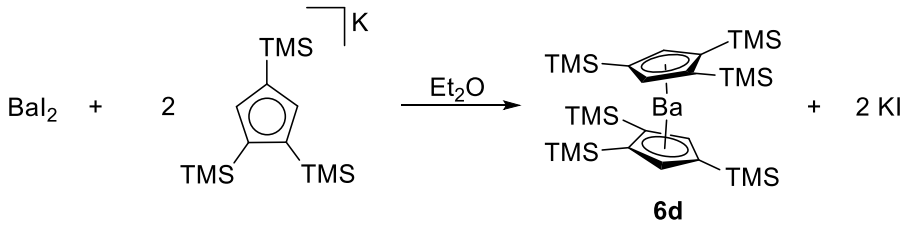

Scheme 52: Synthesis of hexakis(trimethylsilyl)barocene (**6d**) as carried out by Harvey *et al*.[66]

Using thf instead of diethylether as solvent in the synthesis of $^{TMS3}Cp_2Ba$, only $^{TMS3}CpBaI(thf)_x$ was formed, implying that the metallocene itself is too bulky to react with thf. When exposed to air, this barium complex (**6d**) decomposed rapidly. In the crystal, the barium centre reveals contacts to methyl groups of a neighboring tris(trimethylsilyl)cyclopentadienyl ligand similar to the observed methyl-barium contacts in Cp^*_2Ba (**6b**) (Figure 18).[66]

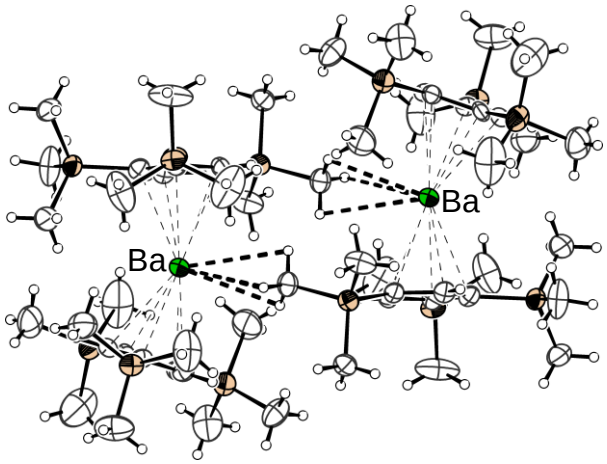

Figure 18: Molecular structure of hexakis(trimethylsilyl)barocene[66] (**6d**) in the crystal (thermal ellipsoids at 50% probability level).

Owing to the bulkiness of the ligand, $^{TMS3}Cp_2Ba$ (**6d**) exhibits a comparably less bended geometry in the solid state (δ = 162.2°) though Ba···HCH_2 contacts are present similar to contacts observed in Cp^*_2Ba (δ = 131.0°).[66] Factors for such differences in structural features can be of multiple origin, for example packing effects in the crystal and attractive dispersion forces. For the heaviest alkaline earth metal element, barium, *iso*propyl substituted metallocenes are well known. The ligand with the slightest steric demand, tri-*iso*propylcyclopentadiene, was introduced to barium chemistry by Burkey *et al*. in 1993 (Scheme 53).[69]

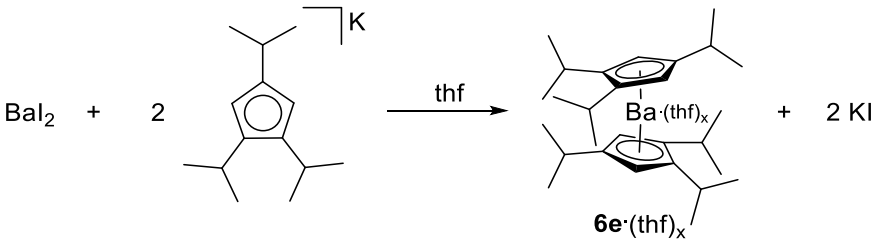

Scheme 53: Synthesis of hexa-*iso*propylbarocene thf adduct (**6e·**$(thf)_x$) as carried out by Burkey *et al*.[69]

Remarkably, even upon sublimation of the thf adduct the base free metallocene (**6e**) was not obtained. By application of the “toluene-reflux method” the unsolvated metallocene could be obtained, which is surprising since other barocenes can be readily sublimed to afford the base free metallocene. The unsolvated metallocene (**6e**) was described as a waxy solid analogously to the corresponding $^{3}Cp_2Mg$ (*vide supra*) and according to this observation, no crystal structure of this complex could be determined.[69] The octa-*iso*propylbarocene (**6f**) (Scheme 54) was reported two years before the hexa-*iso*propylbarocene (**6e**) in 1991 by Williams and coworkers.[67]

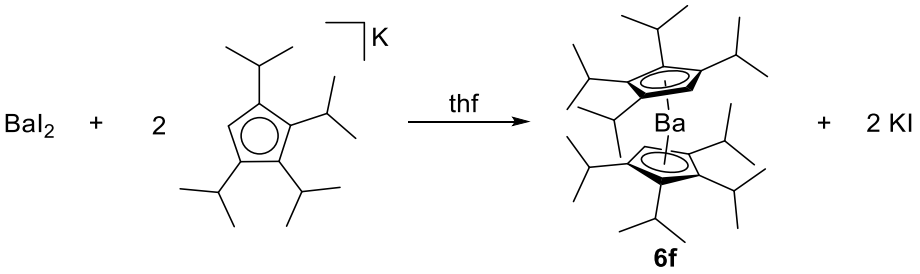

Scheme 54: Synthesis of octa-*iso*propylbarocene (**6f**) as conducted by Williams *et al*.[67]

It is noteworthy that the octa-*iso*propylbarocene (**6f**) was obtained after workup as a base free metallocene, which can be sublimed at comparably low temperatures (363 K, 10^{-3} mbar), although thf was used for the synthesis. This is owing to the fact of the higher steric demand of the tetra-*iso*propylcyclopentadienyl ligand in comparison to the tri-*iso*-propylcyclopentadienyl ligand ensuring a more effective shielding of the central atom toward reactants and a more effective packing in the crystal. The authors attributed an elevated sensitivity of $^{4}Cp_2Ba$ (**6f**) toward air oxidation compared to the calcium analogue $^{4}Cp_2Ca$ to a larger radius of Ba(II) compared to Ca(II). In the molecular structure of $^{4}Cp_2Ba$, a bent

geometry is revealed (δ = 154.3°) with Ba-Cp^{cent} distances marginally shortened in comparison to those observed for Cp*$_2$Ba (see Table 5). Williams *et al*. stated that multiple reasons are conceivable for the increased angle δ in ^{4}Cp$_2$Ba (**6f**) in comparison to the one obtained in Cp*$_2$Ba (**6b**): Differences in the electronic structure and steric demand of the ligands.[67] The per-*iso*propylated cyclopentadienyl ligand, ^{5}Cp, was introduced to barium chemistry in 1998 by the Sitzmann group. Their synthesis started from the penta-*iso*propylcyclopentadiene radical and barium metal in liquid ammonia (Scheme 55).[68]

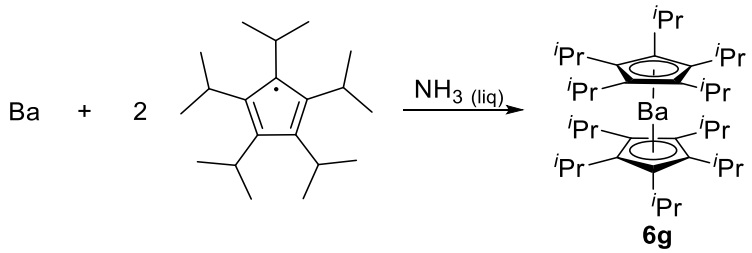

Scheme 55: Synthesis of deca-*iso*propylbarocene (**6g**) as carried out by Sitzmann *et al*.[68]

Sitzmann *et al*. managed to crystallize the deca-*iso*propylbarocene (**6g**). Taking deeper insight into the structural characteristics of ^{5}Cp$_2$Ba, **6g**, an almost coplanar geometry on barium is detected (δ = 179.9°) with a staggered arrangement of the ligands and Ba-Cp^{cent} distances similar to what is found in ^{TMS3}Cp$_2$Ba (**6d**). This complex is the only structurally characterized example of a group 2 metallocene bearing ^{5}Cp ligands. The enormous steric demand of this ligand is presumably the main reason for ^{5}Cp$_2$Ba to exhibit a coplanar structure in the crystal. Upon expose to air, deca-*iso*propylbarocene, **6g**, decomposes slowly, the authors stated the corresponding calcocene and strontocene to be air-stable for several weeks.[68] Analogously to the synthesis of di-*tert*-butylcalcocene (**4h**) and -strontocene (**5g**), the barium derivate (**6h**) was synthesized by metal vapor technique (Scheme 56).[44]

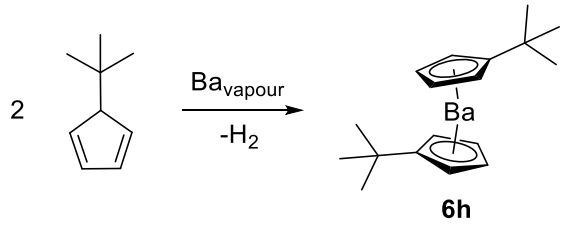

Scheme 56: Metal vapor synthesis of di-*tert*-butylbarocene (**6h**) as conducted by Gardiner *et al*.[44]

Heating of the raw product to 593 K (10^{-4} mmHg) resulted in sublimation of **6h** as a glass-like solid. Dissolution of this metallocene in thf gave rise to the according thf adduct with only loosely bonded thf molecules which could be removed by warming up the adduct to 313 K *in vacuo* to obtain the base free barium complex.[44] The phenomenon of decreasing metal-donor solvent bond strength going down group 2 from beryllium to barium might be a reason for the simplicity of removement of thf from **6h**. Justified by the low steric demand of the two *tert*-butyl groups, all di-*tert*-butylmetallocenes of group 2 exhibit pyrophoricity.[44] Possessing an elevated level of steric demand in comparison to di-*tert*-butylbarocene, **6i** was synthesized by Hatanpää *et al*. in 2007 (Scheme 57).[79]

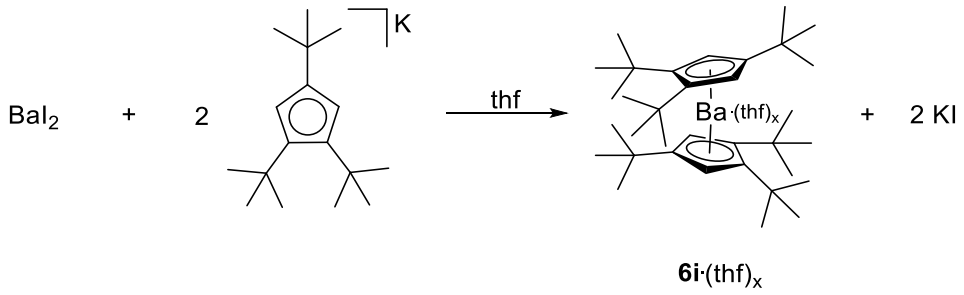

Scheme 57: Synthesis of hexa-*tert*-butylbarocene (**6i**) as carried out by Hatanpää *et al*.[79]

To obtain the base free metallocene **6i**, can be heated while applying vacuum or dissolving the adduct in toluene and distill off the solvent. This complex crystallized in two different polymorphs depending on the circumstances: By sublimation (433-493 K; $5 \cdot 10^{-2}$ mbar), one molecule in the asymmetric unit of **6i** was observed while by slow crystallization from toluene, four independent molecules were found in the asymmetric unit. Interestingly, the conformer obtained by crystallization from toluene exhibits Ba-CH_3 contacts, forming a network in the crystal, which the other conformer did not possess (Figure 19).[79]

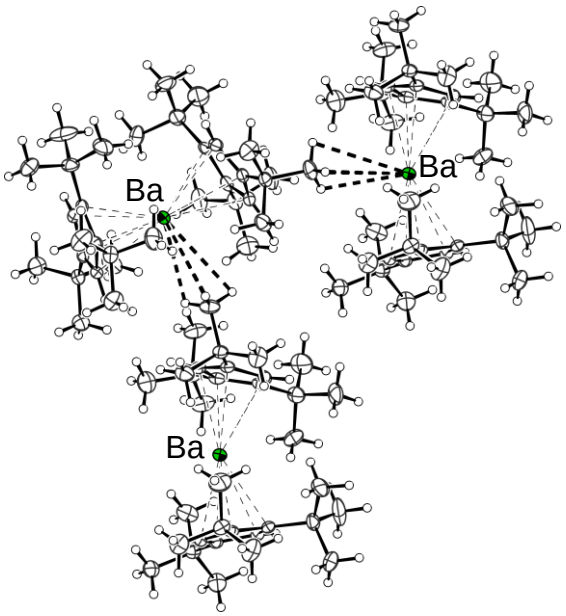

Figure 19: Molecular structure of hexa-*tert*-butylbarocene (**6i**)[79] in the crystal (thermal ellipsoids at 50% probability level).

Remarkably, this is the third structure of barocenes which reveals this behavior in the solid state, where a barium-methyl interaction can be determined. The conformer with only one molecule in the asymmetric unit of **6i** where Ba-CH_3 contacts were observed, exhibits a smaller angle δ (159.7°) in comparison to the range of the angles δ obtained in the other conformer (161.3 – 164.9°). However, since this difference is not significant, no definite conclusions should be drawn in meanings of the contribution of the agostic interaction to the angle δ.[79] Harder reported the polymeric barate complex **6j** which was synthesized by reaction of a Wittig reagent with cyclopentadiene and barocene. In the solid state, the barium atom exhibits a hapticity of η^5 to each cyclopentadienyl ligand (Figure 20).[83]

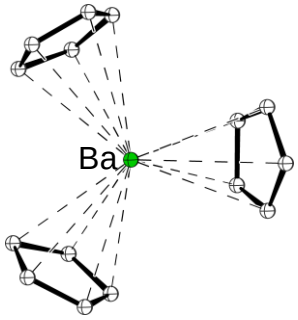

Figure 20: Molecular structure of $(Cp_3Ba)^-$ (**6j**)[83] in the crystal (counterion omitted for clarity, ball-and-stick representation).

The Ba-Cp^{cent} distances vary between 287.41(27) pm and 296.91(19) pm, which is significantly elongated in comparison to barocenes (see Table 5).[83] In 1994, Tanner *et al*. synthesized octaphenylbarocene, $^{Ph4}Cp_2Ba$ (**6k**), by deprotonation of the tetraphenyl cyclopentadienyl ligand with barium bis(trimethylsilylamide) (Scheme 58).[84]

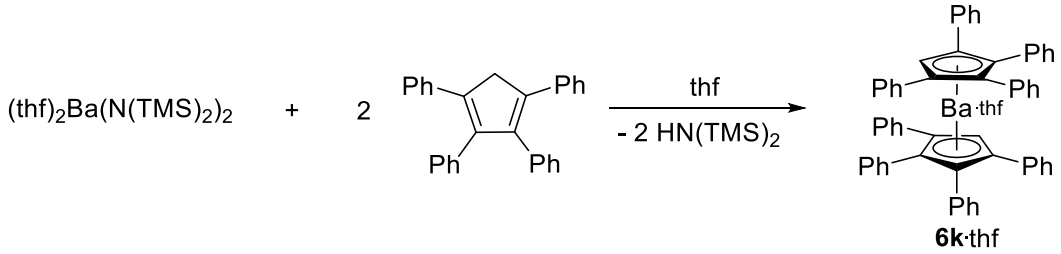

Scheme 58: Synthesis of octaphenylbarocene thf adduct (**6k**·thf) as conducted by Tanner *et al*.[84]

Attempts to synthesize this metallocene (**6k**) by salt metathesis reaction of barium(II)iodide with tetraphenylcyclopentadienylpotassium in dme failed. Surprisingly, approaches to sublime the metallocene yielded in decomposition of the product and formation of the free ligand.[84] The decaaryl substituted metallocenes of barium are well investigated since they all could be structurally characterized. In this class of compounds, the Cp^{BIG} representative with the least steric demand is **6l** which was reported by Deacon *et al*. in 2008 (Scheme 59).[70]

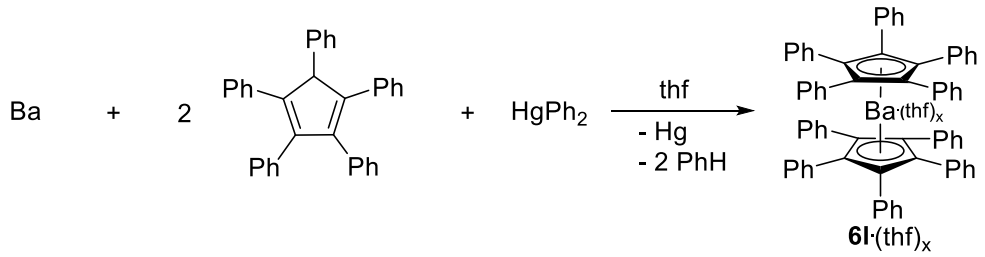

Scheme 59: Synthesis of decaphenylbarocene thf adduct (**6l**·$(thf)_x$) as carried out by Deacon *et al*.[70]

To obtain the base free metallocene, the decaphenylbarocene thf adduct (**6l**·$(thf)_x$) can be dissolved in hexane and sonicated at 323 K for 24 h. Analogously to decaphenylcalcocene (**4b**), **6l**, exhibits low solubility in aliphatic and aromatic solvents. The authors proposed C-H···C(π) interactions in the solid state as the driving force for the successful formation of this

metallocene. In the crystal structure of decaphenylbarocene, a coplanar arrangement (δ = 179.9°) of the cyclopentadienyl ligands is observed and Ba-Cp^{cent} distances comparable to those observed in deca(*para*-*n*-butylphenyl)barocene (*vide infra*), but significantly shortened compared to the Ba-Cp^{cent} distances observed in $^{5}Cp_2Ba$ (**6g**).[70] One approach to increase the solubility of these decaphenylmetallocenes is substitution of the phenyl rings in *para*-position. The barocene, **6m**, was synthesized by Orzechowski *et al*. in 2008 following this idea (Scheme 60).[80]

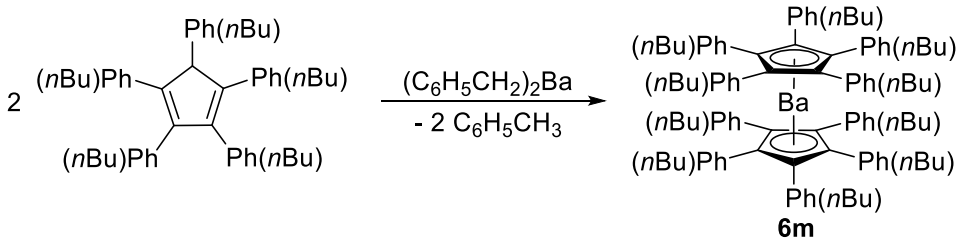

Scheme 60: Synthesis of deca(*para*-*n*-butylphenyl)barocene (**6m**) using dibenzylbarium as conducted by Orzechowski *et al*.[80]

6m exhibits high solubility even in aliphatic solvents such as hexane or pentane supporting the concept of substitution in *para*-position of the phenyl group in these metallocenes to be working.[80] As could be seen in the crystal structure of the analogous strontocene, the penta(*para*-*n*-butylphenyl)cyclopentadienyl ligands are interacting with each other with a network of C···H contacts. In the molecular structure of this metallocene bearing Cp^{BIG} ligands, a coplanar structure was revealed (δ = 179.9°).[80] Another barocene possessing Cp^{BIG} ligands is **6n**, which was synthesized *via* barium amalgam by Schulte *et al*. in 2020 (Scheme 61).[58]

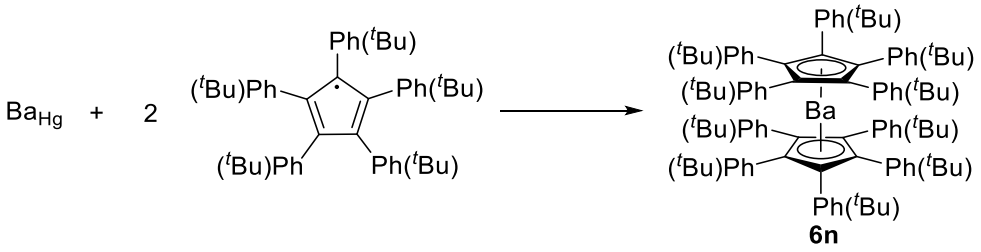

Scheme 61: Synthesis for deca(*para*-*tert*-butylphenyl)barocene (**6n**) carried out by Schulte and coworkers.[58]

By inspection of the crystal structure of **6n**, an almost coplanar arrangement of both cyclopentadienyl ligands is observed (δ = 178.3°) and Ba-Cp^{cent} distances slightly shortened in comparison to those observed for **6m**.[80] It is worth mentioning that all phenyl substituted barocenes exhibit (almost) coplanar structures mostly owing to the steric hindrance of the cyclopentadienyl ligands and that C···H interactions in these metallocenes provide a great contribution to the stability of these barocenes.[58,80] Structurally characterized barocenes with donor moieties connected to the cyclopentadienyl ligand are rare since only the butenyl substituted **6o** and **6p** and **6q** are known.[59,85] Methoxy- and pyridinyl substituted barocenes were synthesized analogously to the calcium and strontium congeners by Hays and coworkers in 1996.[76] Unfortunately, the authors were not able to report any structural characteristics of these two barocenes (Scheme 62).[76]

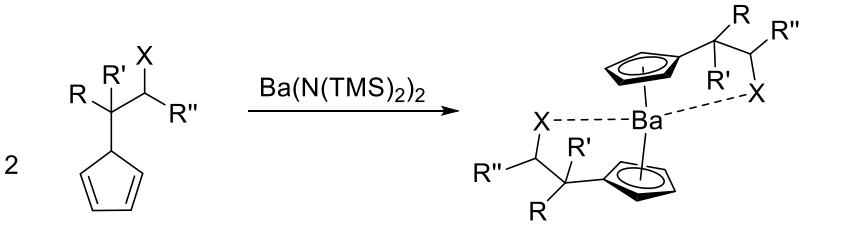

Scheme 62: Synthesis of methoxy- and pyridinyl substituted barocenes (**6r**, **6s**) as carried out by Hays *et al*.[76]

In 2004, Hatanpää *et al*. reported the two donor substituted barocenes $^{Me2NC2H4}Cp^{\#}_2Ba$ (**6p**) and $^{EtOC2H4}Cp^{\#}_2Ba$ (**6q**) (Scheme 63).[85]

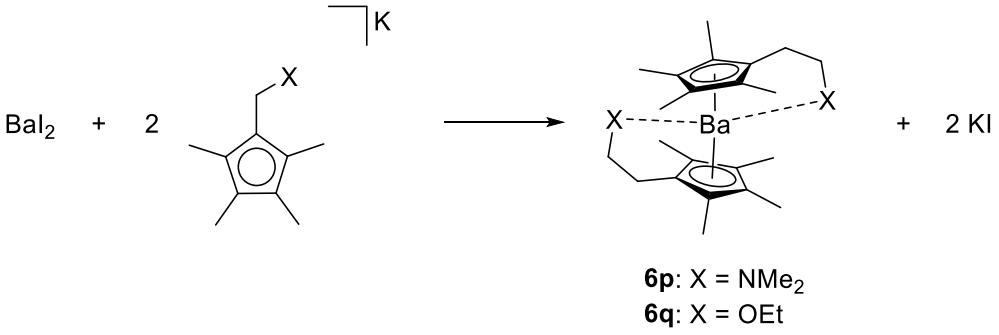

Scheme 63: Synthesis of $^{Me2NC2H4}Cp^{\#}_2Ba$ (**6p**) and $^{EtOC2H4}Cp^{\#}_2Ba$ (**6q**) as conducted by Hatanpää *et al*.[85]

The solid state structures of these two compounds revealed contacts of the barium atom to the corresponding donor moieties. The Ba-Cp^{cent} distances and bending angles δ of these complexes are similar and resemble the structural features for **6o** (*vide infra*).[85] Ester substituted barocenes (**6t**, **6u**) were published by Li *et al*. in 2013 who synthesized these metallocenes under usage of barium bis(trimethylsilylamide) (Scheme 64).[72]

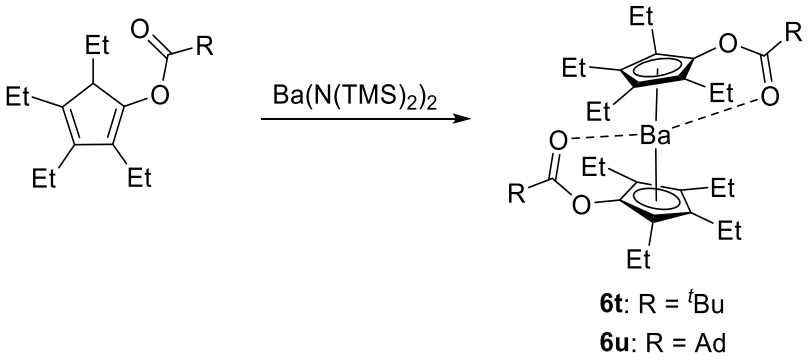

Scheme 64: Synthesis of ester substituted barocenes (**6t**, **6u**) as carried out by Li *et al*.[72]

Only the diethylether adduct of the adamantyl substituted derivate (**6u**·OEt_2) could be structurally characterized unravelling one coordinated diethylether molecule and two carbonyl oxygen atoms of the ester groups.[72] The *tert*-butyl substituted barocene (**6t**) reported by Li *et al*. was presented to be a good Cp transfer reagent by transmetalation of this compound with iron(II)chloride to obtain the corresponding ferrocene.[72] The group established in their report another ligand system solely for barium (Scheme 65).[72]

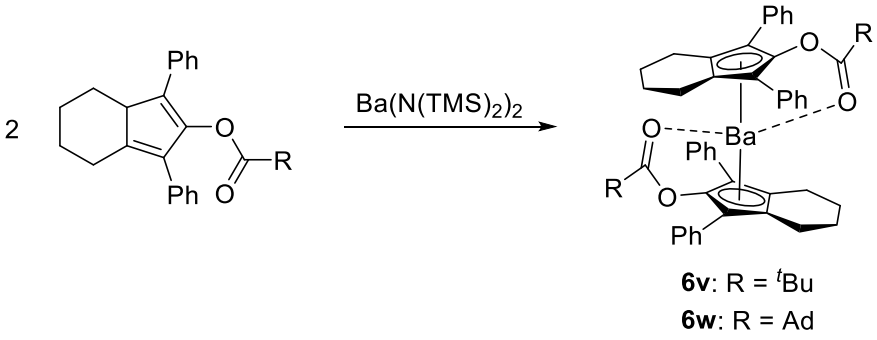

Scheme 65: Synthesis of another ester substituted barocene (**6v**, **6w**) as carried out by Li *et al*.[72]

Upon exposure to air, **6v** and **6w** decomposed readily in contrast to the related ester substituted calcocenes and strontocenes.[72] Since there are two reports of metallocenes of barium with olefin barium contacts making these compounds interesting for possible applications in catalysis, these complexes are presented next. The first report of such a compound dates stems from 2004, when Schumann *et al*. synthesized a butenyl substituted barocene (**6o**) (Scheme 66).[59]

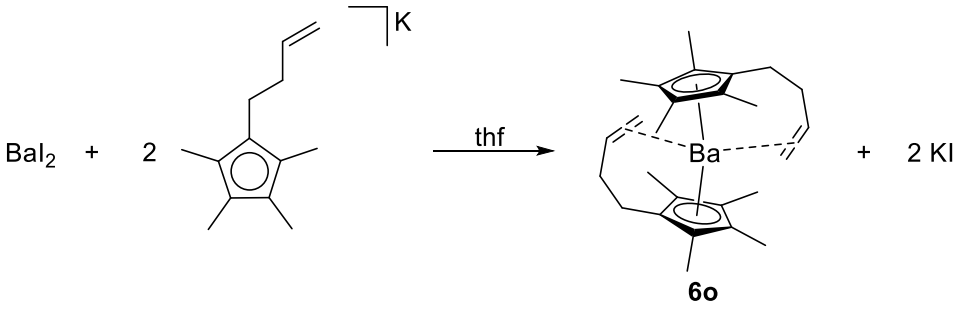

Scheme 66: Synthesis of butenyl substituted barocene (**6o**) reported by Schumann *et al*.[59]

In analogy to the corresponding calcocene (**4v**) and strontocene (**5o**), this barocene (**6o**) exhibits metal olefin contacts in the solid state, which origins were already discussed (*vide supra*). Interestingly, when dissolving the barocene in thf-d_8, the barium olefin contacts were broken and thf was coordinated to the barium centre which was reflected by ^{13}C NMR spectroscopy. This experiment highlights the weakness of the olefin alkaline earth metal interaction in these butenyl substituted metallocenes.[59] The second example of a barocene with barium olefin interaction was reported by Wiecko *et al*. in 2008 (Scheme 67).[86]

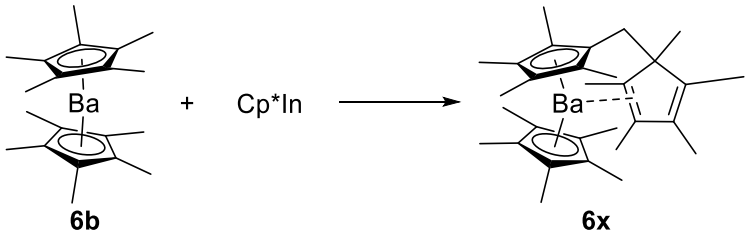

Scheme 67: Synthesis of Cp* based barocene olefin (**6x**) complex as conducted by Wiecko *et al*.[86]

The reaction of decamethylbarocene (**6b**) with Cp*In was carried out without solvent in a sealed glas tube at 413 to 423 K for several days. Wiecko *et al*. suggested a mechanism

including a radical C-H activation process and formation of indium metal during reaction. Crystals suitable for X-ray analysis grew simply over reaction time in the glas tube revealing barium olefin interactions (Figure 21).

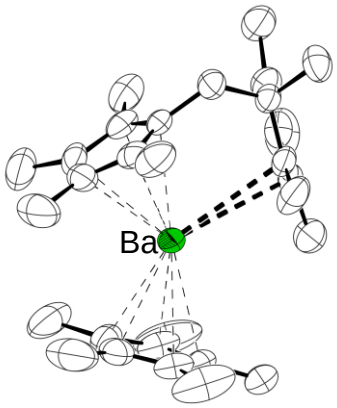

Figure 21: Molecular structure of $(C_5Me_4CH_2C_5Me_5)BaCp^*$ (**6x**)[86] in the crystal (hydrogen atoms omitted for clarity, thermal ellipsoids at 50% probability level).

Quantum chemical calculations carried out by the authors at the MP2/def2-TZVPP level of theory determined the interaction energy of the barium centre with the olefin moiety to 13.3 kcal·mol^{-1}.[86] In the crystal structures of both olefin barocene complexes, bent geometries are revealed with similar Ba-Cp^{cent} distances (see Table 5).

In total, there are 24 barocenes in literature of which 14 are structurally characterized. Interestingly, barocenes with bulky cyclopentadienyl ligands exhibit contacts between methyl groups and the central barium atom which can be observed in Cp'''_2Ba (**6i**), $^{TMS3}Cp_2Ba$ (**6d**) and Cp^*_2Ba (**6b**).[63,66,79] This is presumably due to the large coordination sphere present at the barium atom in comparison to calcium and strontium. Also, the tendency of the ease of loss of coordinating donor solvents reaches a peak at barocenes, where, for example in the case of decamethylbarocene, simply applying vacuum on the compound yields the base free metallocene. The only examples of coplanar barocenes are the ones bearing aryl substituted cyclopentadienyl ligands (Cp^{BIG}) and the superbulky penta-*iso*propylcyclopentadienyl ligand (^5Cp).[58,68,70,80] This is intriguing to observe because it seems that only these extremely bulky ligands can overcome the trend of barocenes to be bent in the solid state.

Table 5: Selected structural parameters and references of barocenes.

Compound	Cp^{cent}-Ba-Cp^{cent} δ[°][a]	Cp^{cent}-Ba [pm][a]	Reference
Cp_2Ba (**6a**)	108.9 – 110.1[81]	291.85(1)[81]	[10,81]
Cp^*_2Ba (**6b**)	131.0[63]	270.03(6); 275.67(4)[63]	[63,77,82]
$^{TMS2}Cp_2Ba$ (**6c**)	-	-	[65]
$^{TMS3}Cp_2Ba$ (**6d**)	162.2	274.45(3); 276.16(3)	[66]
$^{3}Cp_2Ba$ (**6e**)	-	-	[69]
$^{4}Cp_2Ba$ (**6f**)	154.3	267.66(12); 267.94(9)	[67]
$^{5}Cp_2Ba$ (**6g**)	179.9	274.86(5)	[68]
Cp'_2Ba (**6h**)	-	-	[44]
Cp'''_2Ba (**6i**)	159.7 – 164.9	268.90(6); 276.34(4)	[79]
$[Cp_3Ba]^-[Bu_4P]^+$ (**6j**)	106.4 – 114.6	287.41(27) – 296.91(19)	[83]
$^{Ph4}Cp_2Ba$ (**6k**)	-	-	[84]
$^{Ph5}Cp_2Ba$ (**6l**)	179.9	266.97(1)	[70]
$^{(p\text{-}n\text{BuPh})5}Cp_2Ba$ (**6m**)	179.9	266.66(1)	[80]
$^{(p\text{-}t\text{BuPh})5}Cp_2Ba$ (**6n**)	178.3	264.11(3); 264.17(3)	[58]
$^{H2C=CHC2H4}Cp^{\#}_2Ba$ (**6o**)	139.1	271.51(4); 272.06(4)	[59]
$^{Me2NC2H4}Cp^{\#}_2Ba$ (**6p**)	137.9	271.29(4); 271.58(4)	[85]
$^{EtOC2H4}Cp^{\#}_2Ba$ (**6q**)	138.9	271.16(4); 272.81(4)	[85]
$^{MeOC2H4}Cp_2Ba$ (**6r**); $^{PyCH2CMe2}Cp_2Ba$ (**6s**)	-	-	[76]
$^{(t\text{Bu})OCO[Et4]}Cp_2Ba$ (**6t**); $^{(Ad)OCO[Et4]}Cp_2Ba$ (**6u**); $^{(t\text{Bu})OCO[Ph2][(CH2)4)]}Cp_2Ba$ (**6v**); $^{(Ad)OCO[Ph2][(CH2)4)]}Cp_2Ba$ (**6w**)	-	-	[72]
$(C_5Me_4CH_2C_5Me_5)BaCp^*$ (**6x**)	138.6	270.37(4); 270.45(4)	[86]

[a]: Only given in the case of η^5 coordination of cyclopentadienyl ligand to barium atom.

1.7 Lewis Base Adducts of Magnesocenes

Since magnesocenes are of particular interest for the present work, the discussion of Lewis base adducts of group 2 metallocenes will be limited to magnesocenes (Figure 22).

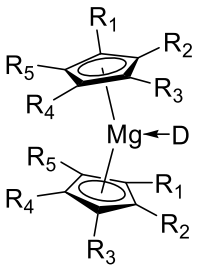

$R_{1\text{-}5}$ = H; D = R_2O, R_3N, R_3P, RCN, Py
$R_{1\text{-}4}$ = Me; R_5 = H; D = NHC
$R_{1\text{-}5}$ = Me; D = NHC
R_1 = $SiMe_3$; R_3 = ^{t}Bu; D = NHC

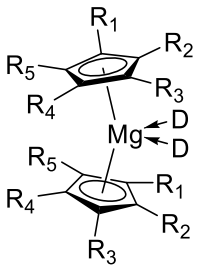

$R_{1\text{-}5}$ = H; D = R_2O, R_3N
$R_{1\text{-}5}$ = H; D = R_2O, R_3N

Figure 22: Overview of Lewis base adducts of magnesocenes (hapticity of η^5/η^5 chosen for schematic depiction).

The first report of Lewis base adducts of magnesocene dates back to 1986, where Lehmkuhl *et al*. investigated the coordination chemistry of magnesocene under usage of different oxygen, nitrogen and phosphorus donors.[87] None of the adducts of magnesocene possibly formed in these experiments could be characterized by single crystal X-ray crystallography by Lehmkuhl and coworkers, but the authors conducted ^{25}Mg NMR spectroscopy on all complexes reported and sorted different donors by their donor strength on the basis of the signals observed in ^{25}Mg NMR spectra.[87] In the case of the Lewis base adduct of magnesocene with trimethylphosphine, Lehmkuhl *et al*. were not able to obtain the corresponding adduct in pure form presumably due to the weak interaction between the phosphorus atom and the magnesium centre.[87] In 2008, Jaenschke *et al*. were able to crystallize selected complexes which were reported by Lehmkuhl *et al*. more than 20 years ago. The adducts of magnesocene with acetonitrile and 1,2-dimethoxyethane (dme) both exhibit hapticities of η^5/η^5 of magnesium to the cyclopentadienyl ligands (Figure 23).[60]

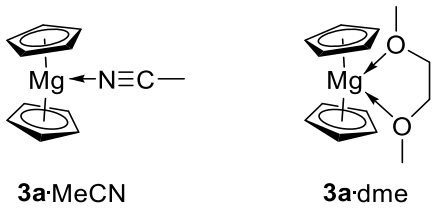

3a·MeCN **3a**·dme

Figure 23: Lewis base adducts of magnesocene with: left: acetonitrile (**3a**·MeCN); right: 1,2-dimethoxyethane (**3a**·dme).[60]

These complexes were easily formed by adding the donor to solutions of magnesocene in toluene (acetonitrile) or thf (1,2-dimethoxyethane).[60] Remarkably, the Mg-Cp^{cent} distances of the adduct formed with dme are elongated in comparison to those observed for the acetonitrile adduct (see Table 6), presumably due to the elevated steric hindrance of dme compared to acetonitrile. Also, the bending in the dme adduct is more pronounced than in the acetonitrile adduct which might also speak for steric reasons. By adding diglyme to a solution of magnesocene in thf, the corresponding adduct, **3a**·diglyme, is formed which exhibits a hapticity of η^5/η^2 in the solid state (Figure 24).[60]

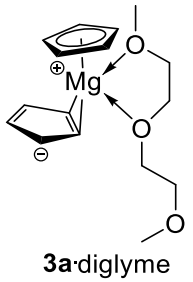

3a·diglyme

Figure 24: Lewis base adduct of magnesocene with diglyme (**3a**·diglyme).[60]

The same hapticity is observed for the corresponding adduct with 1,4-dioxane, **3a**·dioxane, which exhibits a polymeric structure in the solid state. In the adduct of magnesocene with tmeda, **3a**·tmeda, the two cyclopentadienyl ligands exhibit an η^5/η^1 coordination mode (Figure 25).[60]

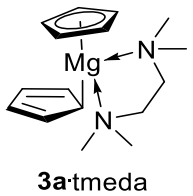

3a·tmeda

Figure 25: Lewis base adduct of magnesocene with tmeda (**3a**·tmeda).[60]

The difference in hapticity between the dme adduct (η^5/η^2) and the tmeda adduct (η^5/η^1) can be attributed to the elevated donor ability of the nitrogen atoms in tmeda and, by that, a stronger bonding of tmeda to the magnesocene resulting in a stronger weakening of the magnesium-Cp bond. Another example of a Lewis base adduct of magnesocene exhibiting an η^5/η^1 hapticity is the bis thf adduct (Figure 26).[29]

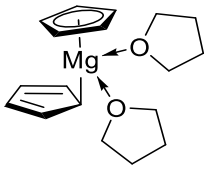

3a·$(thf)_2$

Figure 26: Lewis base adduct of magnesocene with two thf molecules (**3a**·$(thf)_2$).[29]

This bis thf adduct, **3a**·$(thf)_2$, was obtained by Jaenschke *et al*. in 2003 by dissolving magnesocene in thf and adding a small amount of hexane to trigger precipitation of the corresponding adduct.[29] The mono thf adduct was reported by Kim *et al*. in 2007 exhibiting an η^5/η^5 hapticity in the solid state (Figure 27).[88]

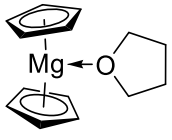

3a·thf

Figure 27: Lewis base adduct of magnesocene with one thf molecule (**3a**·thf).[88]

In the solid state, this adduct (**3a**·thf) exhibits a bent geometry at magnesium (δ = 137.5°) and a Mg-Cp^{cent} distance comparable to what is found for the Mg-Cp^{cent} distance in the bis thf adduct of magnesocene (**3a**·(thf)$_2$). In 1996, Olmstead *et al*. reported of a mixed adduct of magnesocene with thf and *tert*-butylamine (Figure 28).[89]

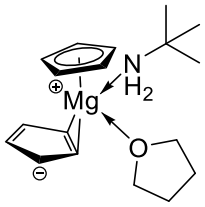

3a·(^{t}BuNH$_2$)(thf)

Figure 28: Lewis base adduct of magnesocene with one thf molecule and one *tert*-butylamine molecule (**3a**·(^{t}BuNH$_2$)(thf)).[89]

The synthesis of this mixed adduct was conducted by adding a mixture of thf and *tert*-butylamine to magnesocene and refluxing this mixture over night.[89] At the beginning of the 2000s, Xia *et al*. synthesized several adducts of amines with magnesocenes. The synthetic procedure to obtain these adducts was dissolving the magnesocene in toluene, adding the corresponding amine and stirring this solution overnight. In their first study from 2002, the authors were able to crystallize the adduct of magnesocene with 2,4-dimethylpentylamine (Figure 29).[90]

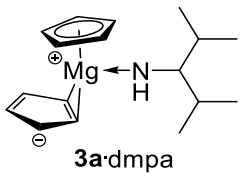

3a·dmpa

Figure 29: Lewis base adduct of magnesocene with 1-*Iso*propyl-2-methylpropylamine (**3a**·ipmpa).[90]

Interestingly, this amine adduct, **3a**·ipmpa, can be sublimed without loss of Lewis base, which is surprising since sublimation of the bis thf adduct of magnesocene, **3a**·(thf)$_2$, results in retrieving the base free magnesocene (**3a**).[87,90] In this complex, an interaction between

the hydrogen atoms at the nitrogen of the amine and the cyclopentadienyl ligand was observed contributing to the stability of this compound (Figure 30).[90]

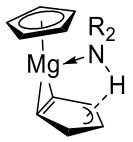

Figure 30: Interaction of N-H with cyclopentadienyl ligand in magnesocene amine adduct.[90]

The Lewis base adduct of magnesocene with 2,4-dimethylpentylamine, **3a**·ipmpa, exhibits an η^5/η^2 hapticity in the solid state presumably due to the interaction of the N-H functionality with the cyclopentadienyl ligand (Figure 30).[90] Similar structures of magnesocene amine adducts are observed for **3a**·H_2NCy and **3a**·(H_2NBn)$_2$ (both η^5/η^2 hapticity in the solid state) which were also reported by Xia *et al*. in 2003.[91] An interesting special case of an amine adduct of magnesocene is the adduct with *iso*propylbenzylamine, **3a**·HN^{i}PrBn, where a hapticity of η^5/η^5 is observed in the solid state (Figure 31).[91]

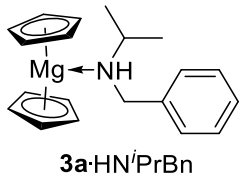

3a·HN^{i}PrBn

Figure 31: Lewis base adduct of magnesocene with *iso*propylbenzylamine (**3a**·HN^{i}PrBn).[91]

The authors stated that no N-H interaction with the cyclopentadienyl ligand could be observed in the solid state structure of this adduct leading to the conclusion that the slippage observed in other magnesocene amine adducts is required for the interaction between the magnesocene and the amine moiety. Another factor might be the steric hindrance incorporated by the benzyl and the *iso*propyl group attached to the nitrogen atom. As early as 1998, Arduengo *et al*. reported of a series of group 2 metallocene adducts with *N*-heterocyclic carbenes (NHCs).[92] They also reacted **3m** with Me_4NHC to yield the corresponding adduct (**3m**·Me_4NHC) (Figure 32).[92]

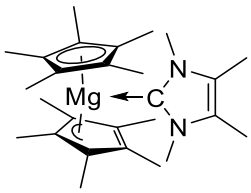

3m·Me_4NHC

Figure 32: Lewis base adduct of decamethylmagnesocene (**3m**) with Me_4NHC (**3m**·Me_4NHC).[92]

The authors concluded the Mg-NHC carbon bond to reveal a covalent character compared to the bonding characters of the later group 2 metals with the NHC carbon atom.[92] In the solid state, an η^5/η^3 like arrangement of the cyclopentadienyl rings can be observed for this complex (**3m**·Me_4NHC).[92] This fact is surprising since the NHC is a much better σ donor compared to a primary amine and should weaken the Mg-Cp bond more effectively, but on the other hand, Me_4NHC is a comparably small molecule because of the planar imidazolium framework. Other adducts of NHCs with magnesocenes were reported by Schumann *et al*. in 2001 (Figure 33).[49]

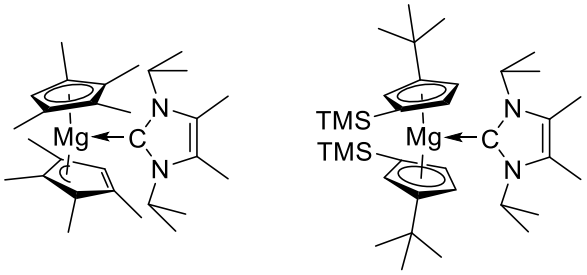

3n·^{i}Pr$_2$Me$_2$NHC **3t**·^{i}Pr$_2$Me$_2$NHC

Figure 33: Lewis base adduct of: left: octamethylmagnesocene with ^{i}Pr$_2$Me$_2$NHC (**3n**·^{i}Pr$_2$Me$_2$NHC); right: 1-trimethylsily-3-*tert*-butylmagnesocene with ^{i}Pr$_2$Me$_2$NHC (**3t**·^{i}Pr$_2$Me$_2$NHC).[49]

Schumann and coworkers were able to obtain crystals in the case of the NHC adduct of octamethylmagnesocene with ^{i}Pr$_2$Me$_2$NHC, **3n**·^{i}Pr$_2$Me$_2$NHC, and observed a hapticity of η^5/η^3 in the solid state analogous to the hapticity observed in the NHC adduct of decamethylmagnesocene with Me_4NHC (**3m**·Me_4NHC) reported by Arduengo and coworkers.[49,92] In the case of the adduct observed by Arduengo *et al*., the Mg-Cp^{cent} distance is slightly shorter than in the case of the adduct reported by Schumann *et al*. which can be justified by the elevated steric hindrance of the *iso*propyl groups in comparison to the methyl groups of

the NHCs used under neglection of the only marginal differences in the bulkiness of the ligands utilized on magnesium.

In conclusion, the potential of magnesocenes in coordinating various donors could be demonstrated and, in some cases, interactions of hydrogen atoms of amines with cyclopentadienyl ligands were observed. The magnesium atom in these metallocenes exhibits significant Lewis acidic character underpinned by the ionic character of the Mg-Cp bond. This bonding character is also evident from the different ring slippages observed in the Lewis base adducts of the magnesocenes. In the adduct of magnesocene with trimethylphosphine, the bonding between the phosphorus atom and the magnesium atom seems to be weak, according to the HSAB principle, due to the inisolability of the adduct in pure form. In summary, magnesocenes reveal an intriguing and fruitful coordination chemistry with a high potential for future bond activation processes as can be seen in the different coordination modes observed in the adducts presented in this chapter.

Table 6: Selected structural parameters and references of Lewis base adducts of magnesocenes.

Compound	Cp^{cent}-Mg-Cp^{cent} δ[°][b]	Cp^{cent}-Mg [pm][b]	Reference
$Cp_2Mg{\cdot}thf$ (**3a**·thf)	137.5	214.68(26)	[88]
$Cp_2Mg{\cdot}(thf)_2$ (**3a**·$(thf)_2$); $Cp_2Mg{\cdot}PMe_3$ (**3a**·PMe_3)[a]	-	213.74(8)[29]	[29,87]
$Cp_2Mg{\cdot}(NH_2{}^tBu)(thf)$ (**3a**·$(NH_2{}^tBu)(thf)$)	-	215.52(11)	[89]
$Cp_2Mg{\cdot}Py$ (**3a**·Py)	-	-	[87]
$Cp_2Mg{\cdot}(dmso)_6$ (**3a**·$(dmso)_6$)	-	-	[29]
$Cp_2Mg{\cdot}H_2NCH{}^iPr_2$ (**3a**·$H_2NCH{}^iPr_2$)	-	211.01(23)	[90]
$Cp_2Mg{\cdot}H_2NCy$ (**3a**·H_2NCy)	-	210.95(9)	[91]
$Cp_2Mg{\cdot}HN{}^iPrBn$ (**3a**·$HN{}^iPrBn$)	134.1	218.26(10); 221.64(14)	[91]
$Cp_2Mg{\cdot}(H_2NBn)_2$ (**3a**·$(H_2NBn)_2$)	-	217.15(11)	[91]
$Cp_2Mg{\cdot}NHRR'$ (R = H, R' = ^{i}Pr; R = H, R' = ^{t}Bu; R = H, R' = $CH_2C_6H_5$; R = R' = Et; R = R' = $CH_2C_6H_5$; R = R' = C_6H_{11})	-	-	[90,91]
$Cp_2Mg{\cdot}MeCN$ (**3a**·MeCN)	147.6	212.25(13)	[60]
$Cp_2Mg{\cdot}dme$ (**3a**·dme)	140.0	227.4(7); 221.4(1)	[60,87]
$Cp_2Mg{\cdot}diglyme$ (**3a**·diglyme)	-	214.96(3)	[60]
$Cp_2Mg{\cdot}dioxane$ (**3a**·dioxane)	-	211.37(7)	[60,87]
$Cp_2Mg{\cdot}tmeda$ (**3a**·tmeda)	-	215.41(7)	[60,87]
$Cp_2Mg{\cdot}pmdta$ (**3a**·pmdta); $Cp_2Mg{\cdot}15\text{-crown-}5$ (**3a**·15-crown-5)	-	-	[60]
$Cp^*{}_2Mg{\cdot}Me_4NHC$ (**3m**·Me_4NHC)	-	216.52(9)	[92]
$Cp^{\#}{}_2Mg{\cdot}{}^iPr_2Me_2NHC$ (**3n**·$^iPr_2Me_2NHC$)	-	218.38(4)	[49]
$^{TMStBu}Cp_2Mg{\cdot}{}^iPr_2Me_2NHC$ (**3t**·$^iPr_2Me_2NHC$)	-	-	[49]

[a]: No structural characterization available; [b]: Only given in the case of η^5 coordination of cyclopentadienyl ligand to magnesium atom.

1.8 Group 14 Metallocenes

Metallocenes of group 14 elements may also be referred to as tetrelocenes. This notion is based on the words tetrel, the name for the elements of group 14, and metallocene. This term seems appropriate for group 14 metallocenes since only lead and tin are metals and the lighter congeners silicon and germanium are metalloids, so consequently their metallocenes should be called “metalloidocenes”. The term tetrelocene for group 14 metallocenes will be used in this thesis.

Since tetrelocenes possess the general formula R_2E (E = Si-Pb), the question arises of whether these compounds can also be considered as tetrylenes. In general, tetrylenes can react as σ donors,[93,94] which can be seen especially in the rich chemistry of *N*-heterocyclic carbenes,[95,96] under oxidative addition or insertion reactions[94,97] and they can act as Lewis acids[94,98,99] due to their vacant p orbital. In the case of “classical” tetrylenes, the lone pair usually corresponds to the HOMO of the molecule and the LUMO often corresponds to a vacant p-type orbital, at least partially located, at the tetrel atom. Similar to "classical" tetrylenes, tetrelocenes possess a vacant p-type orbital, located at the central atom, giving them acceptor abilities. The lone pair, on the other hand, is of higher s character and therefore exhibits only weak, if any, σ donor abilites (Figure 34).

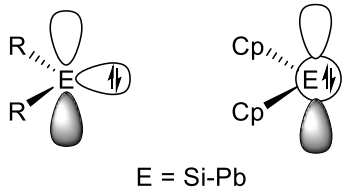

Figure 34: Depiction of the frontier orbitals for a singlet tetrylene (left) and a tetrelocene (right).

As can be seen in the MO diagram for tetrelocenes (Figure 36), the HOMO and HOMO−1 correspond to the π framework of the cyclopentadienyl ligands and the lone pair is lower in energy elucidating its inertness which represents an important difference between “classical” tetrylenes and tetrelocenes. Very recently, this was confirmed by a DFT study on the electronic structure of tetrylenes reported by Nechaev.[100] The difference in the electronic properties and coordintion modes of the tetrel atom in tetrelocenes and "classical" tetrylenes is also depicted by their corresponding heteronuclear NMR chemical shifts (Figure 35).

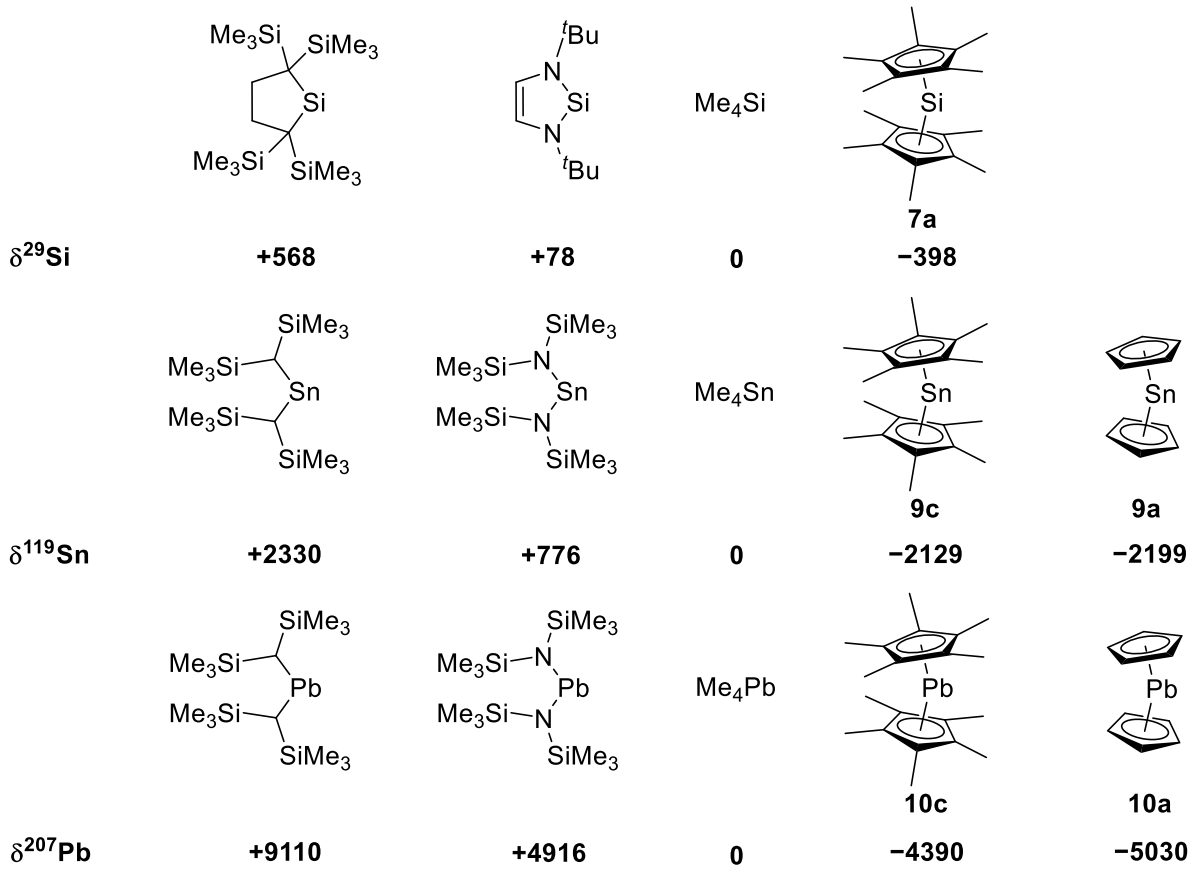

Figure 35: NMR chemical shifts of selected silylenes, stannylenes, plumbylenes and group 14 cyclopentadienyl compounds.[101–109]

Typically, tetrylenes with dicoordinated tetrel atoms exhibit more or less downfield shifted signals in corresponding heteronuclear NMR spectra. This is quite the opposite for tetrelocenes, which typically exhibit very upfield shifted resonances. This is due to the fact that in tetrelocenes, the energy difference between the lone pair and the vacant p orbital is significantly higher than it is for most other tetrylenes, which results in a small paramagnetic term (σ^p) resulting in unusually upfield shifted ^{29}Si, ^{119}Sn and ^{207}Pb NMR signals.[110] Furthermore, the upfield shift of the signals is in line with the hypercoordination of the tetrel atom in tetrelocenes, which exhibits a coordination number of 10.[107,111]

Although of comparably high s character, the lone pair in tetrelocenes exhibits steric demand which is one possible reasoning for the bent structure of these compounds in accordance with the VSEPR model. Another explanation for the bent structure of the tetrelocenes is derived from MO theory (Figure 36).

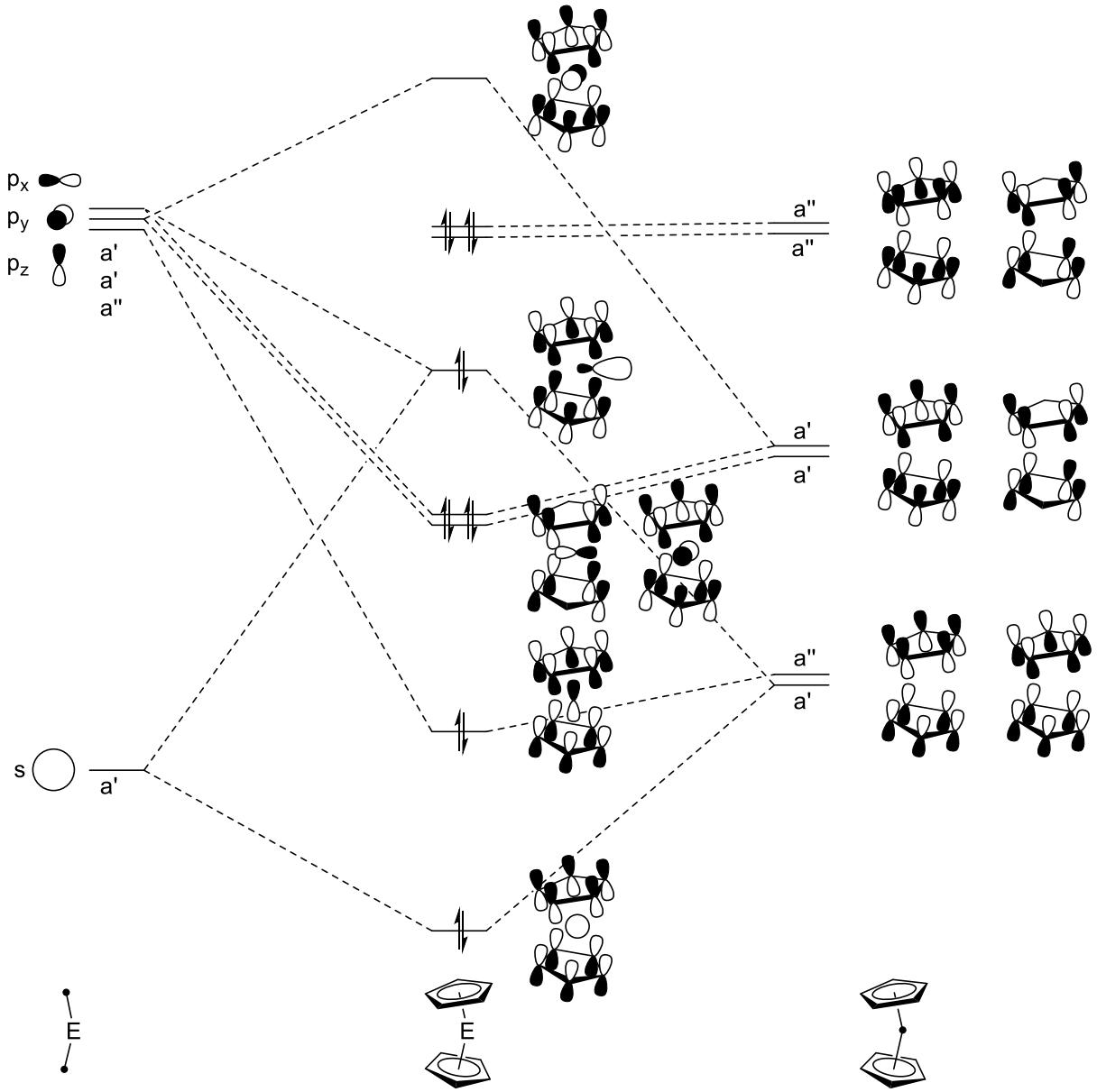

Figure 36: Qualitative molecular orbital diagram for tetrelocenes.

The LUMO is an antibonding combination of the p_y orbital with the π system of the cyclopentadienyl ligand. The s orbital forms a bonding and an antibonding linear combination with the π systems of the cyclopentadienyl ligand. By mixing of the p_x orbital with the s orbital in the formally antibonding linear combination, a “dumbbell-shaped” sp hybrid orbital is obtained which represents the lone pair and give this linear combination bonding character. This mixing results in the bending of tetrelocenes. If tetrelocenes would possess a coplanar structure, this MO would be exclusively antibonding and the lone pair would exhibit 100% s character (Figure 37).[20,112]

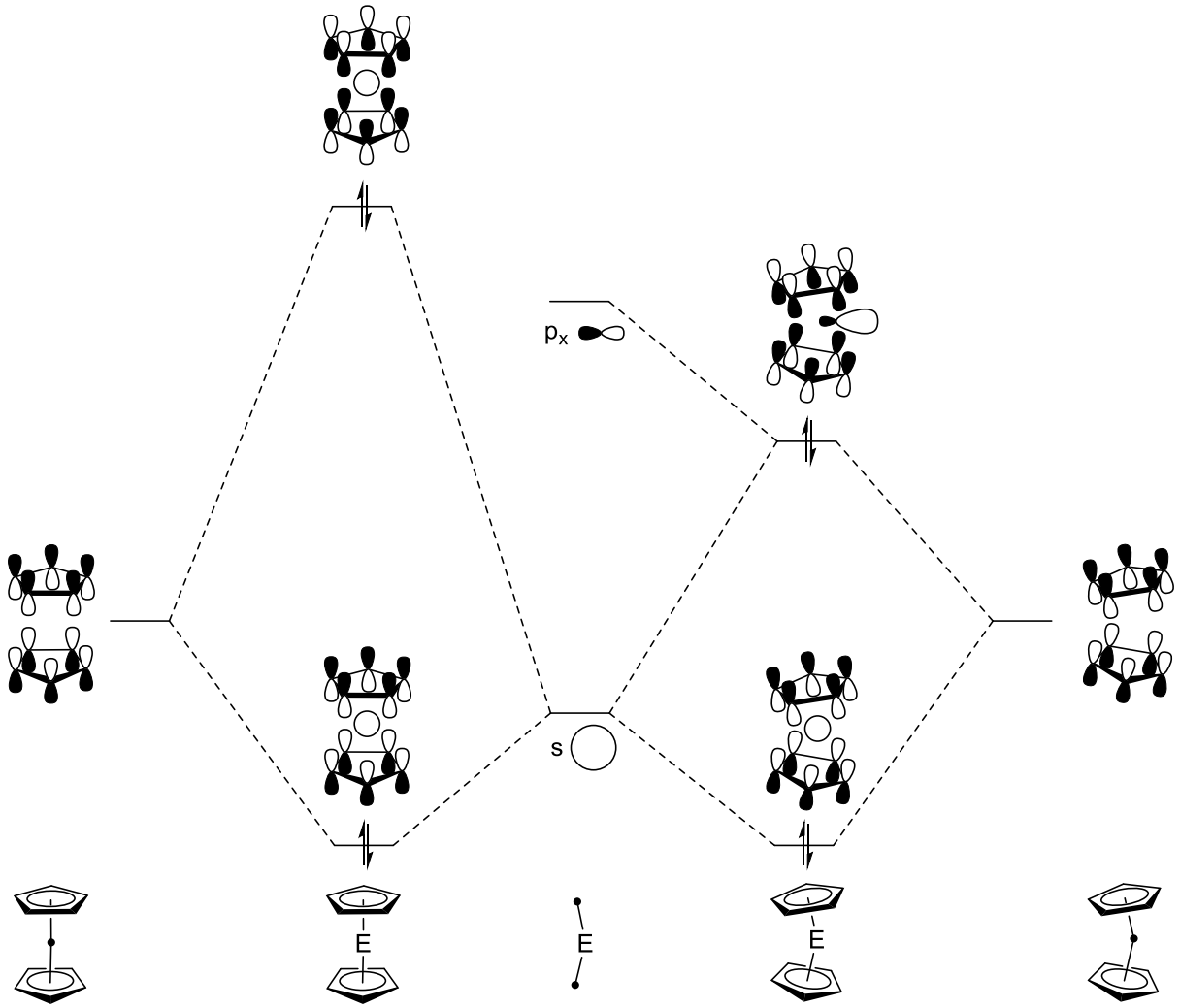

Figure 37: Section of the qualitative molecular orbital diagram of tetrelocenes comparing the interactions of the s and p_x orbital with total symmetric orbitals of the cyclopentadienyl ligand for coplanar and bent structures.

This antibonding interaction of the s orbital with the cyclopentadienyl ligand would be higher in energy for which reason the coplanar structure of tetrelocenes is disfavored and thus, the bent structure of these compounds is favored. However, it should be noted that the decamethylsilicocene exhibits a coplanar and a bent structure in the solid state in the same unit cell demonstrating the low energy difference between these two conformers.[113]

Even though historically the first tetrelocenes that were discovered, were stannocene and plumbocene, followed by germanocene and last silicocene, the discussion of the group 14 metallocenes in this chapter will start with the silicocenes and end at the plumbocenes, following their atomic numbers in the periodic table.

Decamethylsilicocene, Cp^*_2Si (**7a**), was obtained by reduction of bis(pentamethylcyclopentadienyl)dichlorosilane with alkali naphthalene salts. By protonation of **7a** and subsequent reaction with lithium cyclopentadienides, the corresponding heteroleptic silicocenes were obtained (Scheme 68).

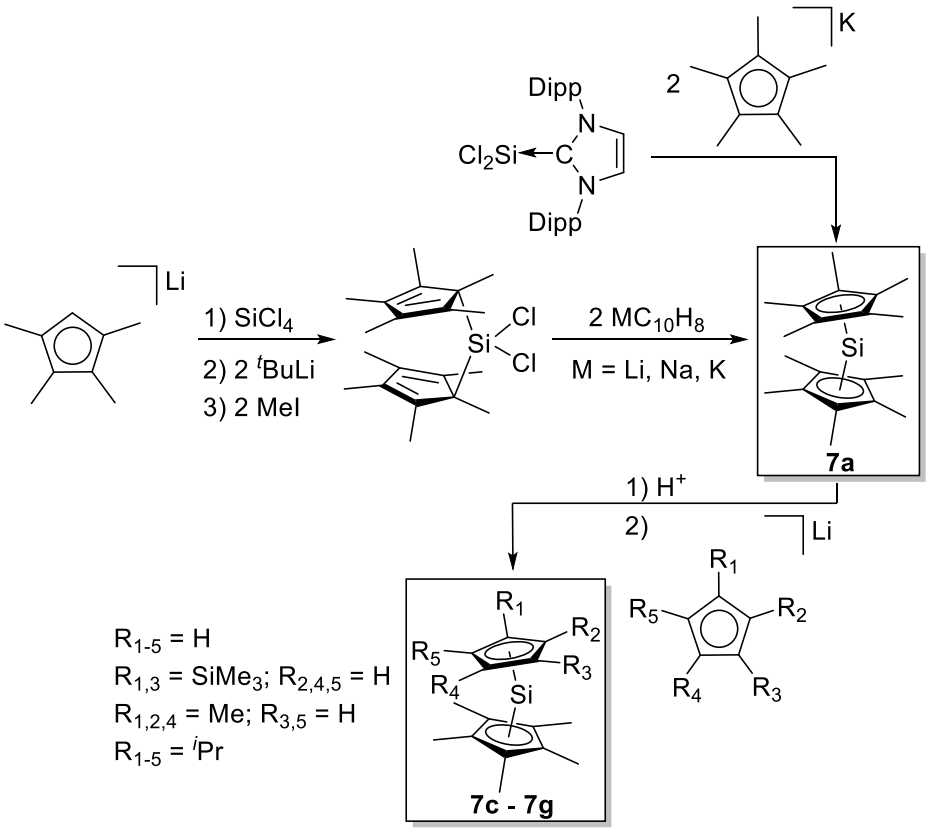

Scheme 68: Overview of synthetic pathways to silicocenes.

The first silicocene to be discovered, Cp^*_2Si (**7a**), was also the first diorgano silicon(II) compound which was stable and isolable at room temperature. Jutzi and coworkers reported of this compound in 1986, eight years before Denk *et al*. reported the synthesis and characterization of the first stable *N*-heterocyclic silylene.[103,114] The synthesis for decamethylsilicocene is challenging since it includes a multistep protocol and reduction of the bis(pentamethylcyclopentadienyl)dichlorosilane with alkali naphthalene salts.[114] Considering that there was no suitable precursor of Si(II) available, Jutzi *et al*. started the synthesis of Cp^*_2Si (**7a**) from silicontetrachloride (see Scheme 68).[113,114]

In the structure in the solid state, two different conformers of decamethylsilicocene are observed: one conformer exhibits a coplanar arrangement of the cyclopentadienyl ligands (δ =

179.9°), the other conformer exhibits a bent geometry (δ = 167.4°) (Figure 38).[114] The reason for the existence of both conformers in the crystal are most likely an only marginal difference in energy of both of the conformers so that packing effects become important.

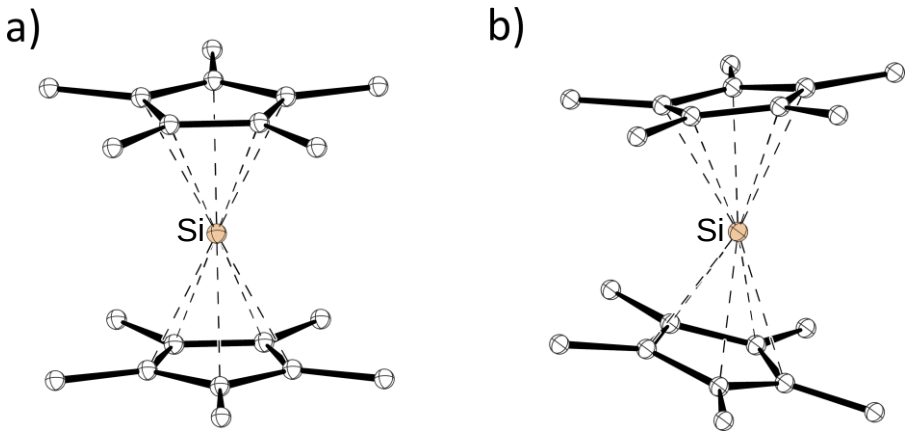

Figure 38: Molecular structures of the a) coplanar and b) bent conformers of decamethylsilicocene (**7a**)[114] in the crystal (hydrogen atoms omitted for clarity, ball-and-stick representation).

Jutzi and coworkers described Cp^*_2Si, **7a**, as thermally stable, since it could be sublimed in oil pump vacuum, and was even air stable for a short period of time.[113,114] In 2018, Ghana *et al*. described another synthesis route to decamethylsilicocene starting from a NHC-stabilized Si(II) precursor which could be transmetalated with pentamethylcyclopentadienylpotassium to obtain Cp^*_2Si (Scheme 69).[115]

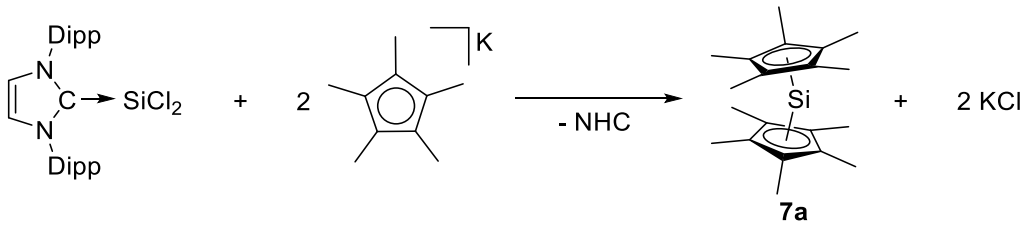

Scheme 69: Synthesis of decamethylsilicocene as conducted by Ghana *et al*.[115]

The authors were able to obtain pure Cp^*_2Si, **7a**, by workup with hexane at 213 K since the NHC almost insoluble in cold hexane.[115] This synthetic route seems to exhibit the advantage of only one step, but it should be noted that the synthesis of the NHC-stabilized

dichlorosilylene also requires significant synthetic effort.[116] In 2006, Jutzi *et al*. synthesized several homoleptic and heteroleptic silicocenes starting from the pentamethylcyclopentadienylsilicon cation (**7b**$B(C_6F_5)_4^-$). By reaction of Cp^*Si^+ with cyclopentadienyllithium, the heteroleptic silicocene Cp*SiCp, **7c**, was achieved (Scheme 70).[117]

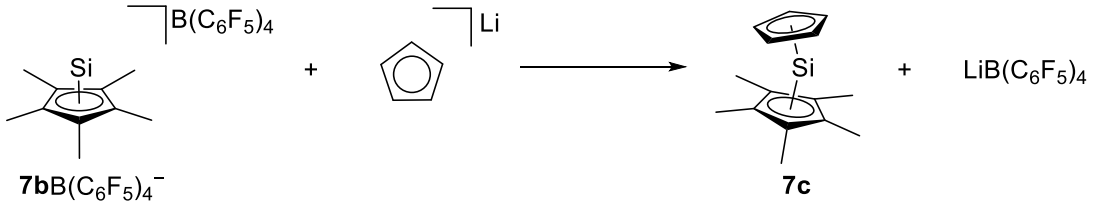

Scheme 70: Synthesis of Cp*SiCp (**7c**) as carried out by Jutzi and coworkers.[117]

This heteroleptic metallocene was described as thermally unstable since it decomposed at temperatures above 243 K and could be characterized only by NMR spectroscopy, where a signal at −336 ppm in the ^{29}Si NMR spectrum indicated the formation of Cp*SiCp (**7c**).[117] This is an important difference to the other tetrelocenes for all of which the unsubstituted metallocenes are known (see Table 8). Also, a heteroleptic silicocene with the bis(trimethylsilyl)cyclopentadienyl ligand was reported which was obtained in a similar process (Scheme 71).[117]

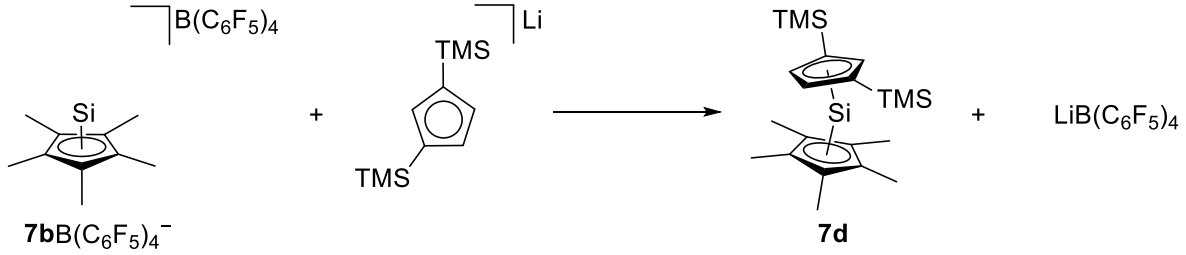

Scheme 71: Synthesis of $Cp^*Si^{TMS2}Cp$ (**7d**) as conducted by Jutzi and coworkers.[117]

The central silicon atom in $Cp^*Si^{TMS2}Cp$, **7d**, exhibited a signal in the ^{29}Si NMR spectrum at −337 ppm, fitting in the row of ^{29}Si NMR shifts of silicocenes (see Table 7). The authors stated that this metallocene was thermally stable, but not as stable as Cp^*_2Si (**7a**) presumably due to less effective encapsulation reached by the two trimethylsilyl groups attached to

the cyclopentadienyl ring in comparison to the pentamethylcyclopentadienyl ligand.[117] By reaction of Cp*Si$^+$ with 1,2,4-trimethylcyclopentadienyllithium, a mixture of the homoleptic complexes Cp*$_2$Si, ^{Me3}Cp$_2$Si and the heteroleptic compound Cp*Si^{Me3}Cp was obtained, from which the products could not be seperated (Scheme 72).[117]

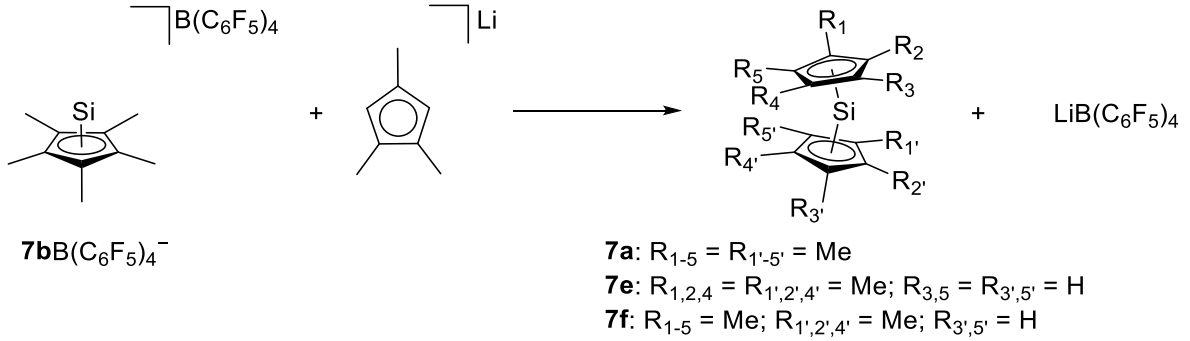

Scheme 72: Reaction of Cp*Si$^+$ with 1,2,4-trimethylcyclopentadienyllithium as conducted by Jutzi *et al*.[117]

In 1992, Jutzi and Bunte reported of the reaction of decamethylsilicocene, **7a**, with catechol which afforded, as the authors concluded, the protonated decamethylsilicocene (Cp*$_2$SiH$^+$) (Scheme 73).[118]

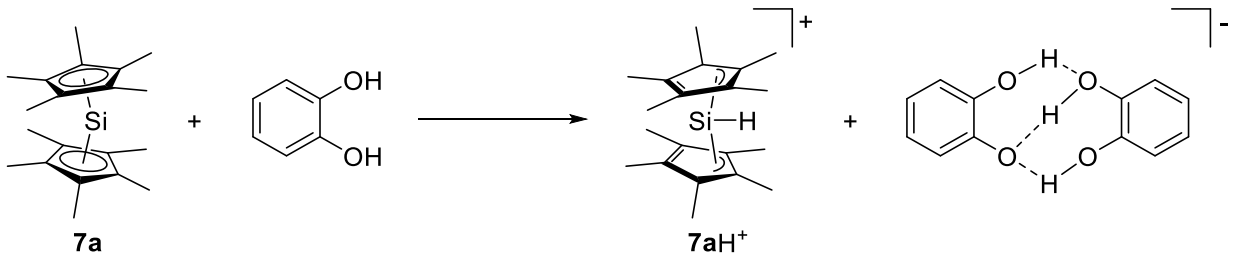

Scheme 73: Synthesis of Cp*$_2$SiH$^+$ (**7a**H$^+$) as reported by Jutzi and Bunte.[118]

The product of this reaction is not easy to expect since protonation of tetrelocenes usually leads to the corresponding half-sandwich cationic complexes (CpE$^+$) under elimination of a cyclopentadienyl ligand (see Chapter 1.3). The authors reported a doublet at −12.1 ppm ($J_{H\text{-}Si}$ = 302 Hz) in the ^{29}Si NMR spectrum, which is a clear hint against a cyclopentadienyl substituted silyliumylidene (see Table 9). In the ^{1}H and ^{13}C NMR spectra of Cp*$_2$SiH$^+$, **7a**H$^+$, only one set of signals for the methyl groups was observed providing evidence for η^5 π

complexed cyclopentadienyl rings and fast haptotropic rearrangement in solution which was corroborated by quantum chemical calculations.[118,119] Since no structural characterization of this cationic complex could be conducted, the postulated structure by Jutzi and Bunte must be doubted also considering that the expected reaction between a silylene with an alcohol would be an oxidative addition.[118] For decamethylsilicocene, **7a**, reaction studies were undertaken by Theil *et al*. in 2002, who reacted Cp^*_2Si with transition metal complexes, namely and (triphenylphosphine)gold chloride (Scheme 74) and cyclopentadienyl(triphenylphosphine)nickel chloride (Scheme 75).[120]

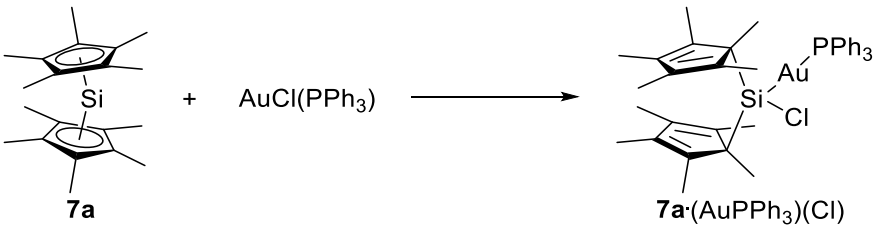

Scheme 74: Reaction of Cp^*_2Si (**7a**) with $AuCl(PPh_3)$.[120]

Theil and coworkers were able to crystallize the gold complex (**7a**·$(AuPPh_3)(Cl)$) revealing an oxidative addition reaction product. The gold atom exhibits a quasilinear arrangement of Si-Au-PPh_3 (171.3°), which can be attributed to repulsive interactions between the gold atom and the Cp* ligand. In the crystal structure, the silicon atom is σ bonded to the pentamethylcyclopentadienyl ligands which is expected for a tetravalent silicon atom. Also, the signal in ^{29}Si NMR spectrum was in line with the observed structure since a signal was detected at 77.6 ppm which is common for transition metal silyl complexes.[120] This product of an oxidative addition to the silicon centre demonstrates the unsuitability of decamethylsilicocene as a σ donor and the inertness of the lone pair at the silicon atom. This reactivity can be justified by the fact that the lone pair of Cp^*_2Si is not the HOMO (Figure 36). Interestingly, a gold(I)chloride complex of a *N*-heterocyclic silylene exists where this silylene acts as a σ donor.[121] The reaction of decamethylsilicocene with cyclopentadienyl(triphenylphospine)nickel chloride also lead to an oxidative addition reaction product under loss of triphenylphosphine and formation of a nickel complex (Scheme 75).[120]

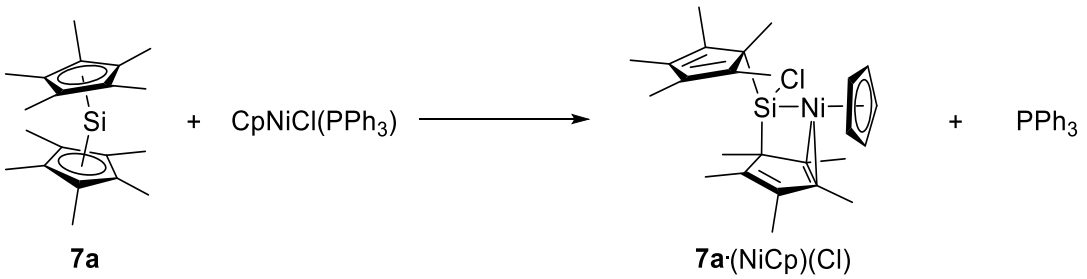

Scheme 75: Reaction of Cp^*_2Si (**7a**) with $CpNiCl(PPh_3)$.[120]

In the molecular structure of the nickel complex, **7a**·(NiCp)(Cl), the nickel atom is η^5 coordinated to the unsubstituted cyclopentadienyl ligand and η^2 coordinated to the Cp* ligand which can also be observed by NMR spectroscopy. The signal in the ^{29}Si NMR spectrum was observed at 8.6 ppm which is the typical region for such a complex.[120]

Other examples of oxidative addition reactions were reported by Theil *et al*. when they reacted Hg_2Cl_2 with decamethylsilicocene in 2000 (Scheme 76).[122]

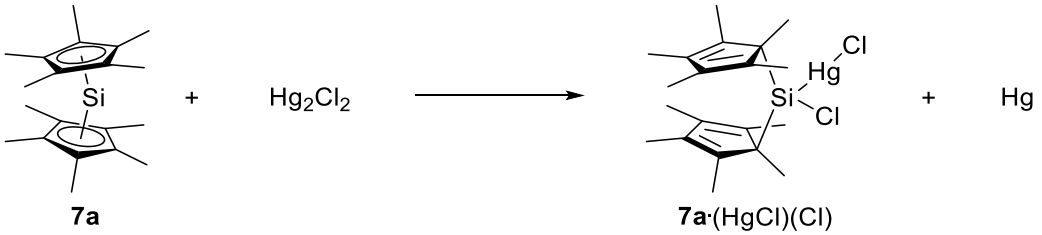

Scheme 76: Reaction of Cp^*_2Si (**7a**) with Hg_2Cl_2.**[122]**

The silicon atom of decamethylsilicocene inserted in the Hg-Cl bond to yield the oxidative addition reaction product. The ^{29}Si NMR spectrum exhibited a signal at 53.4 ppm, which is comparable to the signal observed for the gold complex which was already discussed (*vide supra*). Both the pentamethylcyclopentadienyl ligands in this mercury compound are σ bonded to the silicon atom.[122] Other oxidative addition reactions of Cp^*_2Si (**7a**) with aldehydes, ketones, nitriles, methyl thiocyanate, dimethyl cyanamide and 2,4-dimethylphenyl cyanate were reported by Jutzi *et al*. in 1996 (Figure 39).[123,124]

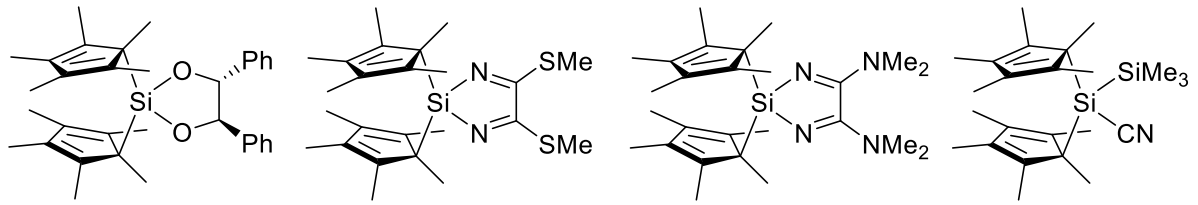

7a·[OCHPh]$_2$ **7a**·[NCSMe]$_2$ **7a**·[NCNMe$_2$]$_2$ **7a**·(SiMe$_3$)(CN)

Figure 39: Structurally characterized products of oxidative addition reactions between Cp*$_2$Si and (from left to right): benzaldehyde, methyl thiocyanate, dimethyl cyanamide and trimethylsilyl cyanide.[123,124]

In all of the structurally characterized products, the tetravalent silicon atom is σ bonded to the cyclopentadienyl ligands in the solid state. The signals in the ^{29}Si NMR spectra of these compounds range from 22.6 to −26.9 ppm, which is significantly downfield shifted compared to the signal for Cp*$_2$Si (see Table 7), but typical for such tetravalent silicon species.[123,124]

A milestone was achieved by synthesizing the Cp*Si$^+$ cation (**7b**) which was obtained by Jutzi *et al*. in 2004.[102] With this important synthetic building block in hand, silicocenes with varying substitution patterns at the cyclopentadienyl ligands were reported by Jutzi *et al*. in 2006.[117] Their study revealed the enormous influence of the steric demand of the cyclopentadienyl ligand on the stability of the obtained silicocene since Cp*Si^{5}Cp (**7g**) is even air stable for a short period of time while Cp*SiCp (**7c**) is only stable at temperatures below 243 K.[117] Reactivity studies of decamethylsilicocene, in which oxidative addition reactions were observed, revealed the character of the tetrylene-type compound decamethylsilicocene to be different from *N*-heterocyclic silylenes since no complexes with decamethylsilicocene as a donor were reported to date.[97,120,122–124] By starting from NHC-stabilized SiCl$_2$, Ghana *et al*. were able to, at first sight, simplify the synthetic procedure to decamethylsilicocene, but it should be noted that the synthesis of NHC-stabilized SiCl$_2$ is not simple.[115]

Table 7: ^{29}Si NMR shifts, selected structural parameters and references for silicocenes.

Compound	δ ^{29}Si [ppm]	Cp^{cent}-E-Cp^{cent} δ[°][a]	Cp^{cent}-E [pm][a]	Reference
Cp^*_2Si (**7a**)	−398	179.9, 167.4	211.38(2); 211.96(23); 212.05(23)	[113–115,125,126]
Cp*SiCp (**7c**)	−336	-	-	[117]
$Cp^*Si^{(1,3\text{-}TMS)2}Cp$ (**7d**)	−337	-	-	[117]
$^{Me3}Cp_2Si$ (**7e**)	−311	-	-	[117]
$Cp^*Si^{Me3}Cp$ (**7f**)	−333	-	-	[117]
^{5}CpSiCp* (**7g**)	−420	179.6	217.15(10); 218.38(10)	[117]

[a]: Only given in the case of η^5 coordination of cyclopentadienyl ligand to silicon.

The predominant part of the heavier tetrelocenes (Ge-Pb) was obtained *via* transmetalation of group 1 cyclopentadienides with corresponding group 14 element halides (Scheme 77). Most of the metallocenes of group 14 known to date exhibit alkyl or silyl substituted cyclopentadienyl ligands. According to the similarity of the synthetic procedures conducted to obtain the metallocenes of the heavier tetrels (Ge-Pb) and their similarities in reactivity, these heavier tetrelocenes are discussed together.

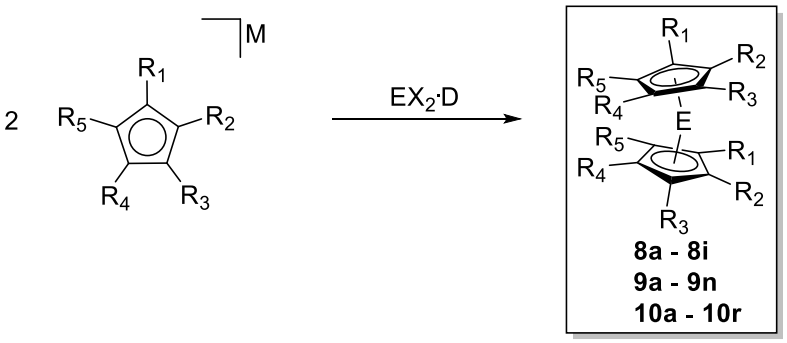

E = Ge; X = Br; D = Et_2O; M = Na; $R_{1\text{-}5}$ = H. E = Sn; X = Cl; D = dmf; M = Li; $R_{1\text{-}5}$ = H. E = Pb; X = NO_3; D = dmf; M = Na; $R_{1\text{-}5}$ = H. E = Ge; X = I; D = C_6H_6; M = K; R_1 = Me; $R_{2\text{-}5}$ = H. E = Sn; X = Cl; D = thf; M = K; R_1 = Me; $R_{2\text{-}5}$ = H. E = Pb; X = OAc; D = dme; M = K; R_1 = Me; $R_{2\text{-}5}$ = H. E = Pb; X = Cl; D = thf; M = Li; $R_{1\text{-}4}$ = Me; R_5 = H. E = Ge; X = Cl; D = dioxane; M = Li; $R_{1\text{-}5}$ = Me. E = Sn; X = Cl; D = thf; M = Li; $R_{1\text{-}5}$ = Me. E = Pb; X = Cl; D = thf; M = Li; $R_{1\text{-}5}$ = Me. E = Pb; X = Cl; D = thf; M = Li; R_1 = Et; $R_{2\text{-}5}$ = Me. E = Pb; X = Cl; D = thf; M = Li; R_1 = ^{i}Pr; $R_{2\text{-}5}$ = Me. E = Pb; X = Cl; D = thf; M = Li; R_1 = *n*Bu; $R_{2\text{-}5}$ = Me. E = Ge; X = Cl; D = dioxane; M = Li; R_1 = TMS; $R_{2\text{-}5}$ = H. E = Pb; X = Cl; D = thf; M = Li; R_1 = TMS; $R_{2\text{-}5}$ = H. E = Ge; X = Cl; D = dioxane; M = Li; $R_{1,3}$ = TMS; $R_{2,4,5}$ = H. E = Pb; X = Cl; D = thf; M = Li; $R_{1,3}$ = TMS; $R_{2,4,5}$ = H. E = Ge; X = Cl; D = dioxane; M = Li; $R_{1,2,4}$ = TMS; $R_{3,5}$ = H. E = Pb; X = Cl; D = thf; M = Li; $R_{1,2,4}$ = TMS; $R_{3,5}$ = H. E = Sn; X = Cl; D = thf; M = K; $R_{1,2,4}$ = ^{i}Pr; $R_{3,5}$ = H. E = Pb; X = I; D = thf; M = K; $R_{1,2,4}$ = ^{i}Pr; $R_{3,5}$ = H. E = Sn; X = Cl; D = thf; M = K; $R_{1\text{-}4}$ = ^{i}Pr; R_5 = H. E = Pb; X = Cl; D = thf; M = Na; $R_{1\text{-}4}$ = ^{i}Pr; R_5 = H. E = Sn; X = Cl; D = thf; M = Li; $R_{1\text{-}5}$ = ^{i}Pr. E = Pb; X = Cl; D = thf; M = Na; $R_{1\text{-}5}$ = ^{i}Pr. E = Sn; X = Cl; D = thf; M = Li; R_1 = ^{t}Bu; $R_{2\text{-}5}$ = H. E = Ge; X = Cl; D = dioxane; M = Li; $R_{1,3}$ = ^{t}Bu; $R_{2,4,5}$ = H. E = Sn; X = Cl; D = thf; M = Li; $R_{1,3}$ = ^{t}Bu; $R_{2,4,5}$ = H. E = Pb; X = Cl; D = thf; M = Li; $R_{1,3}$ = ^{t}Bu; $R_{2,4,5}$ = H. E = Pb; X = Cl; D = thf; M = Li; $R_{1,2,4}$ = ^{t}Bu; $R_{3,5}$ = H. E = Ge; X = Cl; D = dioxane; M = Li; R_1 = Me_2Si^tBu; $R_{2\text{-}5}$ = Me. E = Sn; X = Cl; D = thf; M = Li; R_1 = Me_2Si^tBu; $R_{2\text{-}5}$ = Me. E = Pb; X = Cl; D = Et_2O; M = Li; R_1 = Me_2Si^tBu; $R_{2\text{-}5}$ = Me.

Scheme 77: Transmetalation reactions for syntheses of homoleptic, alkyl and silyl substituted tetrelocenes.

The first room temperature stable, diorgano stannylene- and plumbylene-type compounds, were the metallocenes of these elements. Interestingly, stannocene (**9a**) and plumbocene (**10a**) were discovered long before other stable diorgano tetrylenes were reported.[11,12,127] The metallocene of the lighter, germanocene (**8a**), was first reported by Scibelli *et al*. in 1973[13] and structurally characterized in 1984.[128] The synthesis published by Scibelli and

coworkers started from sodiumcyclopentadienide and germanium(II)bromide (Scheme 78).[13]

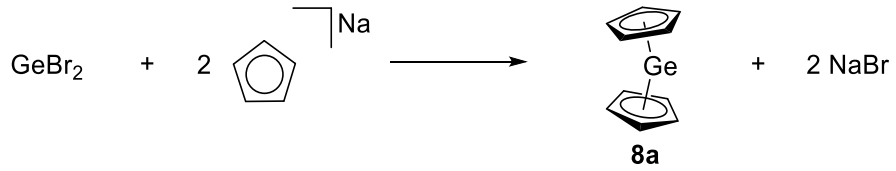

Scheme 78: Synthesis of germanocene (**8a**) as conducted by Scibelli *et al*.[13]

In the original report by Scibelli *et al*., the authors stated that the synthesis, carried out in tetrahydrofuran as solvent and sodiumcyclopentadienide as Cp transfer reagent, did not afford “monomeric” material. Contrary to that observation, Grenz *et al*. reported the synthesis of germanocene, **8a**, with sodiumcyclopentadienide and germanium(II)chloride dioxane complex in tetrahydrofuran to work properly (Scheme 79).[128]

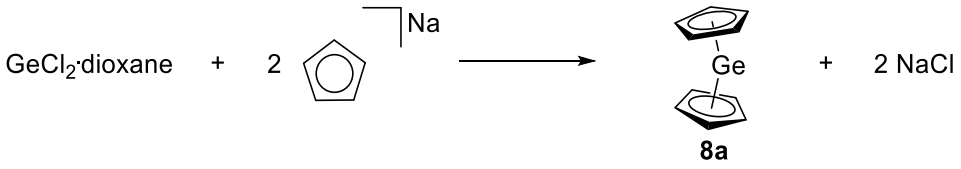

Scheme 79: Synthesis of germanocene (**8a**) as carried out by Grenz *et al*.[128]

The authors stated that **8a** could be sublimed at mild temperatures (333-353 K; 10^{-2} mbar) and by storage at low temperatures, no polymerization could be observed over weeks although it remains unclear what the authors meant by polymerization. In the crystal structure, a bent metallocene is observed (δ = 152.4°) with a Ge-Cp^{cent} distance of 223.37(43) pm.[128]

Stannocene, **9a**, was first reported by Fischer and Grubert in 1956 who synthesized this metallocene by transmetalation of lithiumcyclopentadienide with tin(II)chloride (Scheme 80).[11]

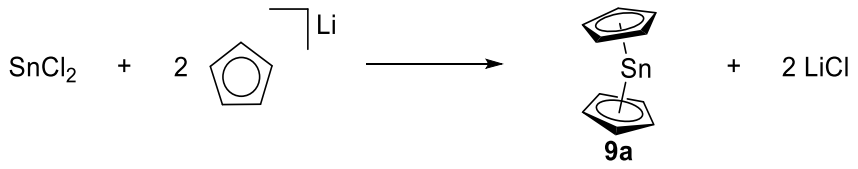

Scheme 80: Synthesis of stannocene (**9a**) as conducted by Fischer and Grubert.[11]

The authors conducted dipole measurements on stannocene (**9a**) and concluded on the basis of these experiments that the structures of ferrocene (**1**) and stannocene (**9a**) in solution were not identical since stannocene exhibited a dipole moment which **1** did not exhibit. In 1981, the structure of stannocene (**9a**) in the solid state could be revealed by Atwood and coworkers.[16] The tin atom in **9a** is complexed in an η^5 fashion to both cyclopentadienyl rings and possesses a monomeric structure in the solid state. In analogy to the geometry of germanocene, **8a**, **9a** exhibits a bent structure in the solid state (δ = 143.8° and 147.1°) but it is more bent than **8a**. In the 1980s and 1990s, ^{119}Sn NMR spectroscopy was conducted with **9a**, revealing a signal at −2199 ppm[107,108] which is shifted significantly upfield compared to other acyclic diorgano substituted stannylenes (δ ^{119}Sn of Sn(CH[TMS]$_2$)$_2$ = +2330 ppm[101]) but in line with the signal for decamethylsilicocene, **7a**, in the ^{29}Si NMR spectrum, which is also significantly upfield shifted compared to other silylenes.[103,113] In lanthanoid chemistry, mild Cp transfer reagents are necessary for the synthesis of cyclopentadienyl compounds of the lanthanoids for which reason Janiak *et al*. demonstrated the applicability of stannocene, **9a**, as Cp transfer reagent in lanthanoid chemistry.[129] Another report of **9a** acting as Cp transfer reagent stems from 2017, when Lohrey *et al*. made usage of this tetrelocene to transfer the cyclopentadienyl ligand to a rhenium complex.[130] Since **9a** exhibits a lone pair, attempts to coordinate Lewis acids were conducted in the years after the discovery of stannocene. In 1970, Harrison and Zuckerman reported of the adduct of **9a** with trifluoroborane ($Cp_2Sn{\cdot}BF_3$), which was characterized by elemental analysis, mass spectroscopy and ^{119}Sn Mössbauer spectroscopy.[131] The authors concluded on basis of their analytical data that the adduct was formed (Scheme 81).

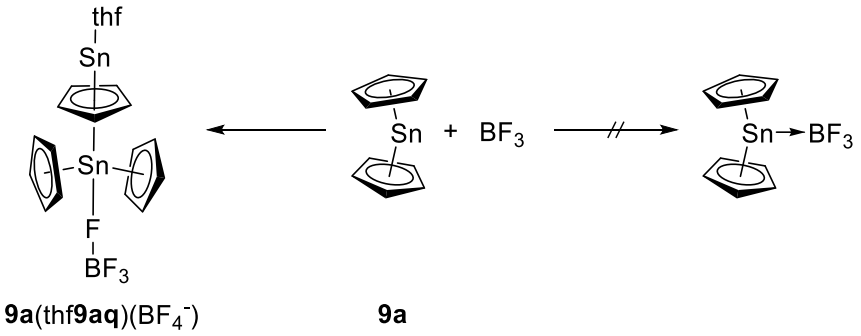

Scheme 81: Reaction of stannocene (**9a**) with trifluoroborane as carried out by Harrison and Zuckerman.[131]

Indeed, Dory *et al*. revised that work in 1985 and were able to demonstrate by X-ray crystallography, that the product formed was not the intended adduct, but **9a**(thf**9aq**)(BF_4^-) (Scheme 81).[132] In 1975, Harrison *et al*. presented the bimetallic complex [$Cp_2Sn(\mu$-$Fe(CO)_4)]_2$, [**9a**(μ-$Fe(CO)_4)]_2$, which was obtained by reaction of **9a** with diironnonacarbonyl (Scheme 82).[133,134]

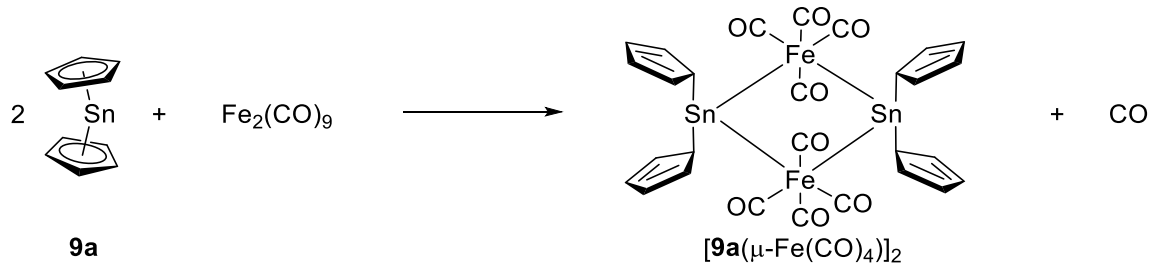

Scheme 82: Synthesis of [$Cp_2Sn(\mu$-$Fe(CO)_4)]_2$ as conducted by Harrison *et al*.[133,134]

The structure of this compound in the solid state revealed a Fe_2Sn_2 ring and σ bonded cyclopentadienyl ligands with Sn-Cp^C distances of 222.06(4) pm and 225.63(2) pm, which is elongated to σ bond lengths observed in **9a**·[$FeCp(CO)_2]_2$ (217 pm and 218 pm[135]). This finding of a σ bonded tin atom is also corroborated by the C-C bond lengths which display two double bonds (133.71(2) pm to 136.89(2) pm). The Sn-Fe distances of 265.07(2) pm and 266.95(3) pm are also elongated compared with those obtained in **9a**·[$FeCp(CO)_2]_2$ (256.8 pm and 257.3 pm[135]).[133,134] An oxidative addition of iodine to **9a** to form Cp_2SnI_2, **9a**I_2 was reported by Bos *et al*. in 1974.[136] In 1976, Cornwell *et al*. published, in addition to [**9a**(μ-$Fe(CO)_4)]_2$, a series of bimetallic complexes which were synthesized by reaction of **9a**

and dimethylstannocene, **9b**, with group 6 metal pentacarbonyl thf complexes or diironnonacarbonyl (Scheme 83).[134] Most of these complexes were only characterized by IR and Mössbauer spectroscopy indicating, according to the authors, a coordination of the group 6 metal pentacarbonyl fragment to the tin atom of stannocenes. Since no structural characterization of these complexes could be conducted, the existence of these complexes must be doubted. Stannocenes cannot exhibit strong σ donor ability (see Figure 36) which is another argument against the existence of these stannocene group 6 pentacarbonyl complexes. On the other hand, for *N*-heterocyclic stannylenes, tungsten pentacarbonyl and iron tetracarbonyl complexes were described.[137,138] By reaction of stannocene, **9a**, with diironnonacarbonyl, [**9a**(μ-Fe(CO)$_4$)]$_2$ was obtained. The structure in the solid state of [**9a**(μ-Fe(CO)$_4$)]$_2$ was not reflected in solution, since a fluxional behavior appeared determined by ^{1}H NMR spectroscopy, where only one signal was observed for the protons of the cyclopentadienyl ligand due to fast sigmatropic rearrangements.[134]

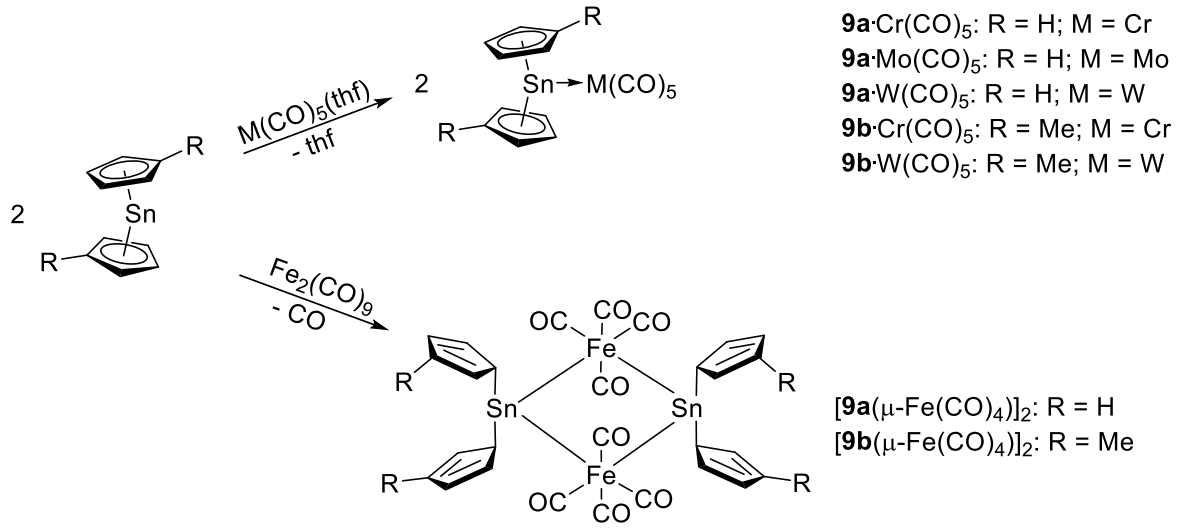

Scheme 83: Syntheses of bimetallic complexes as conducted by Cornwell *et al*.[134]

A related complex, [Cp*$_2$Sn(μ-Fe(CO)$_4$)]$_2$ ([**9c**(μ-Fe(CO)$_4$)]$_2$), was reported by Sriyunyongwat *et al*. in 1986. This compound was characterized by IR, NMR and Mössbauer spectroscopy on which results the authors suggested a similar structure for [**9c**(μ-Fe(CO)$_4$)]$_2$ as it was observed for [**9a**(μ-Fe(CO)$_4$)]$_2$. In 1998, Beswick *et al*. synthesized the Cp$_2$Sn·tmeda, **9a**·tmeda, complex where stannocene acts as a Lewis acid (Scheme 84).[98]

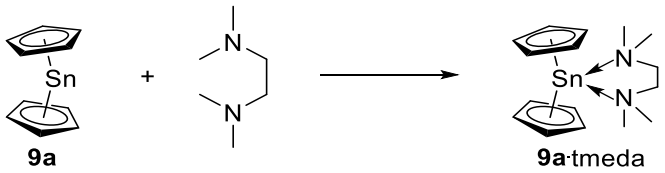

Scheme 84: Synthesis of Cp_2Sn·tmeda (**9a**·tmeda) as carried out by Beswick *et al*.[98]

In this adduct of stannocene, both cyclopentadienyl ligands are η^5 complexed to the tin atom (Figure 40).

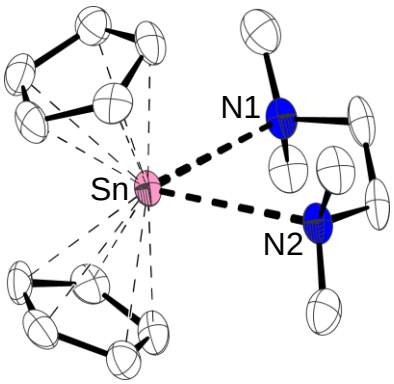

Figure 40: Molecular structure of Cp_2Sn·tmeda (**9a**·tmeda)[98] in the crystal (hydrogen atoms omitted for clarity, thermal ellipsoids at 50% probability level).

By conducting quantum chemical calculations, the authors could corroborate their finding that these adducts were labile.[98] In the solid state structure of **9a**·tmeda, the Sn-Cp^{cent} distance is with 251.63(6) pm elongated in comparison to the ones in free **9a** (237.02(8) - 243.69(8) pm) and the bending angle exhibits a smaller value (δ = 131.4°).[112] In 2001, de Lima *et al*. reacted stannocene, **9a**, with pentamethylcyclopentadienyl lithium and obtained the mixed stannocene CpSnCp* (Scheme 85).[139]

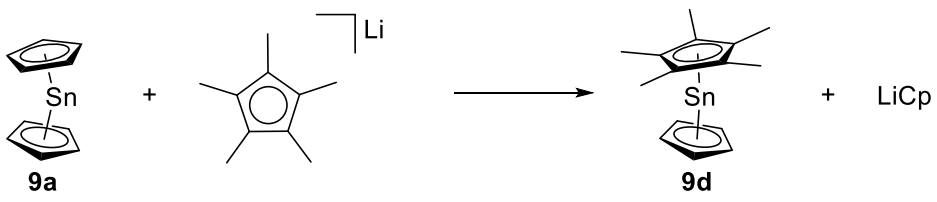

Scheme 85: Synthesis of the mixed stannocene CpSnCp* (**9d**) as conducted by de Lima *et al*.[139]

The authors stated that after extraction of the reaction mixture with diethylether, **9d** could be obtained and the residue could be identified as lithium cylopentadienide. In the ^{119}Sn NMR spectrum of the product, which could be recrystallized from diethylether, a signal appeared at −2129 ppm, which is in the typical region for stannocenes, but very close to the signal for decamethylstannocene (**9c**) (see Table 8). In the ^{1}H NMR spectrum of this complex, signals for methyl groups (δ ^{1}H = 1.8 ppm) and for protons of the cyclopentadienyl ligand (δ ^{1}H = 6.0 ppm) were detected, which is a further hint toward formation of **9d**, but no structural details are available for this compound.[139]

The tetrelocene with the heaviest element, plumbocene (**10a**), was discovered at the same time as stannocene by Fischer and Grubert in 1956. The authors conducted the synthesis starting from lead(II)nitrate and sodiumcyclopentadienide in dimethylformamide (Scheme 86).[12]

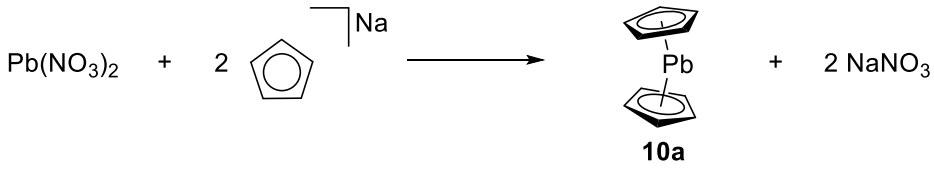

Scheme 86: Synthesis of plumbocene (**10a**) as carried out by Fischer and Grubert.[12]

When exposed to water, plumbocene (**10a**) did not display signs of hydrolysis speaking for an elevated covalent character in the bonding between lead and the cyclopentadienyl ligand in comparison to the bonding character in, for example, magnesocene (**3a**) which decomposes rapidly in water.[12] To shed light onto the geometry of **10a**, the authors carried out dipole measurements and could demonstrate that **10a**, in analogy to the tetrelocenes of the heavier elements germanium and tin, did not exhibit a coplanar structure.[12] In 1966, Panattoni *et al*. revealed the structure of **10a** in the solid state to be a polymeric zig zag structure, which can be justified by the size of the central lead atom leading to a bigger coordination sphere in comparison to germanium and tin in germanocene, **8a**, and stannocene, **9a**, respectively (Figure 41).

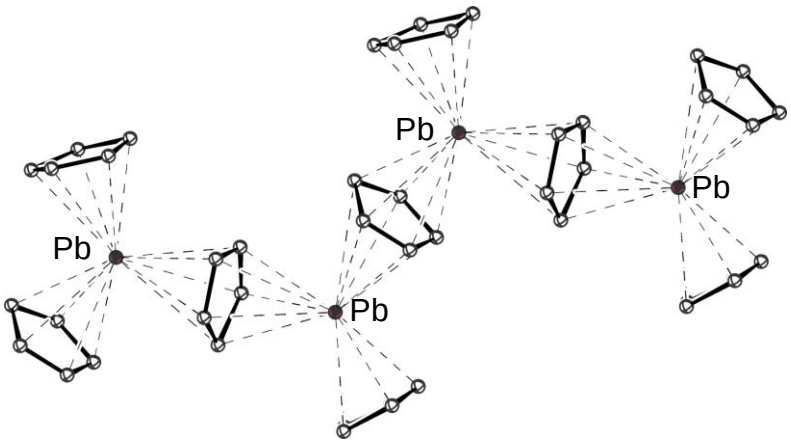

Figure 41: Molecular structure (polymeric zig zag) of plumbocene (**10a**)[15] in the crystal (hydrogen atoms omitted for clarity, ball-and-stick representation).

In the structure of plumbocene, **10a**, in the solid state, the bending angles δ range from 116.9° to 122.9°, which represents a significant stronger bending in comparison to the ones observed for **8a** (δ = 152.4°) and **9a** (δ = 143.8° and 147.1°) presumably also owing to the polymeric structure and intermolecular coordinations.[15,16,128] In 1997, Beswick *et al*. presented a hexagonal phase [**10a**]$_6$ and a polymeric toluene solvate complex of **10a**.[140] In 1998, Overby and coworkers investigated the structures of **10a** and concluded that Panattoni *et al*. refined the zig zag structure in an incorrect space group.[15,141] In 1988, Janiak *et al*. reported the signal in the ^{207}Pb NMR spectrum for **10a** in C_6D_6 solution to be −5030 ppm,[106] which is significantly upfield shifted compared to the signal for many plumbylenes such as Pb(CH[TMS]$_2$)$_2$ (δ ^{207}Pb = +9110 ppm[101]). This is in line with the signal in ^{29}Si NMR for decamethylsilicocene, **7a**, and the signal in ^{119}Sn NMR of **9a**, which are both also significantly upfield shifted. The reactivity of **10a** was examined by Beswick *et al*. by reaction of **10a** with nitrogen donors in 1996 (Scheme 87).[99]

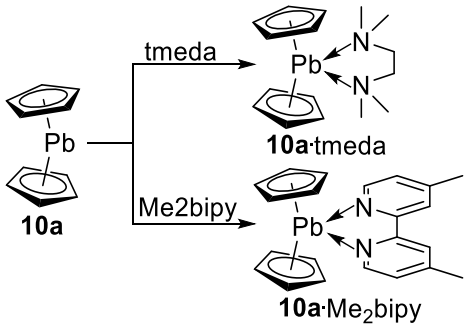

Scheme 87: Synthesis of **10a**·tmeda and **10a**·Me$_2$bipy as carried out by Beswick *et al*.[99]

The authors managed to crystallize both complexes revealing an η^3 arrangement of the cyclopentadienyl ligands in both complexes with a strong tendency toward a hapticity of η^5 (Figure 42).[98,99]

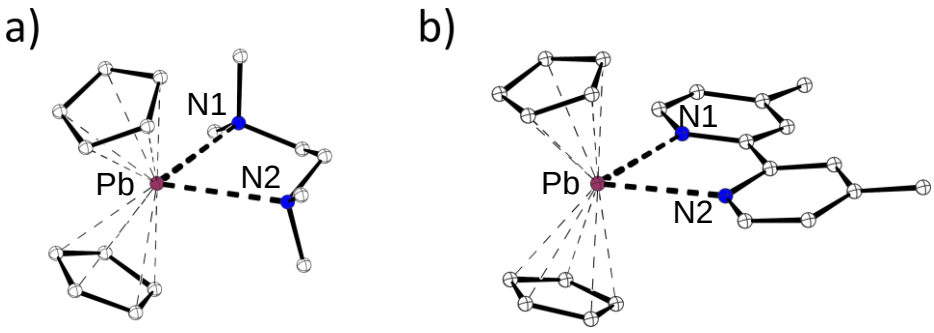

Figure 42: Molecular structures of a) **10a**·tmeda and b) **10a**·Me_2bipy[99] in the crystal (hydrogen atoms omitted for clarity, ball-and-strick representation).

The Pb-Cp^{cent} bond length is elongated in both adducts by about 13 pm in comparison to the Pb-Cp^{cent} bond length in plumbocene, **10a**, which can be explained by the weakening of the Pb-Cp bond by coordination of the nitrogen donor.[99,141] By comparison of the bending angles of both adducts, it should be mentioned that **10a**·tmeda is more bent (δ = 128.8°) than **10a**·Me_2bipy (δ = 139.7°) which might be due to steric pressure of the methyl groups of tmeda. It is worth mentioning in this context that the difference in energy in tetrelocenes between coplanar and bent geometry is small which is nicely demonstrated by the example of **7a** which exists in the form of the coplanar and bent metallocene in one crystal unit (*vide supra*). NMR spectroscopic studies (^{1}H NMR) of **10a**·tmeda at low temperatures (233 K) resulted in release of uncoordinated **10a** hinting toward a weak **10a** tmeda bond. In the case of **10a**·Me_2bipy, the bond between the metallocene and the nitrogen atoms is even weaker since ^{1}H NMR spectra at low temperatures (183 K) exhibited signals for uncoordinated Me_2bipy.[99]

The dimethylgermanocene, **8b**, was discovered in 1978 by Bonny *et al*. who synthesized this complex by transmetalation of methylcyclopentadienyllithium with germanium(II)iodide (Scheme 88).[142]

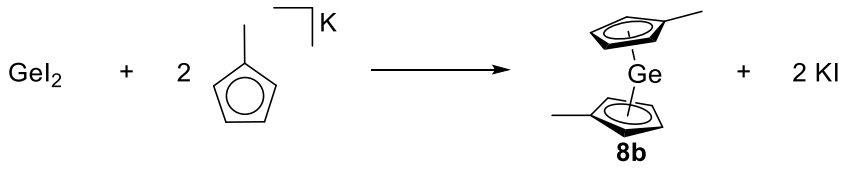

Scheme 88: Synthesis of dimethylgermanocene (**8b**) as conducted by Bonny *et al*.[142]

The authors described the obtained product as a yellow oil similar to the related tin analogue dimethylstannocene, **9b**, which was discovered by Dave *et al*. in 1959 (Scheme 89).[14,142]

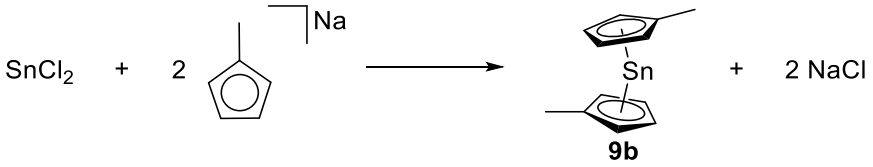

Scheme 89: Synthesis of dimethylstannocene (**9b**) as carried out by Dave *et al*.[14]

The structures of both dimethyltetrelocenes (**8b** and **9b**) were investigated by gas phase electron diffraction (GED) by Almlöf *et al*. in 1983 revealing E-Cp^{cent} distances of 222 pm for **8b** and 240 pm for **9b**, which are both comparable to the distances found in Cp_2Ge, **8a**, and Cp_2Sn, **9a**, by X-ray crystallography.[143] The reported shift for dimethylstannocene in the ^{119}Sn NMR spectrum is also in line with other stannocenes (see Table 8).[142] Interestingly, for the synthesis of dimethylplumbocene, **10b**, lead(II)acetate was used as starting material (Scheme 90).[14]

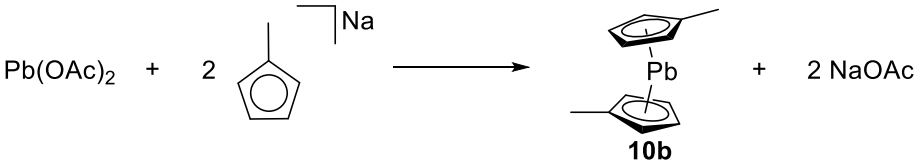

Scheme 90: Synthesis of dimethylplumbocene (**10b**) as carried out by Dave *et al*.[14]

The authors stated that usage of lead(II)acetate as starting material instead of lead(II)chloride was advantageous due to the better solubility of lead(II)acetate in dme.[14]

For all heavier group 14 elements, the decamethylmetallocenes are known (see Table 8). The decamethylgermanocene (**8c**) and decamethylstannocene (**9c**) were first reported in 1980 by Jutzi and coworkers (Scheme 91).[144]

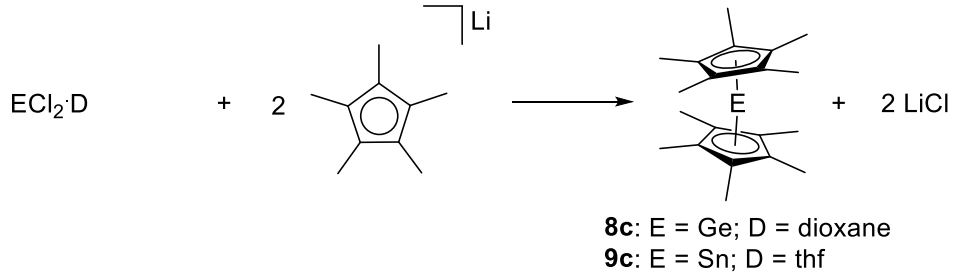

Scheme 91: Synthesis of decamethylgermanocene (**8c**) and decamethylstannocene (**9c**) as conducted by Jutzi *et al*.[144]

An alternative synthetic pathway for both decamethyltetrelocenes was reported by Jutzi *et al*. starting from the corresponding tetrachlorotetrel and Cp*Li and subsequent reduction of the obtained bis(pentamethyl)dichlorogermane or bis(pentamethyl)dichlorostannane, respectively.[145,146] The structure in the solid state of **9c** could be unraveled in 1980 by Jutzi *et al*. displaying a bent geometry (δ = 155.1°) and Sn-Cp^{cent} distances comparable to **9a** (see Table 8).[144] By comparison of the degree of bending in **9c** and stannocene, **9a**, it is obvious that the steric pressure of the methyl groups of the Cp* ligand forces the decamethylstannocene, **9c**, to a more coplanar arrangement of the cyclopentadienyl ligands, but also van der Waals interactions between the Cp* ligands must not be neglected.[147,148] In the ^{119}Sn NMR spectrum for **9c**, a signal at −2129 ppm[111] was observed in line with signals observed for other stannocenes (see Table 8). In 2011, Jutzi *et al*. could demonstrate the suitability of **9c** for the synthesis of small particles by decomposition of this compound in solution to obtain different shaped and sized particles in dependency of the reaction conditions.[149] For decamethylgermanocene, **8c**, the structure could be revealed by Schöpper and by Schenk and Schnepf in 2006.[150,151] The structural parameters displayed no surprising results due to Ge-Cp^{cent} bond lengths similar to the ones observed for germanocene, **8a**, and a bending angle δ of 162.2°, which represents a higher value than that for decamethylstannocene, **9c**, and germanocene (**8a**).[150,151] The synthesis of Cp*$_2$Pb, **10c**, was conducted by Atwood *et al*. in 1981 by reaction of lead(II)chloride with Cp*Li (Scheme 92).[16]

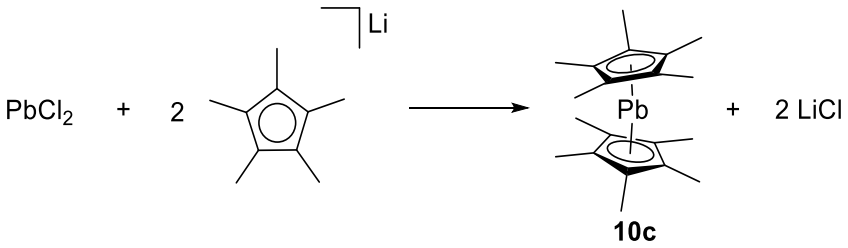

Scheme 92: Synthesis of decamethylplumbocene (**10c**) as carried out by Atwood and coworkers.[16]

The authors described decamethylplumbocene, **10c**, as a red solid which readily sublimed to afford crystals suitable for single crystal X-ray crystallography. In the solid state, **10c** possesses a bent structure (δ = 151.3°) and Pb-Cp^{cent} distances of 247.95(10) pm and 252.34(8) pm.[16] The Pb-Cp^{cent} distances are similar to those observed in the solid state structure of tetrakis(trimethylsilyl)plumbocene, **10d**, but the bending in **10c** is significantly more pronounced in comparison to **10d**. Jutzi and coworkers reported the signal in ^{207}Pb NMR spectrum for decamethylplumbocene, **10c**, at −4384 ppm which is an appropriate region for plumbocenes (see Table 8). In 1996, diethyl(octamethyl)plumbocene, **10e**, was synthesized by Evans and coworkers who used this metallocene as Cp transfer reagent for a samarium complex (Scheme 93).[152]

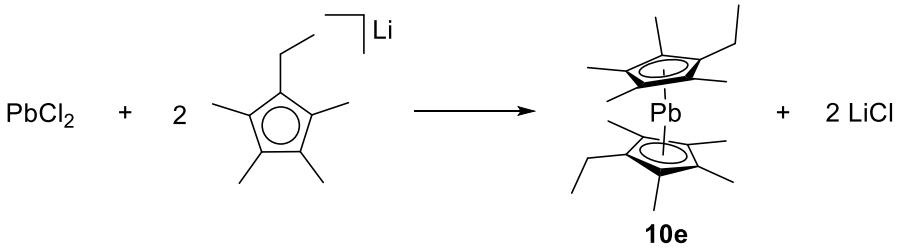

Scheme 93: Synthesis of diethyl(octamethyl)plumbocene (**10e**) as carried out by Evans *et al*.[152]

Surprisingly, the authors described **10e** as a red oil which is structurally closely related to decamethylplumbocene, **10c**, which was a red solid and could be sublimed.[16,152] The same group reported of other plumbocenes bearing $Cp^{\#}$ related ligands, obtained by transmetalation, three years later (Scheme 94).[153]

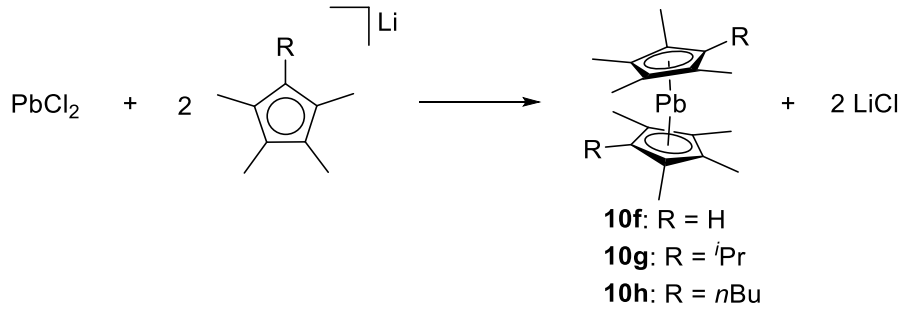

Scheme 94: Synthesis of polyalkylated plumbocenes (**10f**-**h**) as conducted by Evans *et al*.[153]

The authors were able to grow crystals of **10f** suitable for single crystal X-ray crystallography revealing a significantly more bent structure (δ = 139.7°) than Cp*$_2$Pb (δ = 151.3°), **10c**, in the solid state, which might be surprising since only one methyl group is substituted by a proton in **10f** compared to decamethylplumbocene (**10c**). The obtained Pb-Cp^{cent} distances are in line with those observed for **10c** (see Table 8). In 1996 and 2000 Constantine and coworkers synthesized the series of bis(dimethyl-*tert*-butylsilyl)germanocene, -stannocene and -plumbocene (Scheme 95).[154–156]

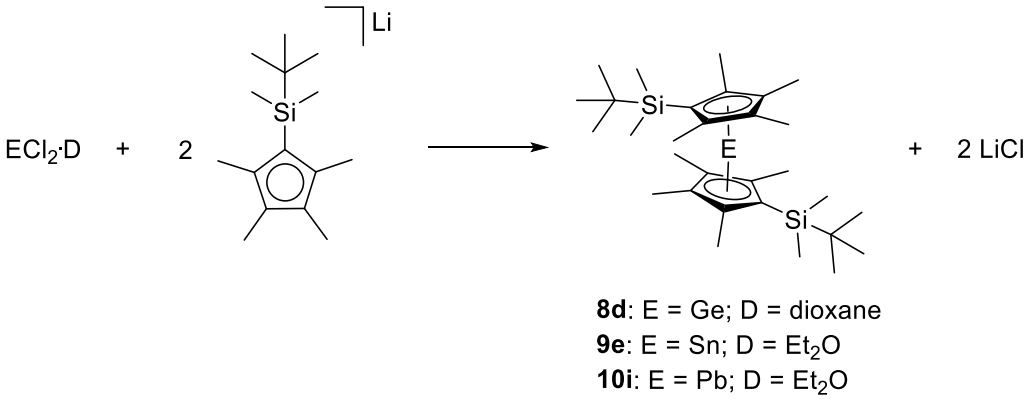

Scheme 95: Synthesis of bis(dimethyl-*tert*-butylsilyl)octamethyltetrelocenes (**8d**, **9e**, **10i**) as conducted by Constantine *et al*.[154–156]

In the solid state, all of these metallocenes (**8d**, **9e**, **10i**) exhibit a coplanar structure (δ = 179.9°) and E-Cp^{cent} distances comparable to the distances observed in the corresponding decamethylmetallocenes (see Table 8). The heteronuclear chemical shifts of **9e** (δ ^{119}Sn = −2204 ppm[154]) and **10i** (δ ^{207}Pb = −4595 ppm[154]) were both observed in regions typical for stannocenes and plumbocenes. The authors stated that **8d** and **10i** were the first examples

of a coplanar germanocene and plumbocene, respectively. By conducting quantum chemical calculations, the authors demonstrated that the ligand used creates about 20% increase of the charge at the germanium atom in **8d**. The trimethylsilyl substituted germanocenes (**8e**-**g**) were synthesized by Jutzi and coworkers by transmetalation of the corresponding lithiumcyclopentadienides with germanium(II)chloride dioxane complex in 1986 (Scheme 96).[157]

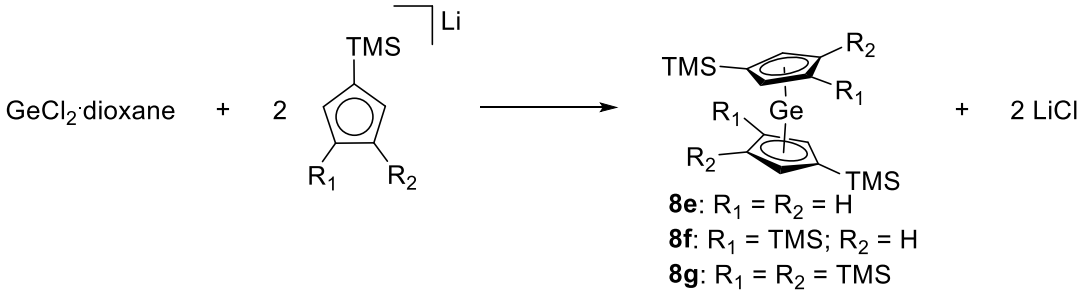

Scheme 96: Synthesis of $^{TMS}Cp_2Ge$, $^{TMS2}Cp_2Ge$ and $^{TMS3}Cp_2Ge$ (**8e**-**g**) as conducted by Jutzi *et al*.[157]

In the case of hexakis(trimethylsilyl)germanocene, **8g**, the authors were able to obtain crystals suitable for single crystal X-ray crystallography revealing a marginally bent structure (δ = 171.8°) presumably due to the steric pressure implemented by the bulky trimethylsilyl groups. The Ge-Cp^{cent} distances are slightly elongated compared to those observed in germanocene (**8a**) (about 1.7 pm). Jutzi *et al*. stated that no rotational barrier was observed since the molecule seems to be fluxional in solution, even at 233 K.[157] Bis(trimethylsilyl)-, tetrakis(trimethylsilyl)- and hexakis(trimethylsilyl)stannocene (**9f**-**h**) were synthesized by Cowley *et al*. in 1983 and 1984 by lithiation of stannocene and stepwise silylation (Scheme 97).[158,159]

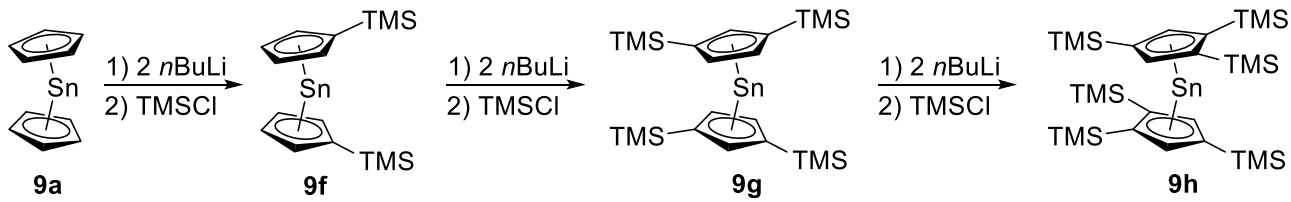

Scheme 97: Synthesis of $^{TMS}Cp_2Sn$, $^{TMS2}Cp_2Sn$ and $^{TMS3}Cp_2Sn$ (**9f**-**h**) as conducted by Cowley *et al*.[158,159]

This synthetic procedure is unique in stannocene chemistry since all other alkyl substituted stannocenes (except an alternative synthetic route for **9c**, *vide supra*) were obtained by transmetalation. For hexakis(trimethylsilyl)stannocene, **9h**, which could also be obtained by transmetalation of tin(II)chloride with two equivalents of tris(trimethylsilyl)cyclopentadienyl-lithium, a crystal structure could be obtained revealing a bending angle δ of 161.7° and Sn-Cp^{cent} distances of 227.24(23) pm and 268.32(33) pm. These values need to be assessed carefully due to the poor quality of the crystals obtained. Remarkably, the bending angle in **9h** is smaller compared to the one observed in the germanium analogue (**8g**) which is a trend that was already displayed in the unsubstituted metallocenes of both elements (see Table 8). The trimethylsilyl substituted plumbocenes were first reported by Jutzi and Schlüter in 1983 in a similar way the corresponding germanocenes (**8e**-**g**) were obtained (Scheme 98).[160]

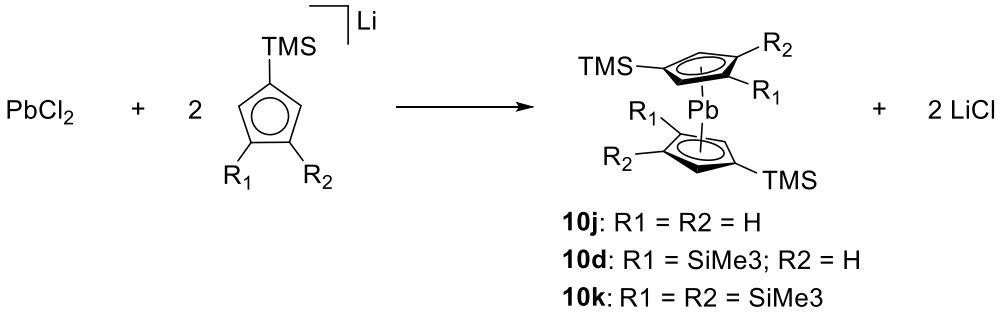

Scheme 98: Synthesis of $^{TMS}Cp_2Pb$, $^{TMS2}Cp_2Pb$ and $^{TMS3}Cp_2Pb$ (**10d**,**j**,**k**) as conducted by Jutzi *et al*.[160]

The authors reported an increasing stability of the trimethylsilyl substituted plumbocenes with increasing number of TMS groups attached to the cyclopentadienyl ligand.[160] Windorff and coworkers were successful in crystallizing bis(trimethylsilyl)plumbocene, **10j**, in 2016. In the structure in the solid state, a polymeric zig zag structure was revealed comparable to the structure of plumbocene with similar Pb-Cp^{cent} distances (248.57(3) pm to 284.00(3) pm) as well as similar bending angles δ (110.2 to 126.4°) and a similar signal observed in the ^{207}Pb NMR spectrum (−4790 ppm).[161] One year later, this compound was used in the synthesis of an uranium complexes as Cp transfer reagent.[162] In 2012, Coles *et al*. were able to structurally characterize the tetrakis(trimethylsilyl)plumbocene, **10d**, revealing a slightly bent geometry (δ = 171.0°) with Pb-Cp^{cent} distances of 245.94(5) pm and 250.46(5) pm.[163]

The fact that this plumbocene is only marginally bent is surprising since hexakis(trimethylsilyl)germanocene, **8g**, exhibits a comparable value for angle δ (171.8°). However, two opposite trends need to be considered in this context: on the one hand, bending in tetrelocenes becomes stronger descending the group 14 and on the other hand, ligands introducing more steric constraint are expected to produce more coplanar geometries in tetrelocenes (see Table 8). Coles and coworkers tended to explain this high value for the bending angle with steric pressure implemented by the trimethylsilyl groups, but in view of the arguments presented above this might not be a satisfying explanation.[163] In the field of the *iso*propyl substituted tetrelocenes of the heavier elements, no example of a germanocene is known to date.

For tin and lead, the hexa(*iso*propyl)-, octa(*iso*propyl)- and deca(*iso*propyl)tetrelocenes are known (see Table 8). In 1995, Burkey and Hanusa reported the syntheses of hexa(*iso*propyl)- and octa(*iso*propyl)stannocene (**9i**, **9j**) (Scheme 99).[164]

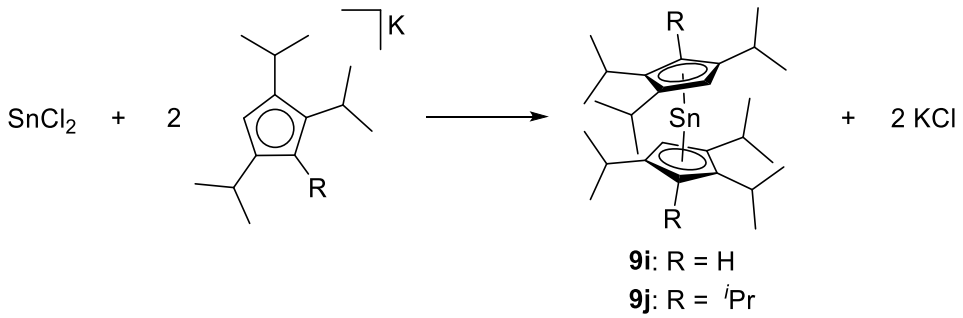

Scheme 99: Synthesis of hexa(*iso*propyl)- and octa(*iso*propyl)stannocene (**9i**; **9j**) as conducted by Burkey and Hanusa.[164]

The authors described hexa(*iso*propyl)stannocene, **9i**, as a yellow oil which could even be distilled (373 K, 10^{-6} mbar) to obtain the metallocene in high purity. This tendency of hexa(*iso*propyl)metallocenes of main group elements to occur as an oil was also observed for $^{3}Cp_2Mg$ (**3h**) and $^{3}Cp_2Ca$ (**4e**) (*vide supra*). These two tetrelocenes exhibited significant different reactivities toward oxygen: whereas **9i** decomposed rapidly in air, the authors stated that **9j** could be exposed for hours to air without serious decomposition which is an interesting result since both metallocenes only differ by two *iso*propyl groups.[164] The structure of **9j** in the solid state could be revealed displaying a bending angle δ of 165.0°, which is, as expected, a bigger value than that observed for stannocene which is consequently

more bent. The Sn-Cp^{cent} distances do not differ dramatically from the ones observed for stannocene (**9a**), which is surprising in view of the different sterics both cyclopentadienyl ligands exhibit.[164] In 1996, Sitzmann and coworkers synthesized deca(*iso*propyl)stannocene, **9k**, in which the central tin atom is completely encapsulated by the super bulky ^{5}Cp ligand (Scheme 100).[165]

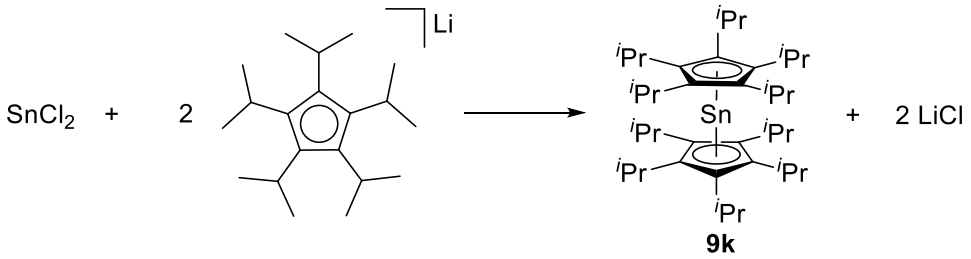

Scheme 100: Synthesis of deca(*iso*propyl)stannocene (**9k**) as conducted by Sitzmann *et al*.[165]

The authors stated that **9k** is inert toward oxidation which is unquestionably a result of the steric demand of the penta(*iso*propyl)cyclopentadienyl ligand (Figure 43).

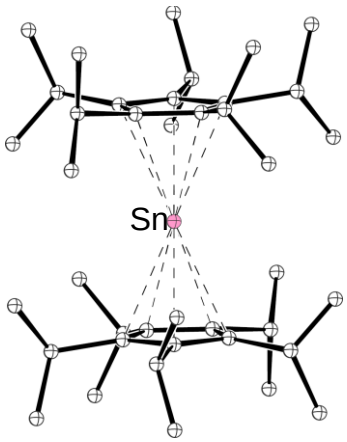

Figure 43: Molecular structure of $^5Cp_2Sn$ (**9k**)[165] in the crystal (hydrogen atoms omitted for clarity, ball-and-stick representation).

By conducting ^{1}H NMR spectroscopy at various temperatures, splitting of the signals for the methyl groups could be observed at 313 K due to existence of metal-close and metal-distant methyl groups. This phenomenon was already discussed in context of $^5Cp_2Ca$ (**4g**) which

exhibited a similar behavior (*vide supra*). The signal of $^{5}Cp_2Sn$, **9k**, in ^{119}Sn CP/MAS NMR spectrum (δ ^{119}Sn = −2262 ppm) is in line with the one observed for other stannocenes (see Table 8).[165] In 2000, Burkey *et al*. reported the synthesis and crystal structure of $^{3}Cp_2Pb$ (**10l**) (Scheme 101).[166,167]

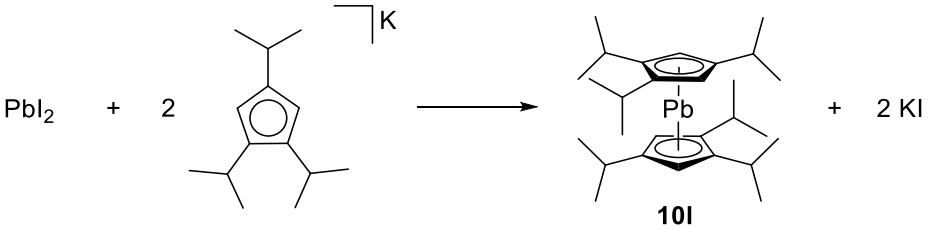

Scheme 101: Synthesis of hexa(*iso*propyl)plumbocene (**10l**) as carried out by Burkey *et al*.[166,167]

This metallocene exhibited a melting point of 307-308 K, which is higher than that observed for the analogous stannocene. By inspection of the structure in the solid state of **10l**, it is noteworthy that this tetrelocene exhibits a coplanar structure (δ = 179.9°) with Pb-Cp^{cent} distances similar to those observed in tetrakis(trimethylsilyl)plumbocene (**10d**). The authors stated the lone pair of the lead center to be stereochemically inactive due to the inert-pair effect, which increases when descending group 14, which might induce the coplanarity of $^{3}Cp_2Pb$ (**10l**).[166,167] Five years before the report of Burkey *et al*. of **10l**, Sitzmann and coworkers published the synthesis of octa(*iso*propyl)- and deca(*iso*propyl)plumbocene (Scheme 102).[168]

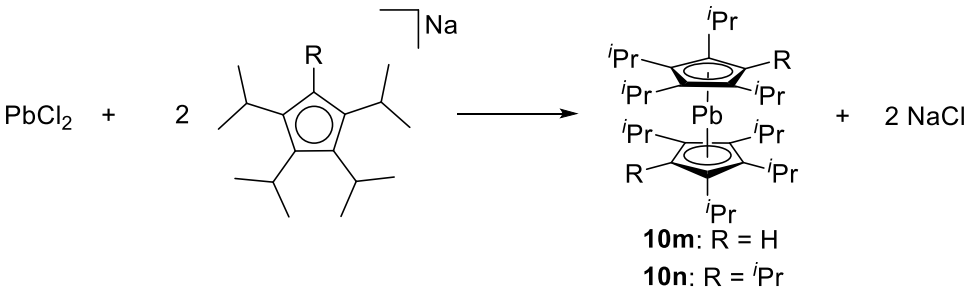

Scheme 102: Synthesis of octa(*iso*propyl)- and deca(*iso*propyl)plumbocene (**10m**; **10n**) as conducted by Sitzmann *et al*.[168]

Both metallocenes were obtained as orange-red (**10m**) and ruby red (**10n**) crystalline solids, but unfortunately no crystals of good quality could be grown. For deca(*iso*propyl)plumbocene, **10n**, the only structural characteristic that could be determined from the data is a Pb-Cp^{cent} distance of 275 pm and an angle δ of approximately 170°, which is surprising in context of the bending angle found in $^{3}Cp_2Pb$ (**10l**), but should not be overestimated due to the poor quality of the structural data of **10n**.[168] The $^{5}Cp_2Pb$, **10n**, exhibited a behavior similar to $^{5}Cp_2Sn$, **9k**, in ^{1}H NMR spectrum at low temperatures due to the existence of metal-close and metal-distant methyl groups.[168] In the ^{207}Pb NMR spectrum, $^{4}Cp_2Pb$, **10m**, displays a signal at −4534 ppm which is in line with other plumbocenes, but $^{5}Cp_2Pb$, **10n**, exhibits a signal at −3293 ppm which seems significantly downfield shifted compared to known plumbocenes (see Table 8).

In the class of tetrelocenes bearing *tert*-butyl substituted cyclopentadienyl ligands, the di-*tert*-butylstannocene, **9l**, the series of tetra-*tert*-butylgermanocene (**8h**), -stannocene (**9m**) and -plumbocene (**10o**) as well as the hexa-*tert*-butylplumbocene (**10p**) are known. The di-*tert*-butylstannocene, **9l**, was synthesized by Hani and Geanangel in 1985 by transmetalation of LiCp' with tin(II)chloride (Scheme 103).[169]

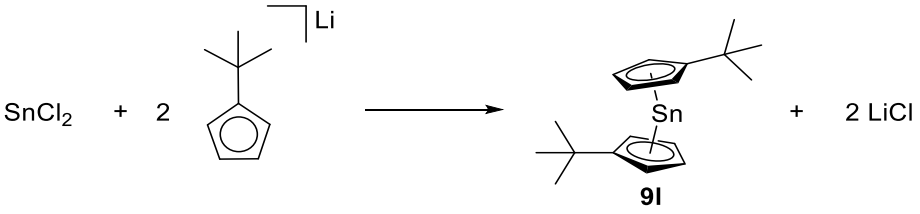

Scheme 103: Synthesis of di-*tert*-butylstannocene (**9l**) as conducted by Hani and Geanangel.[169]

This metallocene, **9l**, was obtained as a brown, air sensitive oil.[169] The series of the tetra-*tert*-butyltetrelocenes Cp''$_2$E (E = Ge-Pb) (**8h**, **9m**, **10o**) was synthesized by Jutzi *et al*. in 1989 by transmetalation of LiCp'' with the corresponding element dichloride (Scheme 104).[170]

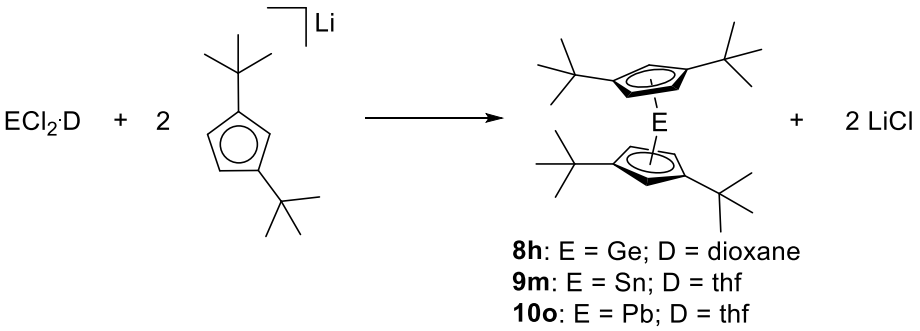

Scheme 104: Synthesis of tetra-*tert*-butyltetrelocenes (**8h**, **9m**, **10o**) as carried out by Jutzi and coworkers.[170]

The reported signals in ^{119}Sn and ^{207}Pb NMR spectra for **9m** (δ ^{119}Sn = −2100 ppm) and **10o** (δ ^{207}Pb = −4756 ppm) fit into the row of signals found for other stannocenes and plumbocenes (see Table 8). The authors stated that all three metallocenes existed as oils at room temperature.[170] In 1995, Sitzmann *et al*. reported the hexa-*tert*-butylplumbocene, **10p**, which was obtained by reaction of di-*tert*-butylcyclopentadienylsodium with lead(II)iodide (Scheme 105).[168]

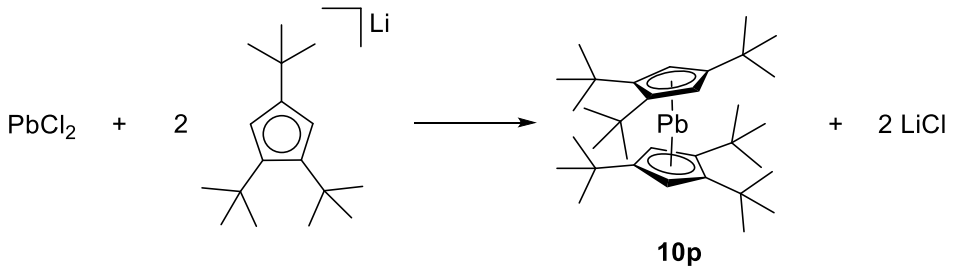

Scheme 105: Synthesis of hexa-*tert*-butylplumbocene (**10p**) as carried out by Sitzmann *et al*.[168]

Unfortunately, no crystals could be grown of this compound by the authors. This metallocene, **10p**, exhibits a signal at −4230 ppm in the ^{207}Pb NMR spectrum, which is in the appropriate region for plumbocenes (see Table 8).[168] In 1989, Jutzi *et al*. reported of the synthesis of [Me$_2$Si[1](η^5-Cp$^{\#}$)(Cp$^{\#}$H)]$_2$E (E = Ge-Pb) (**8i**, **9n**, **10q**) which were obtained by reaction of the monolithiated ligand with the corresponding group 14 precursor (Scheme 106).[171]

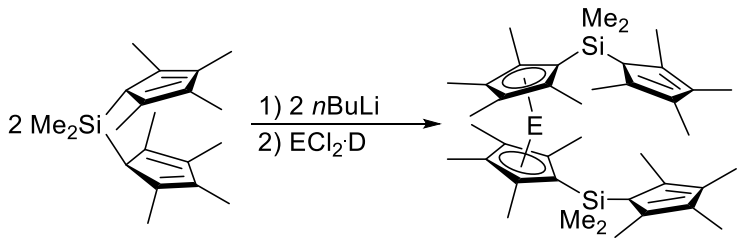

8i: E = Ge; D = dioxane
9n: E = Sn; D = thf
10q: E = Pb; D = thf

Scheme 106: Synthesis of $[Me_2Si[1](\eta^5\text{-}Cp^{\#})(Cp^{\#}H)]_2E$ (**8i**, **9n**, **10q**) as conducted by Jutzi *et al*.[171]

These complexes were characterized by multinuclear NMR spectroscopy exhibiting typical signals in ^{119}Sn and ^{207}Pb NMR spectra, respectively (see Table 8).[171]

In conclusion, the heavier tetrelocenes represent all in all an old class of compounds when taking into account the first representatives which were discovered in the 1950s. To date, 9 germanocenes, 13 stannocenes and 17 plumbocenes were reported of which 17 have been structurally characterized in total. Only few examples of these homoleptic, alkyl and silyl substituted tetrelocenes exhibit a coplanar structure which are $^{(Me2tBuSi)}Cp^{\#}E$ (E = Ge-Pb), $^{5}Cp_2Sn$ (**9k**) and $^{3}Cp_2Pb$ (**10l**) and, in addition, it seems that simple explanations and predictions for the degree of bending in tetrelocenes fail especially when $^{3}Cp_2Pb$ (**10l**) and $^{5}Cp_2Pb$ (**10n**) are compared with each other.[163,168] Interestingly, the E-Cp^{cent} distances do not differ dramatically, even when extremely bulky cyclopentadienyl ligands are attached to the group 14 metal. By inspection of the structures obtained in alkylated and silylated tetrelocenes, it becomes visible that the Cp ligands always exhibit an η^5 hapticity and ring slippage like in the group 2 metallocenes is not present justified by the more covalent bonding character in tetrelocenes. By comparison of the Ge-Cp^{cent} distance of germanocene (**8a**) (223.37(43) pm) with the Fe-Cp^{cent} distance of ferrocene (**1**) (166.06(11) pm[3]) and the Ca-Cp^{cent} distances in calcocene (**4a**) (247.94(4) pm and 259.28(6) pm[61]), it can be seen that due to a more covalent bonding character and participation of d orbitals in ferrocene (**1**), the Fe-Cp bond is stronger compared to the more ionic Ge-Cp bond in germanocene (**8a**) and with increased ionic bonding character in calcocene (**4a**) the Ca-Cp^{cent} bond length is elongated in comparison to the Ge-Cp^{cent} distance. The usage of stannocenes and plumbocenes in lanthanoid chemistry as a Cp transfer reagent is an important application for these metallocenes since they are mild reagents.[129,152,153] No structural prove for a donor complex with

a tetrelocene is reported to date and the only reports of group 6 metal pentacarbonyl complexes of stannocenes are solely characterized by IR and Mössbauer spectroscopy.[134] For stannocene, **9a**, an oxidative addition reaction with iodine was reported in 1974.[136] This result depicts an important difference between stannocenes and “classical” stannylenes: The reactivity of stannocene, **9a**, and plumbocene, **10a**, was probed by Beswick *et al*. who demonstrated the Lewis acidic character of the central atom.[98,99]

The homoleptic, aryl and benzyl substituted tetrelocenes were all obtained by transmetalation of the corresponding alkalicyclopentadienide with group 14 element halides (Scheme 107).

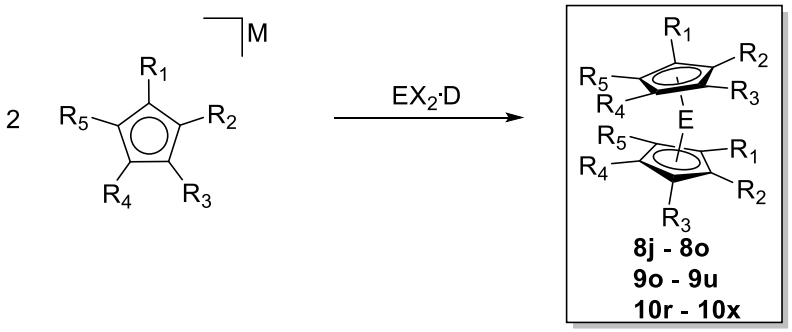

E = Ge; X = I; D = Et_2O; M = Li; R_{1-4} = Ph; R_5 = H. E = Sn/Pb; X = Cl; D = Et_2O; M = Li; R_{1-4} = Ph; R_5 = H. E = Ge; X = I; D = Et_2O; M = Li; R_{1-4} = Ph; R_5 = *p*-^{t}BuPh. E = Sn; X = Cl; D = Et_2O; M = Li; R_{1-4} = Ph; R_5 = *p*-^{t}BuPh. E = Pb; X =OAc; D = Et_2O; M = Li; R_{1-4} = Ph; R_5 = *p*-^{t}BuPh. E = Ge; X = Cl; D = dioxane; M = Li; R_{1-5} = Ph. E = Sn; X = Cl; D = thf; M = Na; R_{1-5} = Ph. E = Pb; X = Cl; D = thf; M = Li; R_{1-5} = Ph. E = Ge; X = I; D = thf; M = Li; R_{1-5} = Bz. E = Sn; X = Cl; D = thf; M = Li; R_{1-5} = Bz. E =Pb; X = OAc; D = thf; M = Li; R_{1-5} = Bz. E = Ge; X = 0.5 Cl; D = *n*Bu_3P; M = K; R_{1-5} = *p*-^{i}PrBz. E = Sn; X = Cl; D = thf; M = Na; R_{1-5} = *p*-*n*BuPh. E = Ge; X = Cl; D = dioxane; M = K; R_{1-5} = *p*-^{t}BuPh. E = Sn; X = I; D = thf; M = K; R_{1-5} = *p*-^{t}BuPh. E = Pb; X = I; D = thf; M = K; R_{1-5} = *p*-^{t}BuPh. E = Sn/Pb; X = Cl; D = thf; M = Na; R_{1-5} = *p*-[$Me(OCH_2)_2C$]Ph. E = Pb; X = Cl; D = thf; M = Na; R_{1-5} = *p*-[$Me(OEt_2)_2C$]Ph.

Scheme 107: Overview of syntheses of homoleptic, aryl substituted tetrelocenes.

The octaphenyltetrelocenes were reported by Schumann *et al*. in 1988, who synthesized these metallocenes (**8j**, **9o**, **10r**) by transmetalation of ^{Ph4}CpLi with group 14 element halides (Scheme 108).[172,173]

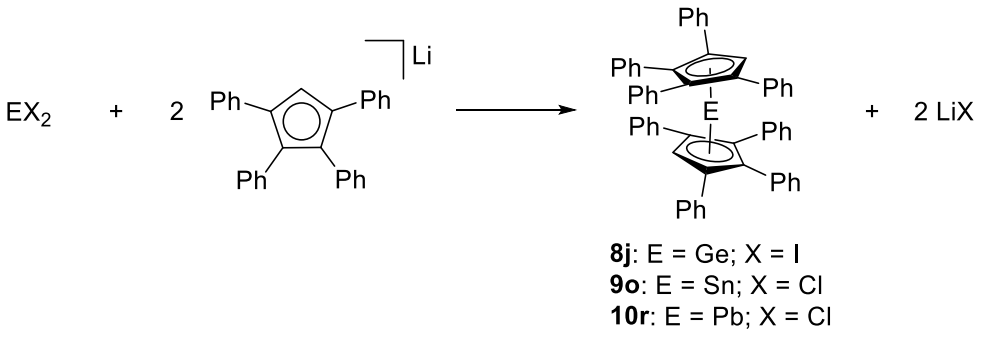

Scheme 108: Synthesis of octaphenyltetrelocenes (**8j**, **9o**, **10r**) as conducted by Schumann *et al*.[172,173]

The authors stated that the stability toward oxidation of the octaphenyltetrelocenes (**8j**, **9o**, **10r**) increases going from germanium to lead as central atom. These metallocenes possess a mediocre solubility in toluene, but still a higher solubility than the related decaphenyltetrelocenes (**8k**, **9p**, **10s**). Schumann and coworkers were not successful in crystallizing these compounds and stated that possible rotamers in solution prevent effective packing in the crystal.[172,173] In the same work, the authors presented the series of air stable bis(*p*ara-*tert*-butylphenyl)octaphenyltetrelocenes (**8l**, **9q**, **10t**) which were obtained by transmetalation (Scheme 109).[172,173]

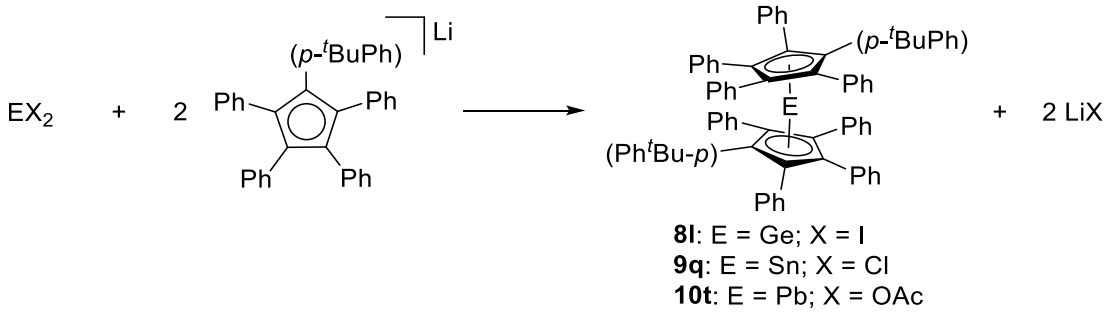

Scheme 109: Synthesis of phenyl substituted tetrelocenes (**8l**, **9q**, **10t**) as carried out by Schumann *et al*.[172,173]

The authors reported of difficulties in the synthesis of the pure metallocenes due to possible formation of the monosubstituted products. Janiak *et al*. reported signals in ^{119}Sn NMR spectra for **9o** (−2200 ppm) and **9q** (−2235 ppm) which are similar to the ones for known stannocenes (see Table 8). The stannocene **9p** was synthesized by Heeg *et al*. in 1984.[174] In 1988, **8k** and **10s** were reported by Heeg and coworkers (Scheme 110).[175]

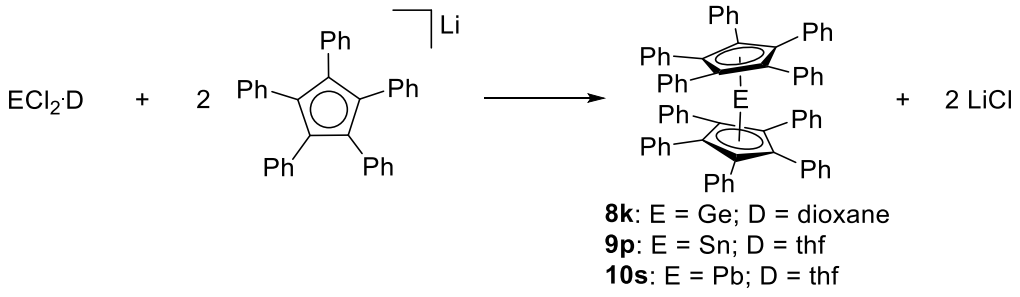

Scheme 110: Synthesis of decaphenyltetrelocenes (**8k**, **9p**, **10s**) as conducted by Heeg and coworkers.[174,175]

The decaphenyltetrelocenes were reported to be air stable and, in the case of decaphenylplumbocene, **10s**, even stable toward hydrolysis. This stability is undoubtedly also due to the poor solubility of the decaphenyltetrelocenes. The authors were able to crystallize decaphenylstannocene, **9p**, which exhibits a coplanar structure in the solide state and a Sn-Cp^{cent} distance of 240.13(4) pm similar to what is observed for Cp^*_2Sn (**9c**). The reported signal in the ^{119}Sn NMR spectrum of −2215 ppm is in the same region as those shifts observed for other stannocenes.[106] The value reported in the ^{207}Pb NMR spectrum by Janiak *et al*. for **10s** (δ ^{207}Pb = −6150 ppm) represents a significantly upfield shifted signal in comparison to known plumbocenes, but it should be mentioned that these measurements were CP/MAS NMR measurements and the inert 6s electrons of lead might be influencing these ^{207}Pb NMR shifts significantly (see Table 8).[106] The series of decabenzyltetrelocenes (**8m**, **9r**, **10u**) was reported by Schumann *et al*. in 1985 (decabenzylgermanocene, **8m**) and 1986 (decabenzylstannocene, **9r**, and -plumbocene, **10v**) (Scheme 111).[176,177]

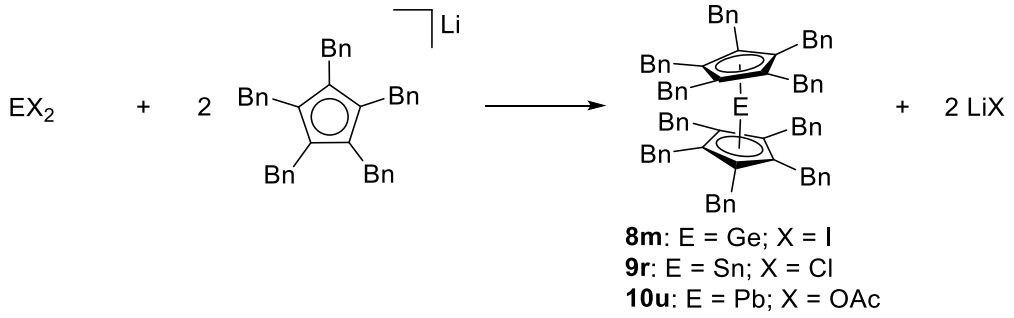

Scheme 111: Synthesis of decabenzyltetrelocenes (**8m**, **9r**, **10u**) as conducted by Schumann *et al*.[176,177]

The authors managed to crystallize the complete series of decabenzyltetrelocenes: The bending increases from decabenzylgermanocene, **8m**, (δ = 162.6°) over decabenzylstannocene, **9r**, (δ = 155.9°) to decabenzylplumbocene, **10u**, (δ = 153.5°) which is an effect that was already discussed in the unsubstituted tetrelocenes (*vide supra*). The bond lengths in the decabenzyltetrelocenes do not differ significantly from those observed in the unsubstituted metallocenes, but the angles δ exhibit higher values displaying a decrease in the degree of bending in the decabenzyltetrelocenes in comparison to the unsubstituted tetrelocenes (see Table 8). Schumann *et al*. justified the significant bending observed in decabenzylstannocene in comparison to decaphenylstannocene by an interaction of the lone pair at the tin atom with the π electrons of the cyclopentadienyl ligand.[177] In 2013,

Naglav *et al*. reported of the synthesis of $^{(p\text{-}i\text{PrBn})5}Cp_2Ge$, **8n**, which was obtained by reaction of a germanium(I)chloride solution stabilized by tri(*n*-butyl)phosphine with $^{(p\text{-}i\text{PrBn})5}CpK$.[178] This product, $^{(p\text{-}i\text{PrBn})5}Cp_2Ge$, **8n**, was also obtained by transmetalation reaction of germanium(II)chloride dioxane complex with $^{(p\text{-}i\text{PrBn})5}CpK$ (Scheme 112).[178]

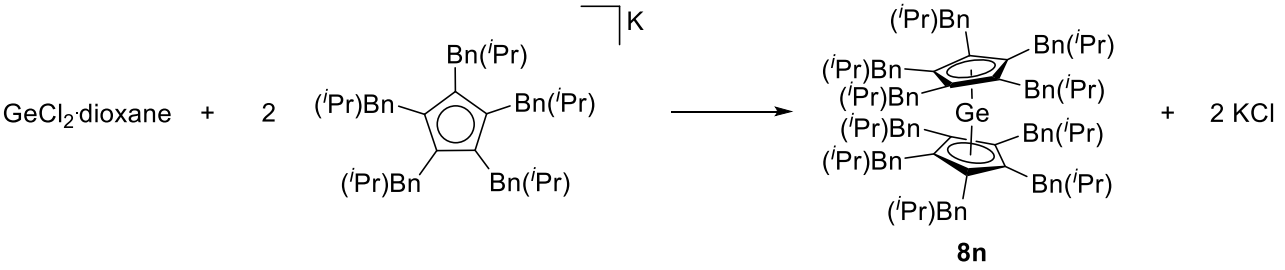

Scheme 112: Synthesis of deca(para-*iso*propylbenzyl)germanocene (**8n**) as conducted by Naglav *et al*.[178]

In the crystal structure, two of the benzyl substituents attached to the cyclopentadienyl ligand point toward the lone pair of the central germanium atom. The bending and the Ge-Cp^{cent} distances of **8n** (δ = 160.9° and 161.6°; Ge-Cp^{cent} = 218.75(3) to 226.01(3) pm) exhibit comparable values to those observed for $^{Bn5}Cp_2Ge$.[177,178] In 2014, Harder and coworkers presented the deca(*para-n*-butylphenyl)stannocene (**9s**) which was synthesized by transmetalation (Scheme 113).[147]

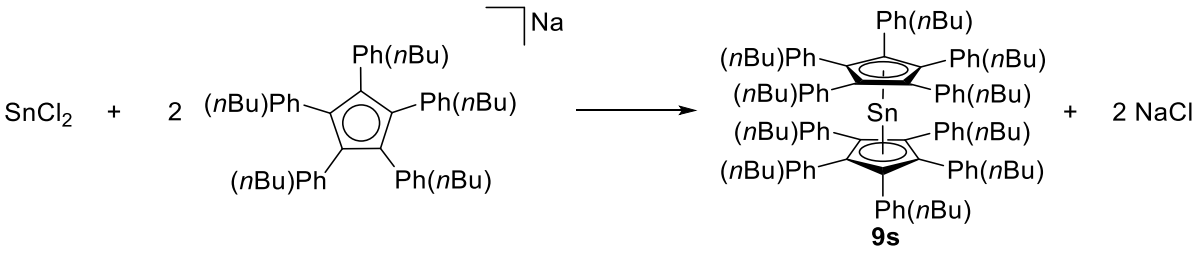

Scheme 113: Synthesis of deca(*para-n*-butylphenyl)stannocene (**9s**) as carried out by Harder *et al*.[147]

In the structure of **9s** in the solid state, a coplanar geometry of the metallocene is displayed with a Sn-Cp^{cent} distance (240.29(1) pm) similar to the ones observed for stannocene (**9a**). The authors also found C-H···C(π) interactions between the cyclopentadienyl ligands and

out-of-plane bending of the aryl substituents toward the metal.[147] These effects were already discussed for Cp^{BIG} complexes of calcium and strontium (*vide supra*). The chemical shift of −2190 ppm in the ^{119}Sn NMR spectrum fits into the row of known stannocenes (see Table 8).[147] With the penta(*para-tert*-butylphenyl)cyclopentadienyl ligand, the series of heavier tetrelocenes (Ge-Pb) could be obtained by Schulte *et al*. in 2020. That work includes a large variety of different metals, also group 2 metals which complexes have been discussed in the chapter of group 2 metallocenes (*vide supra*).[58] The synthesis of these group 14 metallocenes was carried out starting from the corresponding potassiumcyclopentadienide ($^{(p\text{-}t\text{BuPh})5}$CpK) and group 14 element halide (Scheme 114).[58]

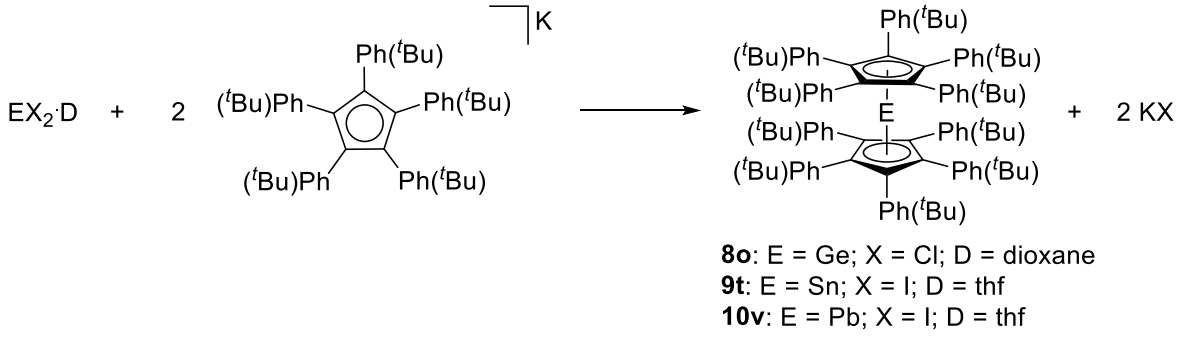

Scheme 114: Synthesis of deca(*para-tert*-butylphenyl)tetrelocenes (**8o**, **9t**, **10v**) as conducted by Schulte *et al*.[58]

The authors reported an alternative synthetic route for the deca(*para-tert*-butylphenyl)stannocene (**9t**) and -plumbocene (**10v**) starting from $^{(p\text{-}t\text{BuPh})5}$Cp radical and tin or lead metal. All tetrelocenes (**8o**, **9t**, **10v**) synthesized in the work of Schulte and coworkers could be crystallized and exhibit coplanar structures in the solid state (δ = 179.9°). The E-Cp^{cent} distances are in the same range as those observed for the corresponding decamethylmetallocenes (E=Ge, Sn). For the deca(*para-tert*-butylphenyl)plumbocene, **10v**, the Pb-Cp^{cent} distance is slightly shortened in comparison to decamethylplumbocene (**10c**) which might be a result of the stereochemically inactive lone pair at lead due to the inert-pair effect and London interactions between the aryl substituted cyclopentadienyl ligands.[58] The effects in these aryl substituted metallocenes have been discussed in the chapter about group 2 metallocenes, especially in strontocene and barocene chemistry (*vide supra*). In 1994, Lowack *et al*. reported on the synthesis of Cp^{BIG} ligands containing ethoxy and dioxa groups. Their synthetic

pathway started from the corresponding potassiumcyclopentadienide and tin(II)chloride or lead(II)chloride (Scheme 115).[179]

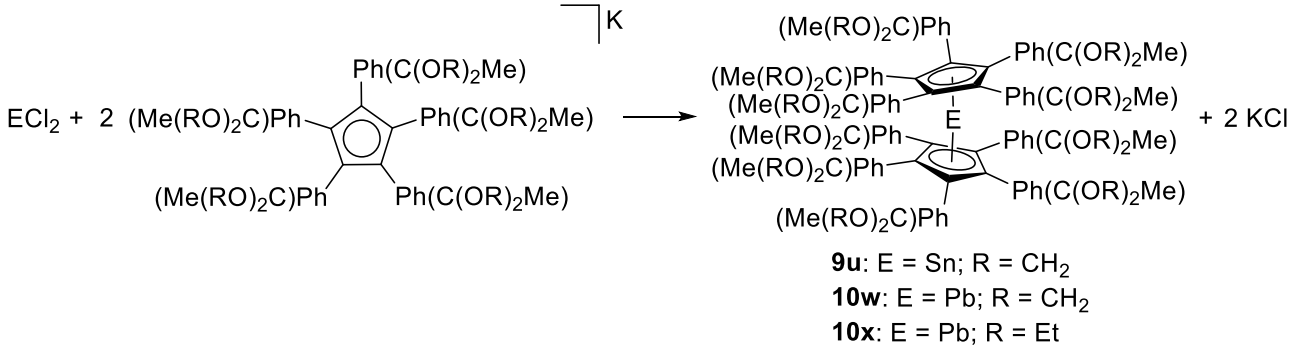

Scheme 115: Synthesis of oxygen containing aryl substituted tetrelocenes (**9u**, **10w**, **10x**) as conducted by Lowack *et al*.[179]

The authors stated that the obtained tetrelocenes (**9u**, **10w**, **10x**) were soluble in dichloromethane and, in the case of the ethoxy substituted plumbocene, **10x**, also soluble in benzene. The stability was reported to be higher than that of unsubstituted stannocene (**9a**) and plumbocene (**10a**), but not as air stable as the decaphenylstannocene (**9p**) or decaphenylplumbocene (**10s**).[179]

In conclusion, the aryl substituted tetrelocenes represent a class of intriguing complexes which properties differ significantly from most of the alkyl and silyl substituted tetrelocenes. These differences can be seen in the inertness of the Cp^{BIG} substituted tetrelocenes which often are air stable and sometimes even stable toward hydrolysis. The aryl substituents exhibit properties which influence the structures of the tetrelocenes by formation of weak interactions. Also important for the stability of aryl substituted metallocenes are London and van der Waals interactions between the cyclopentadienyl ligands, which are weak in themselves but seem to provide significant contribution to the stability of the metallocenes obtained. Exact predictions about the structure are difficult to make since little changes in the aryl substituent might have a great impact on the whole molecule. However, the factors influencing the degree of bending in these aryl substituted tetrelocenes are not fully understood, but several contributions have been presented here and shed light onto this interesting research field.

Rouzaud *et al*. prepared several examples of bis(metallocenes) which were linked by 1,4-phenylene, 1,4-biphenylene or 1,4-thiophene in 2000 and 2002. These complexes were obtained by reaction of the dilithiated ligand with the corresponding pentamethylcyclopentadienyltetrylene chloride (Scheme 116).[180,181]

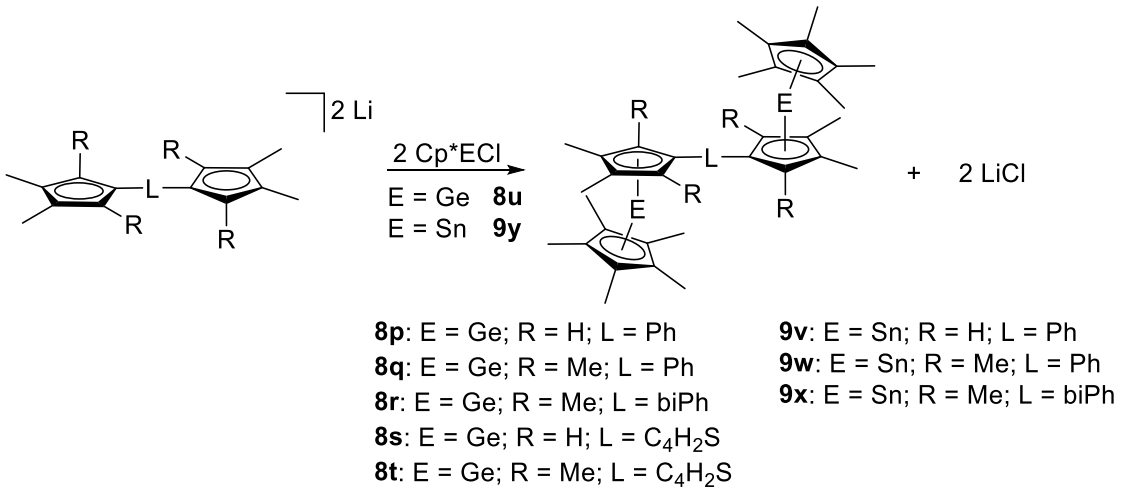

Scheme 116: Synthesis of bis(germanocenes) and bis(stannocenes) as conducted by Rouzaud *et al*.[180,181]

By reaction of phenyl and biphenyl linked bis(germanocenes) with ferrocenium $Cp_2Fe^+BF_4^-$, the corresponding germyliumylidenes were obtained. The authors managed to crystallize the phenyl linked bis(heptamethyl)germanocene (**8p**) from thf (Figure 44).[181]

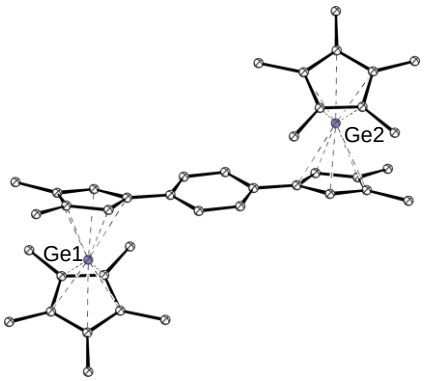

Figure 44: Molecular structure of (0.5μ-PhCp*^{Me2}Cp)Ge (**8p**)[181] in the crystal (hydrogen atoms omitted for clarity, ball-and-stick representation).

The structure in the solid state of **8p** revealed a hapticity of η^5/η^5 and a bent geometry (δ = 158.5°) with Ge-Cp^{cent} distances of: Ge-^{Me2}Cp^{cent}: 228.70(15) pm and Ge-Cp*^{cent}: 210.51(13) pm. The degree of bending in **8p** is comparable to what is observed for germanocene, **8a**, but the Ge-^{Me2}Cp^{cent} is elongated in comparison to the Ge-Cp^{cent} distance in germanocene.[181] The Ge-Cp*^{cent} of **8p** is shortened in comparison to the Ge-Cp^{cent} distances in Cp*$_2$Ge (**8c**) which can be justified by a stronger bond of the germanium atom to the Cp* ligand caused by a weaker bond to the other cyclopentadienyl ligand in **8p** which might be due to steric reasons or a decreased electron density in the phenyl substituted cyclopentadienyl ligand caused by more efficient electron delocalization over the π systems of the cyclopentadienyl ligands bridged by the phenyl linker. Interestingly, only **8p** is stated to be stable in solution, all other reported bis(tetrelocenes) seem to slowly decompose in solution. The signals in ^{119}Sn NMR spectra for **9v** (δ ^{119}Sn = −2110 ppm), **9w** (δ ^{119}Sn = −2128 ppm) and **9x** (δ ^{119}Sn = −2129 ppm) appear in an appropriate region for stannocenes (see Table 8).[181] In 2004, ferrocenyl substituted germanocenes and stannocenes were reported by Joudat *et al*. [182] The synthesis of these compounds started from cyclopentadiene substituted ferrocenes, *n*BuLi and group 14 element chlorides (Scheme 117).[182]

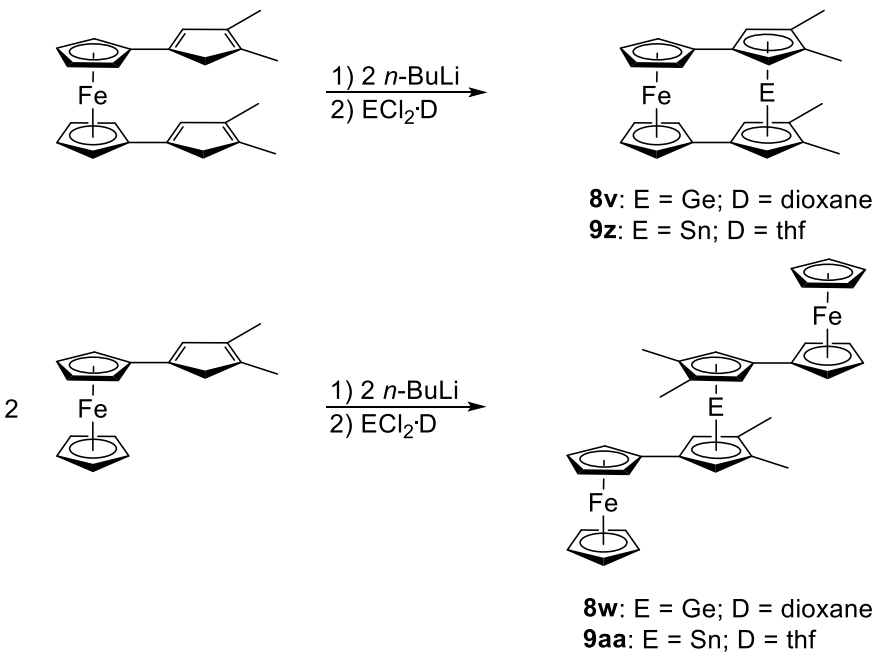

Scheme 117: Synthesis of mono- and bis(ferrocenyl) substituted tetrelocenes (**8v**, **8w**, **9z**, **9aa**) as conducted by Joudat *et al*.[182]

The obtained compounds (**8v**, **8w**, **9z**, **9aa**) were soluble in a broad bandwidth of solvents and stable under inert conditions at room temperature. In the structure in the solid state of **8v**, a bending angle δ of 154.8° and a Ge-Cp^{cent} distance of 221.95(5) pm are observed which are both similar to the values observed for germanocene (**8a**) (see Table 8). The signals in ^{119}Sn NMR spectra for **9z** (−2017 ppm) and **9aa** (−2071 ppm) are in line with the signals for known stannocenes (see Table 8).[182] The only example of a bis(phosphanyl) substituted stannocene (**9ab**) was reported by Cowley *et al*. in 1983. They synthesized this metallocene by lithiation of stannocene and subsequent reaction with (^{i}Pr$_2$N)$_2$PCl (Scheme 118).[158]

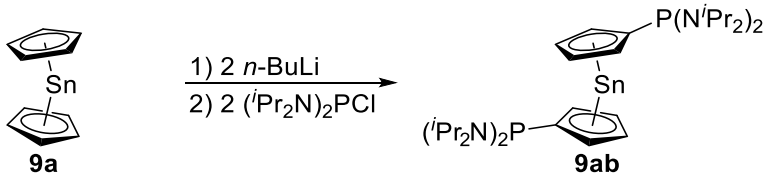

Scheme 118: Synthesis of di(bis[di*iso*propylamino]phosphanyl)stannocene (**9ab**) as carried out by Cowley *et al*.[158]

The structure in the solid state of **9ab** revealed a bending angle δ of 149.0° and Sn-Cp^{cent} distances of 237.88(6) pm and 238.68(6) pm, which is comparable to the angle δ observed in stannocene (**9a**) (δ = 143.8° and 147.1°) as well as the Sn-Cp^{cent} distances in **9a**.[158] In 2001, a stannocene (**9ac**) and a plumbocene (**10y**) with *iso*propyldimethylphosphine groups attached to the cyclopentadienyl ligand were reported by Bellabarba and coworkers (Scheme 119).[183]

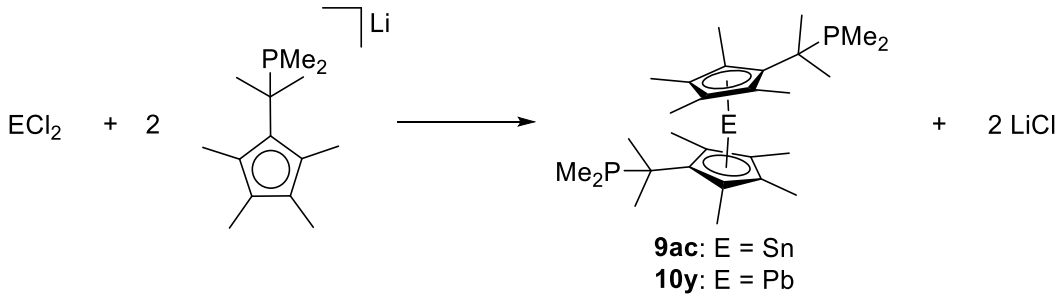

Scheme 119: Synthesis of bis(*iso*propyldimethylphosphine)octamethylstannocene (**9ac**) and -plumbocene (**10y**) as conducted by Bellabarba *et al*.[183]

The authors reported a signal at −2163 ppm in the ^{119}Sn NMR spectrum for **9ac**, which is in line with signals in ^{119}Sn NMR spectra for known stannocenes (see Table 8). The coordination chemistry of this complex was probed by addition of (COD)PtI_2 yielding in polymeric (**9ac**·PtI_2)$_x$, but unfortunately no analytical data was reported by Bellabarba *et al*. for this compound. In the ^{31}P NMR spectrum of **10y**, ^{31}P-^{207}Pb coupling was observed, which might be a prove for the complex to be formed. By addition of [$(C_6F_5)_3B$] to **10y**, the corresponding adduct **10y**·$B(C_6F_5)_3$ was formed, which was investigated by NMR spectroscopy displaying a signal typical for a tetracoordinate boron atom in the ^{11}B NMR spectrum with ^{11}B-^{31}P coupling, whereas no ^{31}P-^{207}Pb coupling was visible any more in the ^{31}P NMR spectrum. Further coordination chemistry studies conducted with (COD)$PdCl_2$ and (COD)PtI_2 resulted in (**10y**·$PdCl_2$)$_x$ and (**9ac**·PtI_2)$_x$, respectively. For (**10y**·$PdCl_2$)$_x$, the formation of the complex should be questioned due to multiple signals in the ^{31}P NMR spectrum which might also stem from different isomers formed according to the suggestion of the authors. The platinum complex, (**9ac**·PtI_2)$_x$, exhibited ^{31}P-^{195}Pt coupling in the ^{31}P NMR spectrum hinting toward formation of the product.[183] The authors did not report any structural data for these tetrelocenes or their coordination chemistry products, for which reason the results of these studies should be assessed carefully. In 1978, Bulten and Budding synthesized the only example of a stannyl substituted stannocene (**9ad**) by reaction of trimethyl(diethylamino)stannane with stannocene (Scheme 120).[184]

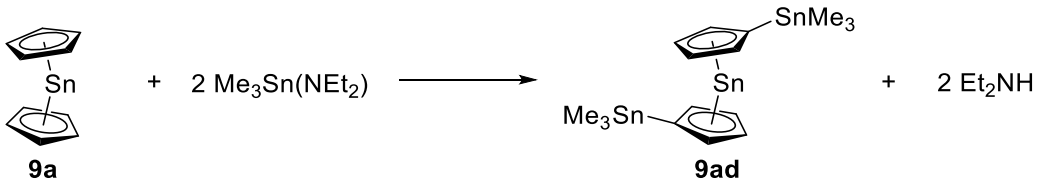

Scheme 120: Synthesis of bis(trimethylstannyl)stannocene (**9ad**) as carried out by Bulten and Budding.[184]

The authors described the product, $^{Me3Sn}Cp_2Sn$ (**9ad**), as an oil which could even be distilled (433 K; 10^{-2} mbar). Since no structural prove for the existence of **9ad** was provided, the formation of this complex must be doubted. Approaches of Bulten and Budding to attach more than one trimethyl(diethylamino)stannyl groups to the cyclopentadienyl rings of stannocene failed.[184]

To this point of the chapter, mostly homoleptic metallocenes have been discussed and a large variety of different substituents was introduced. Beginning with the only examples of heteroleptic germanocenes, ^{TMSx}CpGeCp* (x = 1, 2, 3), which were prepared by Jutzi *et al*. by transmetalation of the corresponding potassiumcyclopentadienide with Cp*GeCl (Scheme 121).[185]

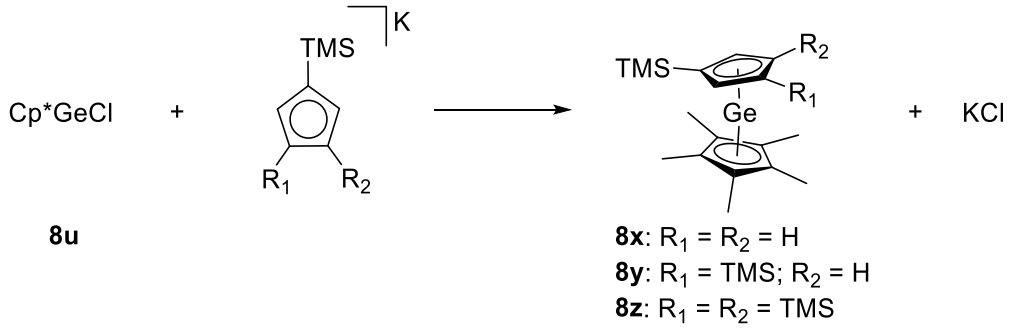

Scheme 121: Synthesis of heteroleptic germanocenes (**8x**-**z**) as conducted by Jutzi *et al*.[185]

Alternatively, these heteroleptic germanocenes could be obtained by reaction of **8aa**BF_4^- with the corresponding silyl substituted potassiumcyclopentadienide, whereas the reaction of **8u** with lithiumcyclopentadienide failed. The authors stated that no redistribution of the heteroleptic complexes to their homoleptic congeners was observed. These germanocenes (**8x**-**z**) exhibit a higher solubility in aliphatic solvents in comparison to **8c**, which is not further surprising in view of the bulkiness of the trimethylsilyl group.[185] In 1982, Cowley *et al*. presented a heteroleptic stannocene (**9ae**) and plumbocene (**10z**). Their synthetic route started from the phosphenium salt $[(^iPr_2N)_2P]^+AlCl_4^-$ with stannocene (**9a**) and plumbocene (**10a**) (Scheme 122).[186]

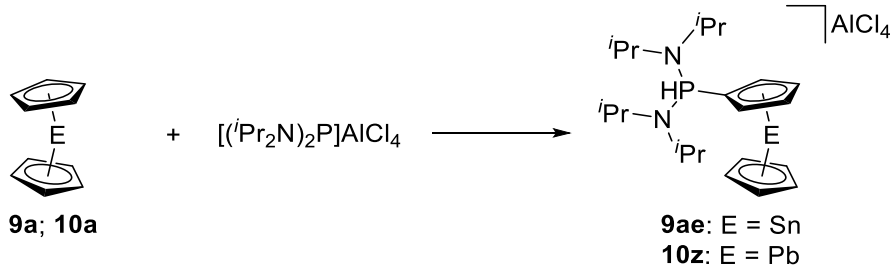

Scheme 122: Synthesis of **9ae** and **10z** as carried out by Cowley *et al*.[186]

A hint for the formation of these complexes was the ^{1}H-^{31}P coupling observed in the ^{31}P NMR spectrum, but no structural characterization could be carried out for these compounds.[186] The synthesis of acetyl and ester substituted heteroleptic stannocenes was reported by Dory *et al*. in 1985 (Scheme 123).[187]

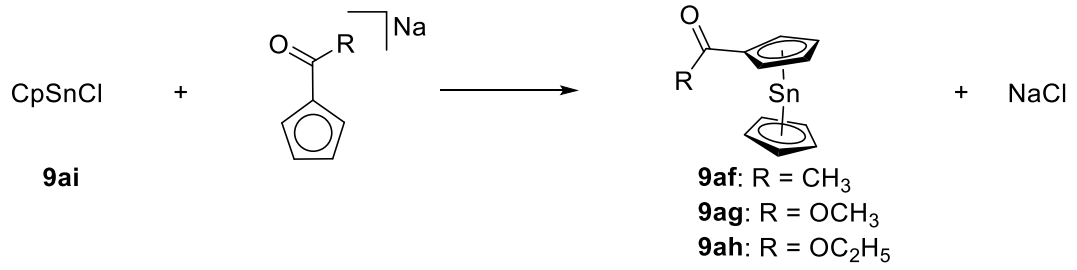

Scheme 123: Synthesis of heteroleptic, acetyl and ester functionalized stannocenes (**9af**-**ah**) as conducted by Dory *et al*.[187]

Unfortunately, no structural characterization could be performed by the authors for which reason it is questionable if these acetyl and ester substituted stannocenes (**9af**-**ah**) exist. Another hint against the existence of these compounds is a report by Jutzi *et al*. in which the authors attempted the synthesis of penta(methoxycarbonyl)stannocene and did not obtain the stannocene, but a tin atom coordinated by four oxygen atoms of the methoxycarbonyl groups which was confirmed by X-ray crystallography.[188] Notably, the authors failed to synthesize the homoleptic stannocenes and only obtained tin(IV)oxide. Because of the elevated electron density on the carbonyl function of the ligands used, they suggested tin(II)chloride to attack that functional group.[187] An example of a heteroleptic complex with an unsubstituted cyclopentadienyl ligand and an aryl substituted one was reported by Heeg *et al*. in 1988 (Scheme 124).[175]

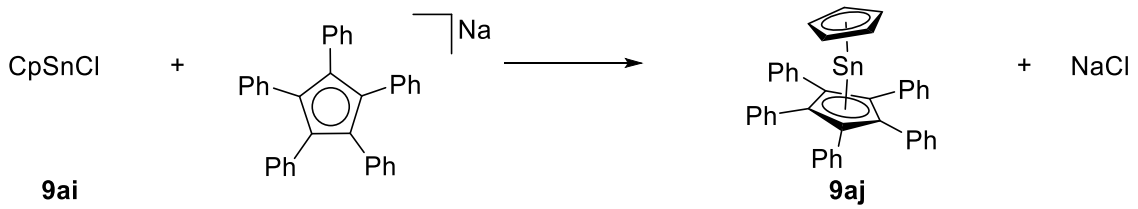

Scheme 124: Synthesis of pentaphenylstannocene (**9aj**) as carried out by Heeg *et al*.[175]

In the structure in the solid state of ^{Ph5}CpSnCp, **9aj**, a bending angle of 151.1° is observed, which is slightly larger than what is observed for stannocene. The distance Sn-^{Ph5}Cp^{cent} is by 9.5 pm longer than that to the unsubstituted Cp ligand (239.20(5) pm) which can be attributed to steric reasons. Notably, the Sn-^{Ph5}Cp^{cent} distance is by 8.6 pm longer than the Sn-Cp^{cent} distance in decaphenylstannocene (240.13(4) pm). This is another hint toward attractive interactions between the cyclopentadienyl ligands in decaphenylstannocene (**9p**).[174,175]

In the last part of this chapter, pnictogenyl substituted heterotetrelocenes and multidecker complexes of group 14 elements will be discussed briefly, even though their relevance for this thesis is limited. The first heterotetrelocene with a pnictogen atom was reported by Kuhn *et al*. in 1992.[189] The authors reported the synthesis of ($^{2,5\text{-}t\text{Bu}}$NC$_4$H$_2$)$_2$Pb (**10aa**) which was obtained by transmetalation (Scheme 125). In the following years, phosphorus and even antimony substituted heterotetrelocenes of germanium (one example), stannocene (three examples) and lead (eight examples) were reported (see Table 8).

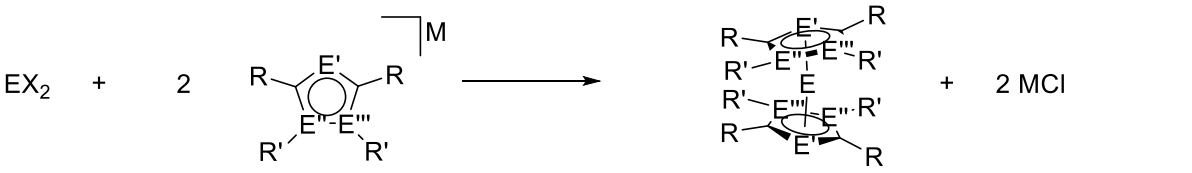

8ab: E = Ge; X = I; E' = P; E'' = E''' = C; R = ^{t}Bu; R' = H; M = Li
9ak: E = Sn; X = Cl; E' = P; E'' = E''' = C; R = ^{t}Bu; R' = H; M = Li
10aa: E = Pb; X = Cl; E' = N; E'' = E''' = C; R = ^{t}Bu; R' = H; M = Li
10ab: E = Pb; X = Cl; E' = P; E'' = E''' = C; R = ^{t}Bu; R' = H; M = Li
10ac: E = Pb; X = Cl; E' = P; E'' = E''' = C; R = ^{t}Bu; R' = Me; M = K
10ad: E = Pb; X = Cl; E' = P; E'' = E''' = C; R = TMS; R' = Me; M = K
10ae: E = Pb; X = Cl; E' = E'' = E''' = P; R = ^{t}Bu; M = Li

Scheme 125: Overview of heterotetrelocenes obtained by transmetalation.

Most of these heterotetrelocenes were obtained by transmetalation, one stannocene by transfer reaction with stannylated triphosphole[190] and one stannocene and one plumbocene by reaction of ECl$_2$ (E = Sn, Pb) with [MeP$_3$C$_3$^{t}Bu$_3$]Li.[191] In the case of the two heteroleptic heteroplumbocenes, 1:1 mixture of the lithiated ligands were mixed with lead(II)chloride and Cp*PbCl (**10af**) was reacted with the lithiated diphosphastibolyl ligand.[192] Since the only

heterogermanocene could not be crystallized, there is no clear evidence for the existence of this compound. The signal in the ^{119}Sn NMR spectrum of the heterotetrelocene ($^{2,5\text{-}t\text{Bu}}P_3C_2)_2Sn$ (**9al**) is significantly downfield shifted (δ ^{119}Sn = −1718 ppm[190]) compared to Cp''$_2$Sn, **9m**, presumably due to the difference in the bonding characteristics.[170,190] This trend can also be seen for the signals in the ^{207}Pb NMR spectra of the heteroplumbocenes, which also exhibit significant downfield shifted signals in the ^{207}Pb NMR spectra compared to other plumbocenes (see Table 8). The distances between the heterocyclopentadienyl ligands and the central atoms is elongated in comparison to the distances observed between cyclopentadienyl ligands and the central atoms presumably due to the difference in the bonding between the central atoms and heterocyclopentadienyl/cyclopentadienyl ligands (see Table 8).

In the field of multidecker group 14 complexes, several reports exist for germanium, tin and lead. In 1999, Beswick *et al*. reported the synthesis of $[Cp_3Sn]^-[Li(12\text{-crown-}4)_2]^+$ (**9am**) which was obtained by reaction of stannocene with lithiumcyclopentadienide and 12-crown-4 ether.[193] In 2005, Jones *et al*. synthesized the tripledecker $[(Cp^*Sn)_2(\mu\text{-}Cp^*)]^+[B(C_6F_5)_4]^-$ (**9an**) by the reaction of $Cp^*Sn^+B(C_6F_5)_4^-$ (**9ao**$B(C_6F_5)_4^-$) with Cp^*_2Sn (**9c**) (Figure 45).[194]

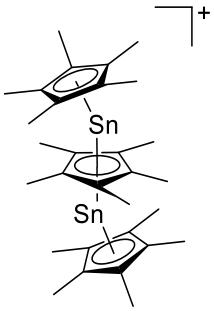

Figure 45: Cationic tin tripledecker compound.

In the ^{1}H NMR spectrum of this compound, only one signal was observed for the methyl groups of the Cp* ligand which came from, according to the authors, a fast equilibrium between the tripledecker complex and the corresponding halfsandwich compound Cp^*Sn^+ (**9ao**) and homoleptic decamethylstannocene (**9c**).[194] In this work, the authors also reported of an analogous compound for lead $[(Cp^*Pb)_2(\mu\text{-}Cp^*)]^+[B(C_6F_5)_4]^-$ (**10ah**).[194] In 2017, Schleep *et al*. reported the synthesis of the first quadruple decker of a main group element

$[Cp_4Sn_3]^{2+}[Al(ptfb)_4^-]_2$ (**9ap**) which was obtained by the reaction of $CpSn^+Al(ptfb)_4^-$ (**9aq**$Al(ptfb)_4^-$) with stannocene (**9a**) (Figure 46).[195]

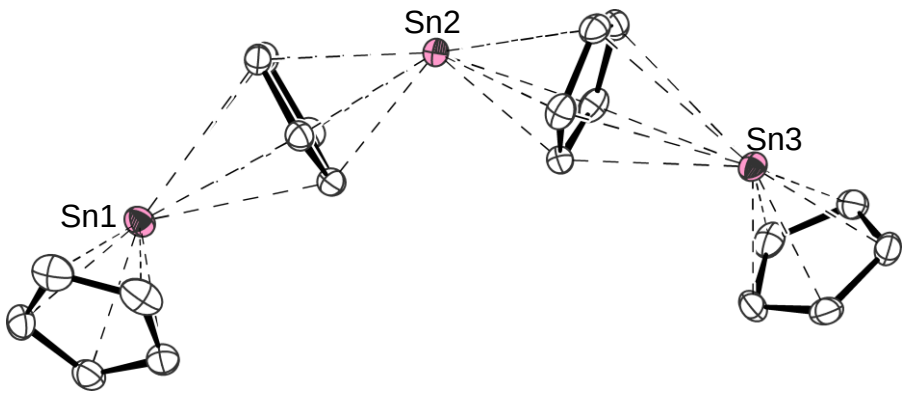

Figure 46: Molecular structure of $[Cp_4Sn_3]^{2+}$[98] in the crystal (hydrogen atoms and counter ions omitted for clarity, thermal ellipsoids at 50% probability level).

Initially, the authors intended the synthesis of a tripledecker complex analogous to the one reported by Jones *et al*. in 2005 (*vide supra*). Surprisingly, only one signal of −2318 ppm was observed in the ^{119}Sn NMR spectrum which is midway between $CpSn^+$ (−2429 ppm[195]) and Cp_2Sn (**9a**) (see Table 8). Also, the ^{1}H NMR spectrum displayed only one signal for the protons of the cyclopentadienyl ligands due to fast equilibrium between the quadruple complex, $CpSn^+$ and Cp_2Sn.[195] In 2020, Schorpp and Krossing synthesized several cationic cyclopentadienyl compounds of germanium and tin, for example the tripledecker complex $[CpGe(\mu\text{-}Cp)GeCp]^+[\mu\text{-}F\{Al(ptfb)_3\}_2]^-$ (**8ac**) and the cationic sandwich complex $[Ga(\mu\text{-}Cp)GeCp]^+[\mu\text{-}F\{Al(ptfb)_3\}_2]^-$ (**8ad**). The mean value of the Ge-Cp^{cent} distances in the tripledecker complex $[CpGe(\mu\text{-}Cp)GeCp]^+[\mu\text{-}F\{Al(pftb)_3\}_2]^-$ (**8ac**) is similar to the Ge-Cp^{cent} distance of neutral germanocenes and also the angle δ is similar to the one observed for germanocene (see Table 8). In $[Ga(\mu\text{-}Cp)GeCp]^+[\mu\text{-}F\{Al(ptfb)_3\}_2]^-$ (**8ad**), the distance between germanium and the terminal cyclopentadienyl ligand is with 194.85(12) pm significantly shorted in comparison to the Ge-Cp^{cent} distance in germanocene (see Table 8) which can be interpreted as a cationic $CpGe^+$ (**8ae**) unit to be present in this structure (Figure 47).

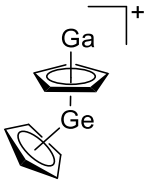

Figure 47: Cationic germanium cyclopentadienyl compound.

The structural characteristics of the stannocene moiety in the polymeric complex $[In(HMB)(\mu\text{-}Cp_2Sn)^+]_n[Al(ptfb)_4^-]_n$ (**9ar**) are similar to those of stannocene and also the signal in the ^{119}Sn NMR spectrum is close to that observed for stannocene (see Table 8). The structure of $[Ga(\mu\text{-}Cp)SnCp]^+[Al(ptfb)_4]^-$ (**9as**) in the solid state is analogous to the one observed for $[Ga(\mu\text{-}Cp)GeCp]^+[\mu\text{-}F\{Al(ptfb)_3\}_2]^-$ (**8ad**). The signal in the ^{119}Sn NMR spectrum for this cationic sandwich complex reveals the cationic nature of this compound since it appears in a region typical for cyclopentadienyl substituted stannyliumylidenes (see Table 11) and also the Sn-Cp^{cent} distance is significantly shortened in comparison to the one observed for stannocene (see Table 8).[196] In 2003, Layfield *et al*. reported the synthesis of $(thf)_2K^+(Cp_3Pb)^-$ (**10ah**) which was obtained by reaction of CpPbCl (**10ai**) with two equivalents cyclopentadienyl potassium. In the solid state, this complex exhibits a honeycomb layer structure. The Pb-Cp^{cent} distances are elongated in comparison to the ones observed for plumbocenes (see Table 8).[197] In 1995, Duer *et al*. reported of the mixed anion sandwich compound $[Li(12\text{-crown-}4)^+]_2[Cp_9Pb_4]^-$ $[Cp_5Pb_2]^-$ (**10aj**) which was synthesized by the reaction of three equivalents plumbocene (**10a**) with one equivalent lithiumcyclopentadienide and two equivalents 12-crown-4. In the crystal structure of this complex, a $[Cp_5Pb_2]^-$ and one $[Cp_9Pb_4]^-$ were obtained (Figure 48).

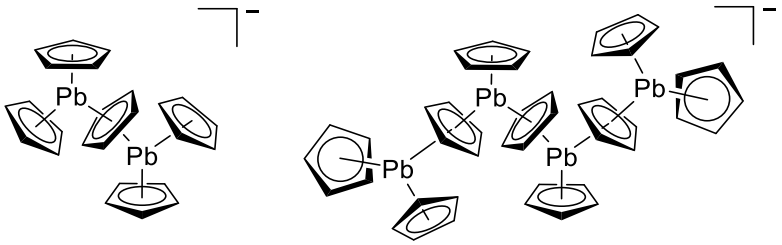

Figure 48: Anionic lead multidecker compound.

Interestingly, three signals were observed in the ^{207}Pb CP/MAS NMR spectrum for this compound which displays the different coordination environments of the lead atoms in this complex.[198] In 1999, Beswick *et al*. reported a series of different lead multidecker complexes, which all exhibit similar structural parameters and were obtained by reaction of plumbocene with lithiumcyclopentadienide and crown ethers or cryptands in different stoichiometries.[193]

Table 8: Heteronuclear NMR shifts, selected structural parameters and references for heavier group 14 metallocenes and related Lewis base adducts.

Compound	δ ^{119}Sn / ^{207}Pb [ppm]	Cp^{cent}-E-Cp^{cent} δ[°][c]	Cp^{cent}-E [pm][c]	Reference
Cp_2Ge (**8a**)	-	152.4	223.37(43)	[13,128]
$^{Me}Cp_2Ge$ (**8b**)	-	-	222[143][b]	[142,143]
Cp^*_2Ge (**8c**)		162.2[150]	220.80(2); 221.66(2)[150]	[144–146,150,151]
$^{(Me2tBuSi)}Cp^{\#}_2Ge$ (**8d**)	-	179.9	221.11(9); 221.15(9)	[154]
$^{TMS}Cp_2Ge$ (**8e**); $^{TMS2}Cp_2Ge$ (**8f**)	-	-	-	[157]
$^{TMS3}Cp_2Ge$ (**8g**)	-	171.8	225.00(21); 225.05(20)	[157]
Cp''_2Ge (**8h**)	-	-	-	[170]
$[Me_2Si[1](\eta^5\text{-}Cp^{\#}; Cp^{\#}H)]_2Ge$ (**8i**)	-	-	-	[171]
$^{Ph4}Cp_2Ge$ (**8j**); $^{(tBuPh)Ph4}Cp_2Ge$ (**8l**)	-	-	-	[172,173]
$^{Ph5}Cp_2Ge$ (**8k**)	-	-	-	[106,175]
$^{Bn5}Cp_2Ge$ (**8m**)	-	162.6[177]	223.87(7); 228.76(6)[177]	[176,177]
$^{(p\text{-}iPrBn)5}Cp_2Ge$ (**8n**)	-	160.9; 161.6	218.75(3); 220.70(4); 224.16(4); 226.01(3)	[178]
$^{(p\text{-}tBuPh)5}Cp_2Ge$ (**8o**)	-	179.9	224.18(2)	[58]
(0.5μ-PhCp*^{Me2}Cp)Ge (**8p**)	-	158.5	210.51(13); 228.70(15)	[181]
(0.5μ-PhCp*$Cp^{\#}$)Ge (**8q**); (0.5μ-biPhCp*$Cp^{\#}$)Ge (**8r**)	-	-	-	[181]
(0.5μ-C_4H_2SCp*^{Me2}Cp)Ge (**8s**); (0.5μ-C_4H_2SCp*$Cp^{\#}$)Ge (**8t**)	-	-	-	[180]
$[^{Fc}(^{Me2}Cp)_2]Ge$ (**8v**)	-	-	-	[182]
$[^{Fc}(^{Me2}Cp)]_2Ge$ (**8w**)	-	154.8	221.95(5)	[182]

$Cp^*Ge^{TMS}Cp$ (**8x**); $Cp^*Ge^{TMS2}Cp$ (**8y**); $Cp^*Ge^{TMS3}Cp$ (**8z**)	-	-	-	[185]
$(^{2,5\text{-}t\text{Bu}}PC_4H_2)_2Ge$ (**8ab**)	-	-	-	[199]
$[CpGe(\mu\text{-}Cp)GeCp]^+$ $[\mu\text{-}F\{Al(ptfb)_3\}_2]^-$ (**8ac**)	-	150.5; 153.4	203.72(3); 256.24(2)	[196]
$[Ga(\mu\text{-}Cp)GeCp]^+[\mu\text{-}F\{Al(ptfb)_3\}_2]^-$ (**8ad**)	-	146.7	194.85(12) (terminal); 267.16(12) (bridging)	[196]
Cp_2Sn (**9a**)	−2199[107,108]	143.8; 147.1[16]	237.02(8); 241.04(9); 243.69(8)[16]	[11,16,107,108,200–204]
$^{Me}Cp_2Sn$ (**9b**)	−2171[142]	-	240[143][b]	[14,142,143,204]
Cp^*_2Sn (**9c**)	−2129[111]; −2137[111][a]; −2140[111][a]	155.1[144]	239.77(4); 240.11(4)[144]	[111,144–146,205,206]
CpSnCp* (**9d**)	−2129	-	-	[139]
$(^{t\text{BuMe2Si}})Cp^{\#}_2Sn$ (**9e**)	−2204[155]; −2236[154][a]	179.9[154]	237.94(16)[154]	[154,155]
$^{TMS}Cp_2Sn$ (**9f**)	-	-	-	[158,159,169]
$^{TMS2}Cp_2Sn$ (**9g**)	-	-	-	[159]
$^{TMS3}Cp_2Sn$ (**9h**)	-	161.7	227.24(23); 268.32(33)	[159]
$^3Cp_2Sn$ (**9i**)	-	-	-	[164]
$^4Cp_2Sn$ (**9j**)	-	165.0	242.25(11); 242.39(12)	[164]
$^5Cp_2Sn$ (**9k**)	−2262[a]	179.9	248.66(5)	[165]
Cp'_2Sn (**9l**)	-	-	-	[169]
Cp''_2Sn (**9m**)	−2100	-	-	[170]
$[Me_2Si[1](\eta^5\text{-}Cp^{\#}; Cp^{\#}H)]_2Sn$ (**9n**)	−2166	-	-	[171]
$^{Ph4}Cp_2Sn$ (**9o**)	−2200[106][a]	-	-	[106,172,173]
$^{Ph5}Cp_2Sn$ (**9p**)	−2215[106][a]	179.9	240.13(4)	[106,174,175]
$(^{t\text{BuPh}})Ph4Cp_2Sn$ (**9q**)	−2235[106][a]	-	-	[106,172,173]
$^{Bn5}Cp_2Sn$ (**9r**)	-	155.9	241.4(1); 243.92(12)	[177]
$(^{p\text{-}n\text{BuPh}})5Cp_2Sn$ (**9s**)	−2190	179.9	240.29(1)	[147]
$(^{p\text{-}t\text{BuPh}})5Cp_2Sn$ (**9t**)	-	179.9	239.95(1)	[58]
$p\text{-}(Me(OCH2)2C)Ph5Cp_2Sn$ (**9u**)	-	-	-	[179]
$(0.5\mu\text{-}PhCp^{*Me2}Cp)Sn$ (**9v**)	−2110	-	-	[180]

(0.5μ-PhCp*Cp$^{\#}$)Sn (**9w**)	−2128	-	-	[180]
(0.5μ-biPhCp*Cp$^{\#}$)Sn (**9x**)	−2129	-	-	[180]
[^{Fc}(^{Me2}Cp)$_2$]Sn (**9z**)	−2017	-	-	[182]
[^{Fc}(^{Me2}Cp)]$_2$Sn (**9aa**)	−2071	-	-	[182]
$^{(i\text{Pr2N})2P}$Cp$_2$Sn (**9ab**)	-	149.0	237.88(6); 238.68(6)	[158]
^{Me2PCMe2}Cp$^{\#}_2$Sn (**9ac**)	−2163	-	-	[183]
[^{Me2PCMe2}Cp$^{\#}_2$Sn·PtI$_2$]$_x$ ([**9ac**·PtI$_2$]$_x$)	-	-	-	[183]
^{Me3Sn}Cp$_2$Sn (**9ad**)	-	-	-	[184]
[$^{(i\text{Pr2N})2PH}$CpSnCp]$^+$[AlCl$_4$]$^-$ (**9ae**)	-	-	-	[186]
^{MeCO}CpSnCp (**9af**); ^{MeOCO}CpSnCp (**9ag**); ^{EtOCO}CpSnCp (**9ah**)	-	-	-	[187]
^{Ph5}CpSnCp (**9aj**)	-	151.1[175]	239.20(5); 248.74(6)[175]	[106,175]
($^{2,5\text{-}t\text{Bu}}$PC$_4$H$_2$)$_2$Sn (**9ak**)	-	169.5; 169.6	243.83(2) – 250.21(2)	[199]
($^{2,5\text{-}t\text{Bu}}$P$_3$C$_2$)$_2$Sn (**9al**)	−1718	-	-	[190]
[Cp$_3$Sn]$^-$[Li(12-crown-4)$_2$]$^+$ (**9am**)	-	114.7; 116.2; 128.8	256.82(8); 266.37(7); 266.43(7)	[193]
[(Cp*Sn)$_2$(μ-Cp*)]$^+$[B(C$_6$F$_5$)$_4$]$^-$ (**9an**)	-	154.7	222.82(5); 261.35(7)	[194]
[Cp$_4$Sn$_3$]$^{2+}$[Al(ptfb)$_4^-$]$_2$ (**9ap**)	−2318	135.4 – 144.6	217.92(4) – 288.23(5)	[195]
[In(HMB)(μ-Cp$_2$Sn)$^+$]$_n$[Al(ptfb)$_4^-$]$_n$ (**9ar**)	−2179	147.9	237.93(21)	[196]
[Ga(μ-Cp)SnCp]$^+$[Al(ptfb)$_4$]$^-$ (**9as**)	−2331	137.1	214.43(8) (terminal); 279.29(8) (bridiging)	[196]
($^{2,4,5\text{-}t\text{Bu}}P_2C_3$)$_2$Sn (**9at**)	-	171.3	249.08(2); 250.93(2)	[191]
Cp$_2$Sn·tmeda (**9a**·tmeda)	-	131.4	251.63(6)	[98]
Cp$_2$Sn·[FeCp(CO)$_2$]$_2$ (**9a**·[FeCp(CO)$_2$]$_2$)	-	-	-	[135]
[Cp$_2$Sn(μ-Fe(CO)$_4$)]$_2$ ([**9a**(μ-Fe(CO)$_4$)]$_2$)	-	-	-	[133,134]
[Cp*$_2$Sn(μ-Fe(CO)$_4$)]$_2$ ([**9c**(μ-Fe(CO)$_4$)]$_2$)	-	-	-	[207]

Cp_2Pb (**10a**)	−5030[106]	112.1 – 135.3[15,140,141]	244.10(6) – 288.76(2)[15,140,141]	[12,15,106,140,141,200–202,208–211]
$^{Me}Cp_2Pb$ (**10b**)	-	-	-	[14,142]
Cp^*_2Pb (**10c**)	−4384[105]; −4390[111]; −4474[111][a]	151.3[16]	247.95(10); 252.34(8)[16]	[16,105,111,212]
$^{TMS2}Cp_2Pb$ (**10d**)	−4958[163]	171.0[163]	245.94(5); 250.46(5)[163]	[160,163]
$^{Et}Cp^{\#}_2Pb$ (**10e**)	-	-	-	[152]
$Cp^{\#}_2Pb$ (**10f**)	-	139.7	241.99(11); 253.84(17)	[153]
$^{i\mathrm{Pr}}Cp^{\#}_2Pb$ (**10g**)	-	-	-	[153]
$^{n\mathrm{Bu}}Cp^{\#}_2Pb$ (**10h**)	-	-	-	[153]
$^{(t\mathrm{BuMe2Si})}Cp^{\#}_2Pb$ (**10i**)	−4595; −4692[a]	179.9	245.96(10)	[156]
$^{TMS}Cp_2Pb$ (**10j**)	−4970[161]	110.2 – 126.4[161]	248.57(3) – 284.00(3)[161]	[160,161]
$^{TMS3}Cp_2Pb$ (**10k**)	-	-	-	[160]
$^{3}Cp_2Pb$ (**10l**)	-	179.9	247.04(3)	[166,167,213]
$^{4}Cp_2Pb$ (**10m**)	−4534	-	-	[168]
$^{5}Cp_2Pb$ (**10n**)	−3293	-	-	[168]
Cp''_2Pb (**10o**)	−4756	-	-	[170]
Cp'''_2Pb (**10p**)	−4230	-	-	[168]
$[Me_2Si[1](\eta^5\text{-}Cp^{\#}; Cp^{\#}H)]_2Pb$ (**10q**)	−4538	-	-	[171]
$^{Ph4}Cp_2Pb$ (**10r**); $^{(t\mathrm{BuPh})Ph4}Cp_2Pb$ (**10t**)	-	-	-	[172,173]
$^{Ph5}Cp_2Pb$ (**10s**)	−6150[106][a]	-	-	[106,175]
$^{Bn5}Cp_2Pb$ (**10u**)	-	153.5	249.91(16); 250.75(16)	[177]
$^{(p\text{-}t\mathrm{BuPh})5}Cp_2Pb$ (**10v**)	-	179.9	245.90(5)	[58]
$^{p\text{-}(Me(OCH2)2C)Ph5}Cp_2Pb$ (**10w**); $^{(Me(OEt)2C)Ph5}Cp_2Pb$ (**10x**);	-	-	-	[179]
$^{Me2PCMe2}Cp^{\#}_2Pb$ (**10y**); $^{Me2PCMe2}Cp^{\#}_2Pb{\cdot}B(C_6F_5)_3$ (**10y**·$B(C_6F_5)_3$); $[^{Me2PCMe2}Cp^{\#}_2Pb{\cdot}PdCl_2]_x$ ([**10y**·$PdCl_2$]$_x$); $[^{Me2PCMe2}Cp^{\#}_2Pb{\cdot}PtI_2]_x$ ([**10y**·PtI_2]$_x$)	-	-	-	[183]
$[^{(i\mathrm{Pr2N})2PH}CpPbCp][AlCl_4]$ (**10z**)	-	-	-	[186]
$(^{2,5\text{-}t\mathrm{Bu}}NC_4H_2)_2Pb$ (**10aa**)	−4142	142.7; 143.9	245.94(7) – 247.63(6)	[189]

($^{2,5\text{-}t\text{Bu}}PC_4H_2)_2Pb$ (**10ab**)	−3163[214]	169.7[199]	250.24(1) – 255.57(1)[199]	[199,214]
($^{2,5\text{-}t\text{Bu}}PC_4Me_2)_2Pb$ (**10ac**)	−2592	174.0	254.53(2); 254.64(2)	[214]
($^{2,5\text{-TMS}}PC_4Me_2)_2Pb$ (**10ad**)	−2728	-	-	[214]
($^{2,5\text{-}t\text{Bu}}P_3C_2)_2Pb$ (**10ae**)	−3752	-	-	[192]
$[(Cp^*Pb)_2(\mu\text{-}Cp^*)]^+[B(C_6F_5)_4]^-$ (**10ag**)	-	152.6	233.77(5); 267.18(6)	[194]
$(thf)_2K\cdot(Cp_3Pb)^-$ (**10ah**)	-	120.0	264.00(1); 264.08(1); 264.09(1)	[197]
$[Li(12\text{-crown-}4)^+]_2[Cp_9Pb_4]^-$ $[Cp_5Pb_2]^-$ (**10aj**)	−4740[a]; −5180[a]; −5270[a]	115.0 – 127.7	254.3 – 291.9	[198]
($^{2,4,5\text{-}t\text{Bu}}P_2C_3)_2Pb$ (**10ak**)	-	170.4	255.22(2); 256.78(2)	[191]
$Cp^*Pb(^{2,5\text{-}t\text{Bu}}P_3C_2)$ (**10al**)	−3951	142.1	235.60(13); 275.37(12) (Pnict)	[192]
$Cp^*Pb(^{2,5\text{-}t\text{Bu}}P_2SbC_2)$ (**10am**)	-	142.2	235.7; 275.5 (Pnict)	[192]
$[Cp_2Pb(\mu\text{-}Cp)Pb^-(\mu\text{-}Cp)Cs(18\text{-crown-}6)^+]$ (**10an**)	-	114.2 – 129.7	254.88(15) – 299.40(21)	[193]
$[Cp_5Pb_2]^-[K(2,2,2\text{-crypt})]^+\cdot(thf)$ (**10ao**)	-	115.6 – 127.1	255.02(23) – 285.16(26)	[193]
$[Cp_5Pb_2]^-[Li(12\text{-crown-}4)_2]^+\cdot(thf)_2$ (**10ap**)	-	111.4 – 127.6	258.35(18) – 296.29(24)	[193]
$[Cp_2Pb(\mu\text{-}Cp)^-Na(15\text{-crown-}5)^+]$ (**10aq**)	-	118.6 – 120.3	261.10(32); 276.02(68)	[193]
$Cp_2Pb\cdot$tmeda (**10a**·tmeda)	-	128.8	258.72(6)	[98,99]
$Cp_2Pb\cdot Me_2$bipy (**10a**·Me_2bipy)	-	139.7	259.00(5)	[98,99]

[a]: Detected by CP/MAS NMR spectroscopy; [b]: Determined by electron diffraction spectroscopy; [c]: Only given in the case of η^5 coordination of cyclopentadienyl ligand or pnictogenyl substituted five membered ring to element.

1.9 Group 14 Halfsandwich Compounds

Complexes of the type CpER, which are related to tetrelocenes, and CpE^+ (E = Si-Pb) are referred to as group 14 halfsandwich compounds. In the field of CpER (R = Cl-I), only examples of the heavier elements germanium, tin and lead exist. The cyclopentadienyltetrel(II) halides represent suitable starting materials for the synthesis of other halfsandwich compounds. In the solid state, these compounds sometimes reveal dimeric or polymeric structures in dependency of the cyclopentadienyl ligand attached to the tetrel atom. The structurally characterized examples of CpER compounds exhibit hapticities of η^1, η^2 or η^3 (see Figure 1) in the solid state.

Cationic cyclopentadienyl compounds of the type CpE^+ formally belong to the class of tetryliumylidenes, which are compounds of the type RE^+ and exhibit two vacant p orbitals and one lone pair making them highly Lewis amphiphilic (Figure 49).

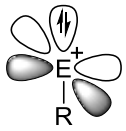

Figure 49: Depiction of frontier orbitals in a tetryliumylidene.

It should be mentioned that these tetryliumylidenes can also be viewed as cluster compounds, in which the tetrel atom contributes its remaining unpaired electron to the bonding in the cluster. If one counts the skeletal electrons according to PSEPT (polyhedral skeletal electron pair theory, sometimes also referred to as Wade's rules), the observed *nido* structure of these compounds is correctly predicted.

Hereinafter, the CpER and CpE^+ systems of group 14 elements will be discussed in descending order from silicon to lead.

In the chemistry of silicon halfsandwich compounds, the Cp^*Si^+ cation (**7b**) has proven to be an useful synthetic building block for further cyclopentadienylsilicon compounds. The pentamethylcyclopentadienylsilicon cation (**7b**$B(C_6F_5)_4^-$) was synthesized in 2004 by the reaction of decamethylsilicocene with $Cp^*H_2^+B(C_6F_5)_4^-$ to afford the corresponding silyliumylidene in a selective reaction (Scheme 126).[102]

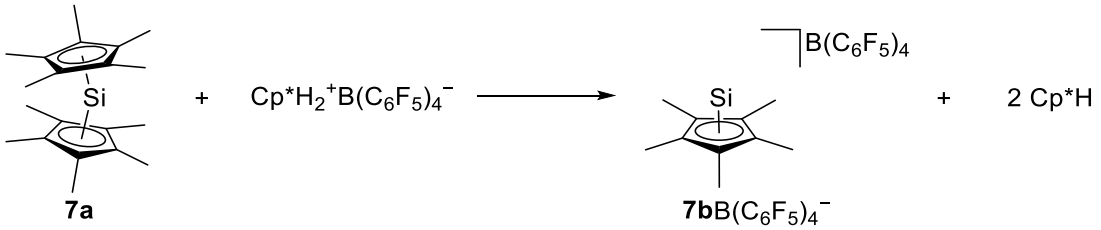

Scheme 126: Synthesis of silyliumylidene $Cp^*Si^+B(C_6F_5)_4^-$ (**7b**$B(C_6F_5)_4^-$) as conducted by Jutzi *et al*.[102]

This silyliumylidene was not stable with tetrafluoroborate as counterion due to formation of the labile Cp*SiF but require the very weakly coordinating $B(C_6F_5)_4^-$ as counterion. Jutzi *et al*. described the obtained Cp^*Si^+ (**7b**) as very sensitive toward oxidation and hydrolysis. The authors were able to perform X-ray crystallographic analysis on this complex revealing an η^5 complexed silicon atom with a Si-Cp^{cent} distance of 176.25(6) pm, which is, as expected, significantly shortened in comparison to the Si-Cp^{cent} distances in **7a** (211.38(2) pm to 212.05(23) pm) due to the elevated electrophilicity of Cp^*Si^+. In the ^{29}Si NMR spectrum of this silyliumylidene, a signal is observed at −400 ppm, which is only shifted by 2 ppm in comparison to decamethylsilicocene. To probe the reactivity of **7b**$B(C_6F_5)_4^-$, Jutzi *et al*. reacted it with lithium bis(trimethylsilyl)amide and obtained the corresponding disilene $Cp^*(N[TMS]_2)Si$ (**7h**), resulting from the dimerization of the initially formed transient silylene, displaying the electrophilic character of this silyliumylidene.[102,113,114] This electrophilic character of **7b**$B(C_6F_5)_4^-$ was further exploited only two years later by Jutzi *et al*. to synthesize new heteroleptic silicocenes which were already discussed (*vide supra*).[117] By reaction of the heteroleptic complex ^{5}CpSiCp* (**7g**) with $(Et_2O)H^+Al(ptfb)_4^-$, the penta-*iso*propylcyclopentadienylsilicon cation $^5CpSi^+Al(ptfb)_4^-$ (**7i**$Al(ptfb)_4^-$) could be obtained (Scheme 127).[117]

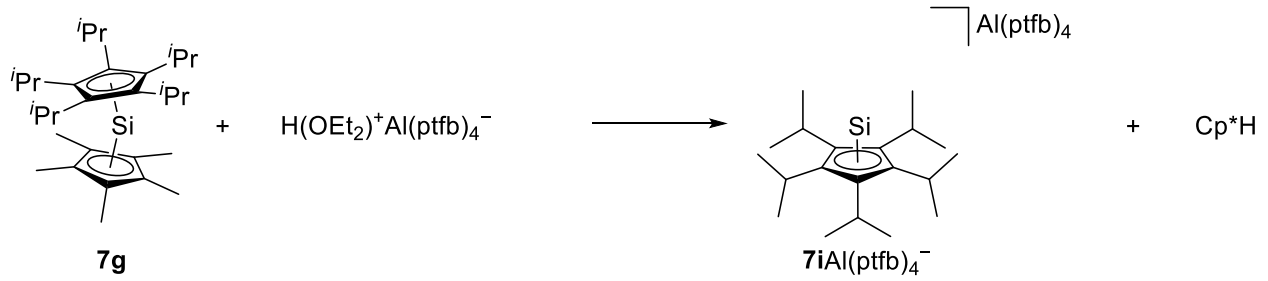

Scheme 127: Synthesis of ^{5}CpSi^{+}Al(ptfb)$_4^-$ (**7i**Al(ptfb)$_4^-$) as carried out by Jutzi *et al*.[117]

Jutzi and coworkers were able to crystallize **7i**Al(ptfb)$_4^-$ but unfortunately those crystals were of poor quality so only the structure for the cationic part could be determined (Figure 50).[117]

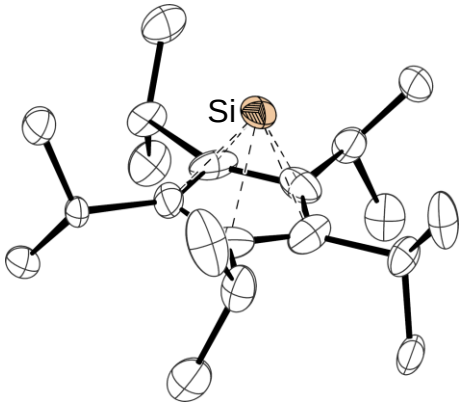

Figure 50: Molecular structures of penta-*iso*propylcyclopentadienylsilicon cation (**7i**)[117] in the crystal (hydrogen atoms and tetra(perfluoroalkoxy)aluminate omitted for clarity, thermal ellipsoids at 50% probability level).

When comparing the structures of the two cyclopentadienylsilicon cations, no significant structural differences can be identified since the Si-Cp^{cent} distances are equal (see Table 9). Inspecting the signals of both cations in the ^{29}Si NMR spectrum, there is also no significant difference. It is still surprising that the signals of decamethylsilicocene and both cations differ only marginally in view of the differences observed in the electronic structure.[117] In 2009, Jutzi *et al*. reacted **7b**B(C$_6$F$_5$)$_4^-$ with Li(2,6-(Trip)$_2$C$_6$H$_3$) and obtained a pentamethylcyclopentadienylsilicon aryl complex (Scheme 128).[215]

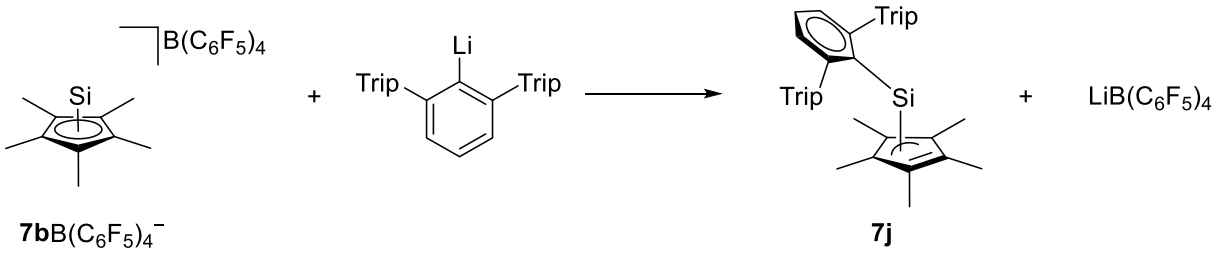

7b$B(C_6F_5)_4^-$ **7j**

Scheme 128: Synthesis of pentamethylcyclopentadienylsilicon(2,6-$(Trip)_2C_6H_3$) (**7j**) as carried out by Jutzi *et al*.[215]

In the structure in the solid state, the aryl substituent is σ bonded to the silicon atom and the Cp* ligand is η^3 complexed to the silicon atom. The Si-Cp^{cent} distances measure 209.64(20) pm, 226.78(19) pm and 228.21(18) pm which is elongated in comparison to the Si-Cp^{cent} distances in decamethylsilicocene (**7a**) (see Table 8). The signal in the ^{29}Si NMR spectrum of Cp*Si(2,6-$(Trip)_2C_6H_3$), **7j**, appears at 52 ppm, which is significantly downfield shifted compared to the signal for decamethylsilicocene or the starting material **7b**$B(C_6F_5)_4^-$ (see Table 8 and Table 9). A fluxional behavior with regards to the hapticity of the cyclopentadienyl ligand of this compound could be demonstrated by the authors under usage of ^{1}H and ^{13}C NMR spectroscopy.[215] One year later, Jutzi *et al*. obtained a bimetallic complex by the reaction of **7b**$B(C_6F_5)_4^-$ and Cp*$Fe(CO)_2^-Na^+$ (Scheme 129).[216]

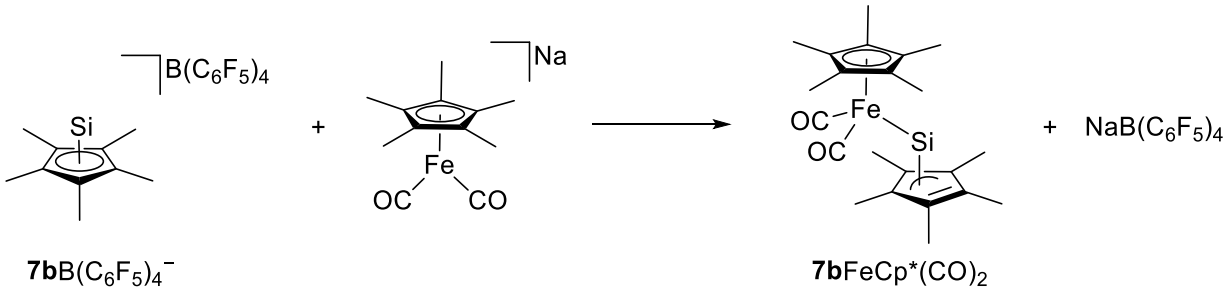

7b$B(C_6F_5)_4^-$ **7b**Fe Cp*$(CO)_2$

Scheme 129: Synthesis of Cp*SiFeCp*$(CO)_2$ (**7b**FeCp*$(CO)_2$) as carried out by Jutzi *et al*.[216]

Interestingly, this reaction takes place selectively only in hexane. If the reaction is conducted in a dme/hexane mixture, **7a**, $[Cp^*Fe(CO)_2]_2$ and elemental silicon are obtained as reaction prod-ucts. In solution, this complex decomposes under oxidative addition of one methyl group of the Cp* ligand attached to the iron atom to form a Si-H and a Si-CH_2 bond. The crystal structure of this compound revealed an η^3 complexed silicon atom with a Fe-Si bond.

The bonding situation between the silicon atom and the pentamethylcyclopentadienyl ligand is similar to that observed in **7j** with Si-Cp^{C} distances of 213.62(18) pm, 221.03(19) pm and 243.49(19) pm. The Si-Fe bond in this compound is with 236.77(6) pm elongated in comparison to $H_3SiFeCp^*(CO)_2$ (Si-Fe distance: 228.7(2) pm[217]). The ^{29}Si NMR spectrum of **7b**$FeCp^*(CO)_2$ exhibits a signal at 317 ppm, which is extremely downfield shifted compared to decamethylsilicocene or $Cp^*Si^+B(C_6F_5)_4^-$.[216] In 2011, Jutzi *et al*. demonstrated the potential of **7b**$B(C_6F_5)_4^-$ in the degradation of ethers and were able to isolate adducts of this silyliumylidene with dme and 12-crown-4 ether (Scheme 130).[218]

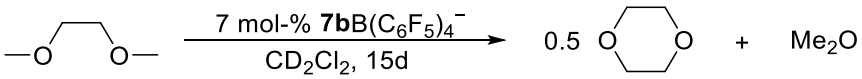

Scheme 130: Degradation of ethers catalyzed by **7b**$B(C_6F_5)_4^-$ on the example of the degradation of dme as conducted by Jutzi *et al*.[218]

The dme adduct of $Cp^*Si^+B(C_6F_5)_4^-$ decomposes slowly under formation of 1,4-dioxane and dimethylether (Scheme 130). In the structures in the solid state of these adducts of **7b**$B(C_6F_5)_4^-$, hapticities of η^5 with a tendency toward η^3 were observed with Si-Cp^{cent} distances of 180.57(5) pm (dme adduct) and 182.57(3) pm and 183.53(66) pm (12-crown-4 adduct) which are marginally elongated in comparison to the Si-Cp^{cent} distance in the starting material. This slightly elongation of the Si-Cp^{cent} distance displays the weak Si-donor bond which is also suggested by the authors in accordance with the ease of loss of dme of the adduct. By performing DFT-calculations, Jutzi *et al*. could demonstrate that in the coordination sphere of the cationic part, two dme molecules are weakly bonded to form 1,4-dioxane and dimethylether. The signals in the ^{29}Si NMR spectra of both adducts exhibit only small deviations from the starting material with −399 ppm for the dme adduct and −402 ppm for the 12-crown-4 adduct.[218] One year later, Leszczyńska *et al*. reported on the reaction of **7b**$B(C_6F_5)_4^-$ with two equivalents $Trip_2Si{=}SiTrip(Li[dme]_2)$ which afforded the neutral silicon cluster Si_6Trip_6.[219] In the same year, Inoue and Leszczyńska presented the synthesis of an imidazolin-2-iminato stabilized pentamethylcyclopentadienyl substituted silylene (**7k**) (Scheme 131).[220]

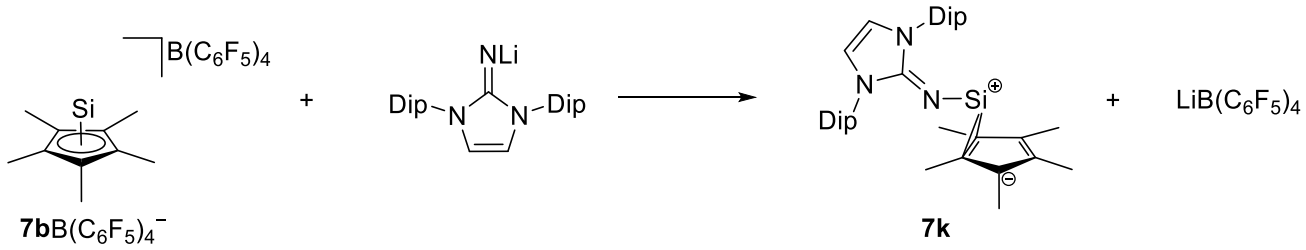

Scheme 131: Synthesis of Cp*Si(NIPr) (**7k**) as carried out by Inoue and Leszczyńska.[220]

In the structure in the solid state of **7k**, the silicon atom is coordinated in an η^2 fashion to the Cp* ligand with Si-Cp^C distances of 212.43(62) pm and 221.79(62) pm. This coordination mode in the solid state is not reflected in solution as can be seen in the ^{1}H NMR and ^{13}C NMR spectra of this compound.[220] A related compound, Cp*(N[TMS]$_2$)Si, **7h**, exhibits a monomeric structure in solution, but a dimeric structure in the solid state.[221] However, this behavior was not found for Cp*Si(NIPr), **7k**, presumably due to the steric demand of the imidazolin-2-iminato ligand. In the ^{29}Si NMR spectrum of this compound, a signal was found at −44 ppm which is significantly downfield shifted in comparison to the starting material as a consequence of the coordination of the imidazolin-2-iminato ligand.[220] By reaction of Cp*Si(NIPr) (**7k**) with B(C$_6$F$_5$)$_3$, the borane adduct Cp*Si(NIPr)[B(C$_6$F$_5$)$_3$] (**7l**) was obtained (Scheme 132).[220]

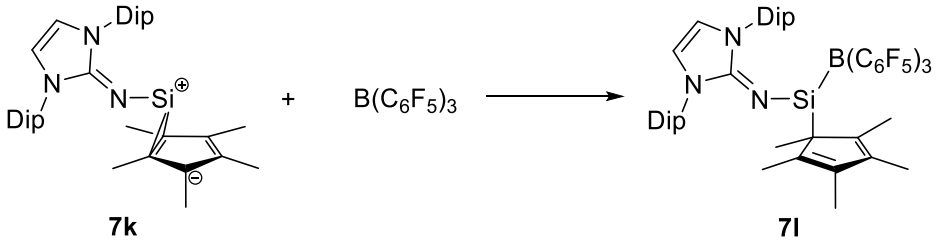

Scheme 132: Synthesis of Cp*Si(NIPr)[B(C$_6$F$_5$)$_3$] (**7l**) as conducted by Inoue and Leszczyńska.[220]

In the solid state structure of **7l**, the silicon atom is σ bonded to the pentamethylcyclopentadienyl ligand with a Si-Cp^C bond length of 190.54(37) pm. The Si-N bond in this compound measures 160.55(31) pm, which is shortened in comparison to 169.00(45) pm found in Cp*Si(NIPr). The authors stated that a π bonding interaction between the silicon and nitrogen atom is present in this borane adduct which was underpinned by DFT calculations.[220]

A silylidyne complex bearing the pentamethylcyclopentadienyl ligand was reported by Ghana *et al*. in 2018 (Scheme 133).[115]

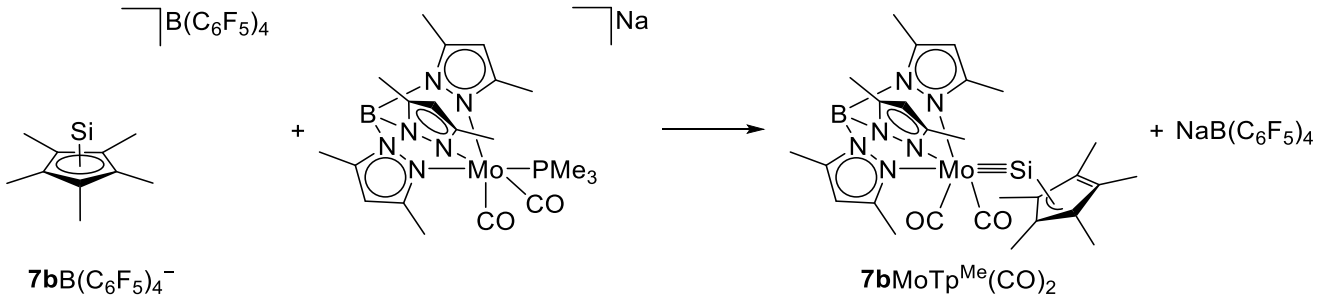

Scheme 133: Synthesis of molybdenum silylidyne complex (**7b**MoTp^{Me}(CO)$_2$) as carried out by Ghana *et al*.[115]

The silylidyne ligand replaces the trimethylphosphine ligand at the molybdenum centre in this complex according to an elevated level of σ donor strength of the silylidyne ligand in comparison to the phosphine ligand and, in addition, **7b** works as an oxidizing reagent for the Na[Tp^{Me}Mo(CO)$_2$PMe$_3$]. In the structure in the solid state, a very short Mo-Si bond length was revealed with 230.92(4) pm speaking for a Mo-Si triple bond (one σ bond, two π bonds) to be present in this complex reflecting perfectly the electronic situation of this silyliumylidene. The silicon atom is complexed in an η^3 fashion to the cylopentadienyl ligand with Si-Cp^C distances of 207.78(17) pm, 215.79(19) pm and 217.10(19) pm, which are significantly shortened in comparison to the Si-Cp^C bond lengths observed for **7b**FeCp*(CO)$_2$ and **7j** indicating stronger Si-Cp^C bonds in **7b**MoTp^{Me}(CO)$_2$ (*vide supra*). The signal in the ^{29}Si NMR spectrum at −272 ppm for this silylidyne complex clearly shows the difference in the bonding of silicon to the transition metal in comparison to the signal for **7b**FeCp*(CO)$_2$ (δ ^{29}Si = 317 ppm) which is shifted significantly downfield.[115] In 2019, Leszczyńska *et al*. reacted Cp*$_2$Si (**7a**) with an anionic silicon cluster (Si$_6$Trip$_5^-$Li$^+$) where the Cp*Si unit could be mounted into this cluster to obtain the cluster Si$_7$Trip$_5$Cp*, which was confirmed by single crystal X-ray crystallography.[222] By reaction of pentamethylcyclopentadienyl tribromosilane with hypersilylpotassium (KSi[TMS]$_3$), Leszczyńska *et al*. obtained the heteroleptic silylene Cp*SiSi(TMS)$_3$ (**7m**) in 2020 (Scheme 134).[223]

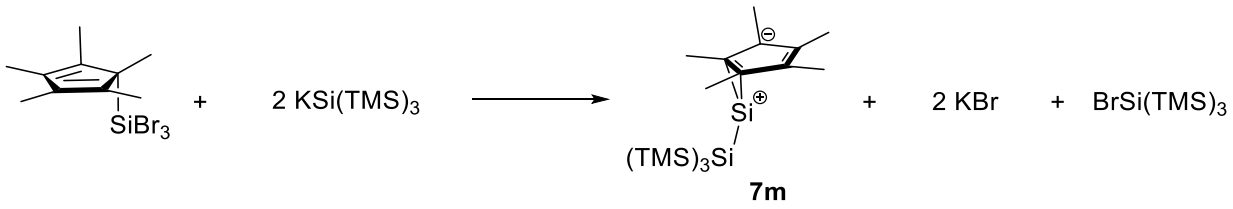

Scheme 134: Synthesis of Cp*SiSi(TMS)$_3$ (**7m**) as conducted by Leszczyńska *et al*.[223]

In the structure in the solid state of **7m**, a monomeric complex was revealed with a silicon atom exhibiting a hapticity of η^2 to the Cp* ligand with bond lengths of 209.97(19) pm and 211.19(19) pm, which are shortened in comparison to the Si-Cp^C distances in **7k** (*vide supra*). In the ^{29}Si NMR of **7m**, a signal at 207 ppm appeared for the silylene type silicon atom which is significantly downfield shifted compared to the signal for **7a** (δ ^{29}Si = −398 ppm), but in the typical region for “classical” silylenes. By conducting DFT calculations, the authors were able to show that the HOMO-LUMO gap of this compound seems to be uncommonly small which was accompanied by the purple color of this silylene in the solid state and the downfield shifted signal in ^{29}Si NMR of **7m**. To prove the high reactivity of this compound as suggested by the small HOMO-LUMO gap, the authors reacted **7m** with ethylene and obtained the corresponding adduct which could also be crystallized and investigated by single crystal X-ray analysis. In the structure in the solid state of this compound, the central silicon atom is σ bonded to the Cp* ligand with a Si-Cp^C distance of 191.17(10) pm. In the ^{29}Si NMR spectrum for this compound, a signal for the Cp* bonded silicon atom is observed at −100 ppm reflecting the change in the bonding mode by oxidative addition of ethylene. In this context, Leszczyńska *et al*. could demonstrate that **7m** activates dihydrogen at room temperature and 1 bar pressure. The reaction of **7m** with Me$_4$NHC afforded **7m**·Me$_4$NHC (Scheme 135).[223]

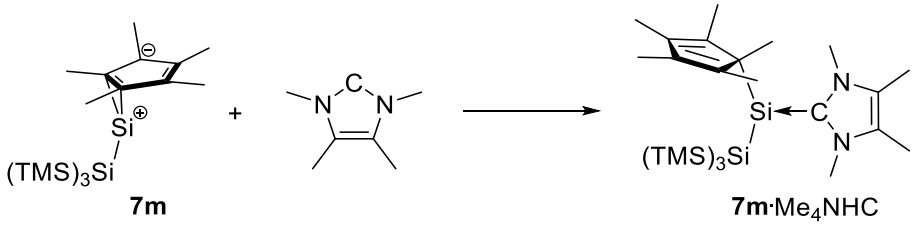

Scheme 135: Synthesis of Cp*Si(Me$_4$NHC)Si(TMS)$_3$ (**7m**·Me$_4$NHC) as conducted by Leszczyńska *et al*.[223]

The structure in the solid state revealed a σ bonded silicon atom with a Si-Cp^C distance of 204.56(11) pm, which is elongated in comparison to the ethylene adduct due to weakening of the Si-Cp bond by coordination of the NHC to the silicon centre. This effect of NHC coordination is also reflected by the signal in the ^{29}Si NMR spectrum which is significantly downfield shifted compared to the starting material **7m** (δ ^{29}Si = 207 ppm). By reaction of **7m** with the heavier homologue of a NHC, a *N*-heterocyclic silylene (NHSi), Leszczyńska *et al*. obtained an unexpected product (Scheme 136).[223]

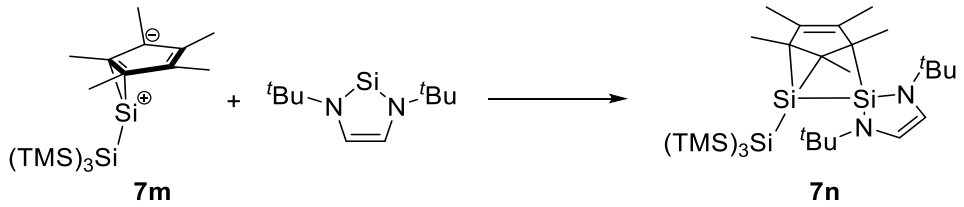

Scheme 136: Reaction between **7m** and ^{t}Bu$_2$NHSi as carried out by Leszczyńska *et al*.[223]

In this product, the former Cp* ligand bridged the two silicon atoms derived from **7m** and ^{t}Bu$_2$NHSi. The ^{29}Si NMR spectrum of this compound derived two signals for the bridged silicon atoms (−106 ppm; −21 ppm).[223] In 2021, Sen *et al*. reacted Cp*(N[TMS]$_2$)Si (**7h**) with aluminum(III)chloride and -bromide as well as with diphenylchlorophosphine (Scheme 137).[224]

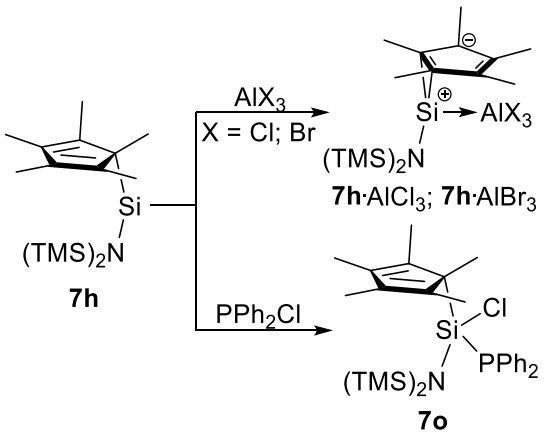

Scheme 137: Synthesis of Lewis adducts of Cp*(N[TMS]$_2$)Si (**7h**) with aluminum(III) halides and oxidative addition of diphenylchlorophospine at silicon center of Cp*(N[TMS]$_2$)Si (**7h**) as conducted by Sen *et al*.[224]

In the crystal structures of the Lewis adducts of **7h** with aluminum(III)chloride and -bromide, donor-acceptor complexes are obtained with almost similar Si-Al bond lengths (**7h**·$AlCl_3$: 246.76(10) pm; **7h**·$AlBr_3$: 246.3(5) pm). In both structures, the silicon atom exhibits a hapticity of η^2 to the cyclopentadienyl ligand with very similar bond lengths (Si-Cp^C bonds range from 203.0(1) pm to 203.7(1) pm). In the structure in the solid state of Cp*Si[$N(TMS)_2$]Cl(PPh_2) (**7o**), the silicon atom is bonded *via* a σ bond to the Cp* ligand with a Si-Cp^C distance of 192.52(18) pm which is similar to the Si-CpC distance observed for Cp*Si(H_2C=CH_2)$Si(TMS)_3$ (191.17(10) pm[223]).[224]

Starting from **7b**$B(C_6F_5)_4^-$, which was obtained by protonation of decamethylsilicocene, several silicon halfsandwich compounds were synthesized in the last decades. Furthermore the application as a catalyst for the degradation of ethers could be demonstrated.[218] For **7m**, the activation of small molecules could be outlined.[223] In 2018, a silylidyne complex (**7b**$MoTp^{Me}(CO)_2$), was presented, verifying the suitability of the Cp*Si fragment as ligand for transition metal complexes.

Table 9: ^{29}Si NMR shifts, selected structural parameters and references of cyclopentadienylsilicon halfsandwich compounds.

Compound	δ ^{29}Si [ppm]	Hapticity Cp η	Cp-Si [pm][a]	Reference
Cp*$Si^+B(C_6F_5)_4^-$ (**7b**$B(C_6F_5)_4^-$)	−400	5	176.25(6)	[102]
Cp*SiFeCp*$(CO)_2$ (**7b**FeCp*$(CO)_2$)	317	3	202.03(5)	[216]
Cp*$Si^+B(C_6F_5)_4^-$·dme (**7b**$B(C_6F_5)_4^-$·dme)	−399	5	180.57(5)	[218]
Cp*$Si^+B(C_6F_5)_4^-$·(12-crown-4) (**7b**$B(C_6F_5)_4^-$·(12-crown-4))	−402	5	182.57(3); 183.53(66)	[218]
Cp*SiMo$Tp^{Me}(CO)_2$ (**7b**$MoTp^{Me}(CO)_2$)	−272	3	187.23(4)	[115]
[Cp*(N[TMS]$_2$)Si]$_2$ ([**7h**]$_2$)	−10	1	194.51(13); 194.72(13)	[102,221]
^{5}CpSi$^+$Al(ptfb)$_4^-$ (**7i**Al(ptfb)$_4^-$)	−397	5	176.11(17)	[117]
Cp*Si(2,6-(Trip)$_2C_3H_6$) (**7j**)	52	3	196.75(5)	[215]
Cp*Si(NIPr) (**7k**)	−44	2	204.98(16)	[220]
Cp*Si(NIPr)[$B(C_6F_5)_3$] (**7l**)	115	1	190.54(37)	[220]

$Cp^*SiSi(TMS)_3$ (**7m**)	207	2	197.80(5)	[223]
$Cp^*Si(H_2C{=}CH_2)Si(TMS)_3$ (**7m**·$H_2C{=}CH_2$)	−100	1	191.16(11)	[223]
$Cp^*Si(Me_4NHC)Si(TMS)_3$ (**7m**·Me_4NHC)	−16	1	204.56(11)	[223]
$(TMS)_3SiSi(\mu\text{-}Cp^*)^tBu_2NHSi$ (**7n**)	−106	2	177.07(22)	[223]
$Cp^*Si[N(TMS)_2]Cl(PPh_2)$ (**7o**)	4 – 6	1	192.52(16)	[224]
$Cp^*SiCl[N(TMS)_2](BCy_3)$ (**7p**)	−6	1	194.33(37)	[224]
$Cp^*Si[N(TMS)_2]\cdot AlCl_3$ (**7h**·$AlCl_3$)	−13	2	189.35(7)	[224]
$Cp^*Si[N(TMS)_2]\cdot AlBr_3$ (**7h**·$AlBr_3$)	−18	2	189.45(29)	[224]

[a]: Given to the centre of silicon-cyclopentadienyl bond.

Descending the group 14, the oxidation state +II becomes more favored which might be the reason why a half-sandwich silicon(II) halide is unknown, and germanium half-sandwich halides are only known for Cp*, while the CpSnX and CpPbX are well-known compounds.

In the field of halide substituted germanium halfsandwich compounds, cyclopentadienylgermanium chloride was never isolated, only *ab initio* calculations to this compound exist.[225] The Cp*GeCl (**8u**) was first synthesized by the group of Jutzi, about ten years after the synthesis of CpSnCl (**9ai**), by reaction of Cp*Li with germanium(II)chloride dioxane complex (Scheme 138).[226]

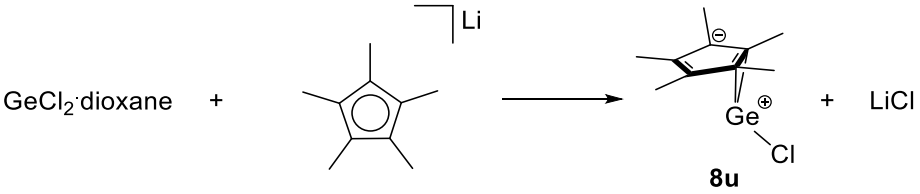

Scheme 138: Synthesis of pentamethylcyclopentadienylgermanium chloride (**8u**) as carried out by Jutzi *et al*.[226]

Alternatively, mixing equimolar amounts of decamethylgermanocene with germanium(II)chloride dioxane complex also afforded **8u**. Since this reaction seemed to be fast, the formed pentamethylcyclopentadienylgermanium chloride must be more stable than decamethylgermanocene (**8c**) and germanium(II)chloride dioxane complex.[226] To shed light onto the structural details of **8u**, a gas phase electron diffraction study (GED) was carried out by Fernholt *et al*. in 1984.[227] The authors reported for **8u** a structure similar to what was observed for CpSnCl (**9ai**) with a Ge-Cl bond of 225.8(12) pm and a hapticity of η^2 or η^3 (three short Ge-Cp^C distances of 230 pm, 254 pm and 268 pm).[227] In 1998, the structure of Cp*GeCl (**8u**) in the solid state could be revealed by Winter and coworkers. The germanium atom exhibits an η^2 bonding mode to the cyclopentadienyl ligand with Ge-Cp^C distances of 221.43(29) pm and 222.10(27) pm (Figure 51).[228]

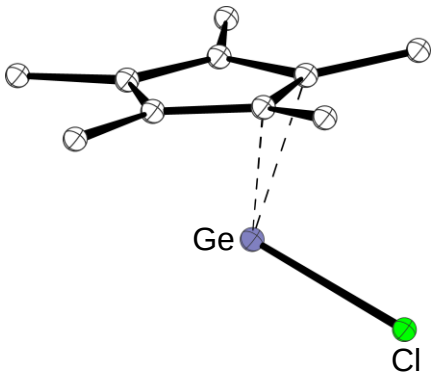

Figure 51: Molecular structure of pentamethylcyclopentadienylgermanium chloride (**8u**)[228] in the crystal (hydrogen atoms omitted for clarity, ball-and-stick representation).

In the solid state, **8u** possesses a monomeric structure (Ge-Cl bond length: 238.40(9) pm; shortest Ge-Cl contact: 415.26(11) pm) without additional Ge-Cl contacts which is in sharp contrast to what is observed in the crystal structures of analogous tin compounds (*vide infra*).[228] In 2010, a detailed study to the structure of **8u** was published by Rohr *et al*. where two different types of structures were reported.[229] One of these structures was similar to that observed by Winter *et al*. and the other was a polymeric structure (crystals were obtained by crystallization from thf) with elongated Ge-Cl bonds (242.95(3) pm) and Ge-Cl contacts (360.67(4) pm) which are significantly shortened in comparison to the Ge-Cl contacts in the structure reported by Winter and coworkers.[228,229] This polymeric structure is similar to the one observed for CpSnCl, **9ai**, reported by Bos *et al*. in 1975.[230] Rohr *et al*. conducted concentration dependent ^{1}H NMR spectroscopy on Cp*GeCl, **8u,** and demonstrated that the formation of higher aggregated species is favored at higher concentrations while at lower concentrations monomeric **8u** is observed in solution.[229] By addition of hydrogen bromide to **8c** the corresponding heteroleptic Cp*GeBr (**8af**) is formed which was reported by Winter *et al*. in 1998 (Scheme 139).[228]

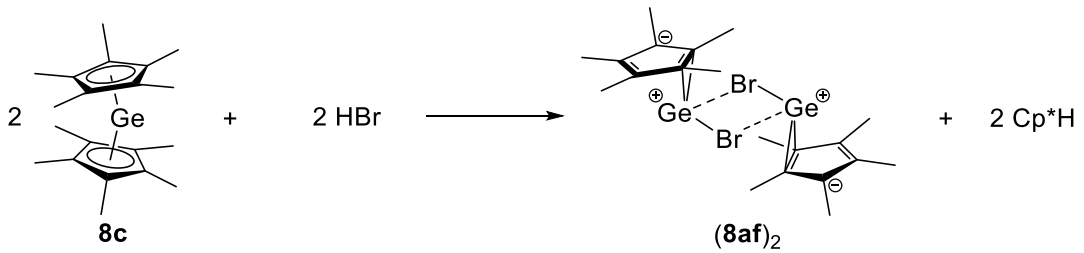

Scheme 139: Synthesis of $(Cp^*GeBr)_2$ $(\mathbf{8af})_2$ as conducted by Winter *et al*.[228]

In the solid state, a dimeric structure was observed for Cp*GeBr (**8af**) with a Ge-Br bond length of 270.56(12) pm and a Ge-Br contact of 313.29(12) pm. The hapticity of the germanium atom in Cp*GeBr can be seen as η^2 (Ge-Cp^C distances of 220.11(47) pm and 229.29(53) pm), similar to that observed in Cp*GeCl, but with a tendency toward η^1. This bromogermylene was slightly less soluble in pentane than the corresponding chlorogermylene.[228] The iodogermylene, Cp*GeI, was reported by Filippou *et al*. in 2002. The authors synthesized this compound by reaction of Cp*GeCl with sodiumiodide (Scheme 140).[231]

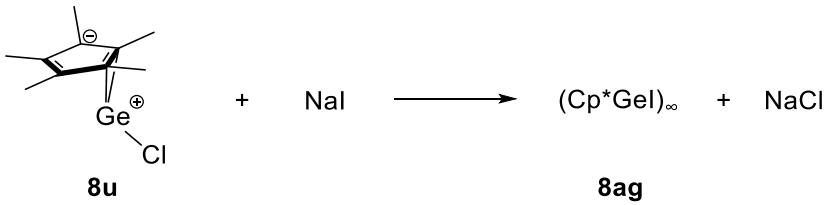

Scheme 140: Synthesis of $(Cp^*GeI)_\infty$ (**8ag**) as conducted by Filippou *et al*.[231]

Filippou and coworkers stated in this work that this iodogermylene (**8ag**) exists as a polymer in the solid state.[231] An example of a germanium halfsandwich compound with a donor substituted cyclopentadienyl ligand was reported by Jutzi *et al*. in 1995. The (dimethylaminoethyl)tetramethylcyclopentadienylgermanium chloride (**8ah**) was prepared by reaction of the corresponding lithium cyclopentadienide with germanium(II)chloride dioxane complex (Scheme 141).[232]

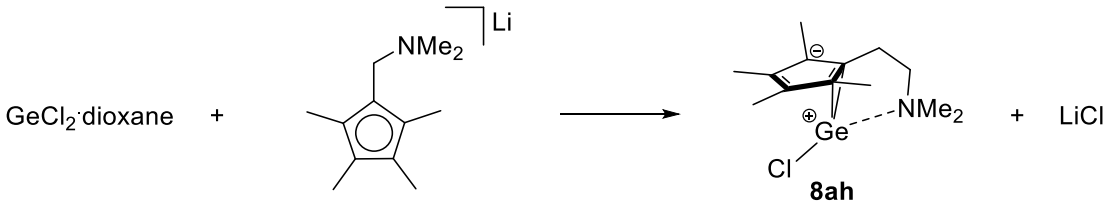

Scheme 141: Synthesis of (dimehtylaminoethyl)tetramethylcyclopentadienylgermanium chloride (**8ah**) as carried out by Jutzi *et al*.[232]

The structure of this amino supported germylene (**8ah**) exhibits a monomeric structure in the solid state with a Ge-Cl bond length of 236.85(14) pm and a Ge-N bond length of 228.61(31) pm (Figure 52).

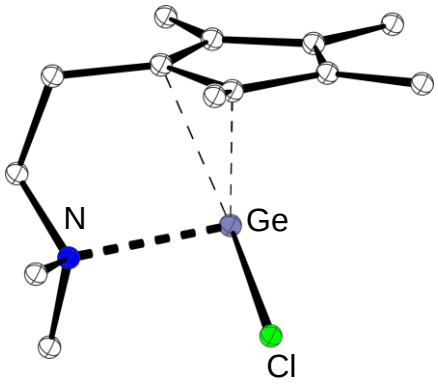

Figure 52: Molecular structure of (dimehtylaminoethyl)tetramethylcyclopentadienylgermanium chloride (**8ah**)[232] in the crystal (hydrogen atoms omitted for clarity, ball-and-stick representation).

By comparison of the Ge-Cl distance in **8ah** with the one observed in Cp*GeCl (**8u**) (Ge-Cl bond length in monomeric Cp*GeCl: 238.40(9) pm[228]), it becomes visible that the Ge-Cl bond in **8ah** is significantly elongated which can be reasoned with the increased electron density caused by the coordination of the amino moiety to the germanium atom and, by that, a weakening of the Ge-Cl bond. The hapticity in **8ah** can be seen as η^2 with a strong tendency toward η^1 (Ge-Cp^C distances of 218.07(37) and 240.19(34) pm), which is different from the η^2 bonding mode observed in **8u**.[228,232] This change in hapticity can also be assigned to the coordination of the dimethylamino group to the germanium atom. **8ah** is stable at room temperature and inert toward air oxidation for several days.[232] The only germyliumylidene bearing an unsubstituted cyclopentadienyl ligand was reported by Schorpp *et al*. in 2020 (Scheme 142).[196]

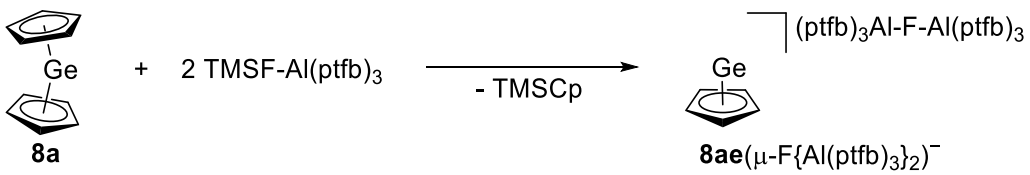

Scheme 142: Synthesis of CpGe$^+$(μ-F{Al(ptfb)$_3$}$_2$)$^-$ (**8ae**(μ-F{Al(ptfb)$_3$}$_2$)$^-$) as carried out by Schorpp *et al*.[196]

The germanium atom in this structure exhibits a hapticity of η^5 with Ge-Cp^{cent} distances of 187.63(19) pm and 189.18(11) pm which is comparable to Ge-Cp^{cent} distances of Cp^*Ge^+ complexes.[196] This is surprising, since the Cp* ligand possesses more steric demand than the unsubstituted cyclopentadienyl ring and therefore, the Ge-Cp* distances should be elongated in comparison to the Ge-Cp distance, but presumably due to the higher electron density obtained at the π system of the Cp* ligand, a relatively strong bond is observed. In 1980, Jutzi *et al*. described the synthesis of the germyliumylidene **8aa**BF_4^- which was synthesized by reaction of decamethylgermanocene, **8c**, with tetrafluoroboric acid (Scheme 143).[144]

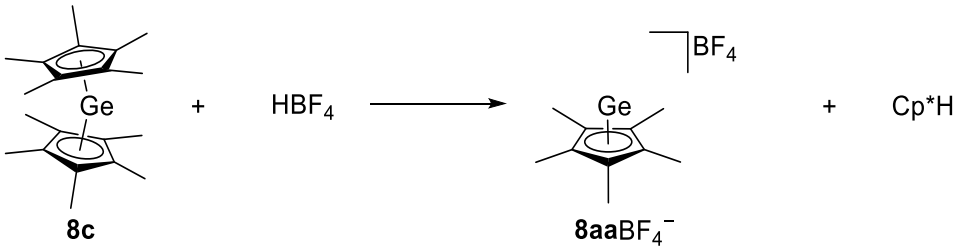

Scheme 143: Synthesis of $Cp^*Ge^+BF_4^-$ (**8aa**BF_4^-) as conducted by Jutzi and coworkers.[144]

As to be expected, germyliumylidene **8aa**BF_4^- was only sparingly soluble in aromatic solvents like toluene, but good soluble in polar solvents.[144] The structure of this cationic complex could be revealed by Winter *et al*. in 1998. In analogy to the silyliumylidene **7b**$B(C_6F_5)_4^-$, the germanium atom exhibits an η^5 coordination to the pentamethylcyclopentadienyl ligand with a Ge-Cp^{cent} distance of 189.73(6) pm. This η^5 bonding mode is corroborated by the high degree of aromaticity in the pentamethylcyclopentadienyl ligand indicated by the equal Cp^C-Cp^C distances.[228] The change in hapticity of the cationic complex **8aa**BF_4^- in comparison to Cp*GeCl (**8u**) can be attributed to the increased electrophilic character of the germyliumylidene compared to the chlorogermylene. In the following years, several germyliumylidenes bearing the pentamethylcyclopentadienyl ligand with various counter ions have been prepared mostly by halide abstraction (Scheme 144), but structurally characterized compounds of this type are rare (*vide infra*).

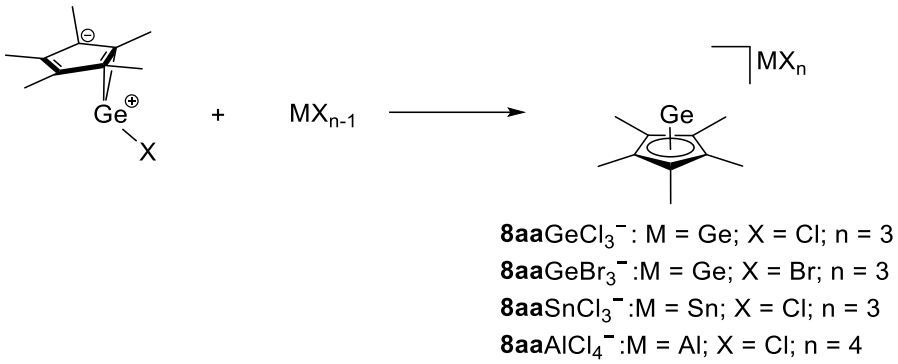

Scheme 144: Syntheses of pentamethylcyclopentadienyl substituted germyliumylidenes by halide abstraction.

In 2002, Rouzaud *et al*. presented the solid state structure of **8aa**$SnCl_3^-$ which was prepared simply by reaction of Cp*GeCl (**8u**) with tin(II)chloride (Scheme 144).[180] The germanium atom in **8aa**$SnCl_3^-$ exhibits an η^5 bonding mode to the pentamethylcyclopentadienyl ligand with a Ge-Cp^{cent} distance of 192.75(39) pm which is almost similar to what is observed for the Ge-Cp^{cent} distance in **8aa**BF_4^- (see Table 10).[180] In 2021, Sen *et al*. were able to structurally characterize **8aa**$AlCl_4^-$, which was obtained by the reaction of Cp*(N[TMS]$_2$)Si (**7h**) with aluminum(III)chloride and germanium(II)chloride dioxane complex (Scheme 145).[224]

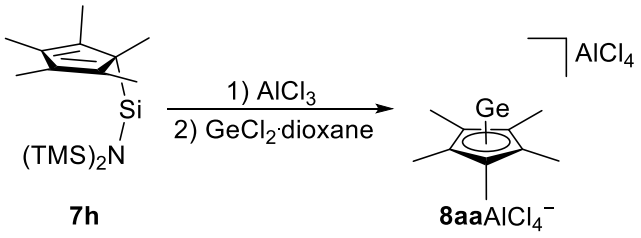

Scheme 145: Synthesis of Cp*$Ge^+AlCl_4^-$ (**8aa**$AlCl_4^-$)as conducted by Sen *et al*.[224]

In the structure in the solid state of **8aa**$AlCl_4^-$, the germanium atom is attached in an η^5 fashion to the cyclopentadienyl ligand with a Ge-Cp^{cent} distance of 191.38(5) pm similar to what was found for related germyliumylidenes (see Table 10).[224] Since the usage of the free Cp* ligand (Cp*H) as a leaving group is a common synthetic pathway in the chemistry of group 14 halfsandwich compounds, Jutzi *et al*. reported the synthesis of **8aa**$^{(COOMe)5}Cp^-$ starting from Cp*$_2$Ge (**8c**) and $H^{(COOMe)5}Cp$ in 1984(Scheme 146).[188]

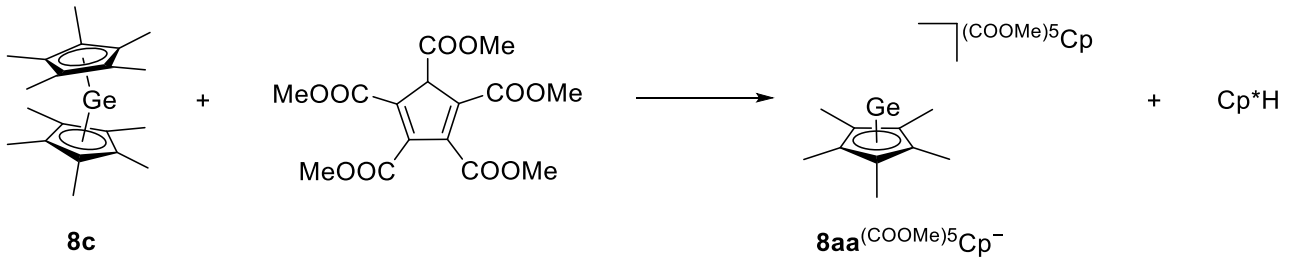

8c **8aa**$^{(COOMe)5}Cp^-$

Scheme 146: Synthesis of $Cp^*Ge^{+(COOMe)5}Cp^-$ (**8aa**$^{(COOMe)5}Cp^-$) as conducted by Jutzi *et al*.[188]

This germyliumylidene, **8aa**$^{(COOMe)5}Cp^-$ was only sparingly soluble in aromatic solvents, but good soluble in dichloromethane which is a hint toward the ionic structure of this compound.[188] Unfortunately, no X-ray crystallographic analysis of this compound could be conducted for which reason the postulated structure should be assessed carefully especially in view of the product obtained by reaction of Cp^*_2Sn (**9a**) with two equivalents of penta(methoxycarbonyl)cyclopentadiene.[188] Another example of a Cp^*Ge^+ (**8aa**) complex was reported by Jutzi *et al*., namely **8aa**OTf^-, which was synthesized starting from Cp*GeCl (**8u**) and TMSOTf (Scheme 147).[233]

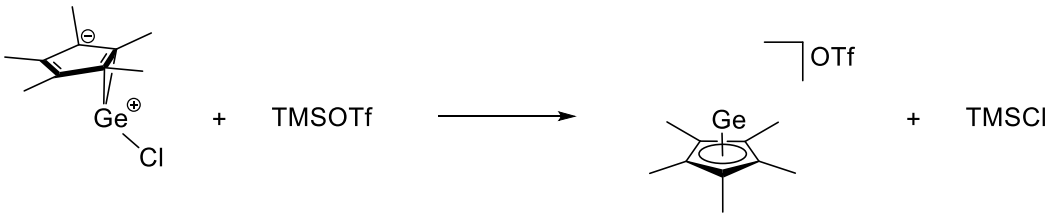

8u **8aa**OTf^-

Scheme 147: Synthesis of $Cp^*Ge^+OTf^-$ (**8aa**OTf^-) as carried out by Jutzi *et al*.[233]

In this reaction, the affinity of the trimethylsilyl group to chlorine is the driving force. In analogy to the synthesis of **8aa**BF_4^-, Jutzi *et al*. synthesized **8ai**BF_4^- by protonation of di-*tert*-butylgermanocene (**8h**) with tetrafluoroboric acid (Scheme 148).[170]

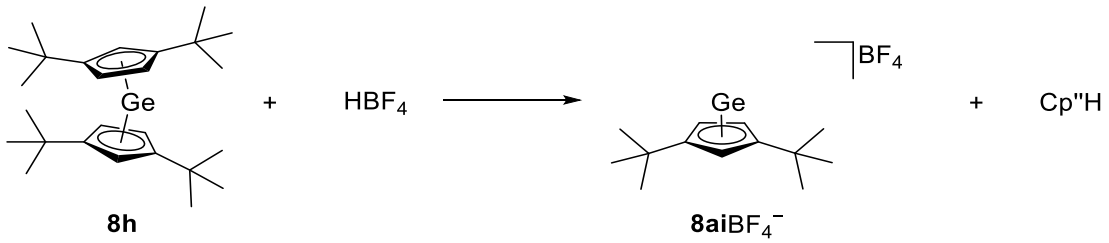

Scheme 148: Synthesis of Cp''Ge^{+}BF$_4^{-}$ (**8ai**BF$_4^{-}$) as conducted by Jutzi *et al*.[170]

This cationic complex, **8ai**BF$_4^{-}$, was soluble in aromatic solvents and exhibited a higher stability toward air oxidation than its Cp* congener.[170] With the more bulky *tert*-butyl substituted Cp ligand, tri-*tert*-butylcyclopentadiene Cp''', the corresponding germyliumylidene, **8aj**GeCl$_3^{-}$, was synthesized by Ding *et al*. in 2021 (Scheme 149).[234]

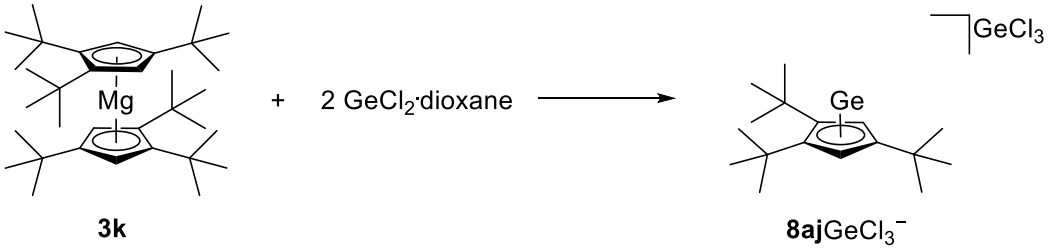

Scheme 149: Synthesis of Cp'''Ge^{+}GeCl$_3^{-}$ (**8aj**GeCl$_3^{-}$) as conducted by Ding *et al*.[234]

In the crystal structure of **8aj**GeCl$_3^{-}$, an η^5 bonding mode of the germanium atom to the cyclopentadienyl ligand with a Ge-Cp^{cent} distance of 193.41(4) pm (Figure 53).

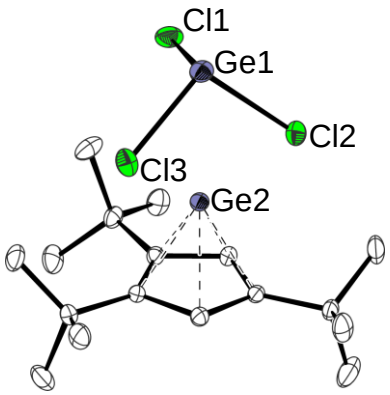

Figure 53: Molecular structure of Cp'''Ge^{+}GeCl$_3^{-}$ (**8aj**GeCl$_3^{-}$)[234] in the crystal (hydrogen atoms omitted for clarity, thermal ellipsoids at 50% probability level).

This structure represents a contact ion pair since the Ge-Cl contacts between the germanium atom attached to the cyclopentadienyl ligand and $GeCl_3^-$ ion measure 316.99(7) to 336.50(8) pm which is significantly less than the sum of the van der Waals radii (386 pm).[234] In 1986 and 1991, the Jutzi group reacted Cp*GeCl with different lithium reagents to obtain heteroleptic germylenes (Scheme 150).[185,235]

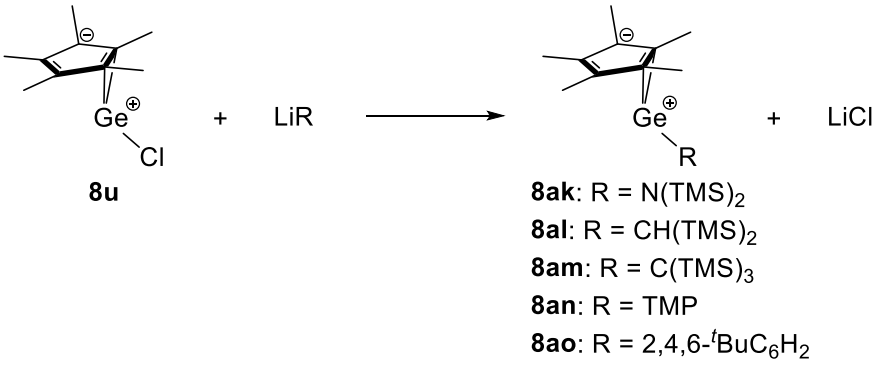

Scheme 150: Syntheses of heteroleptic germylenes as conducted by Jutzi *et al*.[185,235]

All germylenes synthesized are sensitive to air, but **8am** was the most stable of these compounds. Crystallization of **8al** revealed a germanium atom η^2 complexed to the Cp* ligand with Ge-Cp^C distances of 224.24(58) and 224.85(69) pm which is comparable to the Ge-Cp^C distances observed in **8u**.[185,228] In the solid state structure of **8am**, Ge-Cp^C distances of 224.74(11) and 229.45(10) pm in line with a hapticity of η^2 are observed which is only slightly elongated in comparison to the ones observed in **8al**.[185,235] The Ge-C^{TMS} distances are 204.41(60) pm (**8al**) and 213.45(97) pm (**8am**). The difference in the observed Ge-C^{TMS} distances can be explained with the increased steric demand of the ligand in **8am**.[185,235] For **8ao**, a structure similar to the structures of **8al** and **8am** was observed.[235] In 1985, Jutzi *et al*. explored **8u** as ligand for chromium- and tungstenpentacarbonyl complexes (Scheme 151).[236]

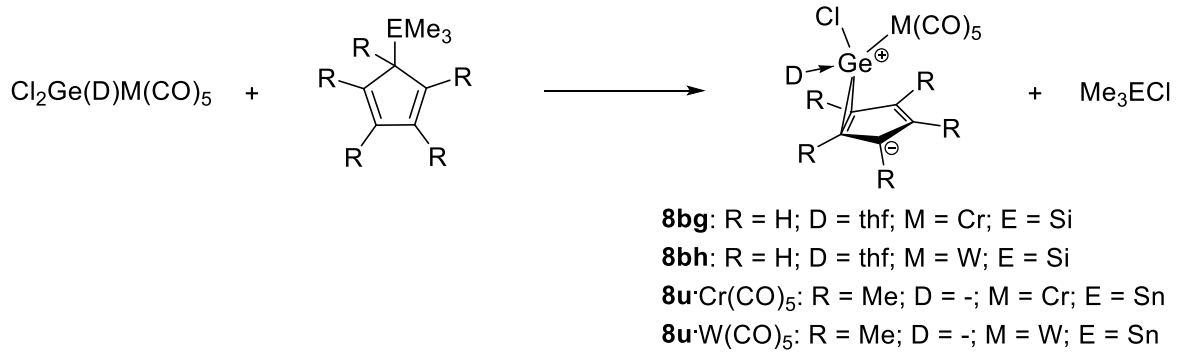

8bg: R = H; D = thf; M = Cr; E = Si
8bh: R = H; D = thf; M = W; E = Si
8u·$Cr(CO)_5$: R = Me; D = -; M = Cr; E = Sn
8u·$W(CO)_5$: R = Me; D = -; M = W; E = Sn

Scheme 151: Syntheses of chromium- and tungstenpentacarbonyl complexes of CpGeCl and Cp*GeCl (**8u**) as conducted by Jutzi *et al*.[236]

Jutzi and coworkers crystallized **8u**·$W(CO)_5$ revealing the potential of **8u** as ligand for transition metal complexes (Figure 54).

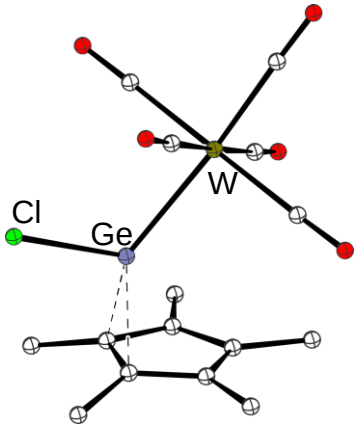

Figure 54: Molecular structure of Cp*GeCl·$W(CO)_5$ (**8u**·$W(CO)_5$)[236] in the crystal (hydrogen atoms omitted for clarity, ball-and-stick representation).

The Ge-Cp^C distances in this tungsten complex measure 215.07(49) pm and the Ge-Cl bond 223.67(25) pm. The germanium atom is η^2 coordinated to the cyclopentadienyl ligand similar to the hapticity observed in Cp*GeCl (**8u**). The Ge-Cl bond and the Ge-Cp^C bonds are significantly shortened in comparison to the Ge-Cl bond in **8u**. At the tungsten fragment, an octahedral coordination environment is observed with a Ge-W bond length of 257.13(27) pm.[236] This tungsten complex reveals the suitability of **8u** as ligand for transition metals. No such complex was obtained for tetrelocenes presumably due to steric reasons and the low energy of the lone pair in these compounds. By addition of aluminum(III)chloride

or germanium(II)chloride dioxane complex to **8u**·$W(CO)_5$, a migration of the tungstenpentacarbonyl fragment to the trichlorogermanide anion was observed as reported by Jutzi *et al*. in 1986.[237] In the same year, Jutzi *et al*. reacted **8u**·$W(CO)_5$ with lithium compounds to functionalize this transition metal complex further (Scheme 152).[238]

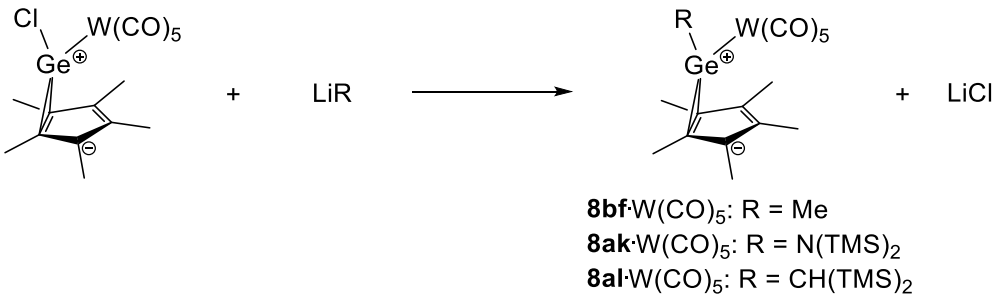

Scheme 152: Syntheses of various substituted tungstenpentacarbonyl germylene complexes as carried out by Jutzi *et al*.[238]

The authors managed to crystallize **8al**·$W(CO)_5$ revealing an η^2 coordination of the germanium atom to the cyclopentadienyl ligand with Ge-Cp^C distances of 219.40(78) pm which is slightly elongated in comparison to the Ge-Cp^C distance in **8u**·$W(CO)_5$. The Ge-C^{TMS} distance measures 198.73(11) pm which is shortened in comparison to the Ge-C^{TMS} distance observed for **8al**. In analogy to the tungsten complex **8u**·$W(CO)_5$, the tungsten atom in **8al**·$W(CO)_5$ possesses an octahedral geometry with a Ge-W bond length of 263.20(27) pm which is elongated in comparison to the Ge-W bond length observed in **8u**·$W(CO)_5$ presumably due to the elevated steric demand.[238] Between 2000 and 2005, the Filippou group reported several examples of insertion products of reactions of pentamethylcyclopentadienylgermanium halides and group 6 metal complexes (Scheme 153).[231,239–241]

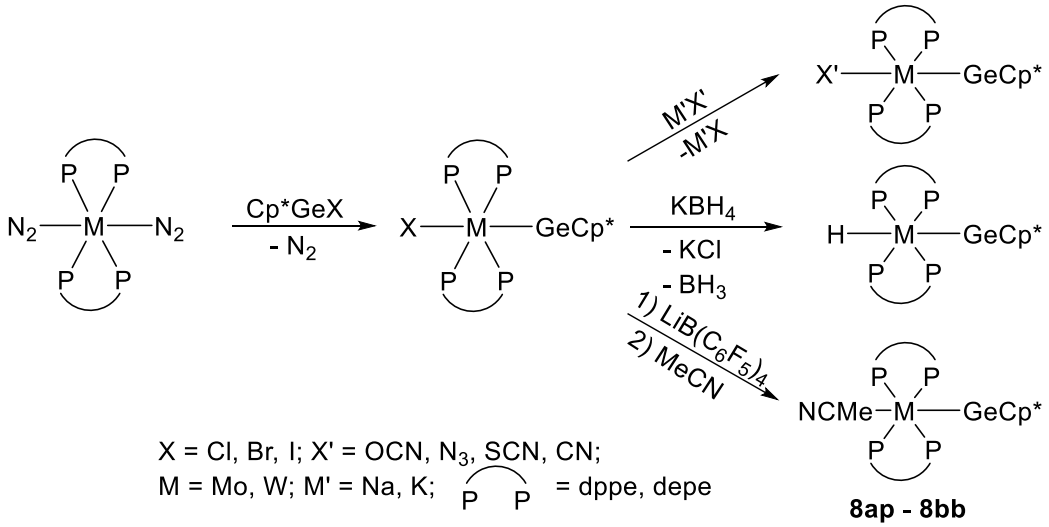

Scheme 153: Syntheses of germylene substituted group 6 metal complexes as conducted by Filippou *et al*.[231,239–241]

Most of these complexes were structurally characterized exhibiting a triple bond between the germanium atom and the group 6 metal centre (range of Ge-M: 227.98(5) to 231.85(6) pm). The germanium atom possesses a hapticity of η^1 in all complexes with a Ge-Cp^C distance ranging from 200.4(2) to 204.9(6) pm.[231,239–241] In 1984, Jutzi *et al*. reacted **8aa**OTf^- with pyridine, bipyridine and pyrazine to probe the electrophilic character of Cp^*Ge^+ (Scheme 154).[242]

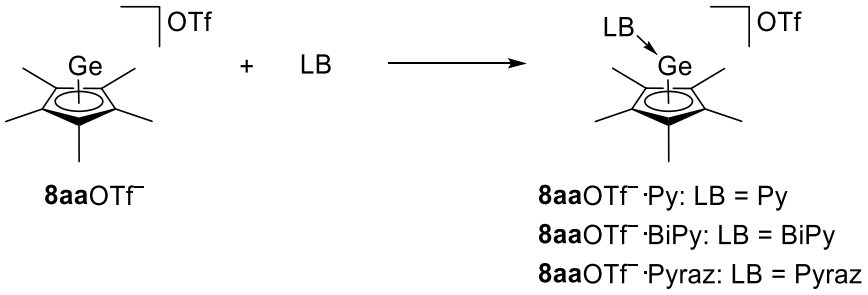

Scheme 154: Syntheses of Lewis base adducts of $Cp^*Ge^+OTf^-$ (**8aa**OTf^-) as carried out by Jutzi *et al*.[242]

The authors demonstrated a correlation between the disproportionation of the obtained adduct and the nucleophilicity of the Lewis base used. Unfortunately, no crystals could be grown of none of these adducts.[242] An unsuspected reaction was reported by Summerscales *et al*. when they reacted the digermyne DipGe≡GeDip with cyclopentadiene and

obtained the heteroleptic complex CpGeDip as the product of this C-H activation (Scheme 155).[243]

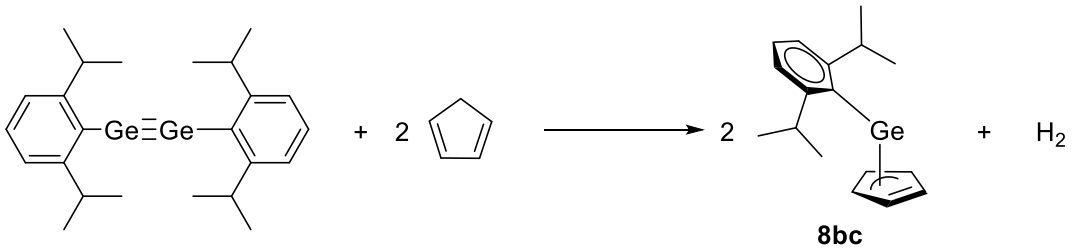

Scheme 155: Synthesis of the heteroleptic germylene CpGeDip (**8bc**) as conducted by Summerscales *et al*.[243]

The authors were able to crystallize this compound revealing an η^3 complexed germanium atom (Figure 55) with a tendency toward η^1 (closest Ge-Cp^C distances: 218.26(14) pm, 232.71(14) pm and 253.16(17) pm).

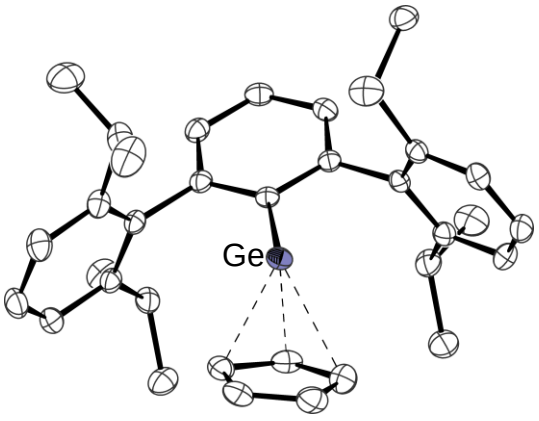

Figure 55: Molecular structure of CpGeDip (**8bc**)[243] in the crystal (hydrogen atoms omitted for clarity, thermal ellipsoids at 50% probability level).

The Ge-C^{Ar} bond in the structure in the solid state of **8bc** measures 203.50(12) pm which is similar to the Ge-C^{Ar} distance observed in (2,6-(^{i}Pr)$_2$C$_6$H$_3$)$_2$Ge (203.33(24) pm and 204.84(27) pm[244]). Although in the solid state an η^3 coordination mode of the germanium atom to the cyclopentadienyl ring is observed, this seems not to be persistent in solution since only one signal appears for the protons of the cyclopentadienyl ligand in the ^{1}H NMR

spectrum.[243] The *Jutzi* group reported of germyliumylidenes exhibiting interactions with an olefin which were synthesized by reacting monolithiated *ansa* ligand $Me_2Si[1](Cp^{\#}H)(Cp^{\#}Li)$ with germanium(II)chloride dioxane complex and subsequent protonation with HBF_4 and HOTf to obtain the corresponding germyliumylidene (Scheme 156).[171]

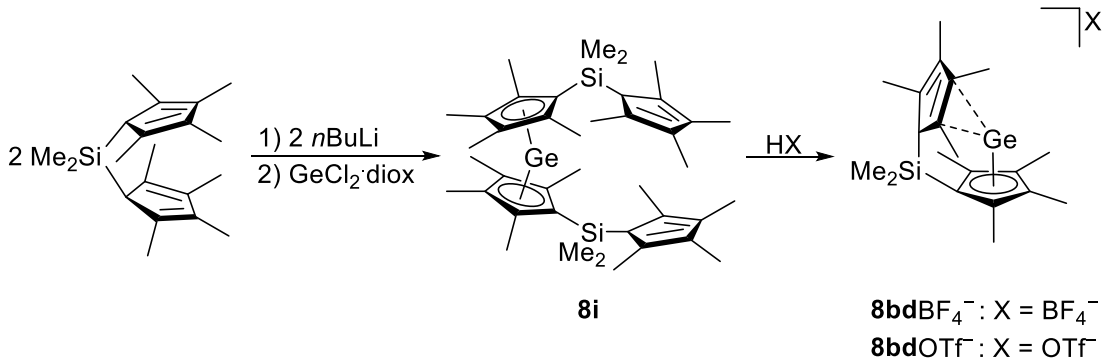

Scheme 156: Syntheses of olefin complexes of germyliumylidenes as conducted by Jutzi *et al*.[171]

By reaction of one equivalent monolithiated *ansa* ligand with one equivalent germanium(II)chloride dioxane complex the corresponding chlorogermylene $Me_2Si[1](Cp^{\#};Cp^{\#}H)GeCl$ (**8be**) was obtained which was reacted again with germanium(II)chloride dioxane complex affording the germyliumylidene **8bd**$GeCl_3^-$.[171] The authors were able to crystallize this complex revealing an interaction between the central germanium atom and a double bond of the cyclopentadiene of the *ansa* ligand (Figure 56).

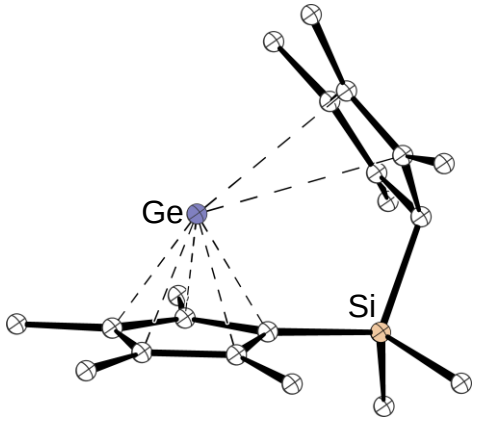

Figure 56: Molecular structure of **8bd**$GeCl_3^-$[171] in the crystal (hydrogen atoms and counter ion omitted for clarity, ball-and-stick representation).

In the crystal structure of **8bd**$GeCl_3^-$ olefin complex, the germanium atom is η^5 complexed to the cyclopentadienyl ring (with a Ge-Cp^{cent} distance comparable to other germyliumylidenes bearing cyclopentadienyl ligands, see Table 10) and η^2 coordinated to a double bond of the cyclopentadiene. These interactions of the cyclopentadiene with the germanium atom were not reflected in the ^1H and ^{13}C NMR spectra of this compound, according to the authors. In view of the comparable long contact of the germanium atom to the double bond (Ge-Cp^C distances: 317.8(1) pm and 334.18(97) pm) of the cyclopentadiene, a weak interaction is predicted.[171]

In summary, the first cyclopentadienylgermanium halide was discovered eleven years after the discovery of cyclopentadienyltin chloride and three of these cyclopentadienylgermanium halide compounds are structurally characterized. In the class of cyclopentadienylgermanium cations, six examples are structurally characterized, of which one example was first reported in 2021. The Ge-Cp bond lengths are similar for Cp*GeCl, **8u**, and [Cp*Geμ-Br]$_2$, (**8af**)$_2$, but differ to the one observed for $^{Me2N(CH2)2}Cp^{\#}GeCl$, **8ah**, presumably due to the coordination of the nitrogen atom to the germanium atom. The hapticities and Ge-Cp^{cent} distances are similar for all five structurally characterized germyliumylidenes. With Cp*GeCl·$W(CO)_5$, **8u**·$W(CO)_5$, the first transition metal complex of a cyclopentadienyl substituted germyliumylidene could be obtained. The *Filippou* group reported several group 6 metal complexes with Cp*Ge as ligand in the 2000s.

Table 10: Selected structural parameters and references of cyclopentadienylgermanium halfsandwich compounds.

Compound	Hapticity Cp η	Cp-Ge [pm][a]	Reference
Cp*GeCl (**8u**)	2	209.84(4)	[226–229]
$^{Me2N(CH2)2}Cp^{\#}GeCl$ (**8ah**)	2	217.61(10)	[232]
[Cp*Geμ-Br]$_2$ ((**8af**)$_2$)	2	212.90(7)	[228]
[Cp*GeI]$_\infty$ (**8ag**)	-	-	[231,240]
Me_2Si[1]($Cp^{\#}$; $Cp^{\#}H$)GeCl (**8be**)	-	-	[171]
Cp*$Ge^+BF_4^-$ (**8aa**BF_4^-)	5	189.73(6)[228]	[144,228]
Cp*$Ge^{+(5COOM)}Cp^-$ (**8aa**$^{(5COOM)}Cp^-$)	-	-	[188]
Cp*$Ge^+GeCl_3^-$ (**8aa**$GeCl_3^-$)	-	-	[226,231,237]

Cp*Ge$^+$GeBr$_3^-$ (**8aa**GeBr$_3^-$)	-	-	[231]
Cp*Ge$^+$AlCl$_4^-$ (**8aa**AlCl$_4^-$)	5	191.38(5)[224]	[224,237]
Cp*Ge$^+$Cl$_3$Ge$^-$·W(CO)$_5$ (**8aa**Cl$_3$Ge$^-$·W(CO)$_5$)	-	-	[237]
Cp*Ge$^+$OTf$^-$ (**8aa**OTf$^-$)	-	-	[233]
Cp*Ge$^+$SnCl$_3^-$ (**8aa**SnCl$_3^-$)	5	192.75(39)	[180]
Cp*Ge$^+$OTf$^-$·Py (**8aa**OTf$^-$·Py); Cp*Ge$^+$OTf$^-$·Pyraz (**8aa**OTf$^-$·Pyraz); Cp*Ge$^+$OTf$^-$·BiPy (**8aa**OTf$^-$·BiPy)	-	-	[242]
CpGe$^+$(μ-F{Al(ptfb)$_3$}$_2$)$^-$ (**8ae**(μ-F{Al(ptfb)$_3$}$_2$)$^-$)	5	187.63(19); 189.18(11)	[196]
Cp''Ge$^+$BF$_4^-$ (**8ai**BF$_4^-$)	-	-	[170]
Cp'''Ge$^+$GeCl$_3^-$ (**8aj**GeCl$_3^-$)	5	193.41(4)	[234]
Cp*GeCH(TMS)$_2$ (**8al**)	2	212.81(14)	[185]
Cp*GeN(TMS)$_2$ (**8ak**); Cp*GeTMP (**8an**)	-	-	[185]
Cp*GeC(TMS)$_3$ (**8am**)	2	215.61(10)	[235]
Cp*Ge(2,4,6-^{t}Bu$_3$C$_6$H$_2$) (**8ao**)	2	220.02(16)	[235]
Cp*GeCl·W(CO)$_5$ (**8u**·W(CO)$_5$)	2	201.81(34)	[236]
CpGe(thf)Cl(Cr(CO)$_5$) (**8bg**); CpGe(thf)Cl(W(CO)$_5$) (**8bh**); Cp*GeCl(Cr(CO)$_5$) (**8u**·Cr(CO)$_5$)	-	-	[236]
Cp*GeCH(TMS)$_2$·W(CO)$_5$ (**8al**·W(CO)$_5$)	2	206.67(12)	[238]
Cp*GeN(TMS)$_2$W(CO)$_5$ (**8ak**·W(CO)$_5$); Cp*GeMe·W(CO)$_5$ (**8bf**·W(CO)$_5$)	-	-	[238]
Cp*Ge≡W(dppe)$_2$Cl (**8ap**); Cp*Ge≡Mo(dppe)$_2$Cl (**8aq**); Cp*Ge≡Mo(dppe)$_2$Br (**8ar**); Cp*Ge≡W(dppe)$_2$Br (**8as**); Cp*Ge≡W(dppe)$_2$I (**8at**); Cp*Ge≡W(dppe)$_2$H (**8au**); Cp*Ge≡W(dppe)$_2$OCN (**8av**); Cp*Ge≡W(dppe)$_2$N$_3$ (**8aw**); Cp*Ge≡W(dppe)$_2$SCN (**8ax**); Cp*Ge≡W(dppe)$_2$CN (**8ay**); [Cp*Ge≡W(dppe)$_2$MeCN][B(C$_6$F$_5$)$_4$] (**8az**); Cp*Ge≡Mo(depe)$_2$Cl (**8ba**); Cp*Ge≡Mo(depe)$_2$Br (**8bb**)	1	200.4(2) – 204.9(6)	[231,239–241]
CpGeDip (**8bc**)	3	212.15(2)	[243]
Me$_2$Si[1](η^5-Cp$^{\#}$; η^2-Cp$^{\#}$H)Ge$^+$GeCl$_3^-$ (**8bd**GeCl$_3^-$)	2, 5	318.84(12) (η^2); 192.55(18) (η^5)	[171]
Me$_2$Si[1](η^5-Cp$^{\#}$; η^2-Cp$^{\#}$H)Ge$^+$BF$_4^-$ (**8bd**BF$_4^-$); Me$_2$Si[1](η^5-Cp$^{\#}$; η^2-Cp$^{\#}$H)Ge$^+$OTf$^-$ (**8bd**OTf$^-$)	-	-	[171]

[a]: Given to the centre of germanium-cyclopentadienyl bond.

In contrast to the lighter tetrel germanium, for tin the halfsandwich compound with the unsubstituted cyclopentadienyl ligand CpSnCl (**9ai**) is known. In general, the cyclopentadienyltin halides are easily obtained by mixing stannocene with the corresponding tin(II)halide or, for CpSnI (**9au**), the reaction of stannocene with iodine. By protonation of decamethylstannocene (**9c**) and $^{(t\text{BuMe2Si})}Cp^{\#}{}_2Sn$ (**9e**) with HBF_4 and HOTf, the corresponding stannyliumylidenes are obtained. The stannyliumylidenes $Cp^*Sn^+BPh_4^-$, **9ao**BPh_4^-, and **9ao**$B(C_6F_5)_4^-$ were obtained by salt metathesis of Cp*SnCl, **9y**, with $NaBPh_4$ and $LiB(C_6F_5)_4$. In addition, with stannocene (**9a**) as starting material, nitrogen containing tin halfsandwich complexes could be obtained.

The first report of tin halfsandwich compounds, which were cyclopentadienyltin chloride (**9ai**) and -bromide (**9av**), dates back to 1972, where Bos *et al*. synthesized CpSnCl (**9ai**) and CpSnBr (**9av**) by ligand exchange reaction between stannocene and tin(II)chloride or tin(II)bromide, respectively (Scheme 157).[245]

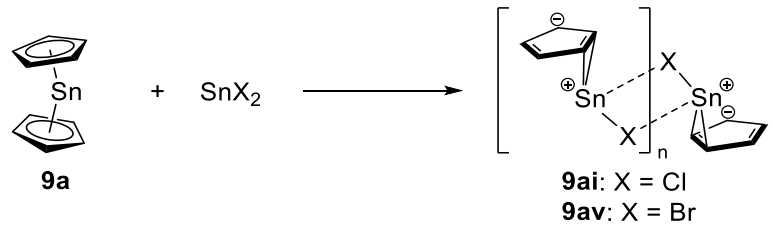

Scheme 157: Syntheses of cyclopentadienyltin halides (**9ai**, **9av**) as conducted by Bos *et al*.[245]

The related cyclopentadienyltin iodide (**9au**) was synthesized by the same group under usage of another synthetic pathway (Scheme 158).[136]

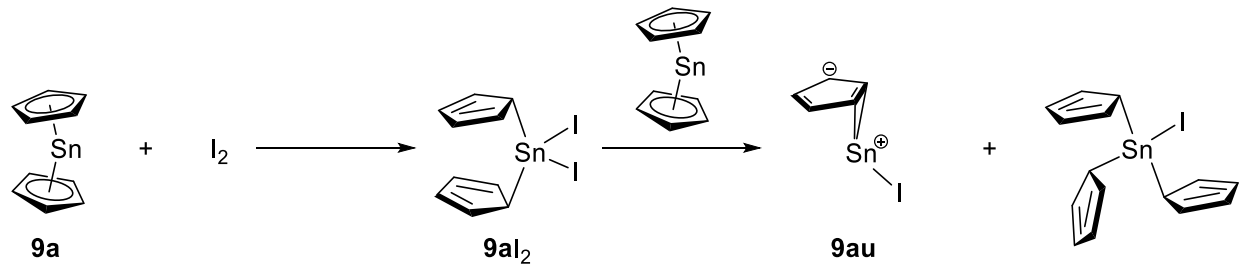

Scheme 158: Synthesis of cyclopentadienyltin iodide (**9au**) as carried out by Bos *et al*.[136]

In the first step of this synthesis, an oxidative addition of iodine to the tin centre of **9a** takes place and in the second step, a redistribution reaction under the addition of stannocene is observed. The structure in the solid state of **9ai** was reported in 1975 by Bos *et al*. revealing a network of Sn-Cl contacts which forms chains in the crystal structure (Figure 57).[230]

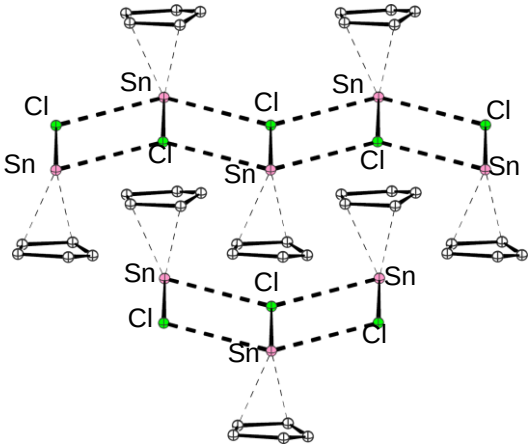

Figure 57: Molecular structure of cyclopentadienyltin chloride (**9ai**)[230] in the crystal (hydrogen atoms omitted for clarity, ball-and-stick representation).

The tin atom is coordinated in an η^2 fashion to the cyclopentadienyl ligand with Sn-Cp^C distances of 244.68(20) and 245.53(18) pm. In this chain type structure, two chloride atoms exhibit contacts to a tin atom (324.02(24) and 326.41(24) pm; both shorter than the sum of van der Waals radii (392 pm) and one Sn-Cl bond (268.01(31) pm) is present. The cyclopentadienyl ligands in CpSnCl possess a low degree of aromaticity which is visible in the large span of C-C bond lengths (121.41(9) to 155.34(11) pm) corroborating the observed hapticity of η^2.[230] In the ^{119}Sn CP/MAS NMR spectrum of CpSnCl (**9ai**), signals were found at −1483 ppm and −1578 ppm,[109] which is significantly upfield shifted compared to $SnCl_2$ (δ ^{119}Sn CP/MAS = −916 ppm[246]), but downfield shifted compared to stannocene (δ ^{119}Sn = −2199 ppm[107,108]). First reports of pentamethylcyclopentadienyltin chloride (**9y**) date back to the end of the 1970s and beginning of the 1980s when Jutzi and coworkers contributed pioneering work to this field, but no structural characterization of these compounds was conducted.[144,205] In 1997, Constantine *et al*. reported on pentamethylcyclopentadienyltin chloride (**9y**) which was synthesized by ligand exchange reaction (Scheme 159).[109]

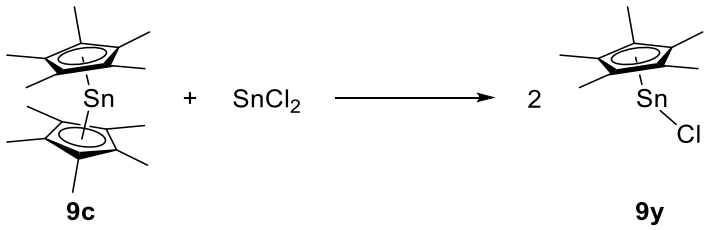

Scheme 159: Synthesis of Cp*SnCl (**9y**) as conducted by Constantine *et al*.[109]

The structure of **9y** in the solid state revealed an η^5 complexed tin atom with Sn-Cp^{cent} distances of 227.03(7) and 228.17(7) pm. This hapticity of η^5 is underpinned by the equal C-C distances in the Cp* ligand (140.86(44) to 144.66(45) pm) unravelling a high degree of aromaticity, though exhibiting a tendency toward η^3 as also suggested by Sen and coworkers.[109,224] The difference in the hapticity between CpSnCl, **9ai**, and Cp*SnCl, **9y**, might stem from the higher electron density present in the Cp* ligand caused by the electron donating methyl groups attached to the cyclopentadienyl ligand and, by that, exhibiting a stronger Sn-Cp bond. In **9y**, the Sn-Cl bond measure 265.67(13) and 269.29(13) pm, which is in line with the Sn-Cl distance in **9ai** (*vide supra*). Analogous to the chain type structure of **9ai**, in **9y** the tin atom possesses two Sn-Cl contacts (Sn-Cl distances: 307.95(13) and 344.43(16) pm) which are both shortened in comparison to the sum of the van der Waals radii (392 pm). The signal in ^{119}Sn NMR spectrum for **9y** (−1644 ppm (CP/MAS)) is comparable to that observed for **9ai** (*vide supra*).[109,230] In 1986 already, Jutzi *et al*. reported on Cp*SnBr (**9aw**) which was synthesized by melting solid samples of decamethylstannocene, **9c**, and Cp*$_2$SnBr$_2$ together. The signal in the ^{119}Sn NMR spectrum for **9aw** is observed at −1630 ppm, in line with the signals for **9ai** and **9y** (*vide supra*).[146] Another tin halfsandwich complex, namely (tBuMe2Si)Cp$^{\#}$SnCl, **9ax**, was reported by Constantine *et al*. in 1997 (Scheme 160).[109]

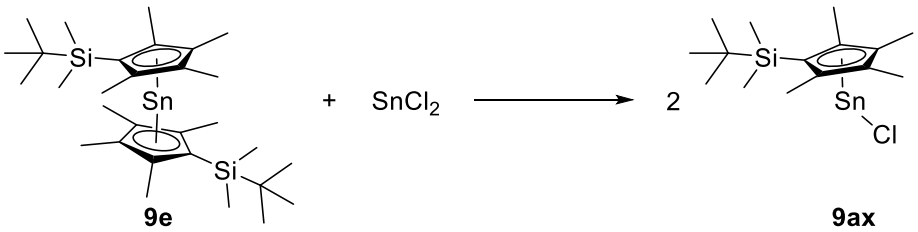

Scheme 160: Synthesis of (tBuMe2Si)Cp$^{\#}$SnCl (**9ax**) as carried out by Constantine *et al*.[109]

The signals in the ^{119}Sn NMR spectra in solution (−1598 ppm) and in the solid state (−1734 ppm) for **9ax** are in line with the signals in ^{119}Sn NMR spectra for other known tin halfsandwich compounds (*vide supra*). Based on the signals in the ^{119}Sn NMR spectra in solution and in the solid state, the authors concluded **9y** and **9ax** to exist as monomers in solution and in the solid state.[109] This halfsandwich compound, **9ax**, was reacted with tin(II)chloride by Constantine *et al*. in 1996. By conducting single crystal X-ray crystallography, the authors were able to characterize the cluster [$^{(t\text{BuMe2Si})}$Cp$^{\#}_6$Sn$_9$Cl$_{12}$] (**9ay**) (Figure 58).[247]

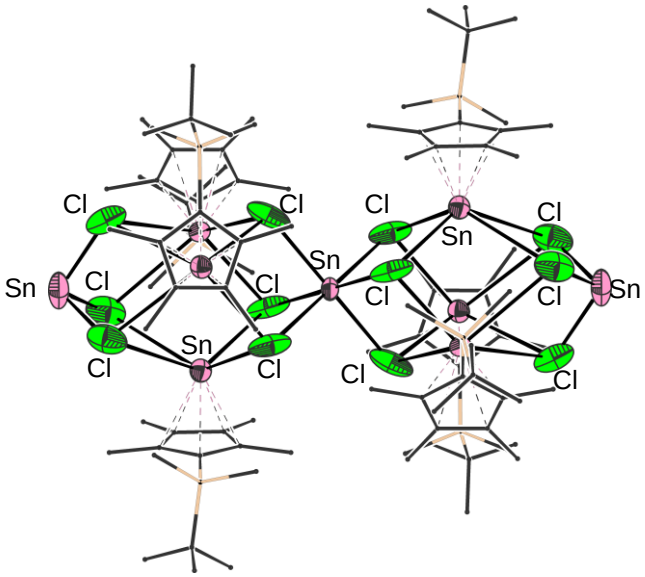

Figure 58: Molecular structure of [$^{(t\text{BuMe2Si})}$Cp$^{\#}_6$Sn$_9$Cl$_{12}$] (**9ay**)[247] in the crystal (hydrogen atoms omitted for clarity, cyclopentadienyl ligand depicted as wireframe, thermal ellipsoids at 50% probability level).

The structure in the solid state consists of two terminal $SnCl_3^-$ units, one central $SnCl_6^{4-}$ unit and six $^{(t\text{BuMe2Si})}$Cp$^{\#}$Sn$^+$ units which is also reflected by the three signals in the ^{119}Sn CP/MAS NMR spectrum ($SnCl_3^-$: −16 ppm; $SnCl_6^{4-}$: −735 ppm; $^{(t\text{BuMe2Si})}$Cp$^{\#}$Sn$^+$: −2075 ppm). In solution, only two signals are observed presumably due to the formation of [$^{(t\text{BuMe2Si})}$Cp$^{\#}$SnCl]$_2$(μ-SnCl$_2$) as the authors stated.[247] A catecholborane substituted tin halfsandwich complex (**9az**) was synthesized by Cassani *et al*. in 2005 (Scheme 161). [248]

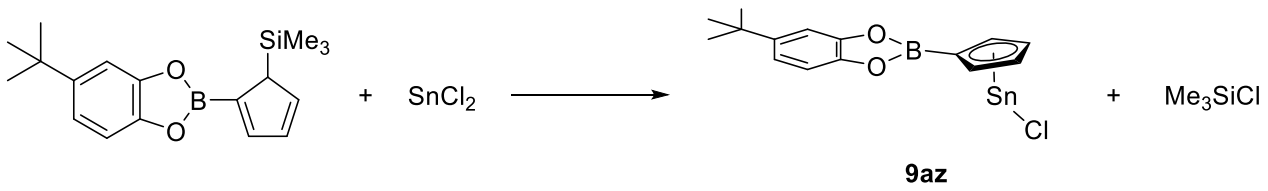

9az

Scheme 161: Synthesis of catecholborane substituted tin halfsandwich complex (**9az**) as conducted by Cassani *et al*.[248]

In the ^{119}Sn NMR spectrum of the product in solution, the authors observed three signals which they assigned to tin(II)chloride (−215 ppm), the heteroleptic halfsandwich complex $^{t\text{BuBcat}}$CpSnCl, **9az**, (−1085 ppm) and the corresponding metallocene (**9ba**) (−2174 ppm) due to a slow equilibrium in solution for which reason all three species can be observed simultaneously (Scheme 162).[248]

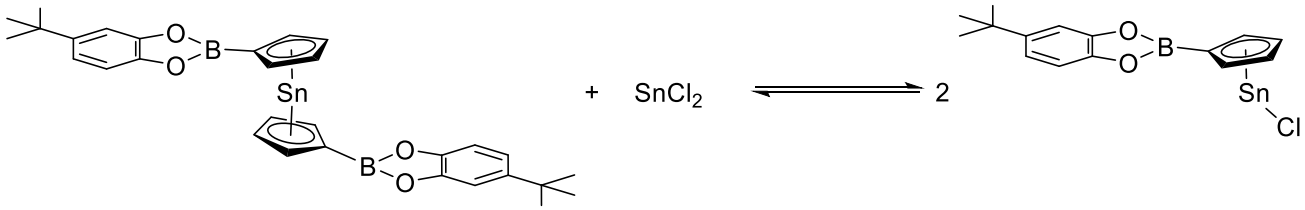

9ba **9az**

Scheme 162: Homoleptic/heteroleptic equilibrium as suggested by *Cassani et al*.[248]

The assignment of the signal at −1085 ppm to the halfsandwich tin compound $^{t\text{BuBcat}}$CpSnCl (**9az**) needs to be assessed carefully since all other known halfsandwich complexes of tin exhibit very similar signals in the ^{119}Sn NMR spectra (see Table 11) in which row this compound does not seem to fit in. It is noteworthy in this context that attempts to isolate tin halfsandwich complexes with highly alkylated cyclopentadienyl ligands (^{3}Cp; ^{4}Cp) were not successful due to redistribution reaction (Scheme 163).[164]

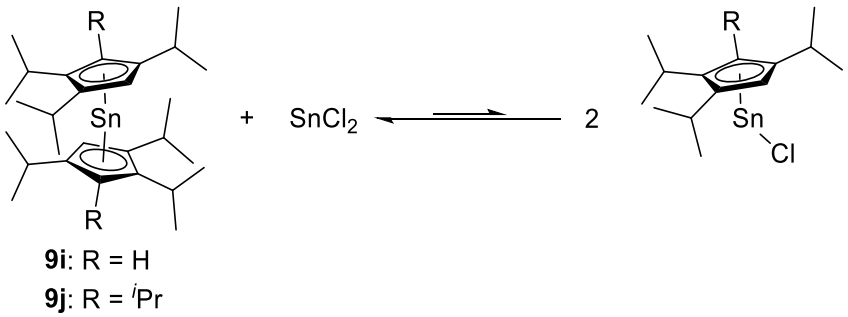

9i: R = H
9j: R = ^{i}Pr

Scheme 163: Redistribution reaction between tri-*iso*propyl- and tetra-*iso*propylcyclopentadienyltin halfsandwich and corresponding sandwich compounds.[164]

Burkey and Hanusa reasoned this observation of lability of ^{3}CpSnCl and ^{4}CpSnCl in solution with an increase of stability of the cationic [$^{3/4}$CpSn]$^{+}$ fragment in comparison to the unsubstituted cyclopentadienyl ligand and, by that, a higher urge to disproportionation in solution.[164] In 1984, Jutzi *et al*. reacted decamethylstannocene (**9c**) with pentamethoxycarbonylcyclopentadiene under the intention to isolate the corresponding cationic halfsandwich complex (Scheme 164).[188]

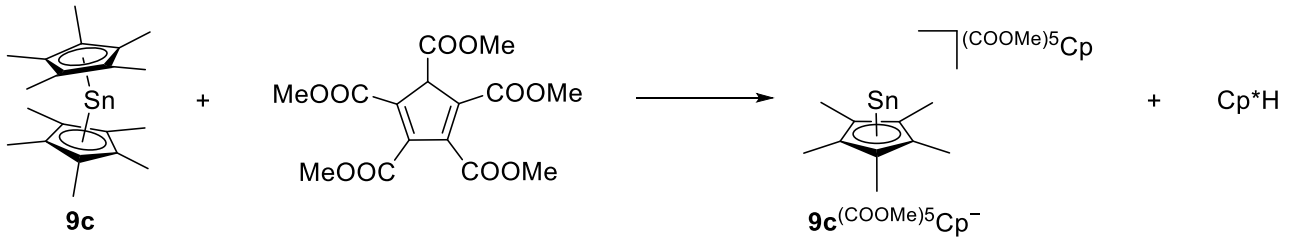

9c

9c$^{(COOMe)5}$Cp^{-}

Scheme 164: Synthesis of Cp*Sn$^{+(COOMe)5}$Cp^{-} (**9a**$^{(COOMe)5}$Cp^{-}) as carried out by Jutzi *et al*.[188]

By addition of two equivalents of pentamethoxycarbonylcyclopentadiene to decamethylstannocene (**9c**), the authors intended the isolation of the corresponding stannocene, but the structure in the solid state revealed a tin atom coordinated by four oxygen atoms and not π complexed to the cyclopentadienyl ligand. This result strongly calls into question if the corresponding cationic halfsandwich complex had formed. A hint which speaks for the formation of **9a**$^{(COOMe)5}$Cp^{-} is the signal for this compound in the ^{119}Sn NMR spectrum which is observed at −2185 ppm being comparable to known CpSn^{+} complexes (see Table 11), but not very different from stannocenes (see Table 8) and without structural characterization of this

tin compound, no definitive conclusions may be drawn.[188] The first stannyliumylidene bearing a cyclopentadienyl ligand was **9ao**BF_4^- which was reported by Jutzi *et al*. in 1979. The synthesis for this compound was carried out analogously to that for $Cp^*Ge^+BF_4^-$ (Scheme 165).[249]

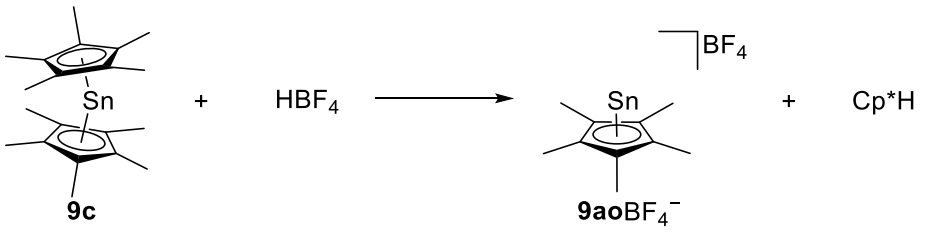

Scheme 165: Synthesis of pentamethylcyclopentadienylstannyliumylidene tetrafluoroborate (**9ao**BF_4^-) as conducted by Jutzi *et al*.[144,249]

In the structure in the solid state of **9ao**BF_4^-, an η^5 coordinated tin atom was revealed exhibiting a Sn-Cp^{cent} distance of 215.70(1) pm which is significantly shorter than the Sn-Cp^{cent} distances in Cp^*_2Sn (239.77(4) and 240.11(4) pm[144]) justified by the increased electrophilic character obtained at the tin atom in **9ao**BF_4^-.[144,249] The solubility of **9ao**BF_4^- in non-polar solvents is, as expected, very limited. The shortest Sn-F contact in **9ao**BF_4^- measures 297.06(3) pm, which is distinctly under the sum of the van der Waals radii (364 pm) indicating the presence of a contact ion pair in the crystal structure of this molecule. The NMR spectroscopic data (^{11}B; ^{19}F) corroborate the ionic structure of **9ao**BF_4^-.[144] A comprehensive work to stannyliumylidenes bearing the cyclopentadienyl ligands was published by Jutzi *et al*. in 1981 (Scheme 166).[51]

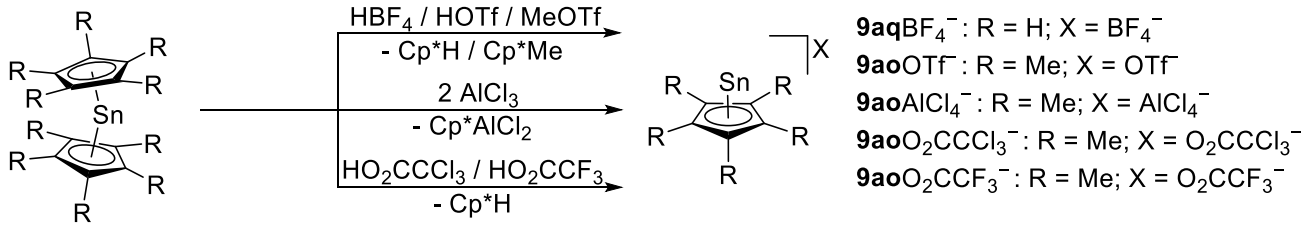

Scheme 166: Syntheses of cyclopentadienyl stannyliumylidenes as carried out by Jutzi *et al*.[51]

Since no structural characterization or heteronuclear NMR spectroscopy was provided to these compounds in the work of Jutzi and coworkers, no statement can be made to the structural details.[51] In 1998, Rhodes and coworkers reported on **9ao**$B(C_6F_5)_4^-$ which was synthesized by transmetalation reaction of Cp*SnCl with $LiB(C_6F_5)_4$ (Scheme 167).[104]

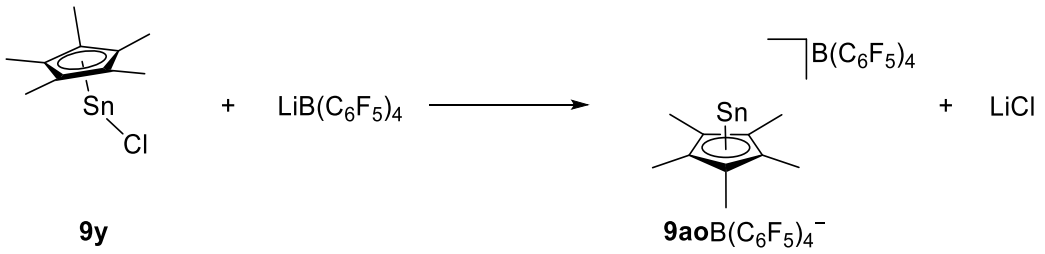

Scheme 167: Synthesis of $Cp^*Sn^+B(C_6F_5)_4^-$ (**9ao**$B(C_6F_5)_4^-$) as conducted by Rhodes *et al*.[104]

The authors reported a signal for **9ao**$B(C_6F_5)_4^-$ at −2219 ppm in the ^{119}Sn NMR spectrum in line with known cyclopentadienyl substituted stannyliumylidenes (see Table 11). Rhodes and coworkers could demonstrate the applicability of **9ao**$B(C_6F_5)_4^-$ as a cocatalyst in the polymerization of α olefins.[104] This compound was structurally characterized by Jones *et al*. in 2005, revealing an η^5 coordinated tin atom with a Sn-Cp^{cent} distance of 211.35(5) pm in line with the Sn-Cp^{cent} distance observed in **9ao**BF_4^- (*vide supra*).[194] In this structure, the tin atom exhibits four contacts to fluorine atoms displaying the high degree of electrophilicity present at the tin centre.[194] A facile synthesis for a Cp^*Sn^+ species was reported by Beckmann *et al*. in 2012 who obtained **9ao**BPh_4^- by reaction of sodiumtetraphenylborate with pentamethylcyclopentadienyltin chloride (Scheme 168).[250]

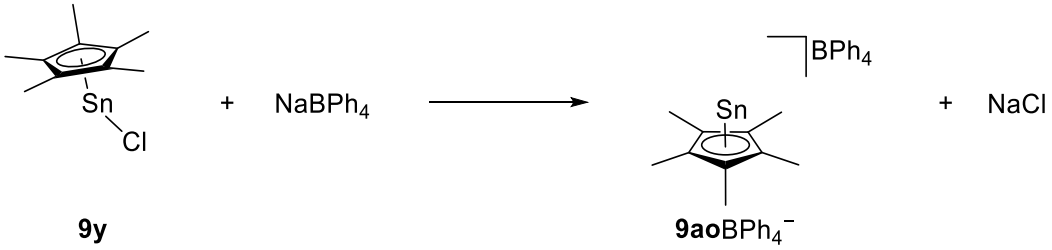

Scheme 168: Synthesis of $Cp^*Sn^+BPh_4^-$ (**9ao**BPh_4^-) as carried out by Beckmann *et al*.[250]

The authors reported signals for **9ao**BPh_4^- in the ^{119}Sn NMR spectra at −2246 ppm (solution) and −2236 ppm (CP/MAS), which are comparable to what is found for related species (see Table 11). In the structure in the solid state of **9ao**BPh_4^-, a hapticity of η^5 was found for the tin atom exhibiting a Sn-Cp^{cent} distance of 219.62(8) pm and two additional contacts to phenyl rings of the tetraphenylborate (Sn-Ph^{cent}: 310.50(17) and 315.10(18) pm; comparable to what is found in $(CpSn{\cdot}C_7H_8)^+Al(ptfb)_4^-$: 300.50(4) pm[195]) (Figure 59).[250]

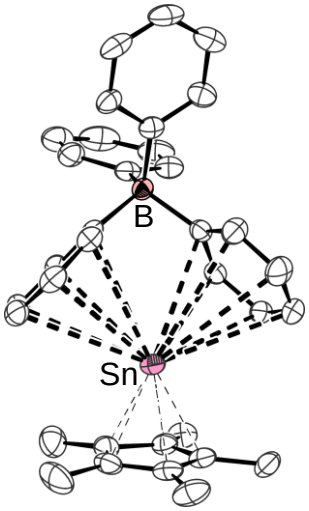

Figure 59: Molecular structure of $Cp^*Sn^+BPh_4^-$ (**9ao**BPh_4^-)[250] in the crystal displaying Sn-Ph contacts (hydrogen atoms omitted for clarity, thermal ellipsoids at 50% probability level).

The stannyliumylidenes **9bb**BF_4^- and **9bb**OTf^- could be reported in 2001 and 2002 by de Lima *et al*. who synthesized this compound analogously to $Cp^*Sn^+OTf^-$ (Scheme 169).[251,252]

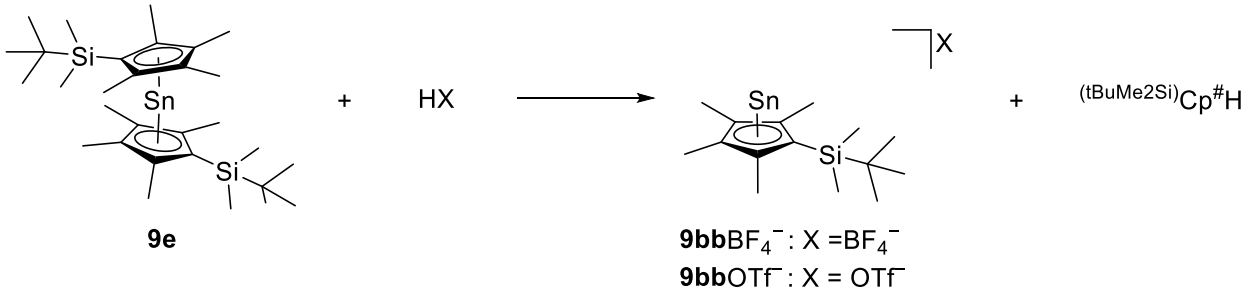

Scheme 169: Syntheses of **9bb**BF_4^- and **9bb**OTf^- as conducted by de Lima *et al*.[251,252]

The structural characteristics of **9bb**BF_4^- are very similar to those observed for **9ao**BF_4^- and also the signal in the ^{119}Sn NMR spectrum (−2289 ppm) exhibits a comparable value as known related stannyliumylidenes (see Table 11).[252] In the structure in the solid state of **9bb**OTf^-, one $^{(t}$BuMe2Si)Cp$^{\#}$Sn$^+$ unit and one [$^{(t}$BuMe2Si)Cp$^{\#}$Sn$(OTf)_2]^-$ are present which can be seen in the difference in the Sn-O^{OTf} distances. Another hint for two chemically distinct tin atoms to exist is the fact that two signals (−2065 ppm and −2301 ppm) in the ^{119}Sn CP/MAS NMR spectrum for **9bb**OTf^- were detected. The Sn-Cp^{cent} distances of 219.15(7) pm and 221.76(10) pm represent comparable values to what is observed in Cp*$Sn^+BPh_4^-$ (219.62(8) pm[250]).[251,252] In 1985, Hani and Geanangel reacted Cp'$_2$Sn with boron trifluoride and obtained as product the stannyliumylidene Cp'$Sn^+BF_4^-$ (**9bc**BF_4^-) (Scheme 170).[169]

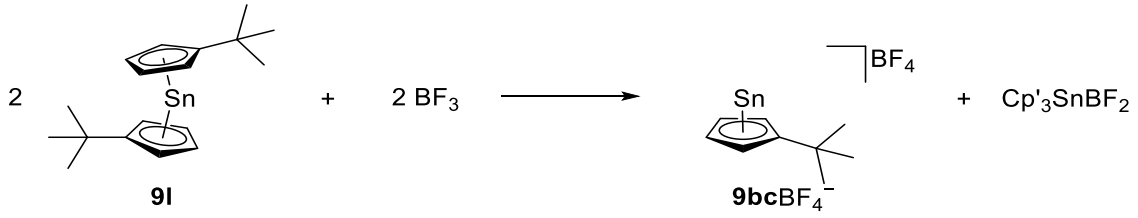

Scheme 170: Synthesis of Cp'$Sn^+BF_4^-$ (**9bc**BF_4^-) as carried out by Hani and Geanangel.[169]

Despite further reports on an adduct of **9a** with BF_3,[131] the authors presented as reaction product **9bc**BF_4^- which could be structurally characterized and exhibits a Sn-Cp^{cent} bond length of 218.17(5) pm which is slightly shortened in comparison to the Sn-Cp^{cent} bond length in **9ao**BPh_4^- (*vide supra*).[169,250] In this structure, the tin atom displays Sn-F contacts similar to the ones observed in, for example, **9ao**BF_4^-.[169,249] In 1989, Jutzi and Dickbreder synthesized Cp''$Sn^+BF_4^-$, **9bd**BF_4^-, analogously to the synthesis of **8ai**BF_4^- (Scheme 171).[170]

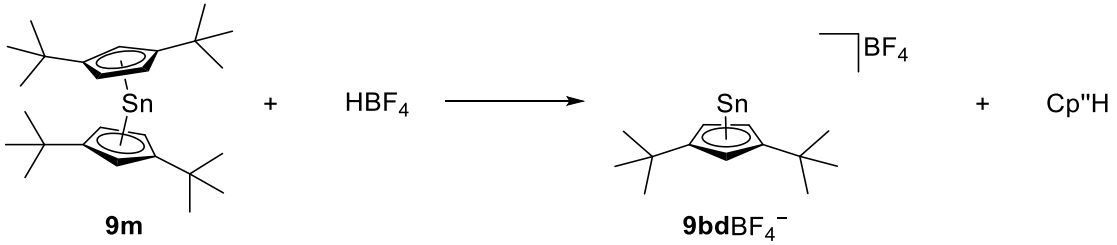

Scheme 171: Synthesis of **9bd**BF_4^- as conducted by Jutzi and Dickbreder.[170]

Unfortunately, no crystal structure could be obtained for this complex, but the signal in the ^{119}Sn NMR spectrum at −2338 ppm speaks for a cyclopentadienyl substituted stannyliumylidene.[170] The complex **9be**$SnCl_3^-$ was synthesized by Ding *et al*. in 2021 (Scheme 172).[234]

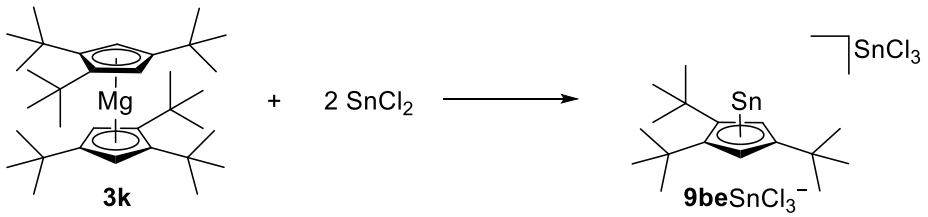

Scheme 172: Synthesis of Cp'''$Sn^+SnCl_3^-$ (**9be**$SnCl_3^-$) as conducted by Ding *et al*.[234]

In the crystal structure of **9be**$SnCl_3^-$, an η^5 coordinated tin atom was revealed with a Sn-Cp^{cent} distance of 220.87(6) pm which is in line with other cyclopentadienyl substituted stannyliumylidenes (see Table 11). The authors stated that the Cp''' ligand is a suitable ligand for ionic complexes since it exhibits an elevated steric demand and is less soluble than other common cyclopentadienyl ligands like Cp* and therefore might suppress the formation of metallocene type structures.[234] In 2017, Schleep *et al*. reported synthesized cyclopentadienyl substituted stannyliumylidenes stabilized by the weakly coordinating anion $Al(ptfb)_4^-$ (Scheme 173).[195]

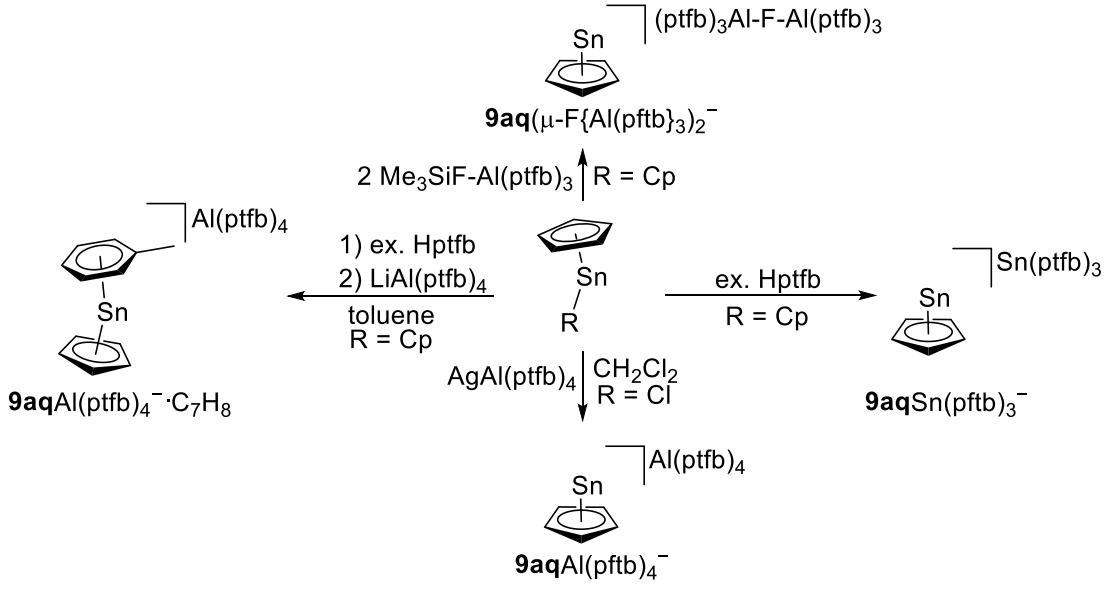

Scheme 173: Cyclopentadienyl substituted stannyliumylidenes obtained by Schleep *et al*.[195]

The stannyliumylidene **9aq**Al(ptfb)$_4^-$ was obtained by salt metathesis of CpSnCl (**9ai**) with AgAl(ptfb)$_4$. Unfortunately, the crystals obtained of **9aq**Al(ptfb)$_4^-$ were of poor quality for which reason discussion of structural parameters is impossible. The signal for this compound in the ^{119}Sn NMR spectrum corroborates the formation of **9aq**Al(ptfb)$_4^-$ (δ ^{119}Sn = −2430 ppm). All stannyliumylidenes obtained by Schleep *et al*. exhibit signals in the ^{119}Sn NMR spectra which are slightly upfield shifted compared with the signals for other cyclopentadienyl substituted stannyliumylidenes (see Table 11). The Sn-Cp^{cent} distance for **9aq**(μ-F{Al(ptfb)$_3$}$_2$)$^-$ measures 210.95(14) pm which is slightly shorter than the Sn-Cp^{cent} distance found in **9ao**B(C$_6$F$_5$)$_4^-$ presumably due to steric reasons.[194,195] In **9aq**Al(ptfb)$_4^-$·C$_7$H$_8$, the Sn-Cp^{cent} distance is with 214.29(4) pm elongated because of the coordination of a toluene molecule (Sn-Ph^{cent}: 300.50(4) pm) to the tin atom displaying the high degree of electrophilicity of this tin atom. The longest Sn-Cp^{cent} distance of these stannyliumylidenes is observed for **9aq**Sn(ptfb)$_3^-$ (222.44(2) pm) which is not further surprising in view of the presence of three Sn-O contacts of the cyclopentadienyl coordinated tin atom to the oxygen atoms of the alkoxy groups weakening the Sn-Cp bond. Based on DFT calculations including fluoride ion affinities (FIA), the authors concluded the CpSn$^+$ fragment to exhibit a higher Lewis acidity than the Cp*Si$^+$ fragment.[195] By reaction of (HMB)Ga$^+$Al(ptfb)$_4^-$ with stannocene, **9a**, CpSn$^+$Al(ptfb)$_4^-$·HMB (**9aq**Al(ptfb)$_4^-$·HMB) could be synthesized by Schorpp *et al*. in 2020 (Scheme 174).[196]

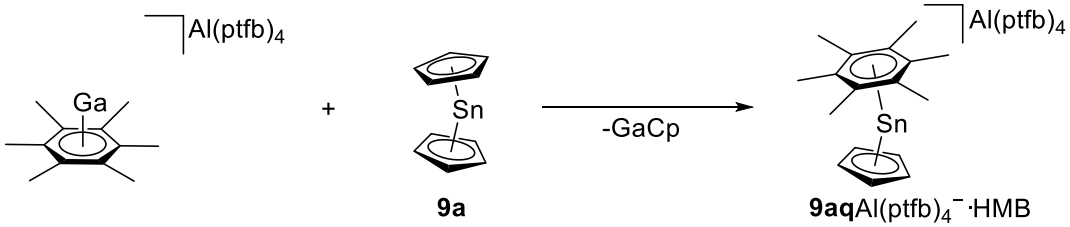

Scheme 174: Synthesis of CpSn$^+$Al(ptfb)$_4^-$·HMB (**9aq**Al(ptfb)$_4^-$·HMB) as conducted by Schorpp *et al*.[196]

In the solid state structure of this cyclopentadienyltin arene complex, an η^5 hapticity to the cyclopentadienyl ligand was revealed, but in view of the poor quality of the structure obtained, due to disorder in the crystal, no structural parameters are discussed.[196] This stannocenium cation exhibits a structure comparable to the toluene adduct of CpSn$^+$, **9aq**Al(pftb)$_4^-$·C$_7$H$_8$, which was reported by Schleep *et al*. in 2017.[195,196] In 1996 and 1997,

Veith and coworkers presented homo- and heterobimetallic bis(*tert*-butoxy) bridged cyclopentadienyltin and -lead complexes which were synthesized by salt metathesis reaction (Scheme 175).[253,254]

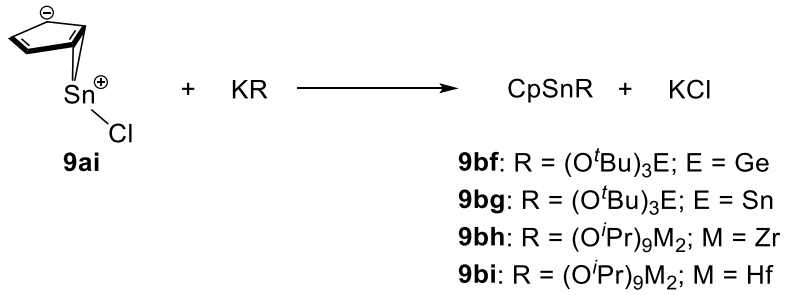

Scheme 175: Syntheses of homo- and heterobimetallic complexes as conducted by Veith *et al*.[253,254]

These complexes exhibit unusual signals in the ^{119}Sn NMR spectra since they are shifted significantly downfield (−261 ppm to −334 ppm) compared to the signal for CpSnCl (**9ai**) (see Table 11) presumably due to coordination of the cyclopentadienyl bonded tin atom to two oxygen atoms, but somewhat similar to the signal of [CpSn(μ-NIPr)]$_2$ (**9bk**) (δ ^{119}Sn = −232 ppm).[253–255] The heterobimetallic compound CpSn(μ-O^{t}Bu)$_2$Ge(O^{t}Bu) (**9bf**) could be crystallized and structurally characterized revealing a hapticity of η^1 with a tendency toward η^3 (Sn-Cp^C: 240.52(19) pm; 267.56(23) pm; 272.89(18) pm) (Figure 60).[253,254]

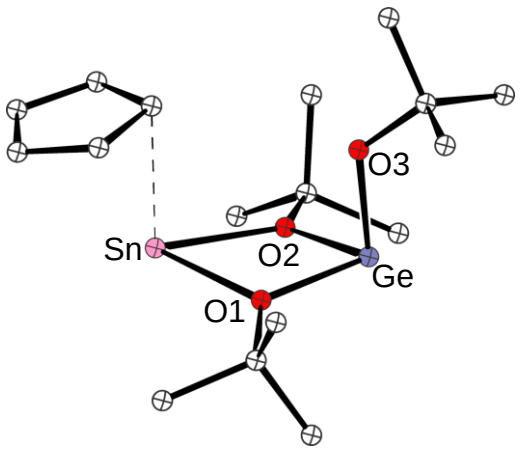

Figure 60: Molecular structure of CpSn(μ-O^{t}Bu)$_2$Ge(O^{t}Bu) (**9bf**)[253] in the crystal (hydrogen atoms omitted for clarity, ball-and-stick representation).

The authors conducted ^{1}H NMR spectroscopy on this complex displaying a fluxional behavior in solution which corroborated the finding of the η^1 hapticity in this complex. Another hint toward this binding mode are the C-C distances found in the cyclopentadienyl ligand.[253,254] In further studies on **9bf**, the trimetallic carbonyl complex CpSn(μ-O^{t}Bu)$_2$Ge(O^{t}Bu)·Mo(CO)$_5$ (**9bj**) could be isolated and structurally characterized. In the structure in the solid state, a hapticity of the tin atom of η^2 could be revealed with Sn-Cp^C distances of 245 pm similar to what was found for the Sn-Cp^C distances in CpSnCl (**9ai**) (*vide supra*). The signal at −185 ppm in the ^{119}Sn NMR spectrum does not differ dramatically from that observed for the starting material.[256] In 2011, Njua *et al*. reported of (^{t}BuO)$_2$ClZr[μ-Cl(CpSn)](μ-O^{t}Bu)$_2$ZrCl(O^{t}Bu)$_2$ (**9bl**) which was synthesized by reaction of CpZrCl$_3$(dme) with Na[Sn(O^{t}Bu)$_3$] and contains a CpSn$^+$ unit (Scheme 176).[257]

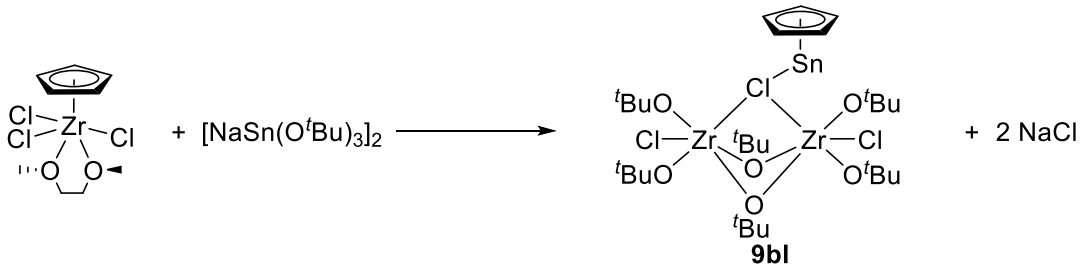

Scheme 176: Synthesis of (^{t}BuO)$_2$ClZr[μ-Cl(CpSn)](μ-O^{t}Bu)$_2$ZrCl(O^{t}Bu)$_2$ (**9bl**) as conducted by Njua *et al*.[257]

The crystal structure of **9bl** revealed an η^5 coordinated tin atom with Sn-Cp^{cent} distance of 228.18(3) pm and a span of C-C bonds in the cyclopentadienyl ligand of 134.21(51) pm to 139.44(51) pm speaking for a high degree of aromaticity on the cyclopentadienyl ligand, although a tendency toward η^3 is indicated by the differences in the Sn-Cp^C bond lengths (246.25(29) pm to 268.41(38) pm). The Sn-Cp^{cent} distance is significantly elongated in comparison to other stannyliumylidenes bearing cyclopentadienyl ligands (see Table 11) for which reason the hapticity of η^5, as suggested by the authors, must be assessed carefully. The Lewis acid base chemistry of **9ao**OTf$^-$ and **9ao**BF$_4^-$ was investigated by addition of different Lewis bases by Kohl *et al*. in 1984 (Scheme 177).[242]

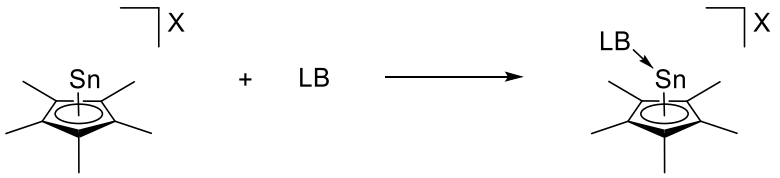

9aoOTf⁻·Py: X = OTf⁻; LB = Py
9aoOTf⁻·BiPy: X = OTf⁻; LB = BiPy
9aoOTf⁻·Pyraz: X = OTf⁻; LB = Pyraz
9aoBF_4^-·BiPy: X = BF_4^-; LB = BiPy

Scheme 177: Synthesis of Lewis acid base adducts of **9ao**OTf⁻ and **9ao**BF_4^- as conducted by Kohl *et al*.[242]

The authors were able to crystallize the adducts **9ao**OTf⁻·Py and **9ao**OTf⁻·BiPy which exhibit significant differences in their structures: While in the pyridine adduct, there still exist Sn-O contacts of the tin atom to two oxygen atoms of the triflate anion, forming a polymeric structure, in the bipyridine adduct there are no Sn-O contacts present presumably due to the chelate effect of bipyridine. These coordination modes also influence the hapticity in these complexes in the solid state: In the pyridine adduct, the hapticity of the tin atom can be regarded as η^3 (Sn-Cp^C: 242.61(2) pm; 244.70(2) pm; 254.50(3) pm), while in the bipyridine adduct, the hapticity can be seen as η^2 (Sn-Cp^C: 241.21(3) pm and 254.96(4) pm). These hapticities can be attributed to the coordination of the Lewis bases and, thereby a weakening of the Sn-Cp bond.[242] In 1993, Paver *et al*. isolated {CpSnN=C(NMe_2)$_2$}$_2$ (**9bm**) as a product of the reaction between stannocene (**9a**) and lithium (bis(dimethylamino)methylene)amide (Scheme 178).[258]

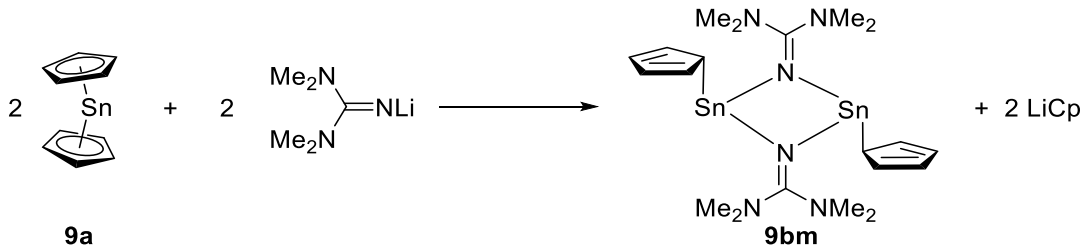

9a **9bm**

Scheme 178: Synthesis of cyclopentadienyltin (bis(dimethylamino)methylene)amide (**9bm**) as conducted by Paver *et al*.[258]

The signal for **9bm** in the ^{119}Sn NMR spectrum appears at 2069 ppm, which is very uncommon compared to related complexes (δ ^{119}Sn for **9bk**: −232 ppm). In the structure in the

solid state, a hapticity of η^1 is observed with a tendency, according to the authors, toward η^3 (Sn-CpC: 239.18(56) pm; 266.69(54) pm; 283.31(60) pm) which is not clearly reflected by the C-C distances in the cyclopentadienyl ligand (span of C-C distances: 134.46(92) pm to 140.47(81) pm). The Sn_2N_2 moiety forms a planar ring with Sn-N distances of 209.18(27) pm and 219.70(32) pm. By conducting ^{1}H NMR spectroscopy at variable temperatures, the authors demonstrated a *cis*/*trans* equilibrium of the cyclopentadienyl ligands.[258] A related compound, $[CpSn(\mu\text{-NIPr})]_2$, **9bk**, was synthesized by Ochiai and Inoue in 2017(Scheme 179).[255]

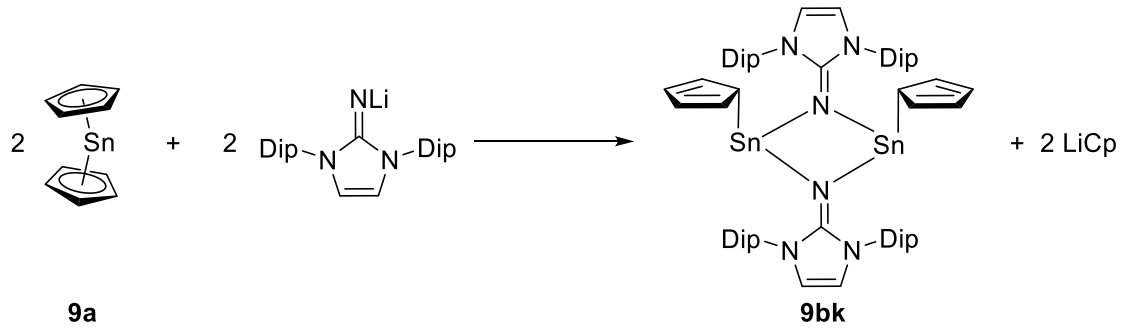

9a **9bk**

Scheme 179: Synthesis of cyclopentadienyltin imino complex (**9bk**) as conducted by Ochiai and Inoue.[255]

The signal in the ^{119}Sn NMR spectrum of −232 ppm is comparable to the one observed for **9bf** synthesized by Veith *et al*. in 1996 (*vide supra*).[253,255] In the crystal structure of **9bk**, an η^1 complexed tin atom is revealed with a Sn-Cp^C distance of 243.78(10) pm, comparable to the shortest Sn-Cp^C distance observed for **9bm** (*vide supra*). The Sn-N distances of 219.18(77) pm and 222.78(70) pm are also similar to the ones observed for **9bm** (*vide supra*). Analogously to the geometry around the tin atom observed in **9bm**, a planar Sn_2N_2 ring appears in the structure of **9bk**. The cyclopentadienyl rings exhibit a *cis* arrangement in **9bk**, which is in contrast to the *trans* arrangement of the cyclopentadienyl ligands in the structure of **9bm**. The authors stated that, again in contrast to **9bm**, no *cis*/*trans* equilibrium exists in solution, presumably due to the steric demand of the di-*iso*propylphenyl groups attached to the nitrogen atoms of the imidazole ring. By addition of dichloromethane to a thf solution of **9bk**, the chlorostannylene $[ClSn(\mu\text{-NIPr})]_2$, was obtained, clearly reflecting the lability of this compound.[255] In 1985, Jutzi *et al*. probed the reactivity of Cp*SnCl, **9y**, toward the pentacarbonyls of chromium and tungsten (Scheme 180).[236]

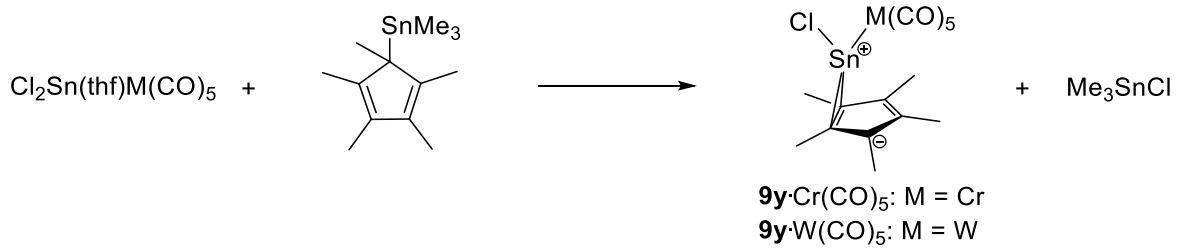

Scheme 180: Synthesis of transition metal complexes of Cp*SnCl (**9y**) as conducted by Jutzi *et al*.[236]

Unfortunately, no crystals could be grown of these two compounds for which reason no discussion on structural details can be undertaken. In the ^{1}H NMR spectra of these complexes, a slight downfield shift of the signals for the methyl groups of the cyclopentadienyl ring was observed in comparison to the uncoordinated Cp*SnCl, **9y**, which was, according to the authors, a hint toward the formation of the chromium(pentacarbonyl) and tungsten(pentacarbonyl) complexes of pentamethylcyclopentadienyltin chloride.[236] Only one year later, Sriyunyongwat *et al*. reported on cyclopentadienyltin halide bridged iron tetracarbonyl complexes (Scheme 181).[207]

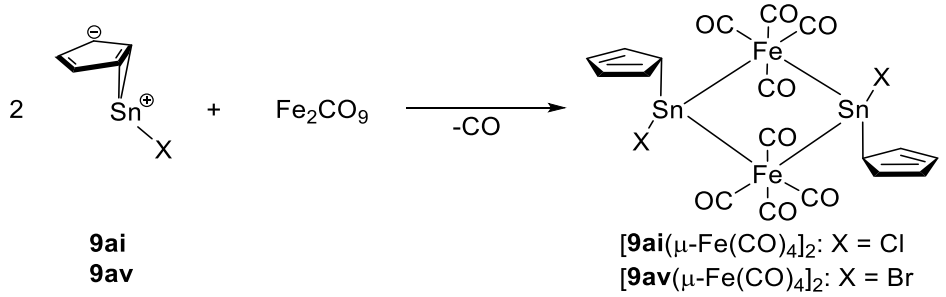

Scheme 181: Synthesis of cyclopentadienyltin halide bridged iron tetracarbonyl complexes as conducted by Sriyunyongwat *et al*.[207]

No structural characteristics of these complexes could be provided, but there is one example of a structure of a related complex where two equivalents stannocene were reacted with diironnonacarbonyl to form [**9a**(μ-Fe(CO)$_4$)]$_2$.[133] In 2011, Summerscales *et al*. obtained a tin halfsandwich compound by the C-H activation reaction of DipSn≡SnDip with cyclopentadiene (Scheme 182).[243]

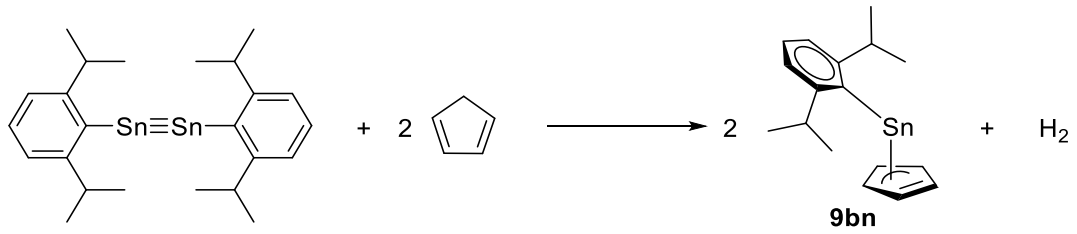

Scheme 182: Synthesis of CpSnDip (**9bn**) as carried out by Summerscales *et al*.[243]

In the ^{119}Sn NMR spectrum of **9bn**, a signal appeared at 94 ppm, which might be in view of the ^{119}Sn NMR signals for the two homoleptic complexes Cp_2Sn (**9a**) (δ ^{119}Sn = −2199 ppm[107,108]) and Dip_2Sn (δ ^{119}Sn = 2235 ppm[244]) a typical region for this heteroleptic stannylene. Unfortunately, the structure in the solid state could not be revealed due to lability of the obtained crystals, but probably it could be analogous to the structure observed for the related germylene CpGeDip (**8bc**) which was reported together with CpSnDip (**9bn**) (*vide supra*).[243] Another example of a tin halfsandwich complex bearing a sterically crowded aryl substituent was reported by Sindlinger *et al*. in 2015 (Scheme 183).[259]

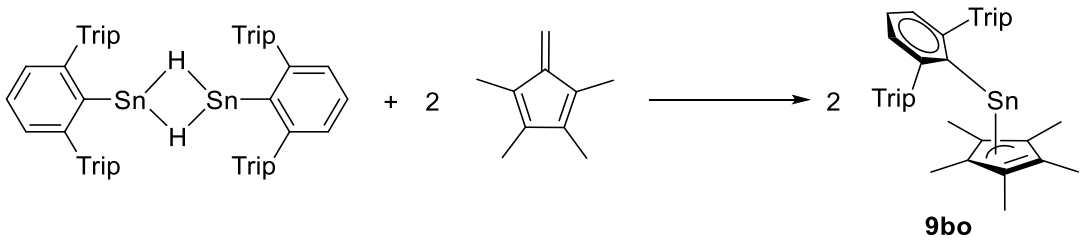

Scheme 183: Synthesis of Cp*Sn(2,6-(Trip)$_2$C$_6$H$_3$) (**9bo**) as conducted by Sindlinger *et al*.[259]

9bo was obtained by hydrostannylation to the exocyclic double bond of the tetramethylfulvene. In the solid state structure of this compound, the tin atom revealed a hapticity of η^3 to the Cp* ligand with Sn-Cp^C distances of 239.82(21) pm, 254.28(20) pm and 255.93(19) pm.[259] In the ^{119}Sn NMR spectrum of this stannylene type compound, a signal appeared at −26 ppm, which is in view of the signal for CpSnDip (**9bn**) a typical region for this type of compound.[243,259] In 1989, the Jutzi group reported of stannyliumylidenes with olefin interactions analogous to the corresponding germyliumylidenes.[171] These complexes were synthesized in the same manner as the corresponding germanium compounds (Scheme 156).[171]

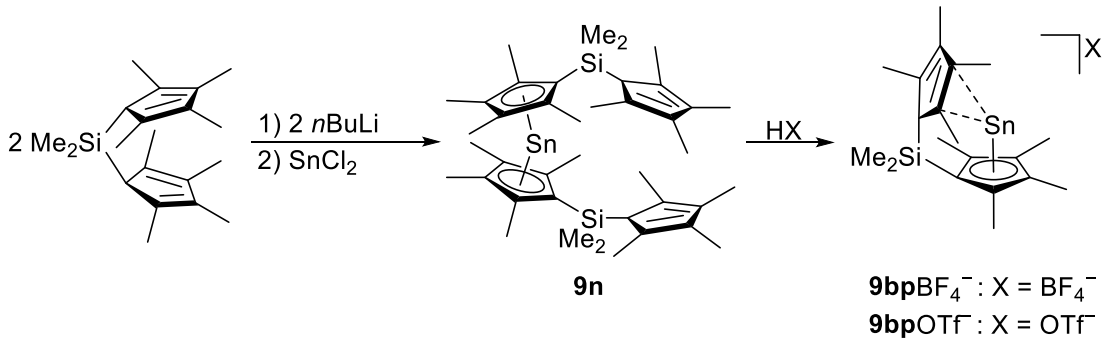

Scheme 184: Syntheses of olefin complexes of stannyliumylidenes as conducted by Jutzi *et al*.[171]

The stannyliumylidene **9bp**BF_4^- could be crystallized by the authors unravelling a structure comparable to the one observed for the germanium analogue with Sn-Cp^C distances of 316.94(67) pm and 330.16(66) pm to the double bond of the cyclopentadiene, which is significantly shorter than these distances in the corresponding germyliumylidene olefin complex.[171] In addition, the authors reported of the synthesis of the halfsandwich complex Me_2Si[1]($Cp^{\#}$; $Cp^{\#}H$)SnCl (**9bq**) which exhibits a signal at −1579 ppm in the ^{119}Sn NMR spectrum comparable to other tin halfsandwich compounds (see Table 11).[171]

In conclusion, the tin halfsandwich compounds represent the largest group in the class of group 14 halfsandwich complexes. The first in the class of tin halfsandwich compounds were the cyclopentadienyltin halides which were synthesized in the 1970s.[136,230,245] In solution, cyclopentadienyltin chloride displays a homoleptic/heteroleptic equilibrium, which is not observed for Cp*SnCl.[109] All cyclopentadienyl substituted stannyliumylidenes exhibit a hapticity of η^5 and approximately equal Sn-Cp^{cent} distances to the cyclopentadienyl ligand and even an example of a stannyliumylidene bearing an unsubstituted cyclopentadienyl ring could be obtained (see Table 11). The stannyliumylidene $Cp^*Sn^+OTf^-$ **9ao**OTf^-,was reacted with pyridine and bipyridine revealing Lewis adducts of this halfsandwich complex. In contrast to cyclopentadienyl substituted germylenes, no example of tin halfsandwich transition metal complexes could be structurally characterized. Two examples of tin halfsandwich complexes bearing a cyclopentadienyl ring and a bulky aryl group were reported in the 2010s.

Table 11: ^{119}Sn NMR shifts, selected structural parameters and references of cyclopentadienyltin halfsandwich compounds.

Compound	δ ^{119}Sn [ppm]	Hapticity Cp η	Cp-Sn [pm][b]	Reference
Cp*SnCl (**9y**)	−1612; −1644[109][a]	5	225.59(10)[224]; 227.03(7)[109]; 228.17(7)[109]	[109,144,205,224]
CpSnCl (**9ai**)	−1483; −1578[109][a]	2	232.47(20)	[109,136,230,245]
CpSnI (**9au**)	-	-	-	[136]
CpSnBr (**9av**)	-	-	-	[245]
Cp*SnBr (**9aw**)	−1630	-	-	[146]
$^{(t\text{BuMe2Si})}$Cp$^{\#}$SnCl (**9ax**)	−1598; −1734[a]	-	-	[109]
$^{(t\text{BuMe2Si})}$Cp$^{\#}_6$Sn$_9$Cl$_{12}$ (**9ay**)	−123; −1856; -16[a]; −735[a]; -2075[a]	5	220.18(12)	[247]
$^{t\text{BuBcat}}$CpSnCl (**9az**)	−1085	-	-	[248]
Me$_2$Si[1](Cp$^{\#}$; Cp$^{\#}$H)SnCl (**9bq**)	−1579	-	-	[171]
[CpSnCl(μ-Fe(CO)$_4$)]$_2$ ([**9ai**(μ-Fe(CO)$_4$)]$_2$); [CpSnBr(μ-Fe(CO)$_4$)]$_2$; ([**9av**(μ-Fe(CO)$_4$)]$_2$)	-	-	-	[207]
Cp*Sn$^{+5\text{COOM}}$Cp$^-$ (**9ao**$^{5\text{COOM}}$Cp$^-$)	−2185	-	-	[188]
CpSn$^+$BF$_4^-$ (**9aq**BF$_4^-$); Cp*Sn$^+$OTf$^-$ (**9ao**OTf$^-$); Cp*Sn$^+$AlCl$_4^-$ (**9ao**AlCl$_4^-$); Cp*Sn$^+$O$_2$CCF$_3^-$ (**9ao**O$_2$CCF$_3^-$); Cp*Sn$^+$O$_2$CCCl$_3^-$ (**9ao**O$_2$CCCl$_3^-$)	-	-	-	[51]
Cp*Sn$^+$BF$_4^-$ (**9ao**BF$_4^-$)	-	5	215.70(1)	[144,249]
Cp*Sn$^+$B(C$_6$F$_5$)$_4^-$ (**9ao**B(C$_6$F$_5$)$_4^-$)	−2219[104]	5	211.35(5)[194]	[104,194]
Cp*Sn$^+$BPh$_4^-$ (**9ao**BPh$_4^-$)	−2246; −2236[a]	5	219.62(8)	[250]
Cp*Sn$^+$OTf$^-$·Py (**9ao**OTf$^-$·Py)	-	5	223.72(2)	[242]
Cp*Sn$^+$OTf$^-$·BiPy (**9ao**OTf$^-$·BiPy)	-	3	230.64(3)	[242]
Cp*Sn$^+$OTf$^-$·Pyraz (**9ao**OTf$^-$·Pyraz); Cp*Sn$^+$BF$_4^-$·BiPy (**9ao**BF$_4^-$·BiPy)	-	-	-	[242]
CpSn$^+$Sn(ptfb)$_3^-$ (**9aq**Sn(ptfb)$_3^-$)	−2392	5	222.44(2)	[195]
CpSn$^+$Al(ptfb)$_4^-$·C$_7$H$_8$ (**9aq**Al(ptfb)$_4^-$·C$_7$H$_8$)	-	5	214.29(4)	[195]
CpSn$^+$(μ-F{Al(ptfb)$_3$}$_2$)$^-$ (**9aq**(μ-F{Al(ptfb)$_3$}$_2$)$^-$)	−2430	5	210.95(14)	[195]

$CpSn^+Al(ptfb)_4^-$ (**9aq**$Al(ptfb)_4^-$)	−2430	-	-	[195]
$SnCp^+Al(ptfb)_4^-$·HMB (**9aq**$Al(ptfb)_4^-$·HMB)	−2379	-	-	[196]
$^{(t\text{BuMe2Si})}Cp^{\#}Sn^+BF_4^-$ (**9bb**BF_4^-)	−2289	5	214.32(9); 215.07(9)	[252]
$^{(t\text{BuMe2Si})}Cp^{\#}Sn^+OTf^-$ (**9bb**OTf^-)	−2170; −2065[a]; −2301[a]	5	219.15(7); 221.76(10)	[251]
$Cp'Sn^+BF_4^-$ (**9bc**BF_4^-)	-	5	218.17(5)	[169]
$Cp''Sn^+BF_4^-$ (**9bd**BF_4^-)	−2338	-	-	[170]
$Cp'''Sn^+SnCl_3^-$ (**9be**$SnCl_3^-$)	-	5	220.87(6)	[234]
$CpSn(\mu\text{-}O^tBu)_2Ge(O^tBu)$ (**9bf**)	−286	3	239.08(17)	[253]
$CpSn(\mu\text{-}O^tBu)_2Sn(O^tBu)$ (**9bg**)	−80; −363	-	-	[253]
$CpSn[Zr_2(O^iPr)_9]$ (**9bh**)	−261	-	-	[254]
$CpSn[Hf_2(O^iPr)_9]$ (**9bi**)	−334	-	-	[254]
$CpSn(\mu\text{-}O^tBu)_2Ge(O^tBu)\cdot Mo(CO)_5$ (**9bj**)	−185	-	-	[256]
$[CpSn(\mu\text{-}NIPr)]_2$ (**9bk**)	−232	1	243.78(10)	[255]
$(^tBuO)_2ClZr[\mu\text{-}Cl(CpSn)](\mu\text{-}O^tBu)_2ZrCl(O^tBu)_2$ (**9bl**)	-	5	228.18(3)	[257]
$[CpSn(\mu\text{-}N{=}C(NMe_2)_2)]_2$ (**9bm**)	2069[258]	1	239.18(56)	[258,260]
CpSnDip (**9bn**)	94	-	-	[243]
Cp*Sn(2,6-$(Trip)_2C_6H_3$) (**9bo**)	−26	3	228.24(2)	[259]
Me_2Si[1](η^5-$Cp^{\#}$; η^2-$Cp^{\#}H)Sn^+GeCl_3^-$ (**9bp**$GeCl_3^-$)	-	-	-	[171]
Me_2Si[1](η^5-$Cp^{\#}$; η^2-$Cp^{\#}H)Sn^+BF_4^-$ (**9bp**BF_4^-)	−2184	2, 5	316.53(12) (η^2); 216.29(15) (η^5)	[171]
Me_2Si[1](η^5-$Cp^{\#}$; η^2-$Cp^{\#}H)Sn^+OTf^-$ (**9bp**OTf^-)	−2116	-	-	[171]

[a]: Detected by CP/MAS NMR spectroscopy; [b]: Given to the centre of tin-cyclopentadienyl bond.

The last part of this chapter deals with the halfsandwich compounds of lead, whose halfsandwich halides were obtained by protonation with HX (X = Cl-I; OAc) and mixing of plumbocene with lead(II)chloride in the case of Cp*PbCl. As already described for cyclopentadienyl substituted stannyliumylidenes, the corresponding plumbyliumylidenes can be obtained by protonation of Cp^*_2Pb (**10c**) with HBF_4 and HOTf.

The first report of a lead halfsandwich compound dates back to 1976, when Holliday *et al*. obtained cyclopentadienyllead halides and cyclopentadienyllead acetate by the reaction of plumbocene with the corresponding hydrogen halides or acetic acid (Scheme 185).[261,262]

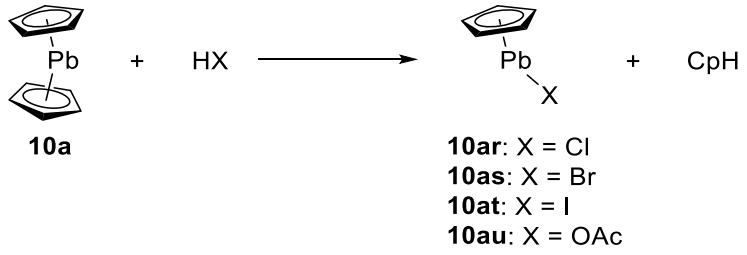

Scheme 185: Syntheses of lead halfsandwich complexes as carried out by Holliday *et al*.[261,262]

The authors described the obtained lead complexes as insoluble in most solvents, more air stable than plumbocene and thermally stable. A polymeric structure in the solid state is anticipated similar to the structure of plumbocene in the solid state but with bridging halide atoms.[261,262] In 1989, Jutzi *et al*. reported on a synthetic route for pentamethylcyclopentadienyllead chloride in analogy to the synthesis for germanium and tin halfsandwich compounds (Scheme 186).[105]

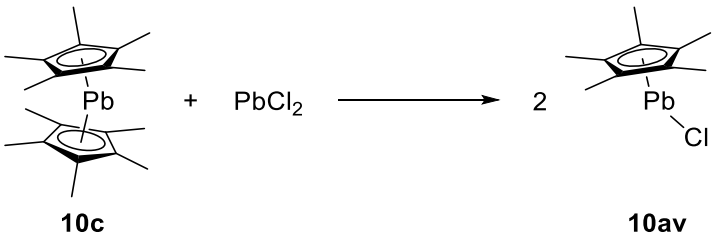

Scheme 186: Synthesis of pentamethylcyclopentadienyllead chloride (**10av**) as conducted by Jutzi *et al*.[105]

The authors stated, that this compound also exhibits a low solubility in most solvents according to a polymeric structure in the solid state. The plumbyliumylidenes **10aw**BF_4^- and **10aw**OTf^- were obtained by the reaction of decamethylplumbocene with the corresponding acid (Scheme 187).[105]

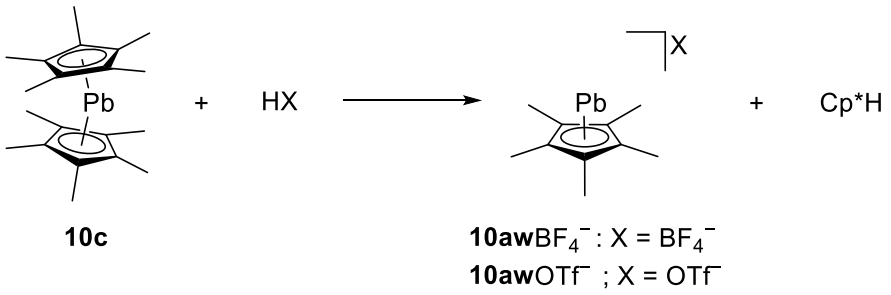

Scheme 187: Syntheses of plumbyliumylidenes as conducted by Jutzi *et al*.[105]

These plumbyliumylidenes exhibit signals of −5042 ppm (**10aw**BF_4^-) and −4962 ppm (**10aw**OTf^-) in the ^{207}Pb NMR spectra which do not differ significantly from those observed for plumbocenes (see Table 8). Crystals suitable for single crystal X-ray crystallography were obtained of **10aw**BF_4^- revealing an η^5 complexed lead atom (Figure 61).[105]

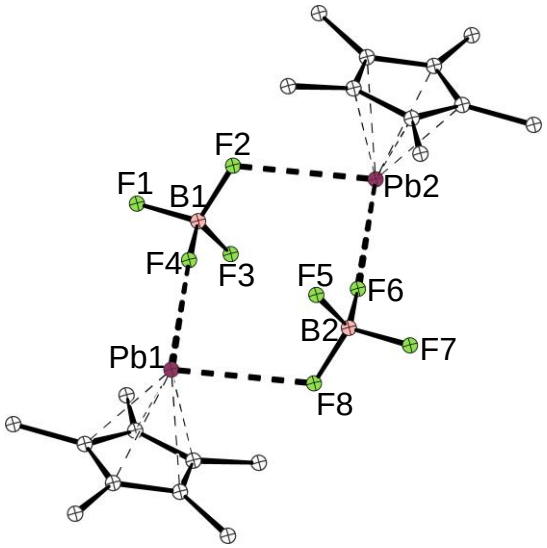

Figure 61: Molecular structure of $Cp^*Pb^+BF_4^-$ (**10aw**BF_4^-)[105] in the crystal (hydrogen atoms omitted for clarity, ball-and-stick representation).

The Pb-Cp^{cent} distance of 226.60(12) pm is greatly shortened in comparison to the Pb-Cp^{cent} distances observed in Cp*$_2$Pb (**10c**) (247.95(10) pm and 252.34(8) pm[16]) due to an increasing electrophilicity at the lead centre. The authors stated that the Pb-F interactions were weak but though this complex could be seen as contact ion pair with two Pb-F contacts at every lead atom (Pb-F distances: 283.04(93) pm and 290.17(87) pm).[105] Another structurally characterized example of a plumbyliumylidene bearing a Cp* ligand was synthesized by Jones *et al*. in 2005 (Scheme 188).[194]

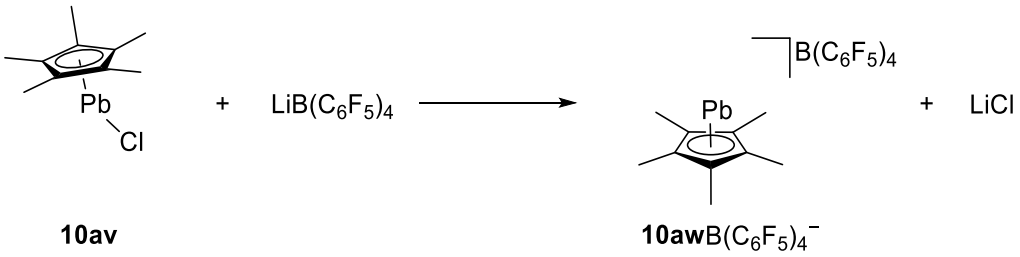

Scheme 188: Synthesis of Cp*Pb$^+$B(C$_6$F$_5$)$_4^-$ (**10aw**B(C$_6$F$_5$)$_4^-$) as conducted by Jones *et al*.[194]

In the solid state structure of **10aw**B(C$_6$F$_5$)$_4^-$, the lead atom exhibits three Pb-F contacts and is η^5 complexed to the pentamethylcyclopentadienyl ligand with a Pb-Cp^{cent} distance of 223.98(6) pm which is comparable to the Pb-Cp^{cent} distance in **10aw**BF$_4^-$ (*vide supra*).[194] The lead compound Cp''Pb$^+$BF$_4^-$ (**10ax**BF$_4^-$) was synthesized by Jutzi and Dickbreder in 1989 in the same manner the corresponding **10aw**BF$_4^-$ was obtained (Scheme 189).[170]

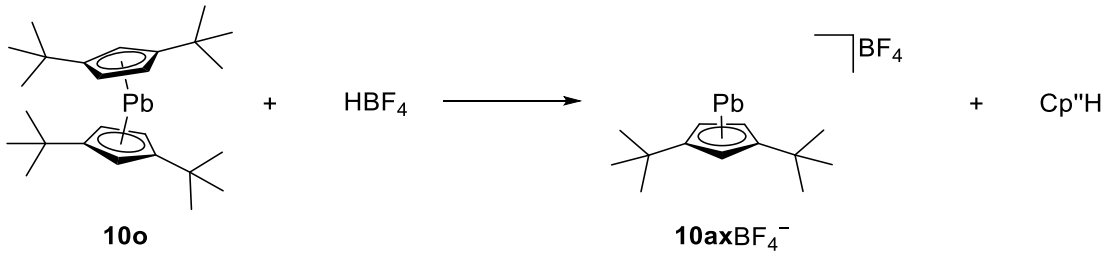

Scheme 189: Synthesis of Cp''Pb$^+$BF$_4^-$ (**10ax**BF$_4^-$) as carried out by Jutzi and Dickbreder.[170]

The authors did not provide structural characteristics to this compound, but the signal of −5462 ppm in the ^{207}Pb NMR spectrum is similar to other cyclopentadienyl substituted

plumbyliumylidenes (see Table 12).[170] The electrophilicity of **10aw**X^- (X = BF_4^-, OTf^-) was investigated by Jutzi *et al*. by addition of bipyridine and naphthyridine to these complexes (Scheme 190).[105]

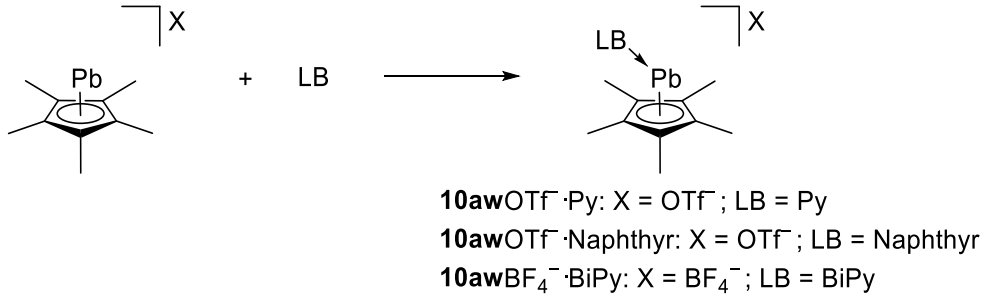

Scheme 190: Synthesis of Lewis base adducts of cyclopentadienyl substituted plumbyliumylidenes as conducted by Jutzi *et al*.[105]

In the case of the bipyridine adducts, the authors suggested structures similar to what was observed in **9ao**OTf^-·BiPy (*vide supra*). The signals in the ^{207}Pb NMR spectra for the obtained adducts were only marginally shifted in comparison to the uncoordinated halfsandwich compounds which was, in accordance to the authors, due to only a little change in electron density at the lead atom. Unfortunately, none of the adducts could be crystallized for which reason further structural discussions are impossible.[105] In 1997, Veith and coworkers synthesized a heterobimetallic complex involving a CpPb moiety (Scheme 191).[254]

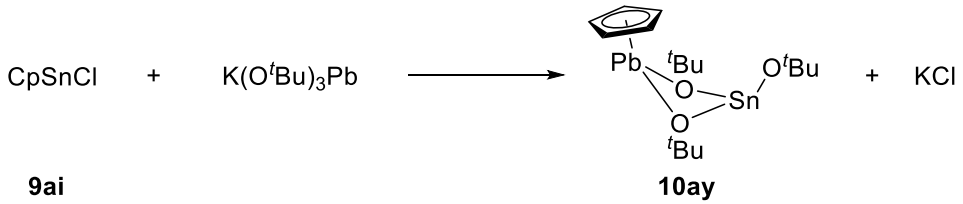

Scheme 191: Synthesis of CpPb(μ-O^{t}Bu)$_2$Sn(O^{t}Bu) (**10ay**) as conducted by Veith *et al*.[254]

The authors intended to synthesize the corresponding tin species, but by redistribution reaction, **10ay** was obtained. In the ^{207}Pb NMR spectrum, a signal appeared at −2092 ppm,

which was significantly downfield shifted compared to other cyclopentadienyllead compounds, but this effect was already observed in the ^{119}Sn NMR spectrum for **9bf** (*vide supra*). The lead atom is complexed in an η^5 fashion to the cyclopentadienyl ligand in the structure of **10ay** in the solid state with a Pb-Cp^{cent} distance of 265.09(21) pm, which is elongated in comparison to other neutral cyclopentadienyllead compounds (see Table 8). In this structure, the lead atom exhibits a contact to another cyclopentadienyl ligand with a Pb-Cp^{cent} distance of 287.46(21) pm, which is elongated but though can be seen as Pb-Cp contact.[254] This behavior of high coordination numbers in cyclopentadienyllead compounds is a known phenomenon which can also be seen in, for example, plumbocene (**10a**).[141] In 1989, the Jutzi group reported of plumbyliumylidenes analogous to the corresponding germyliumylidenes and stannyliumylidenes. These complexes were synthesized in the same manner as the corresponding germanium and tin compounds (Scheme 156).[171]

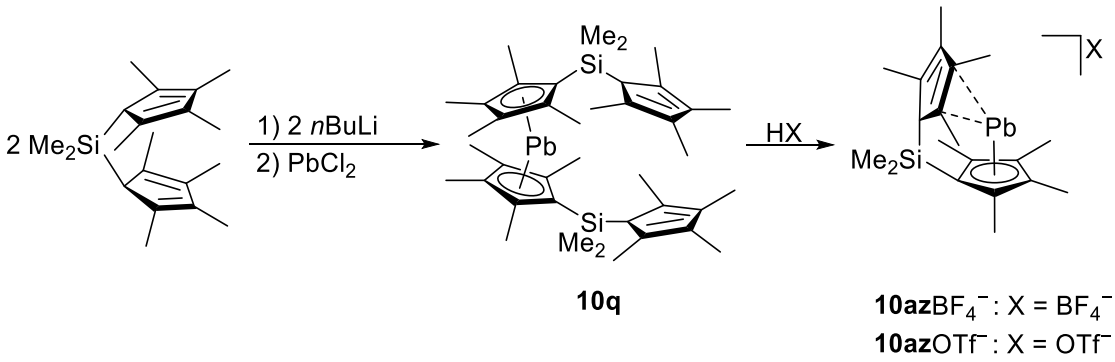

Scheme 192: Syntheses of olefin complexes of plumbyliumylidenes as conducted by Jutzi *et al*.[171]

Unfortunately, no crystals suitable for single crystal X-ray crystallographic analysis could be obtained for which reason the structural characteristics of these plumbyliumylidenes remain uncertain.

In conclusion, the lead halfsandwich complexes represent a small class of compounds with only three examples which are structurally characterized of which two examples are cationic plumbyliumylidenes which both exhibit similar Pb-Cp^{cent} distances (see Table 12). The chemistry of cyclopentadienyl substituted plumbylenes is only sparingly explored in comparison to the chemistry of the corresponding germanium and tin compounds (see Table 10 and Table 11).

Table 12: ^{207}Pb NMR shifts, selected structural parameters and references of cyclopentadienyllead halfsandwich compounds.

Compound	δ ^{207}Pb [ppm]	Hapticity Cp η	Cp-Pb [pm][a]	References
CpPbCl (**10ar**); CpPbBr (**10as**); CpPbI (**10at**); CpPb(O_2CCH_3) (**10au**)	-	-	-	[261,262]
Cp*PbCl (**10av**)	-	-	-	[105]
Cp*Pb$^+$OTf$^-$·BiPy (**10aw**OTf$^-$·BiPy)	−4382	-	-	[105]
Cp*Pb$^+$BF$_4^-$·BiPy (**10aw**BF$_4^-$·BiPy)	−4876	-	-	[105]
Cp*Pb$^+$BF$_4^-$·Naphthyr (**10aw**BF$_4^-$·Naphthyr)	−4504	-	-	[105]
Cp*Pb$^+$B(C_6F_5)$_4^-$ (**10aw**B(C_6F_5)$_4^-$)	-	5	223.98(6)	[194]
Cp*Pb$^+$OTf$^-$ (**10aw**OTf$^-$)	−4962	-	-	[105]
Cp*Pb$^+$BF$_4^-$ (**10aw**BF$_4^-$)	−5042	5	226.60(12)	[105]
Cp''Pb$^+$BF$_4^-$ (**10ax**BF$_4^-$)	−5462	-	-	[170]
CpPb(μ-O^{t}Bu)$_2$Sn(O^{t}Bu) (**10ay**)	−106 (^{119}Sn); −2092 (^{207}Pb)	5	265.09(21)	[254]
Me_2Si[1](η^5-Cp$^{\#}$; η^2-Cp$^{\#}$H)Pb$^+$BF$_4^-$ (**10az**BF$_4^-$)	−4858	-	-	[171]
Me_2Si[1](η^5-Cp$^{\#}$; η^2-Cp$^{\#}$H)Pb$^+$OTf$^-$ (**10az**OTf$^-$)	−4861	-	-	[171]

[a]: Given to the centre of lead-cyclopentadienyl bond.

2. Motivation

Tetrylenes can, in general, react as σ donors or Lewis acids and under oxidative additions or insertion reactions as outlined in the introduction. Stannocene and plumbocene complexes with nitrogen bases were isolated and characterized in 1996 and 1998 revealing the central atom in these tetrelocenes to exhibit mainly Lewis acidic character (Figure 62).[98,99]

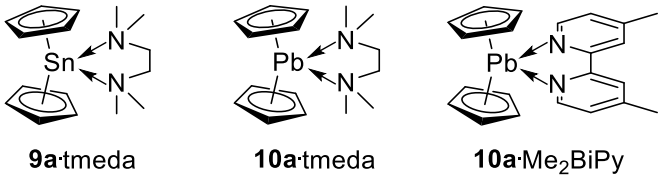

9a·tmeda **10a**·tmeda **10a**·Me_2BiPy

Figure 62: From left to right: Cp_2Sn·tmeda (**9a**·tmeda), Cp_2Pb·tmeda (**10a**·tmeda) and Cp_2Pb·Me_2bipy (**10a**·Me_2BiPy) adducts as reported by *Wright et al*.[98,99]

On the other hand, complexes with non chelating Lewis bases such as adducts of stannocene and plumbocene with strong σ donors were not known at the beginning of this PhD thesis, which lead to the first aim of this thesis (Scheme 193).

Since *N*-heterocyclic carbenes are known to be excellent σ donors and many tetrylene carbene complexes are known to the literature,[95,96,263] the reactions between stannocenes, plumbocene and cyclopentadienyltin(II) halides with carbenes were to be investigated.

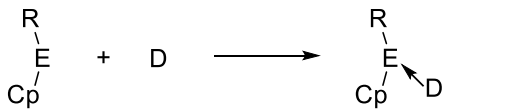

E = Sn; Pb
R = Cl; Br; Cp
D = NHC; cAAC

Scheme 193: Reaction of cyclopentadienyltin and -lead compounds with *N*-heterocyclic carbenes.

In ferrocene chemistry, functionalization of the cyclopentadienyl ligand with various substituents and application of related complexes in different areas is quite common.[73,264–267] As

outlined in the introduction, examples of group 2 and group 14 metallocenes with heteroatomic functionalizated cyclopentadienyl ligands are rare and only one example of a tetrelocene with donor moieties on the cyclopentadienyl rings exists.[158] This lead to the second part of this thesis, which deals with phosphanyl substituted metallocenes of magnesium, antimony and group 14 elements. These phosphanyl functionalized main group metallocenes were to be reacted with small molecules and their coordination chemistry towards different metal fragments was to be explored (Scheme 194).

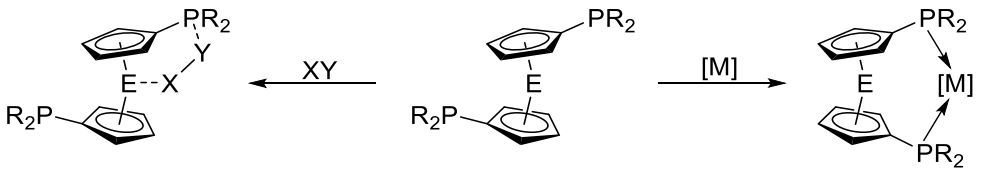

Scheme 194: Reaction of diphosphanylmetallocenes with small molecules and main group and transition metal fragments.

3. Results and Discussion

3.1 Carbene Complexes of Stannocenes

Reprinted with permission from Carsten Müller, Angelika Stahlich, Lisa Wirtz, Claude Gretsch, Volker Huch, André Schäfer, *Inorg. Chem.* **2018**, *57*, 8050-8053. Copyright © (2018) American Chemical Society.

https://doi.org/10.1021/acs.inorgchem.8b01432

The results described within this article are additionally put into context in the Conclusion chapter.

Author contribution:

Carsten Müller:
Lead: Synthesis and characterization of stannocene NHC complexes; writing, reviewing and editing of the supporting information.
Supporting: Writing, reviewing and editing of the manuscript.
Angelika Stahlich:
Supporting: DFT-calculations.
Lisa Wirtz:
Supporting: Synthesis of a stannocene NHC complex.
Claude Gretsch:
Lead: Synthesis and characterization of stannocenophane NHC complexes.
Volker Huch:
Lead: X-ray analysis.
André Schäfer:
Lead: Project administration and supervision; funding acquisition; writing, reviewing and editing of the manuscript; DFT-calculations.
Supporting: Writing, reviewing and editing of the supporting information.

Inorganic Chemistry
Communication
Cite This: Inorg. Chem. 2018, 57, 8050−8053
pubs.acs.org/IC

Carbene Complexes of Stannocenes

Carsten Müller, Angelika Stahlich, Lisa Wirtz, Claude Gretsch, Volker Huch, and André Schäfer*

Faculty of Natural Sciences and Technology, Department of Chemistry, Saarland University, Saarbrücken 66123, Federal Republic of Germany

Supporting Information

ABSTRACT: Several stannocene carbene complexes, **3a**−**3g**, were synthesized and examined in solution by NMR spectroscopy and in the solid state by single-crystal X-ray diffraction. In this new class of metallocene carbene complexes, coordination of the carbene to the tin atom was found to be comparably weak and mostly due to attractive dispersion forces, as indicated by density functional theory calculations. Furthermore, coordination of the N-heterocyclic carbenes results in a weakening of the Sn−Cp bonds, making these complexes very reactive and short-lived at room temperature.

Since the first synthesis and isolation of Wanzlick−Arduengo-type N-heterocyclic carbenes (NHCs),[1−3] they have evolved into one of the most important ligands in transition-metal chemistry.[4−7] In addition, numerous examples of main-group metal complexes with NHCs are known.[8] Furthermore, carbenes have played an important role in the isolation of low-valent main-group compounds in recent years.[4,8−11] Among others, several germylene, stannylene, and plumbylene NHC complexes,[12−22] as well as related stannylene isonitrile complexes,[23] have been reported. However, although NHC complexes of group 2 and 4 metallocenes are known[24−26] and Lewis acid−base adducts of stannocene and plumbocene with tetramethylethylenediamine and bipyridine have been reported,[27,28] highlighting the Lewis acidic character of these metallocenes, the reactivity of group 14 metallocenes (tetrelocenes) toward NHCs is unexplored. On this basis, we were intrigued to study the reactivity of stannocenes, one of the longest known group 14 metallocenes, toward NHCs.

When equimolar amounts of stannocene (**1a**) were mixed with NHCs **2a** and **2b** in deuterated benzene at room temperature and the mixture was examined by multinuclear NMR spectroscopy, new sets of signals were detected. Most characteristic, signals in the ^{13}C NMR spectra at 198.3 ppm (in the case of **2a**) and 209.1 ppm (in the case of **2b**), along with signals at −1824 ppm (in the case of **2a**) and −1936 ppm (in the case of **2b**) in the ^{119}Sn NMR spectra, were observed. These spectroscopic findings indicated the formation of stannocene carbene complexes **3a** and **3b**. To verify these findings, an independent synthesis of complexes **3a** and **3b** by the treatment of **2a**·$SnCl_2$ and **2b**·$SnCl_2$ with 2 equiv of cyclopentadienyllithium was carried out, giving **3a** and **3b**, respectively.[29] In order to investigate the dependence of the complexation reaction on steric demand, dimethylstannocene (**1b**) was reacted with NHCs **2a** and **2b** under identical conditions. The analogues products **3c** and **3d** were obtained, indicating little steric effect of the methyl groups on the cyclopentadienyl rings (Scheme 1).

Scheme 1. Reactions of Stannocenes 1a and 1b with NHCs 2a−2c[a]

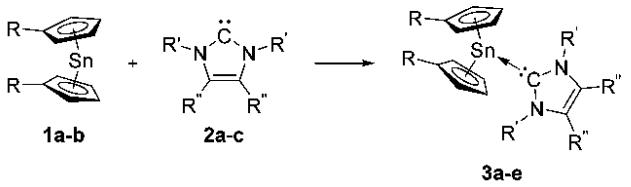

[a] **1a**: R = H. **1b**: R = Me. **2a**: R′ = *i*Pr and R′′ = Me. **2b**: R′ = Mes and R′′ = H. **2c**: R′ = R′′ = Me. **3a**: R = H, R′ = *i*Pr, and R′′ = Me. **3b**: R = Me, R′ = *i*Pr, and R′′ = Me. **3c**: R = H, R′ = Mes, and R′′ = H. **3d**: R = Me, R′ = Mes, and R′′ = H. **3e**: R = R′ = R′′ = Me.

However, when the steric demand is further increased, coordination of an NHC to the tin atom can be prevented. For example, decamethylstannocene (Cp^*_2Sn) does not react with NHCs, just as there is no reaction between **1a** and *N*,*N*′-bis(2,6-diisopropylphenyl)-substituted NHCs. On the other hand, when the steric demand on the NHC is lowered to a minimum, the stannocene carbene complexes become unstable at room temperature. For example, if **1a** is reacted with *N*,*N*′-dimethyl-substituted carbene **2c**, a complex mixture of products is obtained, along with precipitation of metallic tin. However, when **1b** is reacted with NHC **2c** at 248 K, the corresponding complex **3e** can be obtained. **3e** is stable at temperatures below 253 K for several hours and decomposes rapidly upon warming to room temperature. Similar to the stannocenes **1a** and **1b**, the recently reported stannocenophane (**1c**)[30] gives the corresponding NHC complexes **3e** and **3f** with NHCs **2a** and **2b** (Scheme 2).

Scheme 2. Reactions of 1c with NHCs 2a and 2b[a]

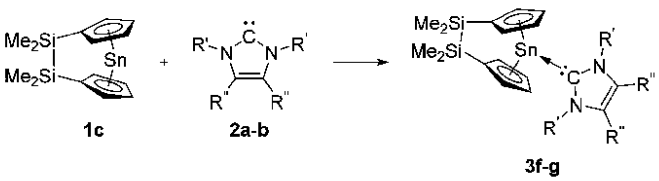

[a] **3f**: R′ = *i*Pr and R′′ = Me. **3g**: R′ = Mes and R′′ = H.

Received: May 24, 2018
Published: June 28, 2018

ACS Publications © 2018 American Chemical Society

DOI: 10.1021/acs.inorgchem.8b01432
Inorg. Chem. 2018, 57, 8050−8053

For all of the carbene complexes **3a**–**3e**, similar NMR spectroscopic parameters are observed (Table S1).[16] The ^{13}C resonances for the carbene carbon atoms experience a high-field shift upon coordination, whereas the ^{119}Sn resonances for **3a**–**3d**, **3f**, and **3g** are downfield-shifted relative to the free stannocenes **1**. To investigate the structure of complexes **3** in more detail, single-crystal X-ray diffraction analysis was performed (Figure 1).

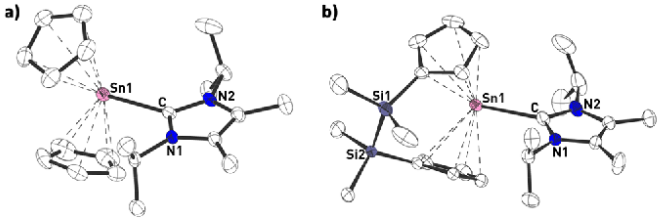

Figure 1. Molecular structures of **3a** (a) and **3f** (b) in the crystal (thermal ellipsoids at the 50% probability level; hydrogen atoms omitted for clarity).

Complexes **3** all show structural similarities in the solid state, which are very long Sn–C^{NHC} bonds compared to 228.0 pm in $(NHC{\cdot}Sn)_2$,[31] 228.7 pm in a NHC·SnR^+ [R = 4-*t*Bu-2,6-$(P(O)(OiPr)_2)_2C_6H_2$],[32] 229.0 pm in **2a**·$SnCl_2$,[33] or 237.9 pm in **2a**·$SnTip_2$ (Tip = 2,4,6-*i*PrC_6H_2),[34] elongated Sn–$Cp^{centroid}$ bonds compared to stannocenes **1a**–**1c**, and an increase in the bending angle α between the cyclopentadienyl ring planes (Table 1 and Figure 2). **3e** exhibits the shortest Sn–C^{NHC} bond of all stannocene carbene complexes **3** as well as the longest Sn–$Cp^{centroid}$ distances. This indicates a relatively strong coordination of the carbene to the tin atom due to little steric bulk in this case, along with weak Sn–Cp bonds. The elongation in the Sn–$Cp^{centroid}$ bonds can be explained by their weakening, due to electron donation from the carbene to the lowest unoccupied molecular orbital (LUMO) of stannocene, which corresponds to an antibonding linear combination of the Sn–Cp bond.[35] This is also the reason for the high reactivity and limited stability of stannocene carbene complexes **3a**–**3g** at room temperature.

In all complexes **3**, unequal Sn–C^{Cp} bond lengths are observed,[38] while there is only one signal in the ^1H and ^{13}C NMR spectra for the cyclopentadienyl moieties in **3a** and **3c**.[29] This indicates a fluxional behavior in solution due to rapid [1,5]-Sn sigmatropic rearrangements, as is common for these types of

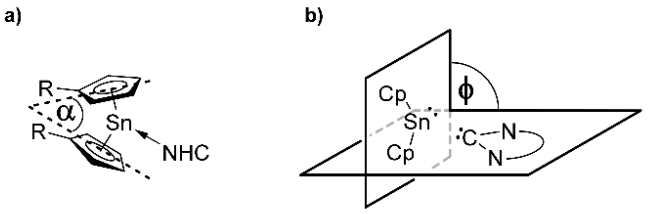

Figure 2. Definition of (a) angle α (angle between cyclopentadienyl planes) and (b) angle φ (angle between the $Cp^{centroid}$–Sn–$Cp^{centroid}$ and NHC planes) in stannocene NHC complexes **3**.

compounds.[39–41] φ angles of 72.2–88.0° between the $Cp^{centroid}$–Sn–$Cp^{centroid}$ and NHC planes in **3** suggest that there is little to no back-bonding from the lone pair at the tin atom to the NHC. This is in agreement with an energetically low-lying lone pair at the tin atom and an energetically high-lying LUMO of the NHC.[29,35,42] To further investigate the bond strengths in these systems, density functional theory (DFT) calculations at the B3LYP-D3/6-311+G(d,p)(C,H,N,Si);SDD-(Sn)/PCM(benzene) level of theory were conducted.[36] The bonding energies of the NHCs **2** to stannocenes **1** in complexes **3** were calculated to be ΔE = 65.9–96.6 kJ·mol^{-1}. When the dispersion force correction terms were omitted [B3LYP/6-311+G(d,p)(C,H,N,Si);SDD(Sn)/PCM(benzene)//B3LYP-D3/6-311+G(d,p)(C,H,N,Si);SDD(Sn)/PCM(benzene)], the calculated BDEs decreased by 70.9–99.8%, indicating that the majority of the complexation energy in complexes **3** can be attributed to attractive dispersion force interactions rather than classical covalent Sn–C^{NHC} bonding.[29] This is in line with recent reports on the importance of dispersion force interactions in many main-group compounds.[43,44] Considering the relatively long Sn–C^{NHC} bonds and the comparably small BDEs, it can be assumed that complexes **3** exist in a dissociative equilibrium with **1** and **2** in solution. This is in agreement with the experimental findings that, upon reaction of **3a** with aluminum chloride, no coordination of $AlCl_3$ to the lone pair at the tin atom is observed, but instead **2a**·$AlCl_3$ along with **1a** is formed, as indicated by ^{27}Al and ^{119}Sn NMR spectroscopy [$\delta(^{27}Al)$ = 107.0; $\delta(^{119}Sn)$ = −2199; Scheme 3].

Furthermore, when 2 equiv of **1a** was mixed with 1 equiv of NHC **2a** or 1 equiv of **1a** was mixed with 2 equiv of NHC **2a** in benzene, only one set of signals is observed in the ^1H, ^{13}C, and ^{119}Sn NMR spectra, indicating a rapid exchange of coordinated and free carbene in solution at room temperature.

Table 1. Relevant Bond Lengths and Angles and Bond Dissociation Energies (BDEs) for 1a–1c and 3a–3g

compound	α (deg)[a]	Sn–$Cp^{centroid}$ (pm)	Sn–C^{NHC} (pm)	φ (deg)[a]	BDE (kJ·mol^{-1})[b]
1a	45.9–46.7[c]	237.0–243.7[c]			
1b	50[d]	240[d]			
1c	47.1–47.3[c]	239.4–242.4[c]			
3a	56.4–59.5[c]	256.1–265.3[c]	245.2–246.6[c]	85.6	70.7
3b	55.2	260.5–262.8[c]	245.1	85.6	72.1
3c	65.3	258.7–262.4[c]	246.5	80.5	88.0
3d	57.7–64.9[c]	253.6–259.5[c]	249.8–250.6[c]	72.2	83.6
3e	67.6	264.5–265.5[c]	238.9	79.1	65.9
3f	56.8	260.2–261.9[c]	248.9	84.8	74.9
3g	62.4	263.5–264.7[c]	248.7	88.0	96.6

[a]See Figure 2 for definitions. [b]BDE is calculated as the difference in the absolute energies between **1**, NHC **2**, and the corresponding stannocene NHC complex **3** at the B3LYP-D3/6-311+G(d,p)(C,H,N,Si);SDD(Sn)/SCRF=PCM(benzene) level of theory.[36] [c]Multiple values are given because more than one molecule is found in the asymmetric unit and/or the bond length or angle is found more than once in the molecule. [d]Value determined by gas electron diffraction.[37]

DOI: 10.1021/acs.inorgchem.8b01432
Inorg. Chem. 2018, 57, 8050–8053

Scheme 3. Reaction of the Stannocene Carbene Complex 3a with Aluminum Chloride

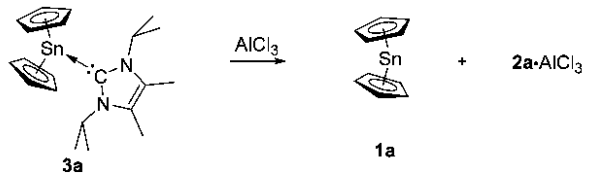

To investigate whether the concept of carbene complexation to stannocenes can be extended to the heavier N-heterocyclic tetrylenes, *N*,*N*′-bis(2,4,6-trimethylphenyl)-substituted N-heterocyclic silylene (**4**)[45,46] and germylene (**5**)[47] were synthesized and reacted with stannocenes **1a** and **1b**.

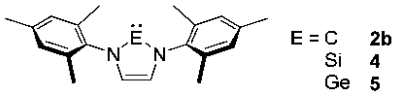

While the reaction of **1a** with **4** resulted in the formation of a mixture of products along with precipitation of tin metal, no reaction was observed by NMR spectroscopy when **1b** was treated with **4**. Corresponding to this, storage of a toluene solution mixture of **1b** + **4** at 248 K yielded only crystals of the starting materials and not of a stannocene silylene complex. Similarly, no reactions were observed between stannocenes **1a** and **1b** and **5**. These results indicate that, unlike for group 2 metallocenes,[48] the complexation of N-heterocyclic tetrylenes to stannocenes is exclusive to NHCs and cannot be observed for their heavier analogues, like **4** and **5**, because of their decreased σ-donor strengths.

In summary, we were able to show that different stannocenes **1** are capable of forming complexes **3** with NHCs **2**. This is in agreement with the carbene germylene and stannylene complexes reported before.[12−15,34] The heavier analogues of NHC **2b**, silylene **4**, and germylene **5** do not form complexes with stannocenes **1a** and **1b** in the same way. Complexes **3a**−**3g** have been studied in solution by multinuclear NMR spectroscopy and in the solid state by single-crystal X-ray diffraction. In solution, it can be assumed that they exist in a dissociative equilibrium. Their solid-state structures reveal a "side-on coordination" of the carbenes to the stannocene moieties, with no back-bonding from the tin atom to the NHC and therefore long Sn−C^{NHC} single bonds, rather than a stannene-type structure. Bonding analysis by DFT calculations shows weak coordination of the carbenes to the tin center with calculated complexation energies between 65.9 and 96.6 kJ·mol^{-1}, 70.9−99.8% of which can be attributed to attractive dispersion force interactions rather than classical covalent bond interactions. Complexes **3** present a new class of stannocene complexes, highlighting the Lewis acidic character of the tin atom and the inertness of its lone pair, which opens up this new field of research. Further studies will focus on other related coordination complexes of group 14 metallocenes.

■ ASSOCIATED CONTENT

Supporting Information

The Supporting Information is available free of charge on the ACS Publications website at DOI: 10.1021/acs.inorgchem.8b01432.

Experimental details, NMR spectroscopic data, and computational details (PDF)

Accession Codes

CCDC 1844881−1844887 contain the supplementary crystallographic data for this paper. These data can be obtained free of charge via www.ccdc.cam.ac.uk/data_request/cif, or by emailing data_request@ccdc.cam.ac.uk, or by contacting The Cambridge Crystallographic Data Centre, 12 Union Road, Cambridge CB2 1EZ, UK; fax: +44 1223 336033.

■ AUTHOR INFORMATION

Corresponding Author

*E-mail: andre.schaefer@uni-saarland.de (A.S.).

ORCID

André Schäfer: 0000-0002-5969-6618

Notes

The authors declare no competing financial interest.

■ ACKNOWLEDGMENTS

Prof. Dr. Guido Kickelbick, Prof. Dr. David Scheschkewitz, Dr. Diego Andrada, and Dr. Carsten Präsang are thanked for their support and helpful discussions. Dr. Michael Zimmer is thanked for his help with NMR experiments. This research was funded by the Deutsche Forschungsgemeinschaft (Emmy Noether Program, SCHA 1915/3-1) and Fonds der Chemischen Industrie.

■ REFERENCES

(1) Wanzlick, H.-W.; Schikora, E. Ein nucleophiles Carben. *Chem. Ber.* **1961**, *94*, 2389−2393.

(2) Wanzlick, H.-W.; Schikora, E. Ein neuer Zugang zur Carben-Chemie. *Angew. Chem.* **1960**, *72*, 494−494.

(3) Arduengo, A. J.; Harlow, R. L.; Kline, M. A stable crystalline carbene. *J. Am. Chem. Soc.* **1991**, *113*, 361−363.

(4) Hopkinson, M. N.; Richter, C.; Schedler, M.; Glorius, F. An overview of N-heterocyclic carbenes. *Nature* **2014**, *510*, 485.

(5) Dröge, T.; Glorius, F. Das Maß aller Ringe − N-heterocyclische Carbene. *Angew. Chem.* **2010**, *122*, 7094−7107.

(6) Díez-González, S.; Marion, N.; Nolan, S. P. N-Heterocyclic Carbenes in Late Transition Metal Catalysis. *Chem. Rev.* **2009**, *109*, 3612−3676.

(7) Hahn, F. E.; Jahnke, M. C. Heterocyclische Carbene − Synthese und Koordinationschemie. *Angew. Chem.* **2008**, *120*, 3166−3216.

(8) Willans, C. E. Non-transition metal N-heterocyclic carbene complexes. *Organometallic Chemistry*; The Royal Society of Chemistry, 2010; Vol. *36*, pp 1−28.

(9) Frenking, G.; Hermann, M.; Andrada, D. M.; Holzmann, N. Donor-acceptor bonding in novel low-coordinated compounds of boron and group-14 atoms C-Sn. *Chem. Soc. Rev.* **2016**, *45*, 1129−1144.

(10) Soleilhavoup, M.; Bertrand, G. Cyclic (Alkyl)(Amino)Carbenes (CAACs): Stable Carbenes on the Rise. *Acc. Chem. Res.* **2015**, *48*, 256−266.

(11) Wurtemberger-Pietsch, S.; Radius, U.; Marder, T. B. 25 years of N-heterocyclic carbenes: activation of both main-group element-element bonds and NHCs themselves. *Dalton Trans.* **2016**, *45*, 5880−5895.

(12) Ruddy, A. J.; Rupar, P. A.; Bladek, K. J.; Allan, C. J.; Avery, J. C.; Baines, K. M. On the Bonding in N-Heterocyclic Carbene Complexes of Germanium(II). *Organometallics* **2010**, *29*, 1362−1367.

(13) Rupar, P. A.; Jennings, M. C.; Baines, K. M. Synthesis and Structure of N-Heterocyclic Carbene Complexes of Germanium(II). *Organometallics* **2008**, *27*, 5043−5051.

(14) Rupar, P. A.; Jennings, M. C.; Ragogna, P. J.; Baines, K. M. Stabilization of a Transient Diorganogermylene by an N-Heterocyclic Carbene. *Organometallics* **2007**, *26*, 4109−4111.

(15) Rupar, P. A.; Jennings, M. C.; Baines, K. M. The reactivity of an anionic gallium N-heterocyclic carbene analogue with a solution stable digermene. *Can. J. Chem.* **2007**, *85*, 141−147.

DOI: 10.1021/acs.inorgchem.8b01432
Inorg. Chem. 2018, 57, 8050−8053

(16) Kocsor, T. G.; Nemes, G.; Saffon, N.; Mallet-Ladeira, S.; Madec, D.; Castel, A.; Escudie, J. N-heterocyclic carbene stabilized phosphaalkenyl(chloro)stannylene. *Dalton Trans.* **2014**, *43*, 2718−2721.
(17) Ekkehardt Hahn, F.; Wittenbecher, L.; Kühn, M.; Lügger, T.; Fröhlich, R. A zwitterionic carbene−stannylene adduct via cleavage of a dibenzotetraazafulvalene by a stannylene. *J. Organomet. Chem.* **2001**, *617*−*618*, 629−634.
(18) Bantu, B.; Pawar, G. M.; Decker, U.; Wurst, K. M.; Schmidt, A. M.; Buchmeiser, M. R. CO_2 and Sn^{II} Adducts of N-Heterocyclic Carbenes as Delayed-Action Catalysts for Polyurethane Synthesis. *Chem. - Eur. J.* **2009**, *15*, 3103−3109.
(19) Al-Rafia, S. M. I.; Malcolm, A. C.; Liew, S. K.; Ferguson, M. J.; Rivard, E. Stabilization of the Heavy Methylene Analogues, GeH_2 and SnH_2, within the Coordination Sphere of a Transition Metal. *J. Am. Chem. Soc.* **2011**, *133*, 777−779.
(20) Al-Rafia, S. M. I.; McDonald, R.; Ferguson, M. J.; Rivard, E. Preparation of Stable Low-Oxidation-State Group 14 Element Amidohydrides and Hydride-Mediated Ring-Expansion Chemistry of N-Heterocyclic Carbenes. *Chem. - Eur. J.* **2012**, *18*, 13810−13820.
(21) Stabenow, F.; Saak, W.; Weidenbruch, M. A zwitterionic carbene-plumbylene adduct. *Chem. Commun.* **1999**, 1131−1132.
(22) Gehrhus, B.; Hitchcock, P. B.; Lappert, M. F. Crystalline (NN)C−M(NN) complexes: synthesis, structure, bonding and lability [M = Si, Ge, Sn or Pb; (NN) = 1,2-$(Bu^tCH_2N)_2C_6H_4$]. *J. Chem. Soc., Dalton Trans.* **2000**, *0*, 3094−3099.
(23) Grützmacher, H.; Freitag, S.; Herbst-Irmer, R. M.; Sheldrick, G. M. Untersuchungen zur Struktur und Reaktivität eines Stannaketenimins. *Angew. Chem.* **1992**, *104*, 459−461.
(24) Kuhn, N.; Al-Sheikh, A. 2,3-Dihydroimidazol-2-ylidenes and their main group element chemistry. *Coord. Chem. Rev.* **2005**, *249*, 829−857.
(25) Arduengo, A. J.; Davidson, F.; Krafczyk, R.; Marshall, W. J.; Tamm, M. Adducts of Carbenes with Group II and XII Metallocenes. *Organometallics* **1998**, *17*, 3375−3382.
(26) Bellemin-Laponnaz, S.; Dagorne, S. Group 1 and 2 and Early Transition Metal Complexes Bearing N-Heterocyclic Carbene Ligands: Coordination Chemistry, Reactivity, and Applications. *Chem. Rev.* **2014**, *114*, 8747−8774.
(27) Armstrong, D. R.; Beswick, M. A.; Cromhout, N. L.; Harmer, C. N.; Moncrieff, D.; Russell, C. A.; Raithby, P. R.; Steiner, A.; Wheatley, A. E. H.; Wright, D. S. Weakly Bonded Lewis Base Adducts of Plumbocene and Stannocene: A Synthetic and Calculational Study. *Organometallics* **1998**, *17*, 3176−3181.
(28) Beswick, M. A.; Cromhout, N. L.; Harmer, C. N.; Raithby, P. R.; Russell, C. A.; Smith, J. S. B.; Steiner, A.; Wright, D. S. Loosely bonded adducts of plumbocene; structures and solution dynamics of [(η-$C_5H_5)_2$Pb·tmeda] and [(η-$C_5H_5)_2$Pb·4,4'-Me_2bipy] (tmeda = $Me_2NCH_2CH_2NMe_2$, 4,4'-Me_2bipy = 4,4'-dimethylbipyridine). *Chem. Commun.* **1996**, 1977−1978.
(29) See the Supporting Information for further details.
(30) Schäfer, A.; Rohe, K.; Grandjean, A.; Huch, V. Synthesis and Structure of [2]Tetrelocenophanes. *Eur. J. Inorg. Chem.* **2017**, *2017*, 35−38.
(31) Jones, C.; Sidiropoulos, A.; Holzmann, N.; Frenking, G.; Stasch, A. An N-heterocyclic carbene adduct of diatomic tin,:Sn = Sn. *Chem. Commun.* **2012**, *48*, 9855−9857.
(32) Wagner, M.; Zöller, T.; Hiller, W.; Prosenc, M. H.; Jurkschat, K. [4-*t*Bu-2,6-{P(O)(O*i*Pr)$_2$}$_2$$C_6H_2$SnL]$^+$: An NHC-Stabilized Organotin(II) Cation and Related Derivatives. *Chem. - Eur. J.* **2013**, *19*, 9463−9467.
(33) Kuhn, N.; Kratz, T.; Bläser, D.; Boese, R. Derivate des Imidazols, XIII. Carben-Komplexe des Siliciums und Zinns. *Chem. Ber.* **1995**, *128*, 245−250.
(34) Schafer, A.; Weidenbruch, M.; Saak, W.; Pohl, S. A carbene-stannylene adduct with a long tin-carbon double bond? *J. Chem. Soc., Chem. Commun.* **1995**, *11*, 1157−1158.
(35) See the Supporting Information for a qualitative molecular orbital diagram of group 14 metallocenes (p S22, Figure S23).
(36) All calculations were performed using the *Gaussian 09*, revision D.01, package of programs; see the Supporting Information for further details, references, and optimized geometries.
(37) Almlöf, J.; Fernholt, L.; Fægri, K., Jr.; Haaland, A.; Schilling, B. E. R.; Seip, R.; Taugbøl, K. The Molecular Structures of 1,1'-Dimethylgermanocene and 1,1'-Dimethylstannocene, $(C_5H_4Me)_2M$; M = Ge and Sn, Determined by Gas Electron Diffraction. Self-consistent Field Molecular Orbital Calculations on Germanocene, $(C_5H_5)_2$Ge. *Acta Chem. Scand.* **1983**, *37a*, 131−140.
(38) While the Cp−Sn bonding in stannocenes **1a**−**1c** is η^5, the Cp−Sn bonding situations in **3a**−**3g** show tendencies toward η^1. However, complexes **3a**−**3g** can still be regarded as π complexes and not as compounds with σ-bonded Cp groups.
(39) Ochiai, T.; Inoue, S. Synthesis of a cyclopentadienyl(imino)-stannylene and its direct conversion into halo(imino)stannylenes. *RSC Adv.* **2017**, *7*, 801−804.
(40) Gridnev, I. D. Sigmatropic and haptotropic rearrangements in organometallic chemistry. *Coord. Chem. Rev.* **2008**, *252*, 1798−1818.
(41) Jutzi, P. The Versatility of the Pentamethylcyclopentadienyl Ligand in Main-Group Chemistry. *Comments Inorg. Chem.* **1987**, *6*, 123−144.
(42) Beswick, M. A.; Palmer, J. S.; Wright, D. S. p-Block metallocenes: the other side of the coin. *Chem. Soc. Rev.* **1998**, *27*, 225−232.
(43) Liptrot, D. J.; Power, P. P. London dispersion forces in sterically crowded inorganic and organometallic molecules. *Nat. Rev. Chem.* **2017**, *1*, 0004.
(44) Wagner, J. P.; Schreiner, P. R. London Dispersion Decisively Contributes to the Thermodynamic Stability of Bulky NHC-Coordinated Main Group Compounds. *J. Chem. Theory Comput.* **2016**, *12*, 231−237.
(45) Zark, P.; Schäfer, A.; Mitra, A.; Haase, D.; Saak, W.; West, R.; Müller, T. Synthesis and reactivity of N-aryl substituted N-heterocyclic silylenes. *J. Organomet. Chem.* **2010**, *695*, 398−408.
(46) Kong, L.; Zhang, J.; Song, H.; Cui, C. N-Aryl substituted heterocyclic silylenes. *Dalton Trans.* **2009**, *28*, 5444−5446.
(47) York, J. T.; Young, V. G.; Tolman, W. B. Heterobimetallic Activation of Dioxygen: Characterization and Reactivity of Novel Cu(I)−Ge(II) Complexes. *Inorg. Chem.* **2006**, *45*, 4191−4198.
(48) Blom, B.; Klatt, G.; Gallego, D.; Tan, G.; Driess, M. Unprecedented silicon(II)→calcium complexes with N-heterocyclic silylenes. *Dalton Trans.* **2015**, *44*, 639−644.

DOI: 10.1021/acs.inorgchem.8b01432
Inorg. Chem. 2018, 57, 8050−8053

3.2 Synthesis, Structure, and Bonding Analysis of Tin(II) Dihalide and Cyclopentadienyltin(II) Halide (Alkyl)(amino)carbene Complexes

Reprinted with permission from Carsten Müller, Diego M. Andrada, Inga-Alexandra Bischoff, Michael Zimmer, Volker Huch, Nils Steinbrück, André Schäfer, *Organometallics* **2019**, *38*, 1052-1061. Copyright © (2019) American Chemical Society.

https://doi.org/10.1021/acs.organomet.8b00861

The results described within this article are additionally put into context in the Conclusion chapter.

Author contribution:

Carsten Müller:
Lead: Synthesis and characterization of CpSnX, cAAC·CpSnX, cAAC·$SnBr_2$ and cAAC·$SnBr_2$·$Fe(CO)_4$ complexes; writing, reviewing and editing of the supporting information.
Supporting: Writing, reviewing and editing of the manuscript; synthesis of cAAC.
Diego M. Andrada:
Lead: DFT-calculations including Energy Decomposition Analysis (EDA) and mechanistic investigations.
Supporting: Writing, reviewing and editing of the manuscript and supporting information.
Inga-Alexandra Bischoff:
Lead: Synthesis of cyclic(amino)(alkyl)carbene ligand (cAAC).
Supporting: Writing, reviewing and editing of the supporting information.
Michael Zimmer:
Lead: CP/MAS NMR analysis.
Volker Huch:
Lead: X-ray analysis.
Nils Steinbrück:
Lead: UV/Vis analysis.
André Schäfer:
Lead: Project administration and supervision; funding acquisition; writing, reviewing and editing of the manuscript.
Supporting: Synthesis of cAAC; writing, reviewing and editing of the supporting information.

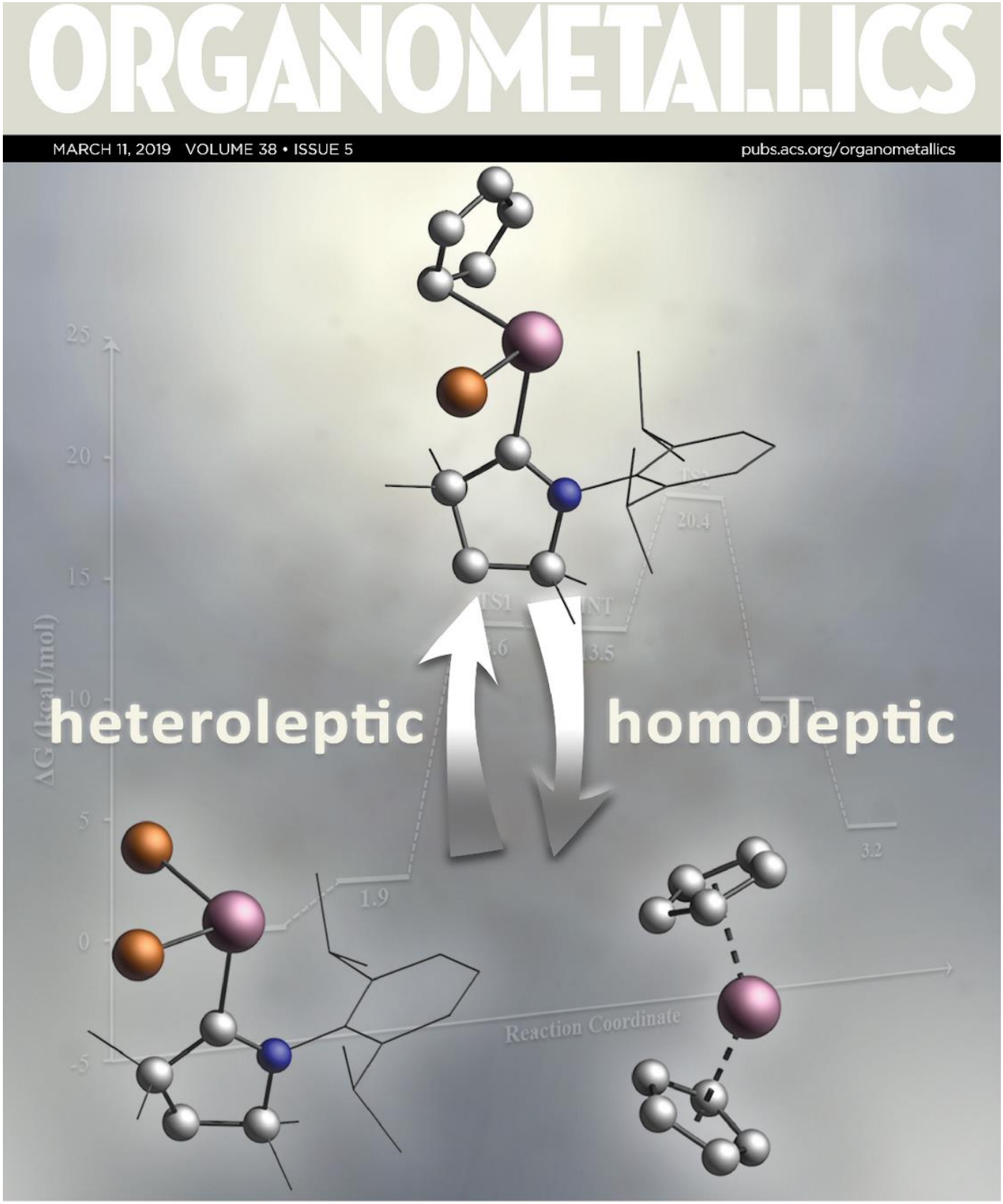
ORGANOMETALLICS
MARCH 11, 2019 VOLUME 38 • ISSUE 5
pubs.acs.org/organometallics
heteroleptic
homoleptic
ΔG (kcal/mol)
Reaction Coordinate
25
20
15
10
5
0
-5
20.4
3.5
3.2
1.9
ACS Publications
Most Trusted. Most Cited. Most Read.
www.acs.org

ORGANOMETALLICS

Article

Cite This: *Organometallics* 2019, 38, 1052−1061

pubs.acs.org/Organometallics

Synthesis, Structure, and Bonding Analysis of Tin(II) Dihalide and Cyclopentadienyltin(II) Halide (Alkyl)(amino)carbene Complexes

Carsten Müller, Diego M. Andrada,* Inga-Alexandra Bischoff, Michael Zimmer, Volker Huch, Nils Steinbrück, and André Schäfer*

Faculty of Natural Sciences and Technology, Department of Chemistry, Saarland University, 66123 Saarbrücken, Federal Republic of Germany

Supporting Information

ABSTRACT: Tin(II) dibromide, **2b**, and cyclopentadienyltin(II) chloride, **2c**, and cyclopentadienyltin(II) bromide, **2d**, were reacted with cyclic (alkyl)(amino)carbene (cAAC), **1**, to give the corresponding complexes cAAC·SnBr$_2$, **3b**, cAAC·SnCpCl, **3c**, and cAAC·SnCpBr, **3d**, which were studied in solution and in the solid state. Although isolatable as crystalline solids, **3c,d** exist in a heteroleptic/homoleptic equilibrium with other tin(II) species, in solution. In addition, the coordination chemistry of **3b** was investigated and the corresponding iron tetracarbonyl complex, **5**, could be isolated and structurally characterized. Furthermore, the mechanism of the equilibrium reaction observed for **3c,d** in solution, as well as the chemical bonding nature of all cAAC complexes were investigated by quantum-chemical calculations within the DFT framework.

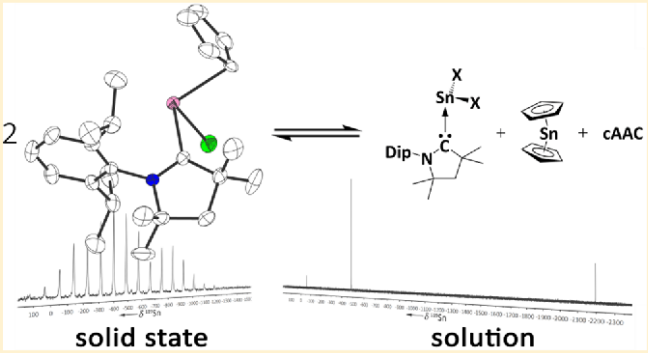

INTRODUCTION

Since their first synthesis, isolation, and characterization,[1] N-heterocyclic carbenes (NHCs) have taken a central stage in chemistry as an extremely versatile class of compounds, which are excellent ligands in transition metal as well as low-valent main group chemistry, due to their strong σ-donating character.[1−5] Thus, in the recent past, the use of NHCs to stabilize highly reactive species has become a hot research field. So far, several examples of hitherto unknown low-valent group 13, 14, and 15 compounds have been experimentally studied in the form of their NHC complexes.[6−22] The related cyclic (alkyl)(amino)carbenes (cAACs), introduced by Bertrand in 2005, have attracted wide attention in this context, since their stronger σ-donor and π-acceptor character provide superior stabilizing abilities with respect to NHCs.[23] Landmark studies in this area have established a solid comparison of the different stabilizing properties of NHCs and cAACs on group 14 halides, such as silicon(II) chloride, germanium(II) chloride, and tin(II) chloride, **3a**.[24−28] It is noteworthy that, although many examples of diorgano germylene and stannylene carbene adducts have been described,[11−14,20] such complexes of group 14 metallocene (tetrelocenes) are almost unknown.[29] Only recently, stannocene, the longest known stable stannylene derivative,[30] has been shown to form complexes with different NHCs, by our group. In these complexes, the carbene coordination to the tin atom weakens the tin Cp bond, making these complexes highly reactive and severely hindering isolation and characterization.[29]

Continuing our research in this area, we were interested in investigating the reactivity of half-sandwich cyclopentadienyltin(II) halide complexes toward carbenes. Herein, we present a combined experimental and computational study in an effort to understand the underlying coordination abilities of carbenes toward a series of cyclopentadienyltin(II) halides.

RESULTS AND DISCUSSION

By reacting stannocene, **4**, with equimolar amounts of tin(II) chloride or tin(II) bromide, the corresponding half-sandwich complexes cyclopentadienyltin(II) chloride, **3c**, and cyclopentadienyltin(II) bromide, **3d**, are obtained quantitatively.[31,32] Based on measurements following the Gutmann−Beckett method, these compounds have a higher Lewis acidity compared to stannocene,[33] making them more reactive toward Lewis bases. Indeed, upon reacting tin half-sandwich complexes **2c,d** with *N,N′*- di-isopropyl-4,5-dimethyl-imidazol-2-ylidene, a coordination of the NHC to the tin atom is indicated by ^{13}C and ^{119}Sn NMR spectroscopy.[36] However, all the attempts to isolate these complexes were unsuccessful, due to rapid decomposition even at low temperatures. The reason for the instability of these complexes could be the relatively weak tin carbene bond. Therefore, we decided to investigate the reactivity of **2b−d** toward cAAC, **1**, since these carbenes possess stronger coordination abilities due to their increased σ-

Received: November 28, 2018
Published: February 19, 2019

ACS Publications © 2019 American Chemical Society

DOI: 10.1021/acs.organomet.8b00861
Organometallics 2019, 38, 1052−1061

donor and π-acceptor character compared to NHCs,[23] as aformentioned.

In analogy to tin(II) chloride, **2a**,[27] tin(II) bromide, **2b**, forms a stable complex, **3b**, with cAAC, **1**, which is isolated in good yields (80%). More interestingly, the related cyclopentadienyl complexes **3c,d** could also be synthesized by treatment of **2c,d** with cAAC, **1**, in THF (Scheme 1) and can

Scheme 1. Synthesis of Complexes 3b−d

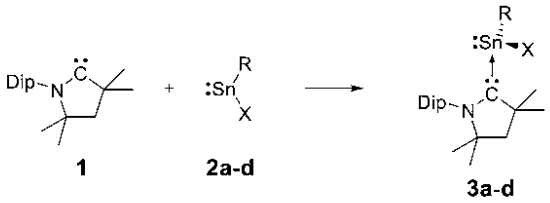

a: R = X = Cl,[27] **b:** R = X = Br;
c: R = Cp, X = Cl; **d:** R = Cp, X = Br

be isolated from a THF/hexane mixture at 248 K in good yields (**3c**: 72%; **3d**: 83%), in the form of yellow to green crystalline solids. Single crystal X-ray diffraction confirms the nature of these complexes (Figure 1).

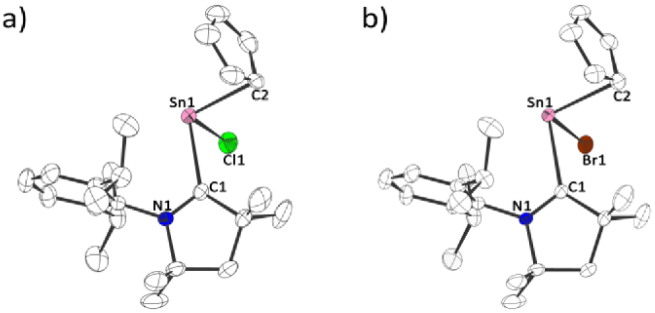

Figure 1. Molecular structure of (a) **3c** and (b) **3d** in the crystal (thermal ellipsoids at 50% probability level; hydrogen atoms omitted for clarity). Selected experimental and calculated [M06-2X/def2-SVP] bond lengths [pm] and angles [deg]: **3c**: N1−C1 129.7 [130.3], C1−Sn1 238.3 [244.3], Sn1−Cl1 252.5 [256.6], Sn1−C2(Cp) 237.9 [242.2], C1−Sn1−Cl1 86.1 [74.8], C1−Sn1−C2 98.5 [94.8], Cl1−Sn1−C2 93.7 [94.0], N1−C1−C3 109.0 [109.2]. **3d**: N1−C1 129.8 [130.3], C1−Sn1 238.3 [244.7], Sn1−Br1 269.1 [274.5], Sn1−C2(Cp) 237.3 [241.6], C1−Sn1−Br1 85.5 [76.6], C1−Sn1−C2 98.3 [95.1], Br1−Sn1−C2 93.8 [93.8], N1−C1−C3 109.0 [109.1].

The coordination of the cyclopentadienyl ligand to the tin atom in **3c** and **3d** is heavily distorted from η^5 and can best be interpreted as η^1. In chloro derivative **3c**, relatively equal C−C bond lengths are observed for the cyclopentadienyl ring carbon atoms (138.8 to 140.4 pm), which suggests some degree of conjugation and preserved aromaticity. In bromo complex **3d**, unequal C−C bond lengths are found within the cyclopentadienyl ring, indicating a diene-type structure (single bonds: 141.2 to 143.3, double bonds: 138.5 to 138.6). In both complexes **3c,d**, the Sn−C^{Cp} distances are significantly different, with one short bond (**3c**: 237.9 pm; **3d**: 237.3 pm), indicating a strong covalent interaction, and longer Sn−C^{Cp} distance to the other C^{Cp} atoms (**3c**: 269.5 to 317.7 pm; **3d**: 269.5 to 317.9 pm). However, for complexes **3c,d**, only one resonance is observed for the cyclopentadienyl moieties in the ^{1}H and ^{13}C NMR spectra at room temperature, due to rapid sigmatropic and haptotropic rearrangements.[35] The Sn−C^{cAAC} bonds in **3c,d** are nearly identical (238.3 pm) and are marginally longer than in dibromo complex **3b** (235.2 pm), which can result from stereoelectronic effects of the cyclopentadienyl ligand (see below) and indicate a slightly weaker Sn−C^{cAAC} bonding interaction in **3c,d** than in **3b**. The ^{13}C NMR chemical shifts for the carbene carbon atoms in **3b−d** are in line with this trend, with a more shielded resonance for **3b** (δ^{13}C = 252.3 ppm) than for **3c,d** (**3c**: δ^{13}C = 265.2 ppm; **3d**: δ^{13}C = 263.3 ppm).

To gain further insight into the electronic structure of the studied compounds, quantum chemical calculations have been carried out.[34] We performed geometry optimization on compound **3c** and **3d** at the M06-2X/def2-SVP level of theory.[37,38] The obtained theoretical structures are in relatively good agreement with the experimental solid state structures. However, it should be noted that the predicted Sn−C^{cAAC} and the Sn−C^{Cp} bond distances deviate by ca. 6 pm. Similar effects have been observed for related complexes before.[27,39] Recomputed optimizations with different functionals (B3LYP+D3(BJ), BP86+D3(BJ), PBE0, TPSSh; Figure S24) led to the same observations. It is noteworthy that the calculations affirm a coordination of the cyclopentadienyl ligand to the tin atom of η^1. The NBO analysis on **3a−d** suggests a donor−acceptor interaction for all the complexes with an electron lone pair localized at the carbene carbon atom and a lone pair at the tin atom (Figure 2).[40] Computed NPA charges reveal negative charges on the tin moiety, while the carbene ligands bear a positive charge (Table 1).

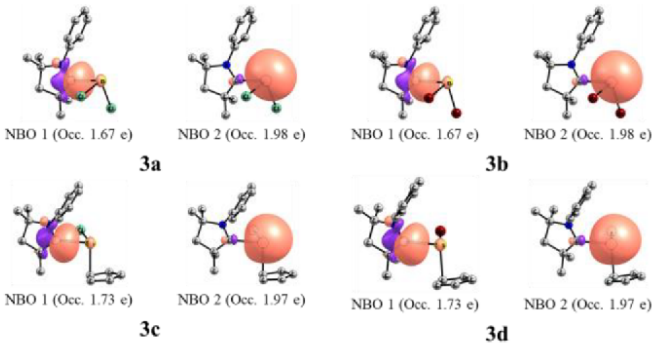

Figure 2. Shape of some relevant natural bond orbitals of **3a−d** at the M06-2X/def2-TZVPP//M06-2X/def2-SVP level of theory.

The Wiberg bond order indicates a stronger Sn−C^{cAAC} interaction for **3a−b** than **3c−d** which is in line with the observed Sn−C^{cAAC} bond length and calculated bond dissociation energies (BDE) at the M06-2X/def2-TZVPP//M06-2X/def2-SVP level of theory (**3a**: 40.6 kcal mol^{-1}, **3b**: 41.2 kcal mol^{-1}, **3c**: 26.3 kcal mol^{-1}, **3d**: 26.8 kcal mol^{-1}).

Table 1. NBO Results at the M06-2X/def2-TZVPP Level of Theory of Compounds 3a−d and 5: Wiberg Bond Order (P) and Partial Charges (q)

	3a	3b	3c	3d	5
q(Sn)	+1.08	+0.97	+1.18	+1.15	+1.21
q(cAAC)	+0.21	+0.21	+0.14	+0.14	+0.24
q(SnXR)	−0.21	−0.21	−0.14	−0.14	+0.18
q(Fe(CO)$_4$)					−0.42
P(C_{carb}−Sn)	0.44	0.44	0.34	0.34	0.43
P(Sn−Fe)					0.43

DOI: 10.1021/acs.organomet.8b00861
Organometallics 2019, 38, 1052−1061

Interestingly, the strength of the Sn−C^{cAAC} bond is influenced by the nature of the halogen atom bonded to the tin atom. Thus, the bromide derivatives **3b,d** show a slightly stronger bonding interaction than the chloride derivatives **3a,c**. On the other hand, bond dissociation energies are ∼15 kcal mol^{-1} weaker when a Cp ligand is bonded to the tin atom.

In order to shed light onto the origins of these differences, energy decomposition analysis (EDA) in combination with natural orbitals for chemical valence (NOCV) has been performed (Table 2 and Table S1).[34,41−43] EDA has proven to be a powerful tool for the understanding of chemical bonding in main-group and transition metal compounds.[43−46] In this method, the bond formation between two or more interacting fragments is divided into three steps (for further details see Computational Details). In the first step, the fragments in their final geometry are placed into the molecule disposition without electronic relaxation to compute the electrostatic interaction (ΔE_{elstat}). In the second step, the wave function is antisymmetrized and renormalized giving the Pauli repulsion within the fragments (ΔE_{Pauli}). In the third step, the molecular orbitals relax into the final state to yield the stabilizing orbital term (ΔE_{orb}). Also, the stabilizing dispersion interaction is directly computed (ΔE_{disp}) when empirical dispersion corrections are used. The sum of all the terms gives the total interaction energy ΔE_{int}. The bond energy (negative of dissociation energy) is calculated as the sum between the interaction energy and the preparation energy (ΔE_{prep}), which is the energy needed to promote the fragments from their relaxed geometry to the geometry and electronic state they have in the final complex.

Thus, the electronic structure of the fragments can be compared with the final electronic structure within the molecule. Many fragmentation schemes can be envisioned. The best fragmentation representations are selected by the means of the orbital interaction term ΔE_{orb}. This term indicates how much the orbitals relax by going from the fragments into the final state in the molecule. Thus, a low absolute value of ΔE_{orb} means that the selected electronic structure of the fragments matches with those in the final molecule. Consequently, the best electronic structure representation is the one that leads to the lower absolute value of ΔE_{orb}. In this regard, we have performed EDA calculations with two possible fragmentations for the C_{carb}-Sn bond, namely, donor−acceptor interaction where the fragments are in their singlet states (Table 2) and electron sharing interaction where the fragments are in their triplet state (Table S1). These studies clearly show a donor−acceptor interaction as the best description for the chemical bonding in **3a,b** with an orbital term of −67.7 and −68.3 kcal mol^{-1} for donor−acceptor bond and −192.2 and −185.1 kcal mol^{-1} for electron-sharing bond, respectively.

Table 2. Energy Decomposition Analysis (EDA-NOCV) of the Sn−C^{cAAC} Bond in 3a−d and 5 at the BP86+D3(BJ)/TZ2P Level of Theory[a]

	3a	3b	3c	3d	5
ΔE_{int}	−54.5	−55.7	−44.3	−46.4	−75.1
ΔE_{Pauli}	142.5	140.5	127.8	127.2	169.9
ΔE_{disp}[b]	−20.1 (10.2%)	−21.3 (10.9%)	−20.5 (11.9%)	−21.6 (12.4%)	−29.3 (12.0%)
ΔE_{elstat}[b]	−109.2 (55.5%)	−106.6 (54.3%)	−94 (54.7%)	−93.7 (54.0%)	−128.4 (52.4%)
ΔE_{orb}[b]	−67.7 (34.4%)	−68.3 (34.8%)	−57.5 (33.4%)	−58.3 (33.6%)	−87.3 (35.6%)
$\Delta E_{orb\ \sigma\text{-}don}$[c]	−50.2 (74.2%)	−51 (74.7%)	−41.3 (71.8%)	−41.9 (71.9%)	−64.1 (73.5%)
$\Delta E_{orb\ LP\text{-}don}$[c]	−3.3 (4.9%)	−3.3 (4.9%)	−3.8 (6.6%)	−3.9 (6.7%)	−5.2 (6.0%)
$\Delta E_{orb\ rest}$[c]	−14.1 (20.9%)	−14 (20.4%)	−12.4 (21.7%)	−12.5 (21.4%)	−17.9 (20.5%)
ΔE_{prep}	6.7	6.9	11	12.1	16.3
$-D_e = \Delta E$	−47.8	−48.9	−33.3	−34.3	−58.8

[a]Energy values given in kcal mol^{-1}. [b]The value in parentheses gives the percentage contribution to the total attractive interactions $\Delta E_{elstat} + \Delta E_{orb} + \Delta E_{disp}$. [c]The value in parentheses gives the percentage contribution to the total orbital interactions ΔE_{orb}.

The computed EDA dissociation energies are ∼5 kcal mol^{-1} higher than those obtained with the M06-2X functional. It should be noted that the ΔE_{prep} values exhibit significant differences between **3a,b** and **3c,d**. The distortion of the SnCpX fragment needs more energy than that for the SnX_2 fragment, as a hapticity shift from η^5 to η^1 occurs. The interaction energy is ∼10 kcal mol^{-1} larger in **3a,b** than in **3c,d**. The Pauli repulsion is ∼15 kcal mol^{-1} higher for the tin(II) dihalide, **3a,b**, derivatives than for cyclopentadienyl derivatives, **3c,d**, in line with their shorter Sn−C^{cAAC} distances. The energy partition of ΔE_{int} also reveals that the total stabilizing interactions are 55% electrostatic, 35% covalent, and 10% dispersion interactions. Interestingly, the numerical data shows a stronger electrostatic and orbital interaction for **3a,b** than for **3c,d**, while the dispersion interactions are similar.

The breakdown of the ΔE_{orb} term into the most important pairwise interactions (Table 2, entries 6−8) shows a strong orbital interaction of −50.2 and −51.0 kcal mol^{-1} for **3a,b** and −41.3 and −41.9 kcal mol^{-1} for **3c,d**, which represents 74% of the orbital term.[34] The largest contribution comes from the σ-donation of the carbene ligand into the vacant *p*-orbital at the tin atom. The interaction is stronger for **3a,b** than for **3c,d**, since they have more Lewis acid character giving their lower LUMO energies (**3a**: ε = −4.37 eV, **3b**: ε = −4.34 eV, **3c**: ε = −3.48 eV, **3d**: ε = −3.15 eV). The remaining pairwise interaction is related to the stabilization interaction between the halide lone pair and the formally vacant *p*-orbital on the carbene carbon atom, explaining the dihedral angle N−C^{cAAC}−Sn−X in these complexes (**3c**: 107.3°, **3d**: 104.3°).

Solid state ^{119}Sn CP-MAS NMR spectra of **3c,d** reveal resonances (δ_{iso}) at δ^{119}Sn = −487 for **3c** and δ^{119}Sn = −486 for **3d**. Analysis of the chemical shift tensors[47] confirms a high chemical shift anisotropy and large span of Ω(**3c**) = $\delta_{11} - \delta_{33}$ = 1070.4 and Ω(**3d**) = $\delta_{11} - \delta_{33}$ = 1052.8 due to the two high field shifted components δ_{22} and δ_{33} and the significantly more deshielded component δ_{11}. Upon dissolving crystals of **3c,d** in THF-D8 and analysis by multinuclear NMR spectroscopy in solution, three signals are observed in the ^{119}Sn NMR spectra in both cases (Figure 3), along with two signals for cyclopentadienyl moieties in the ^{1}H and ^{13}C NMR spectra (**3c**: δ^1H = 5.84, 6.46; δ^{13}C = 111.2, 112.0; **3d**: δ^1H = 5.84, 6.42; δ^{13}C = 111.2, 112.0).[48]

In addition to the signals detected for **3c,d**, which are in line with their solid state ^{119}Sn NMR chemical shifts, the signal at δ^{119}Sn = −2199, along with the resonances at δ^1H = 5.84 and δ^{13}C = 112.0 indicates the formation of stannocene (Cp_2Sn), **4**, while the high field shifted signals can be attributed to tin(II) halide cAAC complexes, **3a,b**.[49] These findings indicate

DOI: 10.1021/acs.organomet.8b00861
Organometallics 2019, 38, 1052−1061

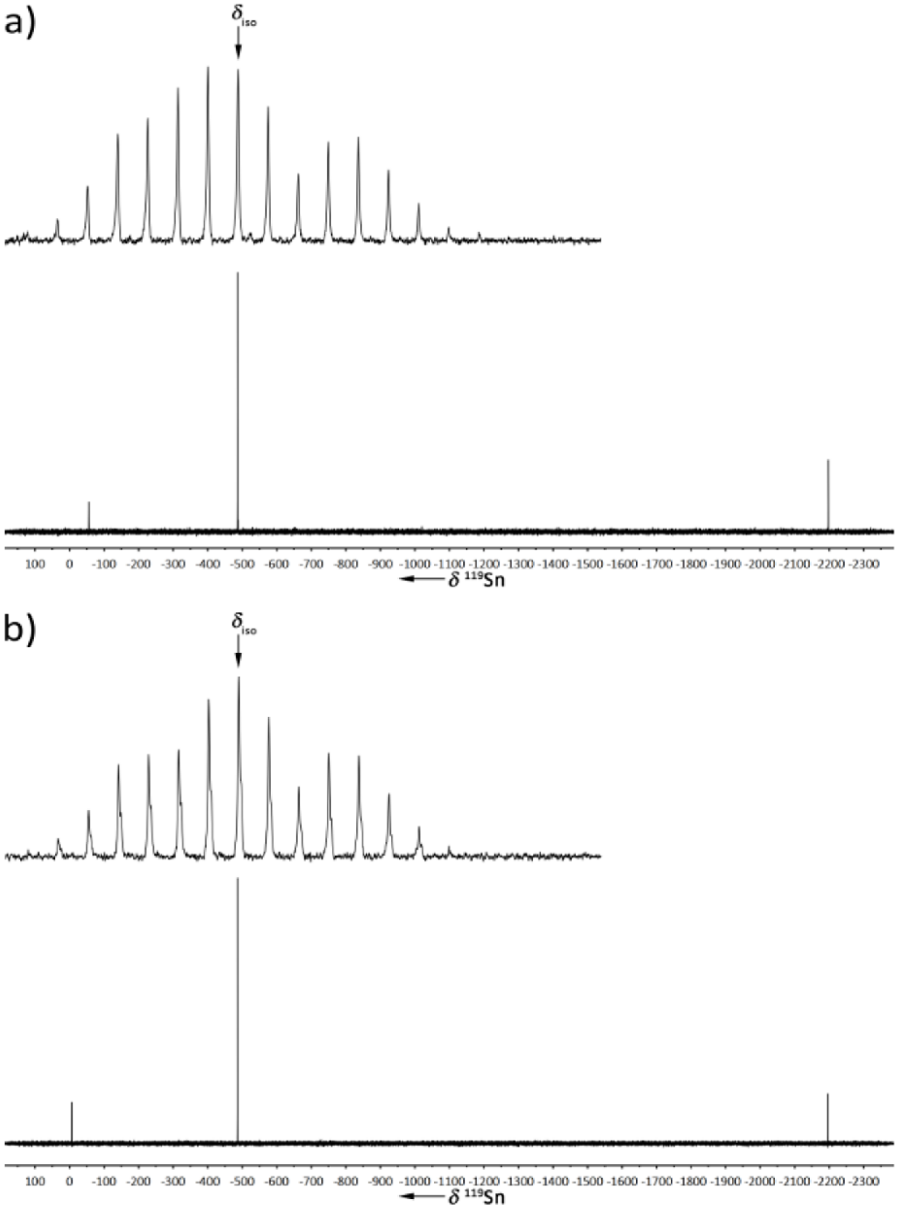

Figure 3. (a) ^{119}Sn NMR spectra derived from **3c** at 299 K, upper trace: ^{119}Sn{^{1}H} CP-MAS spectrum at 13 kHz, lower trace: ^{119}Sn{^{1}H} spectrum in THF-D8; δ^{119}Sn = −56 (**3a**), −486 (**3c**), −2199 (**4**). (b) ^{119}Sn NMR spectra derived from **3d** at 299 K, upper trace: ^{119}Sn{^{1}H} CP-MAS spectrum at 13 kHz, lower trace: ^{119}Sn{^{1}H} spectrum in THF-D8; δ^{119}Sn = −7 (**3b**), −486 (**3d**), −2199 (**4**).

a heteroleptic/homoleptic equilibrium in solution, in which 2 equiv of **3c,d** dissociated into **3a,b** + **1** + **4**, respectively (Scheme 2),[50] which is further supported by an independent synthesis starting from **3b** with **1** and **4**.[51]

Scheme 2. Equilibrium between 3c,d and 3a,b + 4 + 1 in Solution

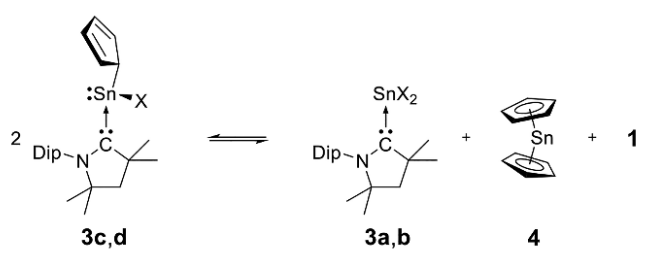

To understand the mechanism of this equilibrium, DFT calculations at the PCM(THF)-M06-2X/def2-TZVPP//M06-2X/def2-SVP level of theory using a model system (simplification of the diisopropylphenyl group on the nitrogen atom by a methyl group) were conducted.

Our calculations suggest that these reactions are slightly endergonic by +1.3 kcal mol^{-1} and +3.5 kcal mol^{-1} for **3c**^{Me} and **3d**^{Me}, respectively. A probable pathway connecting **3c**−**d**^{Me} with **3a**−**b**^{Me} + **1**^{Me} + **4** was located on the potential energy surface (Figure 4).

Since the formation of dimers of cyclopentadienyltin(II) chlorides and pentamethylcyclopentadienylgermanium(II) chlorides is well-known,[32,52−54] dimerization was considered as the starting step.[55] In the energetically lowest dimer structure, one halide atom from one monomer is on top of the carbene carbon atom of the second monomer, due to the aforementioned stabilizing interaction between the lone-pair of the halides and the vacant *p*-orbital at the carbene carbon

DOI: 10.1021/acs.organomet.8b00861
Organometallics 2019, 38, 1052−1061

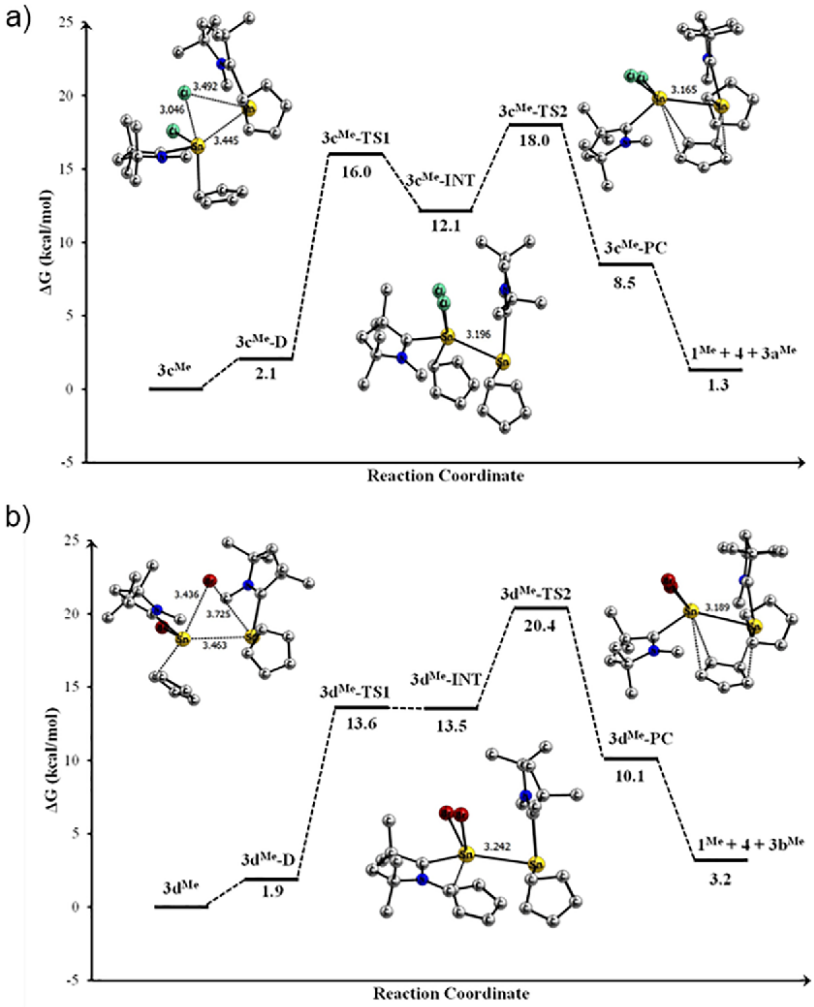

Figure 4. Computed Gibbs energy profiles (Δ*G* at 298.15 K) of the rearrangement reaction of (a) **3c**^{Me} into **4** + **3a**^{Me} + **1**^{Me} and (b) **3d**^{Me} into **4** + **3b**^{Me} + **1**^{Me}. Relative Gibbs energy and bond distances are given in kcal mol^{-1} and Å, respectively. All calculations were performed at the PCM(THF)-M06-2X/def2-TZVPP//M06-2X/def2-SVP level of theory.

atom. The dimerization is slightly endergonic by +2.1 and +1.9 kcal mol^{-1} for **3c**^{Me}**-D** and **3d**^{Me}**-D**, respectively. The reaction mechanism of the redistribution is a stepwise mechanism with the first step consisting of an oxidative addition of the Sn−X bond of one monomer to the Sn atom of the second monomer to give **3c**^{Me}**-INT** and **3d**^{Me}**-INT**. The structures of these intermediates possess a pentacoordinated and a tricoordinated tin atom. In the second step, migration of a Cp ligand from one tin atom to the other takes place, forming the product complex (**3c,d**^{Me}**-PC**). The connecting transition states **3c,d**^{Me}**-TS2** are +5.9 (**3c**^{Me}**-TS2**) and +8.3 (**3d**^{Me}**-TS2**) kcal mol^{-1} higher in energy than the intermediated. The dissociation of the product complex yields the spectroscopically observed products. To the best of our knowledge, this is the first DFT study on the reaction mechanism of such ligand redistribution reactions in main group cyclopentadienide compounds.

Finally, the coordination chemistry of tin(II) bromide carbene complex **3b** toward the iron tetracarbonyl fragment was investigated, by reacting **3b** with diiron nonacarbonyl. Under elimination of iron pentacarbonyl, the corresponding tetracarbonyl complex, **5**, could be obtained (Scheme 3). Crystals of **5**, suitable for single crystal X-ray diffraction, could be obtained from a toluene solution at 248 K (Figure 5b).

Scheme 3. Synthesis of Iron Tetracarbonyl Complex, 5

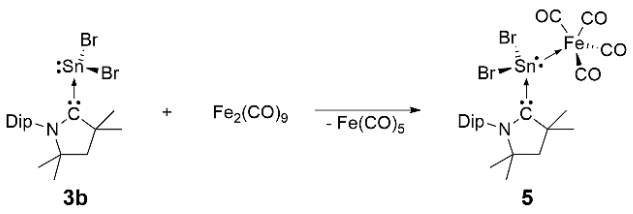

In **5**, a significant shortening of the Sn−C^{cAAC} and Sn−Br bonds can be observed, compared to **3b** (Sn−Br: 261.5 and 262.5 pm (**3b**), 250.5 and 253.6 pm (**5**); Sn−C^{cAAC}: 235.2 pm (**3b**), 225.2 pm (**5**)). The Sn−Fe bond in **5** is 248.3 pm, which is shorter than what is observed in $[Cp_2Sn(Fe(CO)_4)]_2$ (265.1 and 267.0 pm)[56] and for the Sn−Cr bond in IDip·$SnCl_2[Cr(CO)_5]$ (256.8 and 258.3 pm).[57] The Sn−C^{cAAC} bond length in **5** is similar to the Sn−C^{NHC} bond length found in IDip·$SnCl_2[Cr(CO)_5]$ (225.6 and 227.0 pm). Quantum chemical calculations suggest that complex **5** possesses a stronger Sn−C^{cAAC} bond than **3b** and **3d**, namely −58.8 kcal mol^{-1} (Table 2). The dissection of the interaction energy discloses a stronger orbital interaction given the

DOI: 10.1021/acs.organomet.8b00861
Organometallics 2019, 38, 1052−1061

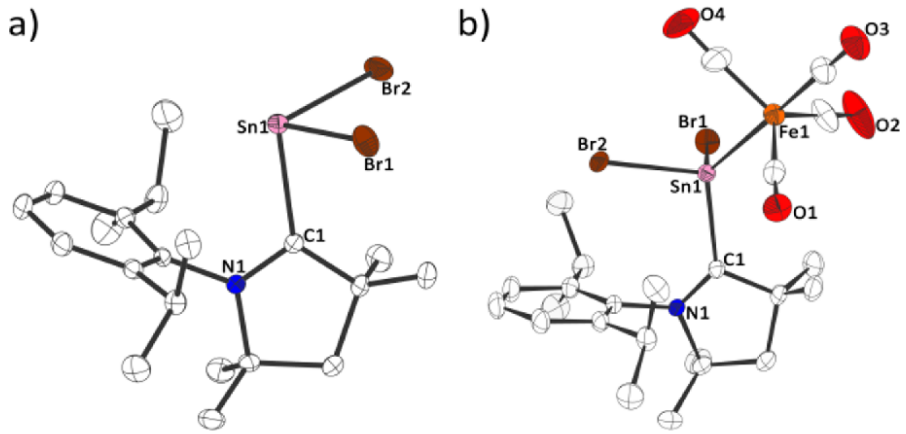

Figure 5. Molecular structure of (a) **3b** and (b) **5** in the crystal (thermal ellipsoids at 50% probability level; hydrogen atoms omitted for clarity). Selected experimental and calculated [M06-2X/def2-SVP] bond lengths [pm] and angles [deg]: **3b**: N1−C1 129.7 [130.1], C1−Sn1 235.2 [239.2], Sn1−Br1 262.5 [266.1], Sn1−Br2 261.5 [264.1], C1−Sn1−Br1 95.1 [83.3], C1−Sn1−Br2 93.1 [92.4], N1−C1−Sn1 117.0 [118.5], N1−C1−C3 109.6 [109.4]. **5**: N1−C1 129.2 [129.6], C1−Sn1 225.2 [231.7], Sn1−Br1 250.5 [256.6], Sn1−Br2 253.6 [260.4], Sn1−Fe 248.3 [256.3], Fe−C3 177.6 [183.3], C3−O3 114.1 [113.5], C1−Sn1−Br1 104.8 [102.7], C1−Sn1−Br2 91.1 [83.8], N1−C1−Sn1 129.6 [130.9], C1−Sn1−Fe 126.9 [125.0].

increased Lewis acidity of the tin moiety by the $Fe(CO)_4$ complexation resulting in a LUMO energy of −5.55 eV.[34]

■ CONCLUSION

In this work, cyclic (alkyl)(amino)carbene complexes of tin(II) bromide, **3b**, and cyclopentadienyltin(II) halides, **3c,d**, were prepared and characterized in solution and in the solid state. Complexes **3c,d** exist in a heteroleptic/homoleptic equilibrium with the corresponding tin(II) dihalide carbene adducts, **3a,b**, along with stannocene, **4**, and cAAC, **1**. This equilibrium was investigated by DFT calculations, suggesting a plausible stepwise mechanism and supporting the spectroscopic observations. Furthermore, the coordination chemistry of complex **3b** was explored and the corresponding iron tetracarbonyl complex, **5**, could be synthesized and structurally characterized. Energy decomposition analysis within the DFT framework showed that the cAAC Sn bond in **3b−d** and **5** is best described as a donor−acceptor interaction.

■ EXPERIMENTAL SECTION

All manipulations were carried out under an argon inert gas atmosphere (argon 5.0), using either standard Schlenk line techniques or a glovebox. Tin dibromide and tin dichloride were purchased from ABCR and used as received. Dicyclopentadiene (90%) was purchased from ABCR, cracked and distilled freshly prior to use. *n*-Butyllithium solution (2.5 M in hexane) was purchased from Acros Organics and used as received. Diiron nonacarbonyl was purchased from Sigma-Aldrich and used as received. Cyclopentadienyl lithium was prepared from cyclopentadiene and n-butyllithium at 195 K. Deuterated benzene and tetrahydrofurane were purchased from ABCR and dried over 4 Å molecular sieves.

1 was prepared by a modified literature procedure.[34] **4** was prepared according to literature known procedures.[30] NMR-spectra were recorded on Bruker Avance III 300 (solution), Bruker Avance III 400 (solution), and Bruker Ascend 400WB (solid state) spectrometers. ^{1}H and ^{13}C NMR spectra were referenced using the solvent signals (δ^1H (C_6HD_5) = 7.20; δ^1H (C_4HD_7O) = 3.58; δ^{13}C (C_6D_6) = 128.0; δ^{13}C (C_4D_8O) = 67.57) and ^{119}Sn NMR spectra were referenced using external standards (δ^{119}Sn ($SnMe_4$) = 0). UV/Vis transmission spectra were recorded with a PerkinElmer Lambda 750 spectrometer with 4 nm increment and 0.2 s integration time. Fourier transformed infrared spectra (FT-IR) were recorded in total reflectance mode with a Bruker Vertex 70 spectrometer from 4500−400 cm^{-1} with a 4 nm increment and 16 scans averaged. Elemental analysis were performed with an Elementar vario micro cube. Single crystal X-ray diffraction analyses were carried out at low temperatures on a Bruker AXS X8 Apex CCD diffractometer operating with graphite monochromated Mo Kα radiation. Structure solution and refinement with anisotropic thermal parameters of all non-hydrogen atoms were performed using SHELX.[58]

Synthesis of 2c,d. Cyclopentadienyl tin(II)halides, **2c,d**, were prepared by a modified literature procedure:[31,32]

Stannocene, **4**, (1.50 g/6.03 mmol) and the corresponding tin(II)halide (**2a**: 1.14 g/6.02 mmol; **2b**: 1.68 g/6.02 mmol) were charged into a Schlenk flask. THF was added, and the resulting solution was stirred overnight. All volatiles were evaporated and the residue washed with hexane. The solvent was evaporated and cyclopentadienyl tin(II)halides, **2c,d**, were obtained as colorless solids. Yield: **2c**: 91%; **2d**: 90%.

2c: ^{1}H NMR (300.13 MHz, C_6D_6, 299 K): δ = 5.84 (s, 10 H, Cp-H); ^{13}C{^{1}H} NMR: (75.47 MHz, C_6D_6, 299 K): δ = 111.2 (Cp); ^{13}C{^{1}H} CP-MAS (13 kHz) NMR (100.65 MHz, 299 K): δ = 113.1 (Cp); ^{119}Sn{^{1}H} CP-MAS (13 kHz) NMR (149.27 MHz, 299 K): δ = −1580.

2d: ^{1}H NMR (300.13 MHz, C_6D_6, 299 K): δ = 5.84 (s, 10 H, Cp-H); ^{13}C{^{1}H} NMR: (100.61 MHz, C_6D_6, 299 K): δ = 111.3 (Cp); ^{13}C{^{1}H} CP-MAS (13 kHz) NMR (100.65 MHz, 299 K): δ = 113.2 (Cp); ^{119}Sn{^{1}H} CP-MAS (13 kHz) NMR (149.27 MHz, 299 K): δ = −1582.

Synthesis of 3b−d. **1** (100 mg/0.35 mmol) and the corresponding tin compound, **2b−d**, (**2b**: 98.0 mg/0.35 mmol; **2c**: 76.0 mg/0.35 mmol; **2d**: 92.0 mg/0.35 mmol) were charged into a Schlenk flask. THF was added, and the solution was stirred until all solids were completely dissolved. The same amount of hexane was added and the resulting solution was stored at 248 K overnight to yield the complexes, **3b−d**, as crystalline solids. Yield: **3b**: 80% (yellow crystals); **3c**: 72% (yellow to green crystals); **3d**: 83% (yellow to green crystals).

3b: ^{1}H NMR (300.13 MHz, THF-D8, 299 K): δ = 1.32 (d, ^3J = 6.6 Hz, 6 H, Dip-Me), 1.34 (d, ^3J = 6.6 Hz, 6 H, Dip-Me), 1.47 (s, 6 H, N−CMe_2), 1.90 (s, 6 H, C−CMe_2), 2.18 (s, 2 H, CH_2), 2.89 (sept, ^3J = 6.6 Hz, 2 H Dip-CH-Me_2), 7.41−7.43 (m, 2 H, *m*-Dip-H), 7.50−7.55 (m, 1 H, *p*-Dip-H); ^{13}C{^{1}H} NMR: (75.47 MHz, THF-D8, 299 K): δ = 24.8 (Me), 27.9 (Me), 29.1 (Me), 29.6 (Me), 30.5 (CHMe_2), 52.4 (CH_2), 61.1 (C_q), 83.1 (C_q), 127.0 (Dip), 132.1 (Dip), 133.6 (Dip), 146.8 (Dip), 252.3 (carbene-C); ^{119}Sn{^{1}H} NMR (111.92 MHz, THF-D8, 299 K): δ = −9; UV/Vis: λ_{max} = 248 nm; Elemental analysis for $C_{20}H_{31}Br_2NSn$: found: C: 42.60%, H: 5.46%, N: 2.67%; calc: C: 42.59%, H: 5.54%, N: 2.48%.

DOI: 10.1021/acs.organomet.8b00861
Organometallics 2019, 38, 1052−1061

3c: Signals observed for cAAC moiety in solution at room temperature are an averaged set of signals derived from different species.[50] ^{1}H NMR (400.13 MHz, C_6D_6/THF-D8, 299 K): δ = 1.00 (s, 6 H, N−C$\underline{Me}_2$), 1.13 (d, ^3J = 6.7 Hz, 6 H, Dip-$\underline{Me}$) 1.27 (bs, 6 H, Dip-$\underline{Me}$), 1.61 (s, 2 H,C$\underline{H}_2$), 1.70 (s, 6 H, C−C$\underline{Me}_2$), 2.82 (bs, Dip-C$\underline{H}$-Me_2), 5.84 (s, 2 H, $\underline{Cp}_2$Sn), 6.46 (s, 3 H, cAAC·$\underline{Cp}$SnCl), 7.00−7.17 (m, 3 H, Dip-$\underline{H}$); ^{13}C{^{1}H} NMR: (75.47 MHz, $\underline{C}_6D_6$/THF-D8, 299 K): δ = 23.7 (bs, Me), 27.0 (bs, Me), 28.5 (Me), 28.9 (Me), 30.2 ($\underline{C}HMe_2$), 51.5 ($\underline{C}H_2$), 81.9 ($\underline{C}_q$), 111.2 ($\underline{Cp}_2$Sn), 112.0 (cAAC·$\underline{Cp}$SnCl), 125.5 (Dip), 130.4 (Dip), 145.9 ($\underline{Dip}$); 265.2 (carbene-C; detected by ^{1}H, ^{13}C-HMBC) (Only 3 signals for the aromatic carbon atoms are observed due to overlapping with the solvent signal.); ^{119}Sn{^{1}H} NMR (111.95 MHz, C_6D_6/THF-D8, 299 K): δ = −2199, −59; ^{119}Sn{^{1}H} NMR (111.92 MHz, THF-D8, 299 K): δ = −2199, −486, −56; ^{13}C{^{1}H} CP-MAS (13 kHz) NMR (100.65 MHz, 299 K): δ = 25.2 (Me), 28.5 (Me), 29.3 (Me), 32.1 ($\underline{C}H$-Me_2), 51.1 ($\underline{C}H_2$), 57.3 ($\underline{C}_q$), 82.5 ($\underline{C}_q$), 111.9 (Cp), 124.4 (Dip), 126.3 (Dip), 130.8 (Dip), 132.2 (Dip), 143.0 (Dip), 145.3 (Dip), 261.0 (carbene-C); ^{119}Sn{^{1}H} CP-MAS (13 kHz) NMR (149.27 MHz, 299 K): δ = −487; Elemental analysis for $C_{25}H_{36}ClNSn$: found: C: 59.09%, H: 7.20%, N: 2.55%; calc: C: 59.49%, H: 7.19%, N: 2.78%. **3d**: Signals observed for cAAC moiety in solution at room temperature is an averaged set of signals derived from different species.[50] ^{1}H NMR (300.13 MHz, C_6D_6/THF-D8, 299 K): δ = 1.02 (s, 6 H, N−C$\underline{Me}_2$), 1.13 (d, ^3J = 6.6 Hz, 6 H, Dip-$\underline{Me}$) 1.27 (d, ^3J = 6.6 Hz, 6 H, Dip-$\underline{Me}$), 1.63 (s, 2 H,C$\underline{H}_2$), 1.72 (s, 6 H, C−C$\underline{Me}_2$), 2.82 (bs, Dip-C$\underline{H}$-Me_2), 5.84 (s, 2 H, $\underline{Cp}_2$Sn), 6.42 (s, 3 H, cAAC·$\underline{Cp}$SnCl), 7.00−7.17 (m, 3 H, Dip-$\underline{H}$); ^{13}C{^{1}H} NMR: (75.47 MHz, $\underline{C}_6D_6$/THF-D8, 299 K): δ = 24.0 (bs, Me), 27.6 (bs, Me), 28.5 (Me), 28.8 (Me), 30.2 (bs, $\underline{C}HMe_2$), 51.5 ($\underline{C}H_2$), 81.9 ($\underline{C}_q$), 111.2 ($\underline{Cp}_2$Sn), 112.0 (cAAC·$\underline{Cp}$SnCl), 125.7 (Dip), 130.5 (Dip), 145.9 ($\underline{Dip}$); 263.3 (carbene-C; detected by ^{1}H,^{13}C-HMBC) (Only 3 signals for the aromatic carbon atoms are observed due to overlapping with the solvent signal.); ^{119}Sn{^{1}H} NMR (149.21 MHz, C_6D_6/THF-D8, 299 K): δ = −2199, −11; ^{119}Sn{^{1}H} NMR (111.92 MHz, THF-D8, 299 K): δ = −2199, −486, −7; ^{13}C{^{1}H} CP-MAS (13 kHz) NMR (100.65 MHz, 299 K): δ = 25.2 (Me), 26.9 (Me), 29.3 (Me), 31.7 ($\underline{C}H$-Me_2), 51.9 ($\underline{C}H_2$), 57.9 ($\underline{C}_q$), 82.6 ($\underline{C}_q$), 112.3 (Cp), 124.5 (Dip), 127.0 (Dip), 131.3 (Dip), 143.3 (Dip), 145.6 (Dip), 260.5 (carbene-C); ^{119}Sn{^{1}H} CP-MAS (13 kHz) NMR (149.27 MHz, 299 K): δ = −489; Elemental analysis for $C_{25}H_{36}BrNSn$: found: C: 53.66%, H: 6.44%, N: 2.74%; calc: C: 54.68%, H: 6.61%, N: 2.55%.

Synthesis of 5. **3b** (80.0 mg, 0.14 mmol) and Fe_2CO_9 (48.0 mg, 0.13 mmol) were charged into a Schlenk flask. Toluene was added and the resulting solution was gently heated, until the color of the solution changed from yellow to red. After storage at 248 K overnight, **5** was obtained in the form of red crystals. Yield: 68%.

^{1}H NMR (300.13 MHz, THF-D8, 299 K): δ = 1.35 (d, ^3J = 6.6 Hz, 6 H, Dip-$\underline{Me}$) 1.33 (s, 2 H, C$\underline{H}_2$), 1.46 (d, ^3J = 6.6 Hz, 6 H, Dip-$\underline{Me}$), 1.55 (s, 6 H, N−C$\underline{Me}_2$), 1.94 (s, 6 H, C−C$\underline{Me}_2$), 2.82 (sept, ^3J = 6.6 Hz, 2 H, Dip-C$\underline{H}$-Me_2), 7.39−7.43 (m, 2 H, *m*-Dip-$\underline{H}$), 7.47−7.54 (m, 1 H, *p*-Dip-$\underline{H}$); ^{13}C{^{1}H} NMR: (75.47 MHz, THF-D8, 299 K): δ = 27.9 (Me), 29.5 (Me), 30.1 (Me), 30.6 ($\underline{C}HMe_2$), 51.0 ($\underline{C}H_2$), 58.5 ($\underline{C}_q$), 87.0 ($\underline{C}_q$) 127.3 (Dip), 132.2 (Dip), 132.9 (Dip), 146.2 (Dip), 215.5 ($\underline{C}$=O), 227.9 (carbene-C); ^{119}Sn{^{1}H} NMR (111.92 MHz, THF-D8, 296 K): δ = 72; IR: 1918 cm^{-1} (CO), 1960 cm^{-1} (CO), 2032 cm^{-1}(CO); UV/Vis: λ_{max} = 223 nm (269 nm); Elemental analysis for $C_{24}H_{31}Br_2FeNO_4Sn$: found: C: 39.47%, H: 4.40%, N: 1.63%; calcd: C: 39.39%, H: 4.27%, N: 1.91%.

Computational Details. All geometries were optimized without symmetry constraint within the DFT (density functional theory) framework using the M06-2X[37] in combination with the Ahlrichs def2-SVP basis function.[38] For comparison, we have also optimized the initial complexes **3b** and **3d** using the BP86+D3(BJ)/def2-SVP,[38,59,60] BP86+D3(BJ)/def2-TZVPP, B3LYP+D3,(BJ)/def2-SVP[61,62] PBE0/def2-SVP[63] and TPSSh/def2-SVP[64−66] levels of theory. These calculations were performed using the Gaussian 16 A.03 software.[67] The stationary points were located with the Berny algorithm[68] using redundant internal coordinates. Analytical Hessians were computed to determine the nature of stationary points (one and zero imaginary frequencies for transition states and minima, respectively)[69] and to calculate unscaled zero-point energies (ZPEs) as well as thermal corrections and entropy effects using the standard statistical-mechanics relationships for an ideal gas.[70] Transition structures (TSs) show only one negative eigenvalue in their diagonalized force constant matrices, and their associated eigenvectors were confirmed to correspond to the motion along the reaction coordinate under consideration using the intrinsic reaction coordinate (IRC) method.[71] The electronic energies were improved by single point calculations at the M06-2X/def2-TZVPP level of theory. Unless otherwise stated, Gibbs energies have been computed at 298.15 K. For these calculations the THF solvent was described by nonspecific solvent effects within the self-consistent reaction field (SCRF) approach in Tomasi's formalism.[72,73] The Wiberg Bond Indices (WBI)[74] and NPA[75,76] atomic partial charges have been calculated at the M06-2X/def2-TZVPP//M06-2X/def2-SVP level of theory using GAUSSIAN 16[67] and GENNBO6.0 programs.[77]

The nature of the chemical bond was investigated by means of an energy decomposition analysis (EDA), which was developed by Morokuma[41] and by Ziegler and Rauk.[42] The EDA focuses on the instantaneous interaction energy ΔE_{int} of a bond A-B between the fragments A and B in the particular electronic reference state at the frozen geometry of the molecule AB.[43] The interaction energy ΔE_{int} is divided into four main components [eq 1].

$$\Delta E_{\text{int}} = \Delta E_{elstat} + \Delta E_{Pauli} + \Delta E_{orb} + \Delta E_{disp} \quad (1)$$

The term ΔE_{elstat} corresponds to the quasiclassical electrostatic interaction between the unperturbed charge distributions of the prepared atoms and is usually attractive. The Pauli repulsion ΔE_{Pauli} arises as the energy change associated with the transformation from the superposition of the unperturbed electron densities $\rho_A + \rho_B$ of the isolated fragments to the wave function,

$$\Psi^0 = N\hat{A}[\Psi_A\Psi_B] \quad (2)$$

which properly obeys the Pauli principle through explicit antisymmetrization ($\hat{A}$ operator) and renormalization (N = constant) of the product wave function. ΔE_{Pauli} comprises the destabilizing interactions between electrons of the same spin on either fragment. The orbital interaction ΔE_{orb} accounts for charge transfer, polarization effects, and electron-pair bonding.[78] In the case that the Grimme dispersion corrections[79,80] are computed the term ΔE_{disp} is added to the equation to count the dispersion interaction between the fragments.

The relaxation of the fragments to their equilibrium geometries at the electronic ground state is termed ΔE_{prep}, because it may be considered as preparation energy for chemical bonding. The addition of ΔE_{prep} to the intrinsic interaction energy ΔE_{int} gives the total energy ΔE, which is—by definition with opposite sign—the bond dissociation energy D_e:

$$\Delta E(-D_e) = \Delta E_{\text{int}} + \Delta E_{prep} \quad (3)$$

The EDA−NOCV method combines the EDA with the natural orbitals for chemical valence (NOCV) to decompose the orbital interaction term ΔE_{orb} into pairwise contributions. The NOCVs Ψ_i are defined as the eigenvector of the valence operator, $\hat{V}$, given by eq 4.

$$\hat{V}\Psi_i = \nu_i\Psi_i \quad (4)$$

In the EDA−NOCV scheme the orbital interaction term, ΔE_{orb}, is given by eq 5,

$$\Delta E_{orb} = \sum_k \Delta E_k^{orb} = \sum_{k=1}^{N/2} \nu_k[-F_{-k,-k}^{TS} + F_{k,k}^{TS}] \quad (5)$$

in which $-F_{-k,-k}^{TS}$ and $-F_{k,k}^{TS}$ are diagonal transition state Kohn−Sham matrix elements corresponding to NOCVs with the eigenvalues $-\nu_k$ and ν_k, respectively. The ΔE_k^{orb} term for a particular type of bond is assigned by visual inspection of the shape of the deformation density

DOI: 10.1021/acs.organomet.8b00861
Organometallics 2019, 38, 1052−1061

$\Delta\rho_k$. The latter term is a measure of the size of the charge deformation, and it provides a visual notion of the charge flow that is associated with the pairwise orbital interaction. The EDA−NOCV scheme thus provides both qualitative and quantitative information about the strength of orbital interactions in chemical bonds.

The EDA−NOCV calculations were carried out with program package ADF2018[81] using DFT functional BP86[59,60] with Grimme dispersion corrections D3(BJ)[79,80] with uncontracted Slater-type orbitals (STOs)[82] with TZ2P quality as basis functions. The latter basis sets for all elements have triple-ζ quality augmented by two sets of polarization functions. An auxiliary set of s, p, d, f, and g STOs was used to fit the molecular densities and to represent the Coulomb and exchange potentials accurately in each SCF cycle.[83] Scalar relativistic effects have been incorporated by applying the zeroth-order regular approximation (ZORA).[84] The EDA-NOCV calculations at the BP86+D3(BJ)/TZ2P level were performed using M06-2X/def2-SVP optimized geometries.

■ ASSOCIATED CONTENT

Supporting Information

The Supporting Information is available free of charge on the ACS Publications website at DOI: 10.1021/acs.organomet.8b00861.

Experimental details, NMR spectra, UV/Vis spectra, IR spectra, X-ray data, computational details, and references (PDF)

Accession Codes

CCDC 1865142−1865145 contain the supplementary crystallographic data for this paper. These data can be obtained free of charge via www.ccdc.cam.ac.uk/data_request/cif, or by emailing data_request@ccdc.cam.ac.uk, or by contacting The Cambridge Crystallographic Data Centre, 12 Union Road, Cambridge CB2 1EZ, UK; fax: +44 1223 336033.

■ AUTHOR INFORMATION

Corresponding Authors

*E-mail: Dr. André Schäfer: andre.schaefer@uni-saarland.de.
*E-mail: Dr. Diego M. Andrada: diego.andrada@uni-saarland.de.

ORCID

André Schäfer: 0000-0002-5969-6618

Notes

The authors declare no competing financial interest.

■ ACKNOWLEDGMENTS

Prof. Dr. Guido Kickelbick is thanked for his support and for help with UV/Vis and IR measurements. Prof. Dr. David Scheschkewitz is thanked for his support and helpful discussions. This research was funded by the Deutsche Forschungsgemeinschaft (Emmy Noether Program, SCHA 1915/3-1) and the Fonds der Chemischen Industrie.

■ REFERENCES

(1) Arduengo, A. J., III; Harlow, R. L.; Kline, M. A. Stable crystalline carbene. *J. Am. Chem. Soc.* **1991**, *113*, 361−363.
(2) Hopkinson, M. N.; Richter, C.; Schedler, M.; Glorius, F. An overview of N-heterocyclic carbenes. *Nature* **2014**, *510*, 485.
(3) Dröge, T.; Glorius, F. The Measure of All Rings-N-Heterocyclic Carbenes. *Angew. Chem.* **2010**, *122*, 7094−7107; *Angew. Chem., Int. Ed.* **2010**, *49*, 6940−6952.
(4) Díez-González, S.; Marion, N.; Nolan, S. P. N-Heterocyclic Carbenes in Late Transition Metal Catalysis. *Chem. Rev.* **2009**, *109*, 3612−3676.
(5) Hahn, F. E.; Jahnke, M. C. Heterocyclic carbenes: synthesis and coordination chemistry. *Angew. Chem.* **2008**, *120*, 3166−3216; *Angew. Chem., Int. Ed.* **2008**, *47*, 3122−3172.
(6) Nesterov, V.; Reiter, D.; Bag, P.; Frisch, P.; Holzner, R.; Porzelt, A.; Inoue, S. NHCs in Main Group Chemistry. *Chem. Rev.* **2018**, *118*, 9678−9842.
(7) Willans, C. E. Non-transition metal N-heterocyclic carbene complexes. *Organometallic Chemistry*; The Royal Society of Chemistry: 2010; Vol. *36*, pp 1−28.
(8) Frenking, G.; Hermann, M.; Andrada, D. M.; Holzmann, N. Donor−acceptor bonding in novel low-coordinated compounds of boron and group-14 atoms C−Sn. *Chem. Soc. Rev.* **2016**, *45*, 1129−1144.
(9) Soleilhavoup, M.; Bertrand, G. Cyclic (Alkyl)(Amino)Carbenes (CAACs): Stable Carbenes on the Rise. *Acc. Chem. Res.* **2015**, *48*, 256−266.
(10) Wurtemberger-Pietsch, S.; Radius, U.; Marder, T. B. 25 years of N-heterocyclic carbenes: activation of both main-group element−element bonds and NHCs themselves. *Dalton Trans.* **2016**, *45*, 5880−5895.
(11) Ruddy, A. J.; Rupar, P. A.; Bladek, K. J.; Allan, C. J.; Avery, J. C.; Baines, K. M. On the Bonding in N-Heterocyclic Carbene Complexes of Germanium(II). *Organometallics* **2010**, *29*, 1362−1367.
(12) Rupar, P. A.; Jennings, M. C.; Baines, K. M. Synthesis and Structure of N-Heterocyclic Carbene Complexes of Germanium(II). *Organometallics* **2008**, *27*, 5043−5051.
(13) Rupar, P. A.; Jennings, M. C.; Ragogna, P. J.; Baines, K. M. Stabilization of a Transient Diorganogermylene by an N-Heterocyclic Carbene. *Organometallics* **2007**, *26*, 4109−4111.
(14) Rupar, P. A.; Jennings, M. C.; Baines, K. M. The reactivity of an anionic gallium N-heterocyclic carbene analogue with a solution stable digermene. *Can. J. Chem.* **2007**, *85*, 141−147.
(15) Kocsor, T. G.; Nemes, G.; Saffon, N.; Mallet-Ladeira, S.; Madec, D.; Castel, A.; Escudie, J. N-heterocyclic carbene stabilized phosphaalkenyl(chloro)stannylene. *Dalton Trans.* **2014**, *43*, 2718−2721.
(16) Hahn, F. E.; Wittenbecher, L.; Kühn, M.; Lügger, T.; Fröhlich, R. A zwitterionic carbene−stannylene adduct via cleavage of a dibenzotetraazafulvalene by a stannylene. *J. Organomet. Chem.* **2001**, *617-618*, 629−634.
(17) Bantu, B.; Pawar, G. M.; Decker, U.; Wurst, K. M.; Schmidt, A. M.; Buchmeiser, M. R. CO_2 and Sn^{II} Adducts of N-Heterocyclic Carbenes as Delayed Action Catalysts for Polyurethane Synthesis. *Chem. - Eur. J.* **2009**, *15*, 3103−3109.
(18) Al-Rafia, S. M. I.; Malcolm, A. C.; Liew, S. K.; Ferguson, M. J.; Rivard, E. Stabilization of the Heavy Methylene Analogues, GeH_2 and SnH_2, within the Coordination Sphere of a Transition Metal. *J. Am. Chem. Soc.* **2011**, *133*, 777−779.
(19) Al-Rafia, S. M. I.; McDonald, R.; Ferguson, M. J.; Rivard, E. Preparation of Stable Low Oxidation State Group 14 Element Amidohydrides and Hydride Mediated Ring Expansion Chemistry of N Heterocyclic Carbenes. *Chem. - Eur. J.* **2012**, *18*, 13810−13820.
(20) Stabenow, F.; Saak, W.; Weidenbruch, M. A zwitterionic carbene−plumbylene adduct. *Chem. Commun.* **1999**, 1131−1132.
(21) Gehrhus, B.; Hitchcock, P. B.; Lappert, M. F. Crystalline (NN)C−M(NN) complexes: synthesis, structure, bonding and lability [M = Si, Ge, Sn or Pb; (NN) = 1,2-$(Bu^tCH_2N)_2C_6H_4$]. *J. Chem. Soc., Dalton Trans.* **2000**, 3094−3099.
(22) Grützmacher, H.; Freitag, S.; Herbst-Irmer, R. M.; Sheldrick, G. M. Investigations of the Structure and Reactivity of a Stannaketenimine. *Angew. Chem.* **1992**, *104*, 459−461; *Angew. Chem., Int. Ed. Engl.* **1992**, *31*, 437−438.
(23) Melaimi, M.; Jazzar, R.; Soleilhavoup, M.; Bertrand, G. Cyclic (Alkyl)(amino)carbenes (CAACs): Recent Developments. *Angew. Chem.* **2017**, *129*, 10180−10203; *Angew. Chem., Int. Ed.* **2017**, *56*, 10046−10068.
(24) Mondal, K. C.; Roesky, H. W.; Schwarzer, M. C.; Frenking, G.; Tkach, I.; Wolf, H.; Kratzert, D.; Herbst Irmer, R.; Niepötter, B.; Stalke, D. Conversion of a Singlet Silylene to a stable Biradical. *Angew.*

DOI: 10.1021/acs.organomet.8b00861
Organometallics 2019, 38, 1052−1061

Chem. **2013**, *125*, 1845−1850; *Angew. Chem., Int. Ed.* **2013**, *52*, 1801−1805.
(25) Niepötter, B.; Herbst Irmer, R.; Kratzert, D.; Samuel, P. P.; Mondal, K. C.; Roesky, H. W.; Jerabek, P.; Frenking, G.; Stalke, D. Experimental Charge Density Study of a Silylone. *Angew. Chem.* **2014**, *126*, 2806−2811; *Angew. Chem., Int. Ed.* **2014**, *53*, 2766−2770.
(26) Li, Y.; Mondal, K. C.; Roesky, H. W.; Zhu, H.; Stollberg, P.; Herbst-Irmer, R.; Stalke, D.; Andrada, D. M. Acyclic Germylones: Congeners of Allenes with a Central Germanium Atom. *J. Am. Chem. Soc.* **2013**, *135*, 12422−12428.
(27) Singh, A. P.; Samuel, P. P.; Mondal, K. C.; Roesky, H. W.; Sidhu, N. S.; Dittrich, B. Lewis Base Stabilized Group 14 Metalylenes. *Organometallics* **2013**, *32*, 354−357.
(28) Li, Y.; Chan, Y.-C.; Li, Y.; Purushothaman, I.; De, S.; Parameswaran, P.; So, C.-W. Synthesis of a Bent 2-Silaallene with a Perturbed Electronic Structure from a Cyclic Alkyl(amino) Carbene-Diiodosilylene. *Inorg. Chem.* **2016**, *55*, 9091−9098.
(29) Müller, C.; Stahlich, A.; Wirtz, L.; Gretsch, C.; Huch, V.; Schäfer, A. Carbene Complexes of Stannocenes. *Inorg. Chem.* **2018**, *57*, 8050−8053.
(30) Fischer, E. O.; Grubert, H. Dicyclopentadienylzinn. *Z. Naturforsch. B* **1956**, *8*, 423−424.
(31) Bos, K. D.; Bulten, E. J.; Noltes, J. G.; Spek, A. L. Cyclopentadienyltin(II) halides. A novel type of divalent organotin compounds. *J. Organomet. Chem.* **1972**, *39*, C52−C54.
(32) Bos, K. D.; Bulten, E. J.; Noltes, J. G.; Spek, A. L. The crystal and molecular structure of cyclopentadienyltin(II) chloride. The bonding of the cyclopentadienyl group in tin(II) compounds. *J. Organomet. Chem.* **1975**, *99*, 71−77.
(33) Measurements in C_6D_6 following the Gutmann−Beckett method Mayer, U.; Gutmann, V.; Gerger, W. *Monatsh. Chem.* **1975**, *106*, 1235−1257 gave $\Delta\delta^{31}$P = 14.9 (**2c**), 15.6 (**2d**), 3.2 (**4**) .
(34) See Supporting Information for further details.
(35) Jutzi, P.; Reumanna, G. Cp* Chemistry of main-group elements. *J. Chem. Soc., Dalton Trans.* **2000**, *0*, 2237−2244.
(36) Upon mixing *N*,*N*′-diisopropyl-4,5-dimethyl-imidazol-2-ylidene (NHC) with **2c**,**d** ^{13}C resonances for the carbene carbon atom and ^{119}Sn resonances indicate a coordination: NHC + **2c**: $\delta^{13}C\{^1H\}$ = 185 (br s), $^{119}Sn\{^1H\}$ = −2099 (br s); NHC + **2d**: $\delta^{13}C\{^1H\}$ = 183 (br s), $^{119}Sn\{^1H\}$ = −2071 (br s).
(37) Zhao, Y.; Truhlar, D. G. The M06 suite of density functionals for main group thermochemistry, thermochemical kinetics, noncovalent interactions, excited states, and transition elements: Two new functionals and systematic testing of four M06-class functionals and 12 other functionals. *Theor. Chem. Acc.* **2008**, *120*, 215−241.
(38) Weigend, F.; Ahlrichs, R. Balanced basis sets of split valence, triple zeta valence and quadruple zeta valence quality for H to Rn: Design and assessment of accuracy. *Phys. Chem. Chem. Phys.* **2005**, *7*, 3297−3305.
(39) Hey, J.; Andrada, D. M.; Michel, R.; Mata, R. A.; Stalke, D. Strong Intermolecular Interactions Shaping a Small Piano Stool Complex. *Angew. Chem.* **2013**, *125*, 10555−10559; *Angew. Chem., Int. Ed.* **2013**, *52*, 10365−10369.
(40) For a complete list of NBOs see Figures S25−S29 in the SI.
(41) Morokuma, K. Molecular Orbital Studies of Hydrogen Bonds. III. C = O···H−O Hydrogen Bond in $H_2CO\cdots H_2O$ and $H_2CO\cdots 2H_2O$. *J. Chem. Phys.* **1971**, *55*, 1236−1244.
(42) Ziegler, T.; Rauk, A. Carbon monoxide, carbon monosulfide, molecular nitrogen, phosphorus trifluoride, and methyl isocyanide as σ donors and π acceptors. A theoretical study by the Hartree-Fock-Slater transition-state method. *Inorg. Chem.* **1979**, *18*, 1755−1759.
(43) For applications see: von Hopffgarten, M.; Frenking, G. Energy decomposition analysis. *Wiley Interdiscip. Rev. Comput. Mol. Sci.* **2012**, *2*, 43−62. Zhao, L. L.; von Hopffgarten, M.; Andrada, D. M.; Frenking, G. Energy decomposition analysis. *Wiley Interdiscip. Rev. Comput. Mol. Sci.* **2018**, *8*, 1345.
(44) Frenking, G.; Hermann, M.; Andrada, D. M.; Holzmann, N. Donor−acceptor bonding in novel low-coordinated compounds of boron and group-14 atoms C−Sn. *Chem. Soc. Rev.* **2016**, *45*, 1129−1144.
(45) Frenking, G.; Tonner, R.; Klein, S.; Takagi, N.; Shimizu, T.; Krapp, A.; Pandey, K. K.; Parameswaran, P. New bonding modes of carbon and heavier group 14 atoms Si−Pb. *Chem. Soc. Rev.* **2014**, *43*, 5106−5139.
(46) Frenking, G.; Wichmann, K.; Froehlich, N.; Loschen, C.; Lein, M.; Frunzke, J.; Rayon, V. M. Towards a rigorously defined quantum chemical analysis of the chemical bond in donor−acceptor complexes. *Coord. Chem. Rev.* **2003**, *238*, 55−82.
(47) **3c**: δ_{11} = 9.5 ± 0.5, δ_{22} = −411.8 ± 20.6, δ_{33} = −1060.9 ± 53.0; **3d**: δ_{11} = 19.1 ± 1.0, δ_{22} = −453.7 ± 22.7, δ_{33} = −1033.7 ± 51.7.
(48) Integration of the resonances for the cyclopentadienyl moieties in the ^{1}H NMR spectra of **3c** suggests a 10:1 (**3c**:**4**) ratio at 253 K and a 1:3.6 (**3c**:**4**) ratio at 296 K.
(49) Mixtures of one and two equivalents of **1** with $SnCl_2$ and $SnBr_2$ in THF-D8 give very similar ^{119}Sn resonances, along with one set of signals in the ^{1}H NMR spectra, indicating a rapid exchange of coordinated and uncoordinated carbene in solution at room temperature (1 eq **1** + $SnCl_2$: δ^{119}Sn = −53;[26] 2 eq **1** + $SnCl_2$: δ^{119}Sn = −59; 1 eq **1** + $SnBr_2$: δ^{119}Sn = −5; 2 eq **1** + $SnBr_2$: δ^{119}Sn = −12).
(50) Only one set of signals is observed for the carbene moiety in ^{1}H and ^{13}C NMR spectra in solution, indicating a fast equilibrium.
(51) Mixing 1 eq of **3b** with 1 eq of **1** and 1 eq of **4** gives rise to two Cp resonances in the ^{1}H NMR spectra at δ^1H (400.13 MHz, C_6D_6, 296 K) = 5.84, 6.64, similar to what is observed for samples derived from **3d**.
(52) Constantine, S. P.; De Lima, G. M.; Hitchcock, P. B.; Keates, J. M.; Lawless, G. A.; Marziano, I. Synthesis and Characterization of $Sn(\eta^5\text{-}C_5Me_5)Cl$ and $Sn\{\eta^5\text{-}C_5Me_4(SiMe_2But)\}Cl$. *Organometallics* **1997**, *16*, 793−795.
(53) Constantine, S. P.; De Lima, G. M.; Hitchcock, P. B.; Keates, J. M.; Lawless, G. A. Synthesis, structure and reactivity of ionogenic $Sn(\eta\text{-}Cp^R)Cl$ derivatives. *Chem. Commun.* **1996**, 2337−2338.
(54) Rohr, A. D.; Kampf, J. W.; Wolfe, J. P.; Banaszak Holl, M. M. Parallelograms and Ladders: Polymorphic Solid-State Structures and Solution Equilibria of Cp*GeCl. *Organometallics* **2010**, *29*, 5004−5009.
(55) Many possible relative postures between the monomers have been considered. For the mechanism the energetically lower energy isomer has been chosen.
(56) Harrison, P. G.; King, T. J.; Richards, J. A. Derivatives of divalent germanium, tin, and lead. Part XII. Crystal and molecular structure of di-μ-bis(cyclopentadienyl)stannyl-bis(tetracarbonyliron). *J. Chem. Soc., Dalton Trans.* **1975**, *20*, 2097−2100.
(57) Al-Rafia, S. M. I.; Shynkaruk, O.; McDonald, S. M.; Liew, S. K.; Ferguson, M. J.; McDonald, R.; Herber, R. H.; Rivard, E. Synthesis and Mössbauer Spectroscopy of Formal Tin(II) Dichloride and Dihydride Species Supported by Lewis Acids and Bases. *Inorg. Chem.* **2013**, *52*, 5581−5589.
(58) Sheldrick, G. *Acta Crystallogr., Sect. A: Found. Crystallogr.* **2008**, *64*, 112−122.
(59) Becke, A. D. Density-functional exchange-energy approximation with correct asymptotic behavior. *Phys. Rev. A: At., Mol., Opt. Phys.* **1988**, *38*, 3098−3100.
(60) Perdew, J. P. Density-functional approximation for the correlation-energy of the inhomogeneous electron-gas. *Phys. Rev. B: Condens. Matter Mater. Phys.* **1986**, *33*, 8822−8824.
(61) Becke, A. D. Density-functional thermochemistry. III. The role of exact exchange. *J. Chem. Phys.* **1993**, *98*, 5648−5652.
(62) Lee, C.; Yang, W.; Parr, R. G. Development of the Colle-Salvetti correlation-energy formula into a functional of the electron density. *Phys. Rev. B: Condens. Matter Mater. Phys.* **1988**, *37*, 785−789.
(63) Adamo, C.; Barone, V. Toward reliable density functional methods without adjustable parameters: The PBE0 model. *J. Chem. Phys.* **1999**, *110*, 6158−6170.
(64) Staroverov, V. N.; Scuseria, G. E.; Tao, J. M.; Perdew, J. P. Comparative assessment of a new nonempirical density functional:

DOI: 10.1021/acs.organomet.8b00861
Organometallics 2019, 38, 1052−1061

Molecules and hydrogen-bonded complexes. *J. Chem. Phys.* **2003**, *119*, 12129−12137.
(65) Tao, J. M.; Perdew, J. P.; Staroverov, V. N.; Scuseria, G. E. Climbing the density functional ladder: Nonempirical meta-generalized gradient approximation designed for molecules and solids. *Phys. Rev. Lett.* **2003**, *91*, 146401−146404.
(66) Staroverov, V. N.; Scuseria, G. E.; Tao, J. M.; Perdew, J. P. Comparative assessment of a new nonempirical density functional: Molecules and hydrogen-bonded complexes. *J. Chem. Phys.* **2004**, *121*, 11507−11507.
(67) Frisch, M. J.; Trucks, G. W.; Schlegel, H. B.; Scuseria, G. E.; Robb, M. A.; Cheeseman, J. R.; Scalmani, G.; Barone, V.; Petersson, G. A.; Nakatsuji, H.; Caricato, M.; Marenich, A. V.; Bloino, J.; Janesko, B. G.; Gomperts, R.; Mennucci, B.; Hratchian, H. P.; Ortiz, J. V.; Izmaylov, A. F.; Sonnenberg, J. L.; Williams-Young, D.; Ding, F.; Lipparini, F.; Egidi, F.; Goings, J.; Peng, B.; Petrone, A.; Henderson, T.; Ranasinghe, D.; Zakrzewski, V. G.; Gao, J.; Rega, N.; Zheng, G.; Liang, W.; Hada, M.; Ehara, M.; Toyota, K.; Fukuda, R.; Hasegawa, J.; Ishida, M.; Nakajima, T.; Honda, Y.; Kitao, O.; Nakai, H.; Vreven, T.; Throssell, K.; Montgomery, J. A.; Peralta, J. E.; Ogliaro, F.; Bearpark, M.; Heyd, J. J.; Brothers, E.; Kudin, K. N.; Staroverov, V. N.; Keith, T. A.; Kobayashi, R.; Normand, J.; Raghavachari, K.; Rendell, A.; Burant, J. C.; Iyengar, S. S.; Tomasi, J.; Cossi, M.; Millam, J. M.; Klene, M.; Adamo, C.; Cammi, R.; Ochterski, J. W.; Martin, R. L.; Morokuma, K.; Farkas, O.; Foresman, J. B.; Fox, D. J. *Gaussian 16*, Revision A.03; Gaussian, Inc.: Wallingford, CT, 2016.
(68) Peng, C. Y.; Ayala, P. Y.; Schlegel, H. B.; Frisch, M. J. Using redundant internal coordinates to optimize equilibrium geometries and transition states. *J. Comput. Chem.* **1996**, *17*, 49−56.
(69) McIver, J. W.; Komornic. A Structure of transition-states in organic reactions - general theory and an application to cyclobutene-butadiene isomerization using a semiempirical molecular-orbital method. *J. Am. Chem. Soc.* **1972**, *94*, 2625−2633.
(70) Atkins, P. W.; De Paula, J. *Physical Chemistry*, 8th ed.; Oxford University Press: Oxford, New York, 2006.
(71) Gonzalez, C.; Schlegel, H. B. Reaction-path following in mass-weighted internal coordinates. *J. Phys. Chem.* **1990**, *94*, 5523−5527.
(72) Miertus, S.; Scrocco, E.; Tomasi, J. Electrostatic interaction of a solute with a continuum - a direct utilization of *ab initio* molecular potentials for the prevision of solvent effects. *Chem. Phys.* **1981**, *55*, 117−129.
(73) Barone, V.; Cossi, M.; Tomasi, J. Geometry optimization of molecular structures in solution by the polarizable continuum model. *J. Comput. Chem.* **1998**, *19*, 404−417.
(74) Wiberg, K. B. Application of pople-santry-segal cndo method to cyclopropylcarbinyl and cyclobutyl cation and to bicyclobutane. *Tetrahedron* **1968**, *24*, 1083−1096.
(75) Reed, A. E.; Weinstock, R. B.; Weinhold, F. Natural-population analysis. *J. Chem. Phys.* **1985**, *83*, 735−746.
(76) Reed, A. E.; Curtiss, L. A.; Weinhold, F. Intermolecular interactions from a natural bond orbital, donor-acceptor viewpoint. *Chem. Rev.* **1988**, *88*, 899−926.
(77) Glendening, E. D.; Badenhoop, J. K.; Reed, A. E.; Carpenter, J. E.; Bohmann, J. A.; Morales, C. M.; Landis, C. R.; Weinhold, F. *GENNBO 6.0*; Theoretical Chemistry Institute, University of Wisconsin: Madison, WI, 2013.
(78) Bickelhaupt, F. M.; Nibbering, N. M. M.; Van Wezenbeek, E. M.; Baerends, E. J. Central bond in the three CN$^{\cdots}$ dimers NC-CN, CN-CN and CN-NC: electron pair bonding and Pauli repulsion effects. *J. Phys. Chem.* **1992**, *96*, 4864−4873.
(79) Grimme, S.; Antony, J.; Ehrlich, S.; Krieg, H. A consistent and accurate ab initio parametrization of density functional dispersion correction (DFT-D) for the 94 elements H-Pu. *J. Chem. Phys.* **2010**, *132*, 154104-1−154104-18.
(80) Grimme, S.; Ehrlich, S.; Goerigk, L. Effect of the Damping Function in Dispersion Corrected Density Functional Theory. *J. Comput. Chem.* **2011**, *32*, 1456−1465.
(81) te Velde, G.; Bickelhaupt, F. M.; Baerends, E. J.; Fonseca Guerra, C.; van Gisbergen, S. J. A.; Snijders, J. G.; Ziegler, T. Chemistry with ADF. *J. Comput. Chem.* **2001**, *22*, 931−967.
(82) Van Lenthe, E.; Baerends, E. J. Optimized Slater type basis sets for the elements 1−118. *J. Comput. Chem.* **2003**, *24*, 1142−1156.
(83) Krijn, J.; Baerends, E. J. *Fit-Functions in the HFS-Method; Internal Report (in Dutch)*; 1984.
(84) Van Lenthe, E.; Baerends, E. J.; Snijders, J. G. Relativistic regular two component Hamiltonians. *J. Chem. Phys.* **1993**, *99*, 4597−4610.

DOI: 10.1021/acs.organomet.8b00861
Organometallics 2019, 38, 1052−1061

3.3 Bonding Situation in Stannocene and Plumbocene N-Heterocyclic Carbene Complexes

Reprinted with permission from Sergi Danés[§], Carsten Müller[§], Lisa Wirtz[§], Volker Huch, Theresa Block, Rainer Pöttgen, André Schäfer, Diego M. Andrada, *Organometallics* **2020**, *39*, 516-527. Copyright © (2020) American Chemical Society.

[§]These authors contributed equally

https://doi.org/10.1021/acs.organomet.9b00667

The results described within this article are additionally put into context in the Conclusion chapter.

Author contribution:

Sergi Danés
Lead: DFT-calculations including Energy Decomposition Analysis (EDA).
Lead: Reviewing and editing of the supporting information.
Carsten Müller:
Lead: Synthesis and characterization of plumbocene NHC complex.
Supporting: Reviewing and editing of the manuscript; reviewing and editing of the supporting information.
Lisa Wirtz:
Lead: Synthesis and characterization of stannocenophane and plumbocenophane NHC complexes.
Supporting: Reviewing and editing of the manuscript, reviewing and editing of the supporting information.
Volker Huch:
Lead: X-ray analysis.
Theresa Block:
Lead: Mössbauer spectroscopy.
Rainer Pöttgen:
Supporting: Mössbauer spectroscopy.
Supporting: Writing, reviewing and editing of the manuscript.
André Schäfer:
Lead: Project administration and supervision; funding acquisition; writing, reviewing and editing of the manuscript.
Supporting: Writing, reviewing and editing of the supporting information.
Diego M. Andrada:
Supporting: DFT-calculations including Energy Decomposition Analysis (EDA); writing, reviewing and editing of the manuscript; reviewing and editing of the supporting information.

ORGANOMETALLICS

pubs.acs.org/Organometallics Article

Bonding Situation in Stannocene and Plumbocene N-Heterocyclic Carbene Complexes

Sergi Danés,[§] Carsten Müller,[§] Lisa Wirtz,[§] Volker Huch, Theresa Block, Rainer Pöttgen,* André Schäfer,* and Diego M. Andrada*

Cite This: *Organometallics* 2020, 39, 516−527 Read Online

ACCESS | Metrics & More | Article Recommendations | Supporting Information

ABSTRACT: A detailed experimental and computational study of a series of stannocene and plumbocene N-heterocyclic carbene complexes is presented. This unique class of group 14 Lewis acid−base adducts was obtained from reactions of the corresponding metallocenes and N-heterocyclic carbenes (NHC) and was structurally characterized by single-crystal X-ray diffraction. The obtained structures show a perpendicular pose of the NHC with respect to the metallocene, hence precluding the maximum interaction between the moieties. The nature of the Sn−C^{NHC} and Pb−C^{NHC} bonds has been investigated by applying natural bond orbital (NBO) analysis and energy decomposition analysis (EDA-NOCV). For the sake of comparison, known stannocene and plumbocene Lewis base complexes have been included in the series. The attractive chemical bonding interactions are around 50% electrostatic, 30% covalent, and 20% dispersion. Indeed, dispersion interactions play a determining role the larger the substituents become. The covalent interactions derive from the donation of the carbene ligand into the empty p orbital of the metallocene.

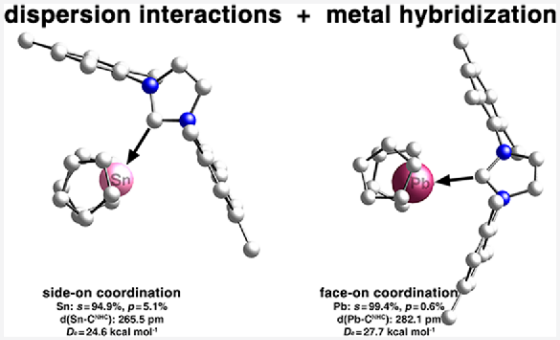

■ INTRODUCTION

Since the first isolation and structural characterization of a persistent, "bottleable", N-heterocyclic carbene (NHC) by Arduengo and co-workers,[1] following the pioneering work of Wanzlick,[2] these compounds have become one of the most important classes of ligands throughout main-group and transition-metal chemistry.[3,4] In main-group chemistry, numerous examples of NHC Lewis adducts have been reported. Particularly, in low-valent p block chemistry, they have seen wide application as strong σ donor ligands, stabilizing and enabling isolation of compounds that are otherwise unstable and nonisolable in the condensed phase. Among others, a well-recognized and particularly important class of such compounds are heavy tetrylene-NHC complexes of the type NHC·ER_2 (E = Si, Ge, Sn, Pb), which are known for various halo- and organo-substituted heavy tetrylenes and represent essential synthons in low-valent main-group chemistry.[5−8]

Surprisingly, the reactivity of the longest known diorganotetrylene-type compounds, stannocene and plumbocene, toward NHCs has been almost unexplored.[9] This might be because these metallocenes are often not regarded as "true" tetrylenes, since they lack any strong σ-donor abilities but rather exclusively exhibit Lewis acidic character. While complexes of plumbocene and stannocene with nitrogen bases have been known since the 1990s and NHC complexes of group 2 and group 4 metallocenes have also been described, the first isolation and structural characterization of group 14 metallocene (tetrelocene) NHC complexes and related compounds has only recently been reported by the Schäfer group (Chart 1).[9−12] It was recognized early on that these complexes show much higher reactivity than their reactants, resulting in low thermal stability and requiring isolation and characterization at low temperatures in some cases. Furthermore, these complexes all exhibit unusually long metal−carbon bonds and the complexation energy of the NHC to the metallocene is rather small. Consequently, these complexes exist in a dissociative equilibrium in solution at room temperature. In the present study, we give a thorough analysis and description of the chemical bonding nature in these species, using ab initio and DFT methods. The E−C^{NHC} and E−N interactions have been analyzed with energy decomposition analysis (EDA) in combination with the natural orbitals for chemical valence (NOCV).

Received: October 9, 2019
Published: February 3, 2020

ACS Publications © 2020 American Chemical Society

Chart 1. Different Stannocene and Plumbocene Lewis Base Complexes

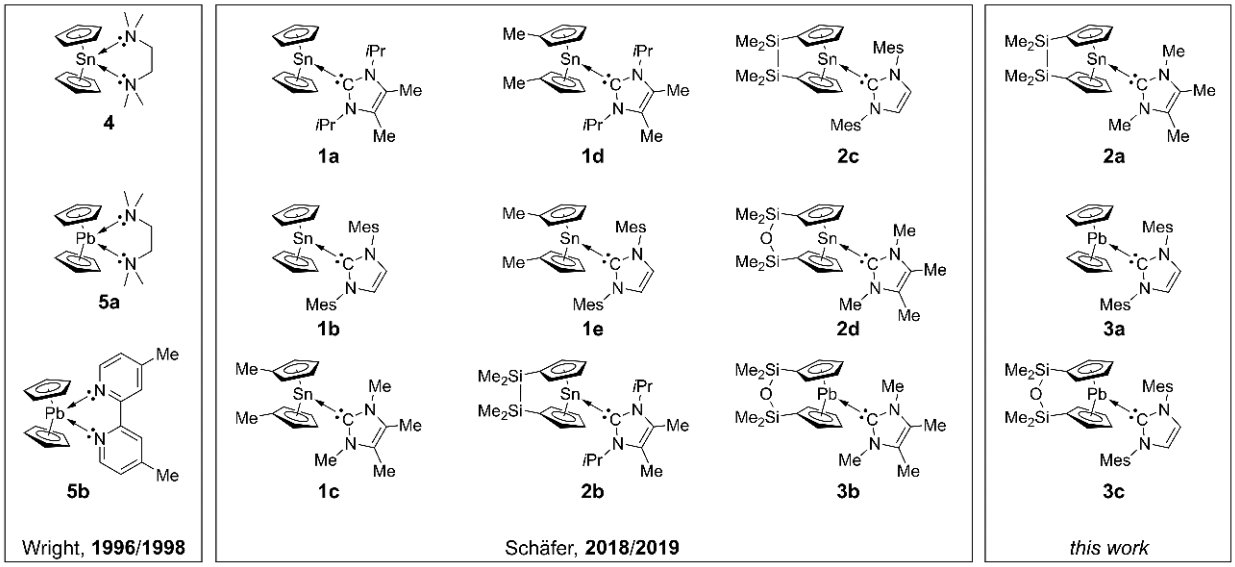

RESULTS AND DISCUSSION

Treatment of a corresponding stannocene or plumbocene with a suitable NHC results in the formation of the corresponding adduct (Scheme 1).

Scheme 1. Synthesis of Stannocene and Plumbocene N-Heterocyclic Carbene Complexes 1a−e, 2a−d, and 3a−c[a]

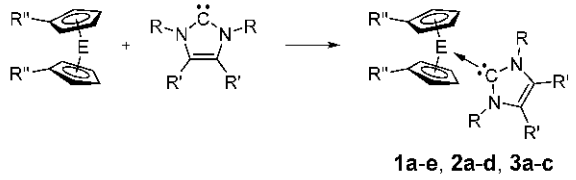

[a]Legend: **1a**, E = Sn, R = *i*Pr, R′ = Me, R″ = H; **1b**, E = Sn, R = Mes, R′ = H, R″ = H; **1c**, E = Sn, R = Me, R′ = Me, R″ = Me; **1d**, E = Sn, R = *i*Pr, R′ = Me, R″ = Me; **1e**, E = Sn, R = Mes, R′ = H, R″ = Me; **2a**, E = Sn, R = Me, R′ = Me, R″ = μ-Si_2Me_4; **2b**, E = Sn, R = *i*Pr, R′ = Me, R″ = μ-Si_2Me_4; **2c**, E = Sn, R = Mes, R′ = H, R″ = μ-Si_2Me_4; **2d**, E = Sn, R = Me, R′ = Me, R″ = μ-Si_2Me_4O; **3a**, E = Pb, R = Mes, R′ = H, R″ = H; **3b**, E = Pb, R = Me, R′ = Me, R″ = μ-Si_2Me_4O; **3c**, E = Pb, R = Mes, R′ = H, R″ = μ-Si_2Me_4O.

As described earlier,[9,12] the stannocene and plumbocene NHC complexes exist in a dissociative equilibrium in solution at room temperature but can be isolated as crystalline solids at low temperatures. In addition to the already reported stannocene- and plumbocene-NHC complexes **1a−e**, **2b−d**, and **3b**,[9,12] we were able to isolate and structurally characterize the 1,3,4,5-tetramethylimidazol-2-ylidene-stannocene adduct **2a** and, more significantly, 1,3-dimesitylimidazol-2-ylidene plumbocene complexes **3a,c** (Figure 1). The latter represent rare examples of bis(cyclopentadienyl)lead(II) carbene complexes and allow for structural comparison to their previously reported tin analogues. The structural features of **2a** are similar to those of the other 1,3,4,5-tetramethylimidazol-2-ylidene stannocene adducts **1c** and **2d**, reported previously.[9]

Strikingly, in the plumbocene-NHC complex **3a**, the coordination of the NHC to the lead atom is significantly different. In all reported stannocene-NHC complexes, as well as in the previously reported plumbocene-NHC complex **3b**, a

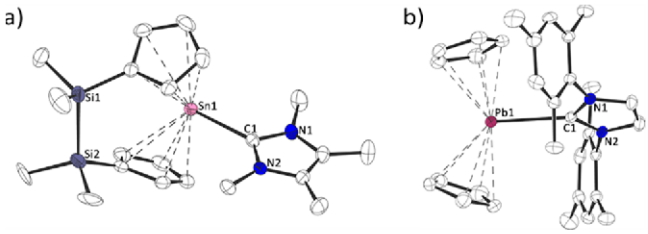

Figure 1. Molecular structures of (a) stannocenophane-NHC complex **2a** and (b) plumbocene-NHC complex **3a** in the solid state (displacement ellipsoids at 50% probability level, H atoms omitted for clarity). Selected experimental bond lengths (pm) and angles (deg): **2a**, Sn−C1 237.6, Sn-$Cp^{centroid}$ 260.5−266.3, ∠Cp−Cp 57.4; **3a**, Pb−C1 272.5, Pb-$Cp^{centroid}$ 257.1−257.7, ∠Cp−Cp 41.7.

"side-on" coordination of the carbene is observed. This has been rationalized by the shape of the frontier molecular orbitals.[9] While the HOMO and HOMO-1 in tetrelocenes correspond to the π system of the cyclopentadienyl ligands, the LUMO exhibits a large coefficient at the central atom in the shape of a p orbital, perpendicular to the Cp−E−Cp plane. In addition, the energetically low lying lone pair spatial demand also contributes to this coordination mode (see Figure 5). In contrast, in the plumbocene-NHC complex **3a** with the N-mesityl-substituted NHC, a "face-on" coordination is observed, which is counterintuitive on the first glance. A similar, yet less pronounced, "face-on" arrangement of the NHC in complex **3c** is observed (Figure 2).

Other structural features in **3a,c** are very long Pb−C^{NHC} bonds of 272.5 pm (**3a**) and 273.4 pm (**3c**), which, in the case of **3a**, is 26 pm longer than in the tin analogue **1b**. The Pb−$Cp^{centroid}$ distances in **3a,c** are elongated in comparison to those in the corresponding plumbocenes (257.1−257.7 pm in **3a** vs 244.1−252.7 pm in Cp_2Pb; 256.0/259.0 pm in **3c** vs 243.0/256.0 pm in μ-$Si_2Me_4O(C_5H_4)_2Pb$), while the C−C bonding distances within the Cp moieties remain relatively uniform, indicating a high degree of aromaticity.[13] The orientation of the NHC plane relative to the Cp−Pb−Cp plane is 64° in **3a** and 58.4° in **3c**, which is significantly smaller than those in all tin-NHC complexes (around 90°).

https://dx.doi.org/10.1021/acs.organomet.9b00667
Organometallics 2020, 39, 516−527

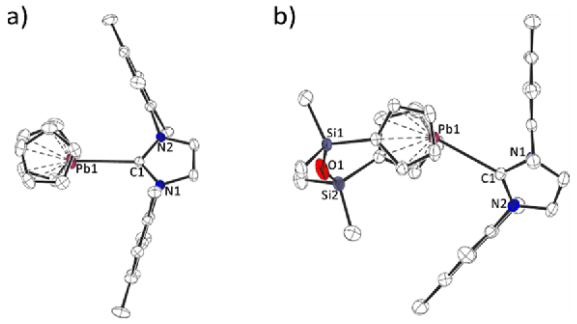

Figure 2. Molecular structures of (a) plumbocene-NHC complex **3a** and (b) plumbocenophane-NHC complex **3c** in the solid state (displacement ellipsoids at 50% probability level, H atoms omitted for clarity).

In order to unravel the bonding situation of compounds **1a–e**, **2a–d**, and **3a–c** as well as of **4** and **5a,b**,[14,15] we performed quantum chemical calculations at the B3LYP+D3/def2-TZVP level of theory (Figure 3). In general, the calculated E–C^{NHC} bonds and Cp–E lengths are ca. 10 pm longer than those experimentally measured. This difference is usually observed in cyclopentadienyl complexes, since their coordination strongly depends on the crystal structure environment (packing effects).[16] As stated before, the tetrelocene-NHC complexes

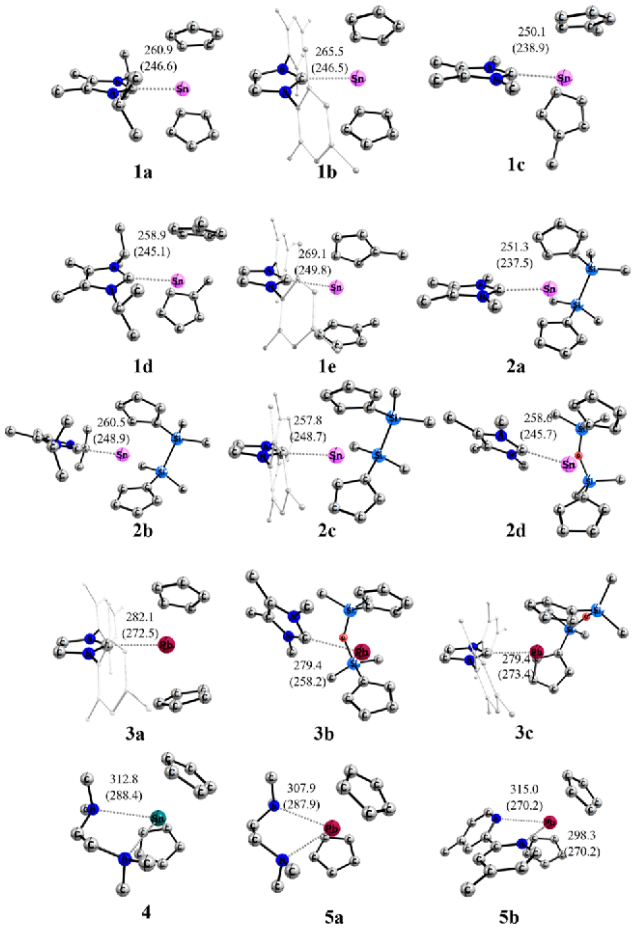

Figure 3. Calculated geometries of complexes **1–5** with selected bond length (in pm) at the B3LYP+D3/def2-TZVP level of theory (experimental values in parentheses).[9,14,15] Hydrogen atoms are omitted for clarity.

exhibit very long Sn–C^{NHC} and Pb–C^{NHC} bonds. Thus, **2a** with the shortest Sn–C^{NHC} bond of this series is slightly longer than in other Sn^{II}–NHC complexes reported elsewhere: for instance, NHC-$SnCl_2$ (235.8 pm).[17,18] The computed Sn–C^{NHC} bond lengths range by 19.0 pm, with complex **1c** having the shortest distance (250.1 ppm) and **1e** (269.1 ppm) exhibiting the longest distance of the series studied here.

All in all the Sn–C^{NHC} and Pb–C^{NHC} bonds found in these metallocene-NHC complexes are along the longest ever structurally characterized two-center–two-electron Sn–C and Pb–C bonds. As is to be expected, the volume of the substituents on the nitrogen atom of the NHC influences the E–C^{NHC} bond distances. In the case of the stannocene complexes, when R = Me the bond is shorter while for R = Mes the bond is longer. The nature of the ansa bridge on some of the tetrelocenophanes does not have a strong influence on the bond distances. A direct comparison of the lead derivatives **3a–c** reveals that the effect of the substituent on the nitrogen atoms of the NHC holds true; although there are only three examples, **3a–c**, with two different NHCs, the Pb–C^{NHC} bond in **3b** is significantly shorter (258.4.4 pm) than in **3a** (272.4 pm) and **3c** (273.4 pm). Noteworthy, plumbocene-NHC complex **3a** displays a different complexation mode, as it is apparently more flexible regarding the complexation place of the carbene ligand than the corresponding stannocene complexes. While all of the stannocene complexes, **1a–e** and **2a–d**, display exclusively a "side-on" complexation of the NHC ligand, the lead analogue **3a** shows a "face-on" coordination, while **3b** exhibits a side-on-coordinated NHC ligand as well and **3c** is somewhat between these two. This is a consequence of many factors such as weak Pb–C^{NHC} bonds, more room on the metal of the metallocene due to longer metal–Cp bonds in the case of lead than in the case of tin, and lower hybridization of the Pb atom than of the Sn atom.

We analyzed the electronic structure of **1–5** by NBO analysis. Table 1 gathers the calculated partial charges and Wiberg bond orders of the E–C^{NHC} and E–N^{ligand} (E = Sn, Pb) bonds. The weakness of the bonding of the carbene ligands to the Sn and Pb atoms is reflected by the Wiberg bond order values (*P*). The bond orders for complexes **1–3** range from 0.3 to 0.4 au, the highest *P* value being for the smallest ligands, in good agreement with the shorter bond lengths.

Examination of the overall charge distribution by natural partial atomic (NPA) charges reveal that the ligands are donating around 0.2 e to the metallocene moiety. For the plumbocene complexes, the NPA values are slightly lower: 0.15 e for **3a** and 0.18 e for **3b**. The NBO orbitals (Figure 4 and Figures S2–S16) show a lone pair on the carbene carbon atom and a lone pair on the metal center. For some complexes, NBO localized E–C^{NHC} single bonds which are strongly polarized toward the carbene carbon atom are observed. The selection of a donor–acceptor representation leads to a non-Lewis occupancy of 2.1% in comparison to 1.9% for the former representation (Table S2). The lone pairs on the Sn and Pb atoms are mostly *s* hybridized, which counts 90 to 95% for Sn, and 98 to 100% for Pb. These hybridization differences might be one of the main reasons for the counterintuitive face-on complexation that is observed in the case of **3a,c**, since there is no directional Pauli repulsion. Second-order perturbation theory within the NBO framework suggests a two-electron stabilization of the carbene lone pair into the vacant p orbital of Sn and Pb. Our calculations estimate values of around −35 to −46 kcal mol^{-1} for E = Sn and −35 kcal mol^{-1} for E = Pb.

https://dx.doi.org/10.1021/acs.organomet.9b00667
Organometallics 2020, 39, 516–527

Table 1. NBO Results for 1−5 at B3LYP+D3/def2-TZVP Level of Theory: Wiberg Bond Order (P, in au), Hybridization, and Partial Charges (q, in e)

	q(E)	q(C^{carb}/N)	q(ECp$_2$)	P(E−C^{carb}/N)	Hyd (E)
1a	1.04	0.12	−0.21	0.35	s (94.5%) p (5.5%)
1b	1.11	0.13	−0.18	0.31	s (94.9%) p (5.1%)
1c	0.98	0.13	−0.24	0.42	s (90.7%) p (9.3%)
1d	1.06	0.11	−0.21	0.36	s (94.1%) p (5.9%)
1e	1.13	0.13	−0.17	0.30	s (96.1%) p (3.9%)
2a	1.16	0.10	−0.18	0.32	s (94.3%) p (5.7%)
2b	1.08	0.09	−0.21	0.34	s (95.1%) p (4.9%)
2c	1.02	0.11	−0.34	0.41	s (91.7%) p (8.2%)
2d	1.06	1.10	−0.22	0.37	s (93.4%) p (6.6%)
3a	1.15	0.12	−0.15	0.25	s (99.4%) p (0.6%)
3b	1.16	0.09	−0.18	0.30	s (98.2%) p (1.8%)
3c	1.21	0.11	−0.15	0.24	s (99.1%) p (0.9%)
4	1.19	−0.42	−0.10	0.06	s (99.9%) p (0.1%)
5a	1.23	−0.43	−0.11	0.06	s (100.0%) p (0.0%)
5b	1.19	−0.43/−0.42	−0.08	0.08/0.06	s (99.8%) p (0.2%)

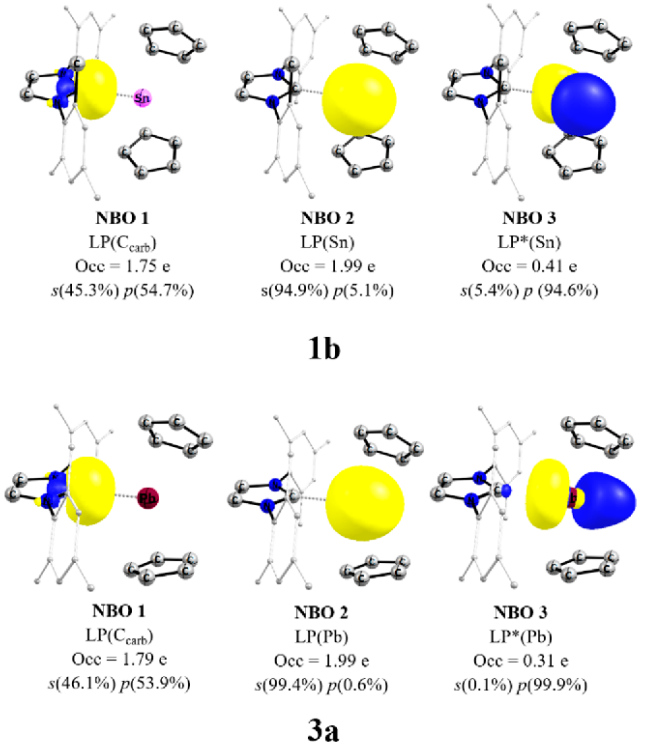

Figure 4. Selected NBO orbitals of compounds **1b** and **3a** at the B3LYP+D3/def2-TZVP level of theory. Hydrogen atoms are omitted for clarity.

The stronger interaction for Sn in comparison to Pb goes in line with the computed occupancy. Thus, tin exhibits a higher p occupancy (0.41 e) than lead (0.31 e). Note that **1c** has the strongest stabilization interaction (62 kcal mol^{-1}), in line with the shortest bond (250.1 pm) of the series.

To examine the strength of the E−C^{NHC} (E = Sn, Pb)) bonds in NHC complexes **1a−e**, **2a−d**, and **3a−c**, we have computed and compared the dissociation energies of this complex series. Table 2 gives the bond energies at the BP86+D3(BJ)/ZORA&TZ2P level of theory using the optimized structures. The computed bond dissociation energies (D_e in Table 2) suggest a small change in the strength of the bond for the different complexes. Despite the small difference, stannocene complexes show a clear trend, which depends on the size of the carbene substituents. Remarkably, opposite to the observation of the bond distances, sterically less demanding carbenes with smaller substituents on the nitrogen atoms exhibit weaker bonds (e.g. **1c**: −16.7 kcal mol^{-1}), whereas sterically more demanding carbenes carrying larger groups on the nitrogen atoms are more strongly bonded (e.g. **2c**: −27.9 kcal mol^{-1}). This goes in line with experimental observations that **1c** is only marginally stable at room temperature and decomposes within minutes to hours in solution, while **2c** is stable under ambient conditions for longer periods.[9] Lead complexes show more strongly bonded NHC ligands in comparison to the tin complexes regardless of whether the bond distances are longer. Thus, the bond length does not directly correlate with the bond strength. This fact has previously been observed for other Lewis pairs.[19,20] Indeed, this result hints at the relative importance of dispersion interactions in order to stabilize these metallocene complexes, explaining, for instance, the carbene position in compound **3b**. It has been demonstrated by Grimme et al.,[21] Schreiner et al.,[22] and Power et al.[23] that bulky groups do provide not only kinetic stability but also thermodynamic stability by their attractive interactions. Further dissection has been performed by energy decomposition analysis (EDA),[24−26] for a more in-depth understanding of the interactions between the metallocenes and the ligand molecules. EDA has proven to be a powerful tool for improving the understanding of chemical bonding in main-group compounds and transition-metal compounds.[6,27−29] Within this method the bond formation between two or more interacting fragments is divided into three steps (see Computational Details). In the first step, the fragments, which are calculated using the frozen geometries within the entire molecule, are placed into the molecule disposition without electronic relaxation to yield the electrostatic interaction (ΔE_{elstat}). In the second step, the wave function is antisymmetrized and renormalized, giving the Pauli repulsion within the fragments (ΔE_{Pauli}). In the third step, the molecular orbitals relax into the final state to yield the stabilizing orbital term (ΔE_{orb}). Also, the stabilizing dispersion interaction can be computed (ΔE_{disp}). The sum of all the terms gives the total interaction energy ΔE_{int}. The dissociation energy can be calculated by combining the interaction energy together with the preparation energy (ΔE_{prep}), which is the energy needed to promote the fragments from their equilibrium geometry to the geometry and electronic state in the compounds.

https://dx.doi.org/10.1021/acs.organomet.9b00667
Organometallics 2020, 39, 516−527

Table 2. Energy Decomposition Analysis (EDA-NOCV) of the E−C^{NHC} bonds (E = Sn, Pb) in Compounds 1−3 at the BP86+D3(BJ)/ZORA&TZ2P Level of Theory[a]

	1a	1b	1c	1d	1e	2a	2b	2c	2d	3a	3b	3c
ΔE_{int}	−30.5	−35.8	−30.1	−31.1	−33.2	−30.2	−33.7	−42.3	−31.7	−32.9	−29.6	−36.5
ΔE_{Pauli}	87.5	72.6	99.4	92.4	69.0	95.9	87.2	88.3	89.5	55.4	58.9	60.2
ΔE_{elstat}[b]	−62.2 (52.7%)	−52.0 (48.0%)	−74.6 (57.6%)	−65.1 (52.7%)	−48.0 (46.9%)	−72.4 (57.5%)	−62.5 (51.7%)	−63.3 (48.5%)	−65.8 (54.3%)	−40.9 (46.3%)	−44.7 (50.5%)	−43.9 (45.4%)
ΔE_{disp}[b]	−16.5 (13.9%)	−22.3 (20.6%)	−11.0 (8.5%)	−17.4 (14.1%)	−22.5 (22.0%)	−10.8 (8.6%)	−17.9 (14.8%)	−25.4 (19.4%)	−15.3 (12.6%)	−23.1 (26.1%)	−17.2 (19.5%)	−26.2 (27.1%)
ΔE_{orb}[b]	−39.3 (33.3%)	−34.0 (31.4%)	−43.9 (33.9%)	−41.1 (33.2%)	−31.8 (31.1%)	−42.9 (34.0%)	−40.5 (33.5%)	−41.9 (32.1%)	−40.1 (33.1%)	−24.3 (27.5%)	−26.6 (30.1%)	−26.6 (27.5%)
$\Delta E_{orb\ \sigma\text{-don}}$[c]	−29.4 (74.6%)	−24.6 (72.3%)	−34.8 (79.2%)	−30.5 (74.3%)	−23.0 (72.3%)	−33.8 (78.9%)	−29.7 (73.4%)	−29.4 (70.1%)	−30.2 (75.3%)	−16.9 (69.4%)	−19.0 (71.5%)	−18.1 (68.2%)
$\Delta E_{orb\ rest}$[c]	−10.0 (25.4%)	−9.4 (27.7%)	−9.1 (20.8%)	−10.5 (25.7%)	−8.8 (27.7%)	−9.0 (21.1%)	−10.8 (26.6%)	−12.5 (29.9%)	−9.9 (24.7%)	−7.4 (30.2%)	−7.6 (28.5%)	−8.4 (31.8%)
ΔE_{prep}	9.3	11.2	13.4	10.2	9.2	11.8	10.5	14.4	10.1	5.2	6.7	5.9
$D_e = -\Delta E$	21.2	24.6	16.7	20.9	24.0	18.4	23.2	27.9	21.6	27.7	23.0	30.6
d(E−C^{NHC})	260.9	265.5	250.1	258.9	269.1	251.3	260.5	257.8	258.6	282.1	279.4	279.4

[a]Energy values are given in kcal mol^{-1} and distances are given in pm. [b]The values in parentheses give the percentage contribution to the total attractive interactions $\Delta E_{elstat} + \Delta E_{orb} + \Delta E_{disp}$. [c]The values in parentheses give the percentage contribution to the total orbital interactions ΔE_{orb}.

As the first approach, we have performed EDA calculations selecting the fragments Cp_2E (E = Sn, Pb) and the different carbenes. The numerical results are presented in Table 2. The interaction energy between the two fragments ranges from −30.1 to −42.3 kcal mol^{-1}. The bond dissociation energy (D_e) of stannocenes follows the same trend, since the preparation energy only involves the deformation of the σ-donating ligand and the metallocene moieties. The total preparation energies are around 10 kcal mol^{-1}, which accounts for the deformation of the stannocene to give room to the interacting carbene. The fact that the plumbocene NHC complexes exhibit more strongly bonded NHC ligands in comparison to the tin analogues is a consequence of a lower preparation energy penalty, which is only 5 kcal mol^{-1} since the potential energy surface of Cp_2Pb is more shallow than that of Cp_2Sn. Further partition of the interaction term shows that the Pauli repulsion in stannocene complexes is stronger than in plumbocene complexes, in line with the shorter bond length.

EDA results suggest that the bonding interactions are on average 60% ionic and 30% covalent with 10% attractive dispersion interactions for the tin compounds, while in the lead compounds the dispersion interactions have higher relevance, with the bonding interactions on average being 50% ionic, 30% covalent, and around 20% dispersion interactions. The ΔE_{disp} term values correlate with the bond energy (D_e) for each series, Sn and Pb (Table 3). For instance, in the tin complexes, values of −22.3 to −25.4 kcal mol^{-1} are calculated as dispersion interactions for complexes with mesityl-substituted NHCs, −17.0 kcal mol^{-1} for complexes with NHCs carrying isopropyl groups, and only −10.8 to −15.3 kcal mol^{-1} for complexes with methyl-substituted carbenes. This highlights the importance of the dispersion interaction for the stability of the complexes. On the other hand, the covalent contribution, which is ca. −40.0 kcal mol^{-1} in the case of the tin complexes and −25.0 kcal mol^{-1} in the case of the lead complexes, represents ∼33% and ∼28% of the stabilizing interaction, respectively. A more detailed insight into the nature of the covalent interactions available from the EDA can be gained in combination with natural orbitals for chemical valence calculations (EDA-NOCV).[30−33] This method decomposes the orbital term ΔE_{orb} into components $\Delta E_{orb\,\rho_i}$ that provide the energetic estimation of a given deformation density ρ_i,

Table 3. Energy Decomposition Analysis (EDA-NOCV) of the E−N^{ligand} Bond (E = Sn, Pb) in Compounds 4 and 5 at the BP86+D3(BJ)/ZORA&TZ2P Level of Theory[a]

	4	5a	5b
ΔE_{int}	−20.1	−24.8	−21.0
ΔE_{Pauli}	31.2	35.9	29.9
ΔE_{elstat}[b]	−21.4 (41.7%)	−27.6 (45.5%)	−24.2 (47.5%)
ΔE_{disp}[b]	−16.2 (31.5%)	−17.4 (28.6%)	−13.5 (26.6%)
ΔE_{orb}[b]	−13.8 (26.9%)	−15.7 (25.9%)	−13.2 (25.9%)
$\Delta E_{orb\ (+,+)\ \sigma\text{-don}}$[c]	−6.7 (48.9%)	−7.7 (48.8%)	−7.3 (55.2%)
$\Delta E_{orb\ (+,-)\ \sigma\text{-don}}$[c]	−3.2 (23.0%)	−3.7 (23.7%)	−2.3 (17.3%)
$\Delta E_{orb\ rest}$[c]	−3.9 (28.2%)	−4.3 (27.6%)	−3.6 (27.5%)
ΔE_{prep}	4.1	4.0	1.7
$D_e = -\Delta E$	16.0	20.8	19.3

[a]Energy values are given in kcal mol^{-1}. [b]The values in parentheses give the percentage contribution to the total attractive interactions $\Delta E_{elstat} + \Delta E_{orb} + \Delta E_{disp}$. [c]The values in parentheses give the percentage contribution to the total orbital interactions ΔE_{orb}.

which is related to a particular electron flow channel, and also the amount of charge transferred $\Delta q_i = |\nu_i|$ for the bonding between the interacting fragments (Table 2). For compounds **1−3**, the main deformation densities are associated with the main orbital interactions (Figure 5 and Figure S17). The eigenvalues ν are a measure for the amount of electrons flowing from one orbital to the other (pairwise). According to these data the main contributions in the case of **1b** and **3a** are associated with the donation of the lone pairs into the vacant p orbitals of the stannocene and plumbocene moieties. The corresponding energies represent around 75% of the total orbital interaction energies. The remaining orbital interactions are attributed to polarization effects. It is worth noting that we found no significant contribution of π-back-donation from the metallocene moiety into these NHC complexes. This effect has been suggested before on the basis of the solid-state structures of stannocene NHC complexes,[9] since the position of the NHC makes an interaction between the stannocene lone pair and the empty p orbital of the NHC impossible. We have recently observed such a behavior when low energy gain by π-back-donation is combined with steric hindrance.[10]

We have taken compounds **4** and **5a,b** to compare the coordination mode. NBO results in Table 1 reveal that the

https://dx.doi.org/10.1021/acs.organomet.9b00667
Organometallics 2020, 39, 516−527

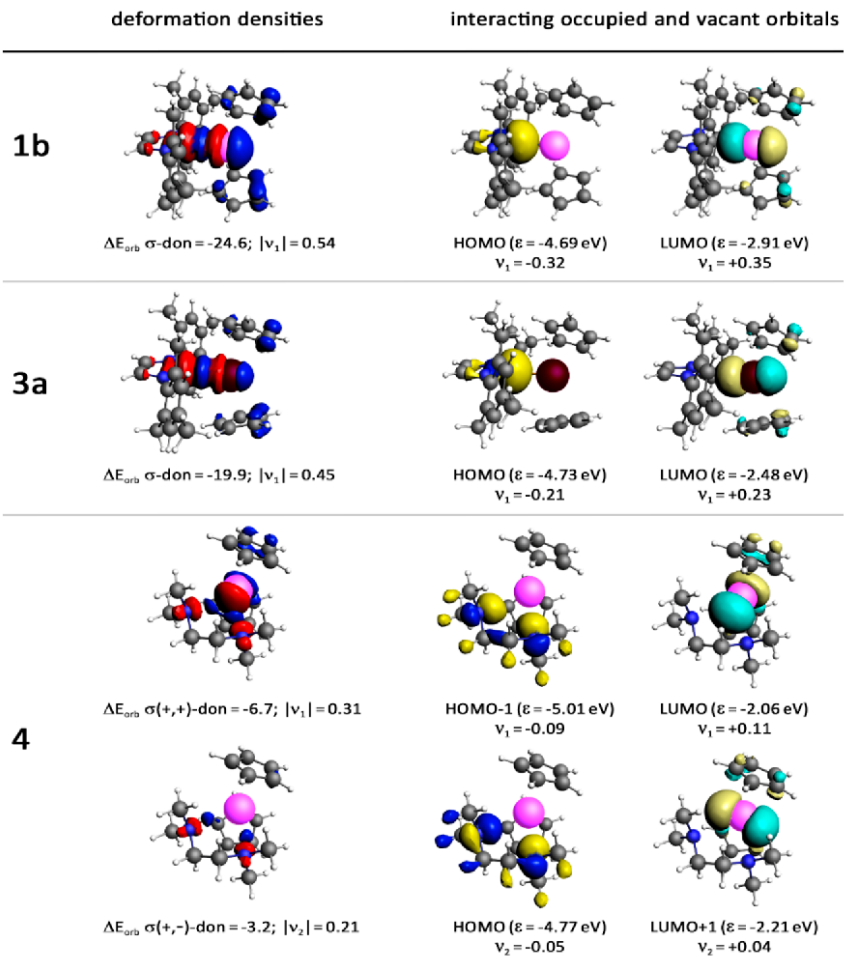

Figure 5. (left) Isodensity plots of deformation densities $\Delta\rho$ (isovalue 0.001 au) of the pairwise orbital interactions between Cp_2E (E = Sn, Pb) moiety and the coordinating ligand (L = NHC^{Mes}, tmeda) for **1b**, **3a** and **4** and associated energies ΔE (in kcal mol^{-1}) and eigenvalues ν (in au). The red color shows charge outflow, and the blue color shows charge density accumulation. (center and right) Isodensity plots of the most relevant interacting occupied and vacant orbitals (isovalue 0.05 au) of the fragments.

metallocene moieties bear less negative charge than in complexes **1**−**3**. The hybridization indicates that two valence electrons of the metal center are in an s orbital and hence the p orbital is able to participate in donor−acceptor interactions. The EDA-NOCV values are summarized in Table 3, while the deformation densities assigned to the orbital interactions are shown in Figure 5. The computed dissociation energies (D_e in kcal mol^{-1}) for **4** and **5a**,**b** are around 10 kcal mol^{-1} higher than those reported by Armstrong et al.[15] A comparison with the carbene complexes **1**−**3** suggests even weaker interactions by around 2 kcal mol^{-1}. As in the former complexes, the lead complex **5a** exhibits a stronger bond in comparison to its tin analogue **4**. Further inspection is given by the preparation and interaction energies. In this case, the energy penalty to deform the fragment to get into the interacting structure is very low and comparable: namely, 4.1 and 4.0 kcal mol^{-1} for **4** and **5a**, respectively. The small binding energy difference comes from the interaction energy (4.7 kcal mol^{-1}). The EDA dissection results in higher Pauli repulsion for the lead complex but also higher stabilization interactions. Herein, the dispersion interaction contributes 30% to the total stabilization interaction, while the electrostatic and orbital interactions contribute around 45% and 25%, respectively. Interestingly, these complexes present two main orbital contributions which come from the positive combination of the nitrogen atom lone pair (+,+) combination which interacts with the one of the empty p orbital of the metallocene and a (+,−) lone pair combination that donates electrons into the other vacant p orbital (Figure 5). These orbital interactions are possible due to the low hybridization degree of the stannocene and plumbocene metal centers. Note that the orbital interaction is slightly higher, in line with the shorter Pb−N distances (Figure 3).

As previously mentioned, the tetrelocene-NHC complexes are significantly more reactive than their initial reactants, as they are only sparsely stable at room temperature. This is related to a general observation of longer Cp−E bond lengths upon complexation of the NHC to the metal center or any other ligand. To understand the origins of this observation, we have used a model where the side substituents on the nitrogen atoms are replaced by hydrogen atoms. This is the smallest substituent possible for the NHC ligands. Note that, in this case, the carbene is disposed in a different manner since the steric hindrance is reduced significantly. Our calculations suggest Cp−E dissociation energies of 549.3 and 526.0 kcal mol^{-1} for stannocene (Cp_2Sn) and plumbocene (Cp_2Pb), respectively. Upon complexation with NHC, the dissociation energy is reduced by more than 100 kcal mol^{-1}: i.e. 411.0 and 404.8 kcal mol^{-1} for Sn and Pb complexes, respectively. This is in line with the experimental observation of the formation of

https://dx.doi.org/10.1021/acs.organomet.9b00667
Organometallics 2020, 39, 516−527

tin metal and imidazolium cyclopentadienyl compounds at room temperature, in some cases. In terms of bond distances, the Sn−Cp bond length is elongated from 246.9 to 279.7 pm upon complexation, while Cp−Pb is lengthened from 254.7 to 266.4 pm. Notably, this affects the stannocene complexes more strongly than the plumbocene complexes. These observations have been ascribed to the donation of the lone pair into the LUMO p orbital of the metal center, which has an antibonding interaction with the Cp groups.[34] We have used EDA on the metal center and Cp group interaction to unravel the origins of such a change. Thus, we have considered a fragmentation scheme where one of the fragments is the E^{2+} or $(E\text{-NHC})^{2+}$ and the other is $(Cp^-)_2$ (Scheme 2 and Table S4). The other

Scheme 2. Cp−E (E = Sn, Pb) Dissociation Energies (D_e) of Metallocenes and Metallocene-NHC Complexes at the BP86+D3(BJ)/TZ2P//B3LYP+D3/def2-TZVP Level of Theory

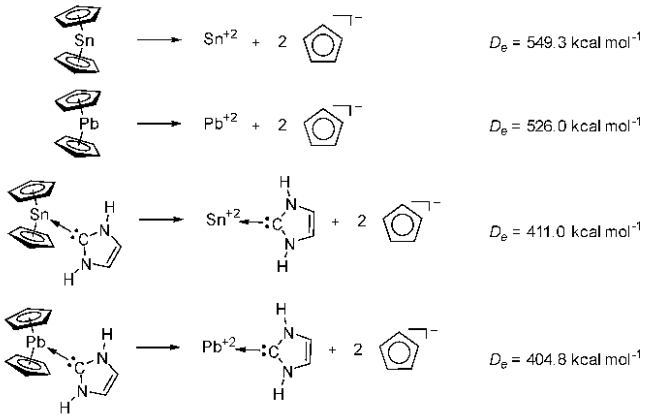

possible dissociation leads to neutral radical fragments E^0 (^3P) and $(Cp)_2$, which is strongly disfavored under experimental conditions. Our results are in good agreement with previous calculations by Rayón et al. on metallocene chemical bonding.[35] The bonding for metallocenes is 70% ionic and 28% covalent with a small dispersion interaction contribution of 2%. The main orbital terms are related to the electron donation of the Cp^- groups to the E^{2+} element. Our results suggest that the lowering of the dissociation energy comes primarily from a weaker interaction energy ΔE_{int}. The stabilization interaction decreases upon complexation since the electrostatic and orbital interactions are weaker. On the one hand, the electrostatic interaction energy decreases by around 70 kcal mol^{-1} since the metal center receives electrons from the carbene ligand. On the other hand, the orbital interaction decreases by ca. 50 kcal mol^{-1} due to weaker donations to the p orbitals of the metal center.

Aside from the metallocene-NHC complexes, dispersion interactions have previously also been described to be very important in case of Si[2]stannocenophane, as the compound exists as a dimer in the solid state, which is believed to be caused by attractive dispersion interactions, rather than a "classical" Sn−Sn bond, as indicated by solution and solid-state CP-MAS ^{119}Sn NMR spectroscopy.[36] The ^{119}Sn Mössbauer spectrum of the sila[2]stannocenophane recorded at 6 K (Figure 6) supports this assumption. The spectrum is well reproduced with a single signal at an isomer shift of δ = 3.734(6) mm s^{-1}, subjected to electric quadrupole splitting of

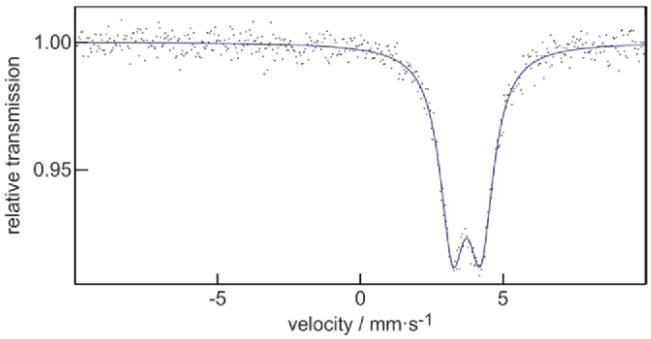

Figure 6. Experimental and simulated ^{119}Sn Mössbauer spectrum of sila[2]stannocenophane at 6 K.

ΔE_Q = 1.00(1) mm s^{-1}. The experimental line width parameter of Γ = 1.08(2) mm s^{-1} is slightly enhanced.

Although, as mentioned previously, the crystal structure contains two crystallographically independent tin sites, they cannot be distinguished in the ^{119}Sn Mössbauer spectrum. Both tin sites exhibit an almost similar electronic environment, and the envelope is observed. This is expressed by the slightly enhanced line width parameter. Significantly, the isomer shift of sila[2]stannocenophane is close to that reported for stannocene (δ = 3.73(6) mm s^{-1}),[37,38] which means that sila[2]stannocenophane does not exhibit any covalent Sn−Sn bond and can be regarded as a divalent tin compound.[39] The electric quadrupole splitting parameter for sila[2]-stannocenophane is increased, in comparison to that of stannocene (ΔE_Q = 0.65(6) to 1.00(1) mm s^{-1}).[37] This is a consequence of the tilt of the Cp ligands due to the ansa bridging, leading to a more asymmetric electron density at the tin nuclei in sila[2]stannocenophane.

We have performed EDA-NOCV calculations to understand the physical factors controlling the interaction between the two sila[2]stannocenophane units (Table S5). EDA calculations suggest that the dissociation energy for the dimer is indeed very weak: namely, −7.6 kcal mol^{-1}. The dissection of the interaction energy discloses that the main contribution is from dispersion interaction (63.1%), while the electrostatic and covalent contributions are very small, 19.4% and 17.5%, respectively. To examine the origins of the dispersion interaction, we have performed energy partitioning within the local correlation methods.[40] We have generated a potential energy plot by the displacement of the sila[2]stannocenophane monomers away from each other from 300 to 700 pm (Chart 2 and Figure 7).

Chart 2. Si[2]stannocenophane Dispersion Dimer

Note that HF/cc-pVTZ predicts no interaction between the monomers. This is in agreement with the EDA calculations, which show weak electrostatic interactions. The effect of correlation is given by the difference of the calculated curves to the HF curve. The SCS-LMP2/cc-pVTZ[41] curves predict an equilibrium distance of 460 pm, while LMP2/cc-pVTZ gives a shorter distance: i.e., 440 ppm. This is expected, since MP2 tends to overestimate dispersion interactions.[42−47] The curves nevertheless are very similar, with energies of −3.6 and −2.3 kcal mol^{-1}, but a shorter equilibrium distance.

https://dx.doi.org/10.1021/acs.organomet.9b00667
Organometallics 2020, 39, 516−527

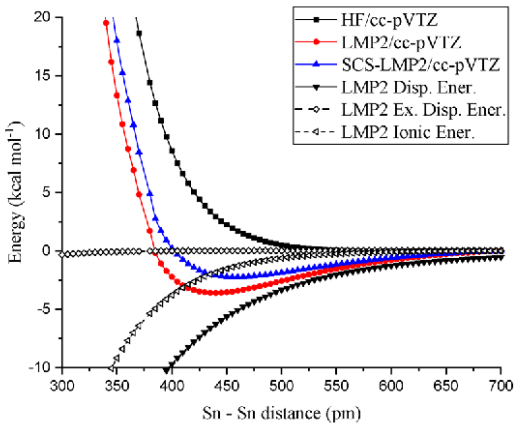

Figure 7. Potential energy curve of the interaction between the sila[2]stannocenophane units. The energy values are given as a function of the Sn1−Sn2 distance.

The local character of occupied and virtual orbitals in the local correlation treatments offers the possibility to dissect intramolecular effects (double excitations from occupied orbitals of one unit into virtual orbitals of the same unit) from intermolecular effects (excitations involving orbitals from both units).[40] Additionally, the intermolecular correlation effects can be decomposed according to different excitation classes: dispersion effects originate from simultaneous monoexcitations at each unit, exchange dispersion is similar but the monoexcitations are from the occupied space of one unit to the virtual space of the other and vice versa, and ionic contributions come from monoexcitations from the occupied space of both units into the virtual space of only one of them. The different classes have been discussed in detail by Schütz et al.[40,48,49] In Figure 7, together with the energy curves, each intermolecular contribution term is also displayed as a function of the distance between the tin atoms. These curves show a continuous favorable interaction with decreasing distance. The main contribution interaction to the correlation energy is the dispersion (−6.6 kcal mol^{-1}), while the ionic excitation and exchange dispersion effects are −0.01 and −2.0 kcal mol^{-1}, respectively.

■ CONCLUSION

In this work, a series of stannocene and plumbocene N-heterocyclic carbene complexes have been studied experimentally and computationally. Their key chemical bonds have been described by natural bond orbital and energy decomposition analysis. The results suggest that the binding is coordinative, having a strong dispersion interaction contribution. The orbital interaction occurs mainly from the donation of the carbene lone pair into the empty p orbital of tin or lead. Remarkably, the carbene ligand disposition toward the main metal center is dominated by the volume of the group on the nitrogen atoms, which preclude the π-back-donation. The complexation weakens the interaction of the metal with the cyclopentadienyl moieties by ca. 100 kcal mol^{-1} and lengthens the E−Cp bonds significantly, by up to ∼25 pm. This has been ascribed to the occupation of the LUMO, which has an antibonding interaction nature with the cyclopentadienyl groups. Dispersion interactions are also the ruling effect to form stannocene dimers for the Si[2]stannocenophane derivatives, where no chemical bond has been found between the tin atoms.

■ EXPERIMENTAL SECTION

All manipulations were carried out under an inert gas atmosphere (argon 5.0), using either Schlenk line techniques or a glovebox. 1,3,4,5-Tetramethylimidazol-2-ylidene,[50] 1,3-dimesitylimidazol-2-ylidene,[51] Si[2]stannocenophane,[36] and plumbocene[52] were prepared following known literature procedures. Deuterated benzene was purchased from ABCR and dried over 400 pm molecular sieves. NMR spectra were recorded on Bruker Avance III 300 (solution NMR), Bruker Avance III 400 (solution NMR), and Bruker Ascend 400WB (solid state NMR) spectrometers. ^{1}H and ^{13}C NMR spectra were referenced using the solvent signals.[53] ^{29}Si, ^{119}Sn, and ^{207}Pb NMR spectra were referenced using external standards ($\delta^{29}_{Si}(SiMe_4)$ 0; $\delta^{119}_{Sn}(SnMe_4)$ 0; $\delta^{207}_{Pb}(PbMe_4)$ 0). Elemental analyses were performed with an Elementar vario microcube instrument. Single-crystal X-ray diffraction analyses were carried out at low temperatures on a Bruker AXS X8 Apex CCD and Bruker AXS D8 Venture diffractometer operating with graphite monochromated Mo Kα radiation. Structure solution and refinement were performed using SHELX.[54] The ^{119}Sn Mössbauer spectroscopy was performed with a $Ca^{119m}SnO_3$ source. Ca. 240 mg of the sample was placed within a thin-walled PMMA container. A palladium foil of 0.05 mm thickness was used to reduce the tin K X-rays concurrently emitted by this source. The measurement (10 days total counting time) was conducted in a continuous flow cryostat system (Janis Research Co LLC) at 6 K. The spectrum was fitted with the NORMOS-90 software package.[55]

Synthesis of 2a. A 2 mL portion of toluene, precooled to 193 K, was added to a mixture of Si[2]stannocenophane (200 mg, 551 μmol) and 1,3,4,5-tetramethylimidazol-2-ylidene (68 mg, 548 μmol). The resulting mixture was stirred for 10 min at 193 K. Storage of this solution at 248 K yielded yellow crystals of stannocenophane carbene complex **2a**. Yield: 22 mg/8%. Anal. Calcd for $C_{21}H_{32}N_2Si_2Sn$: C, 51.75; H, 6.62; N, 5.75. Found: C, 51.41; H, 6.91; N, 6.04. ^{1}H NMR (400.13 MHz, 296 K, C_6D_6): δ 0.54 (s, 12 H, Si-CH_3), 1.28 (s, 6 H, C-CH_3), 3.05 (s, 6 H, N-CH_3), 6.14 (t, $^{3}J_{HH}$ = 2 Hz, 4H, Cp-*H*), 6.42 (t, $^{3}J_{HH}$ = 2 Hz, 4H, Cp-*H*). $^{13}C\{^{1}H\}$ NMR (100.62 MHz, 296 K, C_6D_6): δ −2.6 (Si-CH_3), 8.0 (C-CH_3), 33.5 (N-CH_3), 114.6 (Cp), 114.7 (Cp), 115.9 (*C*═*C*), 117.7 (Cp). $^{29}Si\{^{1}H\}$-INEPT-NMR (79.49 MHz, 296 K, C_6D_6): δ −27.0. No signal could be detected in the ^{119}Sn NMR spectrum in the range of −1650 to −2650 ppm, presumably due to extreme signal broadening.

Synthesis of 3a. A 15 mL portion of toluene was added to a mixture of plumbocene (100 mg, 300 μmol) and 1,3-dimesitylimidazol-2-ylidene (90 mg, 300 μmol). The solution was stirred at room temperature for 10 min and then stored at 248 K overnight, yielding yellow crystals of plumbocene carbene complex **3a**. Yield: 110 mg/57%. Anal. Calcd for $C_{31}H_{34}N_2Pb$: C, 58.01; H, 5.34; N, 4.36. Found: C, 56.79; H, 5.39; N, 4.13 (carbon value was repeatedly reproducibly low, even upon analysis of highly crystalline material). ^{1}H NMR (400.13 MHz, 296 K, C_6D_6): δ 2.09 (s, 12H, *o*-Mes-CH_3), 2.13 (s, 6H, *p*-Mes-CH_3), 5.86 (s, 10H, Cp-*H*), 6.24 (s, 2H, NC-*H*), 6.79 (s, 4H, *m*-Mes-*H*). $^{13}C\{^{1}H\}$ NMR (100.61 MHz, 296 K, C_6D_6): δ 18.1 (*o*-Mes-CH_3), 21.0 (*p*-Mes-CH_3), 110.8 (Cp), 121.0 (C═C), 129.4 (Mes), 135.1 (Mes), 137.6 (Mes), 138.3 (Mes), 226.9 (carbene-*C*). $^{13}C\{^{1}H\}$ CP/MAS (15 kHz) NMR (100.65 MHz, 296 K): δ 17.6 (Mes-CH_3), 21.2 (Mes-CH_3), 24.3 (Mes-CH_3), 109.5, 120.9, 122.1, 128.8, 131.2, 132.4, 133.1, 134.6, 139.2, 239.0 (carbene-C). $^{207}Pb\{^{1}H\}$ CP/MAS (13 kHz) NMR (83.37 MHz, 296 K): δ −4118.

Synthesis of 3c. A solution of plumbocenophane (100 mg, 214 μmol) in 2 mL of toluene was added to a solution of 1,3-dimesitylimidazol-2-ylidene (66.0 mg, 217 μmol) in 2 mL of toluene, and storage of the solution at 248 K yielded yellow crystals of plumbocenophane carbene complex **3c**. Crystals suitable for XRD were obtained from a thf solution at 248 K. Yield: 127 mg/77%. Anal. Calcd for $C_{35}H_{44}N_2OPbSi_2$: C, 54.45; H, 5.74; N, 3.63. Found: C, 54.83; H, 5.70; N, 3.42. ^{1}H NMR (400.13 MHz, 293 K, C_6D_6): δ 0.45 (s, 12H, Si-CH_3), 2.04 (s, 12H, *o*-Mes-CH_3), 2.17 (s, 6H, *p*-Mes-CH_3), 6.02−6.05 (m, 8H, Cp-*H*), 6.13 (s, 2H, N-C*H*), 6.81 (s, 4H, *m*-Mes-*H*). $^{13}C\{^{1}H\}$ NMR (100.63 MHz, 293 K, C_6D_6): δ 2.2 (Si-CH_3), 18.0 (*o*-Mes-CH_3), 21.1 (*p*-Mes-CH_3), 113.9 (Cp), 116.6 (Cp),

https://dx.doi.org/10.1021/acs.organomet.9b00667
Organometallics 2020, 39, 516−527

121.3 (C=C), 129.6 (Mes), 135.0 (Mes), 136.6 (Mes), 138.9 (Mes), 229.7 (carbene-C). $^{13}C\{^1H\}$ CP/MAS(13 kHz) NMR (100.67 MHz, 297 K): δ 0.3 (Si-CH_3), 2.8 (Si-CH_3), 17.7 (Mes-CH_3), 19.2 (Mes-CH_3), 23.3 (Mes-CH_3), 108.4, 110.7, 112.5, 117.6, 121.6, 123.5, 124.3, 130.5, 133.0, 135.7, 140.2, 238.8 (carbene-C). $^{29}Si\{^1H\}$ INEPT NMR (59.63 MHz, 296 K, C_6D_6): δ −7.0; $^{207}Pb\{^1H\}$ NMR (62.51 MHz, 295 K, C_6D_6): δ −4344.

Computational Details. All geometries were optimized without symmetry constraint within the DFT (density functional theory) framework using the B3LYP[56,57] and BP86 functionals[58,59] in combination with the Grimme dispersion corrections D3[60,61] and the Ahlrichs def2-TZVP basis function.[62] For Sn and Pd small-core effective core potentials ECP28MDF and ECP60MDF were included, respectively.[63] These calculations were performed using the Gaussian 16 A03 software suite.[64] The stationary points were located with the Berny algorithm[65] using redundant internal coordinates. Analytical Hessians were computed to determine the nature of stationary points (one and zero imaginary frequencies for transition states and minima, respectively)[66] and to calculate unscaled zero-point energies (ZPEs) as well as thermal corrections and entropy effects using the standard statistical-mechanics relationships for an ideal gas.[67] Unless otherwise stated, Gibbs energies have been computed at 298.15 K. The Wiberg bond indices (WBI)[68] and NPA[69,70] atomic partial charges have been calculated at the B3LYP+D3/def2-TZVP level using GENNBO6.0 programs.[71] The nature of the chemical bonds was investigated by means of the energy decomposition analysis (EDA) method, which was developed by Morokuma[24] and by Ziegler and Rauk.[25,72] The bonding analysis focuses on the instantaneous interaction energy ΔE_{int} of a bond A−B between two fragments A and B in the particular electronic reference state and in the frozen geometry AB. This energy is divided into four main components (eq 1):

$$\Delta E_{int} = \Delta E_{elst} + \Delta E_{Pauli} + \Delta E_{orb} + \Delta E_{disp} \quad (1)$$

The term ΔE_{elst} corresponds to the classical electrostatic interaction between the unperturbed charge distributions of the prepared atoms (or fragments), and it is usually attractive. The Pauli repulsion ΔE_{Pauli} is the energy change associated with the transformation from the superposition of the unperturbed wave functions (Slater determinant of the Kohn−Sham orbitals) of the isolated fragments to the wave function $\Psi_0 = N\hat{A}[\Psi_A\Psi_B]$, which properly obeys the Pauli principle through explicit antisymmetrization ($\hat{A}$ operator) and renormalization (N = constant) of the product wave function. It comprises the destabilizing interactions between electrons of the same spin on either fragment. The orbital interaction ΔE_{orb} accounts for charge transfer and polarization effects.[73] In the case where the Grimme dispersion corrections[60,61] are computed, the term ΔE_{disp} is added to the eq 1. Further details on the EDA method can be found in the literature.[26,74] In the case of the dimers the relaxation of the fragments to their equilibrium geometries at the electronic ground state is termed ΔE_{prep}, because it may be considered as preparation energy for chemical bonding. The addition of ΔE_{prep} to the intrinsic interaction energy ΔE_{int} gives the total energy ΔE, which is—by definition with opposite sign—the bond dissociation energy D_e:

$$\Delta E(-D_e) = \Delta E_{int} + \Delta E_{prep} \quad (2)$$

The EDA-NOCV method combines the EDA with the natural orbitals for chemical valence (NOCV) to decompose the orbital interaction term ΔE_{orb} into pairwise contributions. The NOCVs Ψ_i are defined as the eigenvector of the valence operator, $\hat{V}$, given by eq 3:

$$\hat{V}\Psi_i = \nu_i\Psi_i \quad (3)$$

In the EDA−NOCV scheme the orbital interaction term, ΔE_{orb}, is given by eq 4

$$\Delta E_{orb} = \sum_k \Delta E = \sum_{k=1}^{N/2} \nu_k[- F^{TS}_{-k,k} + F^{TS}_{k,k}] \quad (4)$$

in which $F^{TS}_{-k,-k}$ and $F^{TS}_{k,k}$ are diagonal transition state Kohn−Sham matrix elements corresponding to NOCVs with the eigenvalues—ν_k and ν_k, respectively. The ΔE^{orb}_k term for a particular type of bond is assigned by visual inspection of the shape of the deformation density $\Delta\rho_k$. The latter term is a measure of the size of the charge deformation, and it provides a visual notion of the charge flow that is associated with the pairwise orbital interaction. The EDA-NOCV scheme thus provides both qualitative and quantitative information about the strength of orbital interactions in chemical bonds. The EDA-NOCV calculations were carried out with ADF2018.[74] The basis sets for all elements have triple-ζ quality augmented by two sets of polarization functions and one set of a diffuse function. Core electrons were treated by the frozen-core approximation. This level of theory is denoted BP86+D3(BJ)/TZ2P.[75] Scalar relativistic effects have been incorporated by applying the zeroth-order regular approximation (ZORA).[76]

We performed the second-order local Møller−Plesset perturbation theory (LMP2)[77−85] level of theory calculations by employing the MOLPRO 2019.1[86] software program package. Density fitting (DF) approximations have been used in this local method.[87] The cc-pVTZ basis set was used for carbon, silicon, and tin, while for hydrogen the cc-pVTZ basis set was used.[88,89] In the density fitting calculations reported in this paper, we used the cc-pVTZ/JKJIT and cc-pVTZ/MP2FIT auxiliary fitting basis sets[43] in the DF-HF and DF-LMP2 calculations, respectively. The LMP2 calculations were carried out using Pipek−Mezey localized orbitals.[87] The domains were determined with the use of natural population analysis criteria, with TNPA = 0.03.

■ ASSOCIATED CONTENT

Supporting Information

The Supporting Information is available free of charge at https://pubs.acs.org/doi/10.1021/acs.organomet.9b00667.

Crystallographic details and computational details (PDF)

Cartesian coordinates giving the optimized geometries (XYZ)

Accession Codes

CCDC 1954898−1954900 contain the supplementary crystallographic data for this paper. These data can be obtained free of charge via www.ccdc.cam.ac.uk/data_request/cif, or by emailing data_request@ccdc.cam.ac.uk, or by contacting The Cambridge Crystallographic Data Centre, 12 Union Road, Cambridge CB2 1EZ, UK; fax: +44 1223 336033.

■ AUTHOR INFORMATION

Corresponding Authors

Rainer Pöttgen − *University of Münster, Faculty of Chemistry and Pharmacy, Institute of Inorganic and Analytical Chemistry, 48149 Münster, Federal Republic of Germany*; Email: pottgen@uni-muenster.de

André Schäfer − *Saarland University, Faculty of Natural Sciences and Technology, Department of Chemistry, 66123 Saarbrücken, Federal Republic of Germany*; orcid.org/0000-0002-5969-6618; Email: andre.schaefer@uni-saarland.de

Diego M. Andrada − *Saarland University, Faculty of Natural Sciences and Technology, Department of Chemistry, 66123 Saarbrücken, Federal Republic of Germany*; orcid.org/0000-0003-2515-7859; Email: diego.andrada@uni-saarland.de

Authors

Sergi Danés − *Saarland University, Faculty of Natural Sciences and Technology, Department of Chemistry, 66123 Saarbrücken, Federal Republic of Germany*

https://dx.doi.org/10.1021/acs.organomet.9b00667
Organometallics 2020, 39, 516−527

Carsten Müller − *Saarland University, Faculty of Natural Sciences and Technology, Department of Chemistry, 66123 Saarbrücken, Federal Republic of Germany;* orcid.org/0000-0002-4702-2202

Lisa Wirtz − *Saarland University, Faculty of Natural Sciences and Technology, Department of Chemistry, 66123 Saarbrücken, Federal Republic of Germany*

Volker Huch − *Saarland University, Faculty of Natural Sciences and Technology, Department of Chemistry, 66123 Saarbrücken, Federal Republic of Germany*

Theresa Block − *University of Münster, Faculty of Chemistry and Pharmacy, Institute of Inorganic and Analytical Chemistry, 48149 Münster, Federal Republic of Germany*

Complete contact information is available at: https://pubs.acs.org/10.1021/acs.organomet.9b00667

Author Contributions

[§]S.D., C.M., and L.W. have contributed equally. The names are given in alphabetical order.

Notes

The submitted version has been deposited as a preprint.[90]
The authors declare no competing financial interest.

■ ACKNOWLEDGMENTS

D.M.A. and A.S. thank Prof. Dr. David Scheschkewitz, Prof. Dr. Guido Kickelbick, and Saarland University for support. D.M.A. thanks the European Research Council, ERC (ERC Starting grants, EU805113), for funding. A.S. thanks the Deutsche Forschungsgemeinschaft, DFG, (Emmy Noether-program, SCHA1915/3-1) and the Fonds der Chemischen Industrie, FCI, for funding.

■ REFERENCES

(1) Arduengo, A. J., III; Harlow, R. L.; Kline, M. A stable crystalline carbene. *J. Am. Chem. Soc.* **1991**, *113*, 361−363.
(2) Wanzlick, H. W.; Schönherr, H. J. Direct Synthesis of a Mercury Salt-Carbene Complex. *Angew. Chem., Int. Ed. Engl.* **1968**, *7*, 141−142.
(3) Nesterov, V.; Reiter, D.; Bag, P.; Frisch, P.; Holzner, R.; Porzelt, A.; Inoue, S. NHCs in Main Group Chemistry. *Chem. Rev.* **2018**, *118*, 9678−9842.
(4) Doddi, A.; Peters, M.; Tamm, M. N-Heterocyclic Carbene Adducts of Main Group Elements and Their Use as Ligands in Transition Metal Chemistry. *Chem. Rev.* **2019**, *119*, 6994−7112.
(5) Kundu, S.; Sinhababu, S.; Chandrasekhar, V.; Roesky, H. W. Stable cyclic (alkyl)(amino)carbene (cAAC) radicals with main group substituents. *Chem. Sci.* **2019**, *10*, 4727−4741.
(6) Frenking, G.; Hermann, M.; Andrada, D. M.; Holzmann, N. Donor-acceptor bonding in novel low-coordinated compounds of boron and group-14 atoms C-Sn. *Chem. Soc. Rev.* **2016**, *45*, 1129−1144.
(7) Soleilhavoup, M.; Bertrand, G. Cyclic (Alkyl)(Amino)Carbenes (CAACs): Stable Carbenes on the Rise. *Acc. Chem. Res.* **2015**, *48*, 256−266.
(8) Melaimi, M.; Jazzar, R.; Soleilhavoup, M.; Bertrand, G. Cyclic (Alkyl)(amino)carbenes (CAACs): Recent Developments. *Angew. Chem., Int. Ed.* **2017**, *56*, 10046−10068.
(9) Müller, C.; Stahlich, A.; Wirtz, L.; Gretsch, C.; Huch, V.; Schäfer, A. Carbene Complexes of Stannocenes. *Inorg. Chem.* **2018**, *57*, 8050−8053.
(10) Müller, C.; Andrada, D. M.; Bischoff, I.-A.; Zimmer, M.; Huch, V.; Steinbrück, N.; Schäfer, A. Synthesis, Structure, and Bonding Analysis of Tin(II) Dihalide and Cyclopentadienyltin(II) Halide (Alkyl)(amino)carbene Complexes. *Organometallics* **2019**, *38*, 1052−1061.
(11) Haider, W.; Huch, V.; Schafer, A. Lewis base complexes of sila[2]aluminocenophanes. *Dalton Trans.* **2018**, *47*, 10425−10428.
(12) Wirtz, L.; Jourdain, M.; Huch, V.; Zimmer, M.; Schäfer, A. Synthesis, Structure and Reactivity of Disiloxa[3]tetrelocenophanes. *ACS Omega* **2019**, *4*, 18355−18360.
(13) Feixas, F.; Matito, E.; Poater, J.; Sola, M. Quantifying aromaticity with electron delocalisation measures. *Chem. Soc. Rev.* **2015**, *44*, 6434−6451.
(14) Beswick, M. A.; Cromhout, N. L.; Harmer, C. N.; Raithby, P. R.; Russel, C. A.; Smith, J. S. B.; Steiner, A.; Wright, D. S. Loosely bonded adducts of plumbocene; Structure and solution dynamics of $[(\eta\text{-}C_5H_5)_2Pb.(tmeda)]$ and $[(\eta\text{-}C_5H_5)_2Pb.4,4'\text{-}Me_2bipy]$ (tmeda = $Me_2NCH_2CH_2NMe_2$,4,4′-Me_2bipy = 4,4′-dimethylbipyridine). *Chem. Commun.* **1996**, 1977−1978.
(15) Armstrong, D. R.; Beswick, M. A.; Cromhout, N. L.; Harmer, C. N.; Moncrieff, D.; Russell, C. A.; Raithby, P. R.; Steiner, A.; Wheatley, A. E. H.; Wright, D. S. Weakly bonded Lewis base adducts of plumbocene and stannocene: A synthetic and calculational study. *Organometallics* **1998**, *17*, 3176−3181.
(16) Hey, J.; Andrada, D. M.; Michel, R.; Mata, R. A.; Stalke, D. Strong intermolecular interactions shaping a small piano-stool complex. *Angew. Chem., Int. Ed.* **2013**, *52*, 10365−10369.
(17) Singh, A. P.; Samuel, P. P.; Mondal, K. C.; Roesky, H. W.; Sidhu, N. S.; Dittrich, B. Lewis Base Stabilized Group 14 Metalylenes. *Organometallics* **2013**, *32*, 354−357.
(18) Bantu, B.; Pawar, G. M.; Decker, U.; Wurst, K.; Schmidt, A. M.; Buchmeiser, M. R. CO_2 and Sn^{II} Adducts of N-Heterocyclic Carbenes as Delayed-Action Catalysts for Polyurethane. *Chem. - Eur. J.* **2009**, *15*, 3103−3109.
(19) Bessac, F.; Frenking, G. Chemical bonding in phosphane and amine complexes of main group elements and transition metals. *Inorg. Chem.* **2006**, *45*, 6956−6964.
(20) Loschen, C.; Voigt, K.; Frunzke, J.; Diefenbach, A.; Diedenhofen, M.; Frenking, G. Theoretical studies of inorganic compounds. 19 Quantum chemical investigations of the phosphane complexes $X_3B\text{-}PY_3$ and $X_3Al\text{-}PY_3$ (X = H, F, Cl; Y = F, Cl, Me, CN). *Z. Anorg. Allg. Chem.* **2002**, *628*, 1294−1304.
(21) Grimme, S. Density functional theory with London dispersion corrections. *WIREs Comput. Mol. Sci.* **2011**, *1*, 211−228.
(22) Wagner, J. P.; Schreiner, P. R. London Dispersion in Molecular Chemistry-Reconsidering Steric Effects. *Angew. Chem., Int. Ed.* **2015**, *54*, 12274−12296.
(23) Liptrot, D. J.; Power, P. P. London dispersion forces in sterically crowded inorganic and organometallic molecules. *Nat. Rev. Chem.* **2017**, *1*, 1.
(24) Morokuma, K. Molecular orbital studies of hydrogen bonds III. C=O···H−O hydrogen bond in $H_2CO\cdots H_2O$ and $H_2CO\cdots 2H_2O$. *J. Chem. Phys.* **1971**, *55*, 1236−1244.
(25) Ziegler, T.; Rauk, A. CO, CS, N_2, PF_3, and $CNCH_3$ as σ-donors and π-acceptors - Theoretical-study by the Hartree-Fock-Slater Transition-State method. *Inorg. Chem.* **1979**, *18*, 1755−1759.
(26) Bickelhaupt, F. M.; Baerends, E. J. Kohn-Sham density functional theory: Predicting and understanding chemistry. *Rev. Comp. Chem.* **2007**, *15*, 1−86.
(27) Tonner, R.; Frenking, G. Divalent carbon(0) chemistry, part 1: Parent compounds. *Chem. - Eur. J.* **2008**, *14*, 3260−3272.
(28) Andrada, D. M.; Frenking, G. Stabilization of Heterodiatomic SiC Through Ligand Donation: Theoretical Investigation of $SiC(L)_2$ (L = NHCMe, CAAC(Me), PMe_3. *Angew. Chem., Int. Ed.* **2015**, *54*, 12319−12324.
(29) Engelhardt, F.; Maaß, C.; Andrada, D. M.; Herbst-Irmer, R.; Stalke, D. Benchmarking lithium amide versus amine bonding by charge density and energy decomposition analysis arguments. *Chem. Sci.* **2018**, *9*, 3111.
(30) Michalak, A.; Mitoraj, M.; Ziegler, T. Bond orbitals from chemical valence theory. *J. Phys. Chem. A* **2008**, *112*, 1933−1939.
(31) Mitoraj, M.; Michalak, A. Donor-acceptor properties of ligands from the natural orbitals for chemical valence. *Organometallics* **2007**, *26*, 6576−6580.

(32) Mitoraj, M.; Michalak, A. Applications of natural orbitals for chemical valence in a description of bonding in conjugated molecules. *J. Mol. Model.* **2008**, *14*, 681−687.
(33) Mitoraj, M. P.; Michalak, A.; Ziegler, T. A Combined Charge and Energy Decomposition Scheme for Bond Analysis. *J. Chem. Theory Comput.* **2009**, *5*, 962−975.
(34) Jutzi, P.; Burford, N. Structurally diverse pi-cyclopentadienyl complexes of the main group elements. *Chem. Rev.* **1999**, *99*, 969−990.
(35) Rayón, V. M.; Frenking, G. Structures, bond energies, heats of formation, and quantitative bonding analysis of main-group metallocenes [E(Cp)2] (E = Be-Ba, Zn, Si-Pb) and [E(Cp)] (E = Li-Cs, B-Tl). *Chem. - Eur. J.* **2002**, *8*, 4693−4707.
(36) Schäfer, A.; Rohe, K.; Grandjean, A.; Huch, V. Synthesis and Structure of 2 Tetrelocenophanes. *Eur. J. Inorg. Chem.* **2017**, 35−38.
(37) Harrison, P. G.; Zuckerman, J. J. Tin-119m Mössbauer and nuclear magnetic resonance study of Dicyclopentadienyltin(II). *J. Am. Chem. Soc.* **1969**, *91*, 6885−6886.
(38) Harrison, P. G.; Healy, M. A. Derivatives of divalent germanium, tin and lead: II. Spectroscopic investigation of dicyclopentadienyltin(II) and its methylcyclopentadienyl analogue. *J. Organomet. Chem.* **1973**, *51*, 153−166.
(39) Lippens, P. E. Interpretation of the ^{119}Sn Mossbauer isomer shifts in complex tin chalcogenides. *Phys. Rev. B: Condens. Matter Mater. Phys.* **1999**, *60*, 4576−4586.
(40) Schütz, M.; Rauhut, G.; Werner, H. J. Local treatment of electron correlation in molecular clusters: Structures and stabilities of (H2O)n, n = 2−4. *J. Phys. Chem. A* **1998**, *102*, 5997−6003.
(41) Saebø, S.; Pulay, P. Local configuration interaction: An efficient approach for larger molecules. *Chem. Phys. Lett.* **1985**, *113*, 13−18.
(42) Hill, J. G.; Platts, J. A.; Werner, H. J. Calculation of intermolecular interactions in the benzene dimer using coupled-cluster and local electron correlation methods. *Phys. Chem. Chem. Phys.* **2006**, *8*, 4072−4078.
(43) Grimme, S. On the importance of electron correlation effects for the π-π interactions in cyclophanes. *Chem. - Eur. J.* **2004**, *10*, 3423−3429.
(44) Piacenza, M.; Grimme, S. Van der Waals complexes of polar aromatic molecules: Unexpected structures for dimers of azulene. *J. Am. Chem. Soc.* **2005**, *127*, 14841−14848.
(45) Piacenza, M.; Grimme, S. Van der Waals interactions in aromatic systems: Structure and energetics of dimers and trimers of pyridine. *ChemPhysChem* **2005**, *6*, 1554−1558.
(46) Takatani, T.; David Sherrill, C. Performance of spin-component-scaled Møller-Plesset theory (SCS-MP2) for potential energy curves of noncovalent interactions. *Phys. Chem. Chem. Phys.* **2007**, *9*, 6106−6114.
(47) Van Mourik, T.; Wilson, A. K.; Dunning, T. H., Jr Benchmark calculations with correlated molecular wavefunctions. XIII. Potential energy curves for He_2, Ne_2 and Ar_2 using correlation consistent basis sets through augmented sextuple zeta. *Mol. Phys.* **1999**, *96*, 529−547.
(48) Bistoni, G. Finding chemical concepts in the Hilbert space: Coupled cluster analyses of noncovalent interactions. *Wiley Interdiscip. Rev.: Comput. Mol. Sci.* **2019**, *0*, e1442.
(49) Schneider, W. B.; Bistoni, G.; Sparta, M.; Saitow, M.; Riplinger, C.; Auer, A. A.; Neese, F. Decomposition of Intermolecular Interaction Energies within the Local Pair Natural Orbital Coupled Cluster Framework. *J. Chem. Theory Comput.* **2016**, *12*, 4778−4792.
(50) Kuhn, N.; Kratz, T. Synthesis of imidazol-2-ylidenes by reduction of imidazole-2(3H)-thiones. *Synthesis* **1993**, *1993*, 561−562.
(51) Arduengo, A. J.; Krafczyk, R.; Schmutzler, R.; Craig, H. A.; Goerlich, J. R.; Marshall, W. J.; Unverzagt, M. Imidazolylidenes, imidazolinylidenes and imidazolidines. *Tetrahedron* **1999**, *55*, 14523−14534.
(52) Fischer, E. O.; Grubert, H. Über Aromatenkomplexe von Metallen. IV. Di-cyclopentadienyl-blei. *Z. Anorg. Allg. Chem.* **1956**, *286*, 237−242.
(53) Fulmer, G. R.; Miller, A. J. M.; Sherden, N. H.; Gottlieb, H. E.; Nudelman, A.; Stoltz, B. M.; Bercaw, J. E.; Goldberg, K. I. NMR Chemical Shifts of Trace Impurities: Common Laboratory Solvents, Organics, and Gases in Deuterated Solvents Relevant to the Organometallic Chemist. *Organometallics* **2010**, *29*, 2176−2179.
(54) Sheldrick, G. A short history of SHELX. *Acta Crystallogr., Sect. A: Found. Crystallogr.* **2008**, *64*, 112−122.
(55) Brand, R. A. *Normos: Mössbauer Fitting Program*; Universitat Duisburg: Duisburg, Germany, 2002.
(56) Becke, A. D. Density-functional thermochemistry. III. The role of exact exchange. *J. Chem. Phys.* **1993**, *98*, 5648−5652.
(57) Lee, C.; Yang, W.; Parr, R. G. Development of the Colle-Salvetti correlation-energy formula into a functional of the electron density. *Phys. Rev. B: Condens. Matter Mater. Phys.* **1988**, *37*, 785−789.
(58) Becke, A. D. Density-functional exchange-energy approximation with correct asymptotic behavior. *Phys. Rev. A: At., Mol., Opt. Phys.* **1988**, *38*, 3098−3100.
(59) Perdew, J. P. Density functional approximation for the correlation-energy of the inhomogeneous electron-gas. *Phys. Rev. B: Condens. Matter Mater. Phys.* **1986**, *33*, 8822−8824.
(60) Grimme, S.; Antony, J.; Ehrlich, S.; Krieg, H. A consistent and accurate ab initio parametrization of density functional dispersion correction (DFT-D) for the 94 elements H-Pu. *J. Chem. Phys.* **2010**, *132*, 154104.
(61) Grimme, S.; Ehrlich, S.; Goerigk, L. Effect of the Damping Function in Dispersion Corrected Density Functional Theory. *J. Comput. Chem.* **2011**, *32*, 1456−1465.
(62) Weigend, F.; Ahlrichs, R. Balanced basis sets of split valence, triple zeta valence and quadruple zeta valence quality for H to Rn: Design and assessment of accuracy. *Phys. Chem. Chem. Phys.* **2005**, *7*, 3297−3305.
(63) Metz, B.; Stoll, H.; Dolg, M. Small-core multiconfiguration-Dirac−Hartree−Fock-adjusted pseudopotentials for post-d main group elements: Application to PbH and PbO. *J. Chem. Phys.* **2000**, *113*, 2563−2569.
(64) Frisch, M. J.; Trucks, G. W.; Schlegel, H. B.; Scuseria, G. E.; Robb, M. A.; Cheeseman, J. R.; Scalmani, G.; Barone, V.; Mennucci, B.; Petersson, G. A.; Nakatsuji, H.; Caricato, M.; Li, X.; Hratchian, H. P.; Izmaylov, A. F.; Bloino, J.; Zheng, G.; Sonnenberg, J. L.; Hada, M.; Ehara, M.; Toyota, K.; Fukuda, R.; Hasegawa, J.; Ishida, M.; Nakajima, T.; Honda, Y.; Kitao, O.; Nakai, H.; Vreven, T.; Montgomery, J. A., Jr.; Peralta, J. E.; Ogliaro, F.; Bearpark, M.; Heyd, J. J.; Brothers, E.; Kudin, K. N.; Staroverov, V. N.; Kobayashi, R.; Normand, J.; Raghavachari, K.; Rendell, A.; Burant, J. C.; Iyengar, S. S.; Tomasi, J.; Cossi, M.; Rega, N.; Millam, J. M.; Klene, M.; Knox, J. E.; Cross, J. B.; Bakken, V.; Adamo, C.; Jaramillo, J.; Gomperts, R.; Stratmann, R. E.; Yazyev, O.; Austin, A. J.; Cammi, R.; Pomelli, C.; Ochterski, J. W.; Martin, R. L.; Morokuma, K.; Zakrzewski, V. G.; Voth, G. A.; Salvador, P.; Dannenberg, J. J.; Dapprich, S.; Daniels, A. D.; Farkas, O.; Foresman, J. B.; Ortiz, J. V.; Cioslowski, J.; Fox, D. J. *Gaussian 16, Revision A.03*; Gaussian, Inc.: Wallingford CT,, 2016.
(65) Peng, C. Y.; Ayala, P. Y.; Schlegel, H. B.; Frisch, M. J. Using redundant internal coordinates to optimize equilibrium geometries and transition states. *J. Comput. Chem.* **1996**, *17*, 49−56.
(66) McIver, J. W.; Komornic, A. Structure of Transition-state in organic reactions - General theory and an applications to cyclobutene-butadiene isomerization using a semiempirical molecular-orbital method. *J. Am. Chem. Soc.* **1972**, *94*, 2625−2633.
(67) Atkins, P. W.; De Paula, J. *Physical Chemistry*, 8th ed.; Oxford University Press: 2006.
(68) Wiberg, K. B. Application of People-Santry-Segal CNDO method to cyclopropylcarbinyl and cyclobutyl cation and to bicyclobutane. *Tetrahedron* **1968**, *24*, 1083−1096.
(69) Reed, A. E.; Weinstock, R. B.; Weinhold, F. Natural-population analysis. *J. Chem. Phys.* **1985**, *83*, 735−746.
(70) Reed, A. E.; Curtiss, L. A.; Weinhold, F. Intermolecular interactions from a natural bond orbital, donor-acceptor viewpoint. *Chem. Rev.* **1988**, *88*, 899−926.

https://dx.doi.org/10.1021/acs.organomet.9b00667
Organometallics 2020, 39, 516−527

(71) Glendening, E. D.; Badenhoop, J. K.; Reed, A. E.; Carpenter, J. E.; Bohmann, J. A.; Morales, C. M.; Landis, C. R.; Weinhold, F. *GENNBO 6.0*; Theoretical Chemistry Institute, University of Wisconsin: Madison, WI, 2013.
(72) Ziegler, T.; Rauk, A. Theoretical study of the ethylene-metal bond in complexes between Cu^+, Ag^+, Au^+, Pt^0, or Pt^{2+} and ethylene based on the Hartree-Fock-Slater Transition-State Method. *Inorg. Chem.* **1979**, *18*, 1558−1565.
(73) Bickelhaupt, F. M.; Nibbering, N. M. M.; Van Wezenbeek, E. M.; Baerends, E. J. *J. Phys. Chem.* **1992**, *96*, 4864−4873.
(74) te Velde, G.; Bickelhaupt, F. M.; Baerends, E. J.; Fonseca Guerra, C.; van Gisbergen, S. J. A.; Snijders, J. G.; Ziegler, T. Chemistry with ADF. *J. Comput. Chem.* **2001**, *22*, 931−967.
(75) Krijn, J.; Baerends, E. J. *Fit Functions in the HFS-Method*, 1984.
(76) Van Lenthe, E.; Baerends, E. J.; Snijders, J. G. *J. Chem. Phys.* **1993**, *99*, 4597−4610.
(77) Hetzer, G.; Pulay, P.; Werner, H. J. Multipole approximation of distant pair energies in local MP2 calculations. *Chem. Phys. Lett.* **1998**, *290*, 143−149.
(78) Pulay, P. Localizability of dynamic electron correlation. *Chem. Phys. Lett.* **1983**, *100*, 151−154.
(79) Sæbø, S.; Pulay, P. Local configuration interaction: An efficient approach for larger molecules. *Chem. Phys. Lett.* **1985**, *113*, 13−18.
(80) Hetzer, G.; Schütz, M.; Stoll, H.; Werner, H. J. Low-order scaling local correlation methods II: Splitting the Coulomb operator in linear scaling local second-order Møller-Plesset perturbation theory. *J. Chem. Phys.* **2000**, *113*, 9443−9455.
(81) Saebø, S.; Pulay, P. Fourth-order Møller−Plessett perturbation theory in the local correlation treatment. I. Method. *J. Chem. Phys.* **1987**, *86*, 914−922.
(82) Saebø, S.; Pulay, P. The local correlation treatment. II. Implementation and tests. *J. Chem. Phys.* **1988**, *88*, 1884−1890.
(83) Schütz, M.; Hetzer, G.; Werner, H. J. Low-order scaling local electron correlation methods. I. Linear scaling local MP2. *J. Chem. Phys.* **1999**, *111*, 5691−5705.
(84) Rauhut, G.; Pulay, P.; Werner, H. J. Integral transformation with low-order scaling for large local second-order Møller-Plesset calculations. *J. Comput. Chem.* **1998**, *19*, 1241−1254.
(85) Pulay, P.; Saebø, S. Orbital-invariant formulation and second-order gradient evaluation in Møller-Plesset perturbation theory. *Theor. Chim. Acta* **1986**, *69*, 357−368.
(86) Werner, H.-J.; Knowles, P. J.; Knizia, G.; Manby, F. R.; Schütz, M.; Celani, P.; Korona, T.; Lindh, R.; Mitrushenkov, A.; Rauhut, G.; Shamasundar, K. R.; Adler, T. B.; Amos, R. D.; Bernhardsson, A.; Berning, A.; Cooper, D. L.; Deegan, M. J. O.; Dobbyn, A. J.; Eckert, F.; Goll, E.; Hampel, C.; Hesselmann, A.; Hetzer, G.; Hrenar, T.; Jansen, G.; Köppl, C.; Liu, Y.; Lloyd, A. W.; Mata, R. A.; May, A. J.; McNicholas, S. J.; Meyer, W.; Mura, M. E.; Nicklass, A.; O'Neill, D. P.; Palmieri, P.; Peng, D.; Pflüger, K.; Pitzer, R.; Reiher, M.; Shiozaki, T.; Stoll, H.; Stone, A. J.; Tarroni, R.; Thorsteinsson, T.; Wang, M. *MOLPRO, version 2012.1, a package of ab initio programs*; http://www.molpro.net, 2012.
(87) Schütz, M.; Werner, H. J.; Lindh, R.; Manby, F. R. Analytical energy gradients for local second-order Moøller-Plesset perturbation theory using density fitting approximations. *J. Chem. Phys.* **2004**, *121*, 737−750.
(88) Dunning, T. H., Jr Gaussian basis sets for use in correlated molecular calculations. I. The atoms boron through neon and hydrogen. *J. Chem. Phys.* **1989**, *90*, 1007−1023.
(89) Woon, D. E.; Dunning, T. H., Jr Gaussian basis sets for use in correlated molecular calculations. III. The atoms aluminum through argon. *J. Chem. Phys.* **1993**, *98*, 1358−1371.
(90) Danés, S.; Müller, C.; Wirtz, L.; Huch, V.; Block, T.; Pöttgen, R.; Schäfer, A.; Andrada, D. M. On the Bonding Situation in Stannocene and Plumbocene N-Heterocyclic Carbene Complexes. *ChemRxiv*, **2019**, DOI: 10.26434/chemrxiv.11089097.v1.

https://dx.doi.org/10.1021/acs.organomet.9b00667
Organometallics 2020, 39, 516−527

3.4 Diphosphanylmetallocenes of Main-Group Elements

Carsten Müller, Joshua Warken, Volker Huch, Bernd Morgenstern, Inga-Alexandra Bischoff, Michael Zimmer, André Schäfer, *Chem. Eur. J.* **2021**, *27*, 6500-6510.

https://doi.org/10.1002/chem.202005198

The above cited article was published as an “Open Access” article under the terms of a Creative Commons Attribution-NonCommercial-NoDerivs License. (Creative Commons Attribution-NonCommercial-NoDerivs). Copyright © (2021) The Authors. Published by Wiley-VCH Verlag GmbH & Co. KGaA.

The results described within this article are additionally put into context in the Conclusion chapter.

Author contribution:

Carsten Müller:
Lead: Synthesis and characterization of diphosphanylmagnesocenes, -tetrelocenes, -stibonocenes, related adducts and complexes; writing, reviewing and editing of the manuscript and supporting information.
Equal to A.S.: DFT-calculations.
Joshua Warken:
Supporting: Synthesis and characterization of diphosphanylmagnesocenes and -tetrelocenes; writing, reviewing and editing of the supporting information.
Volker Huch:
Supporting: X-ray analysis.
Bernd Morgenstern:
Lead: X-ray analysis.
Inga-Alexandra Bischoff:
Supporting: Writing, reviewing and editing of the supporting information; synthesis of starting materials.
Michael Zimmer:
Lead: CP/MAS NMR analysis.
André Schäfer:
Lead: Project administration and supervision, funding acquisition.
Equal to C.M.: DFT-calculations.
Supporting: Writing, reviewing and editing of the manuscript and supporting information.

Chemistry–A European Journal
Full Paper
doi.org/10.1002/chem.202005198
Chemistry Europe
European Chemical Societies Publishing

Metallocenes

Diphosphanylmetallocenes of Main-Group Elements

Carsten Müller, Joshua Warken, Volker Huch, Bernd Morgenstern, Inga-Alexandra Bischoff, Michael Zimmer, and André Schäfer*[a]

Abstract: Several 1,1′-diphosphanyl-substituted metallocenes of magnesium (magnesocenes) were synthesized, structurally characterized, and their reactivity and coordination chemistry were investigated. Transmetalation of these magnesocenes gives access to group 14 metallocenes (tetrelocenes), as well as to group 15 stibonocenes. These s- and p-block metallocenes represent a novel class of bis(phosphanyl) ligands, exhibiting Lewis-amphiphilic character. Their coordination chemistry towards different transition-metal and main-group fragments was investigated and different complexes are presented.

Introduction

Phosphines are one of the most important classes of ligands in coordination chemistry throughout the periodic table, owing to their strong σ-donor abilities.[1] Within this class, bidentate ligands in the form of bis(phosphanyl) compounds are widely recognized for their strong binding capabilities owing to the chelate effect.[2a] Modification of the linker between the phosphanyl groups in these bis(phosphines) can have a strong effect on the bite angle, which is of great importance with regards to steric and electronic properties, and thus for applications in coordination chemistry and catalysis.[2b,c] Within this area, 1,1′-diphosphanyl-substituted ferrocenes have developed into a special class of metal-containing redox active ligands, which have been applied for a variety of transition-metal fragments, since their introduction in the late 1960s.[3] The most prominent examples, 1,1′-bis(diphenylphosphanyl)ferrocene, **dppf**, and the 1,1′-bis(diisopropylphosphanyl)ferrocene, **dippf**, are widely recognized for their applications in homogeneous catalysis, for instance, in the form of palladium or platinum complexes, which, nowadays, are even commercially available.[3d,e]

Furthermore, 1,1′-diphosphanyl-substituted metallocenes of other transition metals are also known, for instance, of lanthanum, yttrium, titanium, zirconium, hafnium, niobium, ruthenium, osmium, cobalt,[4] and in addition, of the lanthanoids europium and ytterbium,[5] as well as of a handful of main-group metals[6] (Figure 1). In some cases, weak interactions between the metallocene central atom and P-complexed metal fragments can be observed, which can be important to the reactivity of these complexes.[3c,4l,7] In addition, structurally related heteroleptic complexes of other phosphanyl-functionalized π-ligands like cycloheptatrienyl or phenyl are also known and possess an intriguing coordination chemistry.[8]

As there are several diphosphanyl-substituted metallocenes beyond ferrocenes, mostly exhibiting diphenylphosphanyl or diisopropylphosphanyl groups, a convenient nomenclature for these compounds would be valuable. We suggest to use the popular "dpp" and "dipp" abbreviations for metallocenes possessing a 1,1′-bis(diphenylphosphanyl) or a 1,1′-bis(diisopropylphosphanyl) substitution pattern, derived from the corresponding ferrocene acronyms **dppf** and **dippf**, and combining it with the element symbol. Following this principle, the 1,1′-bis(diphenylphosphanyl)ferrocene, **dppf**, could also be referred to as **dppFe**. This becomes more useful for metallocenes of other metals, for instance, the aforementioned titanium, zirconium, cobalt, and ytterbium species could be referred to as **dppTiCl$_2$**, **dppZrCl$_2$**, **dppCo**, and **dppYb**. In addition, the octamethyl derivatives exhibiting permethylated Cp rings can be denoted by a superscript hash, like in the case of tetramethylcyclopentadienide, Cp$^{\#}$, and pentamethylcyclopentadienide, Cp*, thus 1,1′-bis(diphenylphosphanyl)octamethyl ferrocene[9] could be abbreviated **dpp$^{\#}$Fe**.

As mentioned above, the concept of 1,1′-diphosphanyl-functionalization is limited to a few main-group metallocenes and remains only sparsely explored, aside from dimethylplatinum complexes of thf-adducts of **dppCa**, **dppSr**, and **dppBa**,[6b] and a gold(I) complex of **dppTl$^-$**.[10] This is surprising, as s- and p-block based diphosphanyl-substituted metallocenes present particularly interesting ligands, as the central atom is Lewis-acidic.[11,12] Therefore, these metallocenes can be regarded as

[a] C. Müller, J. Warken, Dr. V. Huch, Dr. B. Morgenstern, I.-A. Bischoff, Dr. M. Zimmer, Dr. A. Schäfer
Faculty of Natural Sciences and Technology, Department of Chemistry
Saarland University, Campus Saarbrücken, 66123 Saarbrücken (Germany)
E-mail: andre.schaefer@uni-saarland.de

Supporting information and the ORCID identification number(s) for the author(s) of this article can be found under: https://doi.org/10.1002/chem.202005198.

© 2021 The Authors. Chemistry - A European Journal published by Wiley-VCH GmbH. This is an open access article under the terms of the Creative Commons Attribution Non-Commercial NoDerivs License, which permits use and distribution in any medium, provided the original work is properly cited, the use is non-commercial and no modifications or adaptations are made.

Chemistry–A European Journal
Full Paper
doi.org/10.1002/chem.202005198
Chemistry Europe
European Chemical Societies Publishing

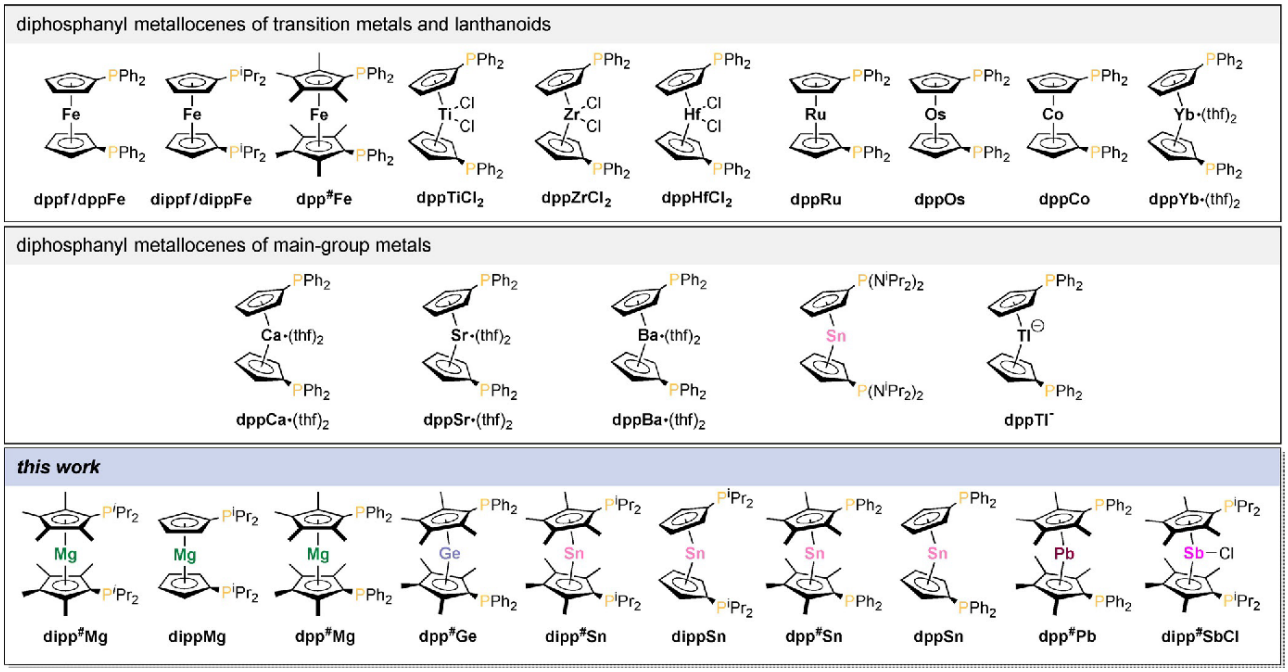

Figure 1. Selected examples of 1,1′-diphosphanyl-substituted metallocenes.

Lewis-amphiphilic ligand systems, with a hard, electron-poor and a soft, electron-rich center.[6b] In general, Lewis-amphiphilic ligands, often based on boron or aluminium, have attracted much attention for their coordination properties, but the use of alkaline earth metals or group 14 elements as Lewis-acidic centers in such ligands is almost unexplored.[13] It should be noted that, so far, the group 2 metallocenes **dppCa**, **dppSr**, and **dppBa**, have only been isolated in the form of their thf adducts in which their Lewis-acidity is quenched by the coordination of the thf molecules.[6b] As group 14 metallocenes (tetrelocenes) are tetrylene-type compounds, and tetrylene complexes of main-group and transition metals have been studied extensively,[14] and following our group's continuous interest in main-group metallocenes, we were intrigued to study diphosphanyl-substituted metallocenes of s- and p-block metals.

Herein, we report the synthesis and structure of different diphosphanylmagnesocenes **1 a–c**, tetrelocenes, **2**, **3 a–c**, **4**, and stibonocenes **5 a**,**b** and present a study of their reactivity towards σ-donors, small molecules, and various metal fragments.

Results and Discussion

Magnesocenes

Diphosphanylmagnesocenes **1 a–c** (**dipp#Mg**, **dippMg**, **dpp#Mg**) were synthesized by the reaction of lithium cyclopentadienide or lithium tetramethylcyclopentadienide with the corresponding chlorophosphines and subsequent treatment with dibutylmagnesium (Scheme 1).

Magnesocenes **1 a–c** are obtained as highly air-sensitive, colorless solids in acceptable to good yields (**1 a**: 38%; **1 b**: 86%; **1 c**: 76%). Notably, the synthesis of a 1,1′-bis(diphenylphosphanyl)magnesocene, **1 d** (**dppMg**), failed, presumably owing to the instability of the protonated ligand Ph_2PCpH.[15] Compounds **1 a–c** show a high degree of solubility in aliphatic and aromatic solvents such as hexane, benzene, and toluene, and were characterized by multinuclear NMR spectroscopy in solution and single-crystal X-ray diffraction analysis in the solid state (Figure 1). In solution, the ^{31}P NMR chemical shifts of **1 a–c**, which range from −2.8 to −25.5 ppm depending on the substitution pattern, are in line with known diphosphanylferrocenes (δ^{31}P(**dppFe**) = −16.6 ppm;[16] δ^{31}P(**dippFe**) = 0.9 ppm[16]). Notably, **1 b** (**dippMg**), exists as a dimer in the solid state (Figure 2 a), owing to its Lewis-amphiphilic nature, although magnesocene phosphine complexes have previously been described as unisolable in pure form.[17] The intermolecular Mg–P distances are 274.32(1) pm and 279.45(1) pm, which are longer than in known phosphorous magnesium complexes[18–20] ((dppmfluMg(μ-*n*Bu))$_2$: 262.71(7) pm (dppmflu = ($Ph_2PCH_2PPh_2$)fluorene)). However, with just a few examples of phosphine-coordinated diorgano-substituted magnesium compounds known,[18–20] and no examples of magnesocene phosphine complexes,[17] this value must be assessed carefully. As only a single signal is observed in the $^{31}P\{^1H\}$ NMR spectrum in solution at room temperature, we assume that it is a rather

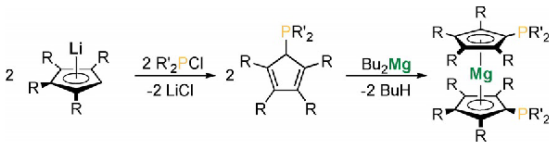

Scheme 1. Synthesis of diphosphanylmagnesocenes **1 a–c.** **1 a**: R = Me; R′ = *i*Pr. **1 b**: R = H; R′ = *i*Pr. **1 c**: R = Me; R′ = Ph.

 © 2021 The Authors. Chemistry - A European Journal published by Wiley-VCH GmbH

Chemistry–A European Journal | Full Paper doi.org/10.1002/chem.202005198 | Chemistry Europe European Chemical Societies Publishing

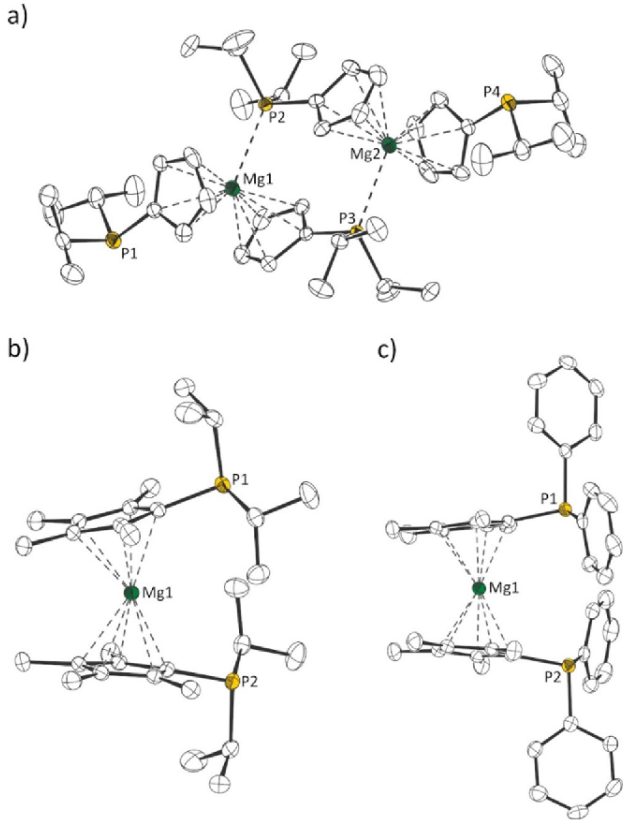

Figure 2. Molecular structures of (a) **1b**-dimer, (b) **1a**, and (c) **1c** in the crystal (displacement ellipsoids at the 50% probability level; H atoms omitted). Selected bond lengths [ppm] and angles [°]: **1b**: Mg1–P2 274.32(1), Mg2–P3 279.45(1), Cp^{cent}–Mg1 211.62(1)/213.39(1)/220.60(1), Cp^{cent}–Mg2 218.36(1)/211.62(1); Cp^{cent}-Mg1-Cp^{cent} 136.627(3), Cp^{cent}-Mg2-Cp^{cent} 135.317(3); **1a**: Cp^{cent}–Mg1 201.36(2); Cp^{cent}-Mg1-Cp^{cent} 159.790(5); **1c**: Cp^{cent}–Mg1 198.66(3)/199.05(3); Cp^{cent}-Mg1-Cp^{cent} 166.539(11).

Table 1. Selected bond lengths, angles, and ^{31}P NMR shifts of **1a–c**, **1b·(thf)$_2$**, **1b·(CS$_2$)$_2$**, **1b·PhNCO**, and **1b·PtMe$_2$**.

Compound	Mg–Cp[a] [pm]	Cp-Mg-Cp[b] [°]	δ ^{31}P [ppm]
1a (**dipp#Mg**)	201.36(2)	159.790(5)	−3.8[c]
1b (**dippMg**)	211.62(1) 213.39(1) 220.60(1)	136.627(3) 135.317(3)	−2.8[c]
1c (**dpp#Mg**)	198.66(3) 199.05(3)	166.539(11)	−25.5[c]
1b·(thf)$_2$	224.05(2) 234.57(2) 248.95(1)	–	−2.3[c]
1b·(CS$_2$)$_2$	215.39(8)	136.611(2)	36.2[c]
1b·PhNCO	218.16(8) 241.50(2) 282.70(2)	–	24.0 −12.6[d]
1b·PtMe$_2$	197.34(6) 198.57(6)	164.409(32)	21.0 ($^1J_{PPt}$ = 1862 Hz)[c]

[a] Corresponding to the bonding mode of the Cp ligand. [b] Corresponding to Cp^{cent} and only given in the case of η^5 bonding. [c] C_6D_6, 162 MHz, 298 K. [d] CP-MAS (13 kHz), 162 MHz, 296 K.

weak interaction and **1b** (**dippMg**) exists in rapid equilibrium with a monomer in solution. As mentioned above, this is in line with previous reports that the isolation of phosphine adducts of magnesocene failed owing to dissociation in solution.[17] The Mg–Cp distances are shorter in case of the permethylated magnesocenes **1c** (**dpp#Mg**) (198.66(3) pm and 199.05(3) pm) and **1a** (**dipp#Mg**) (201.36(2) pm) and longer in the case of **1b** (**dippMg**) (211.62(1) pm and 220.60(1) pm). This can be attributed to steric and electronic factors, as permethylated Cp rings are more electron rich, resulting in stronger Mg–Cp bonds, and on the other hand, phosphine coordination to the magnesium atom in dimer **1b** increases the electron density and steric pressure on the magnesium atom, which weakens the Mg–Cp bonds. The Cp^{cent}-Mg-Cp^{cent} angles in magnesocenes **1a–c** also differ significantly (Table 1). Only a slight bending is observed for **1c** (**dpp#Mg**) (166.5°) and **1a** (**dipp#Mg**) (159.8°), whereas a strong bending is observed in dimeric **1b** (**dippMg**) (135.3° and 136.6°). This highlights the flexibility of the Mg–Cp bonds, owing to their high ionic character. The previously reported diphosphanyl-metallocenes of calcium, **dppCa·(thf)$_2$**, strontium, **dppSr·(thf)$_2$**, and barium, **dppBa·(thf)$_2$**, are monomeric in the solid state, which is a consequence of the coordination of thf molecules to the central atom.[6b] This prompted us to investigate the reactivity of **1b** (**dippMg**) towards thf. As expected, when dissolved in thf, the corresponding bis(thf) adduct, **1b·(thf)$_2$**, is obtained in quantitative yields (Scheme 2).

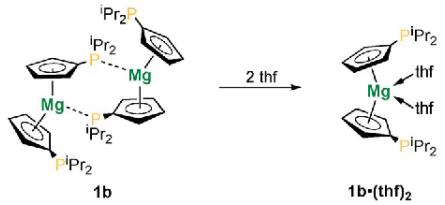

Scheme 2. Reaction of **1b** with thf.

In the solid state, **1b·(thf)$_2$** exhibits one η^5- and one η^2-bonded Cp ligand (Figure 3). Ring slippage of Cp ligands in the solid state is not uncommon for magnesium Cp compounds and is not reflected by NMR spectroscopy in solution. For example, **1b·(thf)$_2$** gives only a single resonance in the ^{31}P NMR spectrum ($\delta^{31}P = -2.3$ ppm) in solution, along with two resonances for Cp protons in the ^1H NMR spectrum. Similar structures have been reported before, for instance, in the case of a magnesocene bis(thf) adduct[21] and also for [1]magnesocenophane bis(thf) adducts.[22]

The Mg–O bond lengths in **1b·(thf)$_2$** are 206.17(2) pm and 208.14(1) pm, comparable to what is found in $Cp_2Mg·(thf)_2$ (208.8 pm and 209.8(2) pm).[21] The Mg–C bond lengths to the

 © 2021 The Authors. Chemistry - A European Journal published by Wiley-VCH GmbH

Chemistry–A European Journal
Full Paper
doi.org/10.1002/chem.202005198
Chemistry Europe
European Chemical Societies Publishing

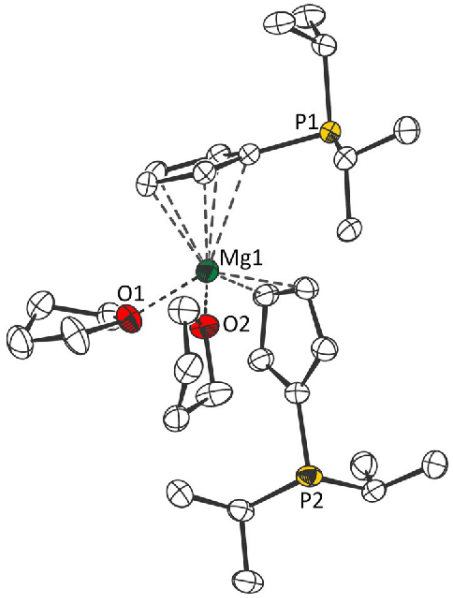

Figure 3. Molecular structure of **1b·(thf)$_2$** in the crystal (displacement ellipsoids at the 50% probability level; H atoms omitted). Selected bond lengths [ppm]: Mg1–O1 208.14(1), Mg1–O2 206.17(2), Cp^{cent}–Mg1 224.05(2).

η^2-coordinated Cp ligand are 234.57(2) pm and 248.95(1) pm, suggesting a tendency towards η^1, and the Mg–Cp^{cent} distance to the η^5-bonded Cp moiety is 224.05(2) pm. Inspection of the frontier orbitals of diphosphanylmagnesocene **1b** (**dippMg**) (Figure 4) highlights its Lewis-amphiphilic character.

HOMO and HOMO−1 exhibit large coefficients at the phosphorus atoms, corresponding to the lone pairs. In comparison, the LUMO is predominantly localized on the magnesium atom, highlighting its Lewis-acidic character. The Lewis-amphiphilicity of **1b** (**dippMg**) prompted us to study its reactivity not only towards metal fragments, but also towards small/organic molecules, as such molecules can often be activated and coordinated by Lewis-amphiphilic frustrated Lewis pair (FLP)-type systems.[24] Indeed, treatment of solutions of **1b** (**dippMg**) with carbon disulfide and phenyl isocyanate, led to formation of the corresponding adducts (Scheme 3). In the case of the CS_2 complex, a downfield shifted doublet in the $^{13}C\{^1H\}$ NMR spectrum at 237.0 ppm (J_{CP} = 37 Hz) was detected, which is comparable to other CS_2 phosphorous adducts.[24a]

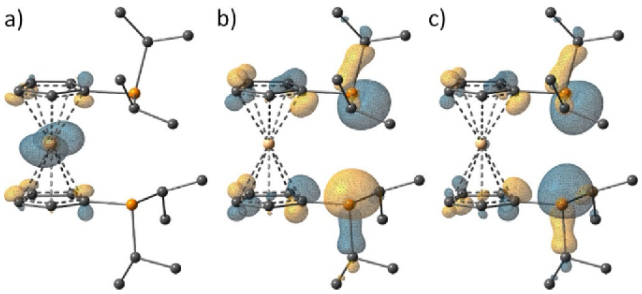

Figure 4. Isosurface plots of (a) LUMO, (b) HOMO, and (c) HOMO−1 of magnesocene **1b** (B3LYP-D3/def2-TZVP,[23] isovalue = 0.05).

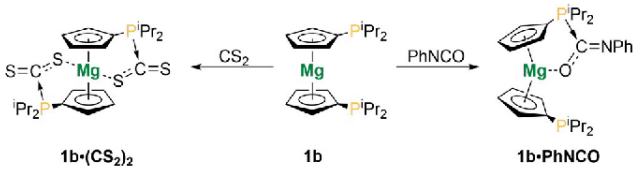

Scheme 3. Reaction of **1b** with CS_2 and PhNCO.

To the best of our knowledge, **1b·(CS$_2$)$_2$** is the first example of a magnesium CS_2 complex of this kind. In the solid state (Figure 5), **1b·(CS$_2$)$_2$** possesses two η^5-coordinated Cp ligands. The P–C bonds in **1b·(CS$_2$)$_2$** are 183.71(124) pm, which is almost identical to Sn/P and B/P FLP CS_2 complexes[24a,c] ((Fxyl)$_2$BCH$_2$P*t*Bu$_2$·CS$_2$: 183.5(8) pm; (F$_5$C$_2$)$_3$SnCH$_2$P*t*Bu$_2$·CS$_2$: 184.7(2) pm), whereas the Mg–S bonds are 249.48(39) pm, which is longer than in a related magnesium dithiocarbonate complex,[24d] but shorter than in a dithiobenzoate complex.[24e] Remarkably, **1b** (**dippMg**) does not undergo a Mg–C insertion reaction with CS_2, in contrast to what is common for Grignard reagents.[24e] Similar to **1b** (**dippMg**), **1b·PhNCO** exhibits a dimeric structure in the solid state[25] with Mg–P bonds of 256.23(1) pm and 273.70(1) pm (Figure S79 in the Supporting Information). The bonding situation of the Cp ligands in **1b·PhNCO** in the solid state is best regarded as η^5 and η^2, like in the afore-discussed bis(thf) adduct **1b·(thf)$_2$**. The Mg–O bond length is 195.65(1) pm, which is slightly shorter than in other magnesium phenyl isocyanate complexes[26] ([(Me$_4$TACD)Mg·PhNCHO]$^+$: 204.3(6) pm (TACD = tetraazacyclododecane)). On the other hand, the P–C bond is 184.80(18) pm, which is slightly shorter than in related FLP complexes of phenyl isocyanate[24c] ((F$_5$C$_2$)$_3$SnCH$_2$P*t*Bu$_2$·PhNCO: 185.0(2) pm). In solution at room temperature, several signals are observed in the ^{31}P NMR spectrum upon dissolving the crystals of **1b·PhNCO** in benzene-D$_6$, presumably owing to decomposition of the complex. In the $^{31}P\{^1H\}$ CP-MAS NMR spec-

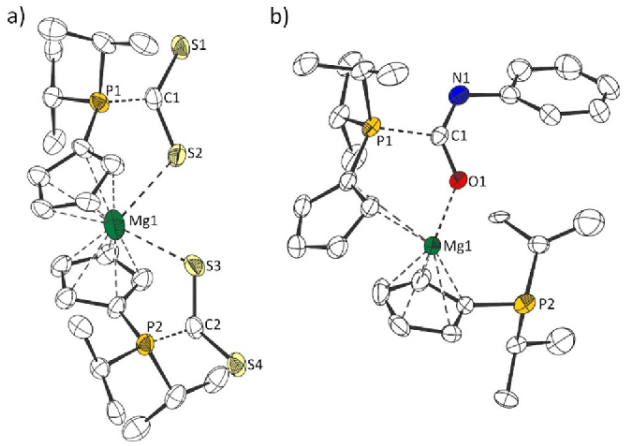

Figure 5. Molecular structure of (a) **1b·(CS$_2$)$_2$** and (b) **1b·PhNCO** in the crystal (displacement ellipsoids at the 50% probability level; H atoms omitted). Selected bond lengths [ppm] and angles [°]: **1b·(CS$_2$)$_2$**: Mg1–S2/S3 249.48(39), Cp^{cent}–Mg1 215.39(8), P1–C1/P2–C2 183.71(124); Cp^{cent}-Mg1-Cp^{cent} 136.611(2); **1b·PhNCO**: Mg1–O1 195.65(1), P1–C1 184.80(18), Cp^{cent}–Mg1 218.16(8).

 © 2021 The Authors. Chemistry - A European Journal published by Wiley-VCH GmbH

Chemistry–A European Journal | Full Paper doi.org/10.1002/chem.202005198 | Chemistry Europe European Chemical Societies Publishing

trum of **1b·PhNCO**, two signals are observed, as one would expect.[25] To assess the bonding energy of phenyl isocyanate to the magnesocene moiety in complex **1b·PhNCO**, we performed DFT calculations at the B3LYP-D3/def2-TZVP level of theory,[23] which suggest a complexation energy of 135.4 kJ mol^{-1}.

It has previously been shown that diphosphanyl-substituted metallocenes of heavy group 2 metals can be used as ligands in platinum complexes. This is particularly interesting, as these ligand systems have highly variable bite angles, owing to the ionic character of the alkaline earth metal Cp bonds. Noteworthy, the reported complexes, **dppCa·(thf)$_2$·PtMe$_2$**, **dppSr·(thf)$_2$·PtMe$_2$**, **dppBa·(thf)$_2$·PtMe$_2$**, all exhibited two thf molecules bound to the group 2 metal. No solvent-free complexes of alkaline earth metals and no complexes of magnesium had previously been described. When (COD)PtMe$_2$ is added to a toluene solution of **1b** (**dippMg**), immediate precipitation of the product **1b·PtMe$_2$** as a colorless solid is observed (Scheme 4), which was obtained in 75% yield.

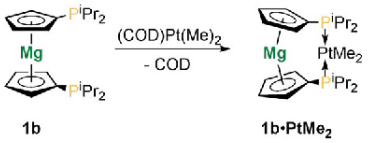

Scheme 4. Reaction of **1b** with (COD)Pt(Me)$_2$.

Compound **1b·PtMe$_2$** is an example of an early–late heterobimetallic complex (ELHB), which have been discussed intensively for their applications in catalysis.[27] Platinum complex **1b·PtMe$_2$** shows a signal at 21.0 ppm in the ^{31}P NMR spectrum, with a platinum coupling of $^1J_{PPt}$ = 1862 Hz (Table 1). This is similar to **dppCa·(thf)$_2$·PtMe$_2$** ($^1J_{PPt}$ = 1878 Hz[6b]) and **dppFe·PtMe$_2$** ($^1J_{PPt}$ = 1903 Hz[28]), and typical for *cis*-bis(phosphine) complexes of dimethylplatinum(II).[29] Notably, in contrast to the previously reported platinum complexes of heavier group 2 diphosphanyl metallocenes,[6b] **1b·PtMe$_2$** can be isolated without solvent coordination to the central atom (Figure 6), retaining the Lewis-acidity of the magnesium atom. The P–Pt bonds in **1b·PtMe$_2$** measure 231.19(4) pm and 232.73(4) pm in the solid state, comparable to those of **dppCa·(thf)$_2$·PtMe$_2$** (229.00(7) pm and 229.15(7) pm).

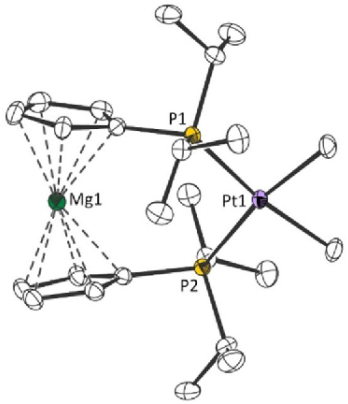

Figure 6. Molecular structure of **1b·PtMe$_2$** in the crystal (displacement ellipsoids at the 50% probability level; H atoms omitted). Selected bond lengths [ppm] and angles [°]: P1–Pt1 231.19(4), P2–Pt1 232.73(4), Cp^{cent}–Mg1 197.34(6)/198.57(6); Cp^{cent}-Mg1-Cp^{cent} 164.409(32), P1-Pt1-P2 105.129(13).

As magnesium Cp compounds are known to be excellent Cp-transfer reagents, we probed the possibility to synthesize other diphosphanylmetallocenes starting from magnesocenes **1a–c**. In the first instance, as proof of concept, we reacted **1b,c** with iron(II) chloride and were able to obtain the corresponding ferrocenes (Scheme 5).[25] Although **dippFe** can more easily be obtained by dilithiation and functionalization of ferrocene, this route is a useful approach for the synthesis of **dpp$^{\#}$Fe**.

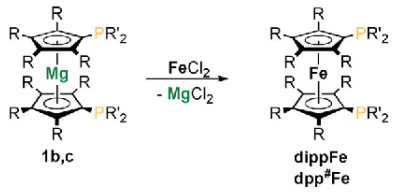

Scheme 5. Transmetalation of **1b,c** with iron(II) chloride (**dippFe**: R = H, R′ = *i*Pr; **dpp$^{\#}$Fe**: R = Me, R′ = Ph).

Tetrelocenes

Following the successful synthesis of ferrocenes **dippFe** and **dpp$^{\#}$Fe** starting from magnesocenes **1b,c**, we were able to prepare diphosphanyltetrelocenes **2** (**dpp$^{\#}$Ge**), **3a–c** (**dipp$^{\#}$Sn**, **dippSn**, **dpp$^{\#}$Sn**), and **4** (**dpp$^{\#}$Pb**) by transmetalation of **1a–c** with the corresponding group 14 dichlorides in acceptable to good yields (Scheme 6).

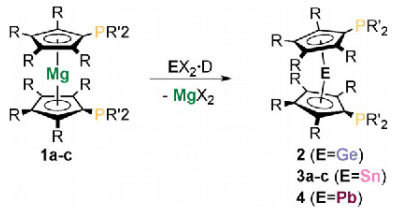

Scheme 6. Synthesis of **2**, **3a–c**, and **4** by transmetalation of **1a–c** with the corresponding group 14 element dichlorides. **2**: R = Me; R′ = Ph. **3a**: R = Me; R′ = *i*Pr. **3b**: R = H; R′ = *i*Pr. **3c**: R = Me; R′ = Ph. **3d**: R = H; R′ = Ph. **4**: R = Me; R′ = Ph.

Bis(diphenylphosphanyl)stannocene, **3d** (**dppSn**), of which the corresponding magnesocene (**dppMg**) could not be prepared, could be obtained in 1% yield by a reaction sequence starting from lithium cyclopentadienide.[25] In contrast to magnesocene **1b** (**dippMg**), stannocene **3b** (**dippSn**) exhibits a monomeric structure in the crystal, just like all diphosphanyltetrelocenes, **2–4**, (Figures 7 and 8). This highlights the decreasing Lewis-acidity of the tetrels compared with magnesium.

The Cp^{cent}-E-Cp^{cent} angles decrease from germanocene **2** (**dpp$^{\#}$Ge**) to stannocene **3c** (**dpp$^{\#}$Sn**) to plumbocene **4** (**dpp$^{\#}$Pb**). This trend, going from lighter to heavier group 14 el-

 © 2021 The Authors. Chemistry - A European Journal published by Wiley-VCH GmbH

Chemistry–A European Journal | Full Paper doi.org/10.1002/chem.202005198 | Chemistry Europe European Chemical Societies Publishing

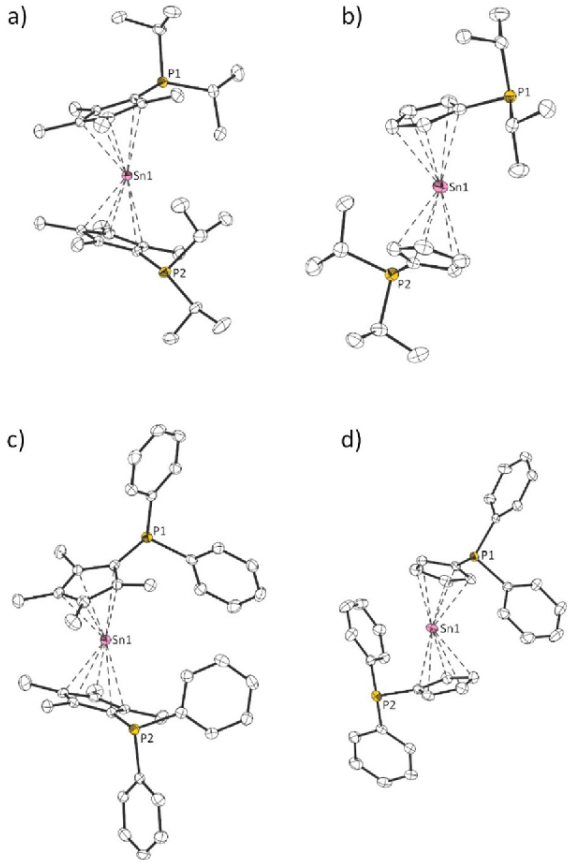

Figure 7. Molecular structures of (a) **3a**, (b) **3b**, (c) **3c**, and (d) **3d** in the crystal (displacement ellipsoids at the 50% probability level, H atoms omitted). Selected bond lengths [ppm] and angles [°]: **3a**: Cp^{cent}–Sn1 237.67(1)/240.43(1); Cp^{cent}-Sn1-Cp^{cent} 156.147(3), **3b**: Cp^{cent}–Sn1 240.39(1)/242.21(1); Cp^{cent}-Sn1-Cp^{cent} 152.593(2); **3c**: Cp^{cent}–Sn1 240.93(1)/242.09(1); Cp^{cent}-Sn1-Cp^{cent} 152.753(3); **3d**: Cp^{cent}–Sn1 242.92(1)/242.93(1); Cp^{cent}-Sn1-Cp^{cent} 146.951(4).

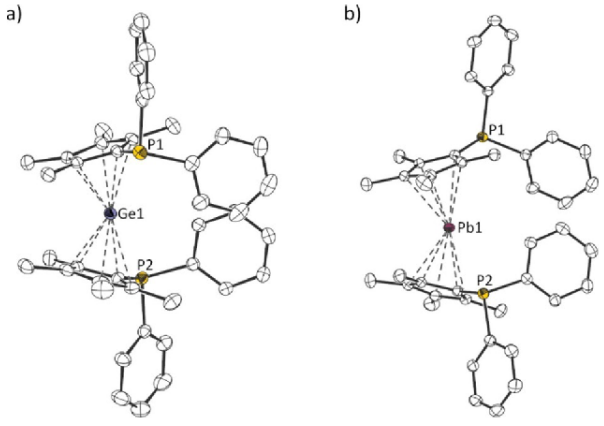

Figure 8. Molecular structures of (a) **2** and (b) **4** in the crystal (displacement ellipsoids at the 50% probability level; H atoms omitted). Selected bond lengths [ppm] and angles [°]: **2**: Cp^{cent}–Ge1 220.20(3)/222.33(3); Cp^{cent}-Ge1-Cp^{cent} 159.932(15); **4**: Cp^{cent}–Pb1 247.82(2)/249.19(2); Cp^{cent}-Pb1-Cp^{cent} 150.575(11).

ements, is a result of decreasing hybridization and less lone-pair character on the central atom. On the other hand, the Cp^{cent}–E bond lengths increase from **2** to **3c** to **4**, which is in line with the increasing size of the central atom. It is noteworthy that **2** (**dpp#Ge**) is the first example of a diphosphanylmetalloidocene, a diphosphanyl-substituted metallocene-type compound based on a metalloid element. Benzene-D_6 solutions of diphosphanyltetrelocenes, **2**–**4**, show similar ^{31}P resonance of −4.8 to −28.7 ppm as magnesocenes **1a**–**c** (Tables 1 and 2), and corresponding ferrocenes[16,30] ($\delta^{31}P$(**dppFe**) = −16.6 ppm; $\delta^{31}P$(**dippFe**) = 0.9 ppm; $\delta^{31}P$(**dpp#Fe**) = −20.1 ppm). The ^{119}Sn NMR chemical shifts of diphosphanylstannocenes **3a**–**d** range from −2134 ppm to −2199 ppm (Table 2), which is similar to stannocene[31] ($\delta^{119}Sn(Cp_2Sn)$ = −2199 ppm) and decamethyl-stannocene[31] ($\delta^{119}Sn(Cp^*_2Sn)$ = −2129 ppm). Diphosphanylplumbocene **4** (**dpp#Pb**) shows a single ^{207}Pb resonance at −4668 ppm, which is in line with other plumbocenes[31] ($\delta^{207}Pb(Cp_2Pb)$ = −5030 ppm; $\delta^{207}Pb(Cp^*_2Pb)$ = −4390 ppm).

Inspection of the frontier orbitals of **3b** (**dippSn**) shows that the HOMO and HOMO−1 correspond predominantly to the lone pairs of the phosphorus atoms, whereas the LUMO is almost exclusively located on the tin atom in the shape of a p-orbital, suggesting that this compound has Lewis-amphiphilic character. The lone pair on the tin atom in the form of the HOMO−7 is comparably low in energy and of high s-character (Figure 9).[12] Qualitatively identical frontier orbitals can be found in all diphosphanyltetrelocenes, **2**–**4**.

To investigate whether **3b** (**dippSn**) does indeed possess Lewis-amphiphilic reactivity as suggested by the frontier orbitals, we reacted it with a σ-donor in the form of an N-heterocyclic carbene (NHC), as well as with different Lewis-acidic metal fragments. We have previously shown that stannocenes can form isolable complexes with different NHCs.[12d] In line with this, stannocene **3b** (**dippSn**) forms a stable carbene complex,

Table 2. Selected bond lengths, angles, ^{31}P, ^{119}Sn, and ^{207}Pb NMR shifts of **2**, **3a**–**d**, **4**.

Compound	E–Cp[a] [pm]	Cp-E-Cp[a] [°]	δ 31P[b] [ppm]	δ 119Sn[c]/ δ 207Pb[d] [ppm]
2 (**dpp#Ge**)	220.20(3) 222.33(3)	159.932(15)	−27.4	–
3a (**dipp#Sn**)	237.67(1) 240.43(1)	156.147(3)	−4.9	−2176
3b (**dippSn**)	240.39(1) 242.21(1)	152.593(2)	−4.8	−2134
3c (**dpp#Sn**)	240.93(1) 242.09(1)	152.753(3)	−27.5	−2199
3d (**dppSn**)	242.92(1) 242.93(1)	146.951(4)	−22.6	−2197
4 (**dpp#Pb**)	247.82(2) 249.19(2)	150.575(11)	−28.7	−4668

[a] Corresponding to $Cp^{centroid}$. [b] C_6D_6, 162 MHz, 298 K. [c] C_6D_6, 149 MHz, 298 K. [d] C_6D_6, 63 MHz, 298 K.

 © 2021 The Authors. Chemistry - A European Journal published by Wiley-VCH GmbH

Chemistry–A European Journal
Full Paper
doi.org/10.1002/chem.202005198
Chemistry Europe
European Chemical Societies Publishing

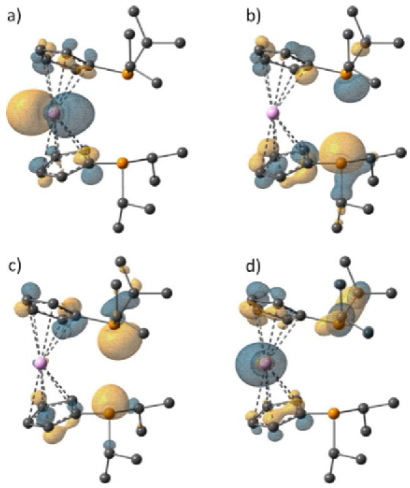

Figure 9. Isosurface plots of (a) LUMO, (b) HOMO, (c) HOMO−1, and (d) HOMO−7 of **3 b** (B3LYP-D3/def2-TZVP;[23] isovalue = 0.05).

3 b·NHC, with 1,3-diisopropyl-4,5-dimethylimidazolin-2-ylidene (Scheme 7).

In **3 b·NHC**, the NHC is side-on coordinated to the metallocene moiety (Figure 10), similar to previously reported stannocene complexes.[12d] The Cp^{cent}–Sn bond lengths (259.31(1) pm and 264.86(1) pm) are significantly elongated compared with **3 b** (240.39(1) pm and 242.21(1) pm) and the Cp^{cent}-Sn-Cp^{cent} angle of **3 b·NHC** (134.8°) is smaller than in **3 b** (**dippSn**) (152.6°), as a result of the NHC coordination. Compound **3 b·NHC** clearly highlights the Lewis-acidic character of the tin atom in **3 b** (**dippSn**).

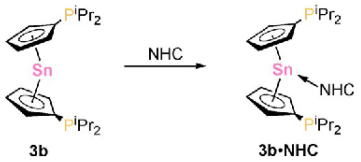

Scheme 7. Reaction of **3 b** with NHC (NHC = 1,3-diisopropyl-4,5-dimethylimidazolin-2-ylidene).

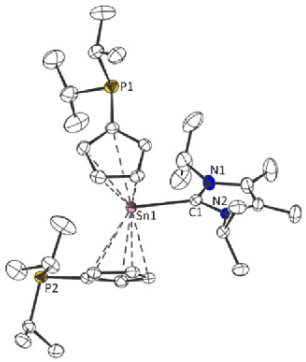

Figure 10. Molecular structure of **3 b·NHC** in the crystal (displacement ellipsoids at the 50% probability level, H atoms omitted). Selected bond lengths [ppm] and angles [°]: Sn1–C1 241.63(0), Cp^{cent}–Sn1 259.31(1)/264.86(1); Cp^{cent}-Sn1-Cp^{cent} 134.767(1).

To probe the applicability of **3 b** (**dippSn**), as a ligand, we reacted it with aluminium(III) chloride, and were able to obtain a corresponding adduct, **3 b·$AlCl_3$**, in 52% yield (Scheme 8).

The solid-state structure reveals that aluminium complex **3 b·$AlCl_3$** possesses a dimeric structure in the solid state (Figure 11 a), owing to the Lewis-acidity of the tin center, which is remarkable as **3 b** (**dippSn**) itself is monomeric in the solid state and phosphine complexes of stannocenes are unknown. Accordingly, **3 b·$AlCl_3$** is the first example of a structurally characterized phosphine adduct of a tetrelocene, and in general, phosphine complexes of stannylenes are extremely rare. The Sn–P distance of 298.78(2) pm is significantly longer than in other phosphine complexes of diaryl- or disilylstannylenes[32,33] (TerSn-μ-aceNaph(P*i*Pr_2): 263.62(6) pm (Ter = 2,6-bis(2,4,6-triisopropylbenzene)xylene, aceNaph = 1,2-dihydroacenaphthylene); ($Me_2Si(SiMe_3)_2Si)_2Sn(PEt_3)$: 260.8(3) pm). The solid-state structure is, however, not persistent in solution at room temperature, as only one set of isopropyl groups is observed in the ^1H and $^{13}C\{^1H\}$ NMR spectra, accompanied by broad signals in the $^{27}Al\{^1H\}$ ($\delta^{27}Al = 111.2$ ppm; $\nu_{1/2} = 121$ Hz) and $^{31}P\{^1H\}$ NMR spectra ($\delta^{31}P = -7.5$ ppm; $\nu_{1/2} = 25$ Hz), along with a single resonance in the $^{119}Sn\{^1H\}$ NMR spectrum ($\delta^{119}Sn = -2172$ ppm), suggesting that the dimeric structure is not maintained in solution but that both phosphorus atoms are equivalent, possibly owing to a fast coordination isomerism. The reaction of stannocene **3 b** (**dippSn**) with 2 equivalents of aluminium(III) chlo-

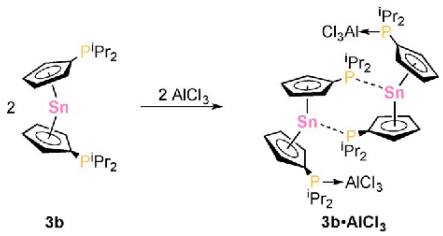

Scheme 8. Reaction of **3 b** with 1 equivalent of $AlCl_3$.

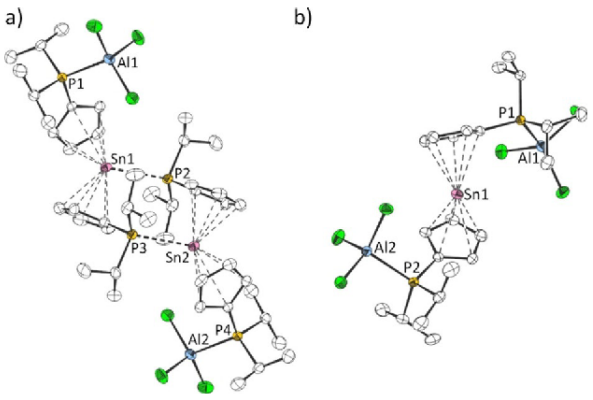

Figure 11. Molecular structures of (a) **3 b·$AlCl_3$** dimer and (b) **3 b·$(AlCl_3)_2$** in the crystal (displacement ellipsoids at the 50% probability level; H atoms omitted). Selected bond lengths [ppm] and angles [°]: **3 b·$AlCl_3$**: Sn1–P2/Sn2–P3 298.78(2), P1–Al1/P4–Al2 240.41(1), Cp^{cent}–Sn1/Cp^{cent}–Sn2 254.00(1)/255.93(1); Cp^{cent}-Sn1-Cp^{cent}/Cp^{cent}-Sn2-Cp^{cent} 130.684(2); **3 b·$(AlCl_3)_2$**: P1–Al1 242.47(1), P2–Al2 240.69(0), Cp^{cent}–Sn1 242.09(0)/242.45(0); Cp^{cent}-Sn1-Cp^{cent} 145.535(1).

 © 2021 The Authors. Chemistry - A European Journal published by Wiley-VCH GmbH

Chemistry–A European Journal | Full Paper doi.org/10.1002/chem.202005198 | Chemistry Europe European Chemical Societies Publishing

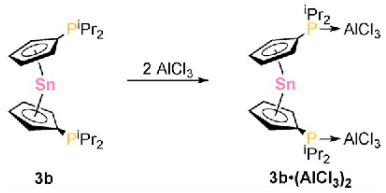

Scheme 9. Reaction of **3 b** with 2 equivalents of $AlCl_3$.

ride yields **3 b·(AlCl$_3$)$_2$**, where both phosphorus atoms are bound to an $AlCl_3$ moiety (Scheme 9, Figure 11 b).

A solution of **3 b·(AlCl$_3$)$_2$** in C_6D_6, exhibits one broad signal in $^{31}P\{^1H\}$ NMR ($\delta^{31}P = -12.2$ ppm; $\nu_{1/2} = 283$ Hz) and $^{27}Al\{^1H\}$ NMR spectrum ($\delta^{27}Al = 110.9$ ppm; $\nu_{1/2} = 189$ Hz), along with only one signal in the $^{119}Sn\{^1H\}$ NMR spectrum ($\delta^{119}Sn = -2178$ ppm). The Al–P bonds in **3 b·AlCl$_3$** and **3 b·(AlCl$_3$)$_2$** are very similar (**3 b·AlCl$_3$**: 240.41(1) pm; **3 b·(AlCl$_3$)$_2$**: 240.69(0) pm and 242.47(1) pm) and are in line with $AlCl_3$·PMe_3[34] (239.2(2) pm). In **3 b·NHC**, the Lewis-acidic character of the tin atom of **3 b** (**dippSn**) is indicated, whereas in **3 b·(AlCl$_3$)$_2$** the Lewis-basicity of the phosphorus atoms is indicated, and especially in **3 b·AlCl$_3$** the Lewis-basic and acidic character are highlighted, displaying the Lewis-amphoterism of **3 b** (**dippSn**).

Following these results, we investigated the reactivity of germanocene **2** (**dpp$^{\#}$Ge**) and stannocene **3 b** (**dippSn**) towards different transition-metal fragments. As tetrelocenes in general usually exhibit flexible bent structures with free rotation around the E–Cp bonds owing to a certain degree of ionic character, diphosphanyltetrelocenes have highly variable bite angles, unlike many transition-metal analogs. Therefore, they should be adaptable to different metal fragments. In this regard, the 14-electron tetracarbonyltungsten(0) fragment proved to be a suitable candidate for a stable stannocene complex. When stannocene **3 b** (**dippSn**) was reacted with $(COD)W(CO)_4$, the corresponding complex **3 b·W(CO)$_4$** was obtained (Scheme 10).

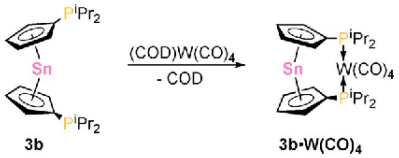

Scheme 10. Reaction of **3 b** with $(COD)W(CO)_4$.

The ^{31}P NMR chemical shift of **3 b·W(CO)$_4$** is observed at 13.4 ppm with ^{183}W satellites with a coupling constant of $^1J_{PW} = 229$ Hz, similar to 1,4-$(Ph_2P)_2(C_4H_8)$·$W(CO)_4$[35b] ($^1J_{PW} = 228.5$ Hz). Remarkably, as a solid, **3 b·W(CO)$_4$**, proved to be air stable for at least 2 h, exemplified by its 18-electron configuration. In the solid state (Figure 12), the tungsten atom reveals a distorted octahedral coordination geometry, with the two phosphorus atoms in *cis*-positions in the equatorial plane, and consequently two CO ligands in *cis*-positions in the equatorial plane and two in the axial positions. The P–W bond lengths of 258.78(20) pm and 259.21(21) pm (Table 3) are similar to

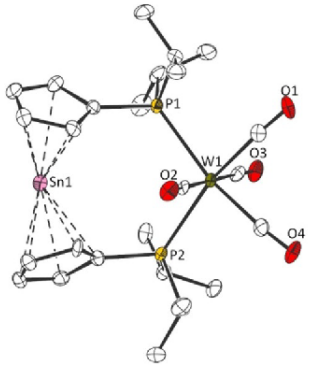

Figure 12. Molecular structure of **3 b·W(CO)$_4$** in the crystal (displacement ellipsoids at the 50% probability level; H atoms omitted). Selected bond lengths [ppm] and angles [°]: P1–W1 259.21(21), P2–W1 258.78(20), Cp^{cent}–Sn1 238.89(6)/241.09(6); Cp^{cent}-Sn1-Cp^{cent} 139.308(26), P1-W1-P2 107.498(65).

Table 3. Selected bond lengths, angles, ^{31}P and ^{119}Sn NMR shifts of complexes **2·PtMe$_2$**, **3 b·NHC**, **3 b·AlCl$_3$**, **3 b·(AlCl$_3$)$_2$**, **3 b·PtMe$_2$**, and **3 b·W(CO)$_4$**.

Compound	E–Cp[a] [pm]	Cp-E-Cp[a] [°]	P-M-P [°]	δ ^{31}P[b] [ppm]	δ ^{119}Sn[c] [ppm]
2·PtMe$_2$	219.77(1) 220.17(1)	162.993(2)	107.338(2)	19.6 ($^1J_{PPt} = 2011$ Hz)	–
3 b·NHC	259.31(1) 264.86(1)	134.767(1)	–	−4.7	–
3 b·AlCl$_3$	254.00(1) 255.93(1)	130.684(2)	–	−7.5	−2172
3 b·(AlCl$_3$)$_2$	242.09(0) 242.45(0)	145.535(1)	–	−12.2	−2178
3 b·PtMe$_2$	237.30(2) 243.11(2)	149.810(4)	105.935(4)	22.0 ($^1J_{PPt} = 1843$ Hz)	−2170
3 b·W(CO)$_4$	238.89(6) 241.09(6)	139.308(26)	107.498(65)	13.4 ($^1J_{PW} = 229$ Hz)	−2176

[a] Corresponding to $Cp^{centroid}$. [b] C_6D_6, 162 MHz, 298 K. [c] C_6D_6, 149 MHz, 298 K.

dppFe·W(CO)$_4$[36] (253.32(16) pm and 256.27(17) pm). Interestingly, the P-W-P bite angle in **3 b·W(CO)$_4$** is 107.5°, which is significantly larger than what is found in comparable compounds[35a,b,36] (**dppFe·W(CO)$_4$**: 95.2°; [*o*-(iPr$_2$P)$_2$(C_6H_4)]·$W(CO)_4$: 79.8° and 80.1°; 1,4-$(Ph_2P)_2(C_4H_8)$·$W(CO)_4$: 91.7°), thus a surprisingly large bite angle and strong deviation from an ideal 90° angle.

As shown before, magnesocene **1 b** (**dippMg**) could be utilized as a ligand for dimethylplatinum(II). To investigate analogous complexes with group 14 metallocene ligands, germanocene **2** (**dpp$^{\#}$Ge**) and stannocene **3 b** (**dippSn**) were reacted with $(COD)PtMe_2$ to give the corresponding complexes **2·PtMe$_2$** and **3 b·PtMe$_2$** (Scheme 11).

Chemical shifts in the $^{31}P\{^1H\}$ NMR spectra of 19.6 ppm (**2·PtMe$_2$**) and 22.0 ppm (**3 b·PtMe$_2$**) with coupling constants of $^1J_{PPt} = 2011$ Hz (**2·PtMe$_2$**) and $^1J_{PPt} = 1843$ Hz (**3 b·PtMe$_2$**; Table 3)

 © 2021 The Authors. Chemistry - A European Journal published by Wiley-VCH GmbH

Chemistry–A European Journal | Full Paper doi.org/10.1002/chem.202005198 | Chemistry Europe European Chemical Societies Publishing

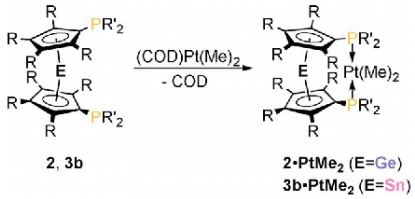

Scheme 11. Reaction of **2** and **3 b** with $(COD)Pt(Me)_2$.

are similar to magnesium complex **1 c·PtMe$_2$** and **dppFe·PtMe$_2$** (see above). The ^{119}Sn NMR chemical shift of **3 b·PtMe$_2$** (δ^{119}Sn = −2170 ppm) is upfield shifted by $\Delta\delta^{119}$Sn = 36 ppm compared with free stannocene **3 b** (**dippSn**).

In the solid-state structures of **2·PtMe$_2$** and **3 b·PtMe$_2$**, the platinum atom shows a slightly distorted square-planar coordination geometry (Figure 13), with a P–Pt bond length similar to **dppFe·PtMe$_2$**[29b] (**2·PtMe$_2$**: 229.40(1) pm and 229.46(1) pm; **3 b·PtMe$_2$**: 232.34(2) pm and 232.80(2) pm; **dppFe·PtMe$_2$**: 229.10(19) pm and 229.48(23) pm), and large P-Pt-P bite angles of 107.3° (**2·PtMe$_2$**) and 105.9° (**3 b·PtMe$_2$**), which are much larger than in the iron analog **dppFe·PtMe$_2$**[29b] (100.8°) and similar to what was observed in tungsten complex **3 b·W(CO)$_4$**. It is worth mentioning that large bite angles of this sort are often discussed with regards to high catalytic activity, for instance, in hydroformylation reactions involving rhodium complexes with bidentate bis(phosphanyl) ligands.[2b,c]

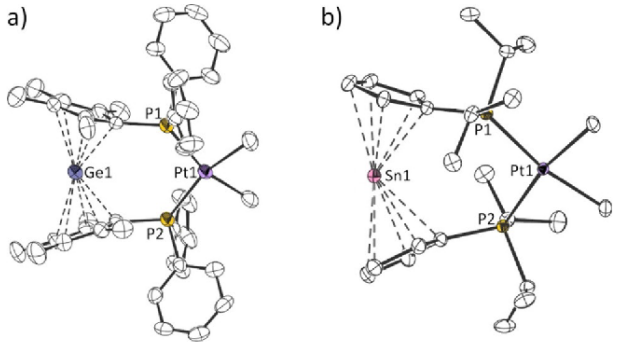

Figure 13. Molecular structures of (a) **2·PtMe$_2$** and (b) **3 b·PtMe$_2$** in the crystal (displacement ellipsoids at the 50% probability level; H atoms omitted). Selected bond lengths [ppm] and angles [°]: **2·PtMe$_2$**: P1–Pt1 229.40(1), P2–Pt1 229.46(1), Cp^{cent}–Ge1 219.77(1)/220.17(1); Cp^{cent}-Ge1-Cp^{cent} 162.993(2), P1-Pt1-P2 107.338(2); **3 b·PtMe$_2$**: P1–Pt1 232.80(2), P2–Pt1 232.34(2), Cp^{cent}–Sn1 237.30(2)/243.11(2); Cp^{cent}-Sn1-Cp^{cent} 149.810(4), P1-Pt1-P2 105.935(4).

A stibonocene and stibonocenium cation

Only a few examples of π-bonded cyclopentadienyl compounds of antimony are known, most of which possess bulky Cp ligands such as $((t\mathrm{Bu})_3C_5H_2)^-$ and $(Me_5C_5)^-$.[37,38] Furthermore, P-functionalized metallocenes of group 15 elements are completely unknown so far. As magnesocenes **1 a–c** have proven to be powerful Cp-transfer reagents in the synthesis of ferrocenes and tetrelocenes, we attempted the synthesis of chlorostibonocene **5 a** (**dipp$^{\#}$SbCl**) starting from magnesocene **1 a** (**dipp$^{\#}$Mg**). Indeed, when magnesocene **1 a** (**dipp$^{\#}$Mg**) is

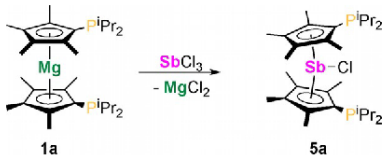

Scheme 12. Reaction of **1 a** with antimony(III) chloride.

treated with antimony(III) chloride in toluene at 198 K, the corresponding diphosphanylchlorostibonocene **5 a** (**dipp$^{\#}$SbCl**) can be obtained (Scheme 12).

Chlorostibonocene **5 a** (**dipp$^{\#}$SbCl**) represents the first example of a diphosphanylmetallocene-type compound based on a group 15 element. To probe the possibility of preparing a highly Lewis-amphiphilic stibonocenium cation, we reacted equimolar amounts of aluminium(III) chloride and chlorostibonocene **5 a** (**dipp$^{\#}$SbCl**) in a toluene/*ortho*-difluorobenzene mixture, and obtained the stibonocenium aluminate salt, **5 b[AlCl$_4$]** ([**dipp$^{\#}$Sb**][**AlCl$_4$**]) (Scheme 13).

In the solid state (Figure 14), chlorostibonocene **5 a** (**dipp$^{\#}$SbCl**) and stibonocenium cation **5 b** (**dipp$^{\#}$Sb$^+$**) both exhibit bent structures with two π-complexed Cp ligands in distorted η^5-coordination mode, with a tendency towards η^3. This is evident from the different Sb–C^{Cp} bond lengths (**5 a**: 259.11(22) pm to 277.68(21) pm; **5 b**: 243.98(17) pm to 275.45(15) pm), although the C^{Cp}–C^{Cp} bond lengths are relatively uniform (**5 a**: 140.08(30) pm to 143.67(29) pm; **5 b**: 141.34(21) pm to 145.25(22) pm), indicating a high degree of π-conjugation. The Cp^{cent}-Sb-Cp^{cent} bending angle is 140.0° in

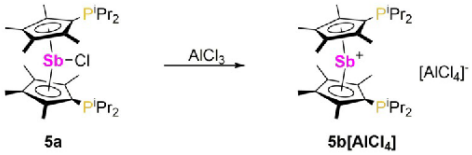

Scheme 13. Reaction of **5 a** with aluminium(III) chloride.

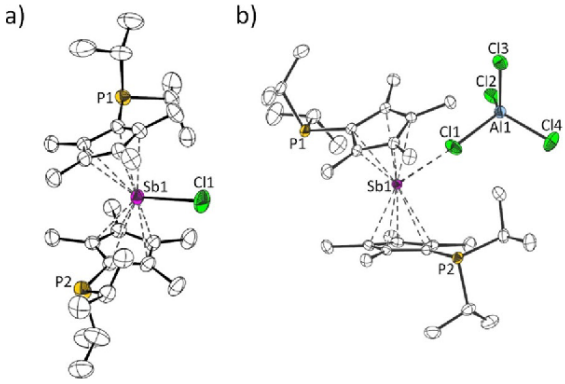

Figure 14. Molecular structures of (a) **5 a** and (b) **5 b[AlCl$_4$]** in the crystal (displacement ellipsoids at the 50% probability level; H atoms omitted). Selected bond lengths [ppm] and angles [°]: **5 a**: Sb1–Cl1 257.71(9), Cp^{cent}–Sb1 238.34(3)/239.16(3); Cp^{cent}-Sb1-Cp^{cent} 139.946(11), **5 b[AlCl$_4$]**: Sb1–Cl1 349.44(5), Cp^{cent}–Sb1 229.63(2)/230.03(3); Cp^{cent}-Sb1-Cp^{cent} 162.346(13).

 © 2021 The Authors. Chemistry - A European Journal published by Wiley-VCH GmbH

Chemistry–A European Journal | Full Paper doi.org/10.1002/chem.202005198 | Chemistry Europe European Chemical Societies Publishing

5a (**dipp#SbCl**) and 162.4° in **5b** (**dipp#Sb+**). Similar structural features are found in Cp^*_2SbCl and $Cp^*_2Sb^+$,[37e] and in the tin analog **3a** (**dipp#Sn**). Interestingly, in contrast to $[Cp^*_2Sb][AlCl_4]$[37e] and $[Me_4Si_2[2](C_5Me_4)_2Sb][AlCl_4]$,[37f] which both exhibit two cation–anion Sb···Cl contacts, **5b[AlCl4]** (**[dipp#Sb][AlCl4]**) reveals only one cation–anion Sb···Cl contact, measuring 349.44(5) pm, which is shorter than in the aforementioned salts[37e,f] (374.40(23) pm to 375.99(21) pm), but significantly longer than the Sb–Cl bond in chlorostibonocene **5a** (**dipp#SbCl**) (257.71(9) pm).

Overall, phosphanyl-functionalized metallocenium cations of group 15 elements represent a new and fascinating class of Lewis-amphiphilic compounds, which will be interesting for small molecule binding as well as ligands for transition-metal fragments in the future.

Conclusion

Herein, we describe a series of new phosphanyl-functionalized metallocenes based on main-group elements. Magnesocenes **1a–c** (**dipp#Mg**, **dippMg**, **dpp#Mg**) are Lewis-amphiphilic compounds and can be used in small molecule activation, as ligands for transition-metal fragments and as Cp-transfer reagents in the preparation of ferrocenes and group 14 and 15 metallocenes. The first results of our reactivity studies include carbon disulfide complex **1b·$(CS_2)_2$**, isocyanate complex **1b·PhNCO**, and platinum complex **1b·$PtMe_2$**. By transmetalation with the corresponding group 14 dichlorides and antimony trichloride, we were able to synthesize a corresponding germanocene **2** (**dpp#Ge**), a series of stannocenes, **3a–d** (**dipp#Sn**, **dippSn**, **dpp#Sn**, **dppSn**), plumbocene **4** (**dpp#Pb**) and the first examples of phosphanyl-functionalized group 15 metallocenes, in the form of chlorostibonocene **5a** (**dipp#SbCl**) and stibonocenium cation **5b** (**dipp#Sb+**). The coordination chemistry of germanocene **2** (**dpp#Ge**) and stannocene **3b** (**dippSn**) was examined and a series of new heterobimetallic complexes with tungsten, platinum, and aluminium fragments could be obtained. In addition, the Lewis-acidity of the tin atom in stannocene **3b** (**dippSn**) is highlighted by the isolation of carbene complex **3b·NHC**.

This work lays the foundation for a new class of main-group metallocene-based bis(phosphanyl) ligands, which possess great potential for future applications as ligands and in different bond-activation processes.

Acknowledgments

We thank Prof. Dr. Guido Kickelbick and Prof. Dr. David Scheschkewitz for their continuous support. Funding by the Deutsche Forschungsgemeinschaft (Emmy Noether Program, SCHA1915/3-1) and the Fonds der Chemischen Industrie is gratefully acknowledged. Dr. Nils Steinbrück is thanked for his help with IR measurements. Susanne Harling is thanked for elemental analysis. Open access funding enabled and organized by Projekt DEAL.

Conflict of interest

The authors declare no conflict of interest.

Keywords: antimony · group 14 · heterobimetallic complexes · magnesium · metallocenes

[1] "Phosphines and related P–C-bonded compounds": D. W. Allen in *Organophosphorus Chemistry*, Royal Society of Chemistry, Cambridge, **2011**, pp. 1–51.

[2] a) A. Pascariu, S. Iliescu, A. Popa, G. Ilia, *J. Organomet. Chem.* **2009**, *694*, 3982–4000; b) P. C. J. Kamer, P. W. N. M. van Leeuwen, J. N. H. Reek, *Acc. Chem. Res.* **2001**, *34*, 895–904; c) Z. Freixa, P. W. N. M. van Leeuwen, *Dalton Trans.* **2003**, 1890–1901.

[3] a) J. H. L. Ong, C. Nataro, J. A. Golen, A. L. Rheingold, *Organometallics* **2003**, *22*, 5027–5032; b) S. L. Martinak, L. A. Sites, S. J. Kolb, K. M. Bocage, W. R. McNamara, A. L. Rheingold, J. A. Golen, C. Nataro, *J. Organomet. Chem.* **2006**, *691*, 3627–3632; c) M. R. Ringenberg, *Chem. Eur. J.* **2019**, *25*, 2396–2406; d) S. W. Chien, T. S. A. Hor in *Ferrocenes, Vol. 2* (Ed.: P. Stepnicka), Wiley, Chichester, **2008**, pp. 33–116; e) T. J. Colacot, S. Parisel in *Ferrocenes, Vol. 3* (Ed.: P. Stepnicka), Wiley, Chichester, **2008**, pp. 117–140; f) G. Marr, T. Hunt, *J. Chem. Soc. C* **1969**, 1070–1072; g) J. J. Bishop, A. Davison, M. L. Katcher, D. W. Lichtenberg, R. E. Merrill, J. C. Smart, *J. Organomet. Chem.* **1971**, *27*, 241–249.

[4] a) R. M. Bellabarba, G. P. Clancy, P. T. Gomes, A. M. Martins, L. H. Rees, M. L. H. Green, *J. Organomet. Chem.* **2001**, *640*, 93–112; b) M. Moriya, R. Fröhlich, G. Kehr, G. Erker, S. Grimme, *Chem. Asian J.* **2008**, *3*, 753–758; c) C. Leblanc, C. Moise, A. Maisonnat, R. Poilblanc, C. Charrier, F. Mathey, *J. Organomet. Chem.* **1982**, *231*, C43–C48; d) B. L. Booth, K. G. Smith, *J. Organomet. Chem.* **1981**, *220*, 229–237; e) W. Tikkanen, J. W. Ziller, *Organometallics* **1991**, *10*, 2266–2273; f) A. W. Rudie, D. W. Lichtenberg, M. L. Katcher, A. Davison, *Inorg. Chem.* **1978**, *17*, 2859–2863; g) D. L. DuBois, C. W. Eigenbrot, A. Miedaner, J. C. Smart, R. C. Haltiwanger, *Organometallics* **1986**, *5*, 1405–1411; h) W. Tikkanen, Y. Fujita, J. L. Petersen, *Organometallics* **1986**, *5*, 888–894; i) C. Cornelissen, G. Erker, G. Kehr, R. Fröhlich, *Organometallics* **2005**, *24*, 214–225; j) J. Szymoniak, M. M. Kubicki, J. Besançon, C. Moise, *Inorg. Chim. Acta* **1991**, *180*, 153–160; k) S. Li, B. Wei, P. M. N. Low, H. K. Lee, T. S. A. Hor, F. Xue, T. C. W. Mak, *J. Chem. Soc. Dalton Trans.* **1997**, 1289–1294; l) O. V. Gusev, A. M. Kalsin, P. V. Petrovskii, K. A. Lyssenko, Y. F. Oprunenko, C. Bianchini, A. Meli, W. Oberhauser, *Organometallics* **2003**, *22*, 913–915; m) T. Miyazaki, Y. Tanabe, M. Yuki, Y. Miyake, Y. Nishibayashi, *Organometallics* **2011**, *30*, 2394–2404; n) A. Antiñolo, T. Expósito, I. del Hierro, D. Lucas, Y. Mugnier, I. Orive, A. Otero, S. Prashar, *J. Organomet. Chem.* **2002**, *655*, 63–69.

[5] a) G. B. Deacon, A. Dietrich, C. M. Forsyth, H. Schumann, *Angew. Chem. Int. Ed. Engl.* **1989**, *28*, 1370–1371; *Angew. Chem.* **1989**, *101*, 1374–1375; b) H. Schumann, J. A. Meese-Marktscheffel, B. Gorella, F. H. Görlitz, *J. Organomet. Chem.* **1992**, *428*, C27–C32; c) R. Broussier, G. Delmas, P. Perron, B. Gautheron, J. L. Petersen, *J. Organomet. Chem.* **1996**, *511*, 185–192; d) G. Lin, W.-T. Wong, *J. Organomet. Chem.* **1996**, *523*, 93–98.

[6] a) A. H. Cowley, J. G. Lasch, N. C. Norman, C. A. Stewart, T. C. Wright, *Organometallics* **1983**, *2*, 1691–1692; b) D. P. Daniels, G. B. Deacon, D. Harakat, F. Jaroschik, P. C. Junk, *Dalton Trans.* **2012**, *41*, 267–277.

[7] a) K. M. Gramigna, J. V. Oria, C. L. Mandell, M. A. Tiedemann, W. G. Dougherty, N. A. Piro, W. S. Kassel, B. C. Chan, P. L. Diaconescu, C. Nataro, *Organometallics* **2013**, *32*, 5966–5979; b) E. P. Warnick, R. J. Dupuis, N. A. Piro, W. Scott Kassel, C. Nataro, *Polyhedron* **2016**, *114*, 156–164.

[8] a) L. B. Kool, M. Ogasa, M. D. Rausch, R. D. Rogers, *Organometallics* **1989**, *8*, 1785–1790; b) M. Ogasa, M. D. Rausch, R. D. Rogers, *J. Organomet. Chem.* **1991**, *403*, 279–291; c) S. K. Mohapatra, S. Büschel, C. Daniliuc, P. G. Jones, M. Tamm, *J. Am. Chem. Soc.* **2009**, *131*, 17014–17023; d) H. Braunschweig, M. Drisch, M. Friedrich, T. Kupfer, K. Radacki, *Organometallics* **2011**, *30*, 5202–5207; e) T. R. Eger, I. Munstein, A. Steiner, Y. Sun, G. Niedner-Schatteburg, W. R. Thiel, *J. Organomet. Chem.* **2016**, *810*, 51–56.

[9] G. Trouve, R. Broussier, B. Gautheron, M. M. Kubicki, *Acta Crystallogr. Sect. C* **1991**, *47*, 1966–1967.

 © 2021 The Authors. Chemistry - A European Journal published by Wiley-VCH GmbH

Chemistry–A European Journal | Full Paper doi.org/10.1002/chem.202005198 | Chemistry Europe European Chemical Societies Publishing

[10] G. K. Anderson, N. P. Rath, *J. Organomet. Chem.* **1991**, *414*, 129 – 135.

[11] a) D. Stalke, *Angew. Chem. Int. Ed. Engl.* **1994**, *33*, 2168 – 2171; *Angew. Chem.* **1994**, *106*, 2256 – 2259; b) S. Harder, *Coord. Chem. Rev.* **1998**, *176*, 17 – 66; c) A. Xia, J. E. Knox, M. J. Heeg, H. B. Schlegel, C. H. Winter, *Organometallics* **2003**, *22*, 4060 – 4069.

[12] a) M. A. Beswick, N. L. Cromhout, C. N. Harmer, P. R. Raithby, C. A. Russell, J. S. B. Smith, A. Steiner, D. S. Wright, *Chem. Commun.* **1996**, 1977 – 1978; b) D. R. Armstrong, M. A. Beswick, N. L. Cromhout, C. N. Harmer, D. Moncrieff, C. A. Russell, P. R. Raithby, A. Steiner, A. E. H. Wheatley, D. S. Wright, *Organometallics* **1998**, *17*, 3176 – 3181; c) M. A. Beswick, J. S. Palmer, D. S. Wright, *Chem. Soc. Rev.* **1998**, *27*, 225 – 232; d) C. Müller, A. Stahlich, L. Wirtz, C. Gretsch, V. Huch, A. Schäfer, *Inorg. Chem.* **2018**, *57*, 8050 – 8053; e) L. Wirtz, M. Jourdain, V. Huch, M. Zimmer, A. Schäfer, *ACS Omega* **2019**, *4*, 18355 – 18360; f) S. Danés, C. Müller, L. Wirtz, V. Huch, T. Block, R. Pöttgen, A. Schäfer, D. M. Andrada, *Organometallics* **2020**, *39*, 516 – 527.

[13] G. Bouhadir, D. Bourissou, *Chem. Soc. Rev.* **2016**, *45*, 1065 – 1079.

[14] a) M. Asay, C. Jones, M. Driess, *Chem. Rev.* **2011**, *111*, 354 – 396; b) J. Baumgartner, C. Marschner, *Rev. Inorg. Chem.* **2014**, *34*, 119 – 152; c) L. Álvarez-Rodríguez, J. A. Cabeza, P. García-Álvarez, D. Polo, *Coord. Chem. Rev.* **2015**, *300*, 1 – 28; d) V. Nesterov, D. Reiter, P. Bag, P. Frisch, R. Holzner, A. Porzelt, S. Inoue, *Chem. Rev.* **2018**, *118*, 9678 – 9842; e) A. Doddi, M. Peters, M. Tamm, *Chem. Rev.* **2019**, *119*, 6994 – 7112; f) Y. Mizuhata, T. Sasamori, N. Tokitoh, *Chem. Rev.* **2009**, *109*, 3479 – 3511 [Corrigendum: Y. Mizuhata, T. Sasamori, N. Tokitoh, *Chem. Rev.* **2010**, *110*, 3850]; g) E. Rivard, *Dalton Trans.* **2014**, *43*, 8577 – 8586.

[15] F. Mathey, J.-P. Lampin, *Tetrahedron* **1975**, *31*, 2685 – 2690.

[16] T. Sixt, M. Sieger, M. J. Krafft, D. Bubrin, J. Fiedler, W. Kaim, *Organometallics* **2010**, *29*, 5511 – 5516.

[17] a) R. Benn, H. Lehmkuhl, K. Mehler, A. Rufińska, *Angew. Chem. Int. Ed. Engl.* **1984**, *23*, 534 – 535; *Angew. Chem.* **1984**, *96*, 521 – 523; b) R. Benn, A. Rufińska, *Angew. Chem. Int. Ed. Engl.* **1986**, *25*, 861 – 881; *Angew. Chem.* **1986**, *98*, 851 – 871; c) H. Lehmkuhl, K. Mehler, R. Benn, A. Rufińska, C. Krüger, *Chem. Ber.* **1986**, *119*, 1054 – 1069.

[18] A. Pape, M. Lutz, G. Müller, *Angew. Chem. Int. Ed. Engl.* **1994**, *33*, 2281 – 2284; *Angew. Chem.* **1994**, *106*, 2375 – 2377.

[19] A. Koch, S. Krieck, H. Görls, M. Westerhausen, *Inorganics* **2016**, *4*, 39.

[20] J. Langer, I. Kosygin, R. Puchta, J. Pahl, S. Harder, *Chem. Eur. J.* **2016**, *22*, 17425 – 17435.

[21] A. Jaenschke, J. Paap, U. Behrens, *Organometallics* **2003**, *22*, 1167 – 1169.

[22] a) P. J. Shapiro, S.-J. Lee, P. Perrotin, T. Cantrell, A. Blumenfeld, B. Twamley, *Polyhedron* **2005**, *24*, 1366 – 1381; b) P. Perrotin, P. J. Shapiro, M. Williams, B. Twamley, *Organometallics* **2007**, *26*, 1823 – 1826; c) P. Perrotin, B. Twamley, P. J. Shapiro, *Acta Crystallogr. Sect. E* **2007**, *63*, m1277 – m1278.

[23] All DFT calculations were performed by using the Gaussian 09 Revision D.01 software suite. See the Supporting Information for further details and references.

[24] a) K. Samigullin, I. Georg, M. Bolte, H.-W. Lerner, M. Wagner, *Chem. Eur. J.* **2016**, *22*, 3478 – 3484; b) I. G. Albuerne, M. A. Alvarez, M. E. García, D. García-Vivó, M. A. Ruiz, *Dalton Trans.* **2017**, *46*, 3510 – 3525; c) P. Holtkamp, F. Friedrich, E. Stratmann, A. Mix, B. Neumann, H.-G. Stammler, N. W. Mitzel, *Angew. Chem. Int. Ed.* **2019**, *58*, 5114 – 5118; *Angew. Chem.* **2019**, *131*, 5168 – 5172; d) R. Lalrempuia, A. Stasch, C. Jones, *Chem. Sci.* **2013**, *4*, 4383 – 4388; e) R. Grubba, W. Wojnowski, K. Baranowska, E. Baum, J. Pikies, *Acta Crystallogr. Sect. E* **2006**, *62*, m2080 – m2081.

[25] See the Supporting Information for further details.

[26] L. E. Lemmerz, A. Wong, G. Ménard, T. P. Spaniol, J. Okuda, *Polyhedron* **2020**, *178*, 114331.

[27] a) V. Ritleng, M. J. Chetcuti, *Chem. Rev.* **2007**, *107*, 797 – 858; b) N. Wheatley, P. Kalck, *Chem. Rev.* **1999**, *99*, 3379 – 3420.

[28] H. R. Shahsavari, M. Rashidi, S. M. Nabavizadeh, S. Habibzadeh, F. W. Heinemann, *Eur. J. Inorg. Chem.* **2009**, 3814 – 3820.

[29] a) C. M. Haar, S. P. Nolan, W. J. Marshall, K. G. Moloy, A. Prock, W. P. Giering, *Organometallics* **1999**, *18*, 474 – 479; b) D. C. Smith, C. M. Haar, E. D. Stevens, S. P. Nolan, W. J. Marshall, K. G. Moloy, *Organometallics* **2000**, *19*, 1427 – 1433.

[30] A. P. Shaw, J. R. Norton, D. Buccella, L. A. Sites, S. S. Kleinbach, D. A. Jarem, K. M. Bocage, C. Nataro, *Organometallics* **2009**, *28*, 3804 – 3814.

[31] C. Janiak, H. Schumann, C. Stader, B. Wrackmeyer, J. J. Zuckerman, *Chem. Ber.* **1988**, *121*, 1745 – 1751.

[32] S. Freitag, K. M. Krebs, J. Henning, J. Hirdler, H. Schubert, L. Wesemann, *Organometallics* **2013**, *32*, 6785 – 6791.

[33] H. Arp, J. Baumgartner, C. Marschner, T. Müller, *J. Am. Chem. Soc.* **2011**, *133*, 5632 – 5635.

[34] J. Burt, W. Levason, M. E. Light, G. Reid, *Dalton Trans.* **2014**, *43*, 14600 – 14611.

[35] a) S.-T. Liu, C.-L. Tsao, M.-C. Cheng, S.-M. Peng, *Acta Crystallogr. Sect. C* **1989**, *45*, 1879 – 1881; b) E. Lindner, R. Fawzi, H. A. Mayer, K. Eichele, W. Hiller, *Organometallics* **1992**, *11*, 1033 – 1043.

[36] L.-C. Song, J.-T. Liu, Q.-M. Hu, G.-F. Wang, P. Zanello, M. Fontani, *Organometallics* **2000**, *19*, 5342 – 5351.

[37] a) W. Frank, *J. Organomet. Chem.* **1991**, *406*, 331 – 341; b) Y. Ehleiter, G. Wolmershäuser, H. Sitzmann, R. Boese, *Z. Anorg. Allg. Chem.* **1996**, *622*, 923 – 930; c) H. Sitzmann, Y. Ehleiter, G. Wolmershäuser, A. Ecker, C. Üffing, H. Schnöckel, *J. Organomet. Chem.* **1997**, *527*, 209 – 213; d) M. Schiffer, B. P. Johnson, M. Scheer, *Z. Anorg. Allg. Chem.* **2000**, *626*, 2498 – 2504; e) R. J. Wiacek, J. N. Jones, C. L. Macdonald, A. H. Cowley, *Can. J. Chem.* **2002**, *80*, 1518 – 1523; f) A. S. D. Stahlich, V. Huch, A. Grandjean, K. Rohe, K. I. Leszczyńska, D. Scheschkewitz, A. Schäfer, *Chem. Eur. J.* **2019**, *25*, 173 – 176; g) O. Coughlin, T. Krämer, S. L. Benjamin, *Dalton Trans.* **2020**, *49*, 1726 – 1730.

[38] a) P. Jutzi, N. Burford, *Chem. Rev.* **1999**, *99*, 969 – 990; b) P. H. M. Budzelaar, J. J. Engelberts, J. H. van Lenthe, *Organometallics* **2003**, *22*, 1562 – 1576.

Manuscript received: December 4, 2020
Accepted manuscript online: January 7, 2021
Version of record online: March 8, 2021

 © 2021 The Authors. Chemistry - A European Journal published by Wiley-VCH GmbH

4. Conclusion

In the first part of this thesis, reactions of *N*-heterocyclic carbenes with stannocenes and plumbocene were conducted and the isolated Lewis adducts (Figure 63) were characterized by multinuclear NMR spectroscopy, X-ray crystallographic analysis and elemental analysis.

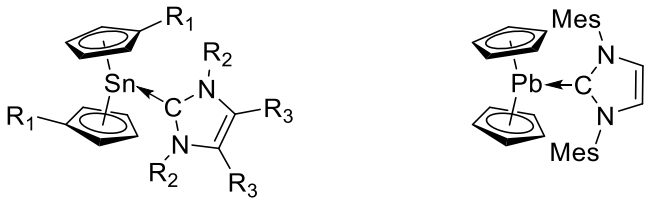

9a·^{i}Pr$_2$Me$_2$NHC: R_1 = H; R_2 = ^{i}Pr; R_3 = Me
9b·^{i}Pr$_2$Me$_2$NHC: R_1 = Me; R_2 = ^{i}Pr; R_3 = Me
9a·MesNHC: R_1 = H; R_2 = Mes; R_3 = H
9b·MesNHC: R_1 = Me; R_2 = Mes; R_3 = H
9b·Me$_4$NHC: R_1 = R_2 = R_3 = Me

10a·MesNHC

Figure 63: Lewis adducts of stannocenes and plumbocene with *N*-heterocyclic carbenes.

Inspection of the Sn-C^{NHC} bond reveals that the complex with the N-methyl substituted NHC (**9b**·Me$_4$NHC) exhibits the shortest Sn-C^{NHC} bond length of all isolated stannocene NHC complexes, which is not surprising in view of the limited steric demand of the NHC. However, it must be mentioned that in general these Sn-C bond lengths are among the longest Sn-C bond lengths in literature. Remarkably, in complex **9b**·MesNHC, the longest Sn-C bond length ever reported could be found. The Sn-Cp^{cent} bond lengths in all carbene complexes are elongated in comparison to uncoordinated stannocenes Cp$_2$Sn (**9a**) and ^{Me}Cp$_2$Sn (**9b**). This observation can be explained by donation of the lone pair of the NHC into the LUMO of stannocene, which represents an antibonding molecular orbital (as outlined in the introduction). Therefore, donation of the lone pair of the NHC into this antibonding molecular orbital weakens the Sn-Cp bonds resulting in an elongation. This weakening of the Sn-Cp bond can also be seen in the decomposition of these stannocene NHC complexes at room temperature over a short period of time. Energy decomposition analysis (EDA) conducted on these carbene complexes revealed that orbital interactions, mainly derived from donation of the lone pair of the NHC into the LUMO of the tetrelocenes, play a major role but that a substantial part of the interaction between NHC and tetrelocenes is also derived from attractive dispersion force interactions. In solution, a dissociative equilibrium between the carbene

complexes, free NHC and free stannocene was found (Scheme 195).

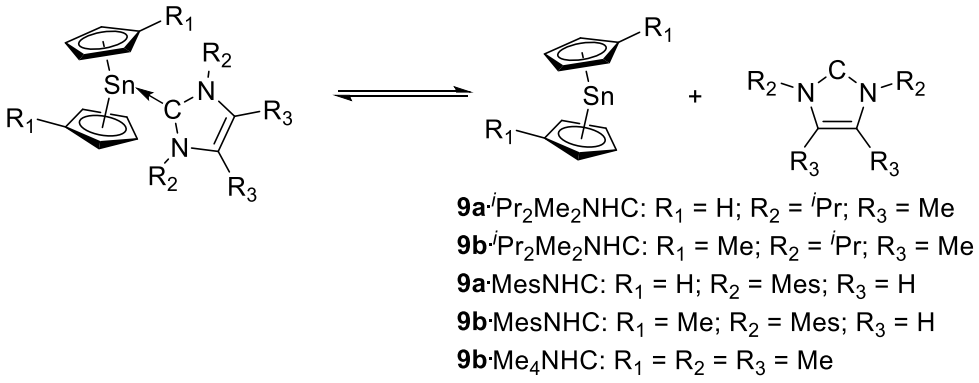

Scheme 195: Equilibrium between carbene complexes and uncoordinated stannocene and NHC.

This is in line with the weak Sn-C^{NHC} and Pb-C^{NHC} interactions as suggested by DFT calculations of the bond dissociation energies (BDE). The results of the first part of this thesis demonstrate that stannocenes and plumbocene exhibit a significant degree of Lewis acidity at the central atom. Noteworthy, the first NHC complex of plumbocene (**10a**·MesNHC) could be obtained which exhibits an unusual face-on coordination of the NHC due to the extremely high s character of the lone pair (>99%) at the lead atom.

Furthermore, halfsandwich cyclopentadienyltin(II)halides were reacted with a cyclic (alkyl)(amino)carbene (cAAC) and the corresponding adducts were isolated and characterized (Figure 64).

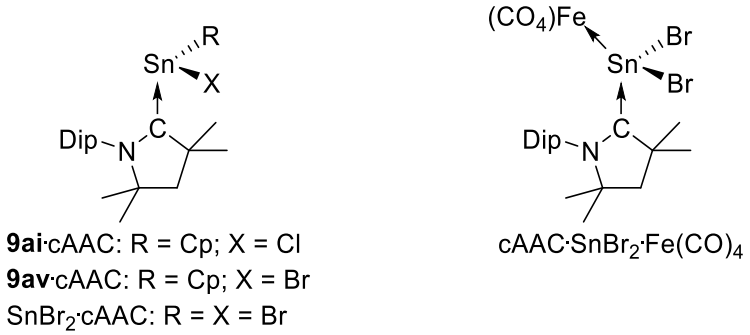

Figure 64: Complexes of tin(II) compounds with cAAC.

In solution, these complexes show a fast equilibrium between different homoleptic and heteroleptic species (Figure 65).

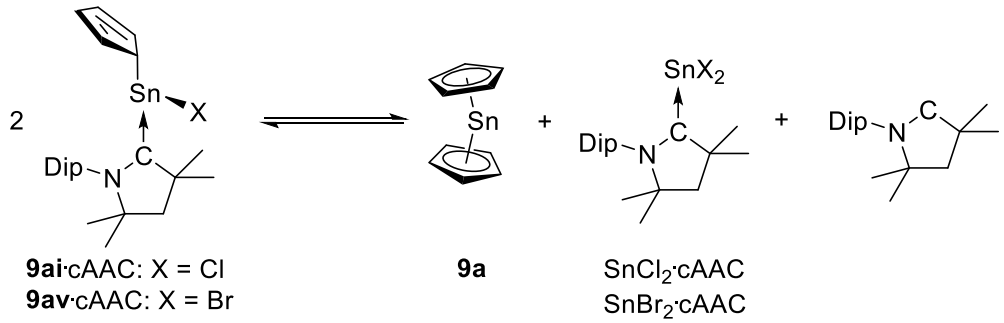

Figure 65: Equilibrium between heteroleptic and homoleptic species as well as free cAAC.

This equilibrium can be monitored by ^{119}Sn NMR in solution, since three signals arise for the different species, while in the ^{119}Sn CP/MAS NMR spectra of **9ai**·cAAC and **9av**·cAAC, only one signal is observed which is in agreement with the one observed for these compounds in solution. Furthermore, the mechanism of this ligand exchange reaction in solution has been investigated by DFT calculations, and energy decomposition analysis (EDA) was performed on these compounds providing evidence for a donor acceptor-type interaction to be present. By reacting $SnBr_2$·cAAC with diironnonacarbonyl, the corresponding transition metal complex cAAC·$SnBr_2$·$Fe(CO)_4$ could be obtained and characterized. This result depicts the suitability of this cAAC supported stannylene as a ligand for transition metals.

In the second part of this thesis, phosphanyl substituted magnesocenes, tetrelocenes, a chlorostibonocene and the corresponding stibonocenium cation were synthesized and structurally characterized (Figure 66).

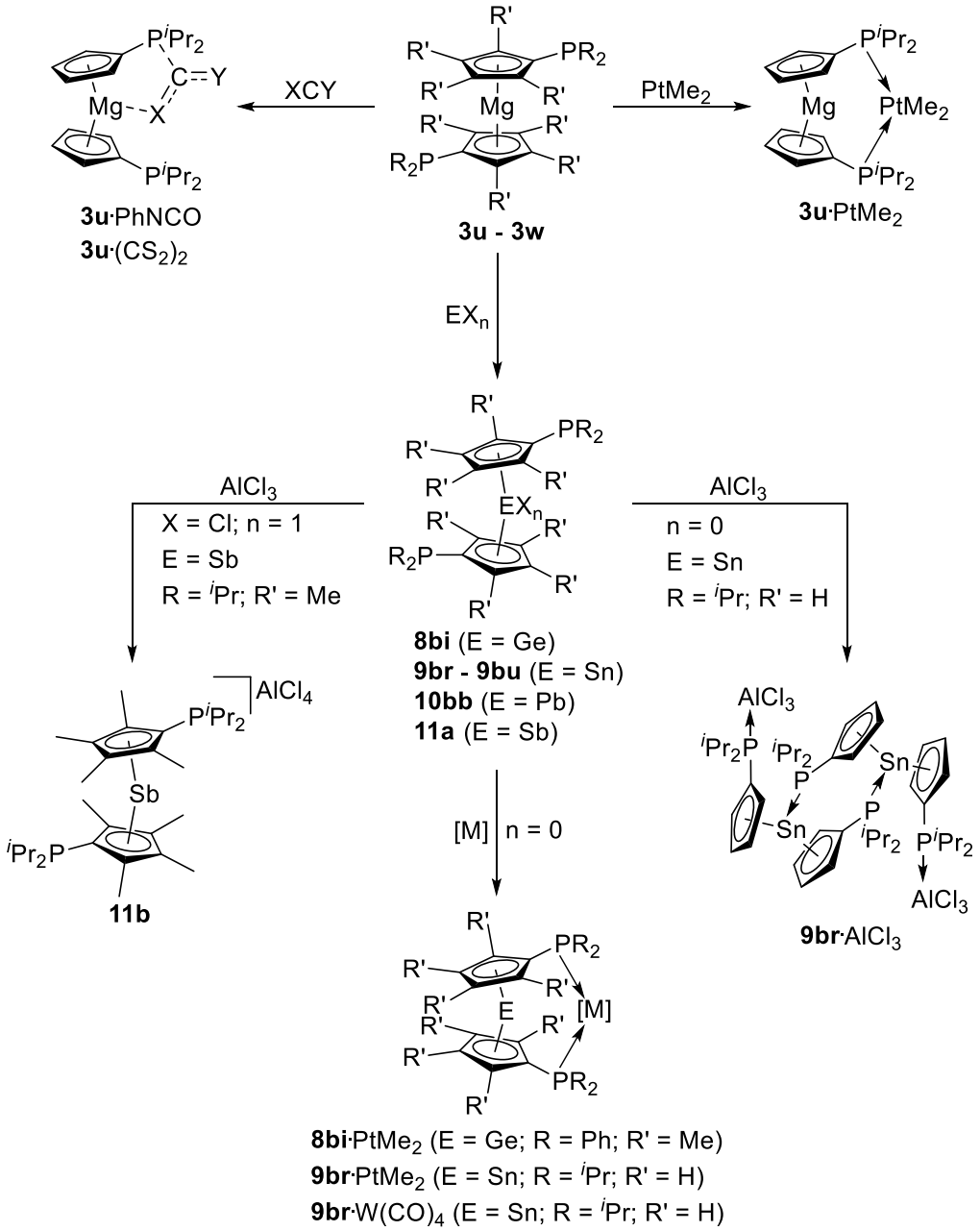

Figure 66: Synthesis of phosphanyl substituted magnesocenes, tetrelocenes and related complexes as well as a chlorostibonocene and related stibonocenium cation.

The magnesocene **3u** exhibits a dimeric structure in the solid state with weak Mg-P bonds representing the first example of a structurally characterized phosphine adduct of a magnesocene. Furthermore, this magnesocene was reacted with carbondisulfide and phenyl isocyanate to form the corresponding adducts **3u**·$(CS_2)_2$ and **3u**·PhNCO which were both structurally characterized and highlight the Lewis amphiphilic character of **3u**. The diphosphanyltetrelocenes were obtained by transmetalation of the corresponding magnesocenes

with group 14 element(II)chlorides. Several examples could be synthesized and characterized revealing monomeric structures of all tetrelocenes in the solid state. An exception is the aluminum(III)chloride adduct of diphosphanylstannocene **9br**·$AlCl_3$, which is dimeric in the solid state and therefore is the first structurally characterized example of a phosphine adduct of a stannocene. Tetrelocenes **8bi** and **9br** were shown to be suitable bidentate ligands for various metal fragments. The complex **9br**·$W(CO)_4$ was found to exhibit a significantly different bite angle P-W-P (107.5°) in the solid state than the related diphosphanylferrocene complex dppFe·$W(CO)_4$ (95.2°) depicting the flexibility of **9br** as ligand. Such large P-M-P bite angles were also found in the solid state structures of **9br**·$PtMe_2$ (107.3°) and **8bi**·$PtMe_2$ (105.9°).

The chlorostibonocene **11a** and the related stibonocenium cation **11b** are the first examples of a phosphanyl substituted group 15 metallocenes and metallocenium cation, respectively.

5. References

[1] S. A. Miller, J. A. Tebboth, J. F. Tremaine, *J. Chem. Soc.* **1952**, 632–635.
[2] T. J. Kealy, P. L. Pauson, *Nature* **1951**, *168*, 1039–1040.
[3] J. D. Dunitz, L. E. Orgel, A. Rich, *Acta Cryst.* **1956**, *9*, 373–375.
[4] G. Wilkinson, M. Rosenblum, M. C. Whiting, R. B. Woodward, *J. Am. Chem. Soc.* **1952**, *74*, 2125–2126.
[5] E. O. Fischer, W. Pfab, *Z. Naturforsch. B* **1952**, *7*, 377–379.
[6] E. O. Fischer, H. P. Hofmann, *Chem. Ber.* **1959**, *92*, 482–486.
[7] G. Wilkinson, F. A. Cotton, *Chem. Ind.-Lond.* **1954**, 307–308.
[8] W. Hafner, E. O. Fischer, *Z. Naturforsch. B* **1954**, *9*, 503–504.
[9] K. Ziegler, H. Froitzheim-Kühlhorn, K. Hafner, *Chem. Ber.* **1956**, *89*, 434–443.
[10] E. O. Fischer, G. Stölzle, *Chem. Ber.* **1961**, *94*, 2187–2193.
[11] H. Grubert, E. O. Fischer, *Z. Naturforsch. B* **1956**, *11*, 423–424.
[12] E. O. Fischer, H. Grubert, *Z. Anorg. Allg. Chem.* **1956**, *286*, 237–242.
[13] J. V. Scibelli, M. D. Curtis, *J. Am. Chem. Soc.* **1973**, *95*, 924–925.
[14] L. D. Dave, D. F. Evans, G. Wilkinson, *J. Chem. Soc.* **1959**, 3684–3688.
[15] C. Panattoni, G. Bombieri, U. Croatto, *Acta Cryst.* **1966**, *21*, 823–826.
[16] J. L. Atwood, W. E. Hunter, A. H. Cowley, R. A. Jones, C. A. Stewart, *J. Chem. Soc., Chem. Commun.* **1981**, 925–927.
[17] P. Štěpnička, *Ferrocenes - Ligands, Materials and Biomolecules*, John Wiley & Sons, Ltd, **2008**.
[18] A. Togni, R. L. Halterman, *Metallocenes: Synthesis Reactivity Applications*, John Wiley & Sons, Ltd, **1998**.
[19] C. Elschenbroich, *Organometallchemie*, Vieweg+Teubner Verlag, **2008**.
[20] P. Jutzi, N. Burford, *Chem. Rev.* **1999**, *99*, 969–990.
[21] W. Haider, V. Huch, B. Morgenstern, A. Schäfer, *ChemistryOpen* **2020**, *9*, 1095–1099.
[22] H. P. Fritz, *Chem. Ber.* **1959**, *92*, 780–791.
[23] A. Almenningen, O. Bastiansen, A. Haaland, *J. Chem. Phys.* **1964**, *40*, 3434–3437.
[24] C.-H. Wong, T.-Y. Lee, K.-J. Chao, S. Lee, *Acta Cryst. B* **1972**, *28*, 1662–1665.
[25] A. Almenningen, A. Haaland, J. Lusztyk, *J. Organomet. Chem.* **1979**, *170*, 271–284.
[26] K. W. Nugent, J. K. Beattie, T. W. Hambley, M. R. Snow, *Aust. J. Chem.* **1984**, *37*, 1601–1606.
[27] C. Wong, T. Y. Lee, T. J. Lee, T. W. Chang, C. S. Liu, *Inorg. Nucl. Chem. Letters* **1973**, *9*, 667–673.
[28] R. Blom, A. Haaland, J. Weidlein, *J. Chem. Soc., Chem. Commun.* **1985**, 266–267.
[29] A. Jaenschke, J. Paap, U. Behrens, *Organometallics* **2003**, *22*, 1167–1169.
[30] J. K. Beattie, K. W. Nugent, *Inorg. Chim. Acta* **1992**, *198–200*, 309–318.
[31] S. J. Pratten, M. K. Cooper, M. J. Aroney, *J. Organomet. Chem.* **1990**, *381*, 147–153.
[32] M. del M. Conejo, R. Fernández, E. Gutiérrez-Puebla, Á. Monge, C. Ruiz, E. Carmona, *Angew. Chem. Int. Ed.* **2000**, *39*, 1949–1951.
[33] K. W. Nugent, J. K. Beattie, L. D. Field, *J. Phys. Chem.* **1989**, *93*, 5371–5377.
[34] M. del Mar Conejo, R. Fernández, D. del Río, E. Carmona, A. Monge, C. Ruiz, A. M. Márquez, J. Fernández Sanz, *Chem. Eur. J.* **2003**, *9*, 4452–4461.
[35] I. Hung, C. L. B. Macdonald, R. W. Schurko, *Chem. Eur. J.* **2004**, *10*, 5923–5935.
[36] E. Weiss, E. O. Fischer, *Z. Anorg. Allg. Chem.* **1955**, *278*, 219–224.
[37] W. Bünder, E. Weiss, *J. Organomet. Chem.* **1975**, *92*, 1–6.
[38] A. W. Duff, P. B. Hitchcock, M. F. Lappert, R. G. Taylor, J. A. Segal, *J. Organomet. Chem.* **1985**, *293*, 271–283.
[39] C. P. Morley, P. Jutzi, C. Krueger, J. M. Wallis, *Organometallics* **1987**, *6*, 1084–1090.
[40] J. D. Fisher, P. H. M. Budzelaar, P. J. Shapiro, R. J. Staples, G. P. A. Yap, A. L. Rheingold, *Organometallics* **1997**, *16*, 871–879.
[41] P. L. Holland, R. A. Andersen, R. G. Bergman, *J. Am. Chem. Soc.* **1996**, *118*, 1092–1104.
[42] D. J. Burkey, T. P. Hanusa, J. C. Huffman, *Adv. Mater. Opt. Electron.* **1994**, *4*, 1–8.
[43] K.-H. Thiele, V. Lorenz, *Z. Anorg. Allg. Chem.* **1990**, *591*, 195–198.
[44] M. G. Gardiner, C. L. Raston, C. H. L. Kennard, *Organometallics* **1991**, *10*, 3680–3686.
[45] C. D. Sofield, R. A. Andersen, *J. Organomet. Chem.* **1995**, *501*, 271–276.
[46] P. B. Duval, C. J. Burns, D. L. Clark, D. E. Morris, B. L. Scott, J. D. Thompson, E. L. Werkema, L. Jia, R. A. Andersen, *Angew. Chem. Int. Ed.* **2001**, *40*, 3357–3361.
[47] C. Bollmann, E. Dehmlow, *Z. Naturforsch. B* **1993**, *48*, 457–460.
[48] F. Weber, H. Sitzmann, M. Schultz, C. D. Sofield, R. A. Andersen, *Organometallics* **2002**, *21*, 3139–3146.
[49] H. Schumann, J. Gottfriedsen, M. Glanz, S. Dechert, J. Demtschuk, *J. Organomet. Chem.* **2001**, *617–618*, 588–600.
[50] J. Vollet, E. Baum, H. Schnöckel, *Organometallics* **2003**, *22*, 2525–2527.
[51] F. X. Kohl, P. Jutzi, *Chem. Ber.* **1981**, *114*, 488–494.
[52] D. Feitler, G. M. Whitesides, *Inorg. Chem.* **1976**, *15*, 466–469.

[53] R. A. Andersen, R. Blom, J. M. Boncella, C. J. Burns, H. V. Volden, *Acta Chem. Scand.* **1987**, *41a*, 24–35.
[54] A. Jaenschke, U. Behrens, *Z. Naturforsch. B* **2014**, *69*, 655–664.
[55] P. J. Shapiro, A. Vij, G. P. A. Yap, A. L. Rheingold, *Polyhedron* **1995**, *14*, 203–209.
[56] M. Westerhausen, N. Makropoulos, B. Wieneke, K. Karaghiosoff, H. Nöth, H. Schwenk-Kircher, J. Knizek, T. Seifert, *Eur. J. Inorg. Chem.* **1998**, *1998*, 965–971.
[57] G. B. Deacon, F. Jaroschik, P. C. Junk, R. P. Kelly, *Organometallics* **2015**, *34*, 2369–2377.
[58] Y. Schulte, H. Weinert, C. Wölper, S. Schulz, *Organometallics* **2020**, *39*, 206–216.
[59] H. Schumann, S. Schutte, H.-J. Kroth, D. Lentz, *Angew. Chem. Int. Ed.* **2004**, *43*, 6208–6211.
[60] A. Jaenschke, J. Paap, U. Behrens, *Z. Anorg. Allg. Chem.* **2008**, *634*, 461–469.
[61] R. Zerger, G. Stucky, *J. Organomet. Chem.* **1974**, *80*, 7–17.
[62] R. A. Andersen, J. M. Boncella, C. J. Burns, R. Blom, A. Haaland, H. V. Volden, *J. Organomet. Chem.* **1986**, *312*, C49–C52.
[63] R. A. Williams, T. P. Hanusa, J. C. Huffman, *Organometallics* **1990**, *9*, 1128–1134.
[64] R. Pal, S. Mebs, M. W. Shi, D. Jayatilaka, J. M. Krzeszczakowska, L. A. Malaspina, M. Wiecko, P. Luger, M. Hesse, Y.-S. Chen, J. Beckmann, S. Grabowsky, *Inorg. Chem.* **2018**, *57*, 4906–4920.
[65] L. M. Engelhardt, P. C. Junk, C. L. Raston, A. H. White, *J. Chem. Soc., Chem. Commun.* **1988**, 1500–1501.
[66] M. J. Harvey, K. T. Quisenberry, T. P. Hanusa, V. G. Young, *Eur. J. Inorg. Chem.* **2003**, *2003*, 3383–3390.
[67] R. A. Williams, K. F. Tesh, T. P. Hanusa, *J. Am. Chem. Soc.* **1991**, *113*, 4843–4851.
[68] H. Sitzmann, T. Dezember, M. Ruck, *Angew. Chem. Int. Ed.* **1998**, *37*, 3113–3116.
[69] D. J. Burkey, R. A. Williams, T. P. Hanusa, *Organometallics* **1993**, *12*, 1331–1337.
[70] G. B. Deacon, C. M. Forsyth, F. Jaroschik, P. C. Junk, D. L. Kay, T. Maschmeyer, A. F. Masters, J. Wang, L. D. Field, *Organometallics* **2008**, *27*, 4772–4778.
[71] C. Ruspic, J. R. Moss, M. Schürmann, S. Harder, *Angew. Chem. Int. Ed.* **2008**, *47*, 2121–2126.
[72] H. Li, W.-X. Zhang, Z. Xi, *Chem. Eur. J.* **2013**, *19*, 12859–12866.
[73] D. Astruc, *Eur. J. Inorg. Chem.* **2017**, *2017*, 6–29.
[74] P. Jutzi, J. Dahlhaus, M. O. Kristen, *J. Organomet. Chem.* **1993**, *450*, C1–C3.
[75] G. A. Molander, H. Schumann, E. C. E. Rosenthal, J. Demtschuk, *Organometallics* **1996**, *15*, 3817–3824.
[76] M. L. Hays, T. P. Hanusa, T. A. Nile, *J. Organomet. Chem.* **1996**, *514*, 73–79.
[77] C. J. Burns, R. A. Andersen, *J. Organomet. Chem.* **1987**, *325*, 31–37.
[78] R. A. Andersen, R. Blom, C. J. Burns, H. V. Volden, *J. Chem. Soc., Chem. Commun.* **1987**, 768–769.
[79] T. Hatanpää, M. Ritala, M. Leskelä, *J. Organomet. Chem.* **2007**, *692*, 5256–5262.
[80] L. Orzechowski, D. F.-J. Piesik, C. Ruspic, S. Harder, *Dalton Trans.* **2008**, 4742–4746.
[81] K. Fichtel, K. Hofmann, U. Behrens, *Organometallics* **2004**, *23*, 4166–4168.
[82] R. A. Williams, T. P. Hanusa, J. C. Huffman, *J. Chem. Soc., Chem. Commun.* **1988**, 1045–1046.
[83] S. Harder, *Angew. Chem. Int. Ed.* **1998**, *37*, 1239–1241.
[84] P. S. Tanner, T. P. Hanusa, *Polyhedron* **1994**, *13*, 2417–2420.
[85] T. Hatanpää, M. Vehkamäki, I. Mutikainen, J. Kansikas, M. Ritala, M. Leskelä, *Dalton Trans.* **2004**, 1181–1188.
[86] M. Wiecko, C. Eidamshaus, R. Köppe, P. W. Roesky, *Dalton Trans.* **2008**, 4837–4839.
[87] H. Lehmkuhl, K. Mehler, R. Benn, A. Rufińska, C. Krüger, *Chem. Ber.* **1986**, *119*, 1054–1069.
[88] D. Y. Kim, Y. Yang, J. R. Abelson, G. S. Girolami, *Inorg. Chem.* **2007**, *46*, 9060–9066.
[89] M. M. Olmstead, W. J. Grigsby, D. R. Chacon, T. Hascall, P. P. Power, *Inorg. Chim. Acta* **1996**, *251*, 273–284.
[90] A. Xia, M. J. Heeg, C. H. Winter, *J. Am. Chem. Soc.* **2002**, *124*, 11264–11265.
[91] A. Xia, J. E. Knox, M. J. Heeg, H. B. Schlegel, C. H. Winter, *Organometallics* **2003**, *22*, 4060–4069.
[92] A. J. Arduengo, F. Davidson, R. Krafczyk, W. J. Marshall, M. Tamm, *Organometallics* **1998**, *17*, 3375–3382.
[93] J. Baumgartner, C. Marschner, *Rev. Inorg. Chem.* **2014**, *34*, 119–152.
[94] Y. Mizuhata, T. Sasamori, N. Tokitoh, *Chem. Rev.* **2009**, *109*, 3479–3511.
[95] M. N. Hopkinson, C. Richter, M. Schedler, F. Glorius, *Nature* **2014**, *510*, 485–496.
[96] V. Nesterov, D. Reiter, P. Bag, P. Frisch, R. Holzner, A. Porzelt, S. Inoue, *Chem. Rev.* **2018**, *118*, 9678–9842.
[97] P. Zark, A. Schäfer, A. Mitra, D. Haase, W. Saak, R. West, T. Müller, *J. Organomet. Chem.* **2010**, *695*, 398–408.
[98] D. R. Armstrong, M. A. Beswick, N. L. Cromhout, C. N. Harmer, D. Moncrieff, C. A. Russell, P. R. Raithby, A. Steiner, A. E. H. Wheatley, D. S. Wright, *Organometallics* **1998**, *17*, 3176–3181.
[99] M. A. Beswick, N. L. Cromhout, C. N. Harmer, P. R. Raithby, C. A. Russell, J. S. B. Smith, A. Steiner, D. S. Wright, *Chem. Commun.* **1996**, 1977–1978.
[100] M. S. Nechaev, *Organometallics* **2021**, *40*, 3408–3423.
[101] B. Wrackmeyer, K. Horchler, H. Zhou, *Spectrochim. Acta A Mol. Biomol. Spectrosc.* **1990**, *46*, 809–816.

[102] P. Jutzi, A. Mix, B. Rummel, W. W. Schoeller, B. Neumann, H.-G. Stammler, *Science* **2004**, *305*, 849–851.
[103] M. Denk, R. Lennon, R. Hayashi, R. West, A. V. Belyakov, H. P. Verne, A. Haaland, M. Wagner, N. Metzler, *J. Am. Chem. Soc.* **1994**, *116*, 2691–2692.
[104] B. Rhodes, J. C. W. Chien, M. D. Rausch, *Organometallics* **1998**, *17*, 1931–1933.
[105] P. Jutzi, R. Dickbreder, H. Nöth, *Chem. Ber.* **1989**, *122*, 865–870.
[106] C. Janiak, H. Schumann, C. Stader, B. Wrackmeyer, J. J. Zuckerman, *Chem. Ber.* **1988**, *121*, 1745–1751.
[107] B. Wrackmeyer, Ē. Kupče, G. Kehr, A. Sebald, *Magn. Reson. Chem.* **1992**, *30*, 964–968.
[108] B. Wrackmeyer, in *Annual Reports on NMR Spectroscopy* (Ed.: G.A. Webb), Academic Press, New York, **1985**, p. 73.
[109] S. P. Constantine, G. M. De Lima, P. B. Hitchcock, J. M. Keates, G. A. Lawless, I. Marziano, *Organometallics* **1997**, *16*, 793–795.
[110] W. Huynh, M. P. Conley, *Dalton Trans.* **2020**, *49*, 16453–16463.
[111] B. Wrackmeyer, A. Sebald, L. H. Merwin, *Magn. Reson. Chem.* **1991**, *29*, 260–263.
[112] M. A. Beswick, J. S. Palmer, D. S. Wright, *Chem. Soc. Rev.* **1998**, *27*, 225–232.
[113] P. Jutzi, U. Holtmann, D. Kanne, C. Krüger, R. Blom, R. Gleiter, I. Hyla-Kryspin, *Chem. Ber.* **1989**, *122*, 1629–1639.
[114] P. Jutzi, D. Kanne, C. Krüger, *Angew. Chem. Int. Ed.* **1986**, *25*, 164–164.
[115] P. Ghana, M. I. Arz, G. Schnakenburg, M. Straßmann, A. C. Filippou, *Organometallics* **2018**, *37*, 772–780.
[116] R. S. Ghadwal, H. W. Roesky, S. Merkel, J. Henn, D. Stalke, *Angew. Chem. Int. Ed.* **2009**, *48*, 5683–5686.
[117] P. Jutzi, A. Mix, B. Neumann, B. Rummel, H.-G. Stammler, *Chem. Commun.* **2006**, 3519–3521.
[118] P. Jutzi, E.-A. Bunte, *Angew. Chem. Int. Ed.* **1992**, *31*, 1605–1607.
[119] T. Müller, P. Jutzi, T. Kühler, *Organometallics* **2001**, *20*, 5619–5628.
[120] M. Theil, P. Jutzi, B. Neumann, A. Stammler, H.-G. Stammler, *J. Organomet. Chem.* **2002**, *662*, 34–42.
[121] S. Khan, S. K. Ahirwar, S. Pal, N. Parvin, N. Kathewad, *Organometallics* **2015**, *34*, 5401–5406.
[122] M. Theil, P. Jutzi, B. Neumann, A. Stammler, H.-G. Stammler, *Organometallics* **2000**, *19*, 2937–2940.
[123] P. Jutzi, D. Eikenberg, B. Neumann, H.-G. Stammler, *Organometallics* **1996**, *15*, 3659–3663.
[124] P. Jutzi, D. Eikenberg, E.-A. Bunte, A. Möhrke, B. Neumann, H.-G. Stammler, *Organometallics* **1996**, *15*, 1930–1934.
[125] P. Jutzi, A. Klipp, A. Mix, B. Neumann, H.-G. Stammler, *Silicon Chem.* **2007**, *3*, 151–156.
[126] P. Jutzi, *Chem. Eur. J.* **2014**, *20*, 9192–9207.
[127] P. J. Davidson, M. F. Lappert, *J. Chem. Soc., Chem. Commun.* **1973**, 317a–317a.
[128] M. Grenz, E. Hahn, W.-W. du Mont, J. Pickardt, J. Pickardt, M. Grenz, E. Hahn, *Angew. Chem. Int. Ed.* **1984**, *23*, 61–63.
[129] C. Janiak, *Z. Anorg. Allg. Chem.* **2010**, *636*, 2387–2390.
[130] T. D. Lohrey, R. G. Bergman, J. Arnold, *Angew. Chem. Int. Ed.* **2017**, *56*, 14241–14245.
[131] P. G. Harrison, J. J. Zuckerman, *J. Am. Chem. Soc.* **1970**, *92*, 2577–2578.
[132] T. S. Dory, J. J. Zuckerman, C. L. Barnes, *J. Organomet. Chem.* **1985**, *281*, c1–c7.
[133] P. G. Harrison, T. J. King, J. A. Richards, *J. Chem. Soc., Dalton Trans.* **1975**, 2097–2100.
[134] A. B. Cornwell, P. P. Harrison, J. A. Richards, *J. Organomet. Chem.* **1976**, *108*, 47–60.
[135] B. P. Biryukov, Yu. T. Struchkov, *J. Struct. Chem.* **1969**, *10*, 86–96.
[136] K. D. Bos, E. J. Bulten, J. G. Noltes, *J. Organomet. Chem.* **1974**, *67*, C13–C15.
[137] S. M. Mansell, R. H. Herber, I. Nowik, D. H. Ross, C. A. Russell, D. F. Wass, *Inorg. Chem.* **2011**, *50*, 2252–2263.
[138] A. Jana, R. Azhakar, H. W. Roesky, I. Objartel, D. Stalke, *Z. Anorg. Allg. Chem.* **2011**, *637*, 1795–1799.
[139] G. M. De Lima, H. G. L. Siebald, J. L. Neto, V. D. De Castro, *Main Group Met. Chem.* **2001**, *24*, 223–228.
[140] M. A. Beswick, C. Lopez-Casideo, M. A. Paver, P. R. Raithby, C. A. Russell, A. Steiner, D. S. Wright, *Chem. Commun.* **1997**, *0*, 109–110.
[141] J. S. Overby, T. P. Hanusa, V. G. Young, *Inorg. Chem.* **1998**, *37*, 163–165.
[142] A. Bonny, A. D. McMaster, S. R. Stobart, *Inorg. Chem.* **1978**, *17*, 935–938.
[143] J. Almlöf, L. Fernholt, K. Fægri, Jr., A. Haaland, B. E. R. Schilling, R. Seip, K. Taugbøl, *Acta Chem. Scand.* **1983**, *37a*, 131–140.
[144] P. Jutzi, F. Kohl, P. Hofmann, C. Krüger, Y.-H. Tsay, *Chem. Ber.* **1980**, *113*, 757–769.
[145] P. Jutzi, B. Hielscher, *J. Organomet. Chem.* **1985**, *291*, c25–c27.
[146] Peter. Jutzi, Bernd. Hielscher, *Organometallics* **1986**, *5*, 1201–1204.
[147] S. Harder, D. Naglav, P. Schwerdtfeger, I. Nowik, R. H. Herber, *Inorg. Chem.* **2014**, *53*, 2188–2194.
[148] S. Labouille, C. Clavaguéra, F. Nief, *Organometallics* **2013**, *32*, 1265–1271.

[149] A. Dreyer, I. Ennen, T. Koop, A. Hütten, P. Jutzi, *Small* **2011**, *7*, 3075–3086.
[150] A. Schöpper, W. Saak, M. Weidenbruch, *J. Organomet. Chem.* **2006**, *691*, 809–810.
[151] C. Schenk, A. Schnepf, *Organometallics* **2006**, *25*, 2378–2380.
[152] W. J. Evans, K. J. Forrestal, J. T. Leman, J. W. Ziller, *Organometallics* **1996**, *15*, 527–531.
[153] W. J. Evans, R. D. Clark, K. J. Forrestal, J. W. Ziller, *Organometallics* **1999**, *18*, 2401–2402.
[154] S. P. Constantine, H. Cox, P. B. Hitchcock, G. A. Lawless, *Organometallics* **2000**, *19*, 317–326.
[155] S. P. Constantine, P. B. Hitchcock, G. A. Lawless, G. M. De Lima, *Chem. Commun.* **1996**, 1101–1102.
[156] S. P. Constantine, P. B. Hitchcock, G. A. Lawless, *Organometallics* **1996**, *15*, 3905–3906.
[157] P. Jutzi, E. Schlüter, M. B. Hursthouse, A. M. Arif, R. L. Short, *J. Organomet. Chem.* **1986**, *299*, 285–295.
[158] A. H. Cowley, J. G. Lasch, N. C. Norman, C. A. Stewart, T. C. Wright, *Organometallics* **1983**, *2*, 1691–1692.
[159] A. H. Cowley, P. Jutzi, F. X. Kohl, J. G. Lasch, N. C. Norman, E. Schlüter, *Angew. Chem. Int. Ed.* **1984**, *23*, 616–617.
[160] P. Jutzi, E. Schlüter, *J. Organomet. Chem.* **1983**, *253*, 313–316.
[161] C. J. Windorff, M. R. MacDonald, K. R. Meihaus, J. W. Ziller, J. R. Long, W. J. Evans, *Chem. Eur. J.* **2016**, *22*, 772–782.
[162] C. J. Windorff, M. R. MacDonald, J. W. Ziller, W. J. Evans, *Z. Anorg. Allg. Chem.* **2017**, *643*, 2011–2018.
[163] M. P. Coles, P. B. Hitchcock, M. F. Lappert, A. V. Protchenko, *Organometallics* **2012**, *31*, 2682–2690.
[164] D. J. Burkey, T. P. Hanusa, *Organometallics* **1995**, *14*, 11–13.
[165] H. Sitzmann, R. Boese, P. Stellberg, *Z. Anorg. Allg. Chem.* **1996**, *622*, 751–755.
[166] D. J. Burkey, T. P. Hanusa, *Inorg. Chem.* **2000**, *39*, 1834–1834.
[167] D. J. Burkey, T. P. Hanusa, J. C. Huffman, *Inorg. Chem.* **2000**, *39*, 153–155.
[168] H. Sitzmann, *Z. Anorg. Allg. Chem.* **1995**, *621*, 553–556.
[169] R. Hani, R. A. Geanangel, *J. Organomet. Chem.* **1985**, *293*, 197–205.
[170] P. Jutzi, R. Dickbreder, *J. Organomet. Chem.* **1989**, *373*, 301–306.
[171] F. X. Kohl, R. Dickbreder, P. Jutzi, G. Müller, B. Huber, *Chem. Ber.* **1989**, *122*, 871–878.
[172] H. Schumann, C. Janiak, J. J. Zuckerman, *Chem. Ber.* **1988**, *121*, 207–218.
[173] H. Schumann, C. Janiak, J. J. Zuckerman, *Chem. Ber.* **1988**, *121*, 1869–1869.
[174] M. J. Heeg, C. Janiak, J. J. Zuckerman, *J. Am. Chem. Soc.* **1984**, *106*, 4259–4261.
[175] M. J. Heeg, R. H. Herber, C. Janiak, J. J. Zuckerman, H. Schumann, W. F. Manders, *J. Organomet. Chem.* **1988**, *346*, 321–332.
[176] H. Schumann, C. Janiak, E. Hahn, J. Loebel, J. J. Zuckerman, *Angew. Chem. Int. Ed.* **1985**, *24*, 773–773.
[177] H. Schumann, C. Janiak, E. Hahn, C. Kolax, J. Loebel, M. D. Rausch, J. J. Zuckerman, M. J. Heeg, *Chem. Ber.* **1986**, *119*, 2656–2667.
[178] D. Naglav, B. Tobey, S. Harder, A. Schnepf, *Z. Anorg. Allg. Chem.* **2013**, *639*, 354–359.
[179] R. H. Lowack, K. Peter, C. Vollhardt, *J. Organomet. Chem.* **1994**, *476*, 25–32.
[180] J. Rouzaud, M. Joudat, A. Castel, F. Delpech, P. Rivière, H. Gornitzka, J. M. Manriquez, I. Chavez, *J. Organomet. Chem.* **2002**, *651*, 44–51.
[181] J. Rouzaud, A. Castel, P. Rivière, H. Gornitzka, J. M. Manriquez, *Organometallics* **2000**, *19*, 4678–4680.
[182] M. Joudat, A. Castel, F. Delpech, P. Rivière, A. Mcheik, H. Gornitzka, S. Massou, A. Sournia-Saquet, *Organometallics* **2004**, *23*, 3147–3152.
[183] R. M. Bellabarba, G. P. Clancy, P. T. Gomes, A. M. Martins, L. H. Rees, M. L. H. Green, *J. Organomet. Chem.* **2001**, *640*, 93–112.
[184] E. J. Bulten, H. A. Budding, *J. Organomet. Chem.* **1978**, *157*, C3–C4.
[185] P. Jutzi, B. Hampel, M. B. Hursthouse, A. J. Howes, *Organometallics* **1986**, *5*, 1944–1948.
[186] A. H. Cowley, R. A. Kemp, C. A. Stewart, *J. Am. Chem. Soc.* **1982**, *104*, 3239–3240.
[187] T. S. Dory, J. J. Zuckerman, M. D. Rausch, *J. Organomet. Chem.* **1985**, *281*, c8–c11.
[188] P. Jutzi, F.-X. Kohl, E. Schlüter, M. B. Hursthouse, N. P. C. Walker, *J. Organomet. Chem.* **1984**, *271*, 393–402.
[189] N. Kuhn, G. Henkel, S. Stubenrauch, *Angew. Chem. Int. Ed.* **1992**, *31*, 778–779.
[190] A. Elvers, F. W. Heinemann, B. Wrackmeyer, U. Zenneck, *Chem. Eur. J.* **1999**, *5*, 3143–3153.
[191] M. Brym, M. D. Francis, G. Jin, C. Jones, D. P. Mills, A. Stasch, *Organometallics* **2006**, *25*, 4799–4807.
[192] J. J. Durkin, M. D. Francis, P. B. Hitchcock, C. Jones, J. F. Nixon, *J. Chem. Soc., Dalton Trans.* **1999**, 4057–4062.
[193] M. A. Beswick, H. Gornitzka, J. Kärcher, M. E. G. Mosquera, J. S. Palmer, P. R. Raithby, C. A. Russell, D. Stalke, A. Steiner, D. S. Wright, *Organometallics* **1999**, *18*, 1148–1153.
[194] J. N. Jones, J. A. Moore, A. H. Cowley, C. L. B. Macdonald, *Dalton Trans.* **2005**, 3846–3851.

[195] M. Schleep, C. Hettich, J. Velázquez Rojas, D. Kratzert, T. Ludwig, K. Lieberth, I. Krossing, *Angew. Chem. Int. Ed.* **2017**, *56*, 2880–2884.
[196] M. Schorpp, I. Krossing, *Chem. Eur. J.* **2020**, *26*, 14109–14117.
[197] R. A. Layfield, M. McPartlin, D. S. Wright, *Organometallics* **2003**, *22*, 2528–2530.
[198] M. J. Duer, N. A. Page, M. A. Paver, P. R. Raithby, M.-A. Rennie, C. A. Russell, C. Stourton, A. Steiner, D. S. Wright, *J. Chem. Soc., Chem. Commun.* **1995**, 1141–1142.
[199] K. Forissier, L. Ricard, D. Carmichael, F. Mathey, *Chem. Commun.* **1999**, 1273–1274.
[200] E. O. Fischer, S. Schreiner, *Chem. Ber.* **1959**, *92*, 938–948.
[201] E. Weiss, *Z. Anorg. Allg. Chem.* **1956**, *287*, 236–241.
[202] A. Almenningen, A. Haaland, T. Motzfeldt, *J. Organomet. Chem.* **1967**, *7*, 97–104.
[203] P. G. Harrison, J. J. Zuckerman, *J. Am. Chem. Soc.* **1969**, *91*, 6885–6886.
[204] P. G. Harrison, M. A. Healy, *J. Organomet. Chem.* **1973**, *51*, 153–166.
[205] P. Jutzi, F. Kohl, *J. Organomet. Chem.* **1979**, *164*, 141–152.
[206] P. Jutzi, B. Hielscher, *Organometallics* **1986**, *5*, 2511–2514.
[207] V. Sriyunyongwat, R. Hani, T. A. Albright, R. Geanangel, *Inorg. Chim. Acta* **1986**, *122*, 91–94.
[208] S. Cradock, W. Duncan, *J. Chem. Soc., Faraday Trans. 2* **1978**, *74*, 194–202.
[209] R. G. Egdell, I. Fragala, A. F. Orchard, *J. Electron Spectrosc. Relat. Phenom.* **1978**, *14*, 467–475.
[210] W. Strohmeier, H. Landsfeld, F. Gernert, *Z. Elektrochem.* **1962**, *66*, 823–827.
[211] C. Gaffney, P. G. Harrison, *J. Chem. Soc., Dalton Trans.* **1982**, 1055–1060.
[212] S. G. Baxter, A. H. Cowley, J. G. Lasch, M. Lattman, W. P. Sharum, C. A. Stewart, *J. Am. Chem. Soc.* **1982**, *104*, 4064–4069.
[213] M. L. Hays, T. P. Hanusa, in *Adv. Organomet. Chem.* (Eds.: F. Gordon, A. Stone, R. West), Academic Press, **1996**, pp. 117–170.
[214] F. Jaroschik, A. Momin, A. Martinez, D. Harakat, L. Ricard, X. F. Le Goff, G. Nocton, *Organometallics* **2016**, *35*, 2032–2038.
[215] P. Jutzi, K. Leszczyńska, B. Neumann, W. W. Schoeller, H.-G. Stammler, *Angew. Chem. Int. Ed.* **2009**, *48*, 2596–2599.
[216] P. Jutzi, K. Leszczyńska, A. Mix, B. Neumann, B. Rummel, W. Schoeller, H.-G. Stammler, *Organometallics* **2010**, *29*, 4759–4761.
[217] W. Malisch, S. Möller, O. Fey, H.-U. Wekel, R. Pikl, U. Posset, W. Kiefer, *J. Organomet. Chem.* **1996**, *507*, 117–124.
[218] K. Leszczyńska, A. Mix, R. J. F. Berger, B. Rummel, B. Neumann, H.-G. Stammler, P. Jutzi, *Angew. Chem. Int. Ed.* **2011**, *50*, 6843–6846.
[219] K. Leszczyńska, K. Abersfelder, M. Majumdar, B. Neumann, H.-G. Stammler, H. S. Rzepa, P. Jutzi, D. Scheschkewitz, *Chem. Commun.* **2012**, *48*, 7820–7822.
[220] S. Inoue, K. Leszczyńska, *Angew. Chem. Int. Ed.* **2012**, *51*, 8589–8593.
[221] P. Jutzi, A. Mix, B. Neumann, B. Rummel, W. W. Schoeller, H.-G. Stammler, A. B. Rozhenko, *J. Am. Chem. Soc.* **2009**, *131*, 12137–12143.
[222] K. I. Leszczyńska, V. Huch, C. Präsang, J. Schwabedissen, R. J. F. Berger, D. Scheschkewitz, *Angew. Chem. Int. Ed.* **2019**, *58*, 5124–5128.
[223] K. I. Leszczyńska, P. Deglmann, C. Präsang, V. Huch, M. Zimmer, D. Schweinfurth, D. Scheschkewitz, *Dalton Trans.* **2020**, *49*, 13218–13225.
[224] N. Sen, N. Parvin, S. Tothadi, S. Khan, *Organometallics* **2021**, *40*, 1874–1883.
[225] A. Haaland, B. E. R. Schilling, S. Hauge, O. Vikane, H. Ohtaki, *Acta Chem. Scand.* **1984**, *38a*, 217–222.
[226] F. X. Kohl, P. Jutzi, *J. Organomet. Chem.* **1983**, *243*, 31–34.
[227] L. Fernholt, A. Haaland, P. Jutzi, F. X. Kohl, R. Seip, *Acta Chem. Scand.* **1984**, *38a*, 211–216.
[228] J. G. Winter, P. Portius, G. Kociok-Köhn, R. Steck, A. C. Filippou, *Organometallics* **1998**, *17*, 4176–4182.
[229] A. D. Rohr, J. W. Kampf, J. P. Wolfe, M. M. Banaszak Holl, *Organometallics* **2010**, *29*, 5004–5009.
[230] K. D. Bos, E. J. Bulten, J. G. Noltes, A. L. Spek, *J. Organomet. Chem.* **1975**, *99*, 71–77.
[231] A. C. Filippou, P. Portius, A. I. Philippopoulos, *Organometallics* **2002**, *21*, 653–661.
[232] P. Jutzi, H. Schmidt, B. Neumann, H.-G. Stammler, *J. Organomet. Chem.* **1995**, *499*, 7–10.
[233] P. Jutzi, B. Hampel, *Organometallics* **1986**, *5*, 730–734.
[234] Y. Ding, P. N. Ruth, R. Herbst-Irmer, D. Stalke, Z. Yang, H. W. Roesky, *Dalton Trans.* **2021**, *50*, 2067–2074.
[235] P. Jutzi, A. Becker, C. Leue, H. G. Stammler, B. Neumann, M. B. Hursthouse, A. Karaulov, *Organometallics* **1991**, *10*, 3838–3842.
[236] P. Jutzi, B. Hampel, K. Stroppel, C. Krüger, K. Angermund, P. Hofmann, *Chem. Ber.* **1985**, *118*, 2789–2797.
[237] P. Jutzi, B. Hampel, *J. Organomet. Chem.* **1986**, *301*, 283–288.
[238] P. Jutzi, B. Hampel, M. B. Hursthouse, A. J. Howes, *J. Organomet. Chem.* **1986**, *299*, 19–27.

[239] A. C. Filippou, A. I. Philippopoulos, P. Portius, D. U. Neumann, *Angew. Chem. Int. Ed.* **2000**, *39*, 2778–2781.
[240] A. C. Filippou, A. I. Philippopoulos, P. Portius, G. Schnakenburg, *Organometallics* **2004**, *23*, 4503–4512.
[241] A. C. Filippou, G. Schnakenburg, A. I. Philippopoulos, N. Weidemann, *Angew. Chem. Int. Ed.* **2005**, *44*, 5979–5985.
[242] F. X. Kohl, E. Schlüter, P. Jutzi, C. Krüger, G. Wolmershäuser, P. Hofmann, P. Stauffert, *Chem. Ber.* **1984**, *117*, 1178–1193.
[243] O. T. Summerscales, J. C. Fettinger, P. P. Power, *J. Am. Chem. Soc.* **2011**, *133*, 11960–11963.
[244] G. H. Spikes, Y. Peng, J. C. Fettinger, P. P. Power, *Z. Anorg. Allg. Chem.* **2006**, *632*, 1005–1010.
[245] K. D. Bos, E. J. Bulten, J. G. Noltes, *J. Organomet. Chem.* **1972**, *39*, C52–C54.
[246] C. L. B. Macdonald, R. Bandyopadhyay, B. F. T. Cooper, W. W. Friedl, A. J. Rossini, R. W. Schurko, S. H. Eichhorn, R. H. Herber, *J. Am. Chem. Soc.* **2012**, *134*, 4332–4345.
[247] S. P. Constantine, G. M. De Lima, P. B. Hitchcock, J. M. Keates, G. A. Lawless, *Chem. Commun.* **1996**, 2337–2338.
[248] M. C. Cassani, M. J. Davies, P. B. Hitchcock, M. F. Lappert, *Inorg. Chim. Acta* **2005**, *358*, 1595–1604.
[249] P. Jutzi, F. Kohl, C. Krüger, *Angew. Chem. Int. Ed.* **1979**, *18*, 59–60.
[250] J. Beckmann, A. Duthie, M. Wiecko, *Main Group Met. Chem.* **2012**, *35*, 179–182.
[251] G. M. De Lima, D. J. Duncalf, S. P. Constantine, *Main Group Met. Chem.* **2002**, *25*, 567–570.
[252] G. M. De Lima, D. J. Duncalf, S. P. Constantine, *Main Group Met. Chem.* **2001**, *24*, 675–680.
[253] M. Veith, C. Mathur, V. Huch, *Organometallics* **1996**, *15*, 2858–2859.
[254] M. Veith, C. Mathur, S. Mathur, V. Huch, *Organometallics* **1997**, *16*, 1292–1299.
[255] T. Ochiai, S. Inoue, *RSC Adv.* **2017**, *7*, 801–804.
[256] M. Veith, C. Mathur, V. Huch, *Phosphorus Sulfur Silicon Relat. Elem.* **1997**, *124*, 489–492.
[257] E. Y. Njua, A. Steiner, L. Stahl, *J. Organomet. Chem.* **2011**, *696*, 3301–3306.
[258] M. A. Paver, D. S. Wright, D. Stalke, *Angew. Chem. Int. Ed.* **1993**, *32*, 428–429.
[259] C. P. Sindlinger, A. Stasch, H. F. Bettinger, L. Wesemann, *Chem. Sci.* **2015**, *6*, 4737–4751.
[260] A. J. Edwards, M. A. Paver, P. R. Raithby, M.-A. Rennie, C. A. Russell, D. S. Wright, *J. Chem. Soc., Dalton Trans.* **1995**, 1587–1591.
[261] A. K. Holliday, P. H. Makin, R. J. Puddephatt, *J. Chem. Soc., Dalton Trans.* **1976**, 435–438.
[262] A. K. Holliday, P. H. Makin, R. J. Puddephatt, J. D. Wilkins, *J. Organomet. Chem.* **1973**, *57*, C45–C46.
[263] D. Bourissou, O. Guerret, F. P. Gabbaï, G. Bertrand, *Chem. Rev.* **2000**, *100*, 39–92.
[264] S. W. Chien, T. S. Andy Hor, in *Ferrocenes*, John Wiley & Sons, Ltd, **2008**, pp. 33–116.
[265] T. J. Colacot, S. Parisel, in *Ferrocenes*, John Wiley & Sons, Ltd, **2008**, pp. 117–140.
[266] U. Siemeling, in *Ferrocenes*, John Wiley & Sons, Ltd, **2008**, pp. 141–176.
[267] P. Štěpnička, M. Lamač, in *Ferrocenes*, John Wiley & Sons, Ltd, **2008**, pp. 237–277.

6. Supporting Information

6.1 Carbene Complexes of Stannocenes

Supplementary Information

for

Carbene Complexes of Stannocenes

1. Experimental Details	S1 – S5
2. NMR Spectra	S6 – S13
3. XRD Data	S14 – S20
4. Computational Details	S21 – S39
5. References	S40

1. Experimental Details

All manipulations were carried out under an argon inert gas atmosphere (argon 5.0), using either standard Schlenk line techniques or a glovebox. Tin dichloride and lithium granules were purchased from ABCR and used as received. Dicyclopentadiene (90%) and methyldicyclopentadiene (90%) were purchased from ABCR, cracked and distilled freshly prior to use. n-butyllithium solution (2.5 M in hexane) was purchased from Acros Organics and used as received. Silicon tetrachloride was purchased from Sigma Aldrich and used as received. Germanium dichloride dioxane adduct was purchased from Strem and used as received. Cyclopentadienyl lithium and methylcyclopentadienyl lithium were prepared from the corresponding cyclopentadiene and n-butyllithium at 195 K. Deuterated benzene was purchased from ABCR and dried over 4 Å molecular sieves.

1c[1] and **2a**-**c**[2-4] were prepared according to literature known procedures.

NMR-spectra were recorded on a Bruker Avance III 300 (solution) and a Bruker Avance III 400 (solution). ^{1}H and ^{13}C NMR spectra were referenced using the solvent signals (δ ^{1}H (C_6HD_5) = 7.20; δ ^{13}C (C_6D_6) = 128.0) and ^{29}Si and ^{119}Sn NMR spectra were referenced using external standards (δ ^{29}Si ($SiMe_4$) = 0; δ ^{119}Sn ($SnMe_4$) = 0). Single crystal X-ray diffraction analysis were carried out at low temperatures on a Bruker AXS X8 Apex CCD diffractometer operating with graphite monochromated Mo Kα radiation. Structure solution and refinement with anisotropic thermal parameters of all non-hydrogen atoms were performed using SHELX[5].

Synthesis of 1a:

Stannocene, **1a**, was prepared by a modified literature procedure.[6]
Tin(II)chloride and CpLi were charged into a schlenk flask. THF, cooled to 273 K in an ice bath, was added and the resulting solution was stirred overnight. All volatiles were evaporated and the residue extracted with toluene. The solvent was evaporated and stannocene, **1a**, was obtained as a colorless solid and was further purified by sublimation.
Yield: 60%
^{1}H NMR (300.13 MHz, C_6D_6, 299 K): δ = 5.83 (s, 10 H, Cp-H); ^{13}C{^{1}H} NMR (75.47 MHz, C_6D_6, 299 K): δ = 111.2 (Cp); ^{119}Sn{^{1}H} NMR (111.71 MHz, C_6D_6, 299 K): δ = -2199.

Synthesis of 1b:

Dimethyl stannocene, **1b**, was prepared by a modified literature procedure.[6-7]
Tin(II)chloride and ^{Me}CpLi were charged into a schlenk flask. THF, cooled to 273 K in an ice bath, was added and the resulting solution was stirred overnight. The solvent was evaporated and the residue extracted with hexane. The solvent was evaporated and dimethyl stannocene, **1b**, was obtained as a red to brown liquid and was purified by flask to flask condensation.
Yield: 53%
^{1}H NMR (300.13 MHz, C_6D_6, 299 K): δ =2.05 (s, 6 H, Cp-CH_3), 5.72-5.76 (m, 8 H, Cp-H); ^{13}C{^{1}H} NMR (75.48 MHz, C_6D_6, 299 K): δ = 14.1 (Cp-CH_3), 108.9 (Cp), 111.5 (Cp), 124.2 (Cp); ^{119}Sn{^{1}H} NMR (111.71 MHz, C_6D_6, 299 K): δ = -2117.

Synthesis of 3a-e:

Method A:
Stannocene (**1a-e**) and *N*-heterocyclic carbene (**2a-c**) were charged into a schlenk flask, toluene was added and the solution was stirred until the compounds had dissolved completely. By addition of an excess of hexane to the toluene solution and storage at 253 K overnight, complexes **3a**-**e** were obtained as crystalline solids.

Method B:
Tin(II)chloride and N-heterocyclic carbene (**2a-c**) were charged into a schlenk flask, THF was added and the solution was stirred overnight. To this solution CpLi was added and the mixture was again stirred overnight. All volatiles were removed in vacuum and the residue was extracted with toluene. By addition of an excess of hexane to the toluene solution and storage at 253 K overnight, complexes **3a**-**e** were obtained as crystalline solids.

3a: colorless crystals, 53% yield.
^{1}H NMR (300.13 MHz, C_6D_6, 299 K): δ = 1.45 (s, 6 H, NCH-(CH_3)$_2$), 1.47 (s, 6 H, NCH-(CH_3)$_2$), 1.72 (s, 6 H, NC-CH_3), 4.08-4.21 (sept, ^{3}J = 6.9 Hz, 2 H, NCH-(CH_3)$_2$), 5.94 (s, 10 H, Cp-H); ^{13}C{^{1}H} NMR (75.48 MHz, C_6D_6, 299 K): δ = 9.2 (NCH-(CH_3)$_2$), 23.8 (NC-CH_3), 49.8 (NCH-(CH_3)$_2$), 111.1 (Cp), 122.3 (NC-CH_3), 198.3 (carbene-C); ^{119}Sn{^{1}H} NMR (111.71 MHz, C_6D_6, 299 K): δ = −1824 ($\nu_{½}$ = 1411 Hz); Elemental analysis for $C_{21}H_{30}N_2Sn$: found: C: 53.41%, H: 6.84%; N: 6.52% calc.: C: 58.77%, H: 7.05%, N: 6.53%.

3b: light green crystals, 73% yield.
^{1}H NMR (300.13 MHz, C_6D_6, 299 K): δ = 1.42 (s, 6 H, NCH-(CH_3)$_2$), 1.45 (s, 6 H, NCH-(CH_3)$_2$), 1.74 (s, 6 H, NC-CH_3), 2.15 (s, 6 H, Cp-CH_3), 4.11-4.25 (sept, ^{3}J = 6.9 Hz, 2 H, NCH-(CH_3)$_2$), 5.79 (m, 4 H, Cp-H), 5.85 (m, 4 H, Cp-H); ^{13}C{^{1}H} NMR (75.48 MHz, C_6D_6, 299 K): δ = 9.1 (NCH-(CH_3)$_2$), 14.6 (Cp-CH_3), 24.2 (NC-

$\underline{C}H_3$), 49.3 (N$\underline{C}$H-$(CH_3)_2$), 108.4 (Cp), 110.1(Cp), 111.5 (Cp), 122.1 (N$\underline{C}$-CH_3), 124.6 (Cp), 202.5 (carbene-$\underline{C}$); ^{119}Sn{^{1}H} NMR (111.71 MHz, C_6D_6, 299 K): δ = −1952 ($\nu_{½}$ = 954 Hz); Elemental analysis for $C_{23}H_{34}N_2Sn$: found: C: 59.16%, H: 7.61%; N: 6.24% calc.: C: 60.42%, H: 7.50%, N: 6.13%.

3c: light yellow crystals, 69% yield.
^{1}H NMR (300.13 MHz, C_6D_6, 299 K): δ = 2.15 (s, 6 H, Mes-*para*-C$\underline{H}_3$), 2.17 (s, 12 H, Mes-*ortho*-C$\underline{H}_3$), 5.90 (s, 10 H, Cp-$\underline{H}$), 6.36 (s, 2 H, NC$\underline{H}$), 6.82 (s, 4 H, Mes-$\underline{H}$); ^{13}C{^{1}H} NMR (75.48 MHz, C_6D_6, 299 K): δ = 17.8 (Mes-$\underline{C}H_3$), 20.7 (Mes-$\underline{C}H_3$), 110.7 (Cp), 121.2 (Mes), 129.1 (Mes), 135.1 (Mes), 138.3 (Mes), 209.1 (carbene-$\underline{C}$); ^{119}Sn{^{1}H} NMR (111.71 MHz, C_6D_6, 299 K): δ = −1936 ($\nu_{½}$ = 190 Hz); Elemental analysis for $C_{31}H_{34}N_2Sn$: found: C: 63.99%, H: 6.17%; N: 5.13% calc.: C: 67.29%, H: 6.19%, N: 5.06%.

3d: yellow crystals, 79% yield.
^{1}H NMR (300.13 MHz, C_6D_6, 299 K): δ = 2.07 (s, 6 H, Mes-*para*-C$\underline{H}_3$), 2.19 (s, 12 H, Mes-*ortho*-C$\underline{H}_3$, 6 H, Cp-C$\underline{H}_3$), 5.71 (m, 4 H, Cp-$\underline{H}$), 5.78 (m, 4 H, Cp-$\underline{H}$), 6.47 (s, 2 H, NC$\underline{H}$), 6.84 (s, 4 H, Mes-$\underline{H}$); ^{13}C{^{1}H} NMR (75.47 MHz, C_6D_6, 299 K): δ = 14.2 (Cp-$\underline{C}H_3$), 18.1 (Mes-$\underline{C}H_3$), 21.0 (Mes-$\underline{C}H_3$), 108.4 (Cp), 111.8 (Cp), 120.7 (Cp), 124.6 (Cp), 129.2 (Mes), 135.4 (Mes), 137.5 (Mes), 138.8 (Mes), 216.9 (carbene-$\underline{C}$); ^{119}Sn{^{1}H} NMR (111.92 MHz, C_6D_6, 299 K): δ = −2063 ($\nu_{½}$ = 41 Hz); Elemental analysis for $C_{39}H_{50}N_2Sn$: found: C: 67.38%, H: 6.51%; N: 5.05% calc.: C: 70.38%, H: 7.57%, N: 4.21%.

3e: orange to brown crystals.
^{1}H NMR (400.13 MHz, C_6D_6, 299 K): δ = 1.34 (s, 6 H, NC-C$\underline{H}_3$), 2.37 (s, 6 H, Cp-C$\underline{H}_3$), 3.09 (s, 6 H, N-C$\underline{H}_3$), 5.97 (m, 4 H, Cp-$\underline{H}$), 6.11 (m, 4 H, Cp-$\underline{H}$); ^{13}C{^{1}H} NMR (75.48 MHz, C_6D_6, 299 K): δ = 8.1 (C-$\underline{C}H_3$), , 15.4 (Cp-$\underline{C}H_3$), 33.6 (N-$\underline{C}H_3$), 107.3 (Cp), 111.6 (Cp), 121.8 ($\underline{C}$-CH_3), 124.1 (Cp), 191.9. (carbene-$\underline{C}$); No ^{119}Sn Signal could be detected, although several attempts were made at temperatures between 298 K and 233 K. This is most likely due to extreme signal broadening.

3f: colorless crystals, 51% yield.
^{1}H NMR (300.13 MHz, C_6D_6, 299 K): δ = 0.41 (s, 12 H, Si-C$\underline{H}_3$), 1.46 (s, 6 H, NCH-($C\underline{H}_3$)$_2$), 1.48 (s, 6 H, NCH-($C\underline{H}_3$)$_2$, 1.73 (s, 6 H, NC-C$\underline{H}_3$), 4.06-4.19 (sept, ^3J = 6.9 Hz, 2 H, NC$\underline{H}$-$(CH_3)_2$), 5.98-6.00 (triplet, ^3J = 2.3 Hz, 4 H, Cp-$\underline{H}$), 6.36-6.37 (t, ^3J = 2.3 Hz, 4 H, Cp-$\underline{H}$); ^{13}C{^{1}H} NMR (75.47 MHz, C_6D_6, 299 K): δ = -2.9 (Si-$\underline{C}H_3$), 8.9 (NCH-($\underline{C}H_3$)$_2$), 24.26 (NC-$\underline{C}H_3$), 49.0 (N$\underline{C}$H-$(CH_3)_2$), 114.1 (Cp), 115.7 (Cp), 117.8 (Cp), 121.9 (N$\underline{C}$-CH_3), 202.5 (carbene-$\underline{C}$); ^{119}Sn{^{1}H} NMR (111.70 MHz, C_6D_6, 299 K): δ = -1981 ($\nu_{½}$ = 403 Hz); ^{29}Si{^{1}H} NMR (59.63 MHz, C_6D_6, 299 K): δ = −26.3; Elemental analysis for $C_{25}H_{41}N_2Si_2Sn$: found: C: 54.59%, H: 7.66%; N: 5.16% calc.: C: 55.15%, H: 7.59%, N: 5.14%.

3g: yellow crystals, 74% yield.
^{1}H NMR (300.13 MHz, C_6D_6, 299 K): δ = 0.39 (s, 12 H, Si-C$\underline{H}_3$) 2.16 (s, 6 H, Mes-*para*-C$\underline{H}_3$), 2.19 (s, 12 H, Mes-*ortho*-C$\underline{H}_3$), 5.87-5.88 (t, ^3J = 2.3 Hz, 4 H, Cp-$\underline{H}$), 6.33-6.35 (m, 4 H, Cp-$\underline{H}$), 6.33-6.35 (m, 2 H, NC$\underline{H}$), 6.83 (s, 4 H, Mes-$\underline{H}$); ^{13}C{^{1}H} NMR (75.48 MHz, C_6D_6, 299 K): δ = -3.0 (Si-$\underline{C}H_3$), 18.1 (Mes-$\underline{C}H_3$), 21.0 (Mes-$\underline{C}H_3$), 114.6 (Cp), 116.2 (Cp), 117.4 (Cp), 120.9 (Cp), 129.3 (Mes), 135.3 (Mes), 137.6 (Mes), 138.1 (Mes), 211.6 (carbene-$\underline{C}$); ^{119}Sn{^{1}H} NMR (111.71 MHz, C_6D_6, 299 K): δ = −1849 ($\nu_{½}$ = 114 Hz); ^{29}Si{^{1}H} NMR (59.63 MHz, C_6D_6, 299 K): δ = −26.5; Elemental analysis for $C_{35}H_{45}N_2Si_2Sn$: found: C: 61.16%, H: 6.67%; N: 4.34% calc.: C: 62.87%, H: 6.78%, N: 4.19%.

Synthesis of 4:

N-heterocyclic Silylene (NHSi), **4**, was prepared by a modified literature procedure.[8-9]
To a solution of 1,2-Bis(2,4,6-trimethylphenylimino)ethane in THF cooled to 273 K lithium granulas were added. Subsequently, the cooling bath was removed and the resulting suspension was stirred for 18 h. The color of the suspension changed from yellow to deep red. Unreacted lithium was removed with tweezers and the solution was cooled to 77 K. Silicon tetrachloride was added through a dropping funnel onto the frozen reaction mixture, which was subsequently allowed to warm to room

temperature. All volatiles were removed in vacuum and the residue was extracted with hexane. After removal of the solvent, the dichlorosilane ($NHSiCl_2$) was obtained as a light orange solid.
Yield: 34%
^{1}H NMR (400.13 MHz, C_6D_6, 299 K): δ = 2.15 (s, 6 H, Mes-C<u>H</u>$_3$), 2.47 (s, 12 H, Mes-C<u>H</u>$_3$), 5.57 (s, 2 H, NC-<u>H</u>), 6.81 (s, 4 H, Mes-<u>H</u>). ^{13}C{^{1}H} NMR (75.48 MHz, C_6D_6, 299 K): δ = 18.9 (Mes-<u>C</u>H$_3$), 20.9 (Mes-<u>C</u>H$_3$), 118.8 (N-<u>C</u>H), 129.8 (Mes), 135.8 (Mes), 136.6 (Mes), 137.3 (Mes); ^{29}Si{^{1}H} NMR (79.49 MHz, C_6D_6, 299 K): δ = -40.7.

The dichlorosilane ($NHSiCl_2$) was mixed with 2.3 eq potassium graphite and THF THF, cooled to 273 K in an ice bath, was added. The reaction mixture was stirred and allowed to warm to room temperature overnight. After evaporation of all volatiles, the residue was extracted with hexane. The hexane solution was concentrated and stored overnight at 253 K. Silylene (NHSi), **4**, was obtained as a light yellow crystalline solid.
Yield: 62%
^{1}H NMR (400.13 MHz, C_6D_6, 299 K): δ = 2.22 (s, 6 H, Mes-*para*-C<u>H</u>$_3$), 2.30 (s, 12 H, Mes-*ortho*-C<u>H</u>$_3$), 6.34 (s, 2 H, NC<u>H</u>), 6.88 (s, 4 H, Mes-<u>H</u>); ^{13}C{^{1}H} NMR (75.48 MHz, C_6D_6, 299 K): δ = 18.5 (Mes-<u>C</u>H$_3$), 21.0 (Mes-<u>C</u>H$_3$), 124.4 (H<u>C</u><u>C</u>H), 129.3 (Mes), 134.8 (Mes), 135.8 (Mes), 140.2 (Mes); ^{29}Si{^{1}H} NMR (79.49 MHz, C_6D_6, 299 K): δ = 77.4.

Synthesis of 5:

N-heterocyclic Germylene (NHGe), **5**, was prepared by a modified literature procedure.[10]
To a solution of 1,2-Bis(2,4,6-trimethylphenylimino)ethane in THF cooled to 273 K lithium granulas were added. Subsequently, the cooling bath was removed and the resulting suspension was stirred for 18 h. The color of the suspension changed from yellow to deep red. Unreacted lithium was removed with tweezers and $GeCl_2$·dioxane was added. After stirring for 2.5 h the solvent was evaporated and the residue extracted with hexane. After removal of the solvent, germylene, **5**, was obtained as an orange solid.
Yield: 65%
^{1}H NMR (400.13 MHz, C_6D_6, 299 K): δ = 2.24 (s, 6 H, Mes-*para*-C<u>H</u>$_3$), 2.28 (s, 12 H, Mes-*ortho*-C<u>H</u>$_3$), 6.62 (s, 2 H, NC<u>H</u>), 6.91 (s, 4 H, Mes-<u>H</u>); ^{13}C{^{1}H} NMR (75.48 MHz, C_6D_6, 299 K): 18.4 (Mes-<u>C</u>H$_3$), 21.0 (Mes-<u>C</u>H$_3$), 125.4 (H<u>C</u><u>C</u>H), 129.3 (Mes), 134.0 (Mes), 135.3 (Mes), 142.8 (Mes).

Table S1. Selected NMR spectroscopic parameters for complexes **3a**-**g**.

compound	$\delta^{13}C^{a}$	$\Delta\delta^{13}C^{b}$	$\delta^{119}Sn^{c}$	$\Delta\delta^{119}Sn^{d}$
3a	198.3	9.2	−1824	375
3b	202.5	4.9	−1952	166
3c	209.1	9.3	−1936	264
3d	216.9	1.5	−2063	55
3e	191.9	21.2		
3f	202.5	5.1	-1981	106
3g	211.6	6.8	-1849	238

[a] 75 MHz, 299 K, C_6D_6 (^{13}C NMR chemical shift of the carbene carbon atom); [b] difference between ^{13}C NMR chemical shift of carbene carbon atom in the complex and in free carbene; [c] 112 MHz, 299 K, C_6D_6; [d] difference between ^{119}Sn NMR chemical shift in the complex and in free stannocene.

2. NMR spectra

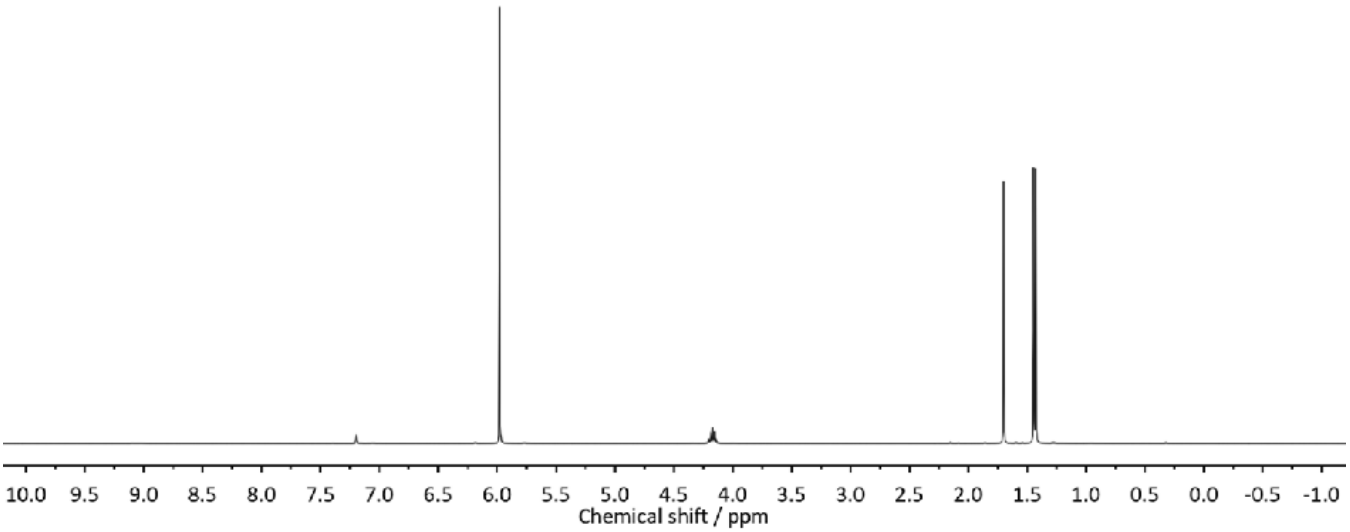

Figure S1: ^{1}H NMR spectrum of **3a**.

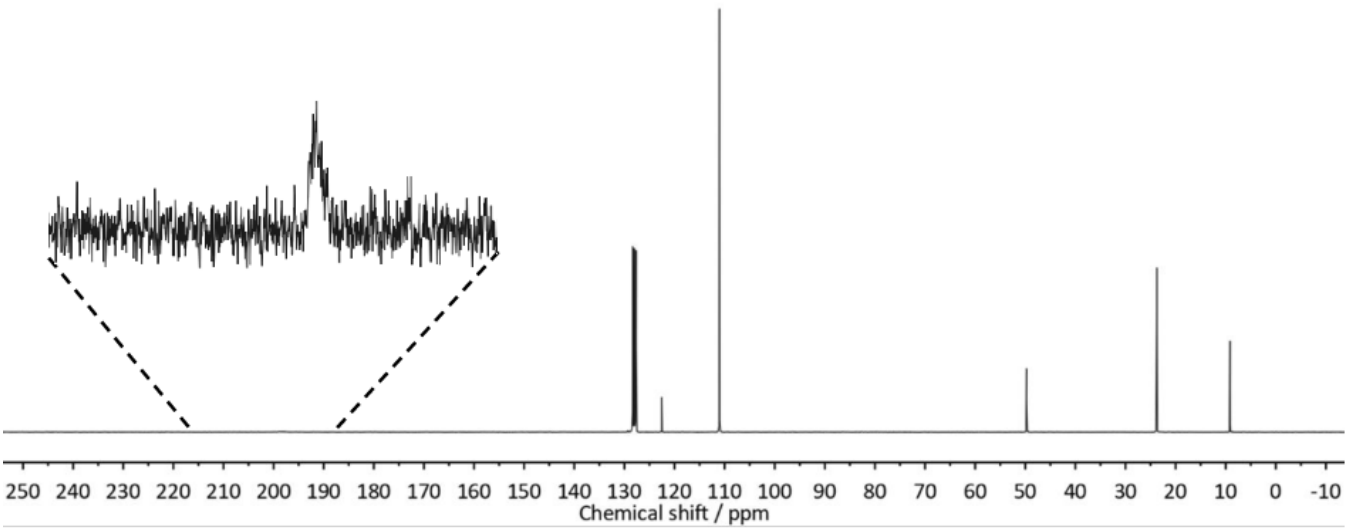

Figure S2: $^{13}C\{^{1}H\}$ NMR spectrum of **3a**.

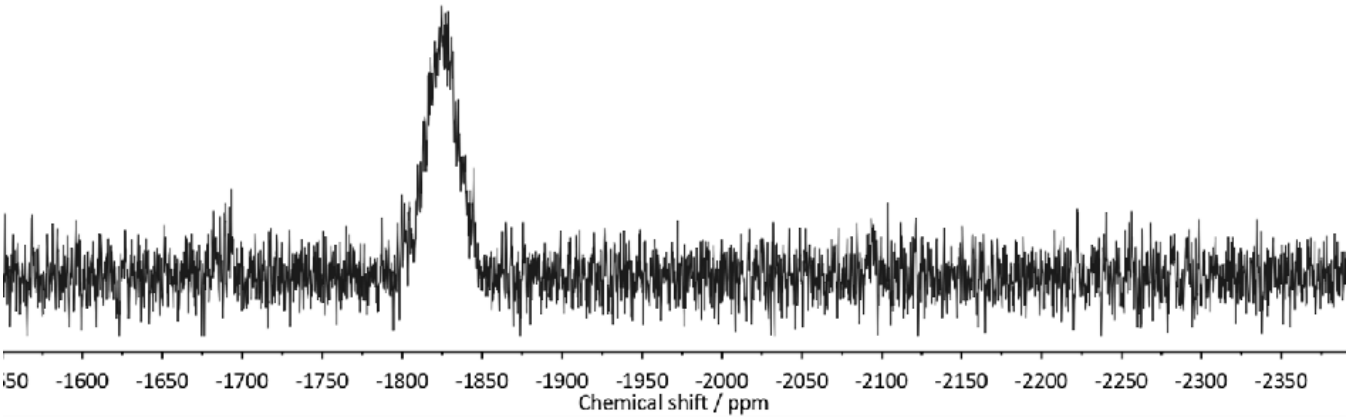

Figure S3: $^{119}Sn\{^{1}H\}$ NMR spectrum of **3a**.

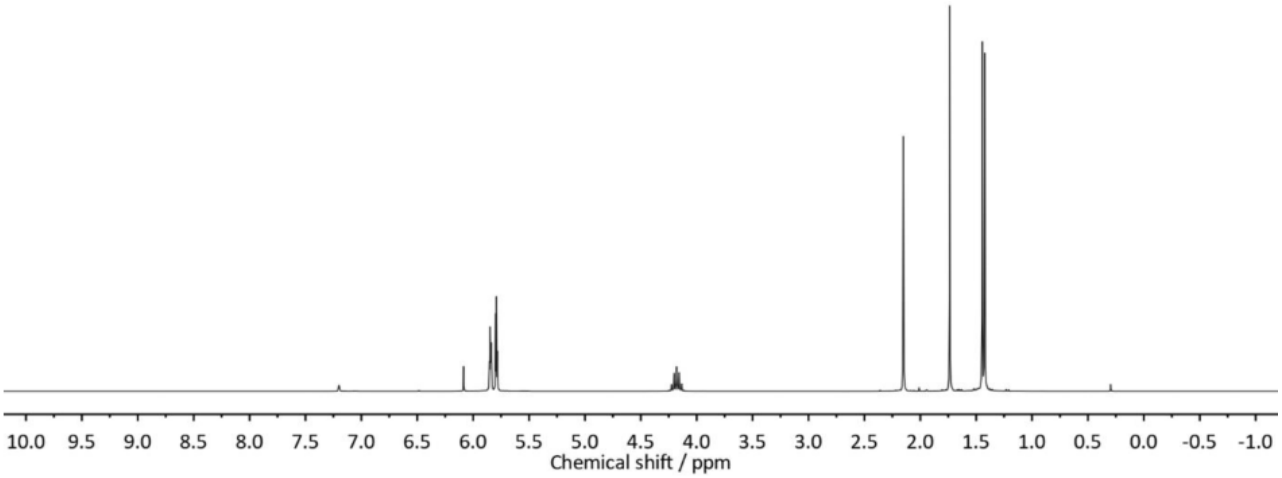

Figure S4: ^{1}H NMR spectrum of **3b**.

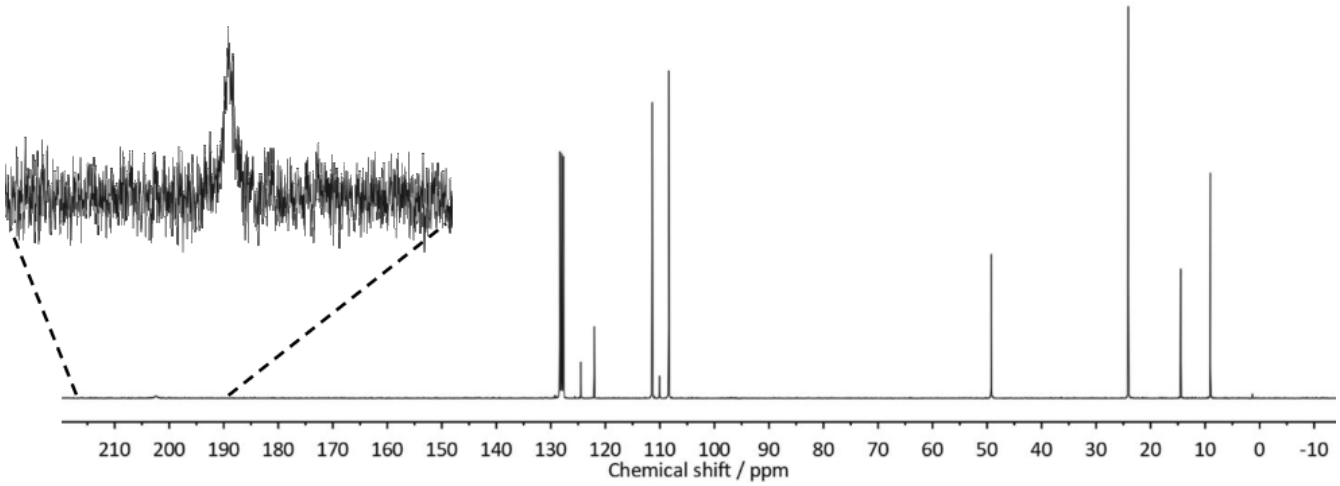

Figure S5: ^{13}C{^{1}H} NMR spectrum of **3b**.

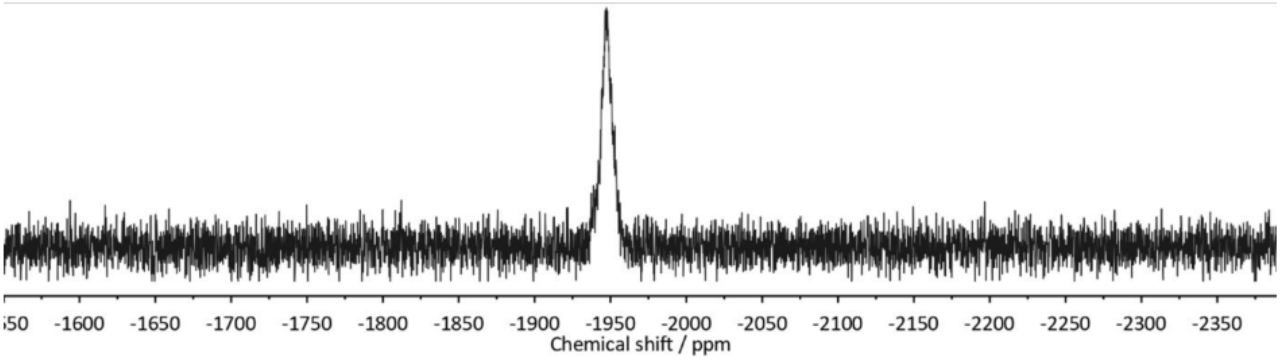

Figure S6: ^{119}Sn{^{1}H} NMR spectrum of **3b**.

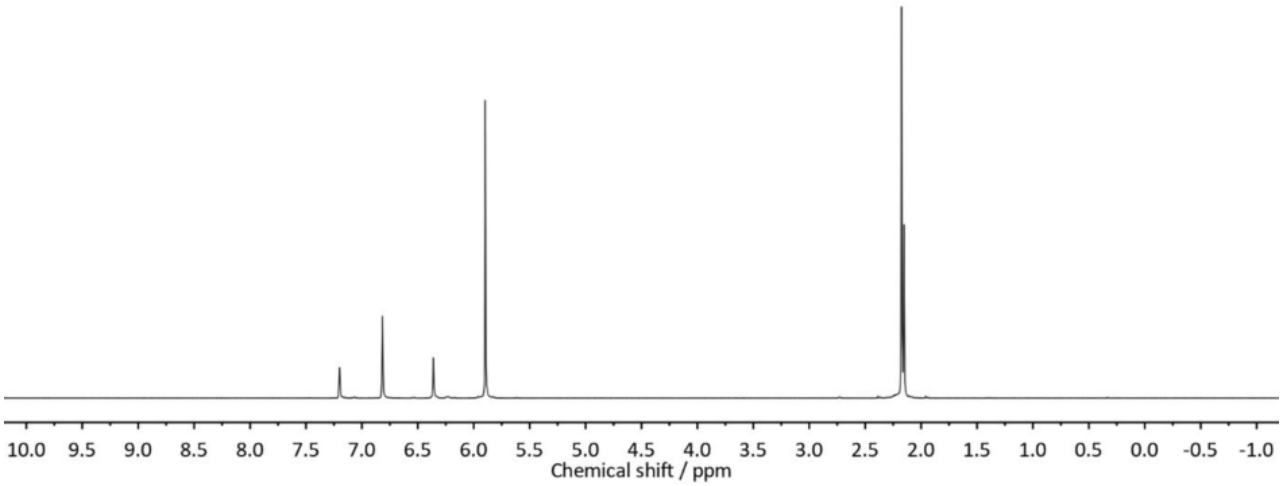

Figure S7: ^{1}H NMR spectrum of **3c**.

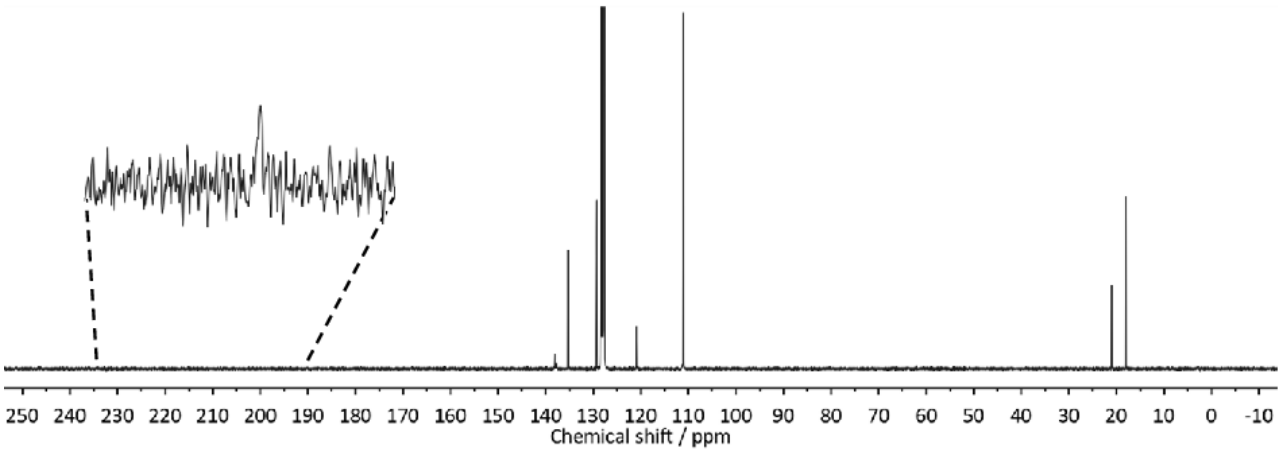

Figure S8: ^{13}C{^{1}H} NMR spectrum of **3c**.

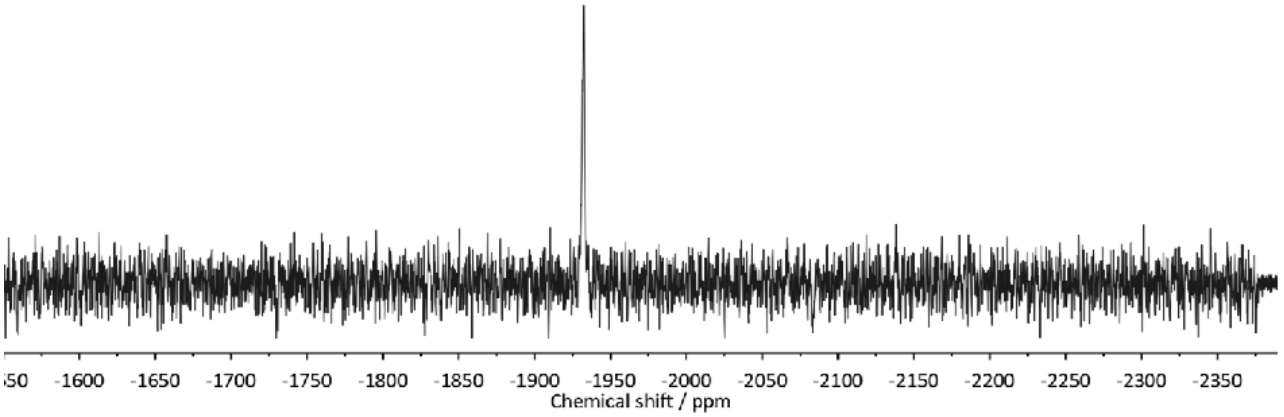

Figure S9: ^{119}Sn{^{1}H} NMR spectrum of **3c**.

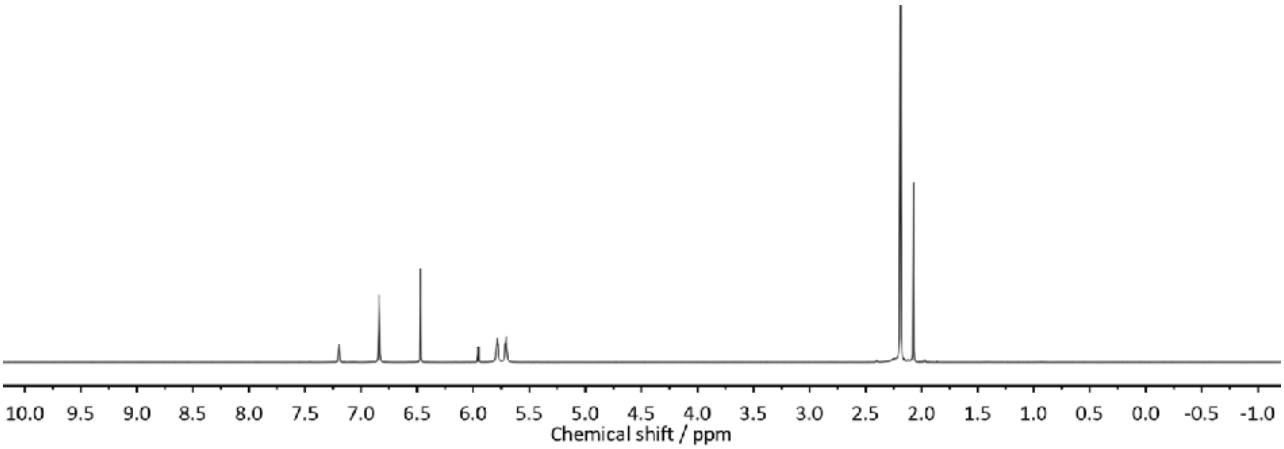

Figure S10: ^{1}H NMR spectrum of **3d**.

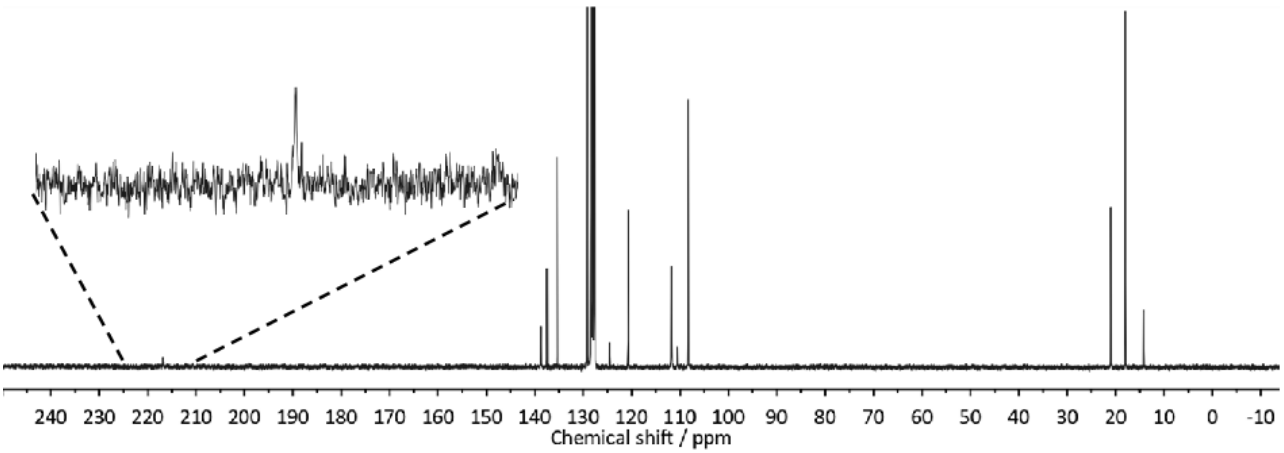

Figure S11: ^{13}C{^{1}H NMR spectrum of **3d**.

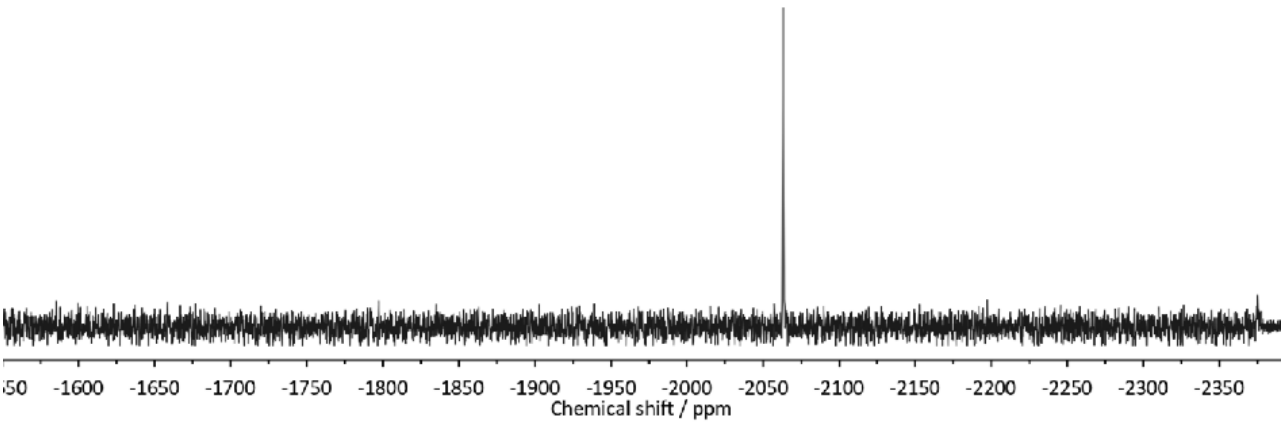

Figure S12: ^{119}Sn{^{1}H} NMR spectrum of **3d**.

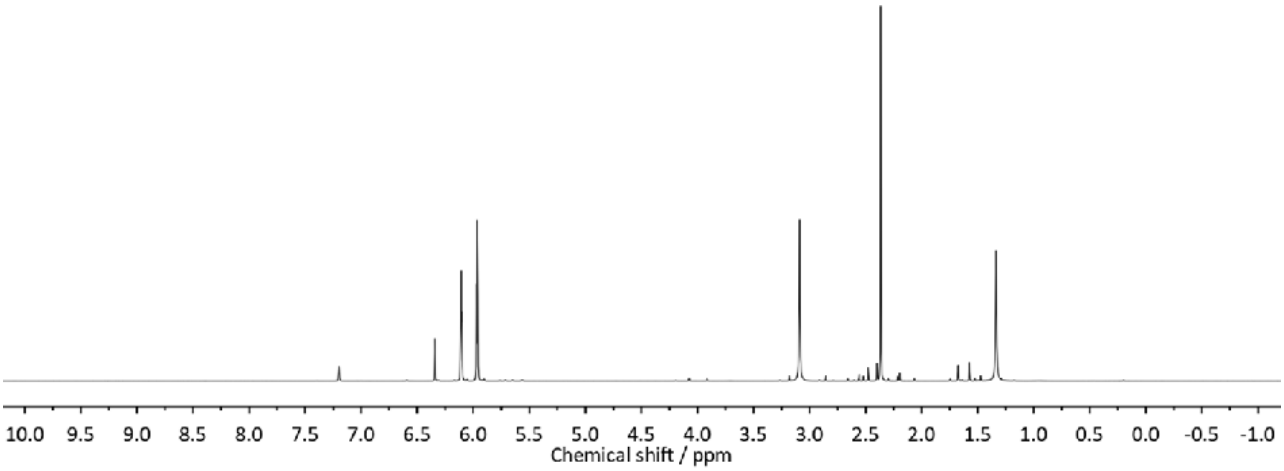

Figure S13: ^{1}H NMR spectrum of **3e** (beginning decomposition is indicated by multiple additional signals).

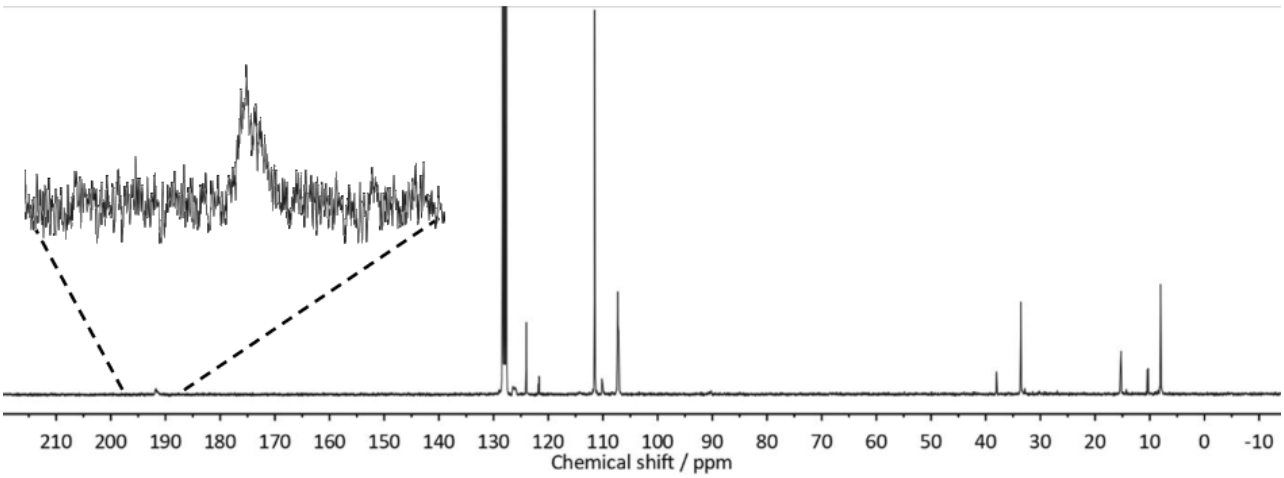

Figure S14: ^{13}C{^{1}H} NMR spectrum of **3e** (beginning decomposition is indicated by additional signals at 10.3, 38.0, 110.1, 121.9, 126.2).

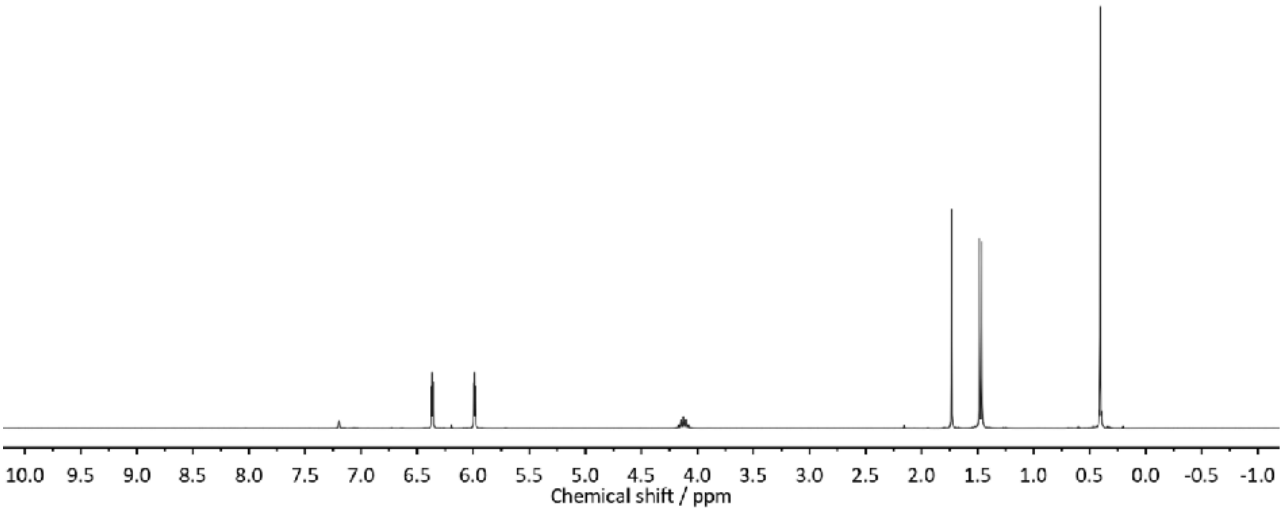

Figure S15: ^{1}H NMR spectrum of **3f**.

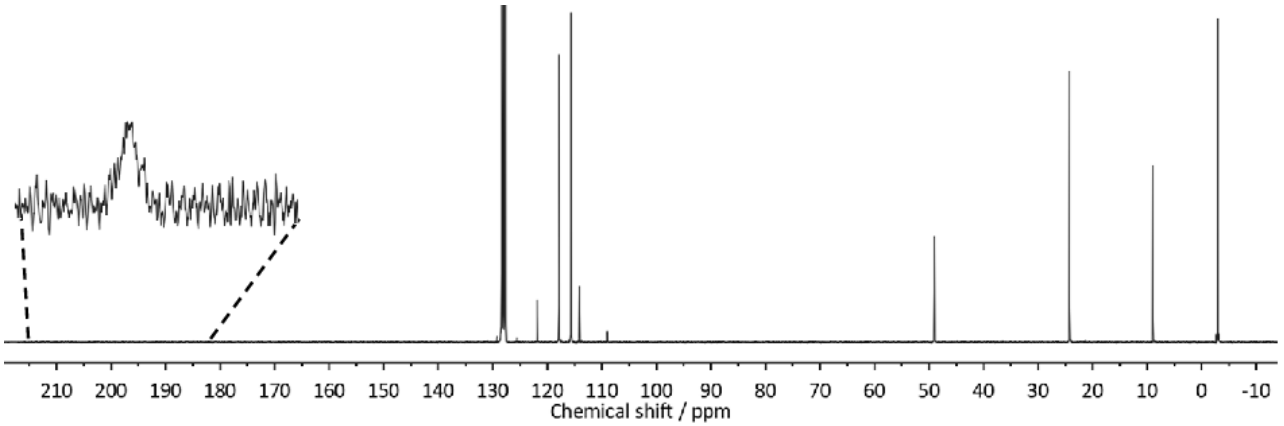

Figure S16: $^{13}C\{^{1}H\}$ NMR spectrum of **3f**.

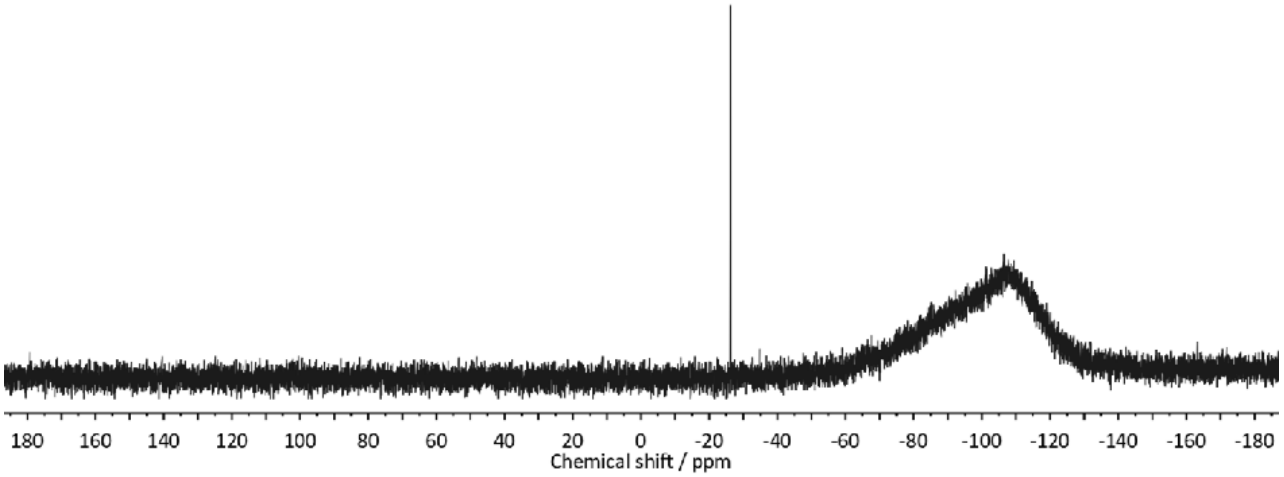

Figure S17: $^{29}Si\{^{1}H\}$ NMR spectrum of **3f**.

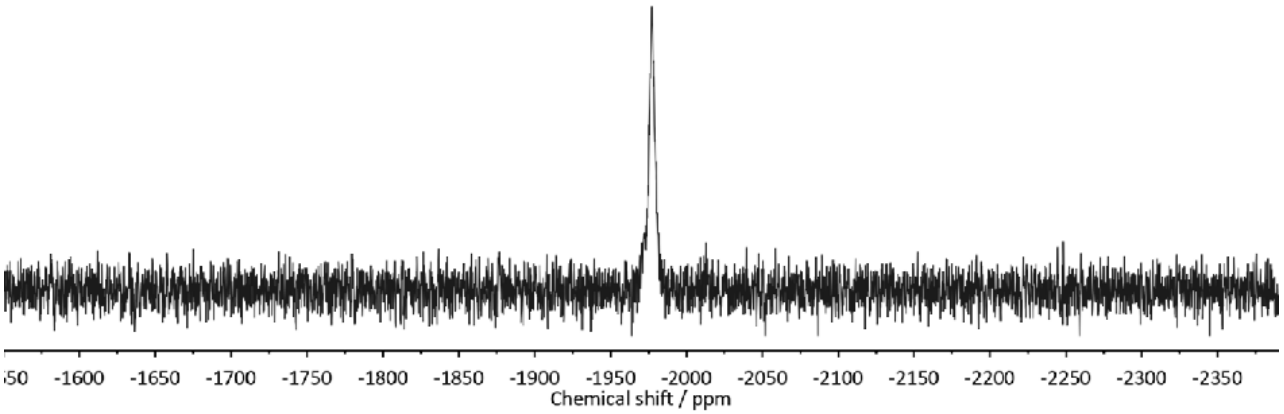

Figure S18: $^{119}Sn\{^{1}H\}$ NMR spectrum of **3f**.

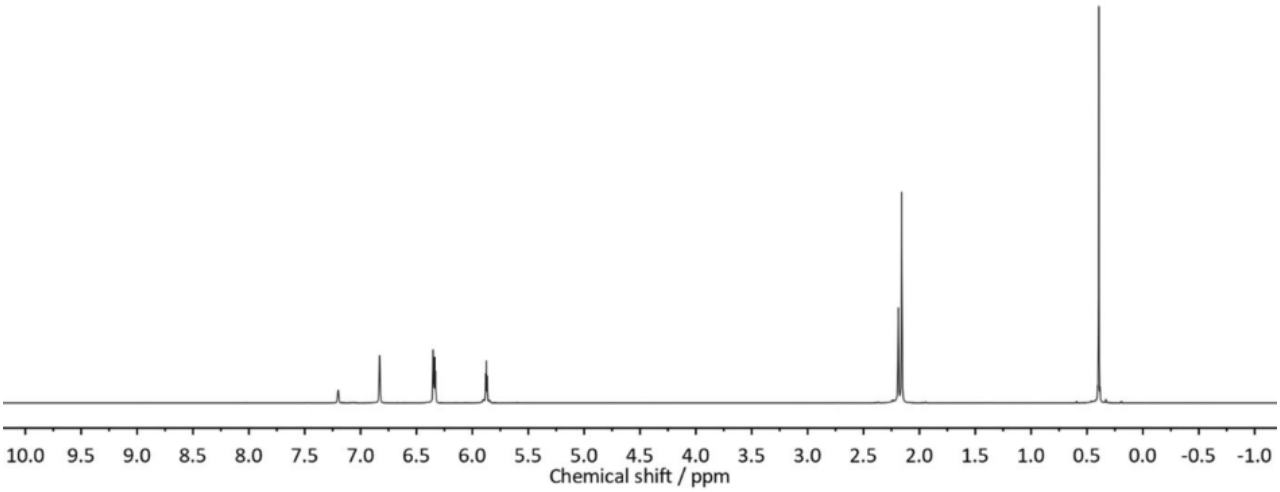

Figure S19: ^{1}H NMR spectrum of **3g**.

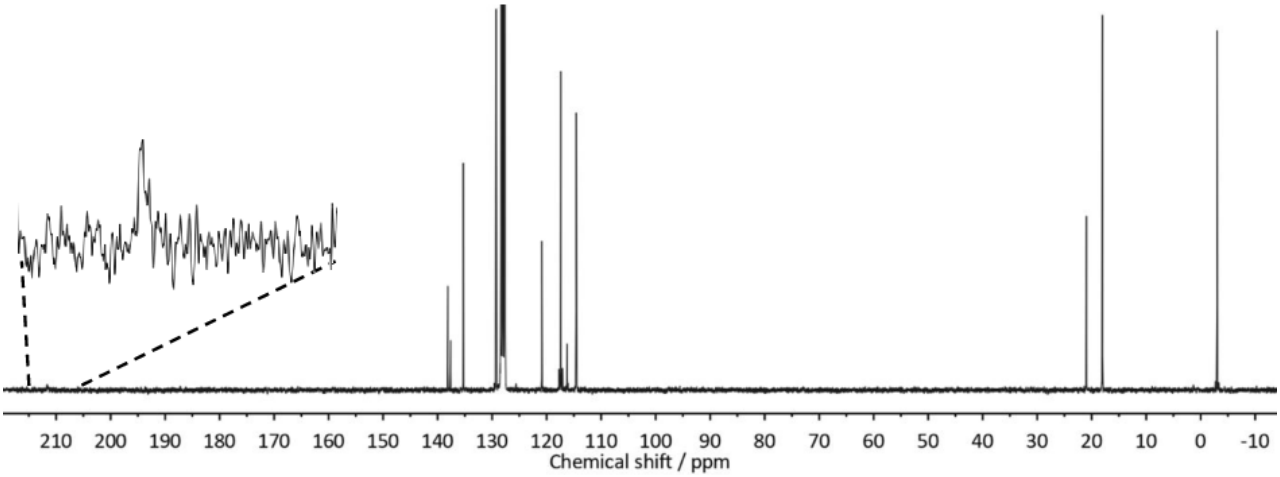

Figure S20: ^{13}C{^{1}H} NMR spectrum of **3g**.

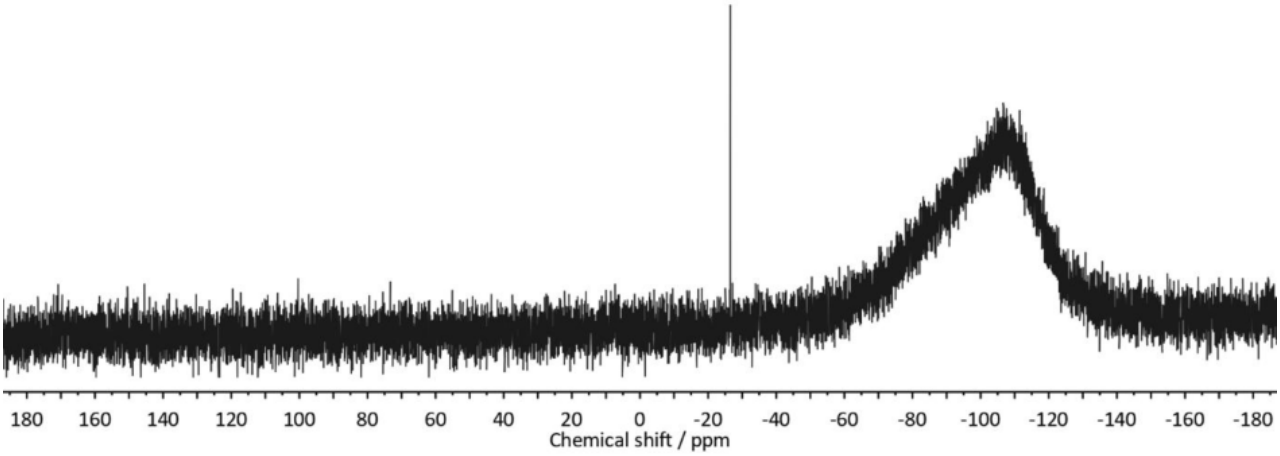

Figure S21: ^{29}Si{^{1}H} NMR spectrum of **3f**.

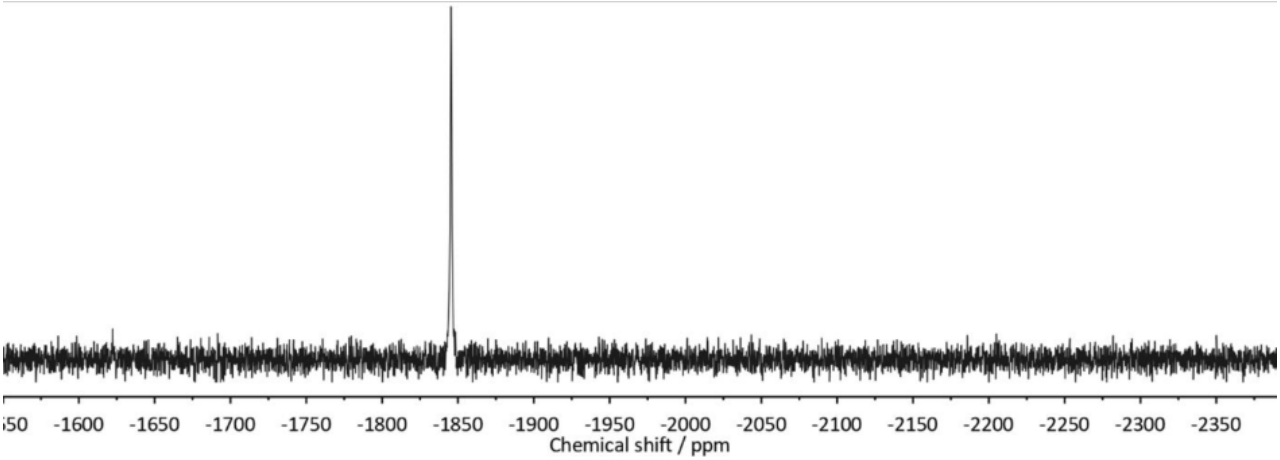

Figure S22: $^{119}Sn\{^{1}H\}$ NMR spectrum of **3g**.

3. XRD Data

All crystal structure data has been deposited with the Cambridge Crystallographic Data Centre (CCDC) and is available free of charge from the Cambridge Structural Database (see CCDC numbers).

Crystallographic data for 3a

CCDC deposition number:	1844881	
Empirical formula:	$C_{21}H_{30}N_2Sn$	
Formula weight:	429.16	
Temperature:	152(2) K	
Wavelength:	0.71073 Å	
Crystal system:	monoclinic	
Space group:	$P2_1/n$	
Unit cell dimensions:	a = 15.7274(11) Å	α = 90°
	b = 14.7260(10) Å	β = 102.406(2)°
	c = 17.8469(12) Å	γ = 90°
Volume:	4036.9(5) $Å^3$	
Z:	8	
Density (calculated):	1.412 mg/m^3	
Absorption coefficient:	1.270 mm^{-1}	
F(000):	1760	
Crystal size:	0.312 x 0.226 x 0.042 mm^3	
Theta range for data collection:	1.567 to 29.174°	
Index ranges:	-21<=h<=21, -14<=k<=20, -24<=l<=23	
Reflections collected:	42408	
Independent reflections:	10868 [R(int) = 0.0607]	
Completeness to theta = 25.242°:	99.8 %	
Absorption correction:	semi-empirical from equivalents	
Max. and min. transmission:	0.7458 and 0.5977	
Refinement method:	full-matrix least-squares on F^2	
Data / restraints / parameters:	10868 / 6 / 456	
Goodness-of-fit on F^2:	1.015	
Final R indices [I>2sigma(I)]:	R1 = 0.0395, wR2 = 0.0805	
R indices (all data):	R1 = 0.0674, wR2 = 0.0916	
Extinction coefficient:	n/a	
Largest diff. peak and hole:	1.655 and -0.661 e.$Å^{-3}$	

Crystallographic data for 3b

CCDC deposition number:	1844882	
Empirical formula:	$C_{23}H_{34}N_2Sn$	
Formula weight:	457.21	
Temperature:	152(2) K	
Wavelength:	0.71073 Å	
Crystal system:	monoclinic	
Space group:	P21/c	
Unit cell dimensions:	a = 9.1199(3) Å	α = 90°
	b = 14.8902(5) Å	β = 91.1084(18)°
	c = 16.4815(6) Å	γ = 90°
Volume:	2237.72(13) $Å^3$	
Z:	4	
Density (calculated):	1.357 mg/m^3	
Absorption coefficient:	1.150 mm^{-1}	
F(000):	944	
Crystal size:	0.515 x 0.346 x 0.252 mm^3	
Theta range for data collection:	1.843 to 37.288°	
Index ranges:	-15<=h<=15, -25<=k<=20, -27<=l<=27	
Reflections collected:	45794	
Independent reflections:	11540 [R(int) = 0.0209]	
Completeness to theta = 25.242°:	100.0 %	
Absorption correction:	semi-empirical from equivalents	
Max. and min. transmission:	0.7473 and 0.6698	
Refinement method:	full-matrix least-squares on F2	
Data / restraints / parameters:	11540 / 0 / 243	
Goodness-of-fit on F^2:	1.105	
Final R indices [I>2sigma(I)]:	R1 = 0.0267, wR2 = 0.0605	
R indices (all data):	R1 = 0.0340, wR2 = 0.0630	
Extinction coefficient:	n/a	
Largest diff. peak and hole:	1.098 and -0.915 $e.Å^{-3}$	

Crystallographic data for 3c

CCDC deposition number:	1844883	
Empirical formula:	$C_{31}H_{34}N_2Sn$	
Formula weight:	553.29	
Temperature:	152(2) K	
Wavelength:	0.71073 Å	
Crystal system:	orthorhombic	
Space group:	P212121	
Unit cell dimensions:	a = 11.0570(4) Å	α = 90°
	b = 15.1919(5) Å	β = 90°
	c = 15.8899(6) Å	γ = 90°
Volume:	2669.14(16) $Å^3$	
Z:	4	
Density (calculated):	1.377 mg/m^3	
Absorption coefficient:	0.978 mm^{-1}	
F(000):	1136	
Crystal size:	0.310 x 0.200 x 0.200 mm^3	
Theta range for data collection:	1.855 to 32.905°	
Index ranges:	-16<=h<=16, -22<=k<=23, -24<=l<=24	
Reflections collected:	38321	
Independent reflections:	9973 [R(int) = 0.0379]	
Completeness to theta = 25.242°:	100.0 %	
Absorption correction:	semi-empirical from equivalents	
Max. and min. transmission:	0.7465 and 0.6930	
Refinement method:	full-matrix least-squares on F^2	
Data / restraints / parameters:	9973 / 0 / 377	
Goodness-of-fit on F^2:	1.008	
Final R indices [I>2sigma(I)]:	R1 = 0.0268, wR2 = 0.0548	
R indices (all data):	R1 = 0.0322, wR2 = 0.0568	
Absolute structure parameter:	0.007(8)	
Extinction coefficient:	n/a	
Largest diff. peak and hole:	0.628 and -0.567 $e.Å^{-3}$	

Crystallographic data for 3d

CCDC deposition number:	1844884	
Empirical formula:	$C_{33}H_{38}N_2Sn$	
Formula weight:	581.34	
Temperature:	142(2) K	
Wavelength:	0.71073 Å	
Crystal system:	monoclinic	
Space group:	P21/n	
Unit cell dimensions:	a = 19.3318(11) Å	α = 90°
	b = 16.3218(10) Å	β = 112.297(3)°
	c = 19.4825(11) Å	γ = 90°
Volume:	5687.7(6) $Å^3$	
Z:	8	
Density (calculated):	1.358 mg/m^3	
Absorption coefficient:	0.922 mm^{-1}	
F(000):	2400	
Crystal size:	0.250 x 0.144 x 0.076 mm^3	
Theta range for data collection:	1.263 to 28.807°	
Index ranges:	-26<=h<=14, -22<=k<=21, -26<=l<=26	
Reflections collected:	55706	
Independent reflections:	14727 [R(int) = 0.0614]	
Completeness to theta = 25.242°:	100.0 %	
Absorption correction:	semi-empirical from equivalents	
Max. and min. transmission:	0.7458 and 0.6997	
Refinement method:	full-matrix least-squares on F^2	
Data / restraints / parameters:	14727 / 0 / 665	
Goodness-of-fit on F^2:	0.991	
Final R indices [I>2sigma(I)]:	R1 = 0.0440, wR2 = 0.0756	
R indices (all data):	R1 = 0.0945, wR2 = 0.0895	
Extinction coefficient:	n/a	
Largest diff. peak and hole:	0.723 and -0.885 $e.Å^{-3}$	

Crystallographic data for 3e

CCDC deposition number:	1844885	
Empirical formula:	$C_{19}H_{26}N_2Sn$	
Formula weight:	401.11	
Temperature:	142(2) K	
Wavelength:	0.71073 Å	
Crystal system:	Monoclinic	
Space group:	P21/n	
Unit cell dimensions:	a = 8.9161(3) Å	α = 90°
	b = 12.8448(4) Å	β = 94.118(2)°
	c = 16.1380(5) Å	γ = 90°
Volume:	1843.44(10) $Å^3$	
Z:	4	
Density (calculated):	1.445 mg/m^3	
Absorption coefficient:	1.385 mm^{-1}	
F(000):	816	
Crystal size:	0.513 x 0.171 x 0.084 mm^3	
Theta range for data collection:	2.028 to 36.363°	
Index ranges:	-14<=h<=14, -19<=k<=21, -26<=l<=26	
Reflections collected:	34893	
Independent reflections:	8944 [R(int) = 0.0207]	
Completeness to theta = 25.242°:	100.0 %	
Absorption correction:	Semi-empirical from equivalents	
Max. and min. transmission:	0.7471 and 0.6151	
Refinement method:	Full-matrix least-squares on F^2	
Data / restraints / parameters:	8944 / 0 / 264	
Goodness-of-fit on F^2:	1.071	
Final R indices [I>2sigma(I)]:	R1 = 0.0331, wR2 = 0.0796	
R indices (all data):	R1 = 0.0415, wR2 = 0.0839	
Extinction coefficient:	n/a	
Largest diff. peak and hole:	3.308 and -1.098 $e.Å^{-3}$	

Crystallographic data for 3f

CCDC deposition number:	1844886	
Empirical formula:	$C_{25}H_{38}N_2Si_2Sn$	
Formula weight:	541.44	
Temperature:	152(2) K	
Wavelength:	0.71073 Å	
Crystal system:	monoclinic	
Space group:	P21/c	
Unit cell dimensions:	a = 10.3388(3) Å	α = 90°
	b = 15.7157(5) Å	β = 101.3846(15)°
	c = 17.0210(5) Å	γ = 90°
Volume:	2711.18(14) $Å^3$	
Z:	4	
Density (calculated):	1.326 mg/m^3	
Absorption coefficient:	1.045 mm^{-1}	
F(000):	1120	
Crystal size:	0.440 x 0.337 x 0.210 mm^3	
Theta range for data collection:	1.780 to 37.952°	
Index ranges:	-17<=h<=17, -27<=k<=20, -29<=l<=25	
Reflections collected:	58823	
Independent reflections:	14694 [R(int) = 0.0236]	
Completeness to theta = 25.242°:	100.0 %	
Absorption correction:	semi-empirical from equivalents	
Max. and min. transmission:	0.7474 and 0.6381	
Refinement method:	full-matrix least-squares on F^2	
Data / restraints / parameters:	14694 / 0 / 281	
Goodness-of-fit on F^2:	1.051	
Final R indices [I>2sigma(I)]:	R1 = 0.0351, wR2 = 0.0792	
R indices (all data):	R1 = 0.0548, wR2 = 0.0871	
Extinction coefficient:	n/a	
Largest diff. peak and hole:	1.386 and -1.008 $e.Å^{-3}$	

Crystallographic data for 3g

CCDC deposition number:	1844887	
Empirical formula:	$C_{35}H_{44}N_2Si_2Sn$	
Formula weight:	667.59	
Temperature:	152(2) K	
Wavelength:	0.71073 Å	
Crystal system:	orthorhombic	
Space group:	P212121	
Unit cell dimensions:	a = 13.5180(3) Å	α = 90°
	b = 14.6994(4) Å	β = 90°
	c = 17.2365(4) Å	γ = 90°
Volume:	3425.00(14) $Å^3$	
Z:	4	
Density (calculated):	1.295 mg/m^3	
Absorption coefficient:	0.841 mm^{-1}	
F(000):	1384	
Crystal size:	0.436 x 0.208 x 0.060 mm^3	
Theta range for data collection:	1.821 to 35.799°	
Index ranges:	-22<=h<=22, -23<=k<=24, -28<=l<=28	
Reflections collected:	121862	
Independent reflections:	15955 [R(int) = 0.0373]	
Completeness to theta = 25.242°:	100.0 %	
Absorption correction:	semi-empirical from equivalents	
Max. and min. transmission:	0.7470 and 0.6794	
Refinement method:	full-matrix least-squares on F^2	
Data / restraints / parameters:	15955 / 0 / 371	
Goodness-of-fit on F^2:	1.038	
Final R indices [I>2sigma(I)]:	R1 = 0.0267, wR2 = 0.0572	
R indices (all data):	R1 = 0.0344, wR2 = 0.0602	
Absolute structure parameter:	-0.012(4)	
Extinction coefficient:	n/a	
Largest diff. peak and hole:	0.456 and -0.339 $e.Å^{-3}$	

4. Computational Details

All calculations were performed using the Gaussian 09, Revision D.01[11] package of programs.
All geometry optimizations have been carried out at the B3LYP[12-15]-D3[16]/6-311+G(d,p)[17-21](C,H,N,Si);SDD[22-23](Sn) level of theory, with and without solvent corrections employing the Polarizable Continuum Model (PCM)[24] with parameters for benzene for, and starting from the corresponding crystal structure. Every optimized structure was confirmed to be a minimum on the potential energy surface by a subsequent frequency analysis (all positive eigenvalues).
In all cases, the calculated Sn-C^{NHC} bond lengths are longer than what is observed experimentally in the crystal structures and the bond lengths increase when solvent corrections are omitted. This is a known phenomenon for DFT calculations of Lewis acid-base-complexes.[25-28]

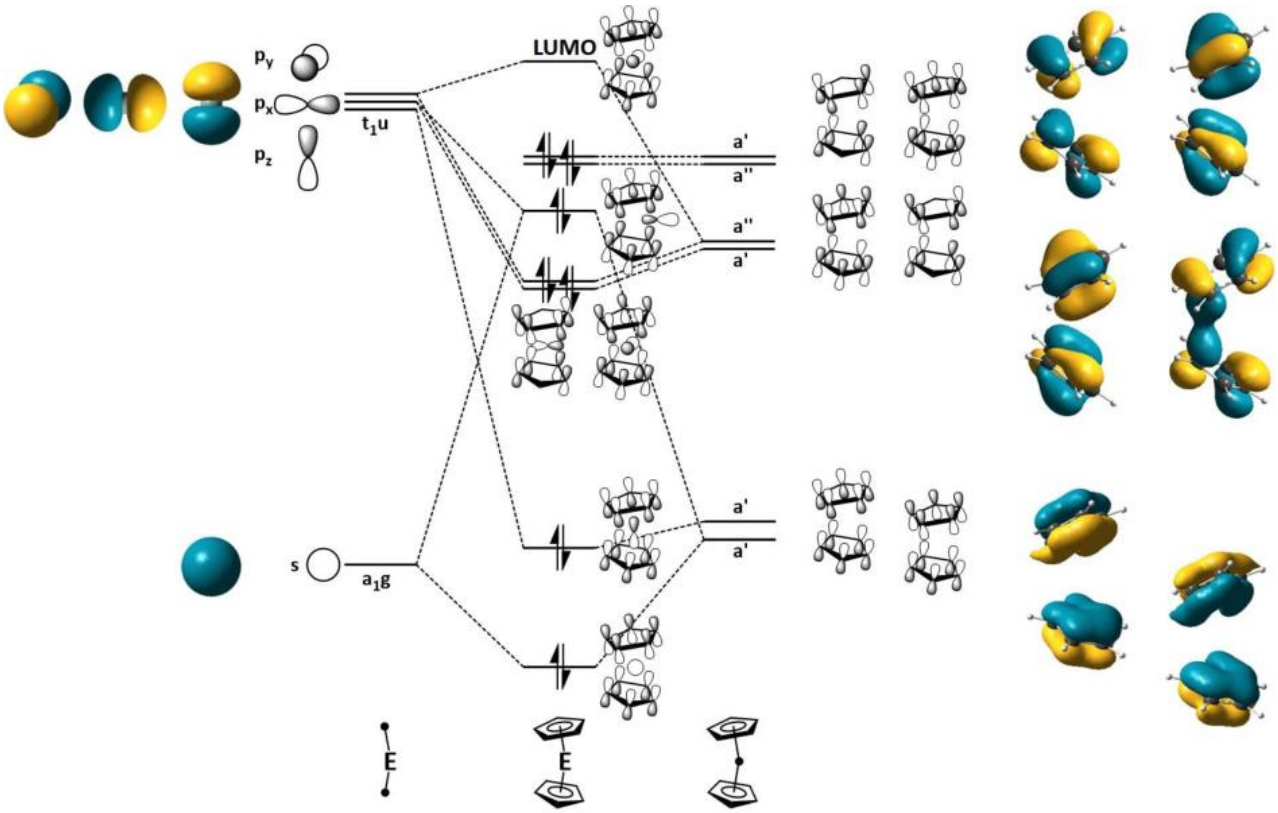

Figure S23: Qualitative molecular orbital diagram for Cp_2E (E = Si-Pb). Orbitals calculated using Cp_2Si as model compound at the B3LYP-D3/cc-pVTZ[29-33] level of theory (isodensity value for surface plots: 0.04).

Table S2: Calculated Sn-C^{NHC} bond lengths and bond dissociation energies (BDEs) for complexes **3a**-**g**.

	B3LYP-D3/6-311+G(d,p)(C,H,N,Si);SDD(Sn)		B3LYP-D3/6-311+G(d,p)(C,H,N,Si);SDD(Sn)/ PCM(benzene)		B3LYP/ 6-311+G(d,p)(C,H,N,Si); SDD(Sn) // B3LYP-D3/ 6-311+G(d,p)(C,H,N,Si); SDD(Sn)/ PCM(benzene)
compound	Sn-C^{NHC}	BDE	Sn-C^{NHC}	BDE	BDE
3a	260.6 pm	66.8 kJ·mol^{-1}	255.3 pm	70.7 kJ·mol^{-1}	12.2 kJ·mol^{-1}
3b	259.3 pm	69.3 kJ·mol^{-1}	254.9 pm	72.1 kJ·mol^{-1}	7.8 kJ·mol^{-1}
3c	255.5 pm	85.1 kJ·mol^{-1}	252.0 pm	88.0 kJ·mol^{-1}	8.1 kJ·mol^{-1}
3d	265.2 pm	82.1 kJ·mol^{-1}	259.1 pm	83.6 kJ·mol^{-1}	0.2 kJ·mol^{-1}
3e	251.4 pm	61.8 kJ·mol^{-1}	247.6 pm	65.9 kJ·mol^{-1}	19.2 kJ·mol^{-1}
3f	261.3 pm	71.8 kJ·mol^{-1}	256.1 pm	74.9 kJ·mol^{-1}	9.9 kJ·mol^{-1}
3g	258.0 pm	95.3 kJ·mol^{-1}	254.0 pm	96.6 kJ·mol^{-1}	3.8 kJ·mol^{-1}

Optimized geometries of Cp_2Si, 1a-c, 2a-c and 3a-g

Cp_2Si (B3LYP-D3/cc-pVTZ)

1	14	0	0.000001	-0.000004	-0.440192
2	6	0	-2.811178	0.278719	-0.893861
3	6	0	-2.245004	1.195170	0.003695
4	6	0	-2.522932	-1.018651	-0.447177
5	1	0	-3.321002	0.530510	-1.809694
6	6	0	-1.588302	0.464329	1.031502
7	1	0	-2.272415	2.269975	-0.076594
8	6	0	-1.768486	-0.926462	0.742476
9	1	0	-2.782991	-1.935797	-0.950726
10	1	0	-1.166445	0.873234	1.935293
11	1	0	-1.446164	-1.746680	1.363279
12	6	0	2.811146	-0.278927	-0.893824
13	6	0	2.244890	-1.195188	0.003876
14	6	0	2.523025	1.018539	-0.447335
15	1	0	3.320937	-0.530906	-1.809624
16	6	0	1.588266	-0.464124	1.031578
17	1	0	2.272209	-2.270008	-0.076243
18	6	0	1.768577	0.926602	0.742333
19	1	0	2.783161	1.935583	-0.951030
20	1	0	1.166389	-0.872844	1.935442
21	1	0	1.446314	1.746944	1.363003

1a (B3LYP-D3/6-311+G(d,p)(C,H),SDD(Sn);SCRF=PCM,benzene)

1	6	0	-1.863815	1.362752	-0.252739
2	6	0	-2.365119	0.417868	-1.193836
3	6	0	-2.921303	-0.666169	-0.472190
4	6	0	1.922256	1.219517	0.645150
5	6	0	2.528740	0.046592	1.176770
6	6	0	2.962657	-0.753337	0.095977
7	6	0	2.630307	-0.093496	-1.106354
8	6	0	1.984637	1.130561	-0.778476
9	6	0	-2.109188	0.842316	1.053087
10	6	0	-2.765564	-0.408860	0.904615
11	50	0	-0.000567	-0.436488	-0.010149
12	1	0	1.671931	1.894745	-1.476328
13	1	0	2.837132	-0.447451	-2.106575
14	1	0	3.449080	-1.715077	0.176865
15	1	0	2.653639	-0.176834	2.227054
16	1	0	-3.371617	-1.547653	-0.906136
17	1	0	-3.084786	-1.051566	1.712899
18	1	0	-1.897863	1.347001	1.985513
19	1	0	-2.357429	0.533329	-2.268674
20	1	0	1.560712	2.065124	1.213509
21	1	0	-1.454095	2.336340	-0.482715

1a (B3LYP-D3/6-311+G(d,p)(C,H),SDD(Sn))

1	6	0	-1.871660	-1.361310	0.250707
2	6	0	-2.365804	-0.414771	1.193673
3	6	0	-2.915957	0.673473	0.474496
4	6	0	1.933196	-1.210095	-0.657656
5	6	0	2.536042	-0.028135	-1.172418
6	6	0	2.958075	0.762300	-0.080795
7	6	0	2.622889	0.087495	1.111939
8	6	0	1.986623	-1.136580	0.766975
9	6	0	-2.115874	-0.837526	-1.053713
10	6	0	-2.764016	0.417245	-0.902367
11	50	0	-0.000557	0.429848	0.009757
12	1	0	1.679819	-1.912507	1.454275
13	1	0	2.825582	0.429687	2.116937
14	1	0	3.441966	1.726128	-0.148229
15	1	0	2.669002	0.206066	-2.219224
16	1	0	-3.363084	1.555455	0.910252
17	1	0	-3.083563	1.061464	-1.709095
18	1	0	-1.913726	-1.344143	-1.987030
19	1	0	-2.361541	-0.533719	2.268038
20	1	0	1.585224	-2.053570	-1.237387
21	1	0	-1.472910	-2.339849	0.478542

1b (B3LYP-D3/6-311+G(d,p)(C,H),SDD(Sn);SCRF=PCM,benzene)

1	6	0	-1.628629	1.270934	1.217961
2	6	0	-2.113888	1.872782	0.026303
3	6	0	-2.839513	0.897525	-0.694317
4	6	0	1.628659	-1.271013	1.217945
5	6	0	2.113894	-1.872813	0.026256
6	6	0	2.839492	-0.897525	-0.694354
7	6	0	2.820234	0.316415	0.029249
8	6	0	2.062565	0.092360	1.216266
9	6	0	-2.062588	-0.092426	1.216267
10	6	0	-2.820279	-0.316431	0.029266
11	50	0	0.000008	0.000029	-0.385155
12	1	0	1.930529	0.802701	2.021564

13	1	0	3.318740	-1.044445	-1.652871
14	1	0	1.956910	-2.900541	-0.270241
15	1	0	-3.318766	1.044477	-1.652827
16	1	0	-1.930546	-0.802780	2.021551
17	1	0	-1.956874	2.900509	-0.270186
18	1	0	1.100546	-1.768700	2.019336
19	1	0	-1.100547	1.768599	2.019386
20	6	0	3.539375	1.584508	-0.331709
21	1	0	3.023585	2.464852	0.060614
22	1	0	4.553564	1.589200	0.083300
23	1	0	3.629683	1.699054	-1.414911
24	6	0	-3.539385	-1.584524	-0.331762
25	1	0	-3.023494	-2.464884	0.060391
26	1	0	-4.553528	-1.589336	0.083357
27	1	0	-3.629803	-1.698937	-1.414969

1b (B3LYP-D3/6-311+G(d,p)(C,H),SDD(Sn))

1	6	0	-1.619099	0.933968	1.430610
2	6	0	-1.885668	1.820485	0.350635
3	6	0	-2.686514	1.129812	-0.592267
4	6	0	1.789397	-1.088823	1.329351
5	6	0	2.221364	-1.815643	0.187762
6	6	0	2.841931	-0.910106	-0.700405
7	6	0	2.812071	0.384058	-0.131505
8	6	0	2.153891	0.279754	1.127914
9	6	0	-2.258787	-0.308318	1.130244
10	6	0	-2.925328	-0.177611	-0.119778
11	50	0	-0.003073	-0.103995	-0.303569
12	1	0	2.044706	1.079401	1.848387
13	1	0	3.260739	-1.157395	-1.666390
14	1	0	2.098925	-2.878554	0.033656
15	1	0	-3.046068	1.532462	-1.529451
16	1	0	-2.303217	-1.171727	1.780650
17	1	0	-1.564458	2.850581	0.283958
18	1	0	1.349393	-1.504262	2.225154
19	1	0	-1.109571	1.181219	2.351268
20	6	0	3.441965	1.624241	-0.697213
21	1	0	2.911654	2.525931	-0.379552
22	1	0	4.480396	1.721170	-0.361069
23	1	0	3.452941	1.605565	-1.789974
24	6	0	-3.781757	-1.221477	-0.777398
25	1	0	-3.465586	-2.231547	-0.504043
26	1	0	-4.829534	-1.114871	-0.474856
27	1	0	-3.747468	-1.140231	-1.866995

1c (B3LYP-D3/6-311+G(d,p)(C,H),SDD(Sn);SCRF=PCM,benzene)

1	50	0	-1.691703	0.000000	0.000000
2	14	0	1.865747	-1.114974	0.397989
3	14	0	1.865747	1.114974	-0.397989
4	6	0	0.172508	-1.822465	-0.019081
5	6	0	-0.754591	-2.443174	0.885499
6	6	0	-1.843551	-2.964377	0.148301
7	6	0	3.222576	-2.160677	-0.408789
8	1	0	3.182504	-3.191885	-0.044701
9	1	0	4.215306	-1.758088	-0.183941
10	6	0	2.063576	-1.159324	2.280824
11	1	0	1.275823	-0.586985	2.778996
12	1	0	3.026345	-0.736562	2.581960
13	1	0	2.017015	-2.188447	2.650683
14	6	0	0.172508	1.822465	0.019081
15	6	0	-0.754591	2.443175	-0.885499
16	6	0	-1.843551	2.964377	-0.148301
17	6	0	-1.632745	2.669861	1.213576
18	6	0	-0.410884	1.959995	1.327303
19	6	0	3.222576	2.160677	0.408789
20	1	0	4.215306	1.758088	0.183941
21	6	0	2.063576	1.159324	-2.280824
22	1	0	3.026345	0.736562	-2.581961
23	1	0	2.017015	2.188447	-2.650683
24	1	0	3.106192	2.182538	1.495937
25	1	0	3.182504	3.191885	0.044701
26	6	0	-0.410884	-1.959995	-1.327302
27	6	0	-1.632745	-2.669861	-1.213576
28	1	0	3.106191	-2.182538	-1.495938
29	1	0	1.275822	0.586985	-2.778996
30	1	0	-2.695951	-3.485361	0.562022
31	1	0	-2.290089	-2.930367	-2.031741
32	1	0	0.047173	-1.641893	-2.254901
33	1	0	-0.613530	-2.536229	1.954088
34	1	0	-2.290089	2.930367	2.031742
35	1	0	0.047173	1.641893	2.254901
36	1	0	-2.695951	3.485361	-0.562022
37	1	0	-0.613530	2.536230	-1.954088

1c (B3LYP-D3/6-311+G(d,p)(C,H),SDD(Sn))

1	50	0	-1.689702	0.000018	0.000001
2	14	0	1.864201	-1.114558	0.399703

3	14	0	1.864213	1.114550	-0.399703
4	6	0	0.170861	-1.818996	-0.017306
5	6	0	-0.756209	-2.442874	0.884988
6	6	0	-1.842380	-2.965761	0.145686
7	6	0	3.220043	-2.164050	-0.403592
8	1	0	3.176832	-3.194881	-0.039084
9	1	0	4.214469	-1.765380	-0.179284
10	6	0	2.061575	-1.154633	2.283075
11	1	0	1.275323	-0.579670	2.780616
12	1	0	3.024911	-0.733894	2.585189
13	1	0	2.012715	-2.182374	2.656372
14	6	0	0.170880	1.819003	0.017307
15	6	0	-0.756184	2.442889	-0.884988
16	6	0	-1.842400	2.965694	-0.145696
17	6	0	-1.630429	2.669647	1.214913
18	6	0	-0.410577	1.956561	1.326439
19	6	0	3.220064	2.164030	0.403594
20	1	0	4.214486	1.765350	0.179286
21	6	0	2.061588	1.154623	-2.283074
22	1	0	3.024920	0.733876	-2.585188
23	1	0	2.012738	2.182364	-2.656371
24	1	0	3.104999	2.188453	1.490797
25	1	0	3.176862	3.194861	0.039086
26	6	0	-0.410601	-1.956547	-1.326437
27	6	0	-1.630428	-2.669679	-1.214919
28	1	0	3.104979	-2.188472	-1.490795
29	1	0	1.275330	0.579668	-2.780616
30	1	0	-2.692753	-3.491299	0.557280
31	1	0	-2.284457	-2.933595	-2.034415
32	1	0	0.049726	-1.640014	-2.253409
33	1	0	-0.615543	-2.539068	1.953275
34	1	0	-2.284474	2.933538	2.034406
35	1	0	0.049754	1.640039	2.253412
36	1	0	-2.692802	3.491180	-0.557296
37	1	0	-0.615514	2.539091	-1.953273

2a (B3LYP-D3/6-311+G(d,p);SCRF=PCM,benzene)

1	6	0	-0.214473	-1.082263	0.020497
2	7	0	-1.152443	-0.108213	-0.133005
3	7	0	0.955888	-0.381157	0.046752
4	6	0	-2.955305	-1.642965	-0.876094
5	6	0	-0.592348	1.173508	-0.185340
6	6	0	-2.603718	-0.370340	-0.106728
7	6	0	0.755601	1.003707	-0.080406
8	6	0	2.238956	-1.103039	0.135325
9	6	0	-1.399456	2.420746	-0.335061
10	6	0	-3.104055	-0.415015	1.341419
11	6	0	1.825633	2.047643	-0.066432
12	6	0	3.013227	-1.056216	-1.186575
13	6	0	3.087356	-0.667935	1.334236
14	1	0	-2.634403	-1.249767	1.867823
15	1	0	-4.189235	-0.547191	1.369467
16	1	0	-2.855141	0.507806	1.871927
17	1	0	-2.587780	-1.589928	-1.903275
18	1	0	-4.041638	-1.766482	-0.897849
19	1	0	-2.507705	-2.516592	-0.401651
20	1	0	-3.077002	0.473665	-0.614810
21	1	0	-0.751654	3.297783	-0.322397
22	1	0	-2.125139	2.535851	0.476556
23	1	0	-1.956401	2.435010	-1.277871
24	1	0	2.277723	2.159340	0.923410
25	1	0	1.404110	3.014772	-0.344110
26	1	0	2.629285	1.829021	-0.772809
27	1	0	1.922022	-2.133527	0.302418
28	1	0	3.377617	-0.051735	-1.413601
29	1	0	2.377920	-1.387725	-2.010815
30	1	0	3.880877	-1.719341	-1.130736
31	1	0	3.911457	-1.373573	1.468394
32	1	0	2.489613	-0.661976	2.248609
33	1	0	3.522844	0.323191	1.196045

2a (B3LYP-D3/6-311+G(d,p))

1	6	0	-0.216550	-1.078999	0.017809
2	7	0	-1.152745	-0.103283	-0.135673
3	7	0	0.953450	-0.377521	0.046325
4	6	0	-2.942310	-1.649098	-0.874385
5	6	0	-0.592681	1.178405	-0.185669
6	6	0	-2.601779	-0.371753	-0.107605
7	6	0	0.754731	1.007804	-0.079480
8	6	0	2.232278	-1.103919	0.135240
9	6	0	-1.399320	2.425618	-0.336089
10	6	0	-3.098480	-0.420076	1.341916
11	6	0	1.825787	2.050354	-0.063243
12	6	0	3.006510	-1.060779	-1.186864
13	6	0	3.082327	-0.671934	1.334254
14	1	0	-2.618850	-1.250546	1.865852
15	1	0	-4.182528	-0.561455	1.374225
16	1	0	-2.855239	0.504438	1.872440
17	1	0	-2.584710	-1.589660	-1.904701
18	1	0	-4.026668	-1.791318	-0.885521

19	1	0	-2.471187	-2.513113	-0.405245
20	1	0	-3.081756	0.469316	-0.615534
21	1	0	-0.752116	3.303344	-0.320641
22	1	0	-2.127712	2.540173	0.473449
23	1	0	-1.953897	2.441454	-1.280549
24	1	0	2.277240	2.161271	0.927261
25	1	0	1.406507	3.018665	-0.341161
26	1	0	2.630384	1.831106	-0.768739
27	1	0	1.908096	-2.132366	0.302061
28	1	0	3.373170	-0.057277	-1.415709
29	1	0	2.368608	-1.391067	-2.009407
30	1	0	3.873017	-1.725781	-1.132481
31	1	0	3.904206	-1.379948	1.470605
32	1	0	2.483404	-0.662969	2.247784
33	1	0	3.522007	0.317628	1.196138

2b (B3LYP-D3/6-311+G(d,p);SCRF=PCM,benzene)

1	6	0	0.000732	0.003709	-0.281604
2	7	0	-1.062766	0.022230	0.578964
3	7	0	1.062135	0.023129	0.581492
4	6	0	-0.678232	0.051714	1.920106
5	6	0	0.674390	0.052280	1.921730
6	6	0	-2.433070	0.007131	0.149072
7	6	0	-3.092413	1.223523	-0.060274
8	6	0	-3.068976	-1.224738	-0.047752
9	6	0	-4.427944	1.184820	-0.468725
10	6	0	-4.403779	-1.216130	-0.457278
11	6	0	-5.100057	-0.023054	-0.668379
12	1	0	-4.951593	2.120228	-0.640583
13	1	0	-4.909138	-2.163202	-0.620391
14	6	0	2.433255	0.007782	0.154278
15	6	0	3.092057	1.224358	-0.058607
16	6	0	3.073443	-1.223743	-0.026734
17	6	0	4.429538	1.185351	-0.458938
18	6	0	4.411306	-1.215500	-0.427886
19	6	0	5.104253	-0.023002	-0.649992
20	1	0	4.954534	2.120619	-0.627967
21	1	0	4.921857	-2.162795	-0.572078
22	1	0	-1.389614	0.068602	2.728491
23	1	0	1.383804	0.069674	2.731832
24	6	0	-2.367631	2.532106	0.130625
25	1	0	-1.993613	2.634569	1.153427
26	1	0	-1.498945	2.590610	-0.530814
27	1	0	-3.024213	3.377535	-0.080466
28	6	0	-2.319283	-2.516834	0.158516
29	1	0	-1.457494	-2.572512	-0.512067
30	1	0	-1.931428	-2.593182	1.178446
31	1	0	-2.963420	-3.377304	-0.028895
32	6	0	-6.553224	-0.042678	-1.077896
33	1	0	-7.202552	-0.133918	-0.200335
34	1	0	-6.833345	0.874643	-1.600509
35	1	0	-6.770589	-0.889106	-1.733953
36	6	0	2.366060	2.532844	0.128128
37	1	0	1.498192	2.588893	-0.534558
38	1	0	1.990635	2.637631	1.150204
39	1	0	3.022223	3.378230	-0.084431
40	6	0	2.328276	-2.516045	0.194282
41	1	0	1.946045	-2.585398	1.216858
42	1	0	1.463152	-2.579386	-0.471277
43	1	0	2.973592	-3.376360	0.010303
44	6	0	6.538405	-0.039606	-1.121892
45	1	0	6.584901	-0.039278	-2.216303
46	1	0	7.084751	0.839068	-0.770895
47	1	0	7.064042	-0.931114	-0.771900

2b (B3LYP-D3/6-311+G(d,p))

1	6	0	0.000594	0.006310	-0.277941
2	7	0	-1.062320	0.037117	0.583747
3	7	0	1.061602	0.038439	0.585996
4	6	0	-0.678135	0.085254	1.924680
5	6	0	0.674508	0.086121	1.926124
6	6	0	-2.431913	0.011774	0.153199
7	6	0	-3.098414	1.222454	-0.063418
8	6	0	-3.058530	-1.224656	-0.042704
9	6	0	-4.433678	1.173455	-0.470516
10	6	0	-4.393185	-1.226488	-0.451199
11	6	0	-5.097765	-0.039163	-0.664620
12	1	0	-4.963220	2.104739	-0.647026
13	1	0	-4.891726	-2.177564	-0.612483
14	6	0	2.431979	0.013098	0.157971
15	6	0	3.095875	1.224032	-0.068347
16	6	0	3.064966	-1.222723	-0.015862
17	6	0	4.433111	1.175009	-0.466968
18	6	0	4.402807	-1.224652	-0.415847
19	6	0	5.102014	-0.037911	-0.645939
20	1	0	4.962475	2.106109	-0.645588
21	1	0	4.908151	-2.175762	-0.553597
22	1	0	-1.389408	0.112610	2.732921
23	1	0	1.384008	0.114353	2.735895
24	6	0	-2.377759	2.535361	0.111524

25	1	0	-1.993145	2.647933	1.129277
26	1	0	-1.516327	2.590471	-0.559829
27	1	0	-3.039608	3.376839	-0.099710
28	6	0	-2.295593	-2.509745	0.157177
29	1	0	-1.443037	-2.557249	-0.525896
30	1	0	-1.892283	-2.580794	1.171458
31	1	0	-2.934491	-3.376540	-0.019618
32	6	0	-6.551203	-0.070384	-1.072364
33	1	0	-7.199092	-0.175437	-0.195238
34	1	0	-6.841620	0.847843	-1.587908
35	1	0	-6.760954	-0.913174	-1.735805
36	6	0	2.371706	2.536334	0.095927
37	1	0	1.512325	2.584955	-0.578514
38	1	0	1.983540	2.654445	1.111731
39	1	0	3.032260	3.377962	-0.118750
40	6	0	2.308829	-2.508402	0.205208
41	1	0	1.912505	-2.568993	1.222943
42	1	0	1.452063	-2.568042	-0.471585
43	1	0	2.950145	-3.374659	0.034716
44	6	0	6.536695	-0.065391	-1.115742
45	1	0	6.585824	-0.066448	-2.210094
46	1	0	7.089336	0.809265	-0.764157
47	1	0	7.055853	-0.959861	-0.763396

2c (B3LYP-D3/6-311+G(d,p);SCRF=PCM,benzene)

1	6	0	0.000000	1.568839	-0.000002
2	7	0	-1.061810	0.712387	-0.000001
3	7	0	1.061810	0.712387	-0.000001
4	6	0	-0.680412	-0.634186	0.000000
5	6	0	-2.445107	1.160751	0.000000
6	6	0	0.680412	-0.634186	0.000000
7	6	0	2.445107	1.160751	0.000000
8	6	0	-1.662973	-1.755937	0.000001
9	6	0	1.662973	-1.755937	0.000001
10	1	0	-2.971002	0.801322	0.888533
11	1	0	-1.146690	-2.716856	0.000006
12	1	0	-2.311125	-1.725697	-0.882176
13	1	0	-2.311130	-1.725691	0.882174
14	1	0	2.311125	-1.725698	-0.882176
15	1	0	1.146690	-2.716856	0.000007
16	1	0	2.311131	-1.725691	0.882174
17	1	0	2.443017	2.248633	-0.000011
18	1	0	-2.971011	0.801302	-0.888518
19	1	0	-2.443017	2.248633	-0.000012
20	1	0	2.971003	0.801321	0.888532
21	1	0	2.971011	0.801303	-0.888519

2c (B3LYP-D3/6-311+G(d,p))

1	6	0	0.000000	-1.569123	0.000001
2	7	0	-1.060686	-0.710958	0.000001
3	7	0	1.060686	-0.710958	0.000001
4	6	0	-0.680181	0.636295	0.000001
5	6	0	-2.440674	-1.164527	-0.000001
6	6	0	0.680181	0.636295	0.000000
7	6	0	2.440674	-1.164527	0.000000
8	6	0	-1.662791	1.757905	0.000000
9	6	0	1.662792	1.757904	0.000000
10	1	0	-2.969641	-0.809147	-0.889002
11	1	0	-1.147347	2.719541	-0.000004
12	1	0	-2.311377	1.728571	0.882202
13	1	0	-2.311382	1.728564	-0.882198
14	1	0	2.311378	1.728570	0.882202
15	1	0	1.147349	2.719540	-0.000005
16	1	0	2.311383	1.728563	-0.882198
17	1	0	2.428633	-2.252373	0.000014
18	1	0	-2.969651	-0.809119	0.888984
19	1	0	-2.428633	-2.252373	0.000016
20	1	0	2.969641	-0.809145	-0.889001
21	1	0	2.969650	-0.809121	0.888985

3a (B3LYP-D3/6-311+G(d,p);SCRF=PCM,benzene)

1	50	0	1.413943	-0.397525	0.148640
2	6	0	-1.117730	-0.192294	-0.107594
3	6	0	1.485755	1.618959	1.729885
4	6	0	0.648396	0.828618	2.598585
5	6	0	1.234007	-0.291714	-2.675197
6	6	0	1.866954	0.837663	-2.038774
7	7	0	-2.043443	-1.168059	0.076546
8	7	0	-1.842231	0.943058	-0.281811
9	6	0	-0.942647	-3.208334	-0.834614
10	6	0	2.847489	1.338732	2.096321
11	6	0	1.483365	0.049596	3.405101
12	6	0	2.218801	-1.253693	-2.917288
13	6	0	3.273760	0.544960	-1.975543
14	6	0	-3.339872	-0.648927	0.027701
15	6	0	-1.756416	-2.604622	0.311427
16	6	0	-3.216382	0.688607	-0.201861

17	6	0	-1.197783	2.237160	-0.599938
18	6	0	2.836318	0.369068	3.098311
19	6	0	3.473898	-0.735088	-2.490030
20	6	0	-4.569993	-1.473725	0.214903
21	6	0	-1.139805	-2.829411	1.694069
22	6	0	-4.296270	1.716231	-0.306063
23	6	0	-1.422146	2.632610	-2.061582
24	6	0	-1.556538	3.341639	0.396284
25	1	0	-0.149919	-2.377557	1.775537
26	1	0	-1.038747	-3.901366	1.880540
27	1	0	-1.773105	-2.400041	2.474007
28	1	0	-1.432773	-3.025940	-1.793601
29	1	0	-0.855849	-4.287745	-0.688452
30	1	0	0.065447	-2.794839	-0.886086
31	1	0	-2.731951	-3.089685	0.304155
32	1	0	-5.456231	-0.842725	0.153930
33	1	0	-4.584429	-1.965677	1.191989
34	1	0	-4.663107	-2.248615	-0.551987
35	1	0	-4.338925	2.350736	0.583128
36	1	0	-5.264140	1.225116	-0.407117
37	1	0	-4.169094	2.365343	-1.173031
38	1	0	-0.139175	2.026899	-0.479808
39	1	0	-2.464137	2.883292	-2.267270
40	1	0	-1.120111	1.822924	-2.728382
41	1	0	-0.816421	3.511334	-2.296222
42	1	0	-0.875849	4.183585	0.249062
43	1	0	-1.441209	2.990619	1.423633
44	1	0	-2.572293	3.714177	0.260900
45	1	0	0.183588	-0.369884	-2.919532
46	1	0	1.441433	1.829379	-1.959541
47	1	0	2.051547	-2.235563	-3.339929
48	1	0	4.031904	1.202979	-1.573351
49	1	0	4.417832	-1.262393	-2.525432
50	1	0	1.166976	2.491161	1.174881
51	1	0	-0.432634	0.844769	2.618818
52	1	0	3.721127	1.791405	1.647638
53	1	0	1.155568	-0.685595	4.128093
54	1	0	3.708253	-0.091052	3.543657

3a (B3LYP-D3/6-311+G(d,p))

1	50	0	1.458049	-0.379277	0.147602
2	6	0	-1.128979	-0.199235	-0.110089
3	6	0	1.475707	1.634123	1.734230
4	6	0	0.628292	0.829785	2.578752
5	6	0	1.213582	-0.286961	-2.663808
6	6	0	1.860470	0.846619	-2.051300
7	7	0	-2.054288	-1.175144	0.075927
8	7	0	-1.857783	0.934157	-0.282061
9	6	0	-0.938643	-3.203971	-0.836883
10	6	0	2.833307	1.340345	2.105668
11	6	0	1.453610	0.030941	3.376313
12	6	0	2.187241	-1.264456	-2.890025
13	6	0	3.264434	0.539640	-1.986028
14	6	0	-3.352667	-0.659272	0.030682
15	6	0	-1.755346	-2.607913	0.311398
16	6	0	-3.232051	0.678045	-0.199007
17	6	0	-1.212147	2.227463	-0.597214
18	6	0	2.809422	0.349993	3.087209
19	6	0	3.448370	-0.752446	-2.476048
20	6	0	-4.580733	-1.486849	0.219840
21	6	0	-1.128825	-2.823119	1.691387
22	6	0	-4.313463	1.704187	-0.302327
23	6	0	-1.436463	2.628035	-2.057596
24	6	0	-1.567785	3.329623	0.402889
25	1	0	-0.147615	-2.352478	1.767640
26	1	0	-1.008713	-3.893139	1.879049
27	1	0	-1.764542	-2.403206	2.474733
28	1	0	-1.437667	-3.034863	-1.793910
29	1	0	-0.831057	-4.281235	-0.686958
30	1	0	0.060319	-2.770687	-0.897945
31	1	0	-2.726704	-3.103021	0.309203
32	1	0	-5.469106	-0.858066	0.161863
33	1	0	-4.593136	-1.980606	1.196368
34	1	0	-4.675260	-2.261364	-0.547701
35	1	0	-4.354008	2.342941	0.584166
36	1	0	-5.282026	1.212729	-0.398444
37	1	0	-4.189562	2.350417	-1.172272
38	1	0	-0.153698	2.014427	-0.478466
39	1	0	-2.478783	2.878809	-2.263668
40	1	0	-1.132063	1.821245	-2.726638
41	1	0	-0.831621	3.508078	-2.290239
42	1	0	-0.890723	4.174312	0.253834
43	1	0	-1.443348	2.977380	1.428695
44	1	0	-2.585500	3.700458	0.274698
45	1	0	0.162274	-0.358500	-2.905712
46	1	0	1.445264	1.843641	-1.984570
47	1	0	2.009017	-2.250126	-3.298474
48	1	0	4.031937	1.198930	-1.604886
49	1	0	4.386469	-1.289453	-2.506232
50	1	0	1.165912	2.517085	1.191247
51	1	0	-0.452661	0.850708	2.593213
52	1	0	3.712347	1.802810	1.678656
53	1	0	1.116784	-0.713271	4.085454

54	1	0	3.675521	-0.120645	3.531858

3b (B3LYP-D3/6-311+G(d,p);SCRF=PCM,benzene)

1	50	0	1.199025	0.198448	0.451238
2	6	0	1.500332	-2.322385	0.222507
3	6	0	1.590947	0.889691	-1.971602
4	6	0	-1.316851	-0.017195	0.103040
5	6	0	0.755615	-2.427765	1.456862
6	6	0	2.897525	-2.240423	0.570526
7	6	0	0.758290	2.031574	-1.663623
8	6	0	2.946873	1.296599	-1.715159
9	7	0	-2.299090	0.510664	0.877653
10	7	0	-1.971833	-0.740774	-0.840942
11	6	0	-1.374187	2.683581	1.672439
12	6	0	1.666645	-2.326531	2.508759
13	6	0	2.978675	-2.213968	1.962670
14	6	0	1.570750	3.050530	-1.160126
15	6	0	2.921603	2.590424	-1.200455
16	6	0	-3.562219	0.115851	0.428594
17	6	0	-2.096954	1.390718	2.055384
18	6	0	-3.359166	-0.677032	-0.660796
19	6	0	-1.250669	-1.431954	-1.933577
20	6	0	1.108397	4.385610	-0.648451
21	6	0	-4.838913	0.522234	1.087195
22	6	0	-1.437587	0.630976	3.208445
23	6	0	-4.376649	-1.390885	-1.490458
24	6	0	-1.484424	-0.759257	-3.288598
25	6	0	-1.512328	-2.939348	-1.947026
26	6	0	4.037290	-2.237996	-0.406454
27	1	0	1.142243	-2.629612	-0.751979
28	1	0	1.309234	0.066740	-2.615709
29	1	0	-0.347390	2.500366	1.353644
30	1	0	-0.316354	-2.546108	1.538728
31	1	0	-0.314148	2.087670	-1.796164
32	1	0	3.825064	0.685875	-1.872235
33	1	0	-1.344742	3.352749	2.535739
34	1	0	-1.894602	3.191341	0.857411
35	1	0	1.417022	-2.306096	3.561591
36	1	0	3.891928	-2.096759	2.532345
37	1	0	3.780602	3.150634	-0.852905
38	1	0	-3.101434	1.664937	2.375731
39	1	0	-0.205539	-1.285568	-1.676710
40	1	0	0.033329	4.513997	-0.800262
41	1	0	1.617032	5.209408	-1.160837
42	1	0	1.306709	4.504636	0.422877
43	1	0	-5.687296	0.082044	0.564036
44	1	0	-4.974493	1.607900	1.079936
45	1	0	-4.884382	0.185303	2.127178
46	1	0	-2.011233	-0.264594	3.458658
47	1	0	-1.393050	1.272291	4.092102
48	1	0	-0.420316	0.323096	2.961882
49	1	0	-4.367029	-2.468461	-1.306949
50	1	0	-4.226702	-1.233255	-2.558954
51	1	0	-5.373713	-1.025105	-1.245305
52	1	0	-0.814263	-1.202588	-4.029173
53	1	0	-1.267331	0.308604	-3.231184
54	1	0	-2.506327	-0.890422	-3.647271
55	1	0	-1.382930	-3.364492	-0.949657
56	1	0	-0.793186	-3.418670	-2.615536
57	1	0	-2.511210	-3.184443	-2.309443
58	1	0	4.936483	-1.798652	0.033631
59	1	0	3.793948	-1.667017	-1.307209
60	1	0	4.291315	-3.255657	-0.727441

3b (B3LYP-D3/6-311+G(d,p))

1	50	0	1.235565	0.193741	0.447095
2	6	0	1.511561	-2.317262	0.187170
3	6	0	1.571441	0.903971	-1.965845
4	6	0	-1.326795	-0.016473	0.107104
5	6	0	0.745081	-2.437632	1.406964
6	6	0	2.902693	-2.235141	0.562537
7	6	0	0.736167	2.041269	-1.648717
8	6	0	2.927812	1.316279	-1.714419
9	7	0	-2.309655	0.504707	0.885800
10	7	0	-1.984645	-0.734882	-0.839313
11	6	0	-1.372317	2.666608	1.691034
12	6	0	1.635997	-2.342778	2.475776
13	6	0	2.956677	-2.220234	1.955802
14	6	0	1.546801	3.060083	-1.144072
15	6	0	2.899078	2.605779	-1.191955
16	6	0	-3.573939	0.112090	0.437115
17	6	0	-2.099296	1.374317	2.068651
18	6	0	-3.372150	-0.673754	-0.657061
19	6	0	-1.261410	-1.419721	-1.933471
20	6	0	1.083202	4.393523	-0.630624
21	6	0	-4.850014	0.514193	1.099702
22	6	0	-1.433997	0.602541	3.210681
23	6	0	-4.390149	-1.382803	-1.490241
24	6	0	-1.496777	-0.743666	-3.286656
25	6	0	-1.516473	-2.928341	-1.950202

26	6	0	4.061497	-2.230583	-0.391361
27	1	0	1.174462	-2.621556	-0.795871
28	1	0	1.292968	0.088442	-2.620685
29	1	0	-0.350858	2.478347	1.359047
30	1	0	-0.327200	-2.564095	1.469250
31	1	0	-0.336932	2.095006	-1.776724
32	1	0	3.808322	0.713204	-1.886238
33	1	0	-1.329639	3.328695	2.559469
34	1	0	-1.896370	3.185291	0.885179
35	1	0	1.367686	-2.337803	3.523906
36	1	0	3.858420	-2.108324	2.543841
37	1	0	3.757575	3.168345	-0.848157
38	1	0	-3.101542	1.649772	2.397363
39	1	0	-0.217242	-1.269419	-1.675025
40	1	0	0.006448	4.518087	-0.774560
41	1	0	1.584037	5.217503	-1.150154
42	1	0	1.290898	4.516675	0.438548
43	1	0	-5.699581	0.078462	0.574078
44	1	0	-4.986016	1.600093	1.101089
45	1	0	-4.896437	0.169965	2.137513
46	1	0	-2.010795	-0.291073	3.461447
47	1	0	-1.374676	1.236926	4.098744
48	1	0	-0.422691	0.287625	2.949806
49	1	0	-4.380573	-2.461935	-1.314626
50	1	0	-4.240707	-1.218412	-2.558025
51	1	0	-5.387740	-1.019092	-1.242786
52	1	0	-0.828293	-1.184703	-4.030304
53	1	0	-1.277430	0.323539	-3.226729
54	1	0	-2.519443	-0.872805	-3.644998
55	1	0	-1.377810	-3.355238	-0.954883
56	1	0	-0.799009	-3.403869	-2.623460
57	1	0	-2.516411	-3.177742	-2.307889
58	1	0	4.950633	-1.789363	0.066725
59	1	0	3.836567	-1.661248	-1.298067
60	1	0	4.323080	-3.248700	-0.704481

3c (B3LYP-D3/6-311+G(d,p);SCRF=PCM,benzene)

1	50	0	0.369221	1.388798	0.000322
2	6	0	0.145264	-1.120695	0.048009
3	6	0	-1.451953	1.639774	-1.664715
4	6	0	-1.159287	1.528240	1.945093
5	7	0	-0.875792	-2.014925	0.147036
6	7	0	1.263693	-1.892508	0.085155
7	6	0	-1.510926	3.074426	-1.494713
8	6	0	-0.606259	1.406356	-2.816260
9	6	0	-1.023655	2.953389	2.143876
10	6	0	-0.211100	0.904452	2.844590
11	6	0	-0.401433	-3.318605	0.236627
12	6	0	-2.277206	-1.684797	0.054176
13	6	0	0.949444	-3.241582	0.200060
14	6	0	2.614583	-1.401248	-0.054787
15	6	0	-0.675223	3.660768	-2.437229
16	6	0	-0.118134	2.631823	-3.253640
17	6	0	0.007505	3.172030	3.047538
18	6	0	0.511349	1.907941	3.478564
19	6	0	-2.842959	-1.578459	-1.227001
20	6	0	-3.034957	-1.519274	1.217495
21	6	0	3.122605	-1.215730	-1.347905
22	6	0	3.375747	-1.151981	1.093263
23	6	0	-4.185022	-1.217197	-1.319958
24	6	0	-2.040909	-1.883843	-2.466677
25	6	0	-4.379103	-1.157959	1.069998
26	6	0	-2.475892	-1.730529	2.602798
27	6	0	4.432802	-0.752983	-1.471327
28	6	0	2.273165	-1.472215	-2.566794
29	6	0	4.682328	-0.691550	0.915672
30	6	0	2.804007	-1.324708	2.476928
31	6	0	-4.964873	-0.983714	-0.182251
32	6	0	5.224934	-0.481009	-0.353133
33	6	0	-6.399181	-0.535642	-0.314778
34	6	0	6.624804	0.058201	-0.514457
35	1	0	-2.052192	1.048814	1.561419
36	1	0	-2.213087	0.955768	-1.311875
37	1	0	-2.094804	3.589482	-0.744898
38	1	0	-0.407125	0.445346	-3.266444
39	1	0	-1.610565	3.712546	1.646582
40	1	0	-0.093251	-0.158750	2.988878
41	1	0	-1.064925	-4.162462	0.315668
42	1	0	1.708813	-4.003215	0.241190
43	1	0	-0.463211	4.718234	-2.524611
44	1	0	0.582045	2.781552	-4.065185
45	1	0	0.386218	4.137985	3.354786
46	1	0	1.333481	1.758641	4.166655
47	1	0	-4.631251	-1.110246	-2.303327
48	1	0	-1.033849	-1.472587	-2.410500
49	1	0	-2.526918	-1.476762	-3.353566
50	1	0	-1.941631	-2.966243	-2.600773
51	1	0	-4.976539	-1.009474	1.964182
52	1	0	-2.481827	-0.796943	3.169231
53	1	0	-1.452969	-2.103319	2.587977
54	1	0	-3.091473	-2.452164	3.146611
55	1	0	4.842816	-0.600356	-2.464465
56	1	0	1.516674	-0.689677	-2.676689

57	1	0	1.746928	-2.427849	-2.502776
58	1	0	2.883211	-1.475029	-3.470842
59	1	0	5.287765	-0.489471	1.793416
60	1	0	3.600707	-1.373917	3.220562
61	1	0	2.197394	-2.228764	2.562935
62	1	0	2.162079	-0.475298	2.726388
63	1	0	-6.448478	0.549520	-0.453277
64	1	0	-6.979858	-0.781339	0.576764
65	1	0	-6.882623	-0.997182	-1.179070
66	1	0	7.088167	-0.303250	-1.435224
67	1	0	7.261946	-0.225731	0.325975
68	1	0	6.609194	1.152179	-0.561503

3c (B3LYP-D3/6-311+G(d,p))

1	50	0	-0.387355	1.403718	-0.115344
2	6	0	-0.120392	-1.131795	0.054580
3	6	0	1.365242	1.801424	1.596094
4	6	0	1.185269	1.344336	-2.019389
5	7	0	0.910017	-2.021739	0.032204
6	7	0	-1.229990	-1.918144	0.066230
7	6	0	1.389582	3.213651	1.286053
8	6	0	0.470682	1.653938	2.723594
9	6	0	1.046981	2.741720	-2.363450
10	6	0	0.261064	0.627410	-2.874463
11	6	0	0.450137	-3.334026	0.037940
12	6	0	2.307192	-1.668875	0.099004
13	6	0	-0.901785	-3.269061	0.057165
14	6	0	-2.585947	-1.428919	0.147651
15	6	0	0.489607	3.860109	2.125396
16	6	0	-0.074953	2.899142	3.013057
17	6	0	0.036544	2.861552	-3.306774
18	6	0	-0.450304	1.557780	-3.621344
19	6	0	2.861523	-1.422127	1.366099
20	6	0	3.071761	-1.613593	-1.069581
21	6	0	-3.112325	-1.136738	1.413427
22	6	0	-3.332327	-1.278109	-1.026872
23	6	0	4.197832	-1.037242	1.430803
24	6	0	2.044670	-1.598861	2.620472
25	6	0	4.411157	-1.224119	-0.950205
26	6	0	2.524644	-1.957751	-2.432643
27	6	0	-4.424393	-0.668928	1.479936
28	6	0	-2.278119	-1.279435	2.660873
29	6	0	-4.642292	-0.809288	-0.905626
30	6	0	-2.740515	-1.550603	-2.385774
31	6	0	4.984550	-0.914376	0.280357
32	6	0	-5.201868	-0.493825	0.332947
33	6	0	6.412968	-0.439500	0.378639
34	6	0	-6.603525	0.055914	0.430403
35	1	0	2.075988	0.914124	-1.576791
36	1	0	2.158673	1.110682	1.341754
37	1	0	1.999296	3.673440	0.521179
38	1	0	0.281430	0.737980	3.263580
39	1	0	1.621852	3.550195	-1.934600
40	1	0	0.149328	-0.445477	-2.913459
41	1	0	1.123285	-4.173853	0.026861
42	1	0	-1.653420	-4.039410	0.066059
43	1	0	0.242871	4.912812	2.097010
44	1	0	-0.818364	3.103447	3.772069
45	1	0	-0.337727	3.788899	-3.719053
46	1	0	-1.251393	1.335738	-4.314397
47	1	0	4.634584	-0.822223	2.400741
48	1	0	1.069001	-1.122729	2.532845
49	1	0	2.556061	-1.169354	3.482087
50	1	0	1.871050	-2.661409	2.821058
51	1	0	5.013230	-1.159811	-1.851290
52	1	0	2.485543	-1.069602	-3.067158
53	1	0	1.519239	-2.373827	-2.386709
54	1	0	3.173203	-2.689519	-2.921913
55	1	0	-4.846999	-0.432412	2.451208
56	1	0	-1.550948	-0.464839	2.725532
57	1	0	-1.719589	-2.218528	2.674306
58	1	0	-2.904529	-1.239282	3.553039
59	1	0	-5.235347	-0.681628	-1.805600
60	1	0	-3.527139	-1.703403	-3.126425
61	1	0	-2.092771	-2.429662	-2.387188
62	1	0	-2.135141	-0.697894	-2.706593
63	1	0	6.447397	0.650073	0.481916
64	1	0	6.987037	-0.706357	-0.510979
65	1	0	6.914959	-0.865593	1.250964
66	1	0	-7.087883	-0.247123	1.361598
67	1	0	-7.224228	-0.279740	-0.403281
68	1	0	-6.586984	1.150724	0.409573

3d (B3LYP-D3/6-311+G(d,p);SCRF=PCM,benzene)

1	50	0	0.296139	1.143015	0.186126
2	6	0	-2.117706	1.287941	0.891301
3	6	0	-0.054850	1.676361	-2.298443
4	6	0	0.134382	-1.433911	-0.034348
5	6	0	-1.734594	0.975425	2.243195
6	6	0	-2.057613	2.724359	0.774822

7	6	0	1.089941	0.811435	-2.482149
8	6	0	0.439109	3.019851	-2.177885
9	7	0	1.254291	-2.202019	0.044237
10	7	0	-0.863694	-2.336387	-0.233047
11	6	0	-1.387994	2.169332	2.880817
12	6	0	-1.585354	3.254627	1.976729
13	6	0	2.238044	1.604251	-2.395164
14	6	0	0.962937	-3.553493	-0.101447
15	6	0	2.575617	-1.683347	0.293710
16	6	0	-0.376152	-3.638246	-0.278898
17	6	0	-2.264029	-2.007949	-0.305786
18	6	0	-1.303382	4.703330	2.261343
19	6	0	2.906432	-1.313702	1.607846
20	6	0	3.481910	-1.568083	-0.764846
21	6	0	-3.036524	-2.121017	0.856529
22	6	0	-2.802204	-1.586673	-1.526464
23	6	0	4.172979	-0.778280	1.832395
24	6	0	1.926236	-1.482665	2.742900
25	6	0	4.739977	-1.025560	-0.485871
26	6	0	3.162584	-2.017240	-2.169669
27	6	0	-4.380497	-1.753814	0.781420
28	6	0	-2.444207	-2.631476	2.146590
29	6	0	-4.151118	-1.226107	-1.550003
30	6	0	-1.957458	-1.533101	-2.773323
31	6	0	5.098601	-0.614948	0.796484
32	6	0	-4.952003	-1.294703	-0.407373
33	6	0	6.442462	0.017216	1.062116
34	6	0	-6.408043	-0.902291	-0.455688
35	6	0	1.836072	2.955401	-2.215405
36	6	0	-0.397101	4.260836	-2.034451
37	1	0	-2.673858	0.635471	0.233031
38	1	0	-1.083232	1.421500	-2.525249
39	1	0	-1.728515	-0.009696	2.685427
40	1	0	-2.325115	3.291294	-0.105870
41	1	0	1.055175	-0.248595	-2.680446
42	1	0	-1.009152	2.260008	3.891484
43	1	0	3.258417	1.246914	-2.427496
44	1	0	1.727097	-4.310614	-0.066460
45	1	0	-1.022268	-4.485864	-0.428922
46	1	0	-1.836889	5.049229	3.153584
47	1	0	-1.613923	5.334529	1.424447
48	1	0	-0.236881	4.885954	2.433585
49	1	0	4.444678	-0.480200	2.840029
50	1	0	1.434569	-2.458215	2.707255
51	1	0	1.138921	-0.723380	2.705735
52	1	0	2.432290	-1.387832	3.704517
53	1	0	5.450427	-0.916404	-1.299484
54	1	0	3.724201	-2.924051	-2.415906
55	1	0	3.447048	-1.247923	-2.890365
56	1	0	2.105103	-2.234564	-2.309524
57	1	0	-4.988464	-1.806914	1.678794
58	1	0	-3.072247	-2.358160	2.995267
59	1	0	-1.442114	-2.234199	2.317412
60	1	0	-2.358391	-3.722949	2.129659
61	1	0	-4.582717	-0.877514	-2.482711
62	1	0	-1.594357	-2.530041	-3.041674
63	1	0	-1.081333	-0.900411	-2.634797
64	1	0	-2.529718	-1.142538	-3.615352
65	1	0	6.831095	-0.269378	2.042329
66	1	0	6.359723	1.109063	1.048912
67	1	0	7.175997	-0.267790	0.305062
68	1	0	-7.044686	-1.787712	-0.557181
69	1	0	-6.616390	-0.245304	-1.302418
70	1	0	-6.707943	-0.386161	0.459348
71	1	0	2.502820	3.801529	-2.103685
72	1	0	-1.414051	4.098321	-2.403005
73	1	0	0.034054	5.089556	-2.603762
74	1	0	-0.479213	4.588559	-0.992130

3d (B3LYP-D3/6-311+G(d,p))

1	50	0	0.289534	1.179150	0.181675
2	6	0	-2.133912	1.287955	0.883961
3	6	0	0.127058	-1.458963	-0.032632
4	1	0	-2.697327	0.651798	0.216362
5	6	0	-1.735151	0.948936	2.222814
6	6	0	-2.041935	2.723025	0.783340
7	7	0	1.246259	-2.229466	0.042304
8	7	0	-0.870588	-2.362999	-0.230252
9	1	0	-1.744327	-0.041272	2.652775
10	6	0	-1.353026	2.127001	2.871927
11	6	0	-1.540169	3.227191	1.986679
12	1	0	-2.313774	3.308067	-0.083995
13	6	0	0.954933	-3.581469	-0.103490
14	6	0	2.566261	-1.707299	0.288705
15	6	0	-0.384717	-3.665824	-0.278179
16	6	0	-2.268060	-2.025304	-0.304940
17	1	0	-0.960323	2.195449	3.878672
18	6	0	-1.238381	4.667198	2.291662
19	1	0	1.719196	-4.338658	-0.071096
20	6	0	2.895602	-1.330170	1.600989
21	6	0	3.469655	-1.585453	-0.771081
22	1	0	-1.031455	-4.512954	-0.428675
23	6	0	-3.044684	-2.131295	0.854204

24	6	0	-2.799490	-1.598139	-1.527139
25	1	0	-1.825472	5.027711	3.143764
26	1	0	-1.471999	5.306403	1.436157
27	1	0	-0.182650	4.820142	2.540249
28	6	0	4.158561	-0.786454	1.822944
29	6	0	1.914478	-1.496658	2.735486
30	6	0	4.725018	-1.035850	-0.494247
31	6	0	3.147927	-2.025208	-2.178515
32	6	0	-4.384502	-1.748779	0.776386
33	6	0	-2.462317	-2.650614	2.145256
34	6	0	-4.143550	-1.223775	-1.553729
35	6	0	-1.948187	-1.547824	-2.769671
36	1	0	4.428373	-0.481662	2.829125
37	6	0	5.082479	-0.620753	0.786319
38	1	0	1.438616	-2.480634	2.712851
39	1	0	1.115686	-0.750455	2.683330
40	1	0	2.415698	-1.380549	3.697471
41	1	0	5.433017	-0.921576	-1.309436
42	1	0	3.743694	-2.902726	-2.449642
43	1	0	3.386550	-1.231344	-2.889468
44	1	0	2.098069	-2.283207	-2.306396
45	1	0	-4.996132	-1.799457	1.671336
46	6	0	-4.946289	-1.278322	-0.411349
47	1	0	-3.083796	-2.361268	2.993615
48	1	0	-1.453012	-2.271386	2.313877
49	1	0	-2.398485	-3.743790	2.132870
50	1	0	-4.571345	-0.875241	-2.488346
51	1	0	-1.526344	-2.531338	-2.997835
52	1	0	-1.110545	-0.860987	-2.648846
53	1	0	-2.533157	-1.221175	-3.630180
54	6	0	6.421610	0.022540	1.049100
55	6	0	-6.375968	-0.798906	-0.449530
56	1	0	6.813691	-0.258184	2.029739
57	1	0	6.331082	1.113761	1.032011
58	1	0	7.157457	-0.259720	0.293156
59	1	0	-7.000015	-1.343182	0.262995
60	1	0	-6.811293	-0.914535	-1.444702
61	1	0	-6.427123	0.263178	-0.187297
62	6	0	1.090071	0.812424	-2.464936
63	1	0	1.052821	-0.245413	-2.674211
64	6	0	2.241097	1.599171	-2.343643
65	6	0	-0.052328	1.684189	-2.311486
66	1	0	3.260534	1.238185	-2.353162
67	6	0	1.843086	2.949853	-2.165787
68	6	0	0.444886	3.022589	-2.167211
69	1	0	-1.077775	1.436931	-2.558308
70	1	0	2.511646	3.790650	-2.031373
71	6	0	-0.389939	4.266949	-2.049887
72	1	0	-1.413006	4.089788	-2.393434
73	1	0	0.027954	5.075118	-2.657454
74	1	0	-0.451847	4.631531	-1.018553

3e (B3LYP-D3/6-311+G(d,p);SCRF=PCM,benzene)

1	50	0	-0.947339	-0.038345	-0.625874
2	6	0	-1.189997	-2.063844	0.747832
3	6	0	-1.541541	1.568339	1.178250
4	6	0	1.455005	-0.132632	-0.034633
5	6	0	-0.556529	-2.903560	-0.254401
6	6	0	-2.623208	-2.224413	0.580911
7	6	0	-0.551984	2.525239	0.712034
8	6	0	-2.804251	2.002944	0.621957
9	7	0	2.444236	-0.257833	-0.953868
10	7	0	2.106997	-0.099907	1.152527
11	6	0	-1.556953	-3.451059	-1.042955
12	6	0	-2.824660	-3.031866	-0.529756
13	6	0	-1.168368	3.414171	-0.159232
14	6	0	-2.563312	3.087797	-0.204536
15	6	0	3.704340	-0.303947	-0.353963
16	6	0	2.249535	-0.358007	-2.397144
17	6	0	3.489493	-0.203379	0.986531
18	6	0	1.472162	0.026457	2.458604
19	6	0	-0.501519	4.514407	-0.935136
20	6	0	4.963871	-0.438659	-1.138951
21	6	0	4.438112	-0.192410	2.135557
22	6	0	-3.671758	-1.662059	1.495949
23	1	0	-0.733322	-1.816542	1.700000
24	1	0	-1.470068	1.017014	2.109165
25	1	0	0.510459	-3.041615	-0.371718
26	1	0	0.494765	2.535298	0.987671
27	1	0	-3.760904	1.532024	0.802283
28	1	0	-1.407394	-4.067433	-1.920215
29	1	0	-3.789888	-3.286538	-0.949692
30	1	0	-3.299897	3.596452	-0.814387
31	1	0	2.789796	0.442239	-2.905341
32	1	0	0.399055	0.084759	2.321276
33	1	0	0.558301	4.591463	-0.676833
34	1	0	-0.965263	5.485985	-0.731586
35	1	0	-0.568636	4.349450	-2.016389
36	1	0	5.825461	-0.462364	-0.471865
37	1	0	5.098946	0.399138	-1.829789
38	1	0	4.972579	-1.359448	-1.729916
39	1	0	4.243016	-1.019531	2.824780
40	1	0	4.366555	0.738157	2.706907

41	1	0	5.464188	-0.288338	1.780960
42	1	0	-4.650808	-1.639933	1.010096
43	1	0	-3.432759	-0.643655	1.814593
44	1	0	-3.769801	-2.267128	2.405744
45	1	0	2.608490	-1.323009	-2.759249
46	1	0	1.189861	-0.269032	-2.622641
47	1	0	1.709636	-0.840029	3.078082
48	1	0	1.815351	0.932930	2.959660

3e (B3LYP-D3/6-311+G(d,p))

1	50	0	-0.974398	-0.060237	-0.618126
2	6	0	-1.100343	-2.072506	0.779726
3	6	0	-1.594996	1.532612	1.173783
4	6	0	1.470452	-0.072202	-0.033229
5	6	0	-0.418749	-2.890766	-0.208377
6	6	0	-2.523725	-2.297951	0.596689
7	6	0	-0.647965	2.523129	0.688548
8	6	0	-2.877869	1.909077	0.618851
9	7	0	2.455945	-0.218811	-0.953945
10	7	0	2.132648	0.005744	1.146547
11	6	0	-1.384116	-3.485821	-1.005169
12	6	0	-2.674409	-3.118943	-0.511753
13	6	0	-1.305032	3.373109	-0.190912
14	6	0	-2.685000	2.989699	-0.223864
15	6	0	3.721603	-0.234496	-0.362763
16	6	0	2.245042	-0.373613	-2.388962
17	6	0	3.515611	-0.090681	0.974566
18	6	0	1.499776	0.172480	2.448232
19	6	0	-0.689245	4.489384	-0.984699
20	6	0	4.976814	-0.386342	-1.151781
21	6	0	4.473385	-0.033547	2.114817
22	6	0	-3.606420	-1.784724	1.500458
23	1	0	-0.667734	-1.799505	1.736282
24	1	0	-1.501122	1.004165	2.116077
25	1	0	0.654435	-2.988199	-0.307595
26	1	0	0.398945	2.582425	0.957490
27	1	0	-3.814301	1.405631	0.815303
28	1	0	-1.196836	-4.102404	-1.874592
29	1	0	-3.621452	-3.420105	-0.941297
30	1	0	-3.445086	3.459688	-0.835275
31	1	0	2.776456	0.408379	-2.934650
32	1	0	0.424738	0.184754	2.312261
33	1	0	0.370313	4.608124	-0.741294
34	1	0	-1.186215	5.444594	-0.782271
35	1	0	-0.764781	4.311793	-2.063364
36	1	0	5.843675	-0.382255	-0.490725
37	1	0	5.102922	0.428685	-1.871376
38	1	0	4.989610	-1.326373	-1.712076
39	1	0	4.302953	-0.848129	2.825713
40	1	0	4.388598	0.908421	2.665482
41	1	0	5.498851	-0.116554	1.754268
42	1	0	-4.576869	-1.786778	0.997167
43	1	0	-3.407731	-0.764213	1.840248
44	1	0	-3.700298	-2.409016	2.397631
45	1	0	2.600468	-1.351391	-2.720253
46	1	0	1.181653	-0.295968	-2.602142
47	1	0	1.769913	-0.654460	3.107694
48	1	0	1.809752	1.114616	2.904408

3f (B3LYP-D3/6-311+G(d,p);SCRF=PCM,benzene)

1	50	0	0.004467	-1.093837	0.174075
2	6	0	0.778794	0.322658	-1.863216
3	6	0	0.733442	0.350220	2.166108
4	6	0	-2.283655	0.056363	0.160837
5	6	0	1.992949	-0.463297	-1.935841
6	6	0	-0.251213	-0.380513	-2.573087
7	6	0	2.110721	-0.022566	1.907730
8	6	0	0.150075	-0.653233	3.008473
9	7	0	-2.539523	1.374631	-0.046513
10	7	0	-3.498146	-0.545672	0.088705
11	14	0	3.659819	0.005816	-1.230414
12	6	0	1.654414	-1.644341	-2.623845
13	6	0	0.290632	-1.597156	-3.011470
14	14	0	3.351796	0.964314	0.915154
15	6	0	2.303016	-1.267320	2.540548
16	6	0	1.114833	-1.648658	3.213183
17	6	0	-3.904318	1.602270	-0.256989
18	6	0	-1.475073	2.400002	0.043123
19	6	0	-4.507820	0.383107	-0.175487
20	6	0	-3.756730	-1.999246	0.231601
21	6	0	4.738111	-1.548742	-1.104131
22	6	0	4.533915	1.256908	-2.364183
23	6	0	5.006918	1.023661	1.838757
24	6	0	2.681144	2.733714	0.725207
25	6	0	-4.528610	2.927755	-0.550936
26	6	0	-1.351340	3.243697	-1.227454
27	6	0	-1.606166	3.238850	1.316959
28	6	0	-5.946220	0.017195	-0.336068
29	6	0	-3.295854	-2.764330	-1.011584
30	6	0	-3.186931	-2.550059	1.539422

31	1	0	-1.260651	-0.027778	-2.738759
32	1	0	-0.850531	-0.628459	3.419946
33	1	0	2.321331	-2.478531	-2.799919
34	1	0	-0.245878	-2.373843	-3.540949
35	1	0	3.210791	-1.856481	2.502170
36	1	0	0.971089	-2.562731	3.774704
37	1	0	-0.565364	1.812009	0.132701
38	1	0	-4.841305	-2.086369	0.293285
39	1	0	4.855193	-2.023263	-2.083809
40	1	0	5.735458	-1.301789	-0.728026
41	1	0	4.290292	-2.280326	-0.425822
42	1	0	3.921574	2.153363	-2.500150
43	1	0	5.497575	1.566203	-1.946136
44	1	0	4.714069	0.821226	-3.352242
45	1	0	5.394659	0.013345	1.998649
46	1	0	5.757104	1.585418	1.273182
47	1	0	4.887699	1.497496	2.818033
48	1	0	2.528688	3.201623	1.703019
49	1	0	3.376553	3.355281	0.153404
50	1	0	1.723800	2.739550	0.196010
51	1	0	-5.613523	2.845570	-0.486947
52	1	0	-4.219403	3.698515	0.156001
53	1	0	-4.282353	3.277856	-1.556671
54	1	0	-2.157443	3.971276	-1.325179
55	1	0	-0.411278	3.799561	-1.191305
56	1	0	-1.336258	2.610423	-2.116405
57	1	0	-1.702412	2.596253	2.194405
58	1	0	-0.710534	3.852947	1.438149
59	1	0	-2.466824	3.908770	1.283369
60	1	0	-6.532675	0.901294	-0.584648
61	1	0	-6.091627	-0.709405	-1.140878
62	1	0	-6.364423	-0.409889	0.580506
63	1	0	-2.211960	-2.719470	-1.132050
64	1	0	-3.585514	-3.814590	-0.927454
65	1	0	-3.753482	-2.349433	-1.912886
66	1	0	-3.533604	-1.961046	2.391201
67	1	0	-3.520129	-3.582264	1.671589
68	1	0	-2.095971	-2.550547	1.546819
69	1	0	0.330648	1.343483	2.027311
70	1	0	0.744115	1.370448	-1.595610

3f (B3LYP-D3/6-311+G(d,p))

1	50	0	-0.046698	-1.108144	0.198454
2	6	0	-0.940831	0.020334	-1.939206
3	6	0	-0.520528	0.637708	2.027416
4	6	0	2.291276	0.029216	-0.059059
5	6	0	-2.179371	-0.715351	-1.777367
6	6	0	-0.008854	-0.824983	-2.630020
7	6	0	-1.915639	0.250100	1.945088
8	6	0	0.134957	-0.248186	2.942406
9	7	0	2.561655	1.341543	-0.284467
10	7	0	3.511733	-0.555024	0.058004
11	14	0	-3.762727	-0.076893	-1.015408
12	6	0	-1.944265	-1.998396	-2.306401
13	1	0	0.987142	-0.546596	-2.947881
14	6	0	-0.626443	-2.067577	-2.825268
15	14	0	-3.238845	1.128359	0.957928
16	6	0	-2.050673	-0.894714	2.757564
17	1	0	1.167547	-0.178212	3.258182
18	6	0	-0.808081	-1.193722	3.368263
19	6	0	3.940552	1.584318	-0.308176
20	6	0	1.485478	2.326451	-0.534974
21	6	0	4.539526	0.380631	-0.089188
22	6	0	3.751238	-1.996788	0.306283
23	6	0	-4.887947	-1.548978	-0.617103
24	6	0	-4.664317	1.068155	-2.236152
25	1	0	-2.649830	-2.818868	-2.291679
26	1	0	-0.169824	-2.935098	-3.283257
27	6	0	-4.789693	1.354307	2.024189
28	6	0	-2.564427	2.841300	0.476485
29	1	0	-2.959069	-1.469976	2.884143
30	1	0	-0.615429	-2.023851	4.034990
31	6	0	4.582798	2.921022	-0.492384
32	1	0	0.577927	1.763407	-0.335241
33	6	0	1.442475	2.760859	-2.002016
34	6	0	1.519101	3.504901	0.442161
35	6	0	5.990036	0.040520	0.006327
36	1	0	4.835786	-2.108038	0.304305
37	6	0	3.201662	-2.856677	-0.834308
38	6	0	3.249187	-2.413371	1.690631
39	1	0	-5.102401	-2.130313	-1.519643
40	1	0	-5.842016	-1.213242	-0.199720
41	1	0	-4.415565	-2.216284	0.109176
42	1	0	-4.030051	1.913121	-2.520141
43	1	0	-5.585785	1.469369	-1.801698
44	1	0	-4.925873	0.525483	-3.150080
45	1	0	-5.168372	0.386753	2.365684
46	1	0	-5.590377	1.849807	1.465955
47	1	0	-4.565148	1.955681	2.910496
48	1	0	-2.303244	3.423260	1.366054
49	1	0	-3.305510	3.406418	-0.096078
50	1	0	-1.667636	2.753469	-0.143905
51	1	0	5.653200	2.797036	-0.658553

52	1	0	4.456932	3.557369	0.387611
53	1	0	4.180779	3.458687	-1.352033
54	1	0	2.312904	3.356871	-2.282330
55	1	0	0.553364	3.373481	-2.171207
56	1	0	1.386333	1.892938	-2.660521
57	1	0	1.669791	3.158813	1.466879
58	1	0	0.560169	4.026317	0.399407
59	1	0	2.298831	4.227417	0.197687
60	1	0	6.595748	0.935394	-0.135920
61	1	0	6.291371	-0.685146	-0.755347
62	1	0	6.247057	-0.375354	0.985469
63	1	0	2.113195	-2.810332	-0.892415
64	1	0	3.487337	-3.899842	-0.677395
65	1	0	3.604686	-2.527343	-1.794881
66	1	0	3.695007	-1.787861	2.467737
67	1	0	3.522680	-3.453662	1.883917
68	1	0	2.164582	-2.328133	1.771954
69	1	0	-0.133181	1.596734	1.713405
70	1	0	-0.853160	1.094915	-1.847033

3g (B3LYP-D3/6-311+G(d,p);SCRF=PCM,benzene)

1	50	0	0.469591	-0.953552	0.084235
2	6	0	-1.138447	-0.445877	-1.818061
3	6	0	-0.919931	-0.133283	2.030002
4	6	0	1.507649	1.347760	-0.198105
5	6	0	-1.706200	-1.781535	-1.825073
6	6	0	-0.005973	-0.451007	-2.706232
7	6	0	-1.783393	-1.299419	2.001909
8	6	0	0.174092	-0.424779	2.919909
9	7	0	1.047115	2.613759	-0.390635
10	7	0	2.857149	1.467210	-0.321887
11	14	0	-3.287157	-2.340848	-1.003097
12	6	0	-0.868407	-2.563587	-2.638197
13	6	0	0.166520	-1.755846	-3.175830
14	14	0	-3.449583	-1.402766	1.161625
15	6	0	-1.154561	-2.277925	2.790974
16	6	0	0.035932	-1.745547	3.351518
17	6	0	2.090360	3.503772	-0.623308
18	6	0	-0.331086	3.021740	-0.261467
19	6	0	3.233213	2.779570	-0.581066
20	6	0	3.792567	0.386025	-0.122457
21	6	0	-3.303023	-4.235297	-0.921910
22	6	0	-4.786308	-1.772104	-2.027215
23	6	0	-4.146326	0.357433	1.013913
24	6	0	-4.616145	-2.455987	2.223971
25	6	0	-1.131934	3.157787	-1.398244
26	6	0	-0.809622	3.310568	1.028172
27	6	0	4.203831	-0.380796	-1.218518
28	6	0	4.265291	0.152146	1.176613
29	6	0	-2.473112	3.513905	-1.208003
30	6	0	-0.615418	2.958683	-2.801482
31	6	0	-2.149573	3.662183	1.163761
32	6	0	0.107462	3.266636	2.224113
33	6	0	5.090047	-1.433203	-0.975755
34	6	0	3.688466	-0.118928	-2.609876
35	6	0	5.143378	-0.914262	1.367604
36	6	0	3.852301	1.035356	2.326542
37	6	0	-3.003181	3.749525	0.057802
38	6	0	5.558367	-1.723375	0.306407
39	6	0	-4.465697	4.062316	0.245561
40	6	0	6.469961	-2.901113	0.547201
41	1	0	-1.659050	0.444364	-1.484957
42	1	0	-1.241448	0.857954	1.741125
43	1	0	0.598379	0.406453	-2.960685
44	1	0	0.953032	0.261843	3.220091
45	1	0	-0.981775	-3.625833	-2.814294
46	1	0	0.961716	-2.095392	-3.827311
47	1	0	-1.518162	-3.285912	2.948406
48	1	0	0.727411	-2.277270	3.992348
49	1	0	1.917446	4.552374	-0.793906
50	1	0	4.263175	3.064964	-0.708010
51	1	0	-2.473038	-4.609186	-0.315939
52	1	0	-3.212980	-4.668386	-1.923410
53	1	0	-4.236168	-4.599056	-0.481267
54	1	0	-4.754014	-2.202231	-3.033408
55	1	0	-4.794769	-0.682490	-2.126133
56	1	0	-5.727167	-2.074847	-1.555573
57	1	0	-4.238327	0.823565	2.000227
58	1	0	-5.134046	0.350246	0.543093
59	1	0	-3.492391	0.989794	0.407668
60	1	0	-4.204020	-3.458170	2.373918
61	1	0	-5.594819	-2.565661	1.746121
62	1	0	-4.762903	-2.001385	3.208671
63	1	0	-3.113489	3.603585	-2.080005
64	1	0	0.456426	2.769373	-2.828866
65	1	0	-0.817340	3.849558	-3.402433
66	1	0	-1.116153	2.115243	-3.281465
67	1	0	-2.540622	3.865853	2.155207
68	1	0	0.615149	2.305382	2.302254
69	1	0	-0.448878	3.431054	3.147037
70	1	0	0.882185	4.035937	2.148557
71	1	0	5.416070	-2.043361	-1.812003
72	1	0	4.355902	-0.552632	-3.356093

73	1	0	3.587717	0.948466	-2.816894
74	1	0	2.701883	-0.571550	-2.737563
75	1	0	5.511115	-1.117634	2.368113
76	1	0	4.204362	0.629438	3.275244
77	1	0	2.767445	1.135581	2.380156
78	1	0	4.262094	2.044050	2.214549
79	1	0	-5.003572	3.160901	0.556957
80	1	0	-4.921851	4.421178	-0.679172
81	1	0	-4.615720	4.818122	1.020485
82	1	0	7.131396	-2.727010	1.398808
83	1	0	7.085790	-3.115783	-0.328964
84	1	0	5.882385	-3.799281	0.764786

3g (B3LYP-D3/6-311+G(d,p))

1	50	0	0.443370	-0.976619	0.114036
2	6	0	-1.120075	-0.431789	-1.804803
3	6	0	-0.946554	-0.133713	2.046543
4	6	0	1.513918	1.350698	-0.189865
5	6	0	-1.688645	-1.767467	-1.828509
6	6	0	0.021320	-0.431446	-2.681753
7	6	0	-1.799131	-1.307169	1.984938
8	6	0	0.135515	-0.431645	2.947412
9	7	0	1.056645	2.614729	-0.406330
10	7	0	2.862068	1.462620	-0.339430
11	14	0	-3.283222	-2.328757	-1.035126
12	6	0	-0.842328	-2.543588	-2.637443
13	6	0	0.197242	-1.732466	-3.159061
14	14	0	-3.460763	-1.403689	1.134688
15	6	0	-1.171426	-2.294195	2.765255
16	6	0	0.003378	-1.760891	3.353887
17	6	0	2.098955	3.495034	-0.678155
18	6	0	-0.317910	3.029086	-0.262409
19	6	0	3.239367	2.767071	-0.637736
20	6	0	3.798521	0.384449	-0.129825
21	6	0	-3.307155	-4.223092	-0.967790
22	6	0	-4.763329	-1.742149	-2.075428
23	6	0	-4.145734	0.362605	0.990229
24	6	0	-4.638547	-2.451226	2.188990
25	6	0	-1.130482	3.172459	-1.390054
26	6	0	-0.783150	3.310497	1.033504
27	6	0	4.219755	-0.386322	-1.218694
28	6	0	4.262078	0.157248	1.173525
29	6	0	-2.468135	3.531746	-1.183519
30	6	0	-0.633858	2.967933	-2.799917
31	6	0	-2.120478	3.664676	1.184796
32	6	0	0.144631	3.248822	2.220388
33	6	0	5.111118	-1.431775	-0.964960
34	6	0	3.704525	-0.140496	-2.612662
35	6	0	5.146639	-0.901114	1.375288
36	6	0	3.813083	1.028680	2.318531
37	6	0	-2.985015	3.760668	0.088648
38	6	0	5.574271	-1.711868	0.320651
39	6	0	-4.445402	4.071853	0.293598
40	6	0	6.492700	-2.881740	0.573803
41	1	0	-1.647066	0.455726	-1.474731
42	1	0	-1.271055	0.859251	1.767632
43	1	0	0.628349	0.427717	-2.924203
44	1	0	0.897817	0.259301	3.278678
45	1	0	-0.954495	-3.603923	-2.823524
46	1	0	0.994762	-2.068065	-3.809473
47	1	0	-1.527590	-3.307718	2.900098
48	1	0	0.687695	-2.296661	3.998381
49	1	0	1.926729	4.539736	-0.871911
50	1	0	4.268291	3.044412	-0.789371
51	1	0	-2.484502	-4.604882	-0.356881
52	1	0	-3.208857	-4.649705	-1.971206
53	1	0	-4.245547	-4.587852	-0.539429
54	1	0	-4.715221	-2.159900	-3.086024
55	1	0	-4.765906	-0.651573	-2.162921
56	1	0	-5.713873	-2.046090	-1.624645
57	1	0	-4.234516	0.826521	1.977892
58	1	0	-5.133198	0.363451	0.518863
59	1	0	-3.486369	0.990607	0.385283
60	1	0	-4.235958	-3.457733	2.335119
61	1	0	-5.617891	-2.550546	1.710332
62	1	0	-4.781876	-2.001097	3.176069
63	1	0	-3.117799	3.626441	-2.048158
64	1	0	0.444243	2.821458	-2.846704
65	1	0	-0.884906	3.837042	-3.414053
66	1	0	-1.106276	2.093271	-3.252425
67	1	0	-2.501381	3.861913	2.181521
68	1	0	0.618638	2.270874	2.302657
69	1	0	-0.396207	3.440998	3.147256
70	1	0	0.944956	3.989905	2.129665
71	1	0	5.444428	-2.045112	-1.796073
72	1	0	4.371242	-0.582658	-3.354710
73	1	0	3.603273	0.924270	-2.832795
74	1	0	2.717387	-0.594081	-2.732120
75	1	0	5.508718	-1.097802	2.379280
76	1	0	4.279916	0.715839	3.253002
77	1	0	2.730321	0.975443	2.445502
78	1	0	4.065052	2.078831	2.143920
79	1	0	-4.980591	3.165826	0.595992

80	1	0	-4.909674	4.445040	-0.621508
81	1	0	-4.588380	4.816844	1.080335
82	1	0	7.163399	-2.688884	1.414268
83	1	0	7.100774	-3.111002	-0.304105
84	1	0	5.911513	-3.777949	0.815474

5. References

[1] Schäfer, A.; Rohe, K.; Grandjean, A.; Huch, V., *Eur. J. Inorg. Chem.* **2017**, *1*, 35-38.
[2] Kuhn, N.; Kratz, T., *Synthesis* **1993**, *06*, 561-562.
[3] Hintermann, L., *Beilstein J. Org. Chem.* **2007**, *3*, 22.
[4] Arduengo, A. J.; Dias, H. V. R.; Harlow, R. L.; Kline, M., *J. Am. Chem. Soc.* **1992**, *114*, 5530-5534.
[5] Sheldrick, G., *Acta Cryst. A* **2008**, *64*, 112-122.
[6] Fischer, E. O.; Grubert, H., *Z. Naturforsch. B* **1956**, *8*, 423-424.
[7] Almlöf, J.; Fernholt, L.; Fægri, J., Knut; Haaland, A.; Schilling, B. E. R.; Seip, R.; Taugbøl, K., *Acta Chem. Scand.* **1983**, 131-140.
[8] Zark, P.; Schäfer, A.; Mitra, A.; Haase, D.; Saak, W.; West, R.; Müller, T., *J. Organomet. Chem.* **2010**, *695*, 398-408.
[9] Kong, L.; Zhang, J.; Song, H.; Cui, C., *Dalton Trans.* **2009**, *28*, 5444-5446.
[10] York, J. T.; Young, V. G.; Tolman, W. B., *Inorg. Chem.* **2006**, *45*, 4191-4198.
[11] Frisch, M. J.; Trucks, G. W.; Schlegel, H. B.; Scuseria, G. E.; Robb, M. A.; Cheeseman, J. R.; Scalmani, G.; Barone, V.; Mennucci, B.; Petersson, G. A.; Nakatsuji, H.; Caricato, M.; Li, X.; Hratchian, H. P.; Izmaylov, A. F.; Bloino, J.; Zheng, G.; Sonnenberg, J. L.; Hada, M.; Ehara, M.; Toyota, K.; Fukuda, R.; Hasegawa, J.; Ishida, M.; Nakajima, T.; Honda, Y.; Kitao, O.; Nakai, H.; Vreven, T.; Montgomery, J. A.; Peralta, J. E.; Ogliaro, F.; Bearpark, M.; Heyd, J. J.; Brothers, E.; Kudin, K. N.; Staroverov, V. N.; Kobayashi, R.; Normand, J.; Raghavachari, K.; Rendell, A.; Burant, J. C.; Iyengar, S. S.; Tomasi, J.; Cossi, M.; Rega, N.; Millam, J. M.; Klene, M.; Knox, J. E.; Cross, J. B.; Bakken, V.; Adamo, C.; Jaramillo, J.; Gomperts, R.; Stratmann, R. E.; Yazyev, O.; Austin, A. J.; Cammi, R.; Pomelli, C.; Ochterski, J. W.; Martin, R. L.; Morokuma, K.; Zakrzewski, V. G.; Voth, G. A.; Salvador, P.; Dannenberg, J. J.; Dapprich, S.; Daniels, A. D.; Farkas; Foresman, J. B.; Ortiz, J. V.; Cioslowski, J.; Fox, D. J., Gaussian 09 Revision D.01., Wallingford CT, **2009.**
[12] Becke, A. D., *J. Chem. Phys.* **1993**, *98*, 5648-5652.
[13] Lee, C.; Yang, W.; Parr, R. G., *Phys. Rev. B* **1988**, *37*, 785-789.
[14] Vosko, S. H.; Wilk, L.; Nusair, M., *Can. J. Phys.* **1980**, *58*, 1200-1211
[15] Stephens, P. J.; Devlin, F. J.; Chabalowski, C. F.; Frisch, M. J., *J. Phys. Chem.* **1994**, *98*, 11623-11627.
[16] Grimme, S.; Antony, J.; Ehrlich, S.; Krieg, H., *J. Chem. Phys.* **2010**, *132*, 154104.
[17] Curtiss, L. A.; McGrath, M. P.; Blaudeau, J. P.; Davis, N. E.; Jr., R. C. B.; Radom, L., *J. Chem. Phys.* **1995**, *103*, 6104-6113.
[18] Binning, R. C.; Curtiss, L. A., *J. Comput. Chem.* **1990**, *11*, 1206-1216.
[19] McGrath, M. P.; Radom, L., *J. Chem. Phys.* **1991**, *94*, 511-516.
[20] McLean, A. D.; Chandler, G. S., *J. Chem. Phys.* **1980**, *72*, 5639-5648.
[21] Krishnan, R.; Binkley, J. S.; Seeger, R.; Pople, J. A., *J. Chem. Phys.* **1980**, *72*, 650-654.
[22] Bergner, A.; Dolg, M.; Küchle, W.; Stoll, H.; Preuß, H., *Mol. Phys.* **1993**, *80*, 1431-1441.
[23] Igel-Mann, G.; Stoll, H.; Preuss, H., *Mol. Phys.* **1988**, *65*, 1321-1328.
[24] Tomasi, J.; Mennucci, B.; Cammi, R., *Chem. Rev.* **2005**, *105*, 2999-3094.
[25] Romm, I. P.; Noskov, Y. G.; Malkov, A. A., *Russ. Chem. Bull.* **2007**, *56*, 1935-1944.
[26] Fujiang, D.; Fowler, P. W.; Legon, A. C., *J. Chem. Soc. Chem. Commun.* **1995**, 113-114.
[27] Phillips, J. A.; Cramer, C. J., *J. Phys. Chem. B* **2007**, *111*, 1408-1415.
[28] Jonas, V.; Frenking, G., *J. Chem. Soc. Chem. Commun.* **1994**, 1489-1490.
[29] Kendall, R. A.; Jr., T. H. D.; Harrison, R. J., *J. Chem. Phys.* **1992**, *96*, 6796-6806.
[30] Woon, D. E.; Jr., T. H. D., *J. Chem. Phys.* **1993**, *98*, 1358-1371.
[31] Peterson, K. A.; Woon, D. E.; Jr., T. H. D., *J. Chem. Phys.* **1994**, *100*, 7410-7415.
[32] Jr., T. H. D., *J. Chem. Phys.* **1989**, *90*, 1007-1023.
[33] Wilson, A. K.; van Mourik, T.; Dunning, T. H., *J. Mol. Struct. THEOCHEM* **1996**, *388*, 339-349.

6.2 Synthesis, Structure, and Bonding Analysis of Tin(II) Dihalide and Cyclopentadienyltin(II) Halide (Alkyl)(amino)carbene Complexes

Supplementary Information

for

Synthesis, Structure, and Bonding Analysis of Tin(II) Dihalide and Cyclopentadienyltin(II) Halide (Alkyl)(amino)carbene Complexes

Carsten Müller, Diego M. Andrada*, Inga-Alexandra Bischoff, Michael Zimmer, Volker Huch, Nils Steinbrück, André Schäfer*

Faculty of Natural Sciences and Technology, Department of Chemistry, Saarland University, 66123 Saarbrücken, Federal Republic of Germany

1. Experimental Details	S1 – S2
2. NMR Spectra	S3 – S9
3. UV-Vis Spectra	S10 – S11
4. IR Spectra	S12
5. XRD Data	S13 – S16
6. Computational Details	S17 – S27
7. References	S28

1. Experimental Details

All manipulations were carried out under an argon inert gas atmosphere (argon 5.0), using either standard Schlenk line techniques or a glovebox. 2,6-di*iso*propylaniline and isobutyraldehyde were purchased from ABCR and used as received. 3-chloro-2-methyl-1-propene was purchased from TCI and used as received. N-butyllithium solution (2.5 M in hexane) was purchased from Acros Organics and used as received. $LiN(SiMe_3)_2$ was purchased from Sigma Aldrich and used as received. Deuterated chloroform, deuterated benzene and heavy water were purchased from ABCR and, in case of chloroform and benzene, dried over 4 Å molecular sieves.

Synthesis of **1**:
Cyclic (amino)(alkyl)carbene (cAAC) **1** has first been described by Bertrand and coworkers.[1,2]
The following reaction sequence is a modification of the corresponding literature known synthesis.

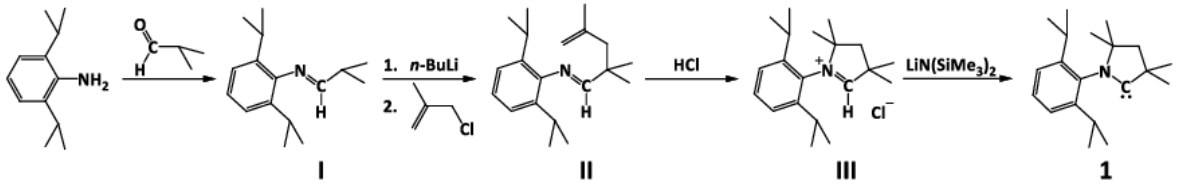

250 g (1.41 mol) 2,6-di*iso*propylaniline (technical grade, 90%) and 400 g (5.55 mol) isobutyraldehyde were mixed and stirred over activated molecular sieves at room temperature for 72 h. Subsequently, the mixture was decanted of the molecular sieves, all volatiles were removed in vacuum and the brown oily residue was distilled in vacuum (0.01 mbar / 363-378 K) to afford imine **I**.
Yield: 89% / 292 g / 1.26 mmol
^{1}H NMR (400.13 MHz, $CDCl_3$, 299 K): δ = 1.32 (d, ^3J = 7 Hz, 12 H, DipCH-(Me)$_2$), 1.38 (d, ^3J = 7 Hz, 6 H, NCH-(Me)$_2$), 2.79-2.91 (m, 1 H, NCH-(Me)$_2$), 3.09 (sept, ^3J = 7 Hz, 2 H, DipCH-(Me)$_2$), 7.16-7.26 (m, 3 H, Dip-H), 7.68 (d, ^3J = 5 Hz, 1 H, NCH-C(Me)$_2$).

57.8 g (250 mmol) of imine **I** were dissolved in diethyl ether and the solution was cooled to 195 K. 100 mL of a 2.5 M solution (250 mmol) of *n*-butyllithium were added. After 10 min the mixture had turn yellow and was allowed to warm to room temperature and stirred for an additional 2 h. The solution was again cooled to 195 K and 22.6 g (250 mmol) 3-chloro-2-methylpropene were slowly added. After 10 min the mixture was allowed to warm to room temperature and was stirred overnight. All volatiles were removed in vacuum and the residue was extracted with hexane. After removal of all volatiles in vacuum, **II** was obtained as a yellow to orange oil that can be used in the next step without further purification (purity as estimated by ^{1}H NMR spectroscopy: >90%).
Yield: 92% / 65.7 g / 230 mmol
^{1}H NMR (400.13 MHz, $CDCl_3$, 299 K): δ = 1.23 (d, J = 6.9 Hz, 12 H, DipCH-Me), 1.34 (s, 6 H, Me), 1.90 (s, 3 H, Me), 2.39 (s, 2 H, CH_2), 3.00 (sept, ^3J = 6.9 Hz, 2 H, DipCH-(Me)$_2$)), 4.83 (m, 1 H, C=CH_2), 4.98 (m, 1 H, C=CH_2), 7.08-7.19 (m, 3 H, Dip-H), 7.65 (s, 1H, N=C-H).

The complete batch of imine **II** from the previous reaction step was dissolved in acetonitrile and cooled to 195 K. 125 mL of a 2 M solution (250 mmol) of HCl in diethyl ether were added dropwise. The resulting suspension was allowed to warm to room temperature and heated to 328 K for 24 h. After cooling to room temperature, the precipitate was collected by filtration and all volatiles were evaporated in vacuum, to obtain a beige solid. This crude product was washed several times with toluene and then dried in vacuum for 4 h at 413 K. Iminium chloride **III** was obtained as a colorless crystalline solid.

Yield: 54% / 43.6 g / 135 mmol

^{1}H NMR (400.13 MHz, D_2O, 299 K): δ = 1.08 (d, ^{3}J = 6 Hz, 6 H, DipCH-(Me)$_2$), 1.35 (d, ^{3}J = 6 Hz, 6 H, DipCH-(Me)$_2$), 1.57 (s, 6H, Me), 1.61 (s, 6H, Me), 2.51 (s, 2H, CH_2), 2.77 (sept, ^{3}J = 7 Hz, 2H, DipCH-(Me)$_2$), 7.51 (d, ^{3}J = 8 Hz, 2H, *m*-Dip-H), 7.63 (t, ^{3}J = 8 Hz, 2H, *p*-Dip-H), 9.23 (s, 1H, NCH-C(Me)$_2$);

10.0 g (31 mmol) Iminium chloride **III** and 5.19 g (31 mmol) lithium bis(trimethylsilyl)amide were charged into a Schlenk flask, 500 mL of hexane were added and the resulting suspension was stirred overnight at room temperature. After filtration, the filtrate was concentrated under reduced pressure until incipient crystallization was observed and then stored at 253 K overnight. The mother liquor was removed and carbene **1** (cAAC) was obtained in form of colorless crystals, which can be stored under an inert atmosphere for at least several weeks.

Yield: 66% / 5.85 g / 20.5 mmol

^{1}H NMR (400.13 MHz, C_6D_6, 299 K): δ = 1.13 (s, 6 H, Me), 1.27 (d, ^{3}J = 6 Hz, 6 H, DipCH-(Me)$_2$), 1.29 (d, ^{3}J = 6 Hz, 6 H, DipCH-(Me)$_2$), 1.49 (s, 6H, Me), 1.59 (s, 2H, CH_2), 3.18 (sept, ^{3}J = 7 Hz, 2H, DipCH-(Me)$_2$), 7.14-7.18 (m, 1H, *p*-Dip-H), 7.21-7.29 (m, 2H, *m*-Dip-H);

^{13}C NMR (100.61 MHz, C_6D_6, 299 K): δ = 21.9 (Me), 26.2 (Me), 28.2 (Me), 29.2 (Me), 29.5 (Dip$C$H-(Me)$_2$), 50.1 (CH$_2$), 58.2 (C_q), 82.5 (C_q), 123.8 (Dip), 128.1 (Dip), 138.0 (Dip), 146.2 (Dip), 313.6 (carbene-C).

2. NMR Spectra

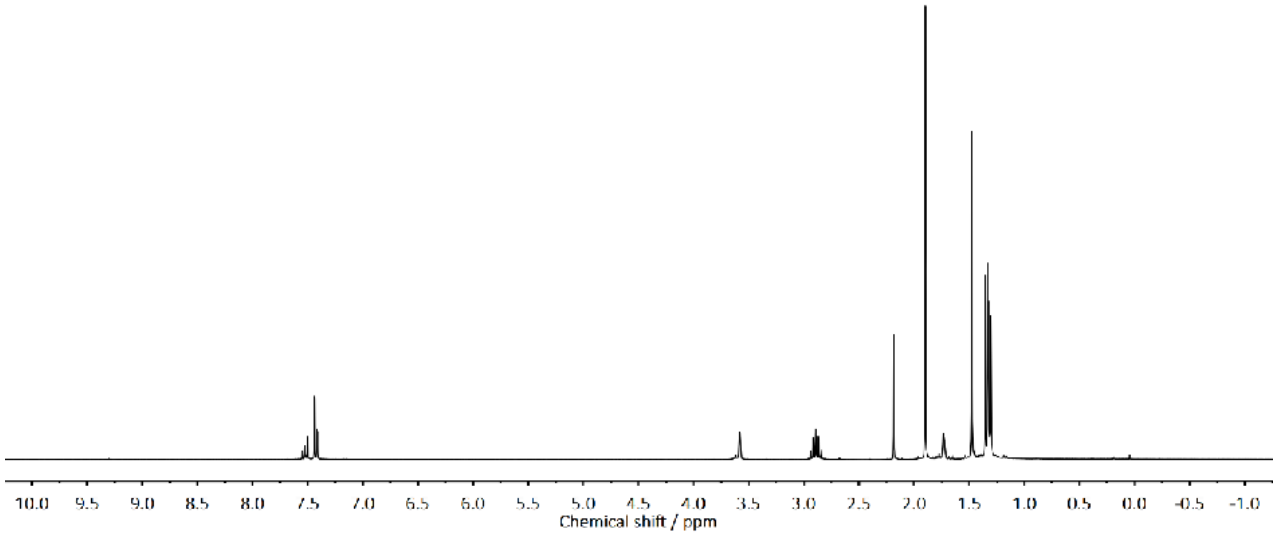

Figure S1: ^{1}H NMR (THF-D8) spectrum of **3b**.

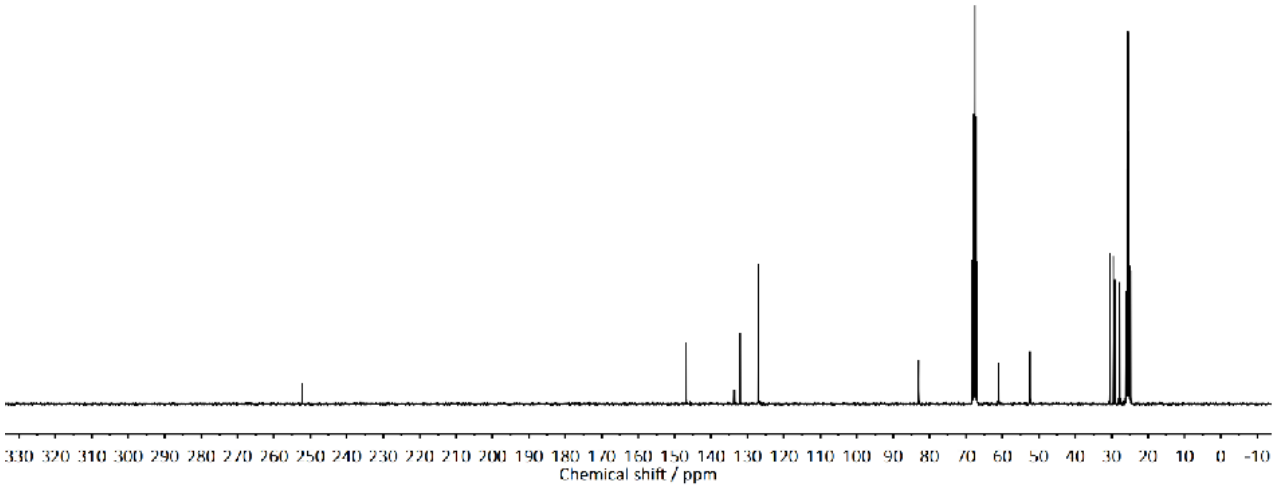

Figure S2: ^{13}C{^{1}H} NMR (THF-D8) spectrum of **3b**.

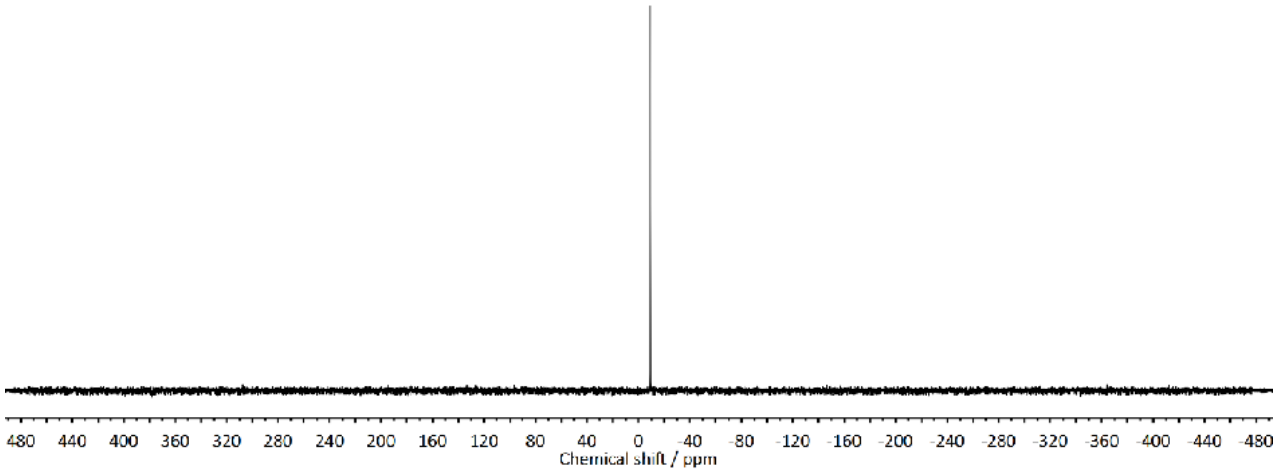

Figure S3: ^{119}Sn{^{1}H} NMR (THF-D8) spectrum of **3b**.

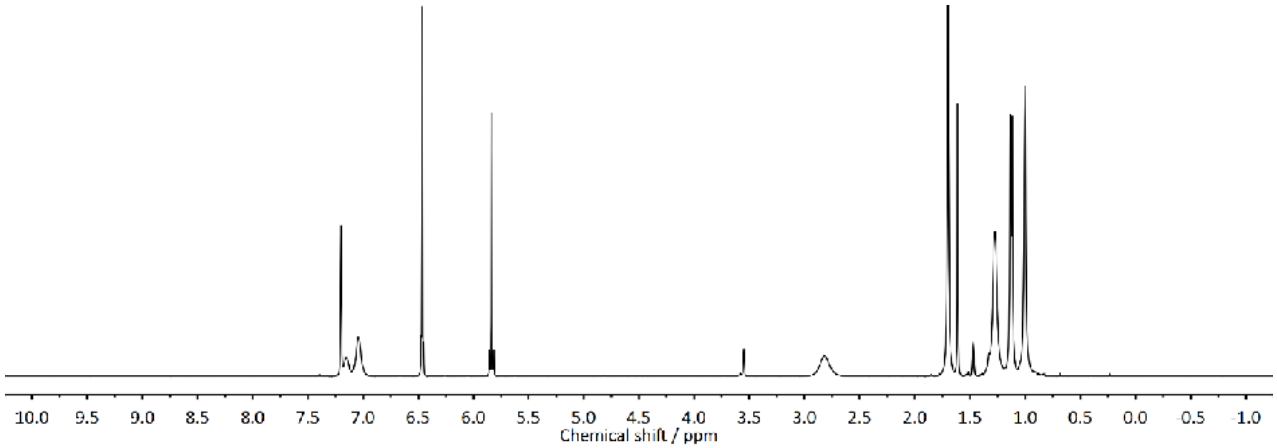

Figure S4: ^{1}H NMR (C_6D_6 / THF-D8) spectrum of **3c**.

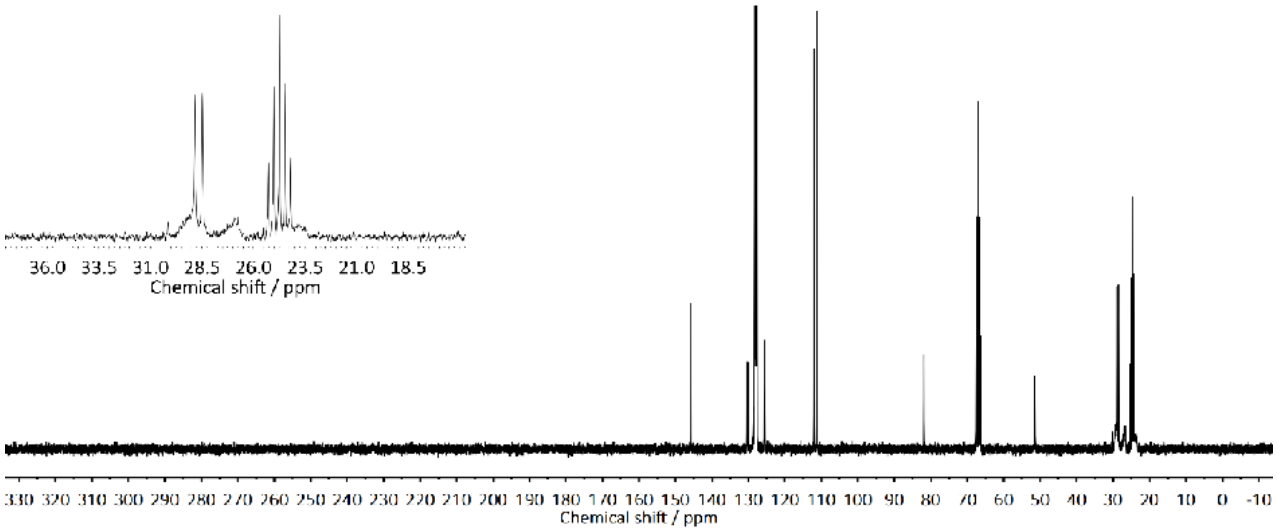

Figure S5: ^{13}C{^{1}H} NMR (C_6D_6 / THF-D8) spectrum of **3c**.

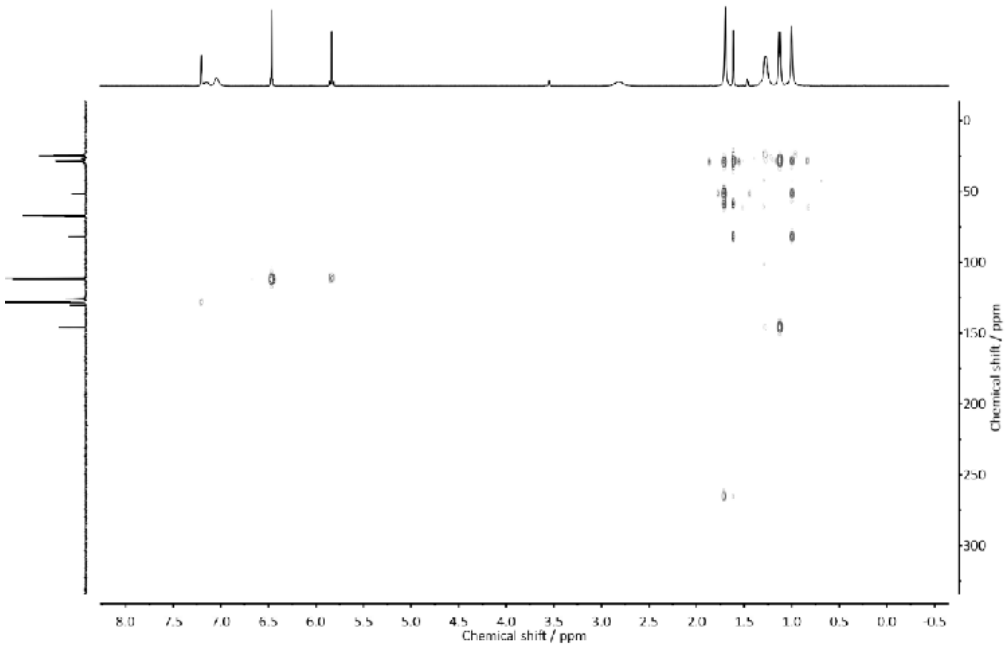

Figure S6: ^{1}H-^{13}C HMBC NMR (C_6D_6 / THF-D8) spectrum of **3c**.

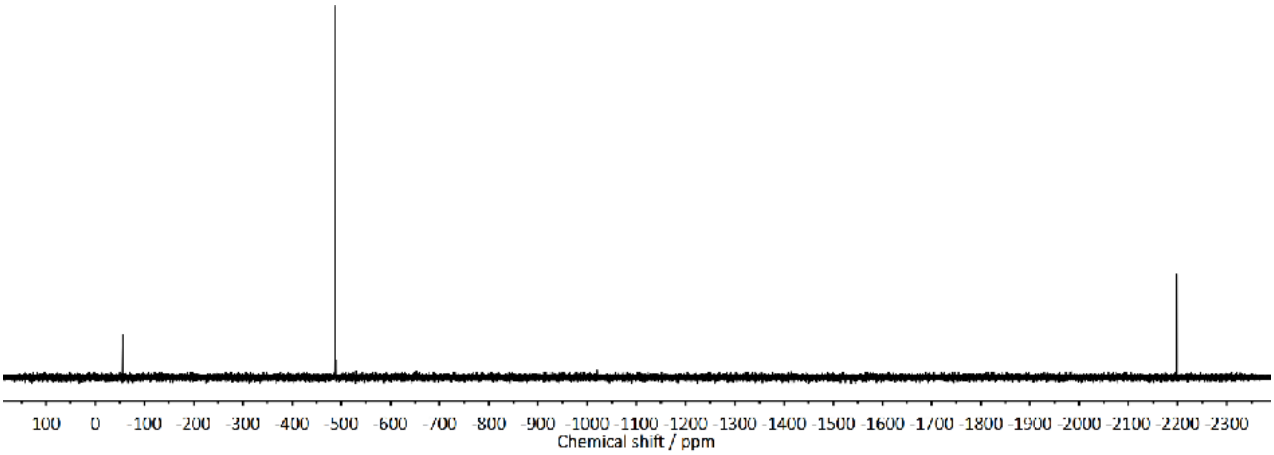

Figure S7: $^{119}Sn\{^{1}H\}$ NMR (THF-D8) spectrum of **3c**.

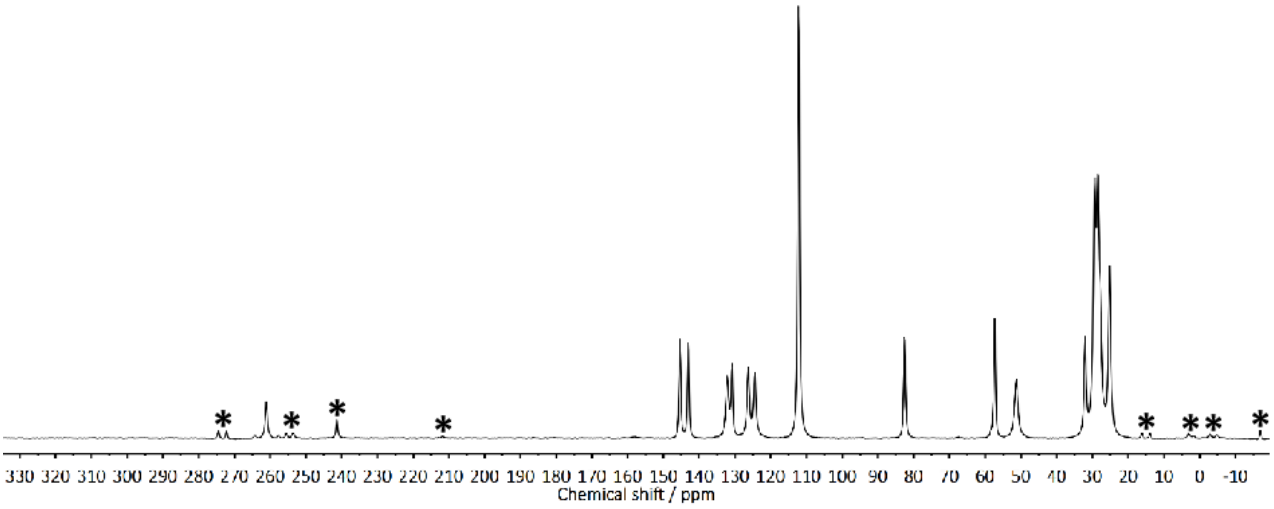

Figure S8: $^{13}C\{^{1}H\}$ Cp-MAS NMR spectra of **3c** at 13 kHz (* spinning sidebands).

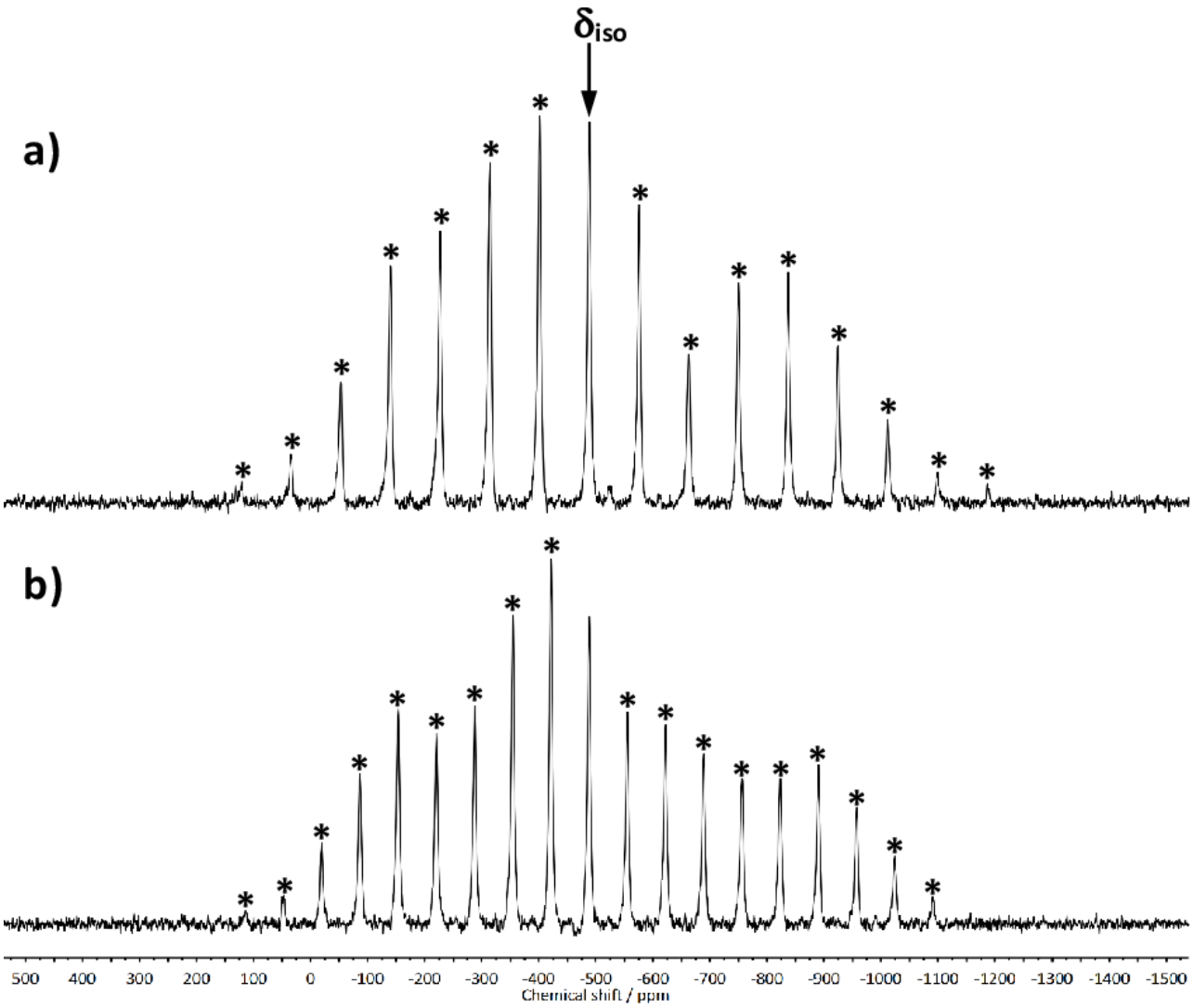

Figure S9: $^{119}Sn\{^{1}H\}$ Cp-MAS NMR spectrum of **3c** at a) 13 kHz and b) 10 kHz (* spinning sidebands).

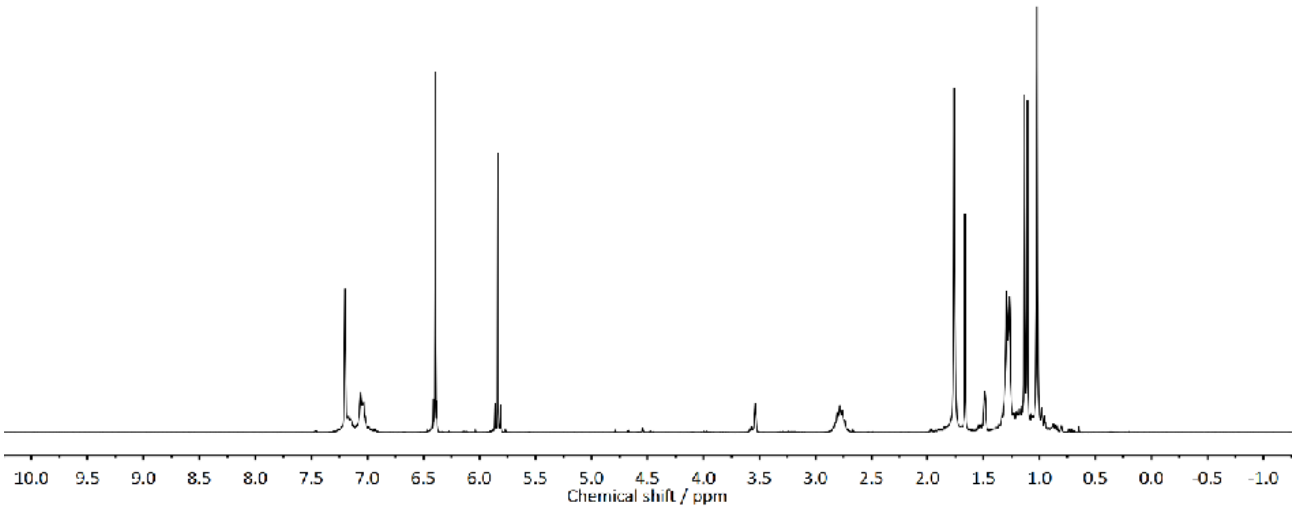

Figure S10: ^{1}H NMR (C_6D_6 / THF-D8) spectrum of **3d**.

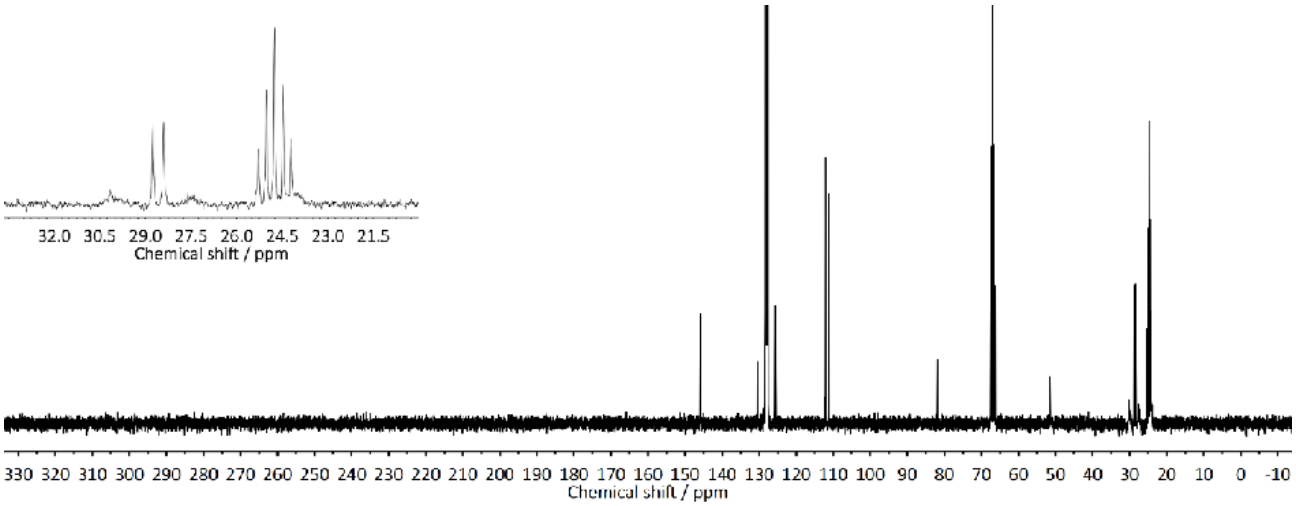

Figure S11: $^{13}C\{^{1}H\}$ NMR (C_6D_6 / THF-D8) spectrum of **3d**.

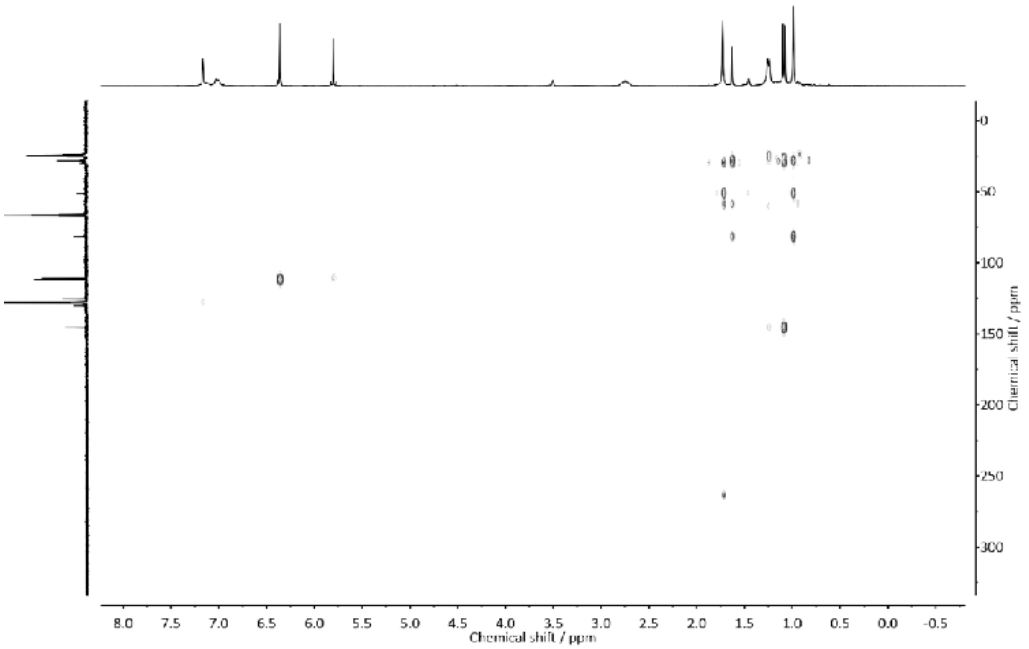

Figure S12: ^{1}H-^{13}C HMBC NMR (C_6D_6 / THF-D8) spectrum of **3d**.

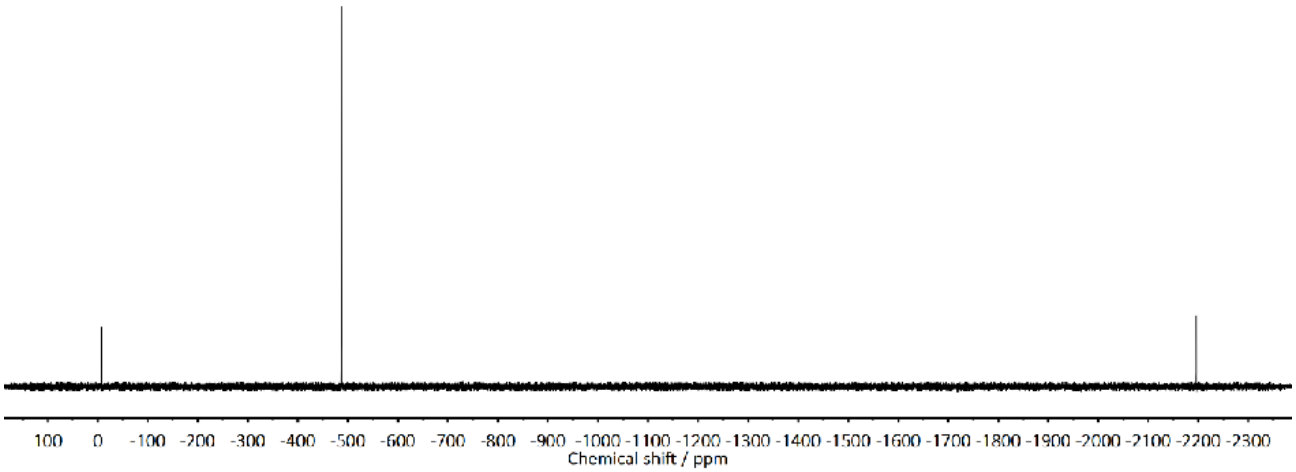

Figure S13: $^{119}Sn\{^{1}H\}$ NMR (THF-D8) spectrum of **3d**.

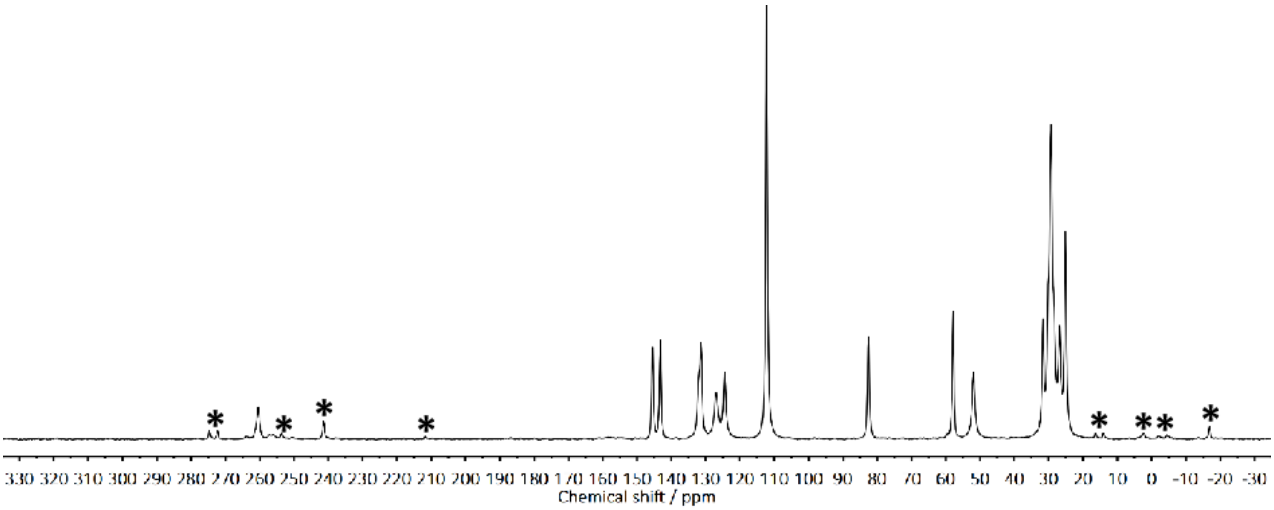

Figure S14: $^{13}C\{^{1}H\}$ Cp-MAS NMR spectra of **3d** at 13 kHz (* spinning sidebands).

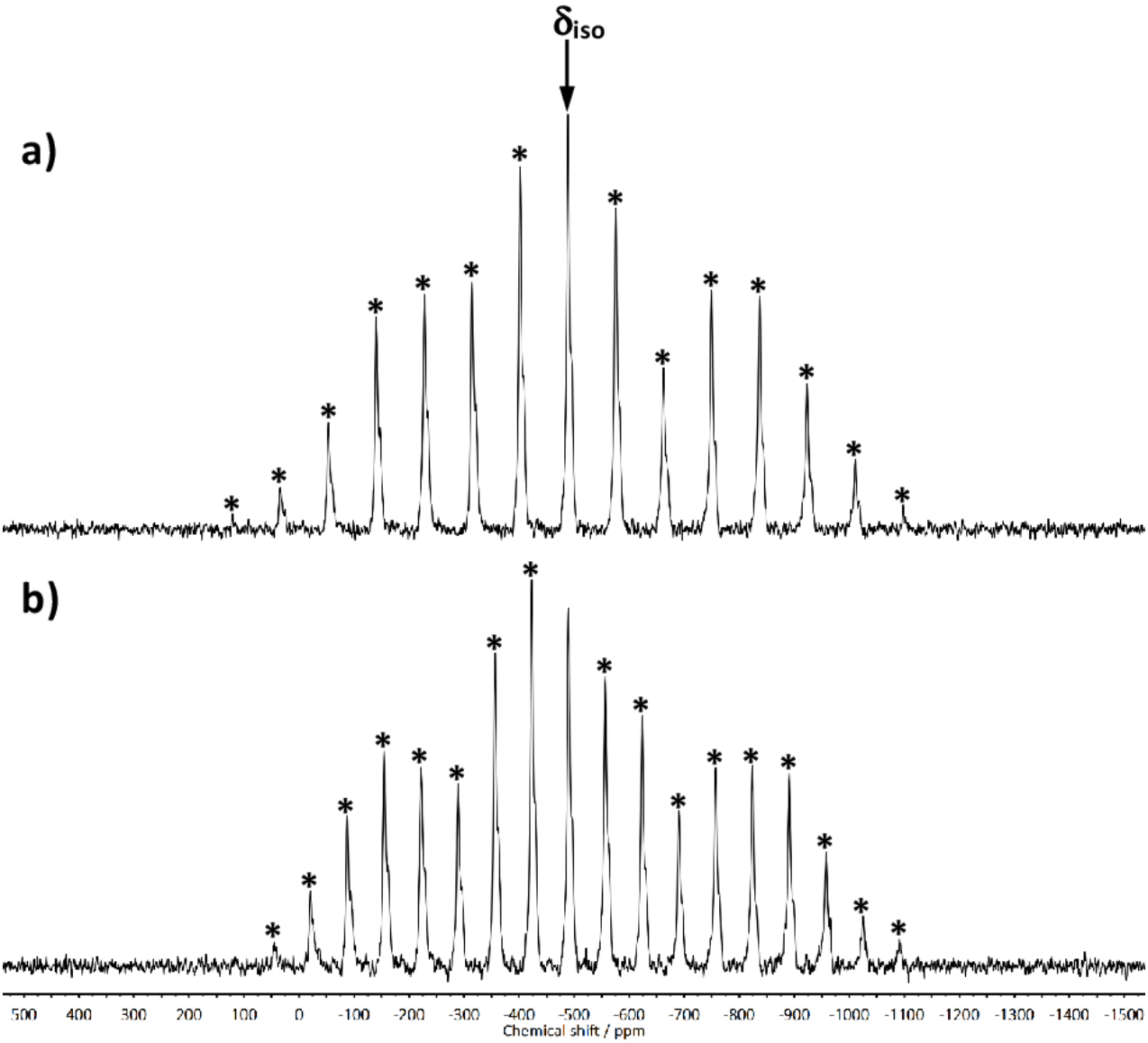

Figure S15: $^{119}Sn\{^{1}H\}$ Cp-MAS NMR spectrum of **3d** at a) 13 kHz and b) 10 kHz (* spinning sidebands).

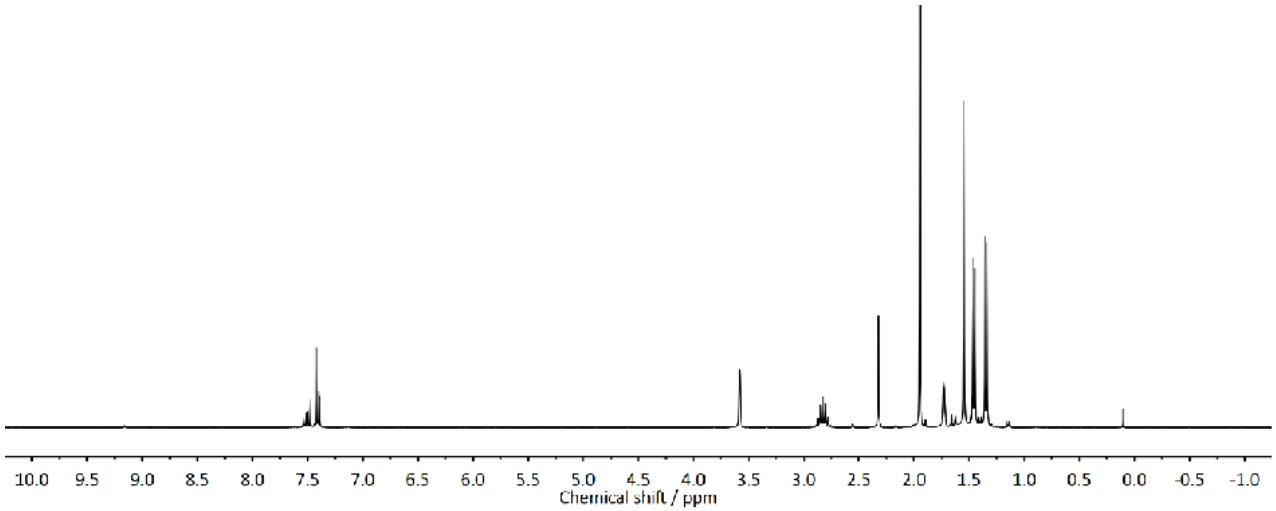

Figure S16: ^{1}H NMR (THF-D8) spectrum of **5**.

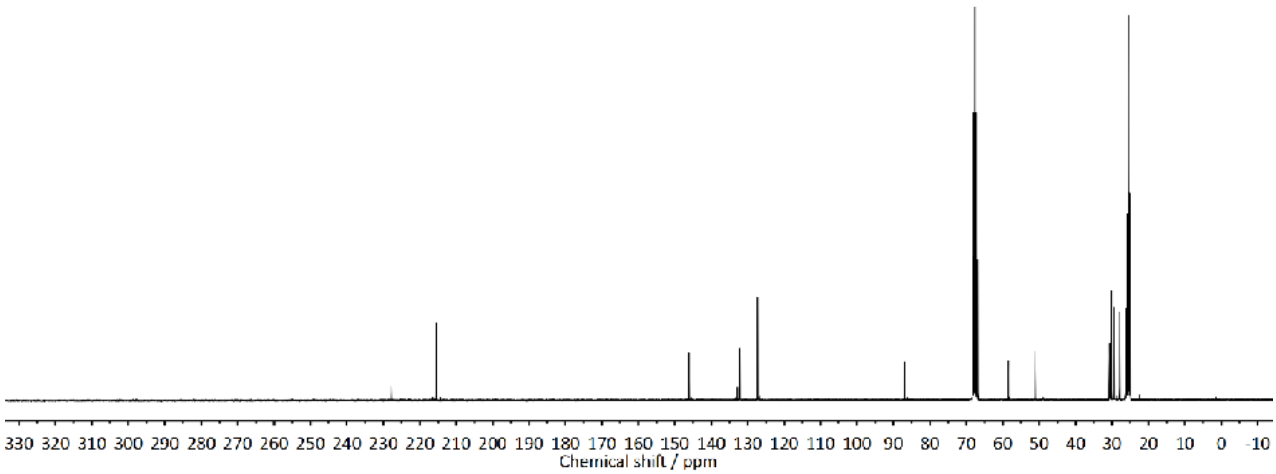

Figure S17: ^{13}C{^{1}H} NMR (THF-D8) spectrum of **5**.

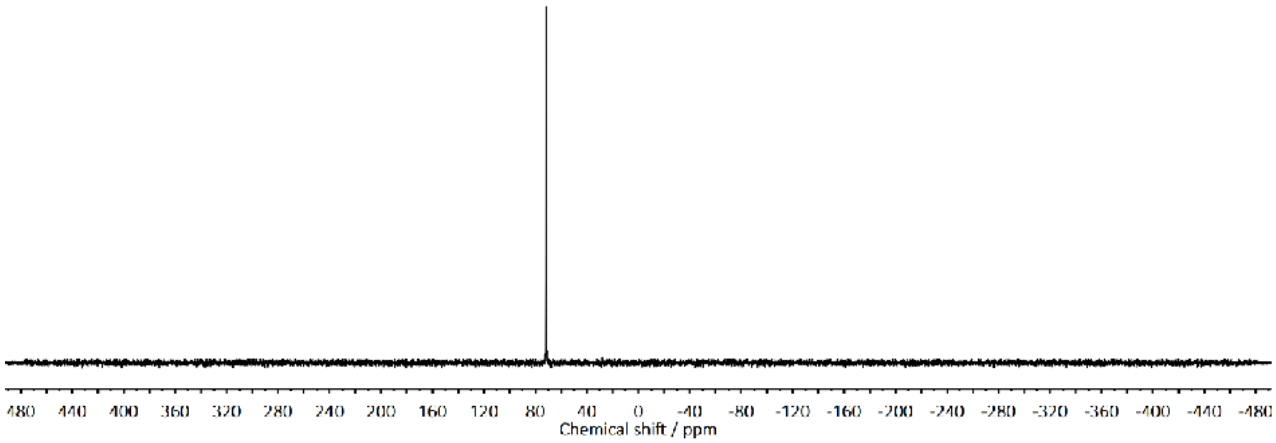

Figure S18: ^{119}Sn{^{1}H} NMR (THF-D8) spectrum of **5**.

3. UV-Vis Spectra

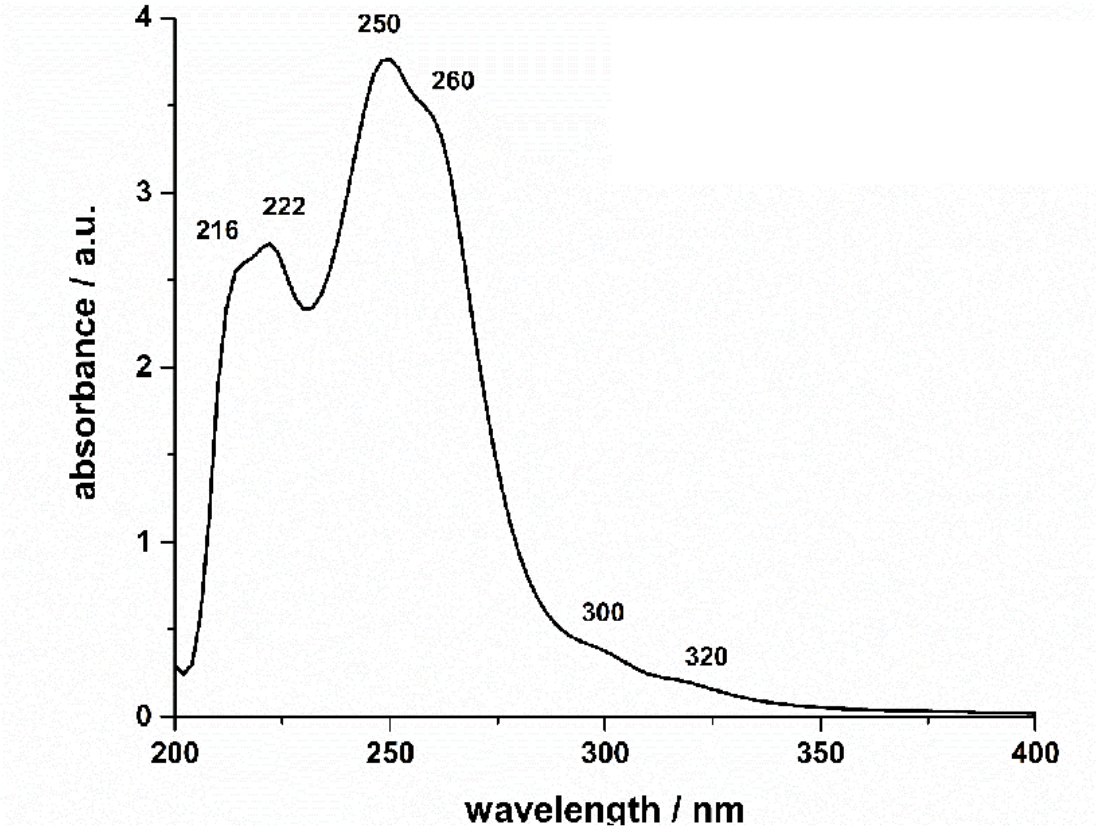

Figure S19: UV-Vis spectra of **3b** in THF.

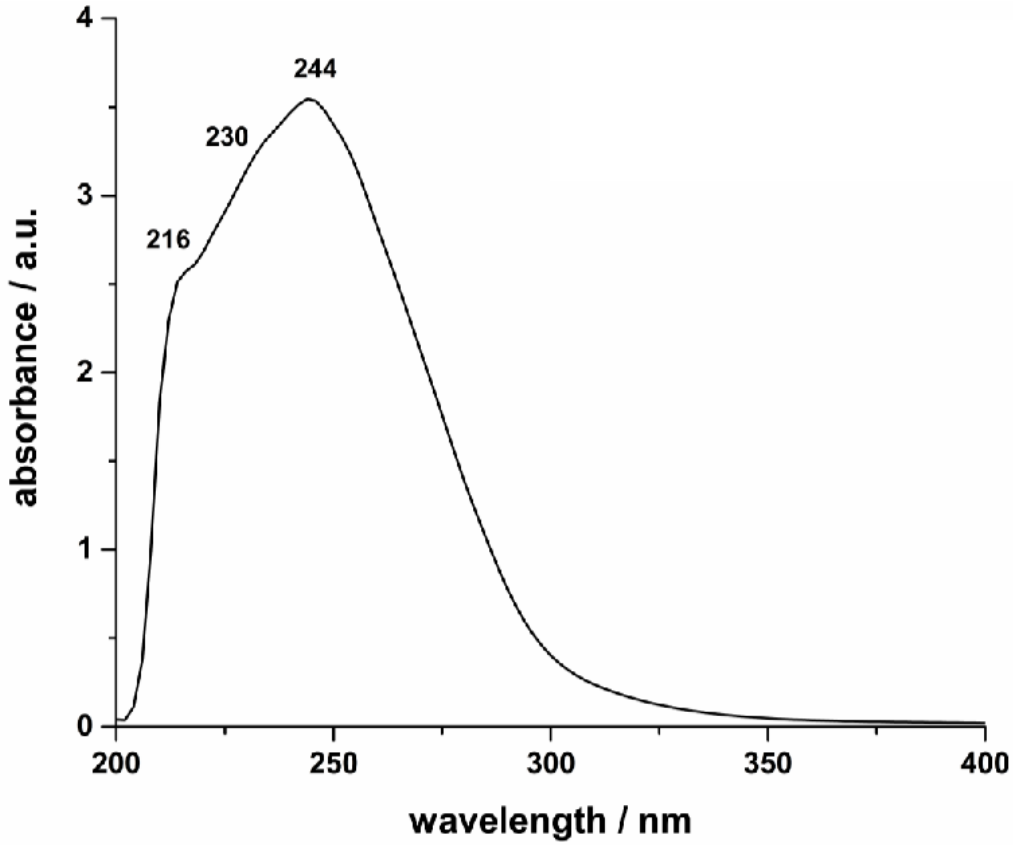

Figure S20: UV-Vis spectra of **3c** in THF.

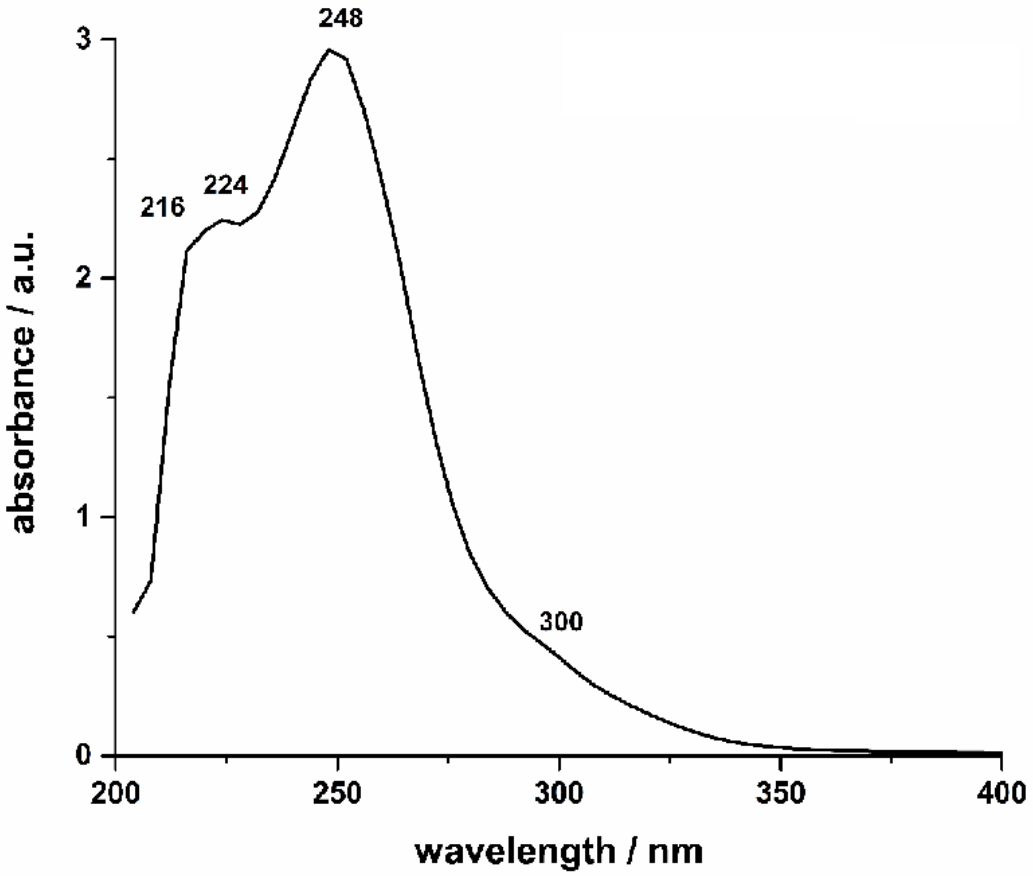

Figure S21: UV-Vis spectra of **3d** in THF.

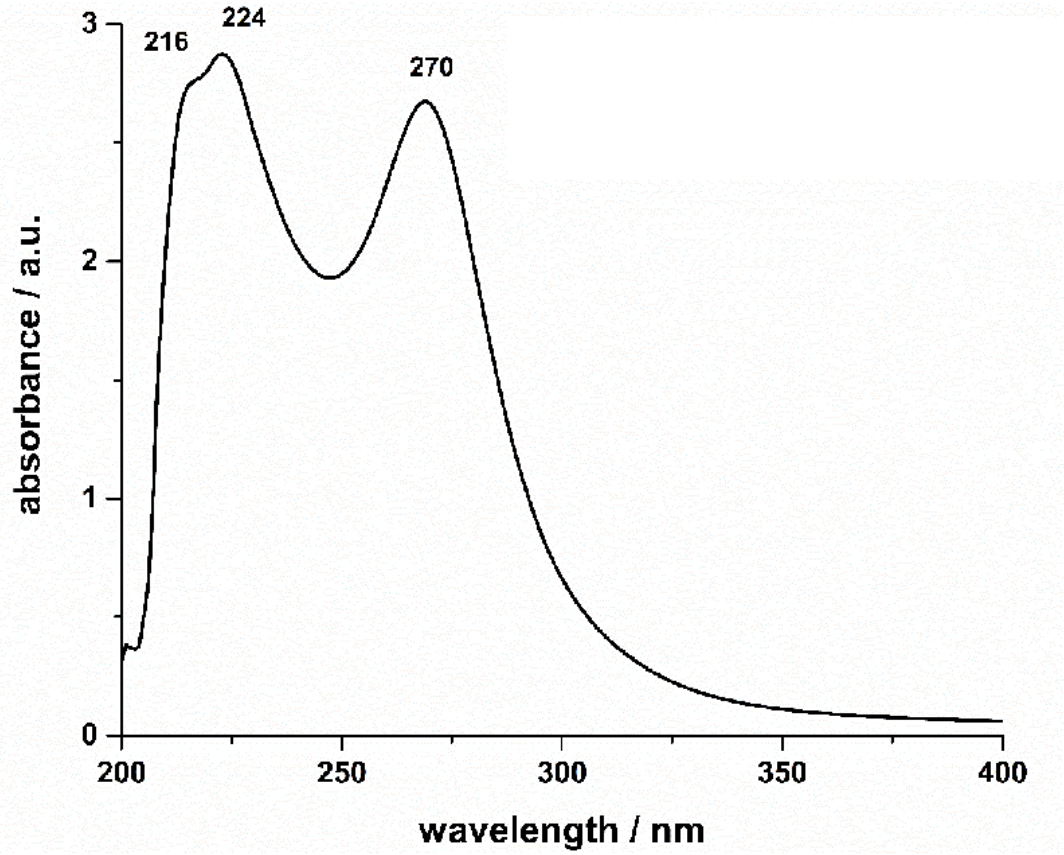

Figure S22: UV-Vis spectra of **5** in THF.

4. IR Spectra

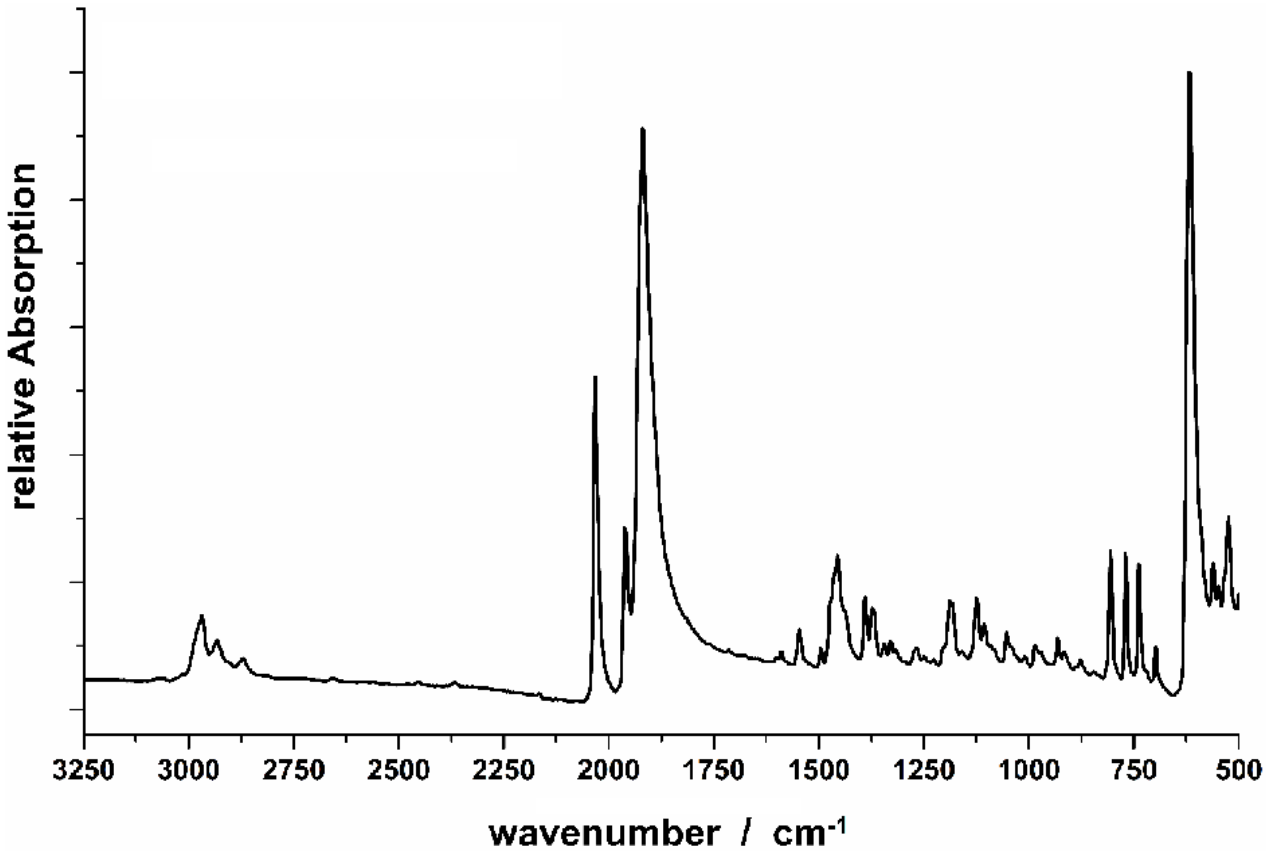

Figure S23: IR spectrum of **5**.

5. XRD Data

All crystal structure data has been deposited with the Cambridge Crystallographic Data Centre (CCDC) and is available free of charge from the Cambridge Structural Database (see CCDC numbers).

Crystallographic data for 3b

CCDC deposition number	1865142	
Empirical formula	$C_{20}H_{31}Br_2NSn$	
Formula weight	563.97	
Temperature	132(2) K	
Wavelength	0.71073 Å	
Crystal system	Monoclinic	
Space group	$P2_1/n$	
Unit cell dimensions	a = 9.7521(2) Å	α= 90°
	b = 17.4105(4) Å	β= 104.9710(10)°
	c = 13.3408(3) Å	γ = 90°
Volume	2188.23(8) $Å^3$	
Z	4	
Density (calculated)	1.712 Mg/m^3	
Absorption coefficient	4.822 mm^{-1}	
F(000)	1112	
Crystal size	0.285 x 0.262 x 0.170 mm^3	
Theta range for data collection	1.966 to 31.624°	
Index ranges	-14<=h<=9, -24<=k<=25, -14<=l<=19	
Reflections collected	29221	
Independent reflections	7355 [R(int) = 0.0206]	
Completeness to theta = 25.242°	100.0 %	
Absorption correction	Semi-empirical from equivalents	
Max. and min. transmission	0.7462 and 0.5938	
Refinement method	Full-matrix least-squares on F^2	
Data / restraints / parameters	7355 / 0 / 341	
Goodness-of-fit on F^2	1.032	
Final R indices [I>2sigma(I)]	R1 = 0.0208, wR2 = 0.0453	
R indices (all data)	R1 = 0.0273, wR2 = 0.0468	
Extinction coefficient	n/a	
Largest diff. peak and hole	1.069 and -0.819 $e.Å^{-3}$	

Crystallographic data for 3c

CCDC deposition number	1865143	
Empirical formula	$C_{25}H_{36}ClNSn$	
Formula weight	504.69	
Temperature	193(2) K	
Wavelength	0.71073 Å	
Crystal system	Monoclinic	
Space group	$P2_1/c$	
Unit cell dimensions	a = 9.1962(2) Å	α= 90°
	b = 15.1678(3) Å	β= 100.8634(11)°
	c = 17.5802(4) Å	γ = 90°
Volume	2408.25(9) $Å^3$	
Z	4	
Density (calculated)	1.392 Mg/m^3	
Absorption coefficient	1.182 mm^{-1}	
F(000)	1040	
Crystal size	0.248 x 0.198 x 0.066 mm^3	
Theta range for data collection	1.787 to 27.718°.	
Index ranges	-12<=h<=12, -19<=k<=19, -22<=l<=16	
Reflections collected	22391	
Independent reflections	5601 [R(int) = 0.0382]	
Completeness to theta = 25.242°	100.0 %	
Absorption correction	Semi-empirical from equivalents	
Max. and min. transmission	0.7456 and 0.6848	
Refinement method	Full-matrix least-squares on F^2	
Data / restraints / parameters	5601 / 30 / 371	
Goodness-of-fit on F^2	1.028	
Final R indices [I>2sigma(I)]	R1 = 0.0304, wR2 = 0.0590	
R indices (all data)	R1 = 0.0443, wR2 = 0.0633	
Extinction coefficient	n/a	
Largest diff. peak and hole	0.477 and -0.363 $e.Å^{-3}$	

Crystallographic data for 3d

CCDC deposition number	1865144	
Empirical formula	$C_{25}H_{36}BrNSn$	
Formula weight	549.15	
Temperature	142(2) K	
Wavelength	0.71073 Å	
Crystal system	Monoclinic	
Space group	$P2_1/c$	
Unit cell dimensions	a = 9.1409(4) Å	α= 90°
	b = 15.3418(7) Å	β= 100.677(2)°
	c = 17.6844(6) Å	γ = 90°
Volume	2437.09(18) $Å^3$	
Z	4	
Density (calculated)	1.497 Mg/m^3	
Absorption coefficient	2.698 mm^{-1}	
F(000)	1112	
Crystal size	0.546 x 0.420 x 0.138 mm^3	
Theta range for data collection	1.771 to 34.935°.	
Index ranges	-14<=h<=12, -24<=k<=24, -28<=l<=28	
Reflections collected	42469	
Independent reflections	10608 [R(int) = 0.0263]	
Completeness to theta = 25.242°	100.0 %	
Absorption correction	Semi-empirical from equivalents	
Max. and min. transmission	0.7469 and 0.5553	
Refinement method	Full-matrix least-squares on F^2	
Data / restraints / parameters	10608 / 24 / 295	
Goodness-of-fit on F^2	1.082	
Final R indices [I>2sigma(I)]	R1 = 0.0272, wR2 = 0.0620	
R indices (all data)	R1 = 0.0371, wR2 = 0.0647	
Extinction coefficient	n/a	
Largest diff. peak and hole	0.855 and -0.819 $e.Å^{-3}$	

Crystallographic data for 5

CCDC deposition number	1865145	
Empirical formula	$C_{24}H_{31}Br_2FeNO_4Sn$, $0.5(C_7H_8)$	
Formula weight	777.92	
Temperature	152(2) K	
Wavelength	0.71073 Å	
Crystal system	Monoclinic	
Space group	$P2_1/n$	
Unit cell dimensions	a = 10.3803(9) Å	α = 90°
	b = 20.1054(16) Å	β = 90.451(4)°
	c = 14.7178(12) Å	γ = 90°
Volume	3071.5(4) $Å^3$	
Z	4	
Density (calculated)	1.682 Mg/m^3	
Absorption coefficient	3.918 mm^{-1}	
F(000)	1540	
Crystal size	0.486 x 0.432 x 0.292 mm^3	
Theta range for data collection	1.715 to 34.334°	
Index ranges	-16<=h<=15, -28<=k<=31, -23<=l<=23	
Reflections collected	93696	
Independent reflections	12834 [R(int) = 0.0245]	
Completeness to theta = 25.242°	100.0 %	
Absorption correction	Semi-empirical from equivalents	
Max. and min. transmission	0.7467 and 0.6153	
Refinement method	Full-matrix least-squares on F^2	
Data / restraints / parameters	12834 / 52 / 357	
Goodness-of-fit on F^2	1.048	
Final R indices [I>2sigma(I)]	R1 = 0.0233, wR2 = 0.0540	
R indices (all data)	R1 = 0.0303, wR2 = 0.0560	
Extinction coefficient	n/a	
Largest diff. peak and hole	0.947 and -0.675 $e.Å^{-3}$	

6. Computational Details

Calculations with different DFT functionals

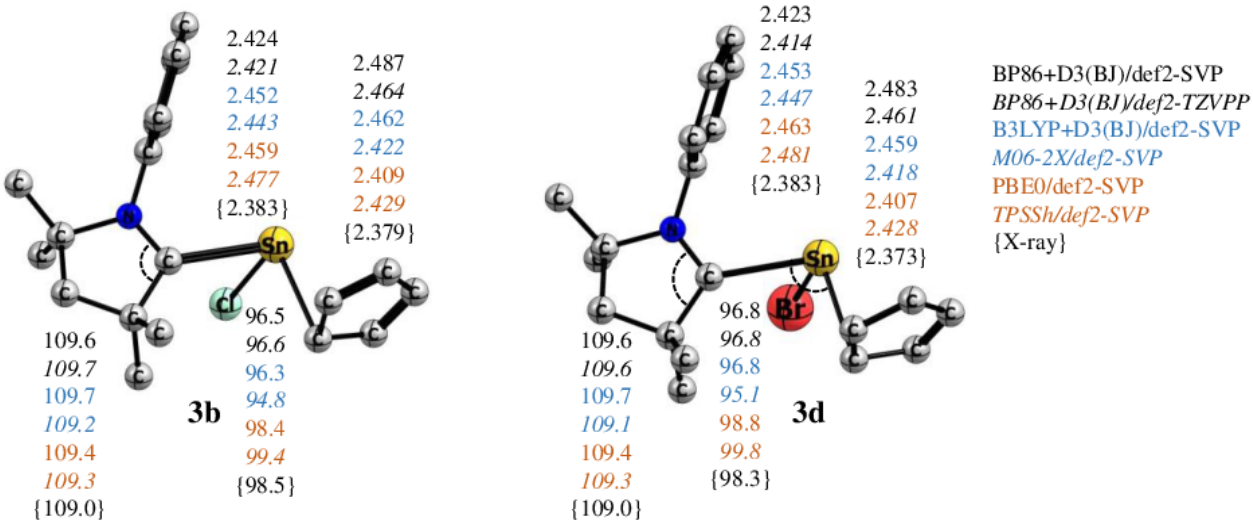

Figure S24. Optimized structure of **3b** and **3d** at the BP86+D3(BJ)/def2-SVP, BP86+D3(BJ)/def2-TZVPP, PBE0/def2-SVP and TPSSh/def2-SVP level of theory. Selected calculated (experimental in parenthesis) bond length and bond angles are in [Å] and [°], respectively. Hydrogen atoms and iso-propyl groups were omitted for clarity.

Bonding Analysis

Orbital	Occ.	Contribution from atoms to the orb	Atomic orbitals
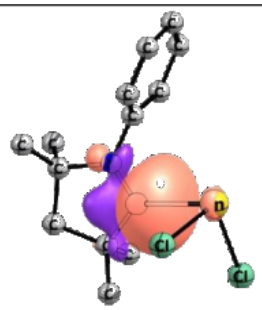	1.67	C	*s*(39.8%), *p*(60.1%), *d*(0.1%)
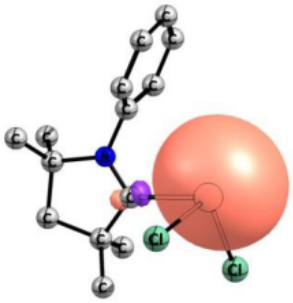	1.98	Sn	*s*(85.6%), *p*(14.4%), *d*(0.01%)
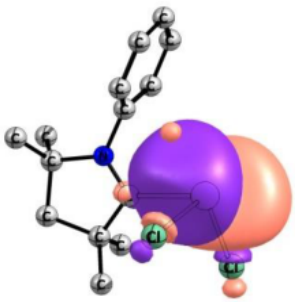	0.41	Sn	*s*(15.2%), *p*(84.6%), *d*(0.2%)
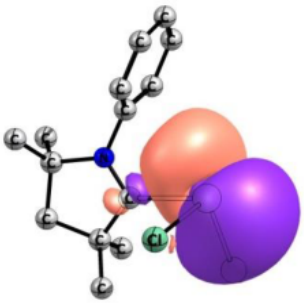	0.27	Sn	*s*(0.2%), *p*(99.1%), *d*(0.7%)
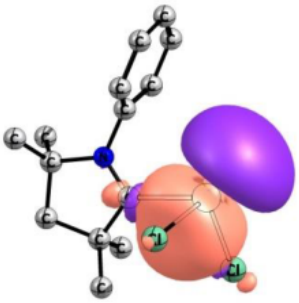	0.24	Sn	*s*(0.2%), *p*(99.4%), *d*(0.4%)

Figure S25. NBO results at the M06-2X/def2-TZVPP//M06-2X/def2-SVP of **3a**. Hydrogen atoms and iso-propyl groups were omitted for carity.

Orbital	Occ.	Contribution from atoms to the orb	Atomic orbitals
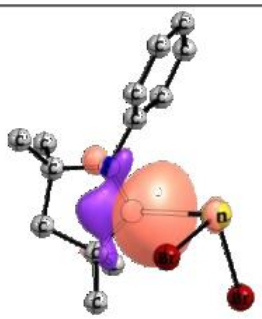	1.67	C	*s*(39.5%), *p*(60.4%), *d*(0.1%)
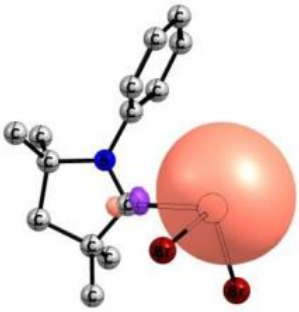	1.98	Sn	*s*(86.7%), *p*(13.3%), *d*(0.01%)
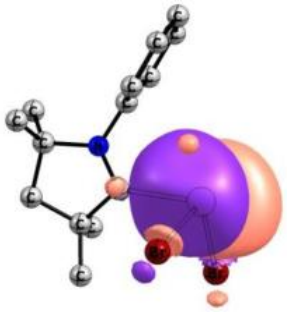	0.44	Sn	*s*(13.7%), *p*(86.0%), *d*(0.2%)
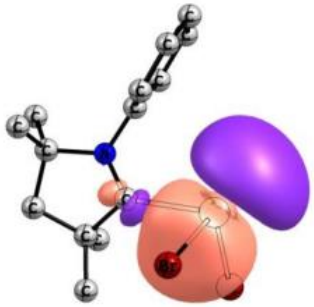	0.32	Sn	*s*(0.1%), *p*(98.7%), *d*(1.2%)
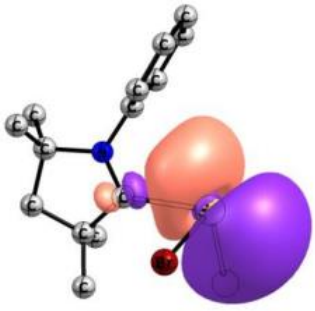	0.26	Sn	*s*(0.3%), *p*(99.2%), *d*(0.5%)

Figure S26. NBO results at the M06-2X/def2-TZVPP//M06-2X/def2-SVP of **3b**. Hydrogen atoms and iso-propyl groups were omitted for carity.

Orbital	Occ.	Contribution from atoms to the orb	Atomic orbitals
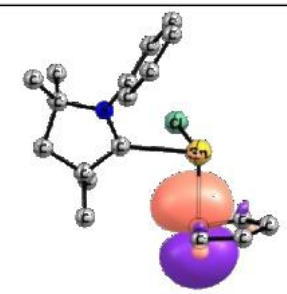	1.25	C	*s*(3.8%), *p*(95.9%), *d*(0.2%)
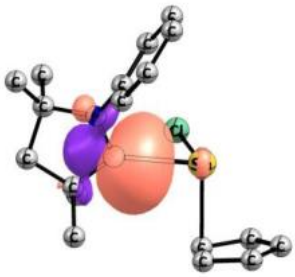	1.73	C	*s*(40.6%), *p*(59.4%), *d*(0.0%)
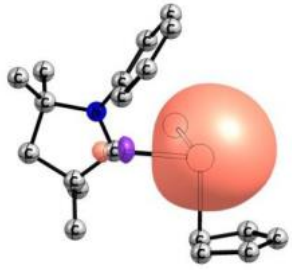	1.97	Sn	*s*(88.5%), *p*(11.4%), *d*(0.1%)
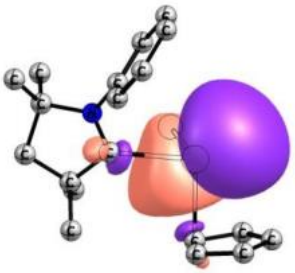	0.37	Sn	*s*(11.9%), *p*(87.9%), *d*(0.2%)
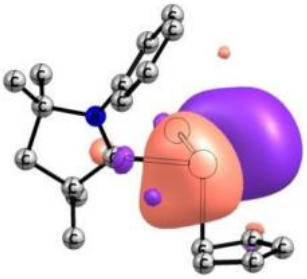	0.25	Sn	*s*(0.2%), *p*(99.4%), *d*(0.4%)
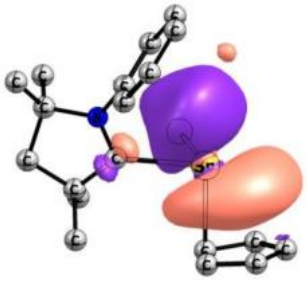	0.19	Sn	*s*(0.3%), *p*(98.9%), *d*(0.8%)

Figure S27. NBO results at the M06-2X/def2-TZVPP//M06-2X/def2-SVP of **3c**. Hydrogen atoms and iso-propyl groups were omitted for carity.

Orbital	Occ.	Contribution from atoms to the orb	Atomic orbitals
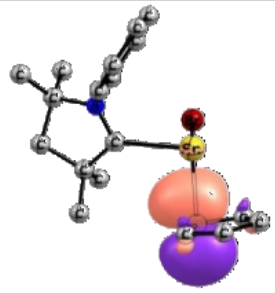	1.25	C	*s*(3.9%), *p*(95.9%), *d*(0.2%)
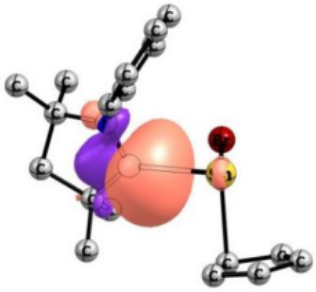	1.73	C	*s*(40.4%), *p*(59.5%), *d*(0.1%)
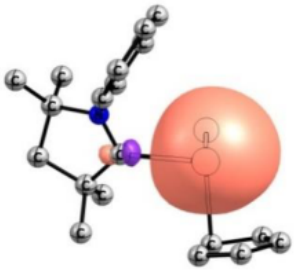	1.97	Sn	*s*(89.1%), *p*(10.9%), *d*(0.0%)
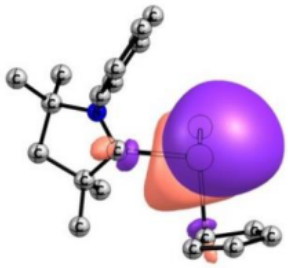	0.39	Sn	*s*(10.9%), *p*(88.9%), *d*(0.2%)
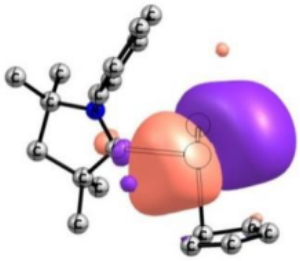	0.27	Sn	*s*(0.4%), *p*(99.0%), *d*(0.6%)
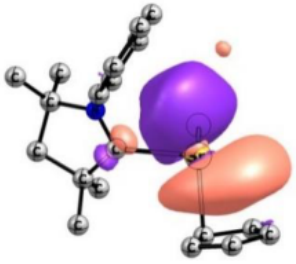	0.19	Sn	*s*(0.3%), *p*(98.8%), *d*(0.8%)

Figure S28. NBO results at the M06-2X/def2-TZVPP//M06-2X/def2-SVP of **3d**. Hydrogen atoms and iso-propyl groups were omitted for carity.

Orbital	Occ.	Contribution from atoms to the orb	Atomic orbitals
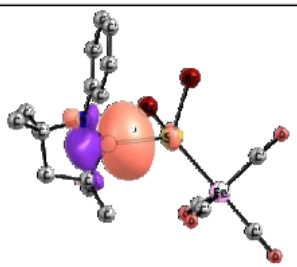	1.65	C	*s*(37.7%), *p*(62.3%), *d*(0.0%)
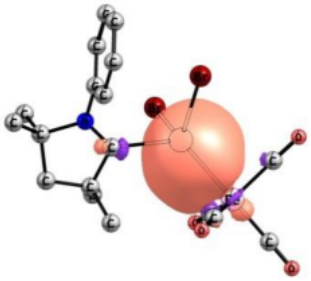	1.87	Sn (63.8%) - Fe (36.2%)	Sn: *s*(86.7%), *p*(13.2%), *d*(0.1%) Fe: *s*(17.8%), *p*(54.8%), *d*(27.4%)
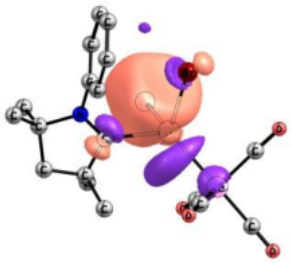	0.47	Sn	*s*(13.1%), *p*(86.8%), *d*(0.1%)
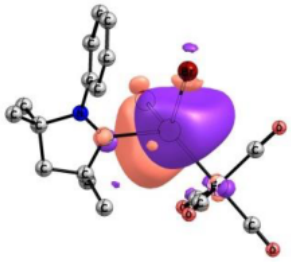	0.37	Sn	*s*(0.1%), *p*(99.6%), *d*(0.3%)
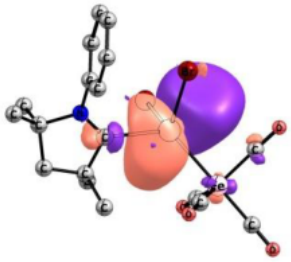	0.33	Sn	*s*(0.3%), *p*(99.5%), *d*(0.2%)
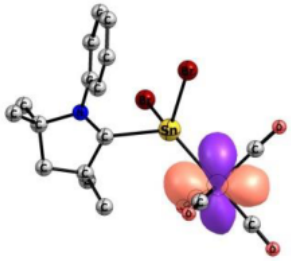	1.87	Fe	*s*(0.0%), *p*(0.1%), *d*(99.9%)

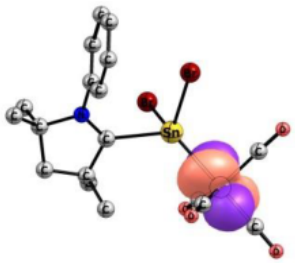

1.86 Fe *s*(0.0%), *p*(0.1%), *d*(99.9%)

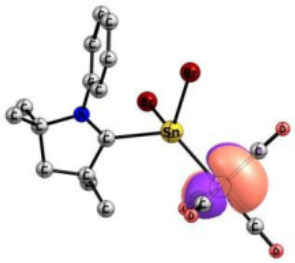

1.72 Fe *s*(0.0%), *p*(3.3%), *d*(96.7%)

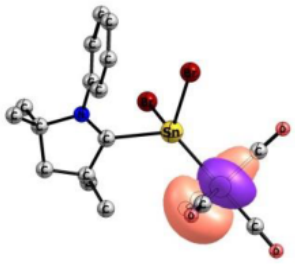

1.67 Fe *s*(0.0%), *p*(4.66%), *d*(95.3%)

Figure S29. NBO results at the M06-2X/def2-TZVPP//M06-2X/def2-SVP of **5**. Hydrogen atoms and iso-propyl groups were omitted for carity.

Table S1. Energy decomposition analysis (EDA) with different fragmentation schemes for **3a** and **3b** complexes at the BP86+D3(BJ)/TZ2P. Energy values are given in kcal/mol.[a]

	3a		**3b**	
	$SnCl_2$ (S); cAAC (S)	$SnCl_2$ (T); cAAC (T)	$SnBr_2$ (S); cAAC (S)	$SnBr_2$ (T); cAAC (T)
ΔE_{int}	-54.5	-178.7	-55.7	-173.3
ΔE_{Pauli}	142.5	124.5	140.5	121.4
ΔE_{disp}[b]	-20.1 (10.2 %)	-20.1 (6.6 %)	-21.3 (10.9 %)	-21.3 (7.2 %)
ΔE_{elstat}[b]	-109.2 (55.5 %)	-91.0 (30.0 %)	-106.6 (54.3 %)	-88.2 (29.9 %)
ΔE_{orb}[b]	-67.7 (34.4 %)	-192.2 (63.4%)	-68.3 (34.8 %)	-185.1 (62.8 %)
ΔE_{prep}	6.7	130.9	6.9	124.4
$-D_e = \Delta E$	-47.8	-47.8	-48.9	-48.9

[a] S and T stand for singlet and triplet reference states, respectively.

[b] The value in parentheses gives the percentage contribution to the total attractive interactions $\Delta E_{elstat} + \Delta E_{orb} + \Delta E_{disp}$.

Deformation densities	cAAC Molecular Orbitals	SnXR Molecular Orbitals

3a

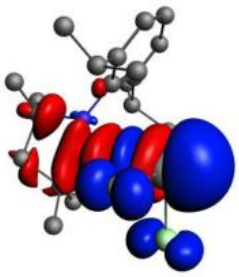

ΔE_{orb} $\rho_{(1)}$= -50.2; $|\nu_1|$=0.73

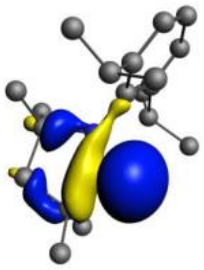

HOMO (ε=-4.15 eV)
ν1= -0.50

→

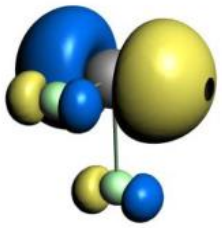

LUMO (ε=-4.37 eV)
ν_1= +0.52

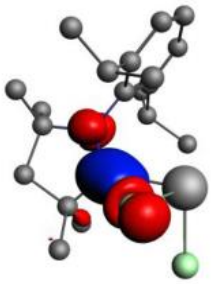

ΔE_{orb} $\rho_{(2)}$= -3.3; $|\nu_2|$=0.22

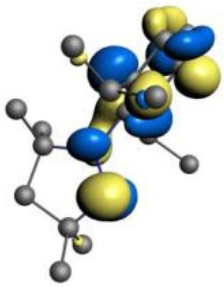

LUMO (ε=-1.43 eV)
ν2= +0.02

←

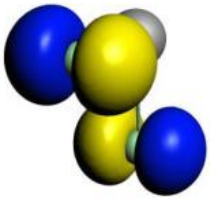

HOMO-2 (ε=-7.33 eV)
ν_2= -0.01

3c

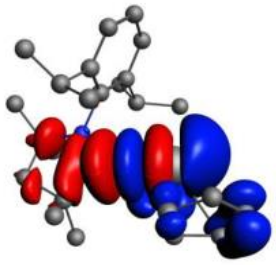

ΔE_{orb} $\rho_{(1)}$= -41.3; $|\nu_1|$=0.67

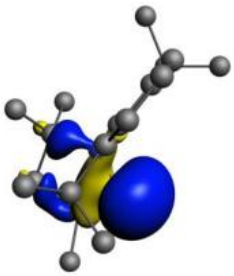

HOMO (ε=-4.15 eV)
ν1= -0.43

→

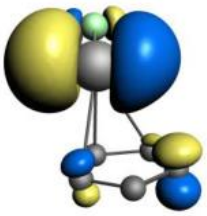

LUMO (ε=-3.48 eV)
ν_1= +0.47

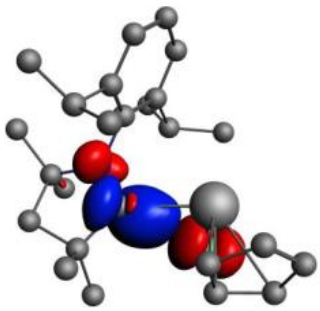

ΔE_{orb} $\rho_{(2)}$= -3.8; $|\nu_2|$=0.25

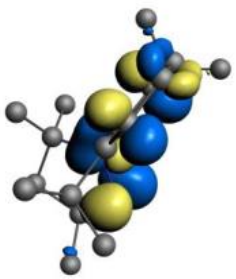

LUMO (ε=-1.47 eV)
ν2= +0.03

←

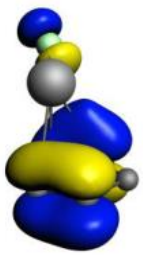

HOMO (ε=--6.15 eV)
ν_2= -0.02

3b

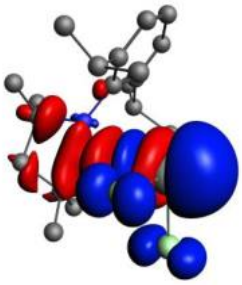

$\Delta E_{orb}\ \rho_{(1)}$= -51.0; $|\nu_1|$=0.75

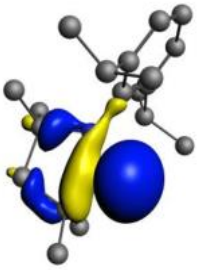

HOMO (ε=-4.15 eV)
ν1= -0.51

→

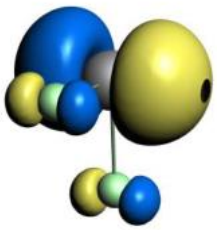

LUMO (ε=-4.34 eV)
ν_1= +0.55

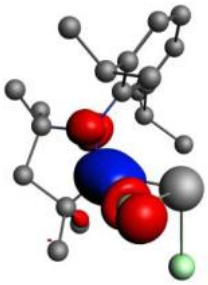

$\Delta E_{orb\ \rho(2)}$= -3.33; $|\nu_2|$=0.24

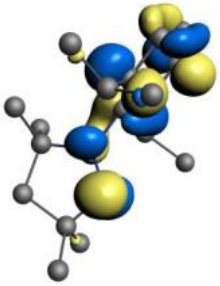

LUMO (ε=-1.43 eV)
ν2= +0.03

←

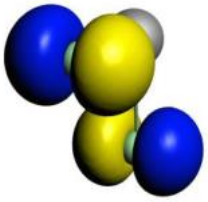

HOMO-2 (ε=--7.19 eV)
ν_2= -0.03

3d

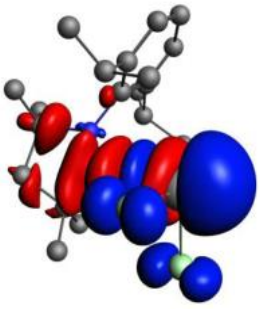

$\Delta E_{orb}\ \rho_{(1)}$= -41.9; $|\nu_1|$=0.68

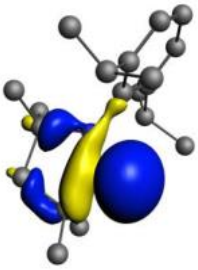

HOMO (ε=-4.14 eV)
ν1= -0.44

→

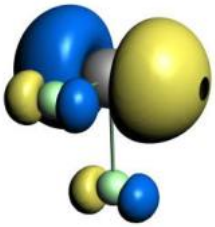

LUMO (ε=-3.15 eV)
ν_1= +0.48

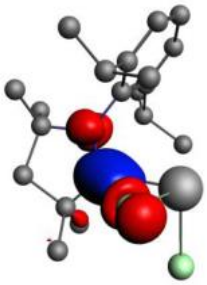

$\Delta E_{orb}\ \rho_{(2)}$= -3.9; $|\nu_2|$=0.27

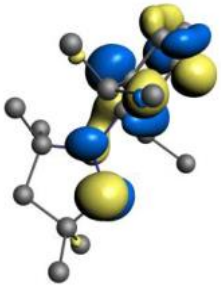

LUMO (ε=-1.48 eV)
ν2= +0.02

←

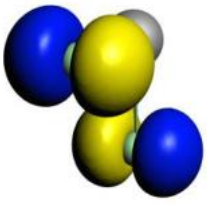

HOMO (ε=-6.08 eV)
ν_2= -0.03

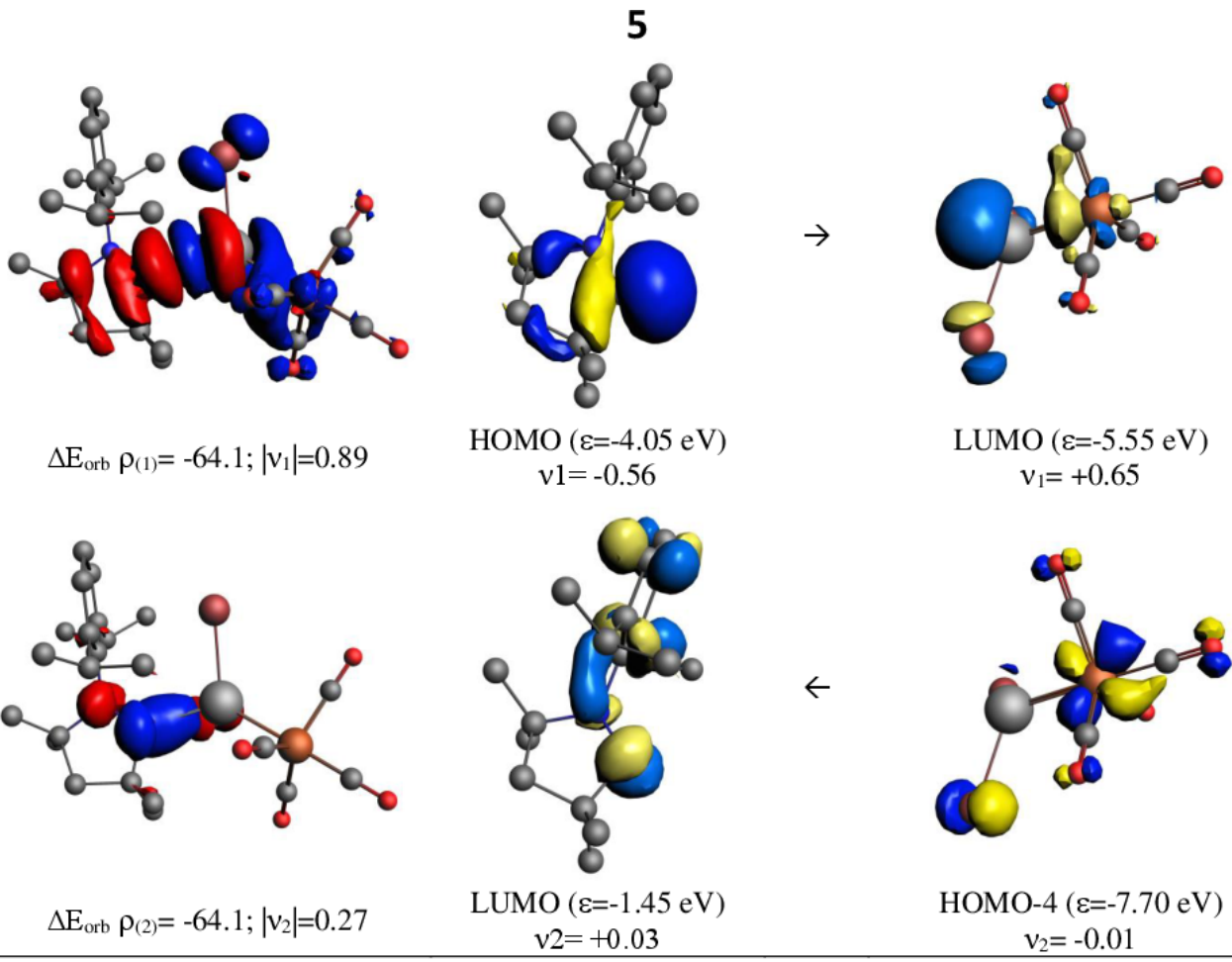

Figure S30. Plot of deformation densities Δρ (isovalue 0.001 a.u.) of the pairwise orbital interactions between SnXR (X = Cl, Br and R = Cp, Cl, Br) and cAAC within compound **3a-d** and **5**, associated energies ΔE (in kcal/mol) and eigenvalues ν (in a.u.). The red colour shows the charge outflow, whereas blue shows charge density accumulation. Shape of the most important interacting occupied and vacant orbitals (isovalue 0.05 a.u.) of the fragments.

Table S2. Energy decomposition analysis (EDA) with different fragmentation schemes for **5** complex at the BP86+D3(BJ)/TZ2P in three different fragmentation schemes. Energy values are given in kcal/mol.[a]

	cAAC(S); $SnBr_2Fe(CO)_4$ (S)	cAAC-$SnBr_2$(S); $Fe(CO)_4$ (S)	cAAC(S); $SnBr_2$(S); $Fe(CO)_4$ (S)
ΔE_{int}	-75.1	-58.4	-117.3
ΔE_{Pauli}	169.9	85.4	240.8
ΔE_{disp}[b]	-29.3 (12.0 %)	-15.8 (11.0 %)	-39.5 (11.0 %)
ΔE_{elstat}[b]	-128.4 (52.4 %)	-61.7 (42.9 %)	-161.7 (45.1 %)
ΔE_{orb}[b]	-87.3 (35.6 %)	-66.3 (46.1 %)	-156.9 (43.8 %)
ΔE_{prep}	16.3	0.4	9.0
$-D_e = \Delta E$	-58.8	-58.0	-108.3

[a] S and T stand for singlet and triplet reference states, respectively.
[b] The value in parentheses gives the percentage contribution to the total attractive interactions $\Delta E_{elstat} + \Delta E_{orb} + \Delta E_{disp}$.

Reaction mechanism

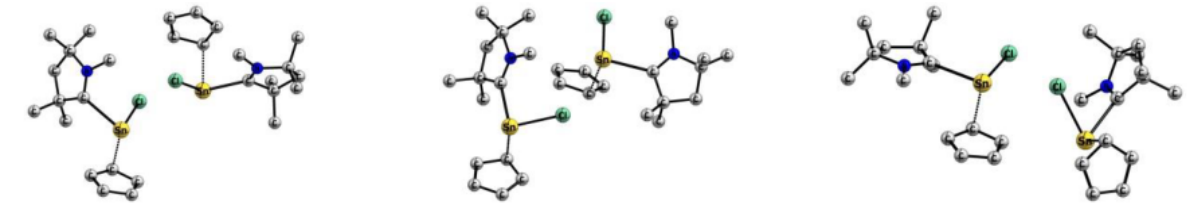

3c-dimer 1
ΔG_R= 8.7 kcal/mol

3c-dimer 2
ΔG_R= 9.8 kcal/mol

3c-dimer 3
ΔG_R= 5.1 kcal/mol

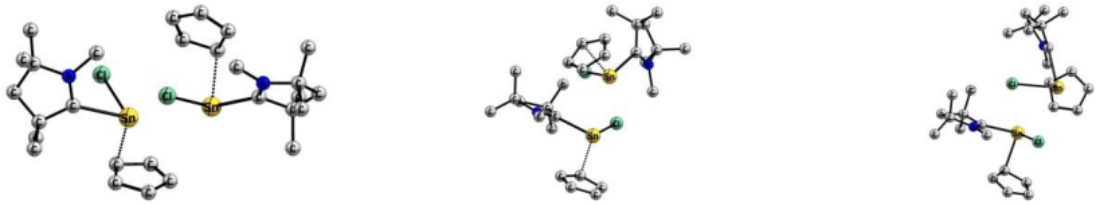

3c-dimer 4
ΔG_R= 8.1 kcal/mol

3c-dimer 5
ΔG_R= 0.0 kcal/mol

3c-dimer 6
ΔG_R= 7.4 kcal/mol

Figure S31. Optimized structure (M06-2X/def2-SVP) and relative Gibbs free energies (PCM(THF)-M06-2X/def2-TZVPP//M06-2X/def2-SVP) of **3c** dimers. Hydrogen atoms were omitted for clarity.

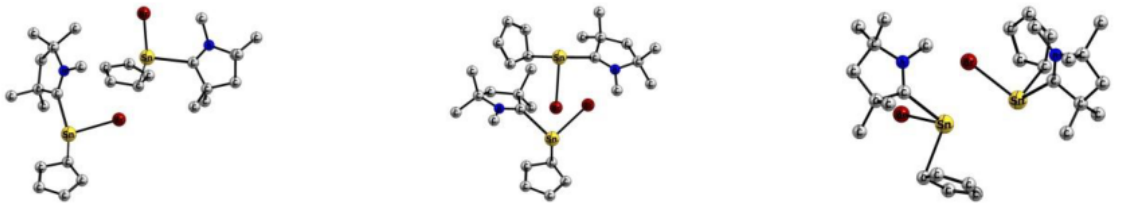

3d-dimer 1
ΔG_R= 12.9 kcal/mol

3d-dimer 2
ΔG_R= 11.7 kcal/mol

3d-dimer 3
ΔG_R= 6.8 kcal/mol

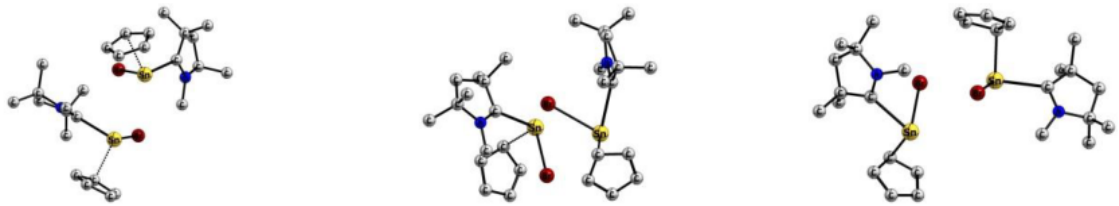

3d-dimer 4
ΔG_R= 7.0 kcal/mol

3d-dimer 5
ΔG_R= 0.0 kcal/mol

3d-dimer 6
ΔG_R= 9.1 kcal/mol

Figure S32. Optimized structure (M06-2X/def2-SVP) and relative Gibbs free energies (PCM(THF)-M06-2X/def2-TZVPP//M06-2X/def2-SVP) of **3d** dimers. Hydrogen atoms were omitted for clarity.

7. References

1. Lavallo, V.; Canac, Y.; Präsang, C.; Donnadieu, B.; Bertrand, G.; Stable Cyclic (Alkyl)(Amino)Carbenes as Rigid or Flexible, Bulky, Electron-Rich Ligands for Transition-Metal Catalysts: A Quaternary Carbon Atom Makes the Difference; *Angew. Chem.* **2005**, *117*, 5851–5855 / *Angew. Chem. Int. Ed.* **2005**, *44*, 5705–5709;
2. Jazzar, R.; Dewhurst, R. D.; Bourg, J.-B.; Donnadieu, B.; Canac, Y.; Bertrand, G.; Conjugate Acids of Cyclic Alkyl Amino Carbenes (CAACs); *Angew. Chem.* **2007**, *119*, 2957-2960 / *Angew. Chem. Int. Ed.* **2007**, *46*, 2899-2902.

6.3 Bonding Situation in Stannocene and Plumbocene N-Heterocyclic Carbene Complexes

Supporting Information

for

On the Bonding Situation in Stannocene and Plumbocene *N*-Heterocyclic Carbene Complexes

Sergi Danés[†§], Carsten Müller[†§], Lisa Wirtz[†§], Volker Huch[†], Theresa Block[‡], Rainer Pöttgen[‡*], André Schäfer[†*], and Diego M. Andrada[†*]

[†]Saarland University, Faculty of Natural Sciences and Technology, Department of Chemistry, Campus Saarbrücken, 66123 Saarbrücken, Federal Republic of Germany

[‡] University of Münster, Faculty of Chemistry and Pharmacy, Institute of Inorganic and Analytical Chemistry, Corrensstrasse 30, 48149 Münster, Federal Republic of Germany

1. Crystallographic Details S2-S4

2. Computational Details S5-S39

1. Crystallographic Details

All crystal structure data is available free of charge from the Cambridge Structural Database (see CCDC numbers).

Crystallographic data for 2a

CCDC deposition number	1954899	
Empirical formula	$C_{21}H_{32}N_2Si_2Sn$	
Formula weight	487.35	
Temperature	152(2) K	
Wavelength	0.71073 Å	
Crystal system	Monoclinic	
Space group	$P2_1/n$	
Unit cell dimensions	a = 8.6474(3) Å	α= 90°
	b = 20.0644(6) Å	β= 97.2700(10)°
	c = 14.0995(5) Å	γ = 90°
Volume	2426.67(14) $Å^3$	
Z	4	
Density (calculated)	1.334 Mg/m^3	
Absorption coefficient	1.159 mm^{-1}	
F(000)	1000	
Crystal size	0.196 x 0.138 x 0.040 mm^3	
Theta range for data collection	1.775 to 28.665°.	
Index ranges	-11<=h<=10, -21<=k<=27, -18<=l<=18	
Reflections collected	25827	
Independent reflections	6229 [R(int) = 0.0316]	
Completeness to theta = 25.242°	100.0 %	
Absorption correction	Semi-empirical from equivalents	
Max. and min. transmission	0.7457 and 0.6885	
Refinement method	Full-matrix least-squares on F^2	
Data / restraints / parameters	6229 / 42 / 351	
Goodness-of-fit on F^2	1.046	
Final R indices [I>2sigma(I)]	R1 = 0.0231, wR2 = 0.0485	
R indices (all data)	R1 = 0.0310, wR2 = 0.0512	
Extinction coefficient	n/a	
Largest diff. peak and hole	0.364 and -0.345 $e.Å^{-3}$	

Crystallographic data for 3a

CCDC deposition number	1954898	
Empirical formula	$C_{31}H_{34}N_2Pb$	
Formula weight	641.79	
Temperature	133(2) K	
Wavelength	0.71073 Å	
Crystal system	Monoclinic	
Space group	$P2_1/n$	
Unit cell dimensions	a = 8.4798(3) Å	α = 90°
	b = 18.1717(7) Å	β = 94.295(2)°
	c = 17.4554(7) Å	γ = 90°
Volume	2682.19(18) $Å^3$	
Z	4	
Density (calculated)	1.589 Mg/m^3	
Absorption coefficient	6.311 mm^{-1}	
F(000)	1264	
Crystal size	0.208 x 0.152 x 0.118 mm^3	
Theta range for data collection	2.529 to 27.134°.	
Index ranges	-10<=h<=10, -23<=k<=23, -22<=l<=22	
Reflections collected	30123	
Independent reflections	5845 [R(int) = 0.0264]	
Completeness to theta = 25.242°	98.4 %	
Absorption correction	Semi-empirical from equivalents	
Max. and min. transmission	0.7455 and 0.5571	
Refinement method	Full-matrix least-squares on F^2	
Data / restraints / parameters	5845 / 0 / 435	
Goodness-of-fit on F^2	1.109	
Final R indices [I>2sigma(I)]	R1 = 0.0195, wR2 = 0.0426	
R indices (all data)	R1 = 0.0213, wR2 = 0.0431	
Extinction coefficient	n/a	
Largest diff. peak and hole	1.358 and -1.187 $e.Å^{-3}$	

Crystallographic data for 3c

CCDC deposition number	1954900	
Empirical formula	$C_{35}H_{44}N_2OPbSi_2$, C_4H_8O	
Formula weight	844.19	
Temperature	143(2) K	
Wavelength	0.71073 Å	
Crystal system	Triclinic	
Space group	P-1	
Unit cell dimensions	a = 8.3597(3) Å	α = 89.476(2)°
	b = 11.4527(4) Å	β = 87.775(2)°
	c = 20.7779(8) Å	γ = 72.792(2)°
Volume	1898.81(12) $Å^3$	
Z	2	
Density (calculated)	1.477 Mg/m^3	
Absorption coefficient	4.540 mm^{-1}	
F(000)	852	
Crystal size	0.184 x 0.063 x 0.046 mm^3	
Theta range for data collection	2.102 to 35.072°.	
Index ranges	-13<=h<=13, -18<=k<=18, -33<=l<=33	
Reflections collected	66433	
Independent reflections	16762 [R(int) = 0.0520]	
Completeness to theta = 25.242°	99.9 %	
Absorption correction	Semi-empirical from equivalents	
Max. and min. transmission	0.7469 and 0.6562	
Refinement method	Full-matrix least-squares on F^2	
Data / restraints / parameters	16762 / 0 / 425	
Goodness-of-fit on F^2	1.076	
Final R indices [I>2sigma(I)]	R1 = 0.0257, wR2 = 0.0550	
R indices (all data)	R1 = 0.0307, wR2 = 0.0563	
Extinction coefficient	n/a	
Largest diff. peak and hole	1.172 and -2.064 $e.Å^{-3}$	

2. Computational Details

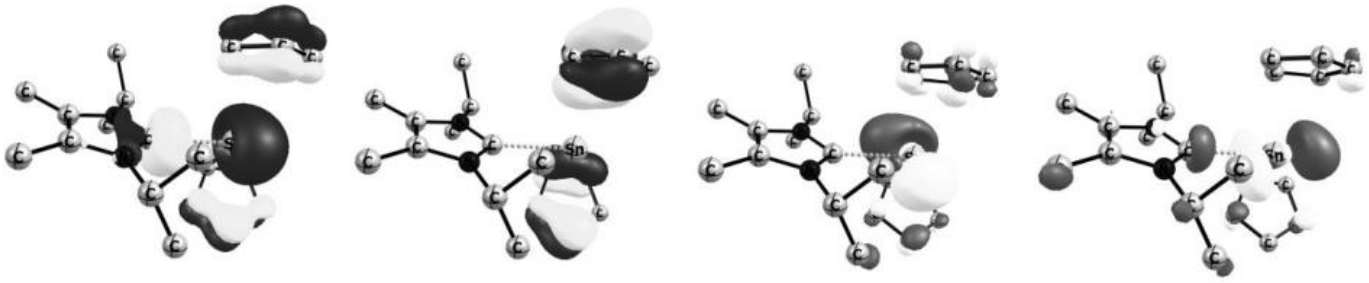

HOMO-4 (ε = -6.61 eV) | HOMO (ε = -5.10 eV) | LUMO (ε = -0.45 eV) | LUMO+4 (ε = 0.45 eV)

1a

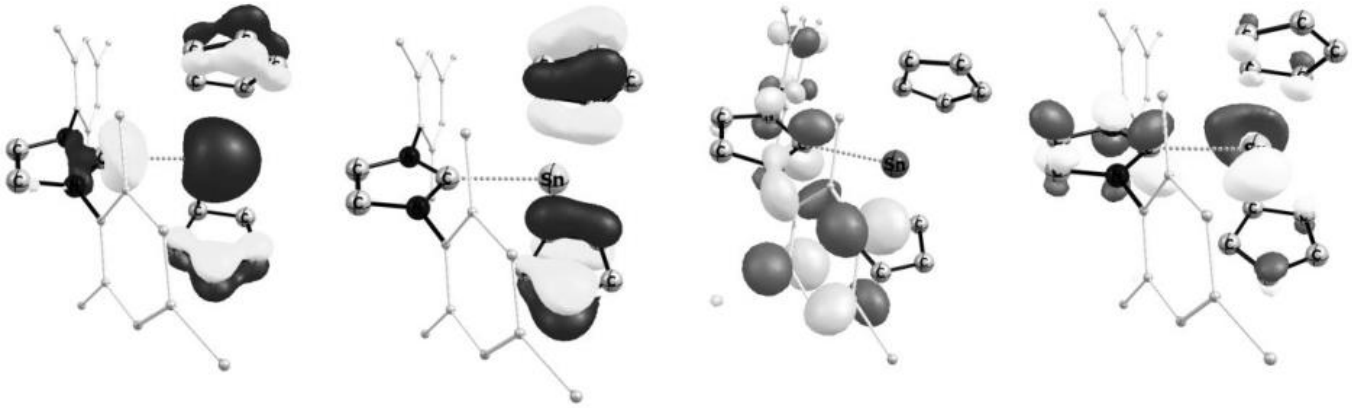

HOMO-4 (ε = -6.60 eV) | HOMO (ε = -4.96 eV) | LUMO (ε = -0.82 eV) | LUMO+5 (ε = -0.12 eV)

1b

HOMO-4 (ε = -6.69 eV) | HOMO (ε = -4.86 eV) | LUMO (ε = -0.51 eV) | LUMO+2 (ε = -0.01 eV)

1c

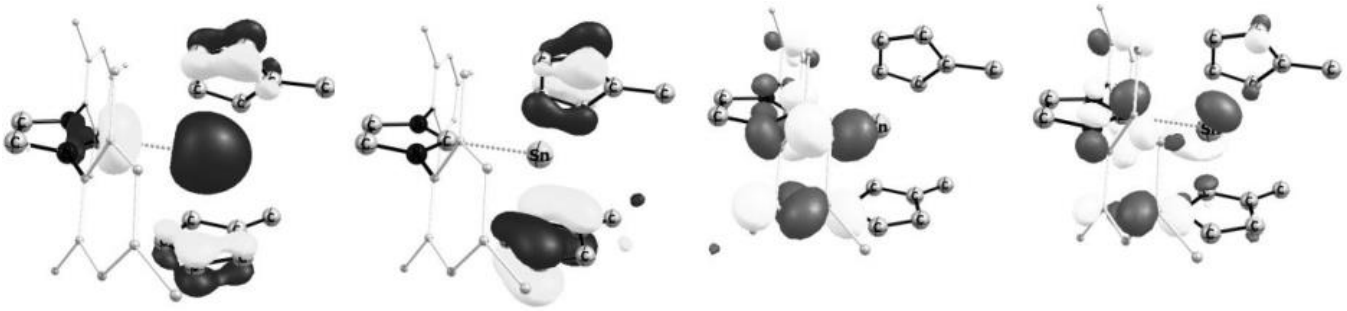

HOMO-4 (ε = -6.45 eV) | HOMO (ε = -4.87 eV) | LUMO (ε = -0.80 eV) | LUMO+4 (ε = -0.63 eV)

1d

HOMO-4 (ε = -6.51 eV) | HOMO (ε = -4.89 eV) | LUMO (ε = -0.39 eV) | LUMO+4 (ε = 0.46 eV)

1e

HOMO-5 (ε = -6.75 eV) | HOMO (ε = -5.06 eV) | LUMO (ε = -0.64 eV) | LUMO+1 (ε = -0.47eV)

2a

HOMO-5 (ε = -6.62 eV) | HOMO (ε = -5.11 eV) | LUMO (ε = -0.67 eV) | LUMO+1 (ε = -0.40 eV)

2b

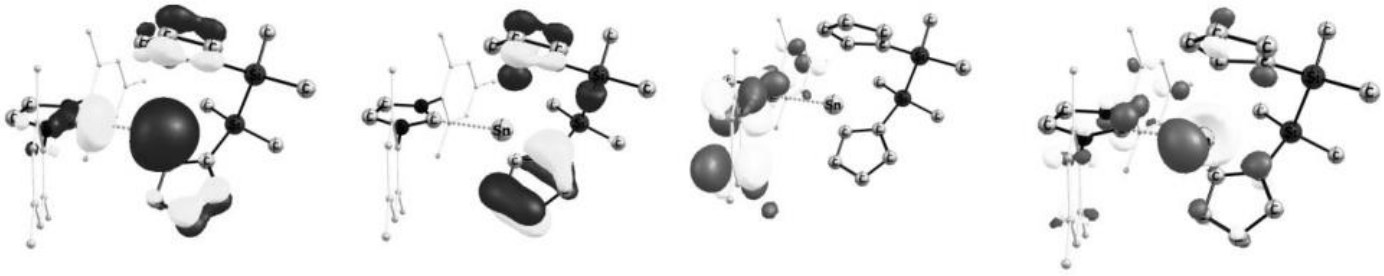

HOMO-5 (ε = -6.77 eV) | HOMO (ε = -5.00 eV) | LUMO (ε = -0.94 eV) | LUMO+5 (ε = -0.48 eV)

2c

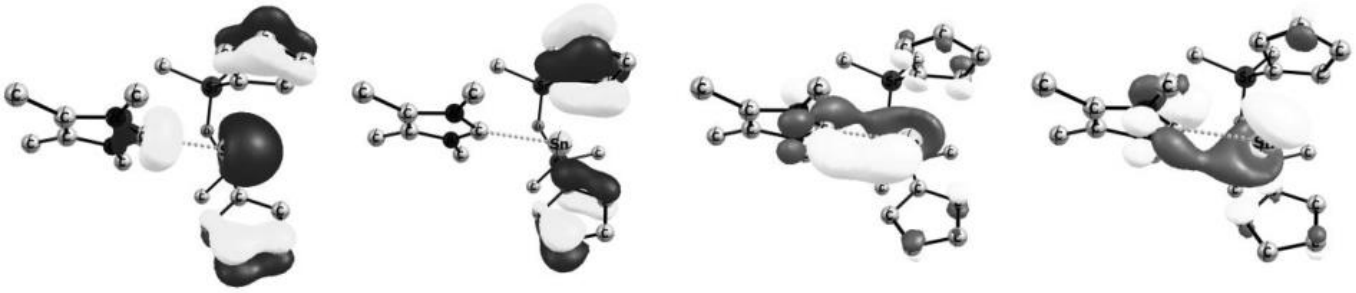

HOMO-4 (ε = -6.75 eV) | HOMO (ε = -5.23 eV) | LUMO (ε = -0.62 eV) | LUMO+1 (ε = -0.32 eV)

2d

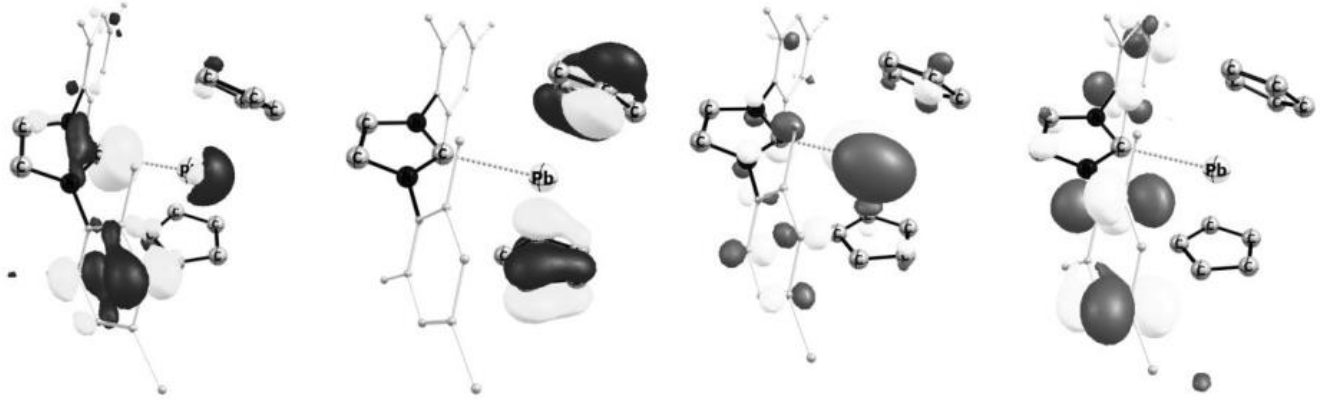

HOMO-5 (ε = -6.96 eV) | HOMO (ε = -5.00 eV) | LUMO (ε = -0.95 eV) | LUMO+1 (ε = -0.80 eV)

3a

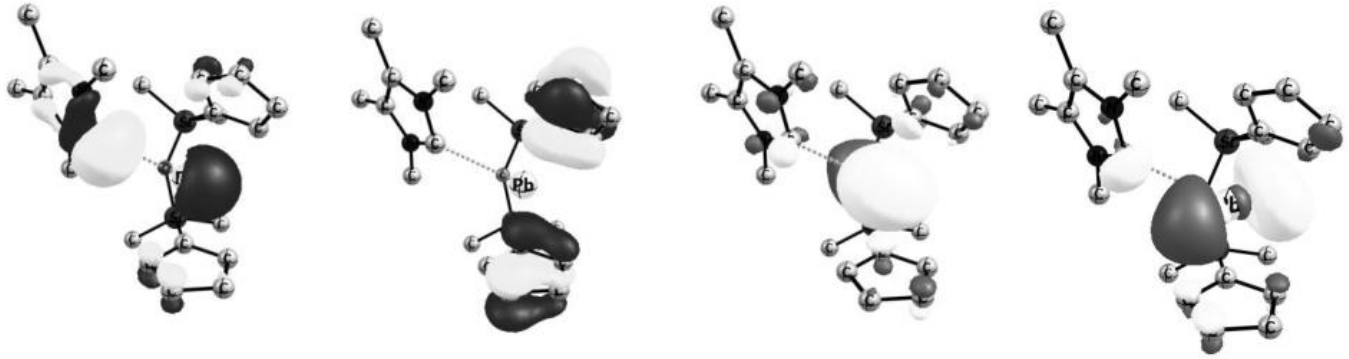

HOMO-5 (ε = -5.59 eV) | HOMO (ε = -5.37 eV) | LUMO (ε = -5.22 eV) | LUMO+2 (ε = -1.07 eV)

3b

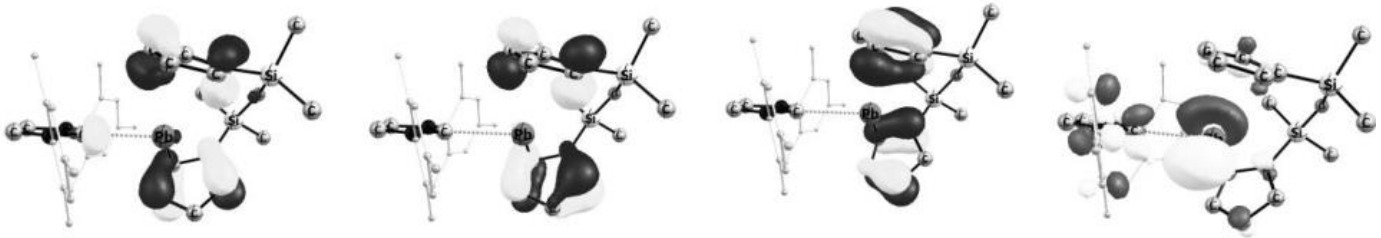

HOMO-2 (ε = -5.48 eV) | HOMO-1 (ε = -5.23 eV) | HOMO (ε = -5.09 eV) | LUMO (ε = -1.06 eV)

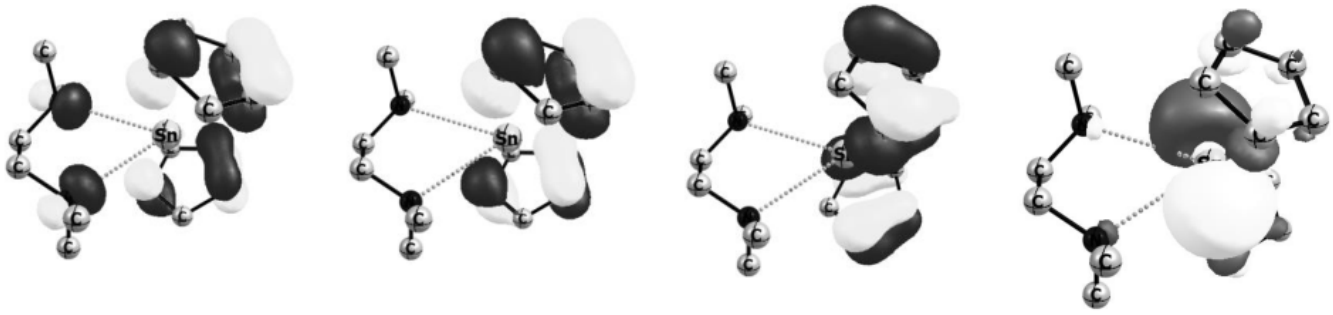

HOMO-2 (ε = -6.01 eV) | HOMO-1 (ε = -5.50eV) | HOMO (ε = -5.50eV) | LUMO (ε = -0.80eV)

4

HOMO-2 (ε = -5.88eV) | HOMO-1 (ε = -5.40 eV) | HOMO (ε = -5.36 eV) | LUMO (ε = -0.86 eV)

5a

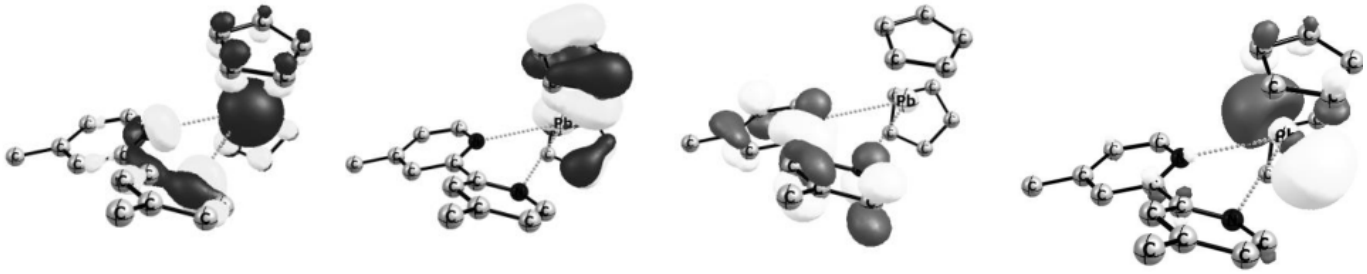

HOMO-4 (ε = -7.23 eV) | HOMO (ε = -5.13 eV) | LUMO (ε = -2.02 eV) | LUMO+3 (ε = -0.70 eV)

5b

Figure S1. Frontier Molecular Orbitals (isosurface 0.05 a.u.) at B3LYP+D3/def2-TZVP of **1-5**. Hydrogen atoms were omitted for clarity.

Table S1. NBO results at the B3LYP+D3/def2-TZVP level of theory of **1-5**: Wiberg bond order (P) and partial charges (q).

	Q(E)	Q(Ccarb)	Q(ECp_2)	Q(L)	P(E-C_{carb})
1a	1.04	0.12	-0.21	0.21	0.35
1b	1.11	0.13	-0.18	0.18	0.31
1c	0.98	0.13	-0.24	0.24	0.42
1d	1.06	0.11	-0.21	0.21	0.36
1e	1.13	0.13	-0.17	0.17	0.30
2a	1.02	0.11	-0.34	0.34	0.41
2b	1.08	0.09	-0.21	0.21	0.34
2c	1.16	0.10	-0.18	0.18	0.32
2d	1.06	1.10	-0.22	0.22	0.37
3a	1.15	0.12	-0.15	0.15	0.25
3b	1.16	0.09	-0.18	0.18	0.30
3c	1.21	0.11	-0.15	0.15	0.24
4	1.19	-0.42	-0.10	0.10	0.06
5a	1.23	-0.43	-0.11	0.11	0.06
5b	1.19	-0.43/-0.42	0.08	0.08	0.08/0.06

Orbital	Occ.	Contribution from atoms to the orb	Atomic orbitals
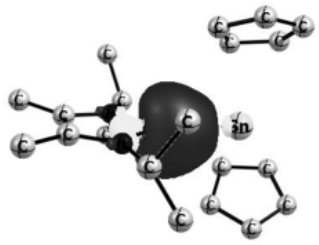	1.93	C_{carb}(87.93%)-Sn (12.07%)	C_{carb}: *s*(40.63%) *p* (59.36%) *d* (0.01%) Sn: *s*(2.37%) *p* (97.34%) *d* (0.21%)
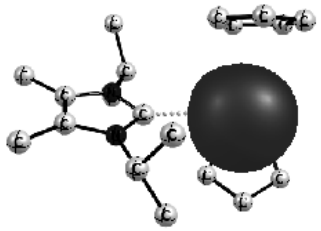	1.98	LP (Sn)	*s*(94.48%) *p* (5.51%) *d* (0.01%)
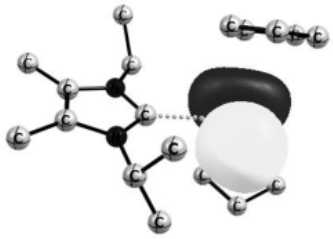	0.39	LP* (Sn)	*s*(3.47%) *p* (96.42%) *d* (0.02%)
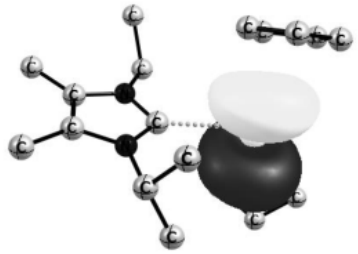	0.19	LP* (Sn)	*s*(0.00%) *p* (99.78%) *d* (0.19%)

Figure S2. NBO results at the B3LYP+D3/def2-TZVP of **1a**. Hydrogen atoms were omitted for clarity.

Orbital	Occ.	Contribution from atoms to the orb	Atomic orbitals
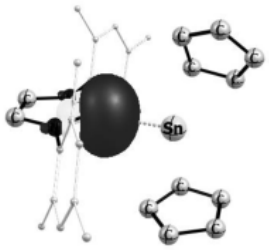	1.75	LP (C_{carb})	*s*(45.30%) *p* (54.68%) *d* (0.01%)
	1.99	LP (Sn)	*s*(94.88%) *p* (5.11%) *d* (0.01%)
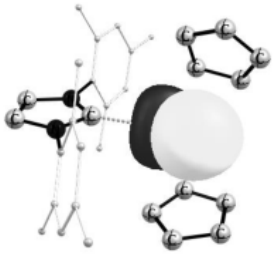	0.41	LP* (Sn)	*s*(5.38%) *p* (94.57%) *d* (0.02%)
	0.29	LP* (Sn)	*s*(0.07%) *p* (99.83%) *d* (0.10%)
	0.18	LP* (Sn)	*s*(0.00%) *p* (99.77%) *d* (0.19%)

Figure S3. NBO results at the B3LYP+D3/def2-TZVP of **1b**. Hydrogen atoms were omitted for clarity.

Orbital	Occ.	Contribution from atoms to the orb	Atomic orbitals
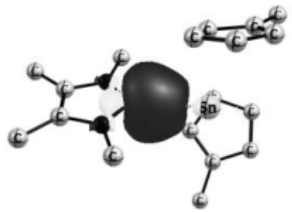	1.95	C_{carb}(85.82%)-Sn (14.18%)	C_{carb}: *s*(40.76%) *p* (59.23%) *d* (0.00%) Sn: *s*(3.79%) *p* (95.99%) *d* (0.14%)
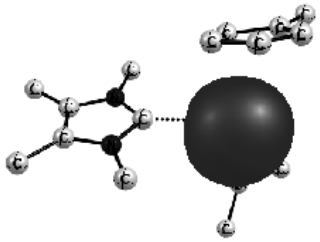	1.98	LP (Sn)	*s*(90.68%) *p* (9.31%) *d* (0.01%)
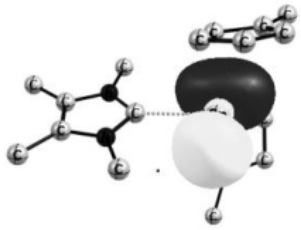	0.43	LP* (Sn)	*s*(5.73%) *p* (94.16%) *d* (0.07%)
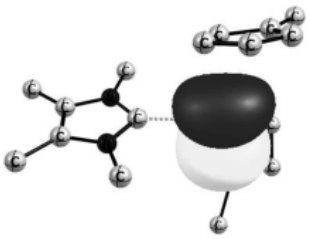	0.21	LP* (Sn)	*s*(0.02%) *p* (99.69%) *d* (0.25%)

Figure S4. NBO results at the B3LYP+D3/def2-TZVP of **1c**. Hydrogen atoms were omitted for clarity.

Orbital	Occ.	Contribution from atoms to the orb	Atomic orbitals
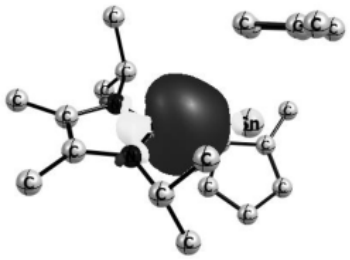	1.94	C_{carb}(87.97%)-Sn (12.03%)	C_{carb}: *s*(40.81%) *p* (59.18%) *d* (0.01%) Sn: *s*(2.65%) *p* (97.07%) *d* (0.03%)
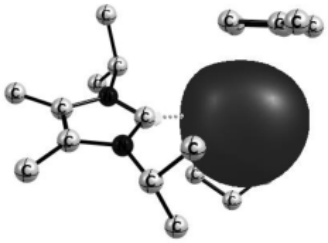	1.98	LP (Sn)	*s*(94.07%) *p* (5.92%) *d* (0.01%)
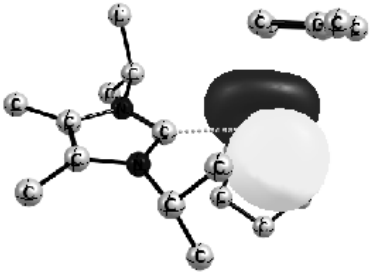	0.39	LP* (Sn)	*s*(3.61%) *p* (96.29%) *d* (0.06%)
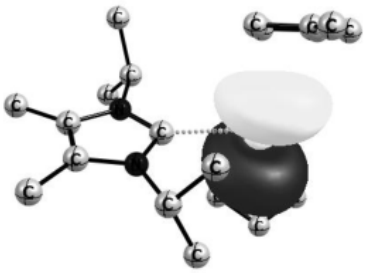	0.19	LP* (Sn)	*s*(0.00%) *p* (99.79%) *d* (0.18%)

Figure S5. NBO results at the B3LYP+D3/def2-TZVP of **1d**. Hydrogen atoms were omitted for clarity.

Orbital	Occ.	Contribution from atoms to the orb	Atomic orbitals
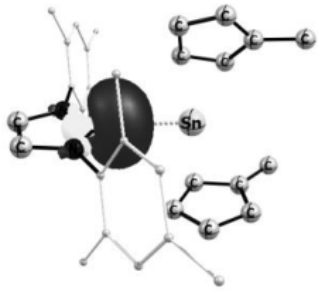	1.76	LP (C_{carb})	*s*(45.26%) *p* (54.73%) *d* (0.01%)
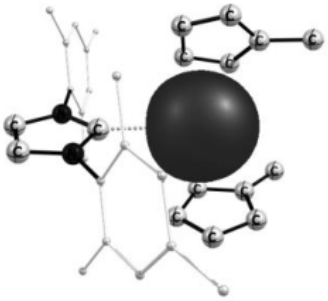	1.99	LP (Sn)	*s*(96.11%) *p* (3.88%) *d* (0.01%)
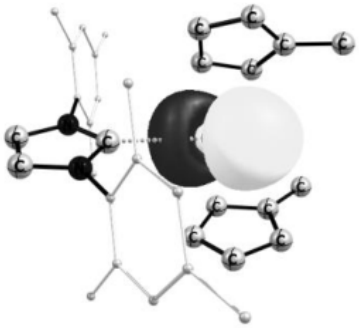	0.39	LP* (Sn)	*s*(4.18%) *p* (95.77%) *d* (0.01%)
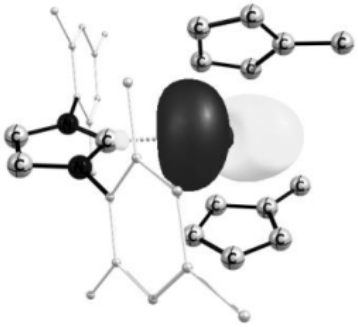	0.29	LP* (Sn)	*s*(0.04%) *p* (99.87%) *d* (0.08%)
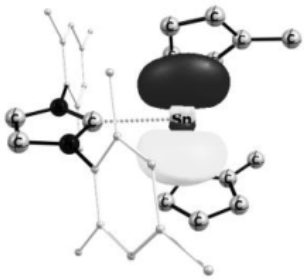	0.17	LP* (Sn)	*s*(0.00%) *p* (99.84%) *d* (0.13%)

Figure S6. NBO results at the B3LYP+D3/def2-TZVP of **1e**. Hydrogen atoms were omitted for clarity.

Orbital	Occ.	Contribution from atoms to the orb	Atomic orbitals
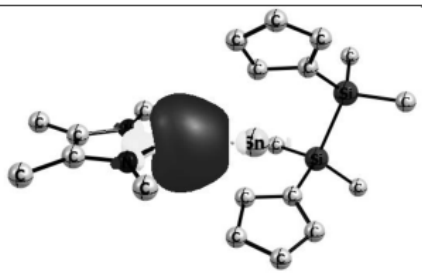	1.95	C_{carb}(86.31%)-Sn (13.69%)	*C_{carb}: s*(40.86%) *p* (59.13%) *d* (0.01%) *Sn: s*(3.30%) *p* (96.46%) *d* (0.15%)
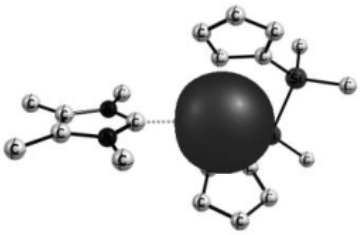	1.98	LP (Sn)	*s*(91.76%) *p* (8.22%) *d* (0.02%)
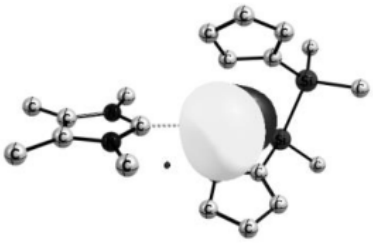	0.40	LP* (Sn)	*s*(5.17%) *p* (94.72%) *d* (0.07%)
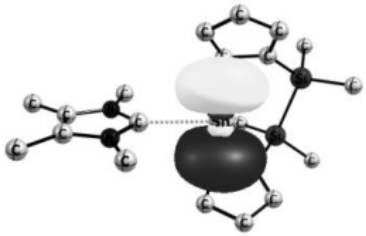	0.20	LP* (Sn)	*s*(0.00%) *p* (99.74%) *d* (0.22%)

Figure S7. NBO results at the B3LYP+D3/def2-TZVP of **2a**. Hydrogen atoms were omitted for clarity.

Orbital	Occ.	Contribution from atoms to the orb	Atomic orbitals
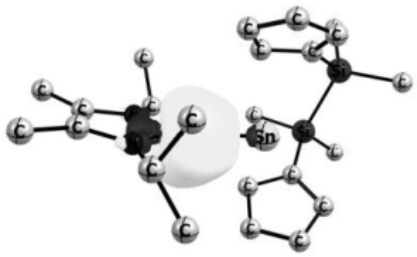	1.94	C_{carb}(88.53%)-Sn (11.47%)	*Ccarb:* *s*(40.73%) *p* (59.26%) *d* (0.01%) *Sn:* *s*(2.18%) *p* (97.52%) *d* (0.22%)
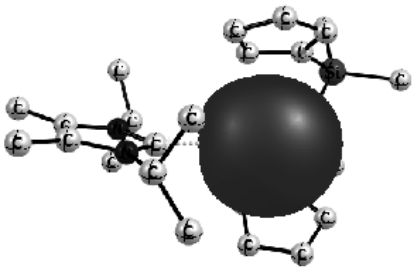	1.98	LP (Sn)	*s*(95.08%) *p* (4.90%) *d* (0.01%)
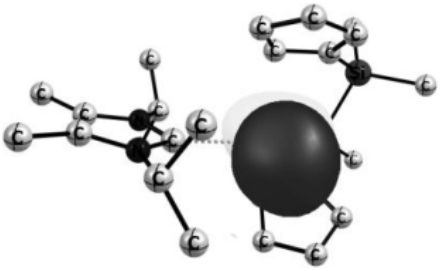	0.36	LP* (Sn)	*s*(3.13%) *p* (96.78%) *d* (0.06%)
	0.19	LP* (Sn)	*s*(0.00%) *p* (99.81%) *d* (0.15%)

Figure S8. NBO results at the B3LYP+D3/def2-TZVP of **2b**. Hydrogen atoms were omitted for clarity.

Orbital	Occ.	Contribution from atoms to the orb	Atomic orbitals
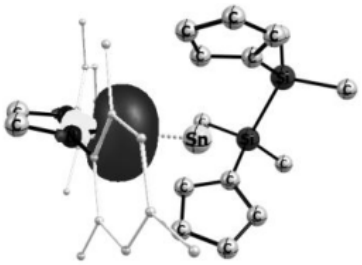	1.75	LP (C_{carb})	*s*(44.04%) *p* (55.94%) *d* (0.01%)
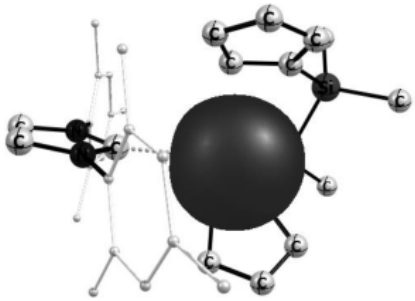	1.98	LP (Sn)	*s*(94.34%) *p* (5.65%) *d* (0.01%)
	0.39	LP* (Sn)	*s*(6.12%) *p* (93.83%) *d* (0.01%)
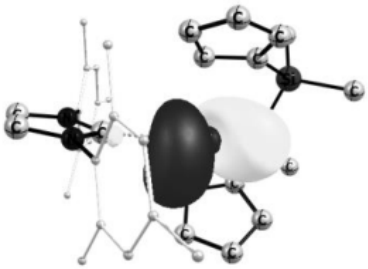	0.26	LP* (Sn)	*s*(00.03%) *p* (99.85%) *d* (0.10%)
	0.18	LP* (Sn)	*s*(0.00%) *p* (99.76%) *d* (0.20%)

Figure S9. NBO results at the B3LYP+D3/def2-TZVP of **2c**. Hydrogen atoms were omitted for clarity.

Orbital	Occ.	Contribution from atoms to the orb	Atomic orbitals
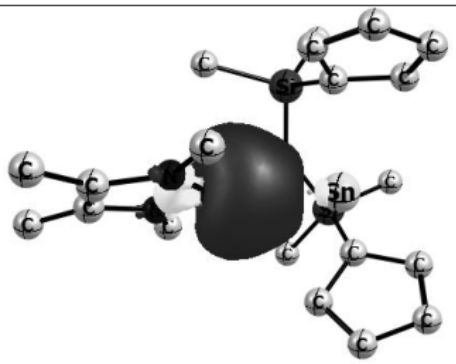	1.94	C_{carb}(87.48%)-Sn (12.52%)	*C_{carb}: s*(40.98%) *p* (59.00%) *d* (0.01%) *Sn: s*(2.35%) *p* (97.39%) *d* (0.18%)
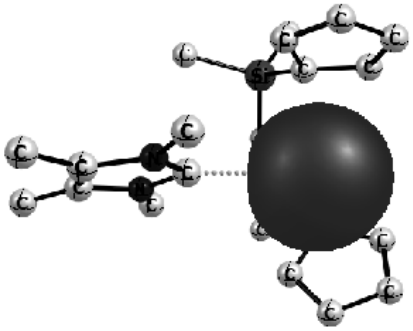	1.98	LP (Sn)	*s*(93.43%) *p* (6.55%) *d* (0.01%)
	0.36	LP* (Sn)	*s*(4.50%) *p* (95.40%) *d* (0.07%)
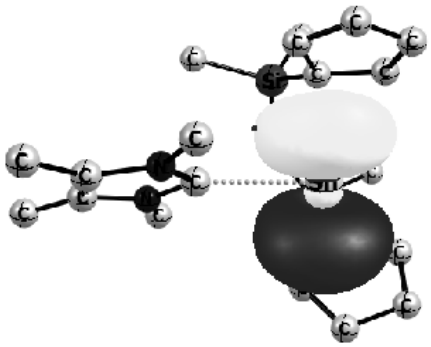	0.18	LP* (Sn)	*s*(0.01%) *p* (99.76%) *d* (0.20%)

Figure S10. NBO results at the B3LYP+D3/def2-TZVP of **2d**. Hydrogen atoms were omitted for clarity.

Orbital	Occ.	Contribution from atoms to the orb	Atomic orbitals
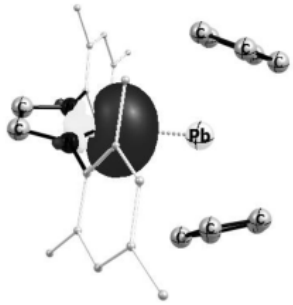	1.79	LP (C_{carb})	*s*(46.07%) *p* (53.91%) *d* (0.01%)
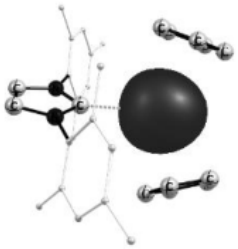	1.99	LP (Pb)	*s*(99.43%) *p* (0.56%) *d* (0.01%)
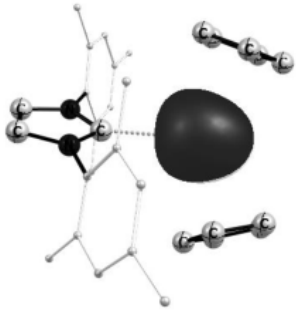	0.37	LP* (Pb)	*s*(0.61%) *p* (99.31%) *d* (0.01%)
	0.31	LP* (Pb)	*s*(0.07%) *p* (99.89%) *d* (0.02%)
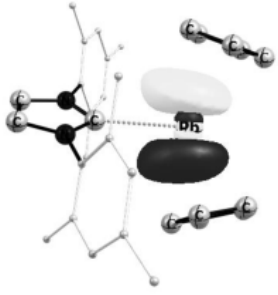	0.16	LP* (Pb)	*s*(0.00%) *p* (99.92%) *d* (0.02%)

Figure S11. NBO results at the B3LYP+D3/def2-TZVP of **3a**. Hydrogen atoms were omitted for clarity.

Orbital	Occ.	Contribution from atoms to the orb	Atomic orbitals
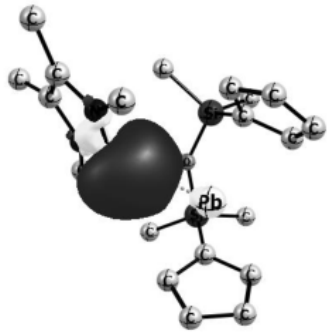	1.94	C_{carb}(89.85%)-Pb (10.15%)	C_{carb}: *s*(0.41%) *p* (99.26%) *d* (0.19%) Pb: *s*(40.64%) *p* (59.33%) *d* (0.03%)
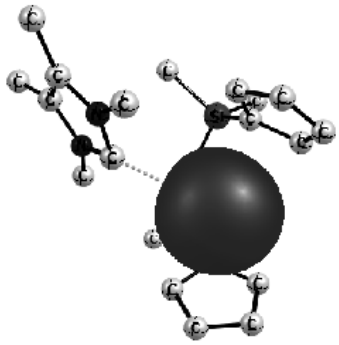	1.99	LP (Pb)	*s*(98.19%) *p* (1.80%) *d* (0.01%)
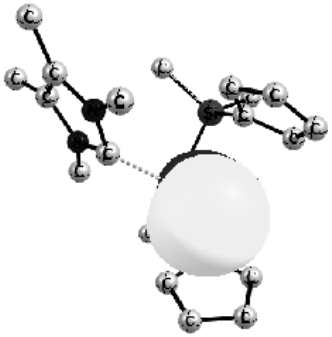	0.33	LP* (Pb)	*s*(1.74%) *p* (98.18%) *d* (0.03%)
	0.16	LP* (Pb)	*s*(0.00%) *p* (99.89%) *d* (0.04%)

Figure S12. NBO results at the B3LYP+D3/def2-TZVP of **3b**. Hydrogen atoms were omitted for clarity.

Orbital	Occ.	Contribution from atoms to the orb	Atomic orbitals
	1.55	LP C_{carb}	C_{carb}: *s*(45.23%) *p* (54.76%) *d* (0.01%)
	1.99	LP (Pb)	*s*(99.06%) *p* (0.93%) *d* (0.01%)
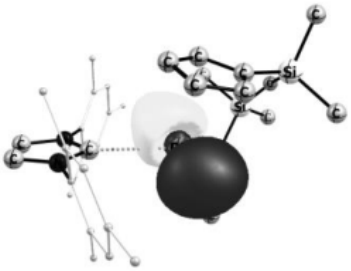	0.34	LP* (Pb)	*s*(1.16%) *p* (98.78%) *d* (0.01%)
	0.27	LP* (Pb)	*s*(0.02%) *p* (99.93%) *d* (0.03%)
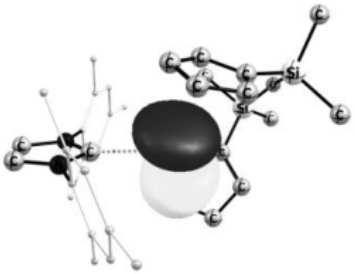	0.15	LP* (Pb)	*s*(0.00%) *p* (99.92%) *d* (0.02%)

Figure S13. NBO results at the B3LYP+D3/def2-TZVP of **3c**. Hydrogen atoms were omitted for clarity.

Orbital	Occ.	Contribution from atoms to the orb	Atomic orbitals
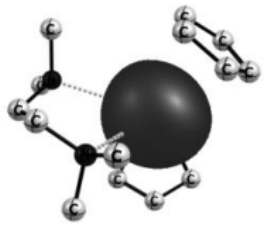	1.99	LP (Sn)	*s*(99.89%) *p* (0.09%) *d* (0.01%)
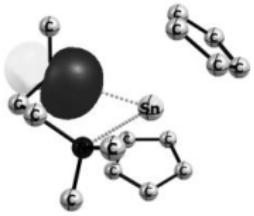	1.84	LP (N)	*s*(16.79%) *p* (83.14%) *d* (0.07%)
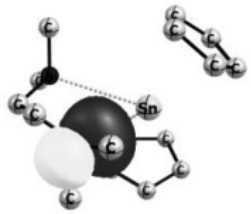	1.84	LP (N)	*s*(16.79%) *p* (83.14%) *d* (0.07%)
	0.34	LP* (Sn)	*s*(0.00%) *p* (99.94%) *d* (0.02%)
	0.28	LP* (Sn)	*s*(0.10%) *p* (99.86%) *d* (0.03%)
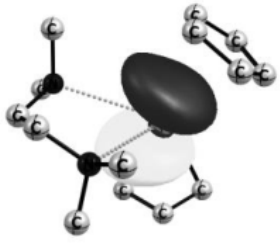	0.15	LP* (Sn)	*s*(0.00%) *p* (99.97%) *d* (0.03%)

Figure S14. NBO results at the B3LYP+D3/def2-TZVP of **4**. Hydrogen atoms were omitted for clarity.

Orbital	Occ.	Contribution from atoms to the orb	Atomic orbitals
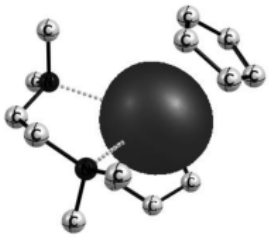	1.99	LP (Pb)	*s*(99.98%) *p* (0.01%) *d* (0.01%)
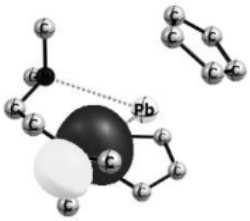	1.85	LP (N)	*s*(16.97%) *p* (82.97%) *d* (0.06%)
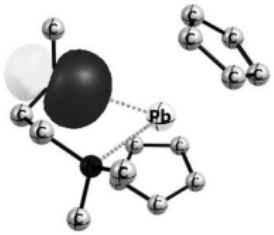	1.85	LP (N)	*s*(16.97%) *p* (82.97%) *d* (0.06%)
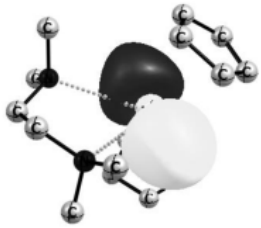	0.32	LP* (Pb)	*s*(0.00%) *p* (99.92%) *d* (0.01%)
	0.27	LP* (Pb)	*s*(0.01%) *p* (99.96%) *d* (0.00%)
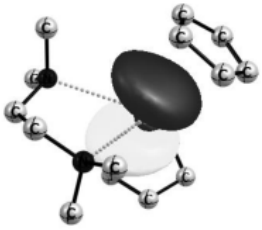	0.15	LP* (Pb)	*s*(0.00%) *p* (99.95%) *d* (0.00%)

Figure S15. NBO results at the B3LYP+D3/def2-TZVP of **5a**. Hydrogen atoms were omitted for clarity.

Orbital	Occ.	Contribution from atoms to the orb	Atomic orbitals
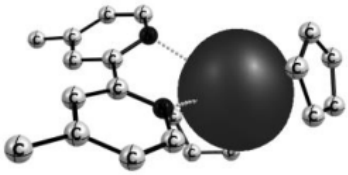	1.99	LP (Pb)	*s*(99.80%) *p* (0.19%) *d* (0.01%)
	1.87	LP (N)	*s*(29.50%) *p* (70.36%) *d* (0.13%)
	1.88	LP (N)	*s*(30.12%) *p* (60.70%) *d* (0.01%)
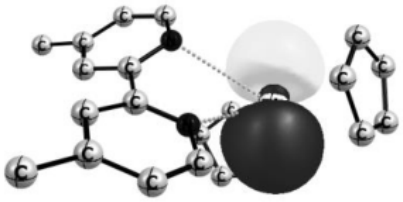	0.36	LP (Pb)	*s*(0.20%) *p* (99.71%) *d* (0.19%)
	0.29	LP (Pb)	*s*(0.01%) *p* (99.94%) *d* (0.02%)
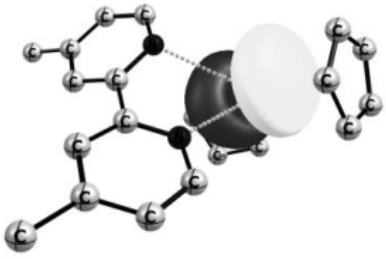	1.88	LP (Pb)	*s*(0.00%) *p* (99.94%) *d* (0.00%)

Figure S16. NBO results at the B3LYP+D3/def2-TZVP of **5b**. Hydrogen atoms were omitted for clarity.

Table S2. Non-Lewis contribution of the of two possible Lewis representation within NBO framework.

	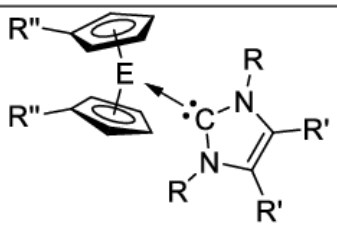	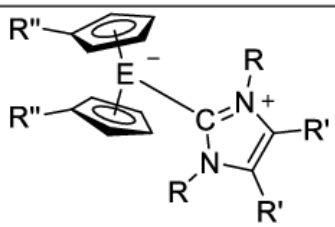
1a	2.131%	1.905%
1b	2.396%	
1c	2.255%	1.922%
1d	1.903%	1.812%
1e	2.331%	
2a	1.823%	1.723%
2b	1.652%	1.652%
2c	2.071%	
2d	1.785%	1.698%
3a	2.231%	
3b	1.620%	1.561%
3c	2.170%	
4	2.026%	
5a	1.712%	
5b	2.359%	

Table S3. NBO Two-electron interactions and associated second-order perturbational energies ($\Delta E^{(2)}$ in kcal mol^{-1}) at the B3LYP+D3/def2-TZVP level of theory of **1-5**.

Compound	Interaction	$\Delta E^{(2)}$ (kcal mol^{-1})
1a	$LP(C_{carb}) \rightarrow LV_1(Sn)$	47.0
	$LP(C_{carb}) \rightarrow LV_2(Sn)$	35.4
1b	$LP(C_{carb}) \rightarrow LV_1(Sn)$	36.6
	$LP(C_{carb}) \rightarrow LV_2(Sn)$	30.9
1c	$LP(C_{carb}) \rightarrow LV_1(Sn)$	62.0
	$LP(C_{carb}) \rightarrow LV_2(Sn)$	42.2
1d	$LP(C_{carb}) \rightarrow LV_1(Sn)$	48.9
	$LP(C_{carb}) \rightarrow LV_2(Sn)$	33.9
1e	$LP(C_{carb}) \rightarrow LV_1(Sn)$	38.1
	$LP(C_{carb}) \rightarrow LV_2(Sn)$	25.1
2a	$LP(C_{carb}) \rightarrow LV_1(Sn)$	54.1
	$LP(C_{carb}) \rightarrow LV_2(Sn)$	46.0
2b	$LP(C_{carb}) \rightarrow LV_1(Sn)$	42.1
	$LP(C_{carb}) \rightarrow LV_2(Sn)$	34.8
2c	$LP(C_{carb}) \rightarrow LV_1(Sn)$	38.6
	$LP(C_{carb}) \rightarrow LV_2(Sn)$	31.8
2d	$LP(C_{carb}) \rightarrow LV_1(Sn)$	46.9
	$LP(C_{carb}) \rightarrow LV_2(Sn)$	35.4
3a	$LP(C_{carb}) \rightarrow LV_1(Pb)$	38.4
	$LP(C_{carb}) \rightarrow LV_2(Pb)$	3.9
3b	$LP(C_{carb}) \rightarrow LV_1(Pb)$	36.0
	$LP(C_{carb}) \rightarrow LV_2(Pb)$	19.9
3c	$LP(C_{carb}) \rightarrow LV_1(Pb)$	31.89
	$LP(C_{carb}) \rightarrow LV_2(Pb)$	6.32
4	$LP(N_1) \rightarrow LV_1(Sn)$	2.6
	$LP(N_1) \rightarrow LV_2(Sn)$	7.7
	$LP(N_2) \rightarrow LV_1(Sn)$	21.5
	$LP(N_2) \rightarrow LV_2(Sn)$	6.8
5a	$LP(N_1) \rightarrow LV_1(Pb)$	2.8

	$LP(N_1) \rightarrow LV_2(Pb)$	8.0
	$LP(N_2) \rightarrow LV_1(Pb)$	19.5
	$LP(N_2) \rightarrow LV_2(Pb)$	6.2
5b	$LP(N_1) \rightarrow LV_1(Pb)$	4.8
	$LP(N_1) \rightarrow LV_2(Pb)$	13.2
	$LP(N_2) \rightarrow LV_1(Pb)$	38.7
	$LP(N_2) \rightarrow LV_2(Pb)$	0.7

	Deformation densities	NHC^R	ECp_2
1a	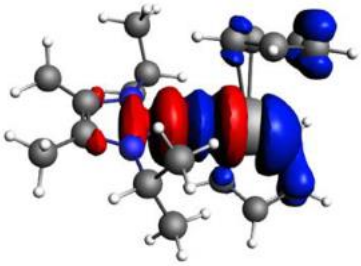	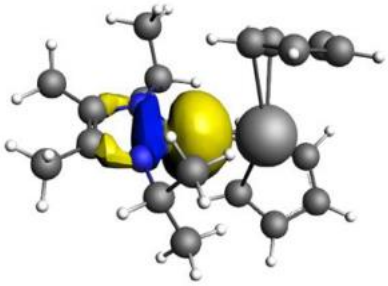	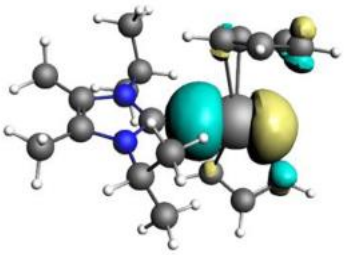
	$\Delta E_{orb\,\rho\,(1)}$ = -29.4 ; |ν_1 |=0.57	HOMO (ε =-4.39 eV) ν_1 = -0.38	LUMO (ε =-2.82 eV) ν_1 = 0.41
1b	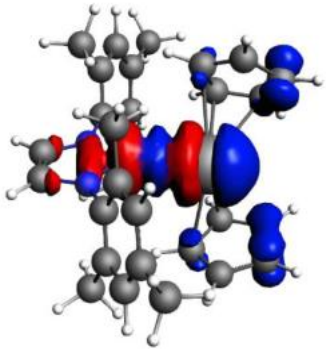	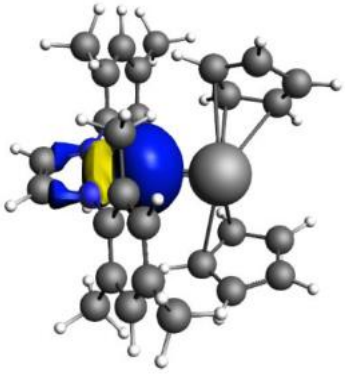	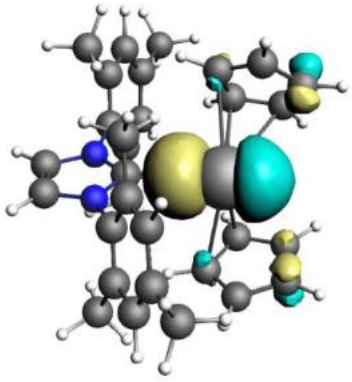
	$\Delta E_{orb\,\rho\,(1)}$ = -24.6 ; |ν_1 |=0.54	HOMO(ε = -4.69 eV) ν_1 = -0.32	LUMO (ε =-2.91 eV) ν_1 = 0.35
1c	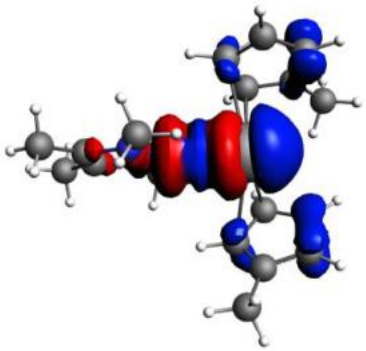	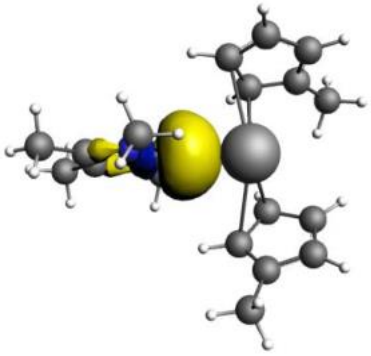	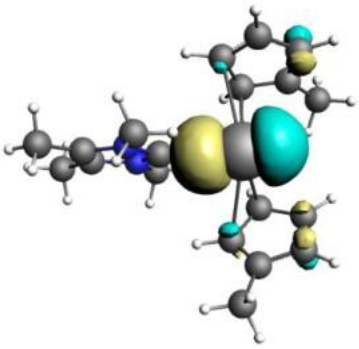
	$\Delta E_{orb\,\rho\,(1)}$ = -34.8 ; |ν_1 |=0.64	HOMO (ε = -4.42 eV) ν_1 = -0.43	LUMO (ε =-2.98 eV) ν_1 = 0.46

1d	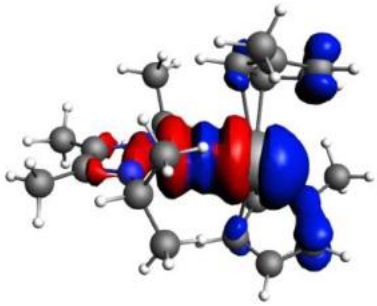	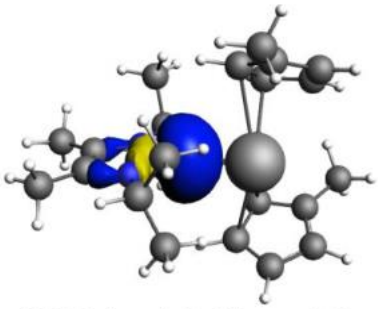	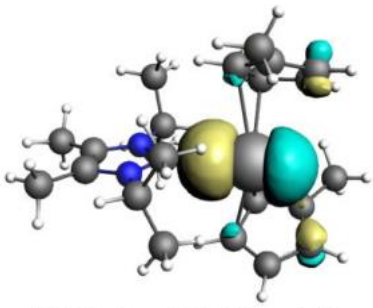
	$\Delta E_{orb\ \rho\ (1)}$ = -30.5 ; |ν_1 |= 0.59	HOMO (ε = -4.38 eV) ν_1 = -0.39	LUMO (ε =-2.76 eV) ν_1 =0.43
1e	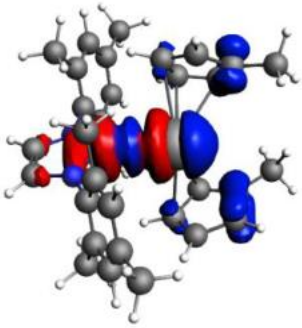	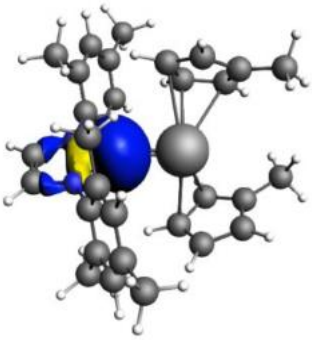	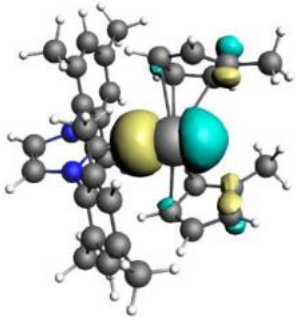
	$\Delta E_{orb\ \rho\ (1)}$ = -23.0 ; |ν_1 |=0.53	HOMO (ε = -4.70 eV) ν_1 = -0.30	LUMO (ε = -2.71 eV) ν_1 = 0.33
2a	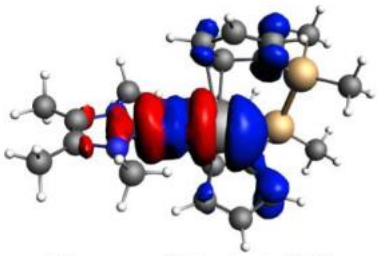	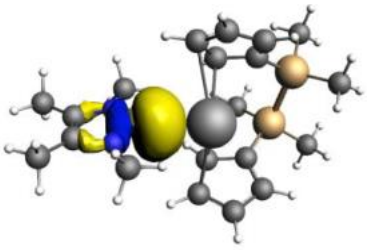	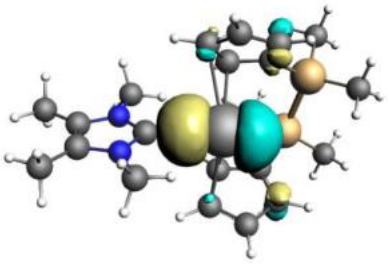
	$\Delta E_{orb\ \rho\ (1)}$ = -33.8 ; |ν_1 |= 0.60	HOMO (ε = -4.43 eV) ν_1 = -0.42	LUMO (ε = -3.04 eV) ν_1 = 0.45
2b	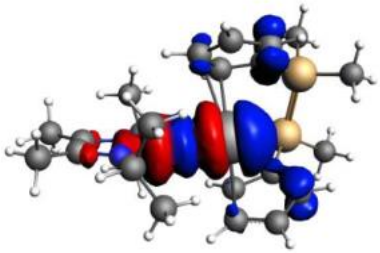	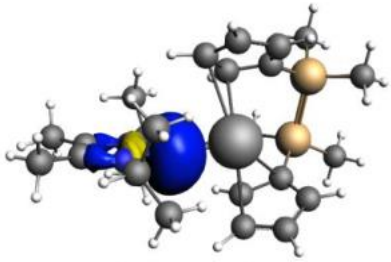	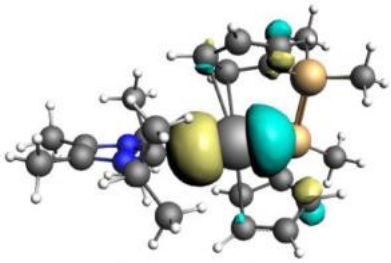
	$\Delta E_{orb\ \rho\ (1)}$ = -29.7 ; |ν_1 |= 0.58	HOMO (ε = -4.37 eV) ν_1 = -0.40	LUMO (ε = -2.94 eV) ν_1 = 0.43

2c	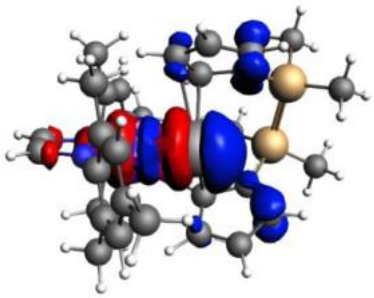 $\Delta E_{orb\ \rho\ (1)}$ = -29.4; $\lvert\nu_1\rvert$ = 0.59	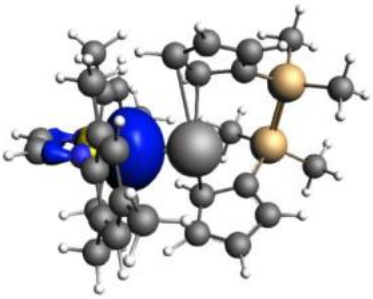 HOMO (ε = -4.66 eV) ν_1 = -0.36	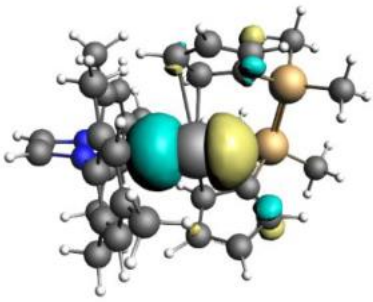 LUMO (ε = -3.14 eV) ν_1 = 0.40
2d	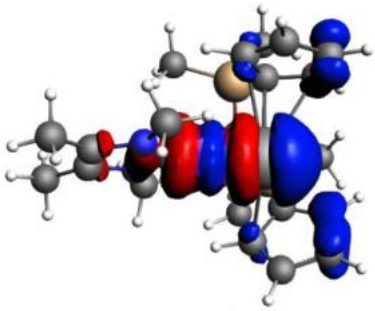 $\Delta E_{orb\ \rho\ (1)}$ = -30.2 ; $\lvert\nu_1\rvert$ = 0.58	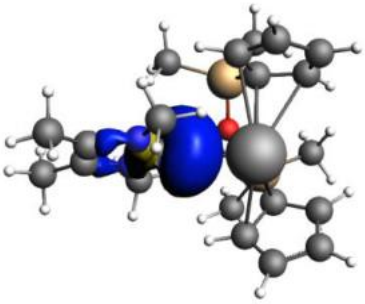 HOMO (ε = -4.44 eV) ν_1 = -0.40	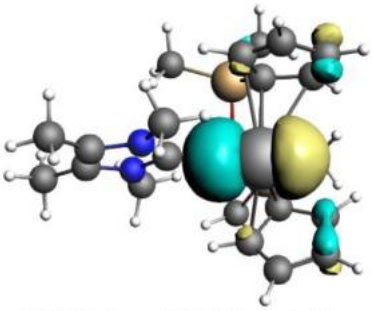 LUMO (ε =-2.95 eV) ν_1 =0.42
3a	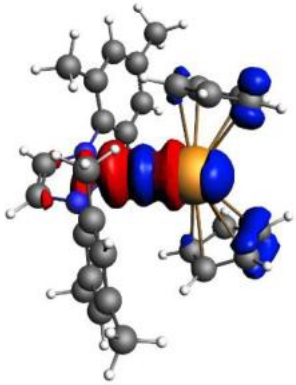 $\Delta E_{orb\ \rho\ (1)}$ = -16.9 ; $\lvert\nu_1\rvert$ =0.45	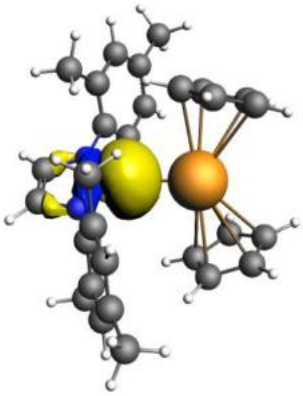 HOMO (ε = -4.73 eV) ν_1 =-0.21	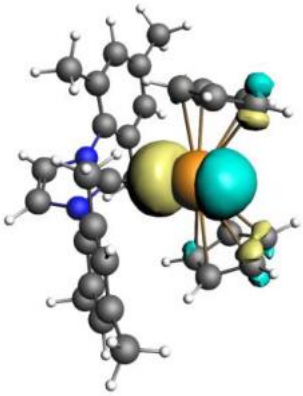 LUMO (ε = -2.48 eV) ν_1 = 0.23
3b	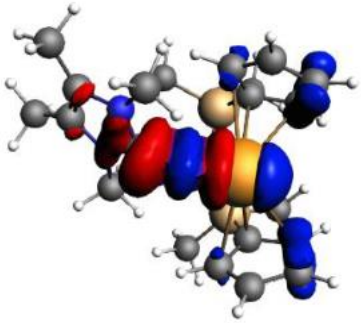 $\Delta E_{orb\ \rho\ (1)}$ = -19.0 ; $\lvert\nu_1\rvert$ = 0.49	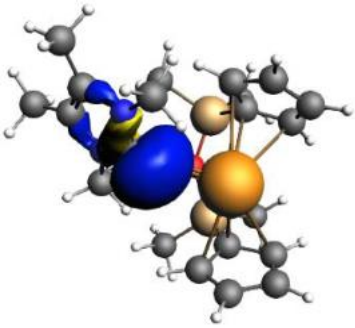 HOMO (ε = -4.46 eV) ν_1 = -0.25	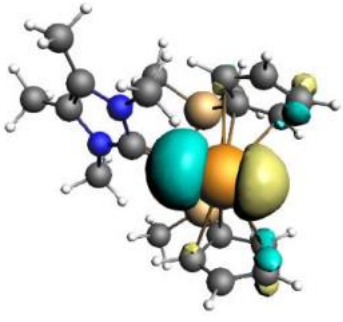 LUMO (ε = -2.71 eV) ν_1 = -0.28

3c	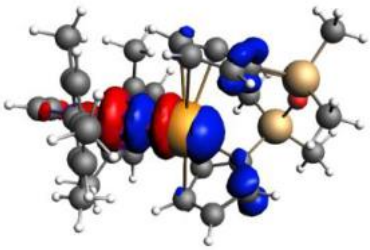	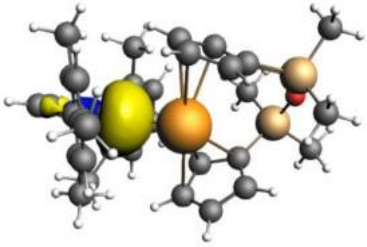	
	$\Delta E_{orb\ \rho\ (1)}$ = -18.1 ; $\lvert\nu_1\rvert$ = 0.49	HOMO (ε = -4.63 eV) ν_1 = -0.22	LUMO (ε = -1.86 eV) ν_1 = -0.24
4	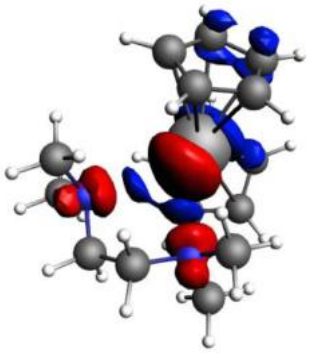	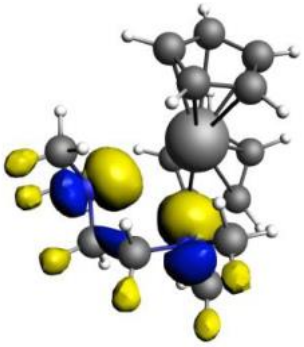	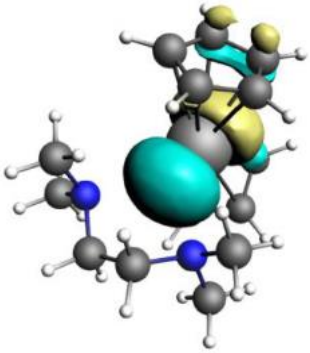
	$\Delta E_{orb\ \rho\ (1)}$ = -6.74 ; $\lvert\nu_1\rvert$ = 0.31	HOMO-1 (ε = -5.01 eV) ν_1 = -0.09	LUMO+1(ε = -2.06 eV) ν_1 = 0.11
	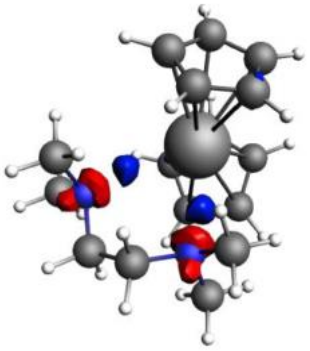	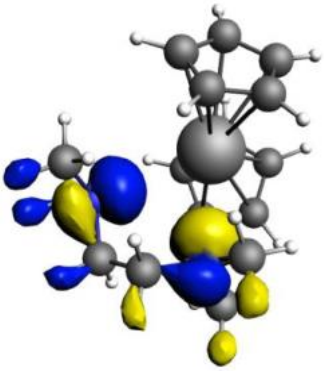	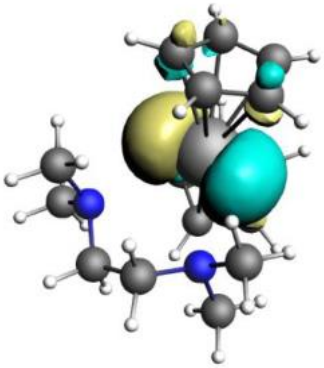
	$\Delta E_{orb\ \rho\ (2)}$ = -3.17 ; $\lvert\nu_2\rvert$ = 0.21	HOMO (ε = -4.77 eV) ν_2 = -0.05	LUMO (ε = -2.21 eV) ν_2 = 0.04
5a	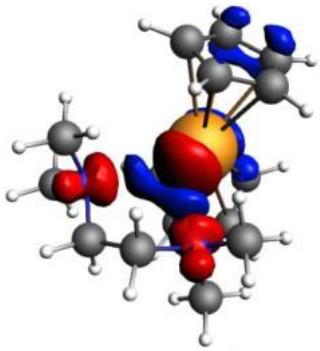	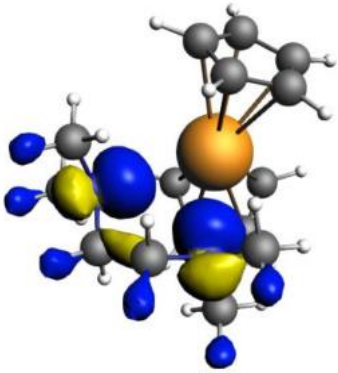	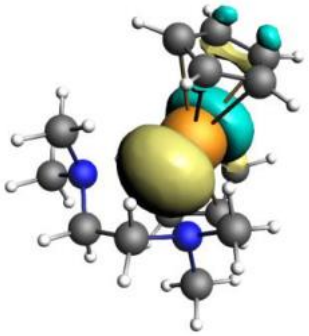
	$\Delta E_{orb\ \rho\ (1)}$ = -7.67 ; $\lvert\nu_1\rvert$ = 0.32	HOMO-1 (ε = -5.02 eV) ν_1 = -0.09	LUMO+1 (ε = -2.20 eV) ν_2 = 0.12

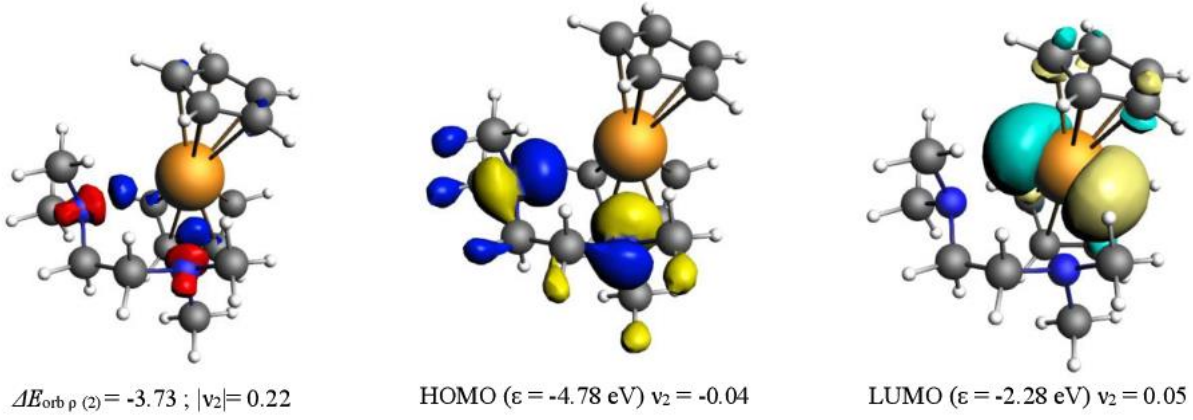

$\Delta E_{orb\,\rho\,(2)}$ = -3.73 ; $|\nu_2|$= 0.22 | HOMO (ε = -4.78 eV) ν_2 = -0.04 | LUMO (ε = -2.28 eV) ν_2 = 0.05

5b

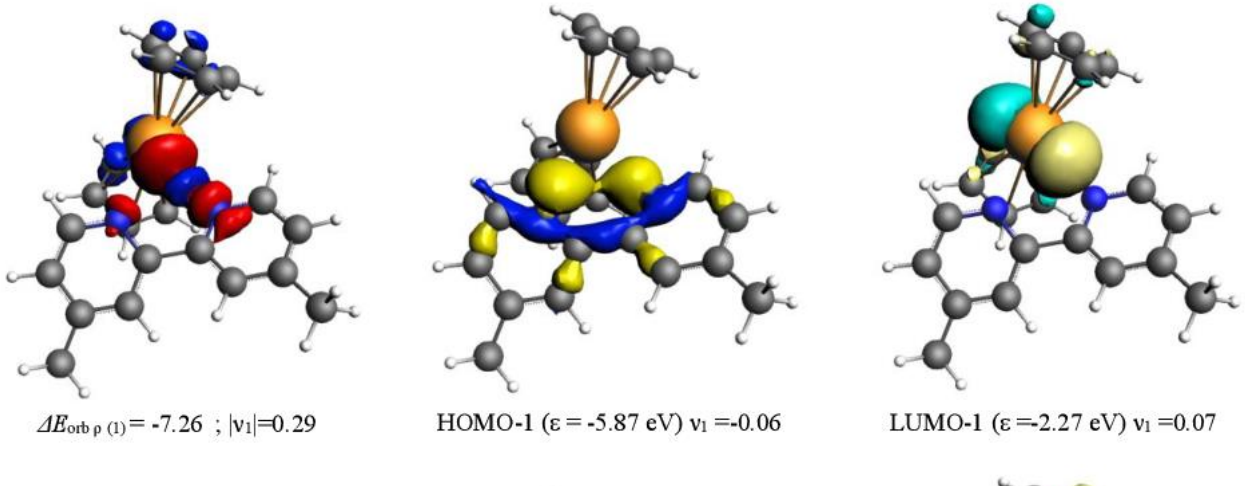

$\Delta E_{orb\,\rho\,(1)}$ = -7.26 ; $|\nu_1|$=0.29 | HOMO-1 (ε = -5.87 eV) ν_1 =-0.06 | LUMO-1 (ε =-2.27 eV) ν_1 =0.07

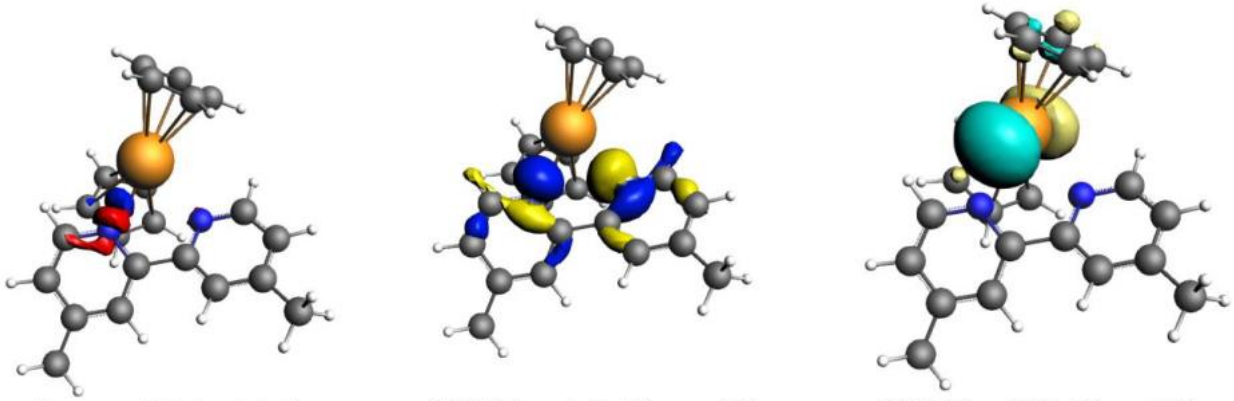

$\Delta E_{orb\,\rho\,(2)}$ =-2.28 ; $|\nu_{1\,\alpha}|$=0.15 | HOMO (ε = -5.66 eV) ν_2 = -0.02 | LUMO (ε = -2.13 eV) ν_2 = 0.02

Figure S17. Deformation densities $\Delta\rho$ (isovalue 0.001 a.u.) of the pairwise orbital interactions between L (NHC, TMEDA, and Bipy) and ECp_2 (E = Sn and Pb) of compound **1-5** (MOs = molecular orbitals). Associated energies ΔE (in kcal/mol) and eigenvalues ν (in a.u.). The red color shows the charge outflow, whereas blue shows charge density accumulation. Shape of the most important interacting occupied and vacant orbitals (isovalue 0.05 a.u.) of the fragments.

Table S4. Energy decomposition analysis (EDA-NOCV) of the E-Cp bonds (E =Sn, Pb) in the metallocene Cp_2Sn and Cp_2Pb, and metallocene Cp_2Sn-NHC and Cp_2Pb-NHC complexes at BP86+D3(BJ)/ZORA&TZ2P level of theory. Energy values are given in kcal mol^{-1}.

Fragments	Cp_2Sn	Cp_2Sn-NHC	Cp_2Pb	Cp_2Pb-NHC
ΔE_{int}	-615.9	-485.6	-590.5	-476.6
ΔE_{Pauli}	117.5	149.2	102.0	93.5
ΔE_{elstat}[a]	-502.8 (68.6%)	-430.7 (67.8%)	-489.7 (70.7%)	-409.2 (71.8%)
ΔE_{disp}[a]	-8.9 (1.2%)	-13.8 (2.2%)	-10.0 (1.4%)	-15.2 (2.7%)
ΔE_{orb}[a]	-221.7 (30.2%)	-190.3 (30.0%)	-192.8 (27.8%)	-145.7 (25.6%)
$\Delta E_{\rho 1}$(a' → p_x)[b]	-60.9 (27.5%)	-78.7 (41.3%)	-52.2(27.1%)	-48.6 (33.4%)
$\Delta E_{\rho 2}$ (a'' → p_y)[b]	-55.6 (25.1%)	-46.9 (24.7%)	-50.2 (26.0%)	-27.1 (18.6 %)
$\Delta E_{\rho 3}$ (a' → p_z)[b]	-37.3 (16.8%)	-16.8 (8.8%)	-34.2 (17.7%)	-25.1 (17.2%)
$\Delta E_{\rho 4}$(a' → d_{yz})[b]	-12.9 (5.8 %)	-8.1 (4.3 %)	-9.9 (5.1 %)	-7.1 (4.9 %)
$\Delta E_{\rho 5}$ (a' → d_{xz})[b]	-12.4 (5.6 %)	-5.1 (2.7 %)	-10.1 (5.2 %)	-3.4 (2.3 %)
$\Delta E_{\rho 6}$ (a' → d_z^2)[b]	-5.4 (2.4 %)	-3.9 (2.0 %)	-4.2 (2.2 %)	-6.3 (4.3 %)
ΔE_{orb}(rest)[b]	-37.2 (16.8 %)	-30.8 (16.2 %)	-32.0 (16.6 %)	-28.1 (19.3 %)
ΔE_{prep}	66.6	74.6	64.5	71.8
$-D_e$	-549.3	-411.0	-526.0	-404.8

[a] The value in parenthesis gives the percentage contribution to the total attractive interactions $\Delta E_{elstat} + \Delta E_{orb} + \Delta E_{disp}$. [b] The value in parenthesis gives the percentage contribution to the total orbital interactions ΔE_{orb}.

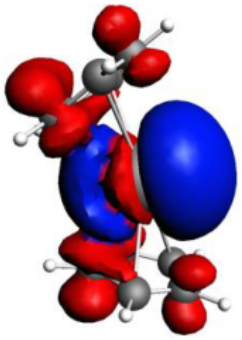

ΔE_1=-60.9; $|\nu_1|$=0.74

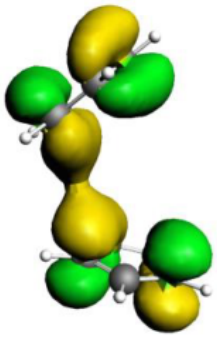

HOMO-3 (ε=3.48 eV)
ν_1=-0.43

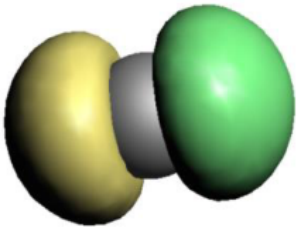

LUMO (ε= -17.97 eV)
ν_1=+0.51

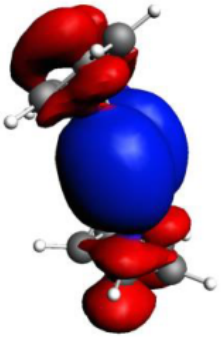

ΔE_2=-55.6; $|\nu_2|$=0.69

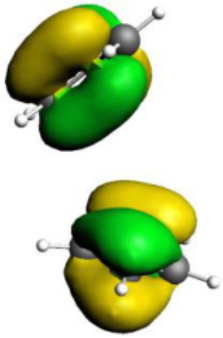

HOMO-2 (ε=3.53 eV)
ν_2=-0.49

LUMO (ε= -17.97 eV)
ν_2=+0.45

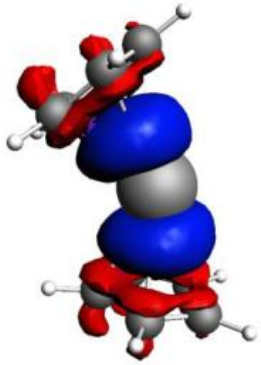

ΔE_3=-37.3; $|\nu_3|$=0.42

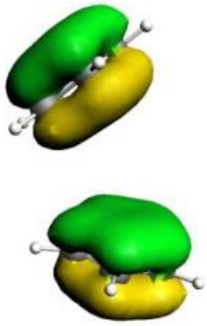

HOMO-4 (ε=0.01 eV)
ν_3=-0.30

LUMO (ε= -17.97 eV)
ν_3=+0.31

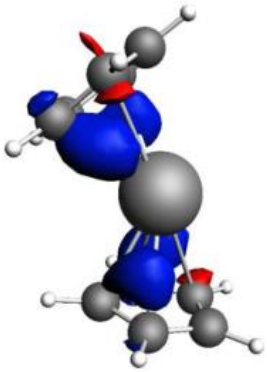

ΔE_4= -12.9; $|\nu_4|$=0.22

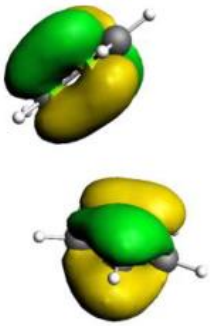

HOMO-1 (ε=3.68 eV)
ν_4=-0.08

LUMO+1 (ε= -8.39 eV)
ν_4=+0.07

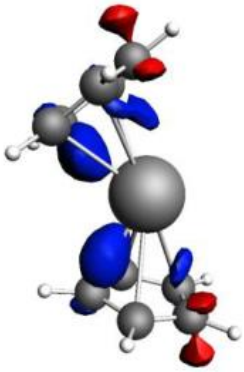

ΔE_5=-12.4; $|\nu_5|$= 0.21

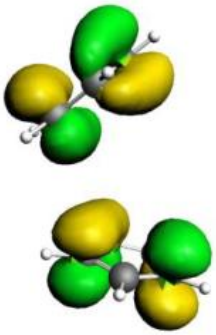

HOMO (ε= 3.76 eV)
ν_5=-0.06

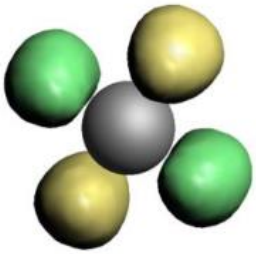

LUMO+1 (ε= -8.39 eV)
ν_5=+0.06

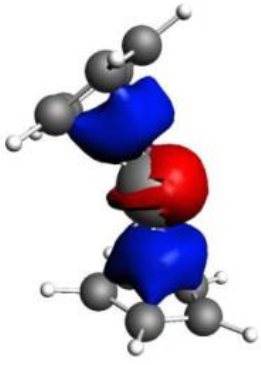

ΔE_6=-5.4; $|\nu_6|$= 0.13

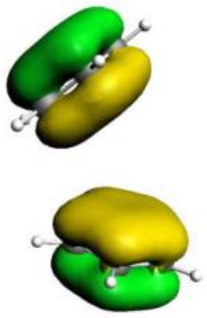

HOMO-5 (ε= -0.15 eV)
ν_6=-0.08

LUMO+1 (ε=-8.39 eV)
ν_6=+0.01

Figure S18. Deformation densities $\Delta\rho$ (isovalue 0.001 a.u.) of the pairwise orbital interactions between $(Sn)^{2+}$ and $(Cp_2)^{2-}$ of compound **Cp_2Sn** (MOs = molecular orbitals). Associated energies ΔE (in kcal/mol) and eigenvalues ν (in a.u.). The red color shows the charge outflow, whereas blue shows charge density accumulation. Shape of the most important interacting occupied and vacant orbitals (isovalue 0.05 a.u.) of the fragments.

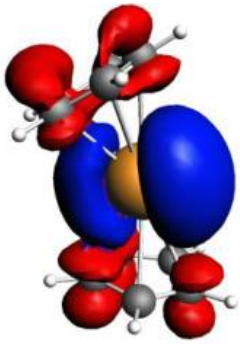

ΔE_1=-52.2; $|\nu_1|$=0.69

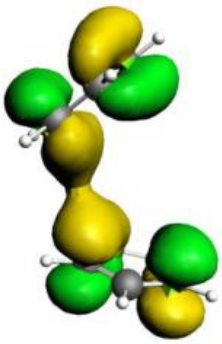

HOMO-3 (ε=3.44 eV)
ν_1=-0.43

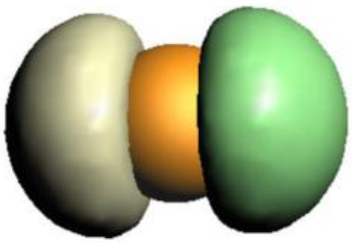

LUMO (ε= -17.20 eV)
ν_1=+0.44

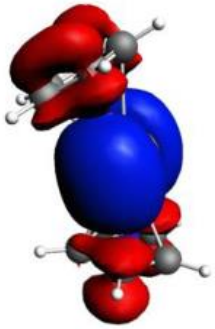

ΔE_2=-50.2; $|\nu_2|$=0.68

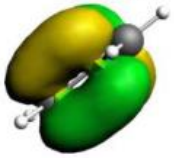

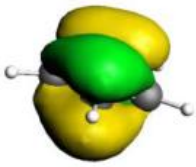

HOMO-2 (ε=3.46 eV)
ν_2=-0.46

LUMO (ε= -17.20 eV)
ν_2=+0.43

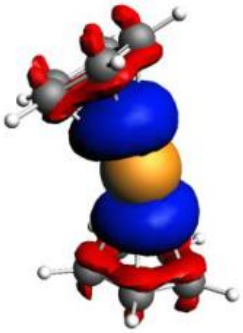

ΔE_3=-34.2; $|\nu_3|$=0.41

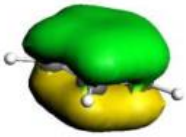

HOMO-4 (ε=-0.11 eV)
ν_3=-0.27

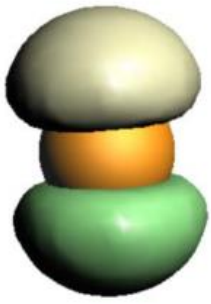

LUMO (ε= -17.20 eV)
ν_3=+0.27

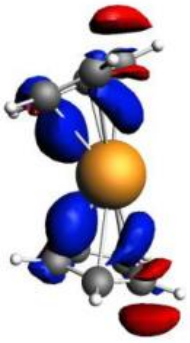

ΔE_4= -10.1; $|\nu_4|$=0.19

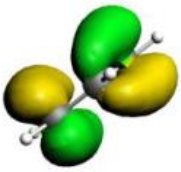

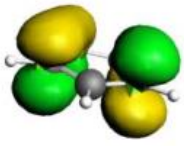

HOMO (ε=3.61 eV)
ν_4=-0.06

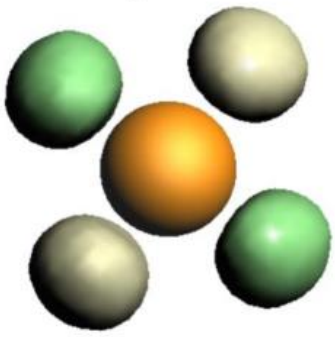

LUMO+1 (ε= -8.49 eV)
ν_4=+0.05

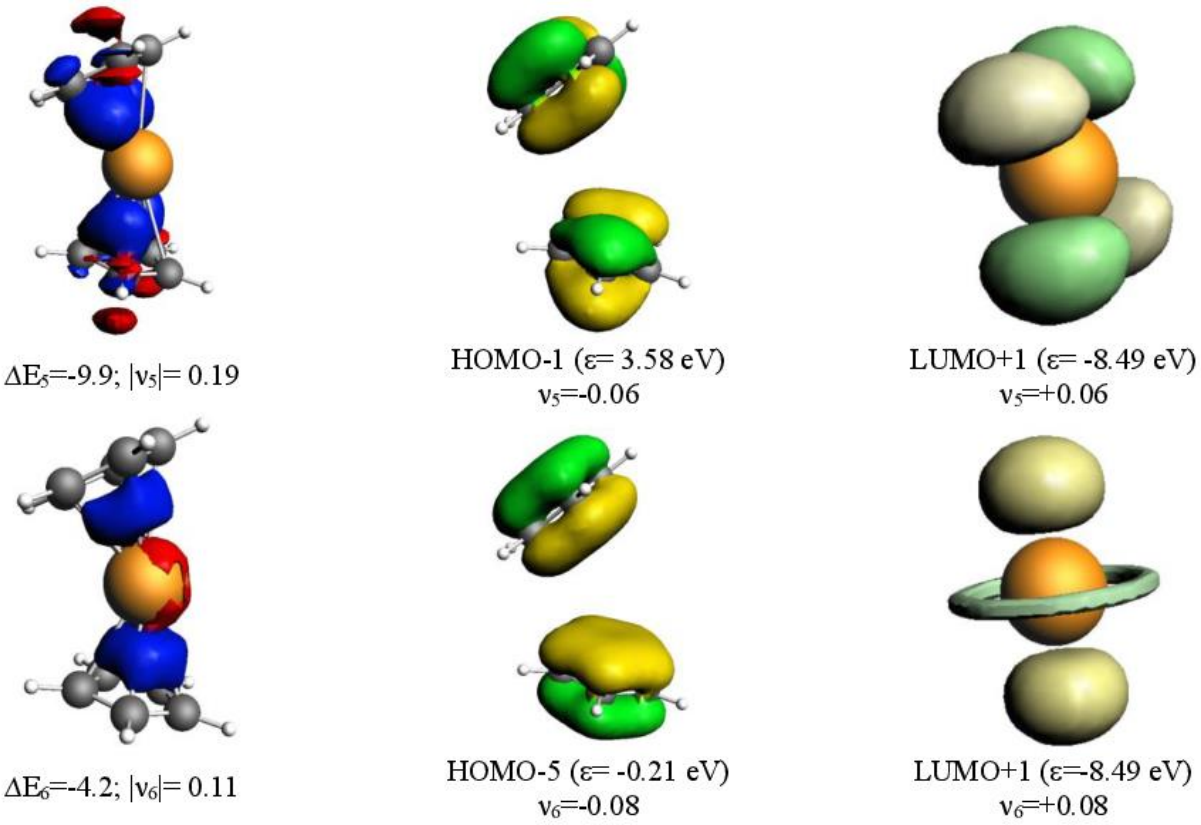

Figure S19. Deformation densities $\Delta\rho$ (isovalue 0.001 a.u.) of the pairwise orbital interactions between $(Pb)^{2+}$ and $(Cp_2)^{2-}$ of compound **Cp_2Pb** (MOs = molecular orbitals). Associated energies ΔE (in kcal/mol) and eigenvalues ν (in a.u.). The red color shows the charge outflow, whereas blue shows charge density accumulation. Shape of the most important interacting occupied and vacant orbitals (isovalue 0.05 a.u.) of the fragments.

$\Delta E_{\rho 1}$(a' → p_x)^b	-60.9 (27.5%)	-78.7 (41.3%)	-52.2(27.1%)	-48.6 (33.4%)
$\Delta E_{\rho 2}$ (a'' → p_y)^b	-55.6 (25.1%)	-46.9 (24.7%)	-50.2 (26.0%)	-27.1 (18.6 %)
$\Delta E_{\rho 3}$ (a' → p_z)^b	-37.3 (16.8%)	-16.8 (8.8%)	-34.2 (17.7%)	-25.1 (17.2%)
$\Delta E_{\rho 4}$(a' → d_{yz})^b	-12.9 (5.8 %)	-8.1 (4.3 %)	-9.9 (5.1 %)	-7.1 (4.9 %)
$\Delta E_{\rho 5}$ (a' → d_{xz})^b	-12.4 (5.6 %)	-5.1 (2.7 %)	-10.1 (5.2 %)	-3.4 (2.3 %)

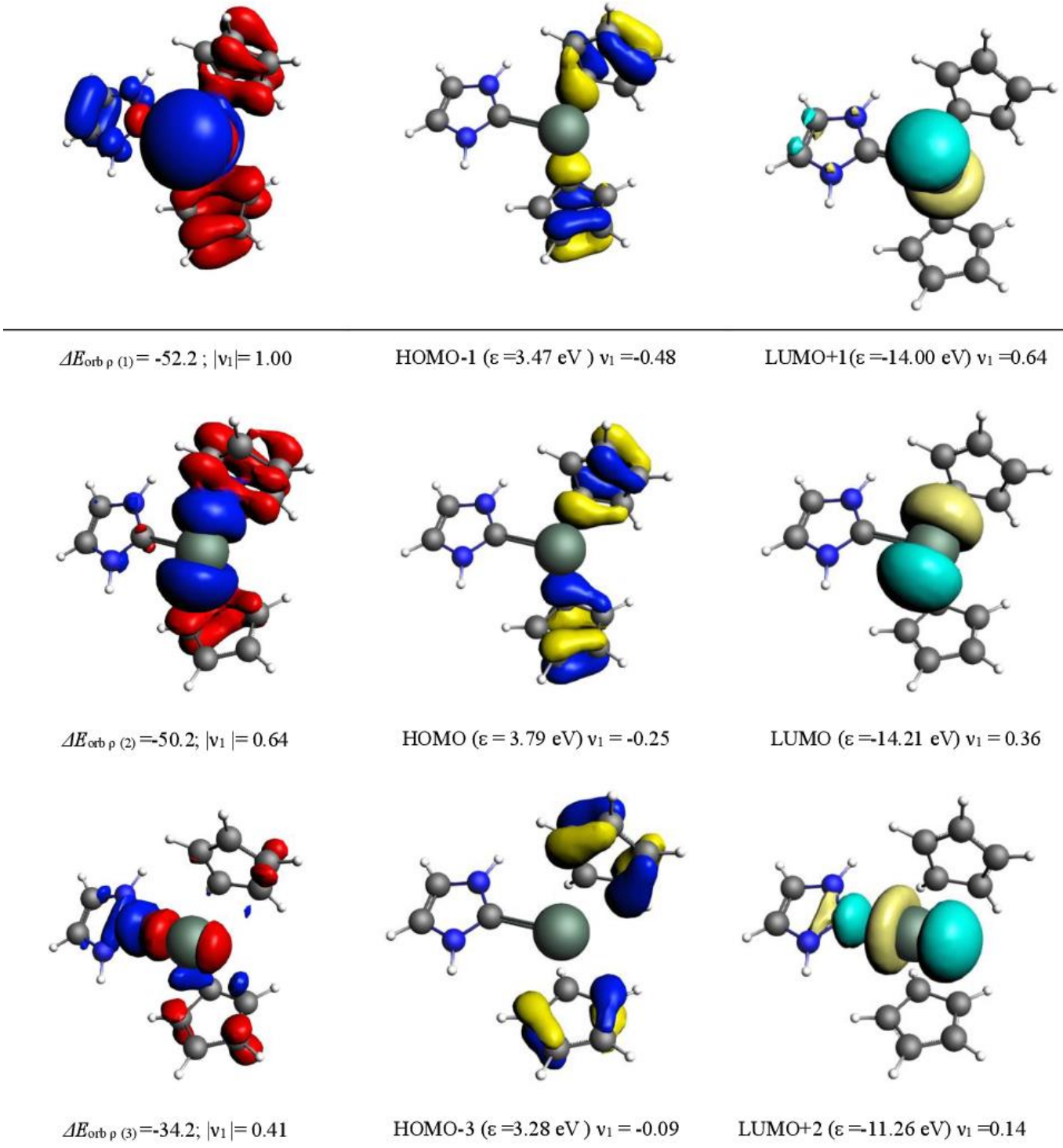

Figure S20. Deformation densities $\Delta\rho$ (isovalue 0.001 a.u.) of the pairwise orbital interactions between $(NHC\text{-}Sn)^{2+}$ and $(Cp_2)^{2-}$ of compound **1M** (MOs = molecular orbitals). Associated energies ΔE (in kcal/mol) and eigenvalues ν (in a.u.). The red color shows the charge outflow, whereas blue shows charge density accumulation. Shape of the most important interacting occupied and vacant orbitals (isovalue 0.05 a.u.) of the fragments.

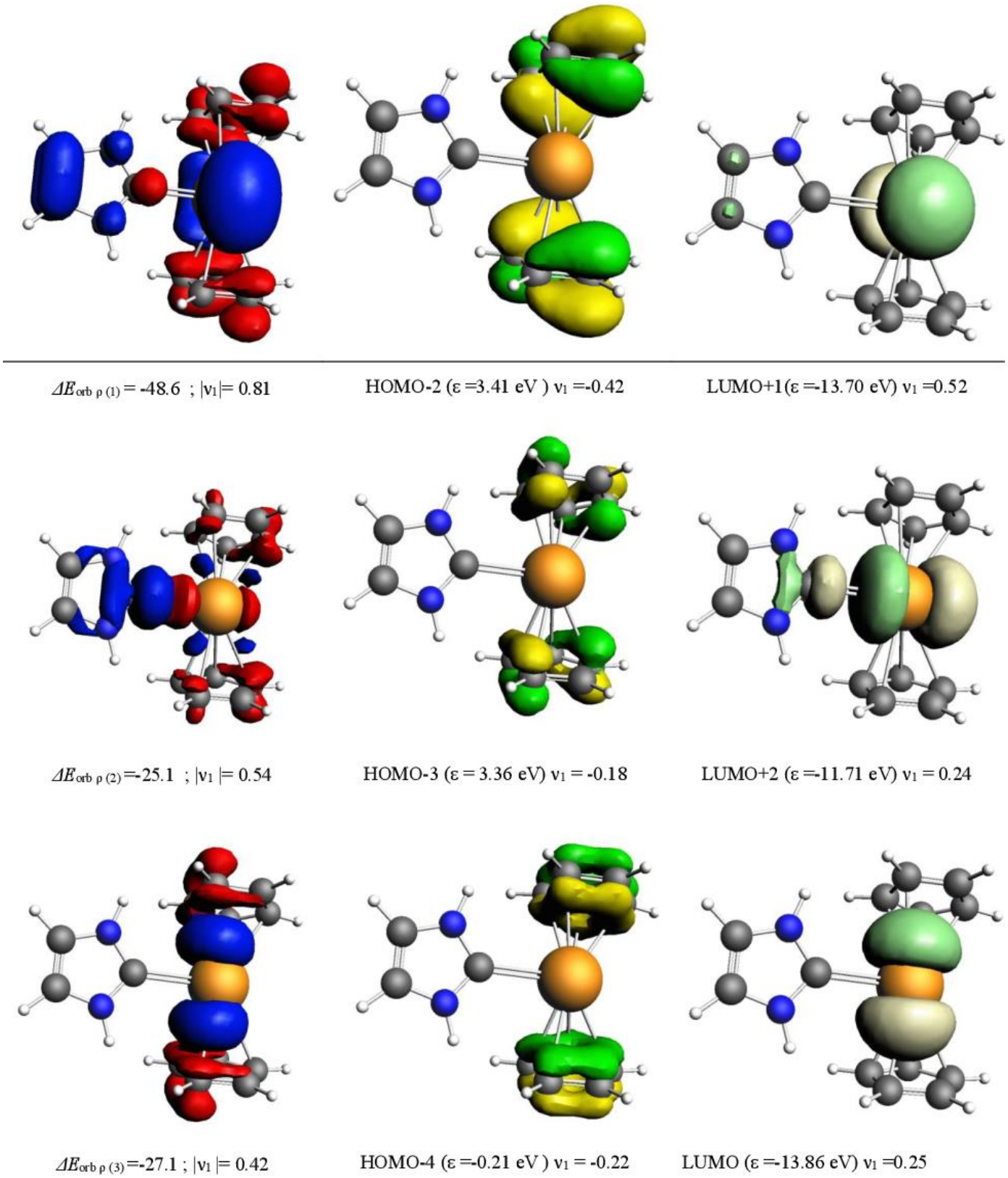

Figure S21. Deformation densities $\Delta\rho$ (isovalue 0.001 a.u.) of the pairwise orbital interactions between $(NHC\text{-}Pb)^{2+}$ and $(Cp_2)^{2-}$ of compound **1M** (MOs = molecular orbitals). Associated energies ΔE (in kcal/mol) and eigenvalues ν (in a.u.). The red color shows the charge outflow, whereas blue shows charge density accumulation. Shape of the most important interacting occupied and vacant orbitals (isovalue 0.05 a.u.) of the fragments.

Table S5. Energy decomposition analysis (EDA-NOCV) of sila[2]stannocenophane dimer 6 at the BP86+D3(BJ) /ZORA&TZ2P level of theory. Energy values are given in kcal/mol.

	6
ΔE_{int}	-7.6
ΔE_{Pauli}	7.1
ΔE_{elstat}[a]	-2.9 (19.4 %)
ΔE_{disp}[a]	-9.3 (63.1 %)
ΔE_{orb}[a]	-2.6 (17.5 %)
ΔE_{prep}	0.2
ΔE (-De)	7.8
d(Sn-Sn)	438.0

[a] The value in parenthesis gives the percentage contribution to the total attractive interactions $\Delta E_{elstat} + \Delta E_{orb} + \Delta E_{disp}$.

6.4 Diphosphanylmetallocenes of Main-Group Elements

Chemistry–A European Journal

Supporting Information

Diphosphanylmetallocenes of Main-Group Elements

Carsten Müller, Joshua Warken, Volker Huch, Bernd Morgenstern, Inga-Alexandra Bischoff, Michael Zimmer, and André Schäfer*[a]

WILEY-VCH

SUPPORTING INFORMATION

Table of Contents

Experimental Procedures	S2	– S8
NMR Spectra	S9	– S44
IR Spectra	S45	
XRD Data	S46	– S66
Computational Details	S67	– S68
References	S69	

SUPPORTING INFORMATION

Experimental Procedures

All manipulations were carried out under an argon inert gas atmosphere (argon 5.0), using either Schlenk line techniques or a glovebox. Solvents were purified and dried using a MBraun Solvent Purification System and activated 4Å molecular sieves. Chlorodiisopropylphosphine was synthesized following a literature known procedure.[1] Tin(II) chloride and antimony(III) chloride were purchased from ABCR and used as received. (1,5-cyclooctadiene)dimethylplatinum, (1,5-cyclooctadiene)tetracarbonyltungsten, iron(II) chloride and aluminum(III) chloride were purchased from Sigma Aldrich and used as received. 1,2,3,4-tetramethylcyclopentenone was purchased from Hangzhou Dayangchem and used as received. *n*-Butyllithium solution (2.5 M in hexane) was purchased from Acros Organics and used as received. (1,4-dioxane)germanium(II) chloride was purchased from Strem and used as received. Carbon disulfide solution (5.0 M in hexane) was purchased from Sigma Aldrich and used as received. 1,2,3,4-tetramethylcyclopentadiene was prepared from 1,2,3,4-tetramethyl-cyclopentenone following a literature known procedure.[2] lithium 1,2,3,4-tetramethylcyclopentadienide was prepared from 1,2,3,4-tetramethylcyclopentadiene and *n*-butyllithium in hexane at 293 K. 1,3-diisopropyl-4,5-dimethylimidazolin-2-ylidene was prepared following a literature known procedure.[3] NMR-spectra were recorded on Bruker Avance III 300 and Bruker Avance III 400. ^{1}H and ^{13}C NMR spectra were referenced using the solvent signals[4] (δ^{1}H (C_6HD_5) = 7.16; δ^{13}C (C_6D_6) = 128.06) and ^{27}Al, ^{31}P, ^{119}Sn and ^{207}Pb NMR-spectra were referenced using external standards (δ^{27}Al($AlCl_3$ in D_2O) = 0; δ^{31}P(85% $H_3PO_{4(aq)}$) = 0; δ^{119}Sn($SnMe_4$) = 0, δ^{207}Pb($PbMe_4$) = 0). Fourier transformed infrared spectra (FT-IR) were recorded in total reflectance mode with a Bruker Vertex 70 spectrometer from 4500−400 cm^{-1} with a 4 nm increment and 16 scans averaged. Single crystal X-ray diffraction analysis were carried out at low temperatures on Bruker AXS X8 Apex CCD and Bruker AXS X8 Venture diffractometers. Structure solution and refinement with anisotropic thermal parameters of all non-hydrogen atoms were performed using SHELX.[5] Elemental analysis were performed on an Elementar vario MICRO cube®.

Synthesis of 1,1'-bis(diisopropylphosphanyl)octamethylmagnesocene 1a (dipp$^{\#}$Mg)

To a solution of lithium 1,2,3,4-tetramethylcyclopentadienide (1.50 g, 11.7 mmol) in 50 mL of thf was added chlorodiisopropylphosphine (1.78 g, 1.85 mL, 11.3 mmol) *via* syringe at room temperature. After stirring overnight, all volatiles were removed *in vacuo* and the residue was extracted with hexane. After evaporation of all volatiles, 1,2,3,4-tetramethylcyclopentadienyl-diisopropylphosphine, dipp$^{\#}$H, was obtained as a mixture of isomers in form of a yellow oil, which was used in the subsequent step without further purification.

Yield: 2.51 g / 93%.

^{1}H-NMR (400.13 MHz, 298 K, C_6D_6): δ = 3.09 (m, 1H, CpH), 2.90 (q, 1H, *J* = 7.40Hz, CpH), 2.16 (s, 2H, $CpCH_3$), 2.03 (s, 4H, $CpCH_3$), 1.91–1.79 (m, 2H, CH), 1.75 (s, 5H, $CpCH_3$), 1.25–0.90 (m, 18H, CH_3).

^{31}P{^{1}H}-NMR (161.98 MHz, 298 K, C_6D_6): δ = 18.4, -7.4, -8.6.

To a solution of tetramethylcyclopentadienyldiisopropylphosphine, dipp$^{\#}$H, (2.51 g, 10.5 mmol) in 50 mL of hexane was added a solution of n-butyl-sec-butyl magnesium (7.5 mL, 5.25 mmol, 0.7 M in hexane) *via* syringe at room temperature. After stirring for 1 hour, all volatiles were removed *in vacuo*, the resulting yellow oily residue was washed with 20 mL of cold hexane and taken up in 20 mL of toluene. Storage of the toluene solution at 253 K resulted in the crystallization of in 1,1'-bis(diisopropylphosphanyl)octamethylmagnesocene, **1a**, in form of colorless crystals.

Yield: 385 mg / 38%.

^{1}H-NMR (400.13 MHz, 298 K, C_6D_6): δ = 2.18 (s, 12H, $CpCH_3$), 2.18–2.07 (m, 4H, CH), 1.98 (s, 12H, $CpCH_3$), 1.15 (d, *J* = 6.9 Hz, 6H, CH_3), 1.10 (d, *J* = 6.9 Hz, 6H, CH_3), 0.98 (d, *J* = 7.0 Hz, 6H, CH_3), 0.94 (d, *J* = 7.0 Hz, 6H, CH_3).

^{13}C{^{1}H}-NMR (100.61 MHz, 298 K, C_6D_6): δ = 121.3 (d, J_{CP} = 10.6 Hz, CpC), 117.1 (d, J_{CP} = 3.2 Hz, CpC), 105.5 (d, J_{CP} = 22.5 Hz, CpC), 25.2 (d, J_{CP} = 11.6 Hz, CH), 22.1 (d, J_{CP} = 23.1 Hz, CH_3), 21.9 (d, J_{CP} = 11.0 Hz, CH_3), 13.2 (d, J_{CP} = 9.7 Hz, CH_3), 11.1 (s, CH_3).

^{31}P{^{1}H}-NMR (161.98 MHz, 298 K, C_6D_6): δ = -3.8.

Synthesis of 1,1'-bis(diisopropylphosphanyl)magnesocene 1b (dippMg)

To a suspension of lithium cyclopentadienide (4.15 g, 57.6 mmol) in 100 mL of hexane was added chlorodiisopropylphosphine (8.70 g, 9.00 mL, 57.0 mmol) *via* syringe at room temperature and the resulting mixture was stirred overnight. After filtration and evaporation of all volatiles, cyclopentadienyldiisopropylphosphine, dippH, was obtained as a mixture of isomers in form of a yellow oil, which was used in the subsequent step without further purification.

Yield: 7.75 g / 75%.

^{1}H-NMR (400.13 MHz, 298 K, C_6D_6): δ = 6.86–6.82 (m, 1H, CpH), 6.66–6.55 (m, 1H, CpH), 6.45 (s, 1H, CpH), 6.31–6.28 (m, 1H, CpH), 2.90 (s, 1H, CpH), 2.74 (s, 1H, CpH), 1.91 (sept, 1H, *J* = 7.1 Hz, *J* = 2.1 Hz, CH), 1.80 (sept, 1H, *J* = 7.1 Hz, *J* = 2.0 Hz, CH), 1.13–0.87 (m, 12H, CH_3).

^{31}P{^{1}H}-NMR (161.98 MHz, 298 K, C_6D_6): δ = -3.4, -5.1.

To a solution of cyclopentadienyldiisopropylphosphine, dippH (7.75 g, 42.5 mmol), in 100 mL hexane was added a solution of n-butyl-sec-butyl magnesium (30 mL, 21.0 mmol, 0.7 M in hexane) *via* syringe at room temperature and stirred for 18 h. The solution was stored at 253 K overnight, resulting in crystallization of 1,1'-bis(diisopropylphosphanyl)magnesocene, **1b**, in form of colorless crystals.

Yield: 7.00 g / 86%.

^{1}H-NMR (400.13 MHz, 298 K, C_6D_6): δ = 6.25–6.17 (m, 8H, CpH), 1.87 (sept, *J* = 6.9 Hz, 4H, CH), 1.06 (d, *J* = 7.1 Hz, 6H, CH_3), 1.02 (d, *J* = 7.1 Hz, 6H, CH_3), 0.96 (d, *J* = 6.9 Hz, 6H, CH_3), 0.93 (d, *J* = 6.9 Hz, 6H, CH_3).

$^{13}C\{^1H\}$-NMR (100.61 MHz, 298 K, C_6D_6): δ = 114.1 (d, J_{CP} = 19.8 Hz, CpC), 113.9 (d, J_{CP} = 12.2 Hz, CpC), 109.7 (d, J_{CP} = 4.1 Hz, CpC), 23.5 (d, J_{CP} = 11.9 Hz, CH), 20.3 (d, J_{CP} = 18.2 Hz, CH_3), 19.7 (d, J_{CP} = 8.7 Hz, CH_3).
$^{31}P\{^1H\}$-NMR (161.98 MHz, 298 K, C_6D_6): δ = -2.8.

Synthesis of 1,1'-bis(diphenylphosphanyl)octamethylmagnesocene 1c (dpp#Mg)

To a solution of lithium 1,2,3,4-tetramethylcyclopentadienide (5.95 g, 46.5 mmol) in 120 mL of thf was added chlorodiphenylphosphine (8.10 mL, 45.0 mmol) *via* syringe at room temperature. After stirring overnight, all volatiles were removed *in vacuo* and the solid residue was extracted with 100 mL of hexane. After evaporation of all volatiles, 1,2,3,4-tetramethylcyclopentadienyldiphenylphosphine, dpp#H, was obtained as a mixture of isomers in form of a yellow oil, which was used in the subsequent step without further purification.
Yield: 11.2 g / 81%.
Analytical data was identical to that reported before.[6,7]
^1H-NMR (400.13 MHz, 298 K, C_6D_6): δ: 7.58–7.51 (m, 4H, PhH), 7.50–7.43 (m, 4H, PhH), 7.13–7.08 (m, 6H, PhH), 7.08–7.03 (m, 6H, PhH), 3.70–3.66 (m, 1H, CpH), 2.90–2.80 (m, 1H, CpH), 2.01 (d, *J* = 1.8 Hz, 3H, $CpCH_3$), 1.80 (s, 6H, $CpCH_3$), 1.65 (s, 3H, $CpCH_3$), 1.63 (s, 3H, $CpCH_3$), 1.54 (s, 6H, $CpCH_3$), 0.85 (d, *J* = 7.6 Hz, 3H, $CpCH_3$).
$^{31}P\{^1H\}$-NMR (161.98 MHz, 298 K, C_6D_6): δ: -0.2, -25.6, -30.7.
To a solution of tetramethylcyclopentadienyldiphenylphosphine, dpp#H (11.2 g, 36.6 mmol), in 100 mL of toluene was added a solution of n-butyl-sec-butyl magnesium (25.0 mL, 17.5 mmol, 0.7 M in hexane) *via* syringe at room temperature. After stirring overnight, the yellow solution was concentrated to approximately half its volume and stored at 253 K overnight, resulting in crystallization of 1,1'-bis(diphenylphosphanyl)octamethylmagnesocene, **1c**, in form of colorless crystals.
Yield: 8.42 g / 76%.
^1H-NMR (400.13 MHz, 298 K, C_6D_6): δ = 7.46–7.40 (m, 8H, PhH), 7.15–7.10 (m, 8H, PhH), 7.06–7.01 (m, 4H, PhH), 1.99 (s, 12H, $CpCH_3$), 1.89 (s, 12H, $CpCH_3$).
$^{13}C\{^1H\}$-NMR (100.61 MHz, 298 K, C_6D_6): δ = 139.2 (d, J_{CP} = 10.6 Hz), 132.1 (d, J_{CP} = 19.1 Hz), 128.8 (d, J_{CP} = 6.3 Hz), 121.5 (d, J_{CP} = 12.0 Hz), 117.6 (d, J_{CP} = 10.0 Hz), 103.6 (d, J_{CP} = 10.7 Hz), 12.1 (d, J_{CP} = 9.0 Hz, $CpCH_3$), 10.7 (s, $CpCH_3$).
$^{31}P\{^1H\}$-NMR (161.98 MHz, 298 K, C_6D_6): δ = -25.5.

Synthesis of 1,1'-bis(diisopropylphosphanyl)magnesocene bis(tetrahydrofurane) adduct 1b·(thf)$_2$ (dippMg·(thf)$_2$)

1,1'-Bis(diisopropylphosphanyl)magnesocene, **1b**, (200 mg, 0.52 mmol) was dissolved in 5 mL of thf and 20 mL hexane were added. The resulting colorless solution was stored at 253 K overnight, yielding colorless crystals of **1b·(thf)$_2$**.
Yield: 184 mg / 70%.
^1H-NMR (400.13 MHz, 298 K, C_6D_6): δ = 6.25–6.27 (m, 8H, CpH), 3.48–3.55 (m, 8H, thf), 1.97 (sept, *J* = 6.9 Hz, 4H, CH), 1.31–1.37 (m, 8H, thf), 1.14 (d, *J* = 7.1 Hz, 6H, CH_3), 1.11 (d, *J* = 7.1 Hz, 6H, CH_3), 1.04 (d, *J* = 6.9 Hz, 6H, CH_3), 1.01 (d, *J* = 6.9 Hz, 6H, CH_3).
$^{13}C\{^1H\}$-NMR (100.61 MHz, 298 K, C_6D_6): δ = 114.5 (d, J_{CP} = 13.7 Hz, CpC), 111.6 (d, J_{CP} = 16.0 Hz, CpC), 107.7 (s, CpC), 68.5 (s, thf), 23.5 (d, J_{CP} = 11.9 Hz), 25.6 (s, thf), 23.6 (d, J_{CP} = 11.3 Hz), 20.5 (d, J_{CP} = 17.5 Hz), 19.8 (d, J_{CP} = 8.5 Hz).
$^{31}P\{^1H\}$-NMR (161.98 MHz, 298 K, C_6D_6): δ = -2.3.

Synthesis of 1,1'-bis(diisopropylphosphanyl)magnesocene carbon disulfide adduct 1b·(CS$_2$)$_2$ (dippMg·(CS$_2$)$_2$)

1,1'-Bis(diisopropylphosphanyl)magnesocene, **1b**, (200 mg, 0.52 mmol) was dissolved in 30 mL hexane and carbon disulfide (2.50 mmol, 0.50 mL of a 5.0 M solution in hexane) was added. The color of the solution immediately turned from colorless to dark red. The solution was stirred for 4 h while **1b·(CS$_2$)$_2$** precipitated as a red solid which was isolated by filtration and washed with 50 mL of hexane.
Yield: 174 mg / 62%.
^1H-NMR (400.13 MHz, 298 K, CD_2Cl_2): δ = 6.75–6.05 (m, 8H, CpH), 3.09–2.97 (m, 4H, CH), 1.38 (d, *J* = 6.9 Hz, 6H, CH_3), 1.34 (d, *J* = 7.0 Hz, 6H, CH_3), 1.23 (d, *J* = 6.9 Hz, 6H, CH_3), 1.19 (d, *J* = 6.9 Hz, 6H, CH_3).
$^{13}C\{^1H\}$-NMR (100.61 MHz, 298 K, CD_2Cl_2): δ = 237.0 (d, J_{CP} = 37.2 Hz, CS_2), 116.8–114.6 (m, CpC), 109.6 (bs, CpC), 87.7 (d, J_{CP} = 88 Hz, Cp), 24.6–22.7 (m, CH), 17.8 (s, CH_3), 16.7 (s, CH_3).
$^{31}P\{^1H\}$-NMR (161.98 MHz, 298 K, CD_2Cl_2): δ = 36.2.

Synthesis of 1,1'-bis(diisopropylphosphanyl)magnesocene phenylisocyanate adduct 1b·PhNCO (dippMg·PhNCO)

1,1'-Bis(diisopropylphosphanyl)magnesocene, **1b**, (200 mg, 0.52 mmol) was dissolved in 5 mL toluene and phenylisocyanate (62.0 mg, 0.52 mmol) was added. The resulting yellow to green solution was stirred for 2 h and subsequently additional 50 mL hexane were added. After storage of the solution at 253 K overnight, the adduct **1b·PhNCO** was obtained as colorless crystals.
Yield: 141 mg / 54%.
$^{13}C\{^1H\}$-CP-MAS(13 kHz)-NMR (100.65 MHz, 296 K) δ = 155.9, 154.7, 148.5, 137.9,129.7, 125.2, 123.5, 119.0, 115.6, 114.4, 105.0, 103.4, 99.8, 98.0, 82.2, 81.3, 25.2–15.9 (m).
$^{31}P\{^1H\}$-CP-MAS(13 kHz)-NMR (162.04 MHz, 296 K): δ = 24.0 (s), -12.6 (s).

SUPPORTING INFORMATION

(Note: Attempts to dissolve the crystals in C_6D_6 at room temperature and obtain solution NMR spectra resulted in the decomposition of **1b·PhNCO**. The resulting NMR spectra indicated a complex mixture of products with free ligand, dippH, among other compounds.)
Elemental analysis: calculated for $C_{29}H_{41}MgNOP_2$: C: 68.85%, H: 8.17%, N: 2.77%; found: C: 67.72%, H: 9.17%, N: 2.60%.

Synthesis of 1,1'-bis(diisopropylphosphanyl)magnesocene dimethylplatinum adduct 1b·PtMe$_2$ (dippMg·PtMe$_2$)
1,1'-Bis(diisopropylphosphanyl)magnesocene, **1b**, (200 mg, 0.52 mmol) and (1,5-cyclooctadiene)dimethylplatinum (172 mg, 0.52 mmol) were mixed and stirred in 10 mL of toluene at 298 K overnight. The resulting yellow solution was stored at 253 K overnight, resulting in crystallization **1b·PtMe$_2$**, in form of colorless crystals.
Yield: 240 mg / 75%.
^{1}H-NMR (400.13 MHz, 298 K, C_6D_6): δ = 6.19 (s, 4H, CpH), 5.85 (s, 4H, CpH), 2.61 (okt, 4H, J = 6.9 Hz, CH), 1.37 (d, 6H, J = 6.9 Hz, CH_3), 1.34 (d, 6H, J = 6.9 Hz, CH_3), 1.27 (t, 5H, J_{HP} = 6.4 Hz, Pt-CH_3), 1.19 (t, 1H, J_{HP} = 6.4 Hz, Pt-CH_3), 0.92 (d, 6H, J = 6.8 Hz, CH_3), 0.89 (d, 6H, J = 6.8 Hz, CH_3).
^{13}C{^{1}H}-NMR (100.61 MHz, 298 K, C_6D_6): δ = 112.7 (t, J_{CPt} = 2.9 Hz, CpC), 111.9 (d, J_{CP} = 16.2 Hz, CpC), 108.2 (t, J_{CPt} = 2.9 Hz, CpC), 24.3-23.9 (m, CH), 19.5-18.9 (m, CH_3), 4.7 (d, J_{CP} = 11.5 Hz, CH_3), 3.7 (d, J_{CP} = 11.6 Hz, CH_3).
^{31}P{^{1}H}-NMR (161.98 MHz, 298 K, C_6D_6): δ = 21.0 (s, J_{PPt} = 1862 Hz).
Elemental analysis: calculated for $C_{24}H_{42}MgP_2Pt$: C: 47.11%, H: 6.92%; found: C: 46.67%, H: 7.18%.

Synthesis of 1,1'-bis(diisopropylphosphanyl)ferrocene (dippFe/dippf)
1,1'-Bis(diisopropylphosphanyl)magnesocene, **1b**, (298 mg, 0.77 mmol) and iron(II) chloride (98.0 mg, 0.77 mmol) were mixed and stirred in 50 mL of thf overnight at room temperature. All volatiles were removed, the resulting residue was extracted with 50 mL of hexane and the precipitate was filtered off. The solution was stored at 253 K overnight, resulting in the crystallization of 1,1'-bis(diisopropylphosphanyl)ferrocene, **dippFe/dippf**, in form of orange crystals.
Yield: 101 mg / 31%.
Analytical data was identical to that reported before.[8]
^{1}H-NMR (400.13 MHz, 298 K, C_6D_6): δ = 4.23–4.14 (m, 8H, CpH), 1.85 (s, 4H, CH), 1.09 (s, 24H, CH_3).
^{31}P{^{1}H}-NMR (161.98 MHz, 298 K, C_6D_6): δ = -1.0.

Synthesis of 1,1'-bis(diphenylphosphanyl)octamethylferrocene (dpp$^\#$Fe/dppomf)
1,1'-Bis(diphenylphosphanyl)octamethylmagnesocene, **1c**, (500 mg, 0.79 mmol) was dissolved in 30 mL thf and a solution of iron(II) chloride (100 mg, 0.79 mmol) in 20 mL thf was added at 198 K. After warming up to room temperature overnight, thf was evaporated and the residue was extracted with 30 mL of benzene. Filtration of the resulting suspension and evaporation of benzene afforded 1,1'-bis(diphenylphosphanyl)octamethylferrocene, **dpp$^\#$Fe/dppomf**, as an orange solid.
Yield: 412 mg / 78%.
Analytical data was identical to that reported before.[9]
^{1}H-NMR (400.13 MHz, 298 K, C_6D_6): δ = 7.68–7.41 (m, 8H, PhH), 7.09–7.00 (m, 8H, PhH), 1.78 (s, 12H, $CpCH_3$), 1.56 (s, 12H, $CpCH_3$).
^{31}P{^{1}H}-NMR (161.98 MHz, 298 K, C_6D_6): δ = -21.6 (s).

Synthesis of 1,1'-bis(diphenylphosphanyl)octamethylgermanocene 2 (dpp$^\#$Ge)
1,1'-Bis(diphenylphosphanyl)octamethylmagnesocene, **1c**, (2.68 g, 4.20 mmol) and (1,4-dioxane)germanium(II) chloride (995 mg, 4.30 mmol) were mixed and stirred in 250 mL of thf overnight at room temperature. All volatiles were removed, and the resulting yellow solid residue was extracted with 50 mL of toluene and the precipitate was filtered off. After removal of all volatiles and the addition of 50 mL hexane, the yellow solution was stored at 253 K overnight, resulting in the crystallization of 1,1-bis(diphenylphosphanyl)octamehtylgermanocene, **2**, in form of colorless crystals.
Yield: 2.21 g / 77%.
^{1}H-NMR (400.13 MHz, 298 K, C_6D_6): δ = 7.59–7.54 (m, 8H, PhH), 7.15–7.09 (m, 8H, PhH), 7.07–7.01 (m, 4H, PhH), 2.00 (s, 12H, $CpCH_3$), 1.88 (s, 12H, $CpCH_3$).
^{13}C{^{1}H}-NMR (100.61 MHz, 298 K, C_6D_6): δ = 138.9 (d, J_{CP} = 10.6 Hz, PhC), 133.3 (d, J_{CP} = 18.5 Hz, PhC), 128.7 (d, J_{CP} = 6.1 Hz, PhC), 128.6 (s, CpC), 122.4 (d, J_{CP} = 4.5 Hz, CpC), 115.0 (d, J_{CP} = 8.9 Hz, CpC), 12.1 (d, J_{CP} = 9.85 Hz, $CpCH_3$), 10.6 (s, $CpCH_3$).
^{31}P{^{1}H}-NMR (161.98 MHz, 298 K, C_6D_6): δ = -27.4 (s).
Elemental analysis: calculated for $C_{42}H_{44}P_2Ge$: C: 73.82%, H: 6.49%; found: C: 68.60%, H: 6.83% (Carbon value was repeatedly and reproducibly low, even upon analysis of crystalline material.).

SUPPORTING INFORMATION

Synthesis of 1,1'-bis(diisopropylphosphanyl)octamethylstannocene 3a (dipp#Sn)

1,1'-Bis(diisopropylphosphanyl)octamethylmagnesocene, **1a**, (500 mg, 1.00 mmol) and tin(II) chloride (190 mg, 1.00 mmol) were mixed and stirred 50 mL of thf overnight at room temperature. All volatiles were removed, and the resulting residue was extracted with 50 mL of toluene. Storage of the solution at 253 K resulted in crystallization of 1,1'-bis(diisopropylphosphanyl)octamethylstannocene, **3a**, in form of yellow crystals.

Yield: 190 mg / 32%.

1H-NMR (400.13 MHz, 298 K, C_6D_6): δ = 2.29–2.15 (m, 4H, CH), 2.22 (s, 12H, $CpCH_3$), , 2.01 (s, 12H, $CpCH_3$), 1.19 (d, J = 6.9 Hz, 6H, CH_3), 1.13 (d, J = 6.9 Hz, 6H, CH_3), 1.10 (d, J = 6.9 Hz, 6H, CH_3), 1.06 (d, J = 6.9 Hz, 6H, CH_3).

$^{13}C\{^1H\}$-NMR (100.61 MHz, 298 K, C_6D_6): δ = 125.9 (d, J = 12.1 Hz, CpC), 121.6 (d, J = 3.7 Hz, CpC), 112.9 (d, J = 22.6 Hz, CpC), 24.5 (d, J = 12.1 Hz, CH), 22.0 (d, J = 22.3 Hz, CH_3), 22.0–21.3 (m, CH_3), 12.9 (d, J = 9.9 Hz, J = 27.1 Hz, CH_3), 10.9 (s, J = 27.1 Hz, CH_3).

$^{31}P\{^1H\}$-NMR (161.98 MHz, 298 K, C_6D_6): δ = -4.9 (s, J_{PSn} = 16.9 Hz).

$^{119}Sn\{^1H\}$-NMR (149.21 MHz, 298 K, C_6D_6): δ = -2176.

Elemental analysis: calculated for $C_{30}H_{52}P_2Sn$: C: 60.72%, H: 8.83%; found: C: 59.50%, H: 8.49% (Carbon value was repeatedly and reproducibly low, even upon analysis of crystalline material.).

Synthesis of 1,1'-bis(diisopropylphosphanyl)stannocene 3b (dippSn)

1,1'-Bis(diisopropylphosphanyl)magnesocene, **1b**, (2.00 g, 5.18 mmol) and tin(II) chloride (980 mg, 5.18 mmol) were mixed and stirred in 50 mL of thf overnight at room temperature. All volatiles were removed, and the resulting residue was extracted with 100 mL of hexane and the precipitate was filtered off. After removal of all volatiles and addition of diethyl ether, the solution was stored at 253 K overnight, resulting in the crystallization of 1,1'-bis(diisopropylphosphanyl)stannocene, **3b**, in form of yellow crystals.

Yield: 1.89 g / 76%.

^1H-NMR (400.13 MHz, 298 K, C_6D_6): δ = 6.10–6.02 (m, 4H, CpH), 5.95–5.85 (m, 4H, CpH) 1.87 (sept, J = 7.0 Hz, 4H, CH), 1.09 (d, J = 7.1 Hz, 6H, CH_3), 1.04 (d, J = 7.1 Hz, 6H, CH_3), 1.01 (d, J = 6.9 Hz, 6H, CH_3), 0.97 (d, J = 6.9 Hz, 6H, CH_3).

$^{13}C\{^1H\}$-NMR (100.61 MHz, 298 K, C_6D_6): δ = 128.4 (d, J = 19.9 Hz, CpC), 117.9 (d, J = 13.9 Hz, CpC), 112.1 (d, J = 4.7 Hz, CpC), 23.5 (d, J = 11.8 Hz, CH), 20.3 (d, J = 17.9 Hz, CH_3), 19.9 (d, J = 8.6 Hz, CH_3).

$^{31}P\{^1H\}$-NMR (161.98 MHz, 298 K, C_6D_6): δ = -4.8 (s, J_{PSn} = 16.0 Hz).

$^{119}Sn\{^1H\}$-NMR (149.21 MHz, 298 K, C_6D_6): δ = -2134 (s, J_{SnP} = 16.0 Hz).

Elemental analysis: calculated for $C_{22}H_{36}P_2Sn$: C: 54.31%, H: 7.54%; found: C: 54.02%, H: 7.17%.

Synthesis of 1,1'-bis(diphenylphosphanyl)octamethylstannocene 3c (dpp#Sn)

1,1'-Bis(diphenylphosphanyl)octamethylmagnesocene, **1c**, (2.01 g, 3.24 mmol) and tin(II) chloride (613 mg, 3.23 mmol) were mixed and stirred in 50 mL of thf for 2 h at room temperature. After removal of all volatiles, the resulting yellow solid residue was extracted with 100 mL of toluene and the precipitate was filtered off. The yellow solution was concentrated to approximately half its volume and stored at 253 K overnight, resulting in the crystallization of 1,1'-bis(diphenylphosphanyl)-octamethylstannocene, **3c**, in form of yellow crystals.

Yield: 1.77 g / 75%.

^1H-NMR (400.13 MHz, 298 K, C_6D_6): δ = 7.58–7.53 (m, 8H, PhH), 7.13–7.07 (m, 8H, PhH), 7.10–7.04 (m, 4H, PhH), 2.06 (s, 12H, $CpCH_3$), 1.93 (s, 12H, $CpCH_3$).

$^{13}C\{^1H\}$-NMR (100.61 MHz, 298 K, C_6D_6): δ = 139.5 (d, J = 10.6 Hz, CpC), 133.3 (d, J = 18.9 Hz, CpC), 133.3 (d, J = 18.9 Hz, J = 13.6 Hz, CpC), 128.6 (d, J = 5.5 Hz, PhC), 127.1 (d, J = 14.7 Hz, PhC), 121.5 (d, J = 5.0 Hz, PhC), 113.1 (d, J = 9.5 Hz, PhC), 12.2 (d, J = 9.7 Hz, $CpCH_3$), 10.7 (s, J = 21.2 Hz, $CpCH_3$).

$^{31}P\{^1H\}$-NMR (161.98 MHz, 298 K, C_6D_6): δ = -27.5 (s, J_{PSn} = 47 Hz).

$^{119}Sn\{^1H\}$-NMR (149.21 MHz, 298 K, C_6D_6): δ = -2203 (s, J_{SnP} = 47 Hz).

Elemental analysis: calculated for $C_{42}H_{44}P_2Sn$: C: 69.15%, H: 6.08%; found: C: 68.08%, H: 5.85% (Carbon value was repeatedly and reproducibly low, even upon analysis of crystalline material.).

Synthesis of 1,1'-bis(diphenylphosphanyl)stannocene 3d (dppSn)

To a suspension of magnesocene (5.05 g, 32.7 mmol) in 250 mL of hexane was added chlorodiphenylphosphine (11.6 mL, 64.4 mmol) *via* syringe at room temperature. After stirring overnight, the suspension was filtered, and all volatiles were removed *in vacuo*. The resulting colorless viscous oil was taken up in 50 mL of hexane and a solution of n butyl lithium (7.90 mL, 19.8 mmol, 2.5 M in hexane) was slowly added *via* syringe at room temperature. The resulting yellow suspension was stirred overnight, filtered and all volatiles were removed *in vacuo*. The resulting yellow residue was mixed with tin(II) chloride (674 mg, 3.60 mmol) and 100 mL of thf were added. The mixture was stirred for 90 min at room temperature. Subsequently, all volatiles were removed in vacuo and the solid red-brown residue was extracted with 50 mL of hexane. The resulting orange solution was concentrated to approximately half its volume and stored at 253 K overnight, resulting in the crystallization of a small amount of 1,1'-bis(diphenylphosphanyl)stannocene, **3d**, in form of orange crystals.

Yield: 132 mg / 1%. (Note: The extremely low yields can probably be attributed to limited stability of cyclopentadienyldiphenylphosphine, dppH,[10] also preventing ligand isolation and characterization.)
^{1}H-NMR (400.13 MHz, 298 K, C_6D_6): δ = 7.51–7.44 (m, 8H, PhH), 7.11–7.01 (m, 12H, PhH), 5.97–5.90 (m, 4H, CpH), 5.76–5.69 (m, 4H, CpH).
^{13}C{^{1}H}-NMR (100.61 MHz,298 K, C_6D_6): δ = 140.6 (d, *J* = 10.6 Hz, PhC), 133.7 (d, *J* = 19.6 Hz, PhC), 128.69–128.48 (m, PhC), 121.3 (d, J = 8.5 Hz, CpC), 118.4 (d, *J* = 15.9 Hz, CpC), 113.2 (d, *J* = 5.7 Hz, CpC).
^{31}P{^{1}H}-NMR (161.98 MHz, 298 K, C_6D_6): δ = -22.60 (s, J_{PSn} = 41.0 Hz).
^{119}Sn{^{1}H}-NMR (149.21 MHz, 298 K, C_6D_6): δ = -2197 (s).
Elemental analysis: calculated for $C_{34}H_{28}P_2Sn$: C: 66.16%, H: 4.57%; found: C: 64.73%, H: 4.92% (Carbon value was repeatedly and reproducibly low. As described above, only limited material was available for analysis.).

Synthesis of 1,1'-bis(diphenylphosphanyl)octamethylplumbocene 4 (dpp#Pb)
1,1'-Bis(diphenylphosphanyl)octamethylmagnesocene, **1c**, (300 mg, 0.47 mmol) and lead(II) chloride (131 mg, 0.47 mmol) were mixed and stirred in 50 mL of thf overnight at room temperature. All volatiles were removed, and the resulting residue was extracted with 30 mL of toluene. After filtration of the suspension, the red solution was stored at 253 K overnight, resulting in the crystallization of 1,1'-bis(diphenylphosphanyl)octamethylplumbocene, **4**, in form of orange crystals.
Yield: 266 mg / 70%.
^{1}H-NMR (400.13 MHz, 298 K, C_6D_6): δ = 7.56–7.50 (m, 8H, PhH), 7.13–7.07 (m, 8H, PhH), 7.05–7.00 (m, 4H, PhH), 2.27 (s, 12H, $CpCH_3$), 2.07 (s, 12H, $CpCH_3$).
^{13}C{^{1}H}-NMR (100.61 MHz, 298 K, C_6D_6): δ = 140.3 (d, *J* = 10.7 Hz, PhC), 133.2 (d, *J* = 18.7 Hz, PhC), 128.7 (s, PhC), 128.7 (d, *J* = 2.2 Hz, CpC), 122.1 (d, *J* = 5.2 Hz, CpC), 113.5 (d, *J* = 9.7 Hz, CpC), 12.0 (d, *J* = 10.1 Hz, $CpCH_3$), 10.5 (s, $CpCH_3$).
^{31}P{^{1}H}-NMR (161.98 MHz, 298 K, C_6D_6): δ = -28.7 (s, J_{PPb} = 46.1 Hz).
^{207}Pb{^{1}H}-NMR (62.79 MHz, 298 K, C_6D_6): δ = -4668 (s, J_{PbP} = 46.1 Hz).
Elemental analysis: calculated for $C_{42}H_{44}P_2Pb$: C: 61.67%, H: 5.42%; found: C: 61.31%, H: 5.85%.

Synthesis of 1,1'-bis(diisopropylphosphanyl)stannocene NHC adduct 3b·NHC (dippSn·NHC)
1,1-Bis(diisopropylphosphanyl)stannocene, **3b**, (300 mg, 0.62 mmol) and 1,3-diisopropyl-4,5-dimethylimidazolin-2-ylidene (112 mg, 0.62 mmol) were mixed and stirred in 50 mL of toluene for 10 minutes at room temperature and stored at 253 K overnight, resulting in crystallization of 1,1'-bis(diisopropylphosphanyl)stannocene NHC adduct, **3b·NHC**, in form of colorless crystals.
Yield: 258 mg / 63%.
^{1}H-NMR (400.13 MHz, 298 K, C_6D_6): δ = 6.28 (q, *J* = 2.4 Hz, 4H, CpH), 6.08–6.02 (m, 4H, CpH), 4.53–4.31 (m, 2H, NC<u>H</u>-$(CH_3)_2$), 2.01 (sept, *J* = 6.8 Hz, 4H, PC<u>H</u>-$(CH_3)_2$), 1.58 (s, 6H, NC-CH_3), 1.35 (d, *J* = 6.4 Hz, 12H, NCH-$(C\underline{H}_3)_2$), 1.21–1.08 (m, 24H, PCH-$(C\underline{H}_3)_2$).
^{13}C{^{1}H}-NMR (75.48 MHz, 298 K, C_6D_6): δ = 200.4 (s, carbene-C), 123.0 (s, N<u>C</u>-CH3), 118.9 (d, *J* = 15.4 Hz, CpC), 109.7 (d, *J* = 5.7 Hz, CpC), 50.6 (s, N<u>C</u>H-$(CH_3)_2$), 23.7 (d, *J* = 11.3 Hz, CH), 20.6 (d, *J* = 18.4 Hz, CH_3), 20.0 (d, *J* = 8.6 Hz. CH_3), 9.2 (s, CH_3).
^{31}P{^{1}H}-NMR (161.98 MHz, 298 K, C_6D_6): δ = -4.7.
^{119}Sn{^{1}H}-NMR (149.21 MHz, 298 K, C_6D_6): no signal could be detected in the range of -600 to -2500 ppm.
Elemental analysis: calculated for $C_{33}H_{56}N_2P_2Sn$: C: 59.83%, H: 8.67%; N: 4.23%; found: C: 59.91%, H: 8.44%, N: 4.10%.

Synthesis of 1,1'-bis(diisopropylphosphanyl)stannocene aluminum(III) chloride adduct 3b·$AlCl_3$ (dippSn·$AlCl_3$)
1,1-Bis(diisopropylphosphanyl)stannocene, **3b**, (500 mg, 1.04 mmol) and aluminum(III) chloride (138 mg, 1.04 mmol) were mixed and stirred in 50 mL of toluene overnight at room temperature. The resulting yellow suspension was filtered and the solution was stored at 253 K overnight, resulting in crystallization of 1,1'-bis(diisopropylphosphanyl)stannocene aluminum(III) chloride adduct, **3b·$AlCl_3$**, in form of colorless crystals.
Yield: 330 mg / 52%.
^{1}H-NMR (400.13 MHz, 298 K, C_6D_6): δ = 6.21 (s, 4H, CpH), 5.87 (s, 4H, CpH), 1.99–1.82 (m, 4H, CH), 1.07 (d, *J* = 7.0 Hz, 6H, CH_3), 1.02 (d, *J* = 7.2 Hz, 6H, CH_3), 0.94 (d, *J* = 7.0 Hz, 6H, CH_3), 0.89 (d, *J* = 6.9 Hz, 6H, CH_3).
^{13}C{^{1}H}-NMR (75.48 MHz, 298 K, C_6D_6): δ = 118.6 (d, *J* = 10.0 Hz, CpC), 113.5 (d, *J* = 7.2 Hz, CpC), 23.2 (d, *J* = 10.5 Hz, CH), 19.0 (d, *J* = 8.4 Hz, CH_3), 18.9 (s, CH_3).
^{27}Al-NMR (78.20 MHz, 298 K, C_6D_6): δ = 111.2.
^{31}P{^{1}H}-NMR (161.98 MHz, 298 K, C_6D_6): δ = -7.5 ($\nu_{½}$ = 25.0 Hz).
^{119}Sn{^{1}H}-NMR (111.92 MHz, 298 K, C_6D_6): δ = -2172.
Elemental analysis: calculated for $C_{22}H_{36}AlCl_3P_2Sn$: C: 43.00%, H: 5.91%; found: C: 42.71%, H: 6.01%.

Synthesis of 1,1'-bis(diisopropylphosphanyl)stannocene bis(aluminum(III)chloride) adduct 3b·$(AlCl_3)_2$ (dippSn·$(AlCl_3)_2$)
1,1-Bis(diisopropylphosphanyl)stannocene, **3b**, (200 mg, 0.42 mmol) and aluminum(III) chloride (111 mg, 0.84 mmol) were mixed and stirred in 50 mL of o-difluorobenzene overnight at room temperature. The resulting yellow suspension was filtered and the solution was

stored at 253 K overnight, resulting in crystallization of 1,1'-bis(diisopropylphosphanyl)stannocene bis(aluminum(III) chloride) adduct, **3b·(AlCl$_3$)$_2$**, in form of colorless crystals.
Yield: 187 mg / 60%.
^{1}H-NMR (400.13 MHz, 298 K, C_6D_6): δ = 6.37 (q, *J* = 2.8 Hz, 4H, CpH), 5.76 (q, *J* = 2.7 Hz, 4H, CpH), 1.96–1.81 (m, 4H, CH), 1.05 (d, *J* = 7.0 Hz, 6H, CH_3), 1.01 (d, *J* = 7.0 Hz, 6H, CH_3), 0.86 (d, *J* = 7.1 Hz, 6H, CH_3), 0.83 (d, *J* = 7.1 Hz, 6H, CH_3).
^{13}C{^{1}H}-NMR (75.48 MHz, 298 K, C_6D_6): δ = 119.5 (d, *J* = 9.0 Hz, CpC), 114.2 (d, *J* = 9.4 Hz, CpC), 102.6 (d, *J* = 51.0 Hz, CpC) 22.7 (d, *J* = 27.4 Hz, CH), 18.0 (s, CH_3).
^{27}Al-NMR (78.20 MHz, 298 K, C_6D_6): δ = 110.9.
^{31}P{^{1}H}-NMR (161.98 MHz, 298 K, C_6D_6): δ = -12.2 ($\nu_{½}$ = 283 Hz).
^{119}Sn{^{1}H}-NMR (111.92 MHz, 298 K, C_6D_6): δ = -2178.
Elemental analysis: calculated for $C_{22}H_{36}Al_2Cl_6P_2Sn$: C: 35.33%, H: 4.85%; found: C: 35.42%, H: 5.06%.

Synthesis of 1,1'-bis(diphenylphosphanyl)octamethylgermanocene dimethylplatinum adduct 2·PtMe$_2$ (dpp$^\#$Ge·PtMe$_2$)
1,1'-Bis(diphenylphosphanyl)octamethylgermanocene, **2**, (200 mg, 0.29 mmol) and (1,5-cyclooctadiene)dimethylplatinum (98.0 mg, 0.29 mmol) were mixed and stirred in 10 mL of hexane overnight at 298 K. The resulting yellow solution was stored at 253 K for overnight, resulting in crystallization of 1,1'-bis(diphenylphosphanyl)octamethylgermanocene dimethylplatinum adduct, **2·PtMe$_2$**, in form of colorless crystals.
Yield: 190 mg / 72%.
^{1}H-NMR (400.13 MHz, 298 K, C_6D_6): δ = 8.35–8.28 (m, 8H, PhH), 7.12–7.07 (m, 8H, PhH), 7.04–6.99 (m, 4H, PhH), 1.72 (s, 12H, $CpCH_3$), 1.69 (s, 12H, $CpCH_3$), 1.32 (t, 6H, J_{HP} = 14.0 Hz, J_{HPt} = 68 Hz, $PtCH_3$).
^{13}C{^{1}H}-NMR (100.61 MHz, 298 K, C_6D_6): δ = 137.1–136.6 (m, PhC), 136.3 (t, J_{CPt} = 12.6 Hz, PhC), 135.8 (t, J_{CPt} = 12.6 Hz, PhC), 130.8–130.7 (m, PhC), 129.5 (s, CpC), 122.2–122.0 (m, CpC), 105.7 (d, *J* = 36.0 Hz, CpC), 13.0 (s, CH_3), 10.3 (t, J_{CPt} = 99 Hz, CH_3).
^{31}P{^{1}H}-NMR (161.98 MHz, 298 K, C_6D_6): δ = 19.6 (s, J_{PPt} = 2011 Hz).
Elemental analysis: calculated for $C_{44}H_{50}P_2GeP_2Pt$: C: 58.17%, H: 5.55%; found: C: 58.12%, H: 5.93%.

Synthesis of 1,1'-bis(diisopropylphosphanyl)stannocene dimethylplatinum adduct 3b·PtMe$_2$ (dippSn·PtMe$_2$)
1,1-Bis(diisopropylphosphanyl)stannocene, **3b**, (160 mg, 0.34 mmol) and (1,5-cyclooctadiene)dimethylplatinum (110 mg, 0.34 mmol) were mixed and stirred in 30 mL of hexane for 4 h at 298 K. The resulting yellow solution was stored at 253 K overnight, resulting in crystallization of 1,1'-bis(diisopropylphosphanyl)stannocene dimethylplatinum adduct, **3b·PtMe$_2$**, in form of colorless crystals.
Yield: 184 mg / 77%.
^{1}H-NMR (400.13 MHz, 298 K, C_6D_6): δ = 6.11–6.04 (m, *J* = 11 Hz, 4H, CpH), 6.00–5.96 (m, 4H, CpH) 2.58 (sept, *J* = 7.0 Hz, 4H, CH), 1.30 (d, *J* = 7.0 Hz, 6H, CH_3), 1.27 (d, *J* = 7.0 Hz, 6H, CH_3), 1.21 (t, J_{HP} = 13 Hz, 5H, $PtCH_3$), 1.13 (t, J_{HP} = 13.0 Hz, 1H, $PtCH_3$), 0.90 (d, *J* = 6.5 Hz, 6H, CH_3), 0.87 (d, *J* = 6.5 Hz, 6H, CH_3).
^{13}C{^{1}H}-NMR (100.61 MHz, 298 K, C_6D_6): δ = 116.0 (t, *J* = 4.8 Hz, CpC), 115.0 (t, *J* = 5.4 Hz, CpC), 111.0 (m, CpC), 25.2–24.7 (m, CH), 19.9–18.9 (m, CH_3).
^{31}P{^{1}H}-NMR (161.98 MHz, 298 K, C_6D_6): δ = 22.0 (s, J_{PSn} = 19.5 Hz, J_{PPt} = 1843 Hz).
^{119}Sn{^{1}H}-NMR (149.21 MHz, 298 K, C_6D_6): δ = -2169.
Elemental analysis: calculated for $C_{24}H_{42}P_2PtSn$: C: 40.81%, 5.99%; found: C: 41.25%, H: 6.22%.

Synthesis of 1,1'-bis(diisopropylphosphanyl)stannocene tungstentetracarbonyl adduct 3b·W(CO)$_4$ (dippSn·W(CO)$_4$)
1,1-Bis(diisopropylphosphanyl)stannocene, **3b**, (350 mg, 0.73 mmol) and (1,5-cyclooctadiene)tetracarbonyltungsten (294 mg, 0.73 mmol) were mixed and stirred in 50 mL of toluene overnight at 373 K. The resulting solution was allowed to cool down to room temperature and was stored at 253 K for 2 h, resulting in crystallization of 1,1'-bis(diisopropylphosphanyl)stannocene-tungstentetracarbonyl adduct, **3b·W(CO)$_4$**, in form of light yellow crystals.
Yield: 245 mg; 43%.
^{1}H-NMR (400.13 MHz, 298 K, C_6D_6): δ = 5.88–5.83 (m, 4H, 2,5-CpH), 5.77–5.71 (m, 4H, 3,4-CpH) 2.32 (sept, *J* = 6.5 Hz, 4H, CH), 1.31 (d, *J* = 7.0 Hz, 6H, CH_3), 1.26 (d, *J* = 6.9 Hz, 6H, CH_3), 0.87 (d, *J* = 7.2 Hz, 6H, CH_3), 0.84 (d, *J* = 6.8 Hz, 6H, CH_3).
^{13}C-NMR (^{13}C: 100.61 MHz; 298 K, C_6D_6): δ = 115.8 (CpC), 114.3 (CpC), 28.7 (CH), 19.1 (CH_3), 18.4 (CH_3) (signals detected by ^{1}H-^{13}C HMBC (^{1}H: 400.13 MHz) and HMQC (^{1}H: 400.13 MHz) spectroscopy).
^{31}P{^{1}H}-NMR (161.98 MHz, 298 K, C_6D_6): δ = 13.4 (s, J_{PSn} = 39.0 Hz, J_{PW} = 229 Hz).
No signal could be detected in ^{119}Sn NMR spectra due to poor solubility of the compound.
IR: ν (cm^{-1}) = 2005 (C=O), 1882 (C=O), 1866 (C=O), 1835 (C=O).
Elemental analysis: calculated for $C_{26}H_{36}O_4P_2SnW$: C: 40.19%, H: 4.67%; found: C: 40.65%, H: 4.76%.

Synthesis of 1,1'-bis(diisopropylphosphanyl)octamethylchlorostibonocene 5a (dipp$^\#$SbCl)
1,1-Bis(diisopropylphosphanyl)octamethylmagnesocene **1a**, (500 mg, 1.00 mmol) and antimony(III) chloride (229 mg, 1.00 mmol) were separately dissolved in 20 mL of toluene each. The solution of **1a** was cooled to 193 K and the antimony(III) chloride solution was

added, resulting in a red suspension. Stirring was continued for 2 h at 193 K and 2 h at 293 K. The colorless precipitate was filtered off, toluene was evaporated *in vacuo* and the red residue was taken up in 100 mL of hexane. Storage of the intense red solution at 253 K overnight yielded crystals of 1,1'-bis(diisopropylphosphanyl)octamethylchlorostibonocene ,**5**, in form of large red blocks.
Yield: 285 mg; 45%.
^{1}H-NMR (300.13 MHz, 298 K, C_6D_6): δ = 2.24 (s, 12H, $CpCH_3$), 2.24–2.21 (m, 4H, CH), 2.02 (s, 12H, $CpCH_3$), 1.17 (d, J = 7.0 Hz, 6H, CH_3), 1.12 (d, J = 7.0 Hz, 6H, CH_3), 1.07 (d, J = 7.0 Hz, 6H, CH_3), 1.02 (d, J = 7.0 Hz, 6H, CH_3).
^{13}C{^{1}H}-NMR (75.48 MHz, 298 K, C_6D_6): δ = 133.8 (d, J_{CP} = 12.9 Hz, CpC), 125.5 (d, J_{CP} = 29.0 Hz, CpC), 123.5 (s, CpC), 24.6 (d, J_{CP} = 12.4 Hz, CH), 22.2–21.8 (m, CH_3), 14.2 (d, J_{CP} = 9.8 Hz, CH_3), 11.5 (s, CH_3).
^{31}P{^{1}H}-NMR (121.49 MHz, 298 K, C_6D_6): δ = -4.7.
Elemental analysis: calculated for $C_{30}H_{52}ClP_2Sb$: C: 57.02%, H: 8.29%; found: C: 55.55%, H: 8.29% (Carbon value was repeatedly and reproducibly low, even upon analysis of crystalline material.).

Synthesis of 1,1'-bis(diisopropylphosphanyl)octamethylstibonocenium tetrachloroaluminate 5b[AlCl$_4$] (dipp$^{\#}$Sb[AlCl$_4$])
1,1'-Bis(diisopropylphosphanyl)octamethylchlorostibonocene **5a**, (250 mg, 0.40 mmol) and aluminum(III) chloride (53.0 mg, 0.40 mmol) were dissolved in a mixture of 12 mL toluene and 3 mL ortho-difluorobenzene. The resulting orange solution was stirred for 4 h at room temperature, concentrated to approximately three quarters of its volume and then stored at 253 K overnight to yield 1,1'-Bis(diisopropylphosphanyl)octamethylstibonocenium tetrachloroaluminate, **5b[AlCl$_4$]**, as orange crystals.
Yield: 161 mg; 53 %.
^{1}H-NMR (400.13 MHz, 298 K, CD_2Cl_2): δ = 2.34 (s, 12H, $CpCH_3$), 2.33–2.30 (m, 4H, CH), 2.28 (s, 12H, $CpCH_3$), 1.15 (d, J = 7.1 Hz, 6H, CH_3), 1.11 (d, J = 7.0 Hz, 6H, CH_3), 1.00 (d, J = 7.0 Hz, 6H, CH_3), 0.96 (d, J = 7.0 Hz, 6H, CH_3).
^{13}C{^{1}H}-NMR (100.61 MHz, 298 K, CD_2Cl_2): δ = 135.3 (d, J_{CP} = 10.6 Hz, CpC), 131.4 (s, CpC), 127.4 (d, J_{CP} = 38.9 Hz, CpC), 24.3 (d, JCP = 12.1 Hz, CH), 21.7 (d, J_{CP} = 9.6 Hz, CH_3), 21.4 (s, CH_3), 21.2 (s, CH_3), 12.7 (d, J_{CP} = 8.8 Hz, CH_3), 10.9 (s, CH_3).
^{27}Al-NMR (104.26 MHz, 298 K, CD_2Cl_2): δ = 103.7.
^{31}P{^{1}H}-NMR (161.97 MHz, 298 K, CD_2Cl_2): δ = -3.6.
Elemental analysis: calculated for $C_{30}H_{52}AlCl_4P_2Sb$: C: 47.09%, H: 6.85%; found: C: 46.89%, H: 6.99%.

NMR Spectra

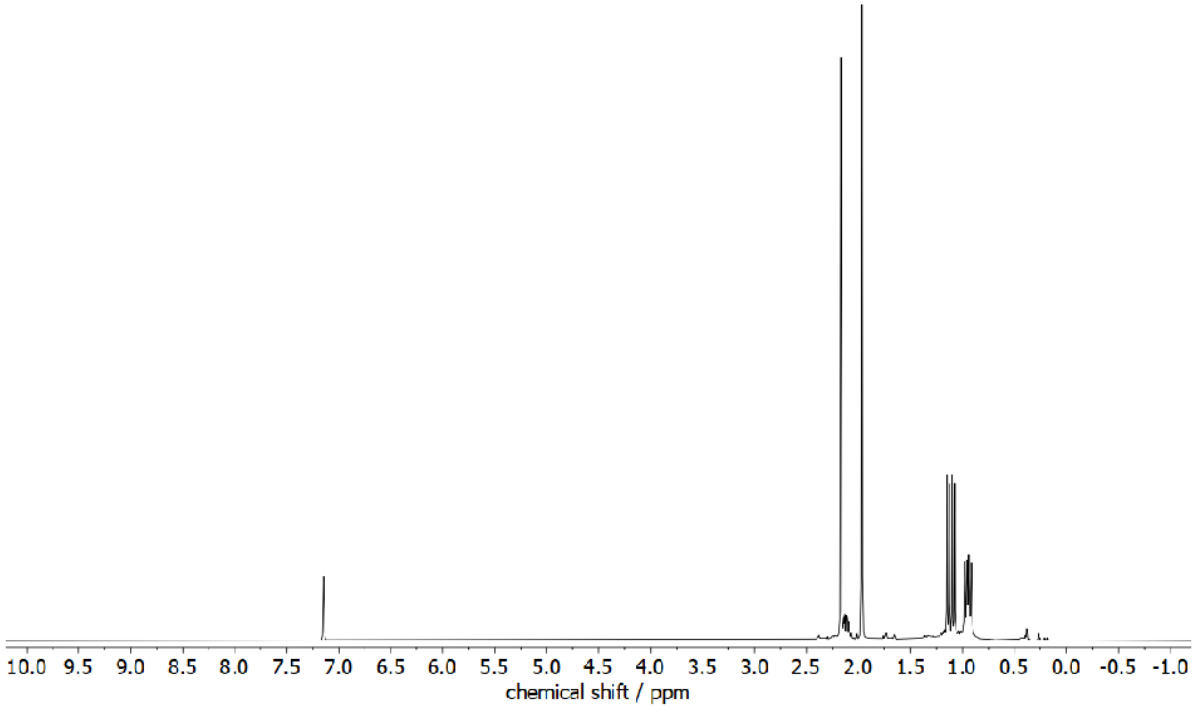

Figure S1: ^{1}H NMR spectrum (C_6D_6) of **1a**.

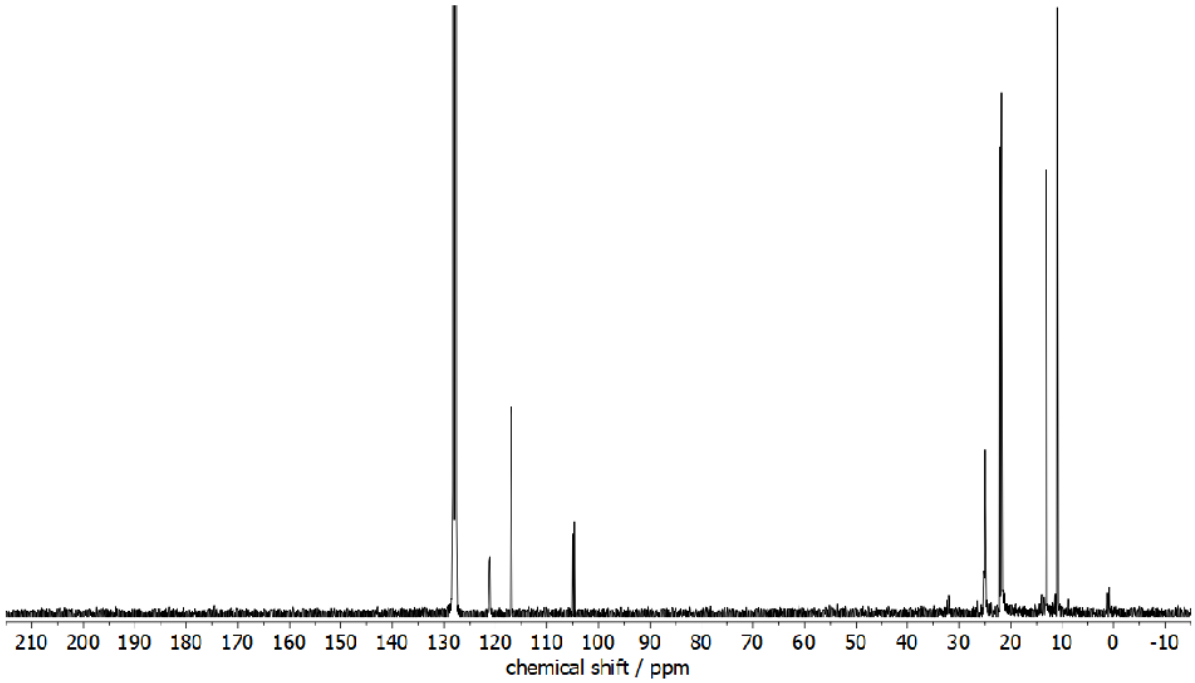

Figure S2: $^{13}C\{^{1}H\}$ NMR spectrum (C_6D_6) of **1a**.

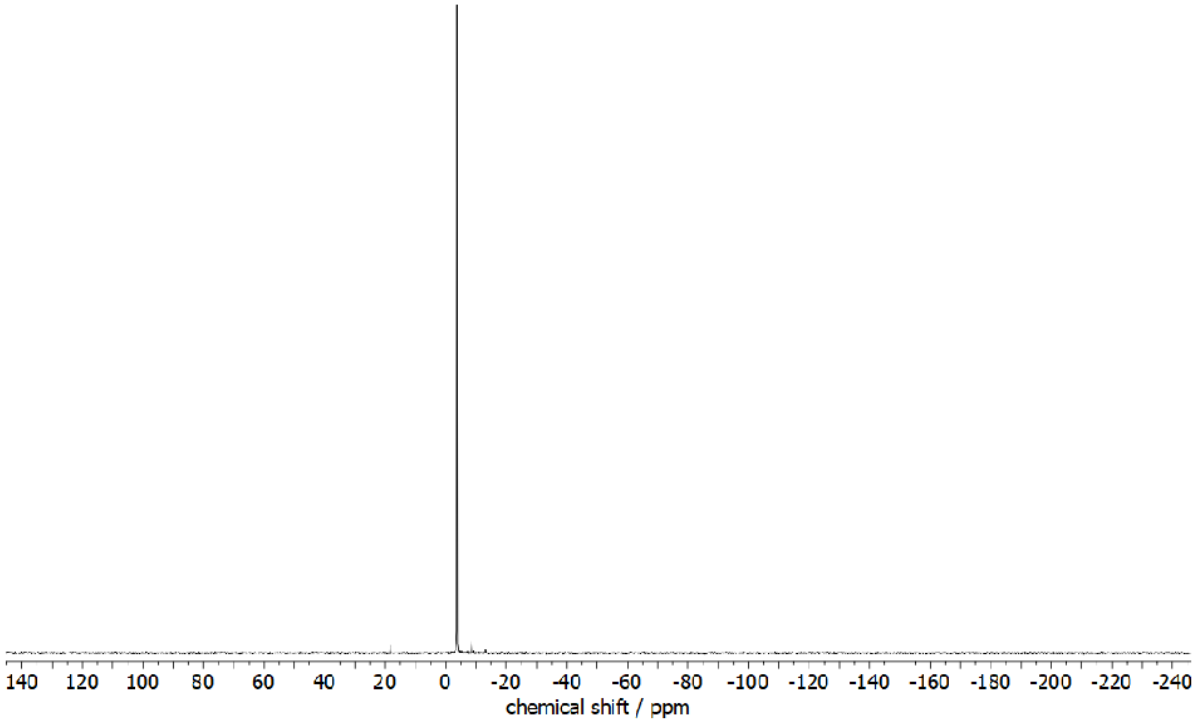

Figure S3: $^{31}P\{^{1}H\}$ NMR spectrum (C_6D_6) of **1a**.

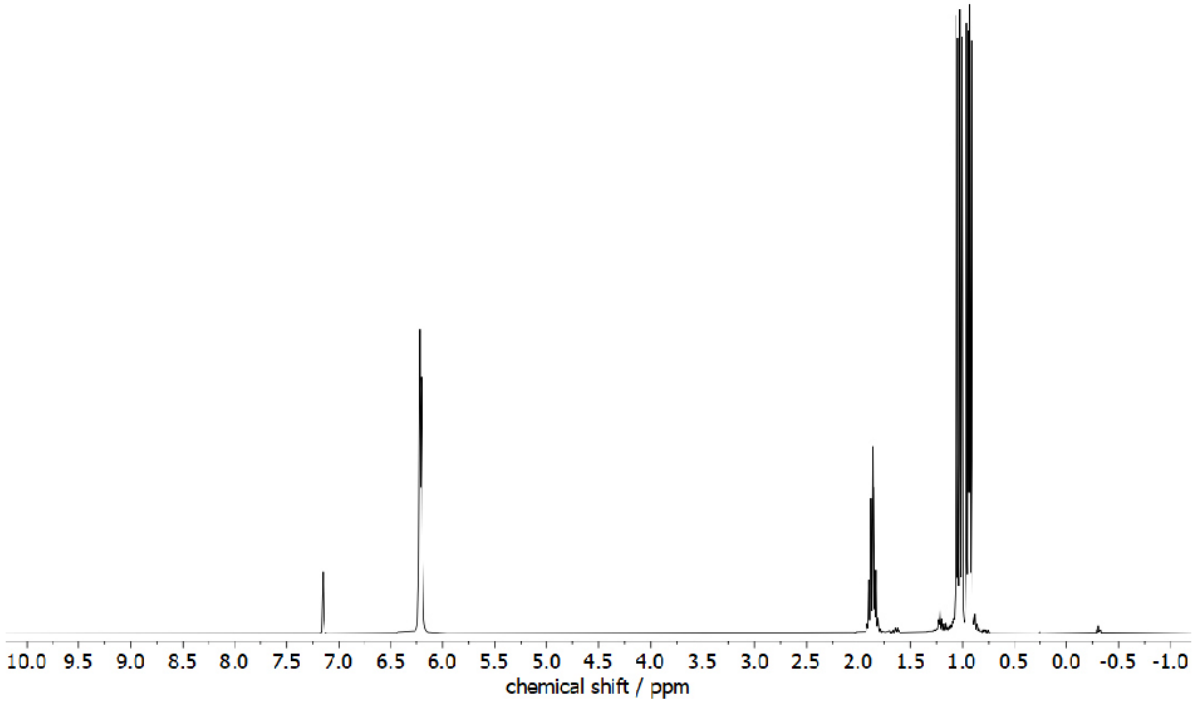

Figure S4: ^{1}H NMR spectrum (C_6D_6) of **1b**.

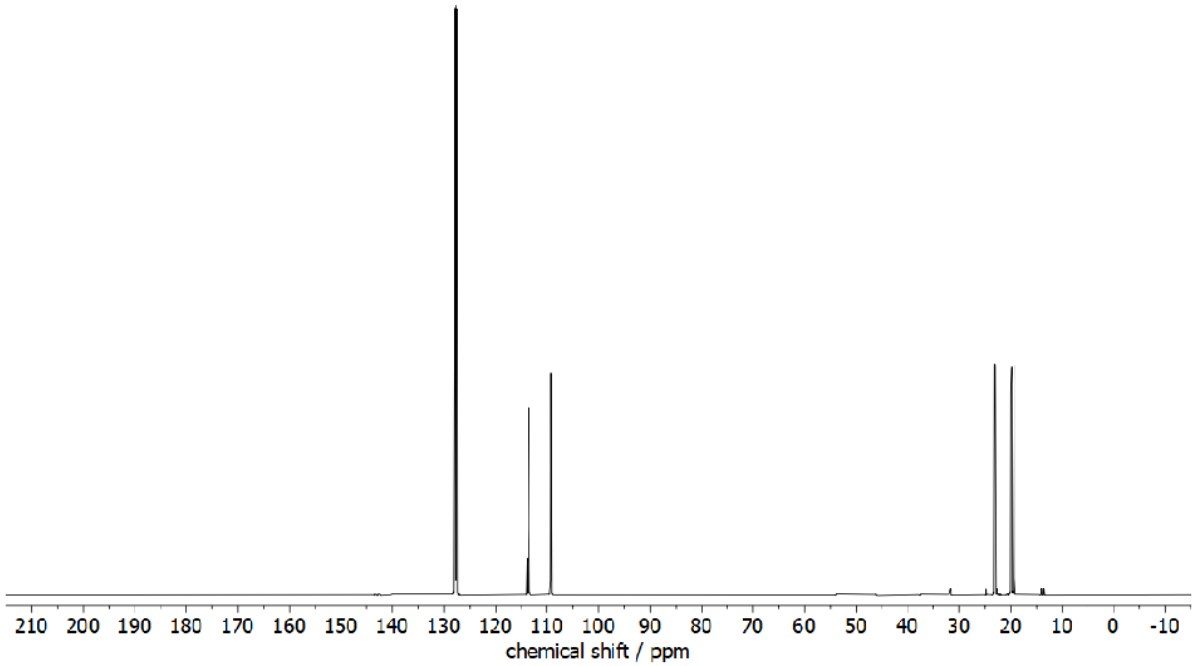

Figure S5: $^{13}C\{^{1}H\}$ NMR spectrum (C_6D_6) of **1b**.

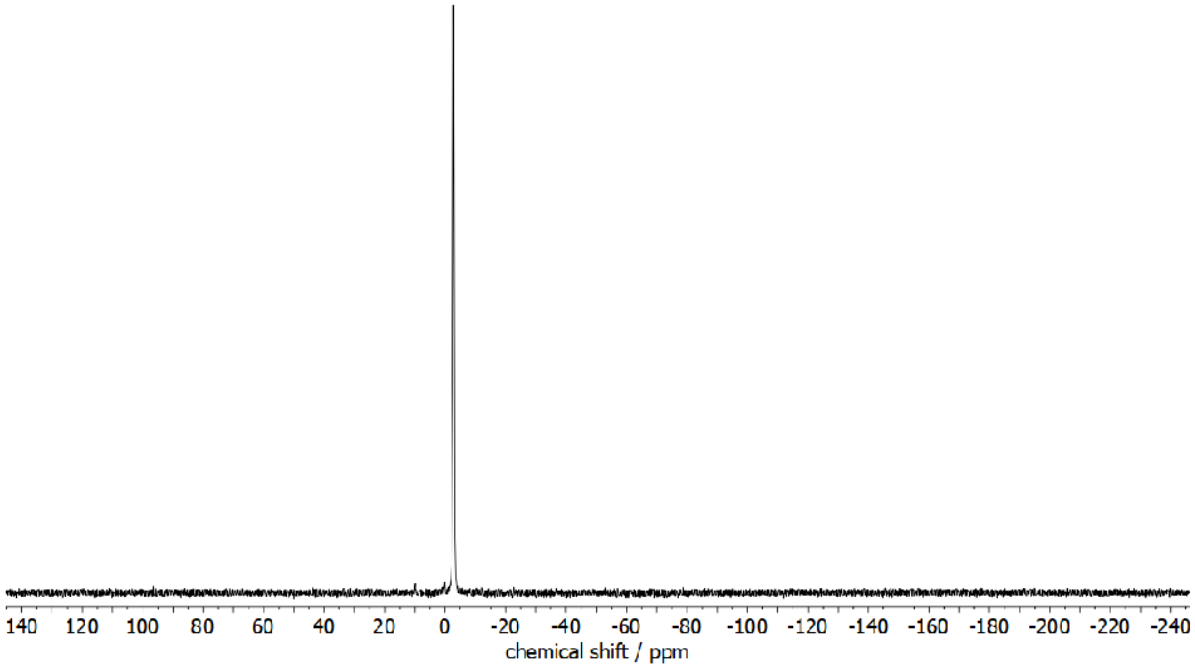

Figure S6: $^{31}P\{^{1}H\}$ NMR spectrum (C_6D_6) of **1b**.

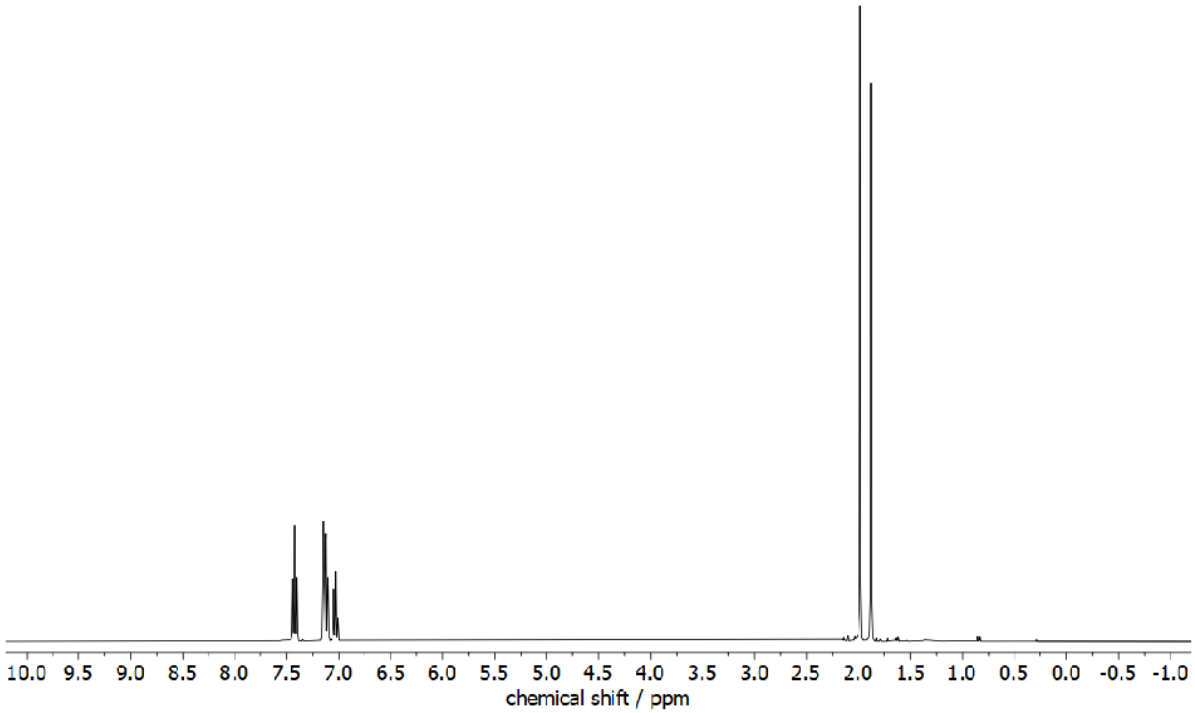

Figure S7: ^{1}H NMR spectrum (C_6D_6) of **1c**.

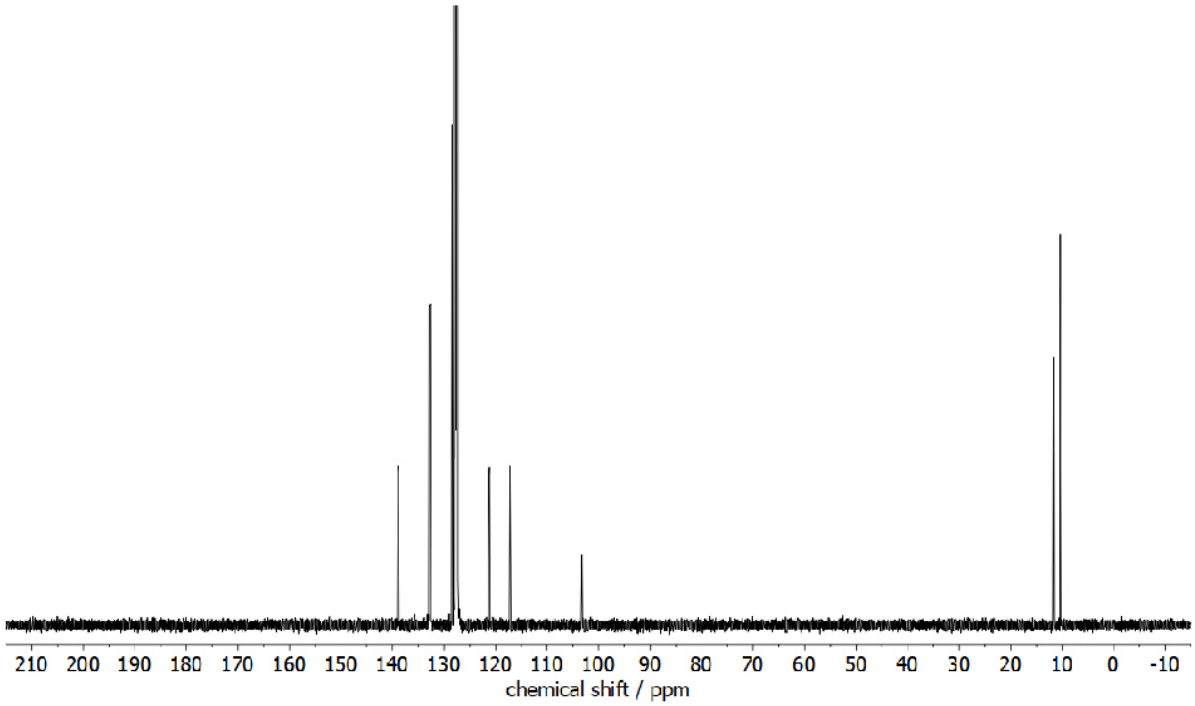

Figure S8: $^{13}C\{^{1}H\}$ NMR spectrum (C_6D_6) of **1c**.

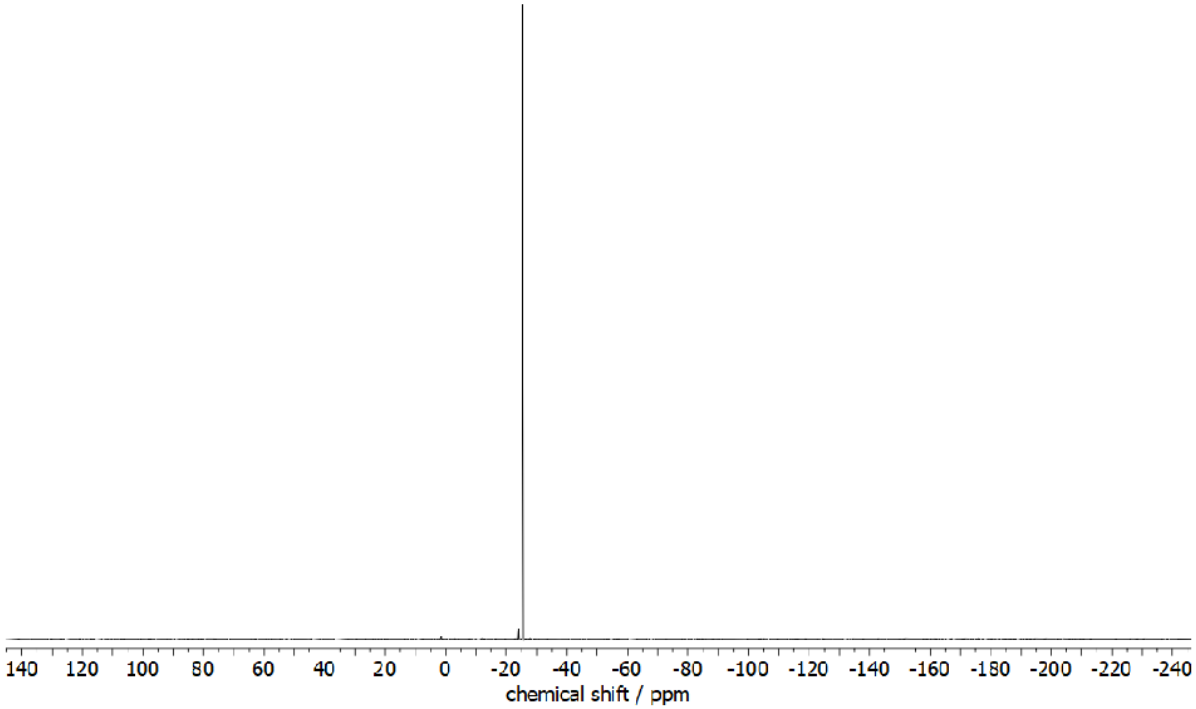

Figure S9: $^{31}P\{^{1}H\}$ NMR spectrum (C_6D_6) of **1c**.

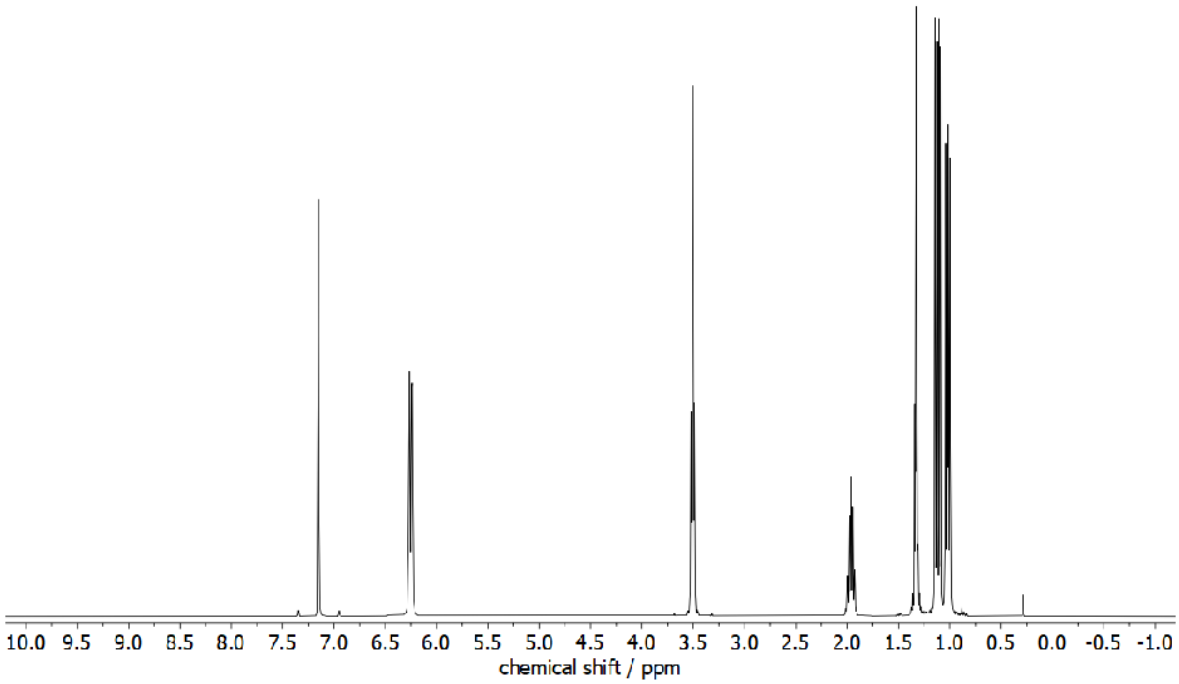

Figure S10: ^{1}H NMR spectrum (C_6D_6) of **1b·(thf)$_2$**.

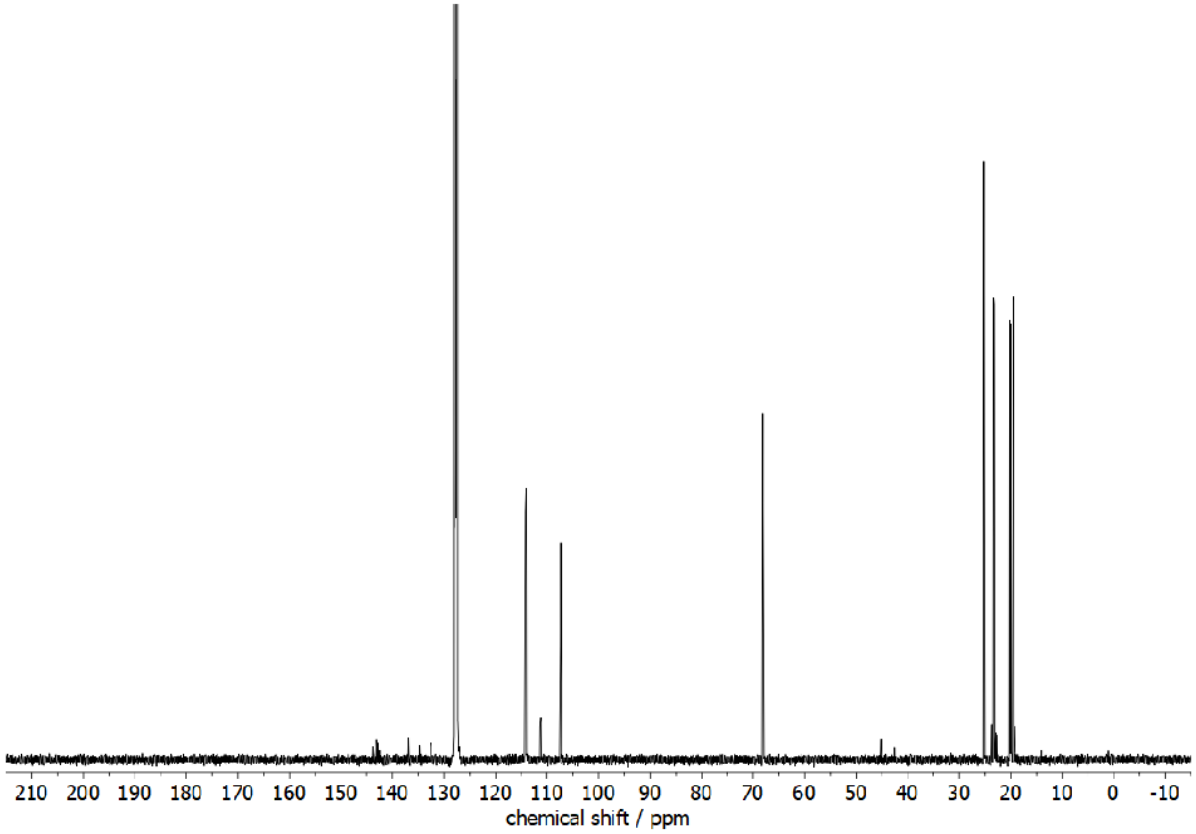

Figure S11: $^{13}C\{^{1}H\}$ NMR spectrum (C_6D_6) of **1b·(thf)$_2$**.

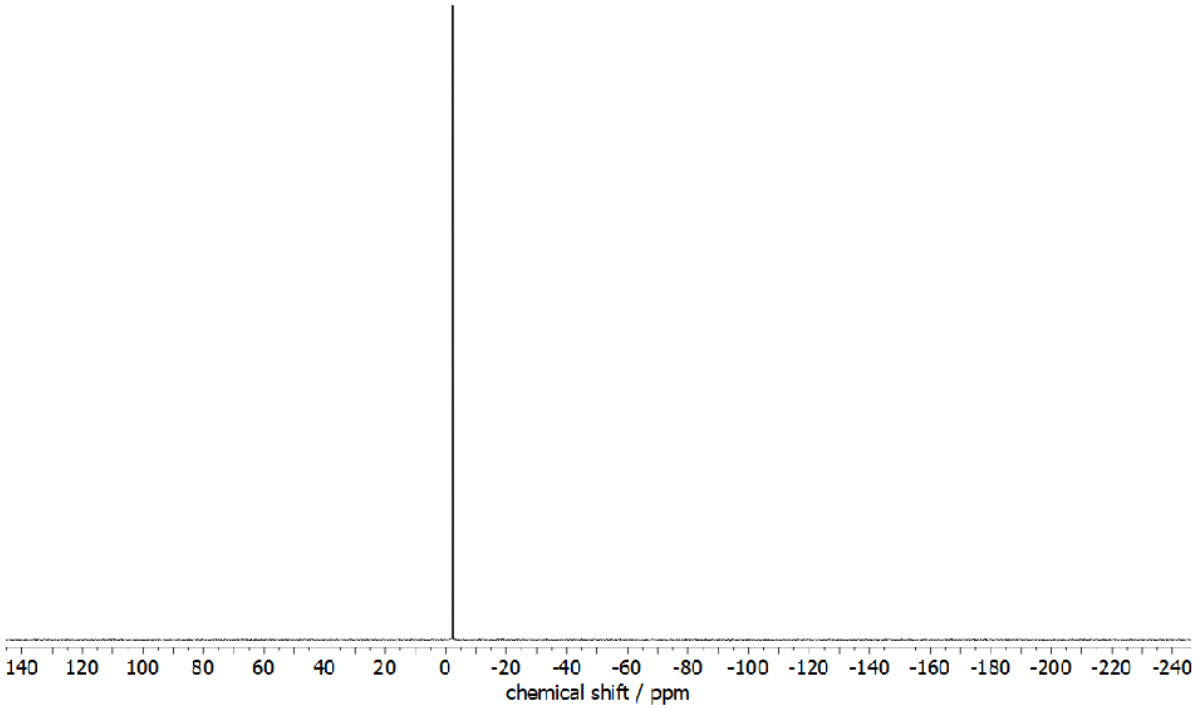

Figure S12: $^{31}P\{^{1}H\}$ NMR spectrum (C_6D_6) of **1b·(thf)$_2$**.

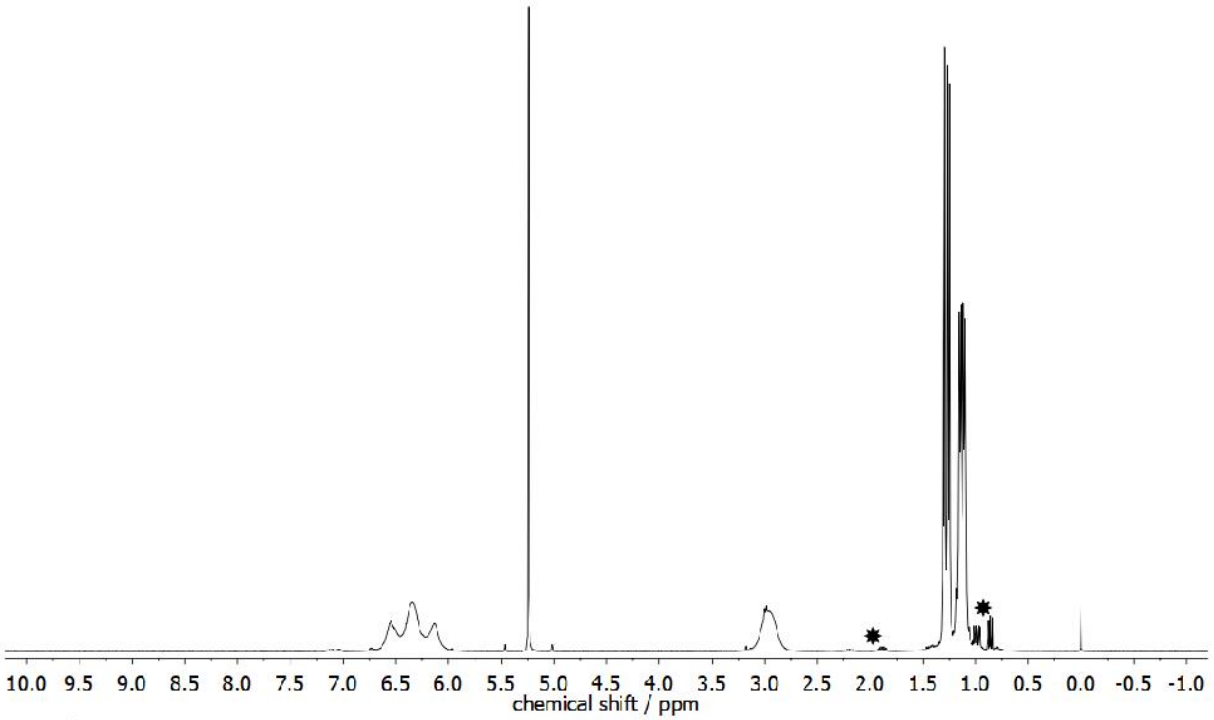

Figure S13: ^{1}H NMR spectrum (CD_2Cl_2) of **1b·(CS$_2$)$_2$** (✸ free ligand).

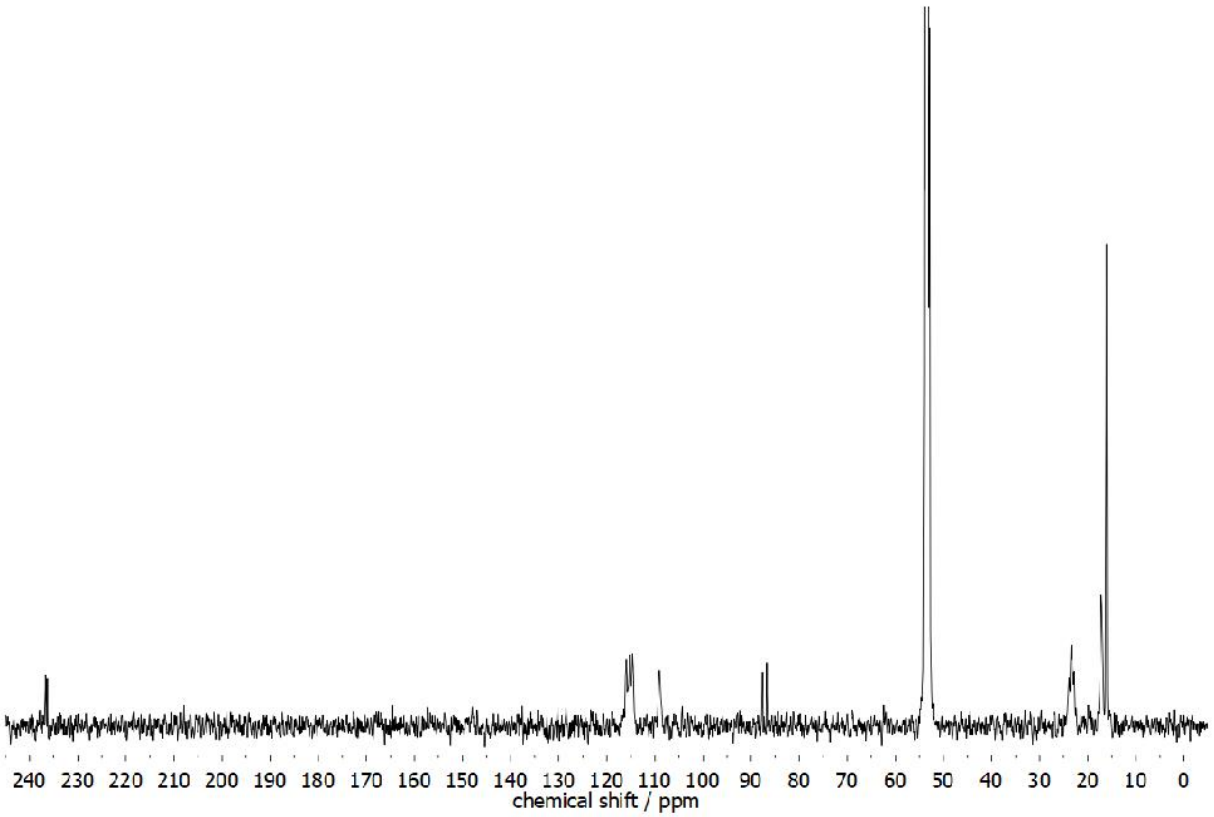

Figure S14: $^{13}C\{^{1}H\}$ NMR spectrum (CD_2Cl_2) of **1b·(CS$_2$)$_2$**.

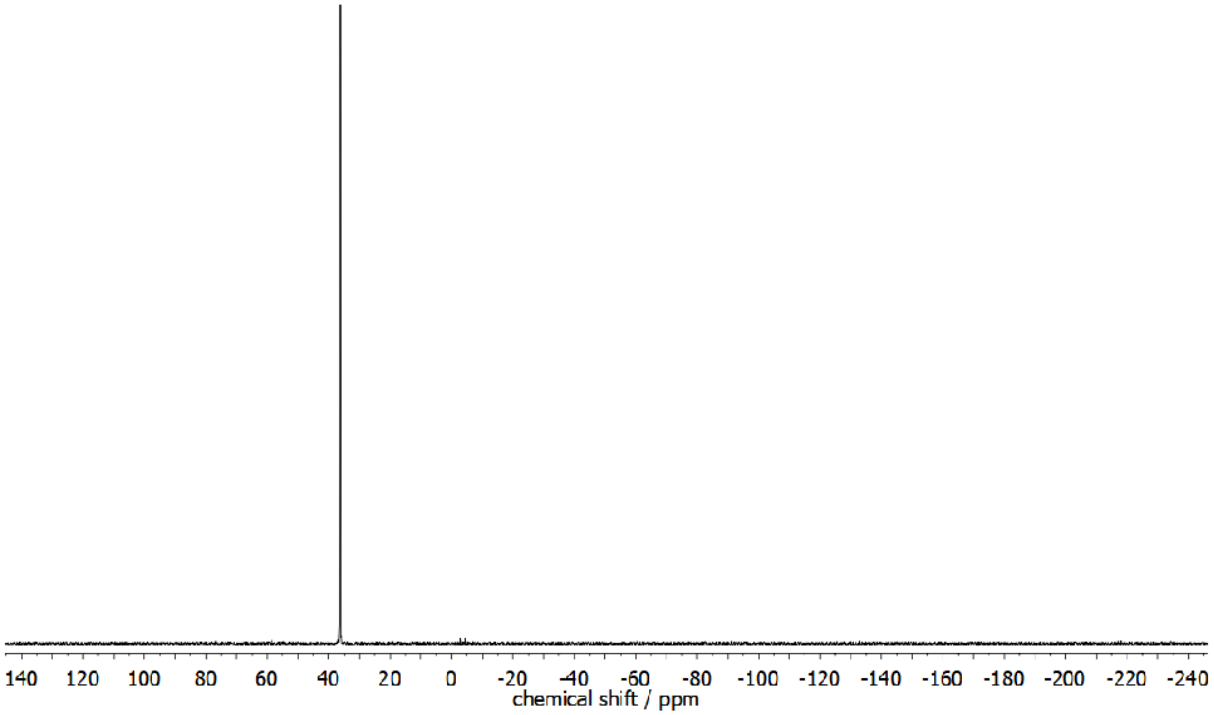

Figure S15: $^{31}P\{^{1}H\}$ NMR spectrum (CD_2Cl_2) of **1b·(CS$_2$)$_2$**.

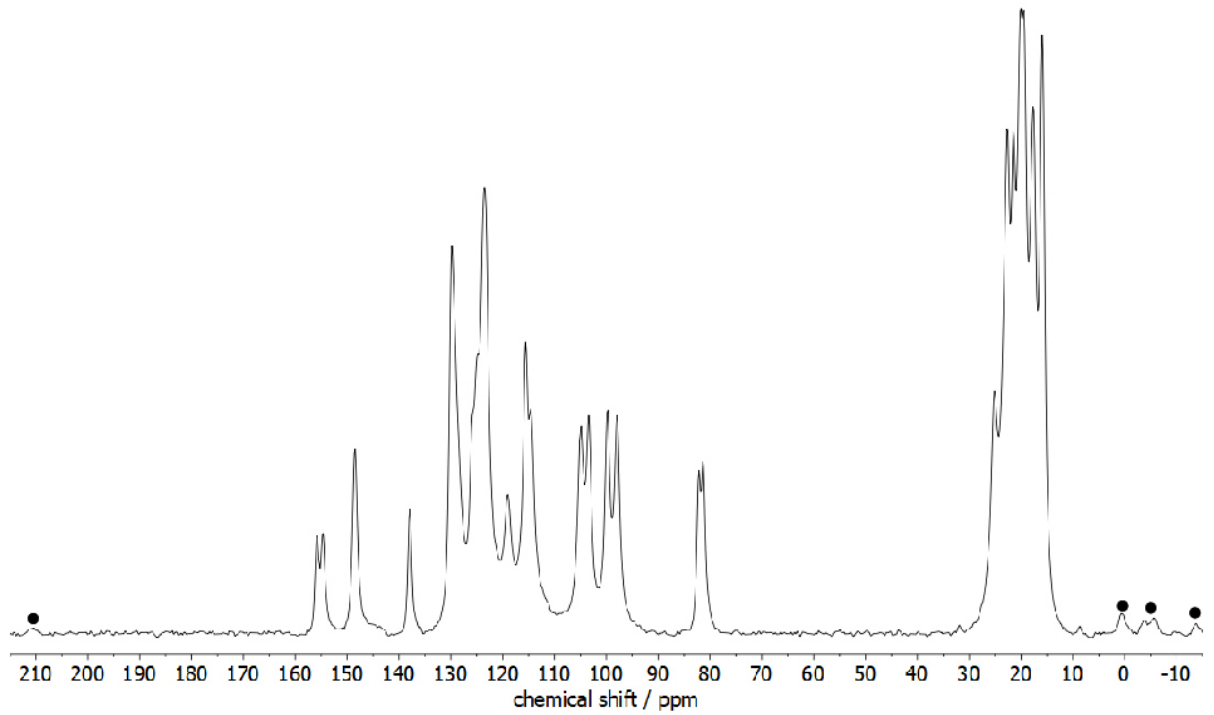

Figure S16: $^{13}C\{^{1}H\}$ CP-MAS NMR spectrum of **1b·PhNCO** (● spinning sidebands).

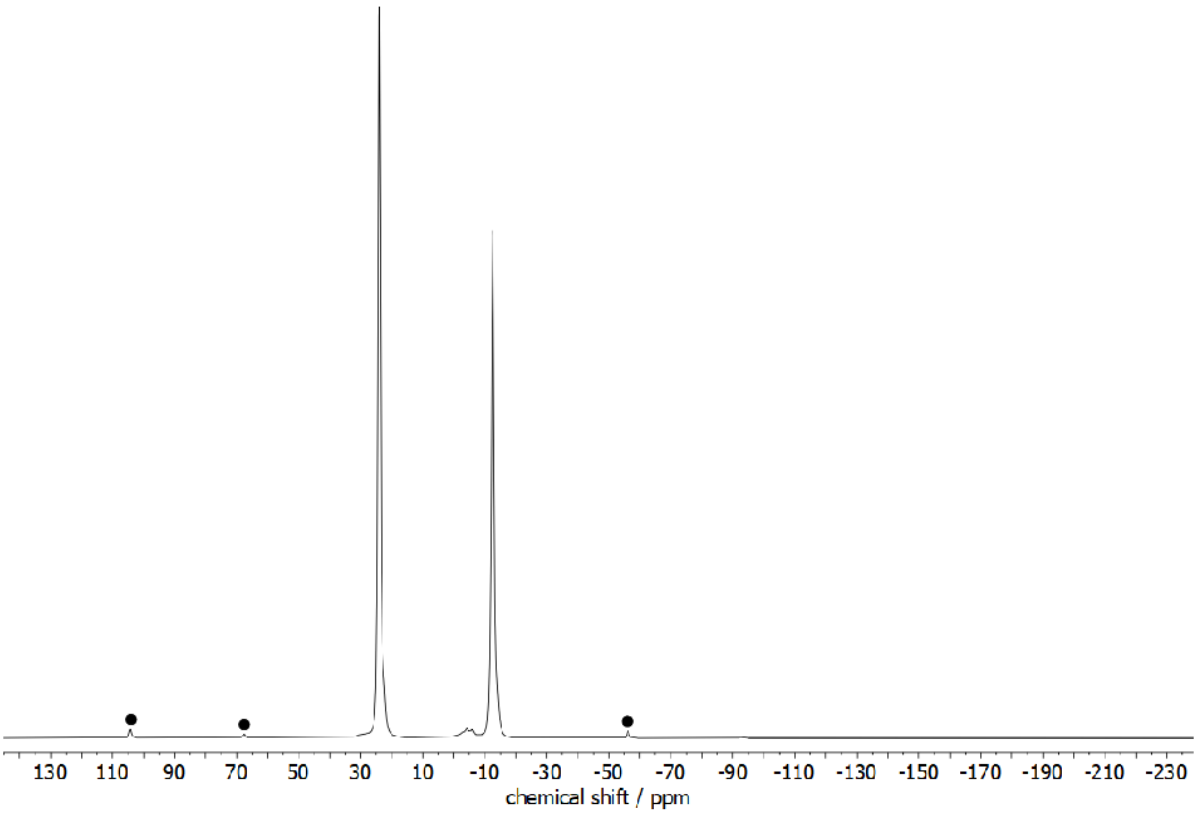

Figure S17: $^{31}P\{^{1}H\}$ CP-MAS NMR spectrum of **1b·PhNCO** (● spinning sidebands).

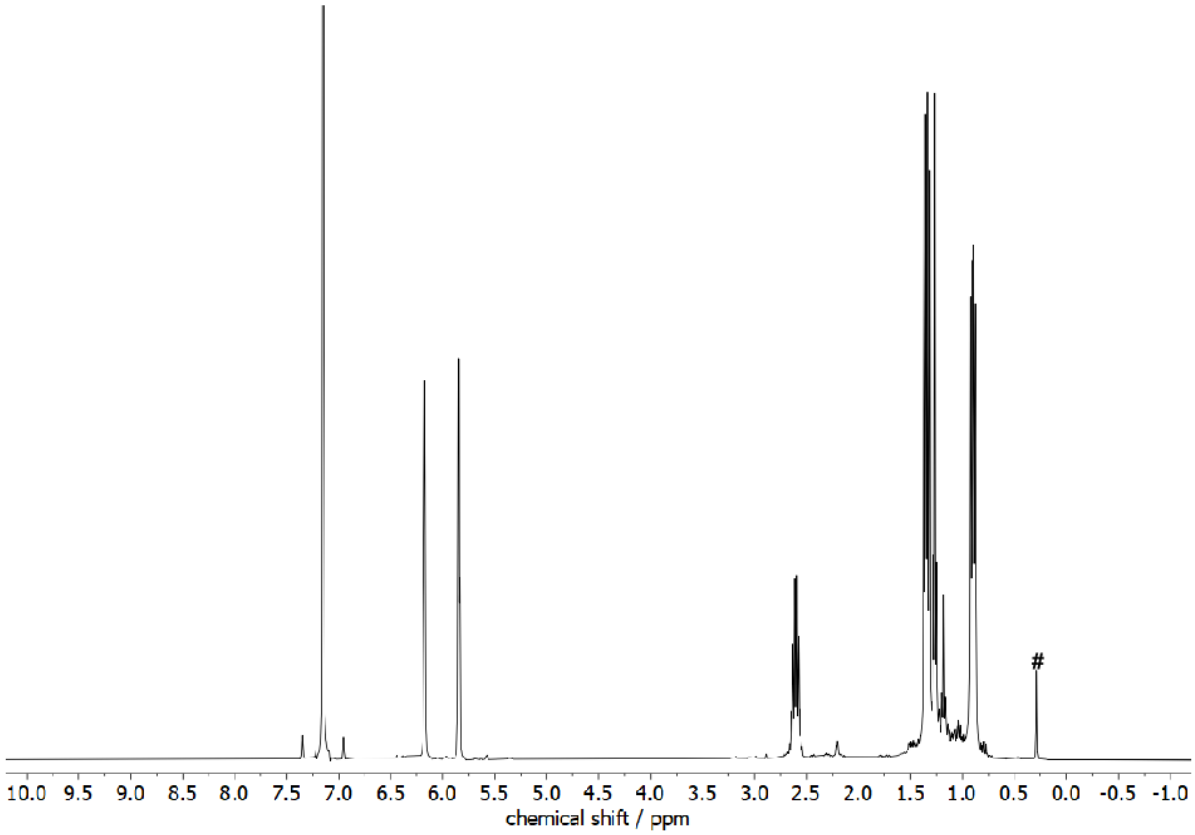

Figure S18: ^{1}H NMR spectrum (C_6D_6) of **1b·Pt(Me)$_2$** (**#** silicon grease).

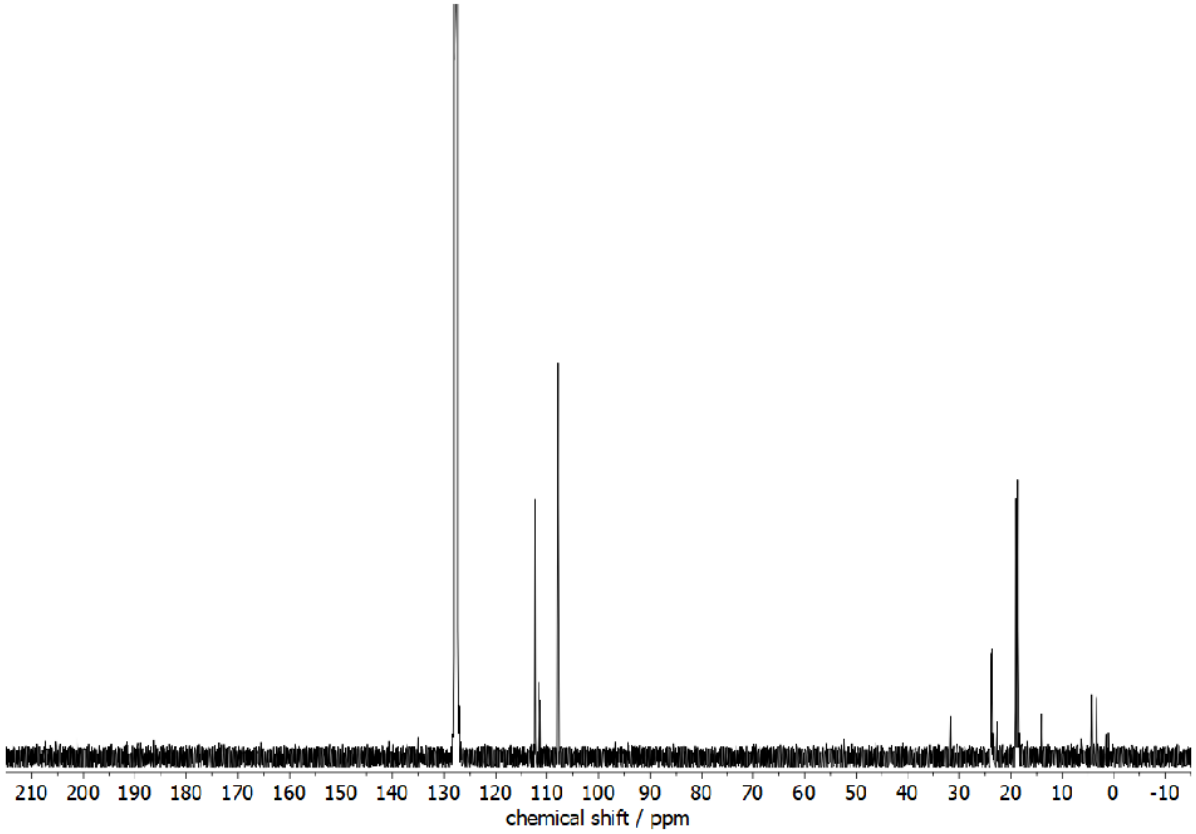

Figure S19: $^{13}C\{^{1}H\}$ NMR spectrum (C_6D_6) of **1b·Pt(Me)$_2$**.

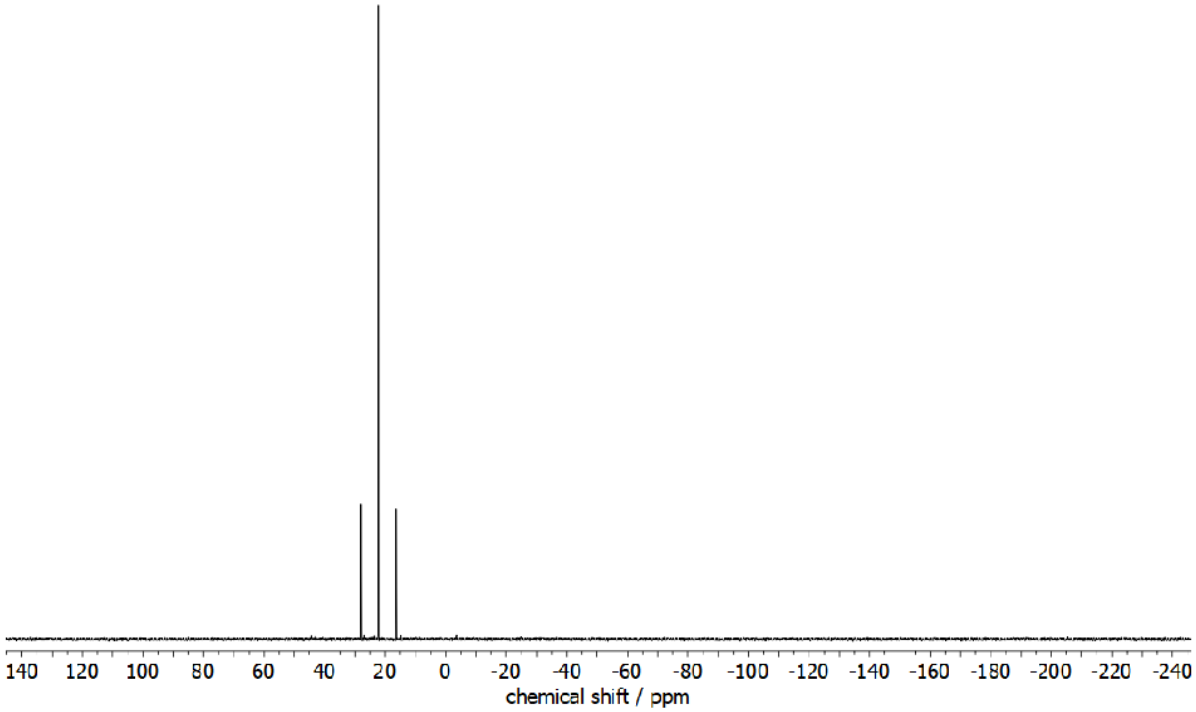

Figure S20: $^{31}P\{^{1}H\}$ NMR spectrum (C_6D_6) of **1b·Pt(Me)$_2$**.

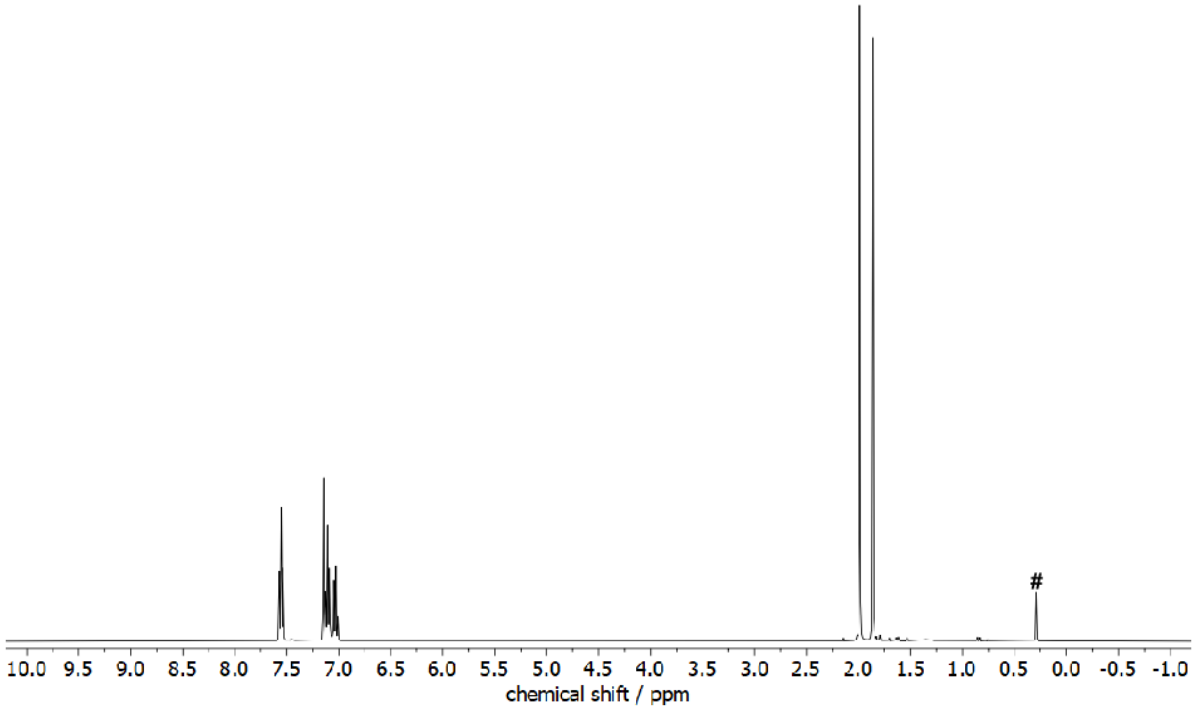

Figure S21: ^{1}H NMR spectrum (C_6D_6) of **2** (**#** silicon grease).

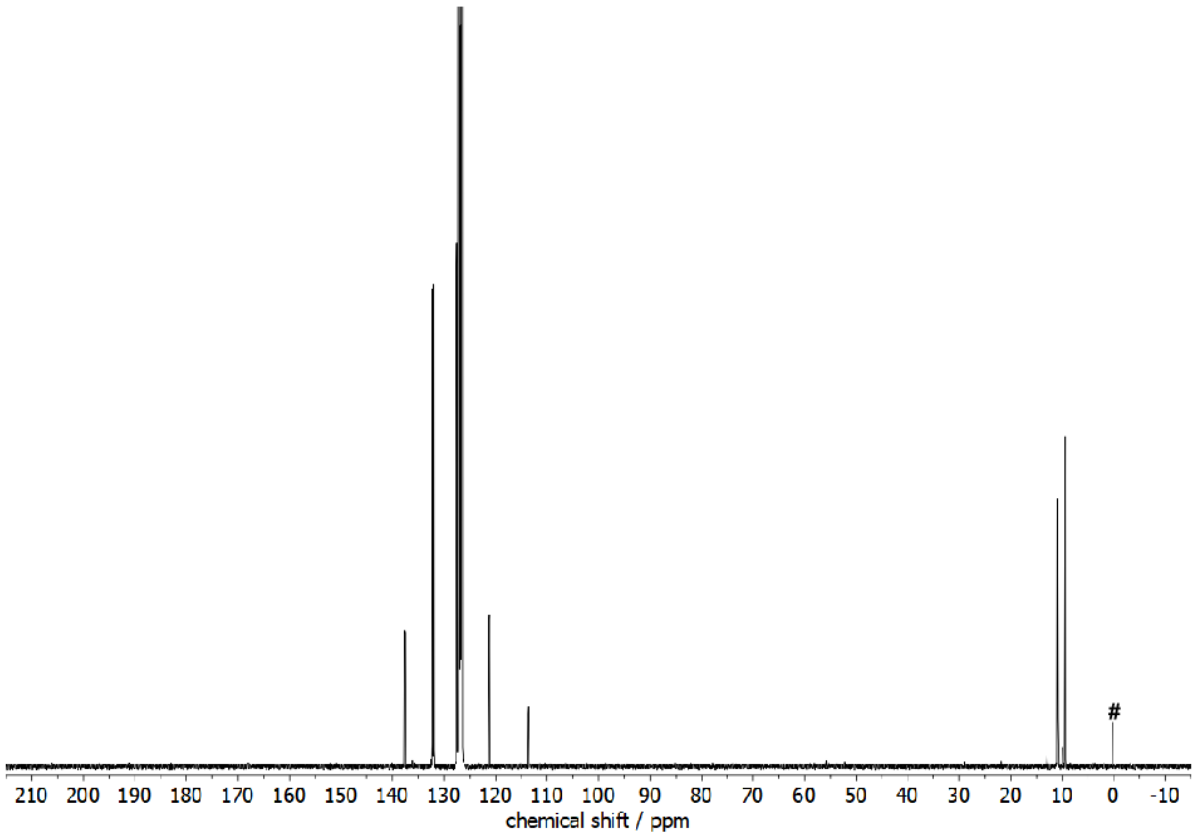

Figure S22: ^{13}C{^{1}H} NMR spectrum (C_6D_6) of **2** (**#** silicon grease).

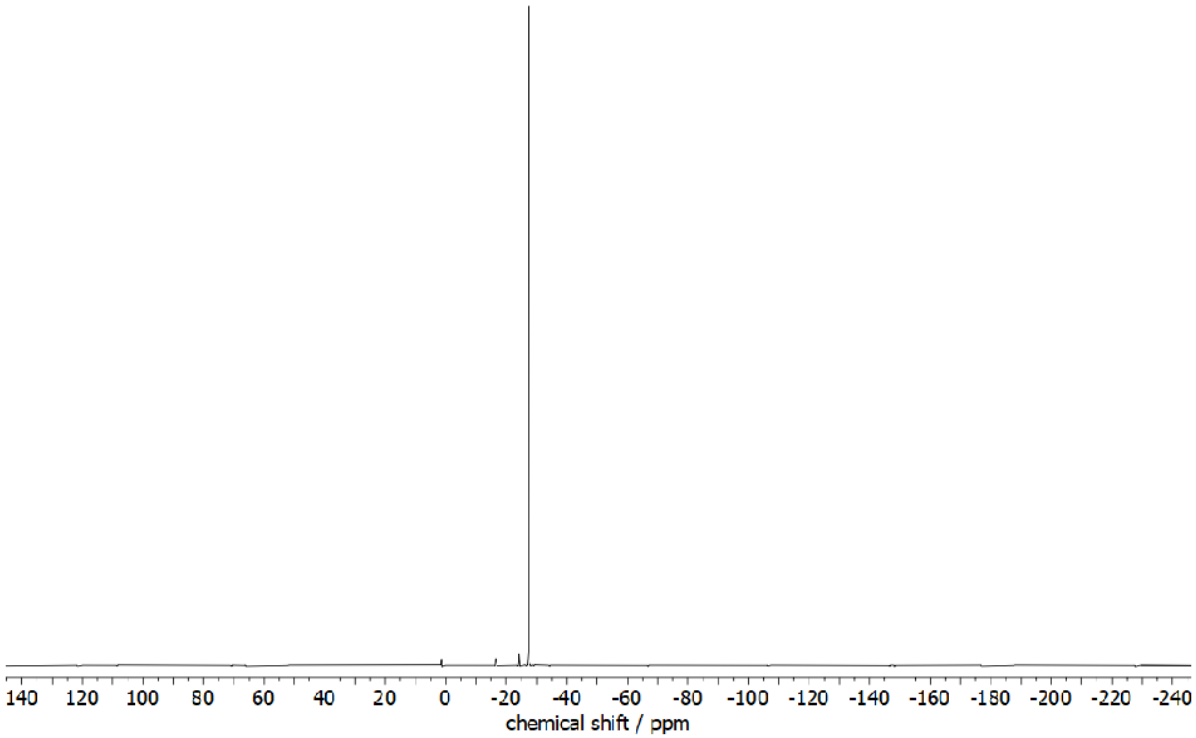

Figure S23: $^{31}P\{^{1}H\}$ NMR spectrum (C_6D_6) of **2**.

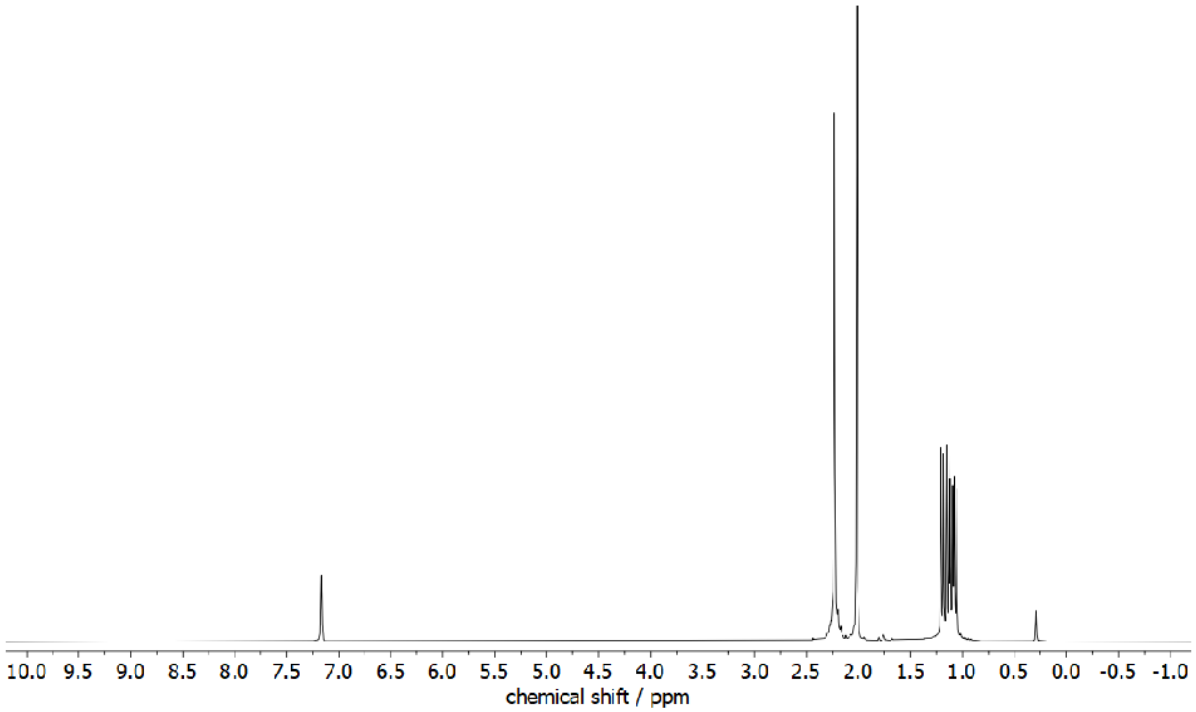

Figure S24: ^{1}H NMR spectrum (C_6D_6) of **3a**.

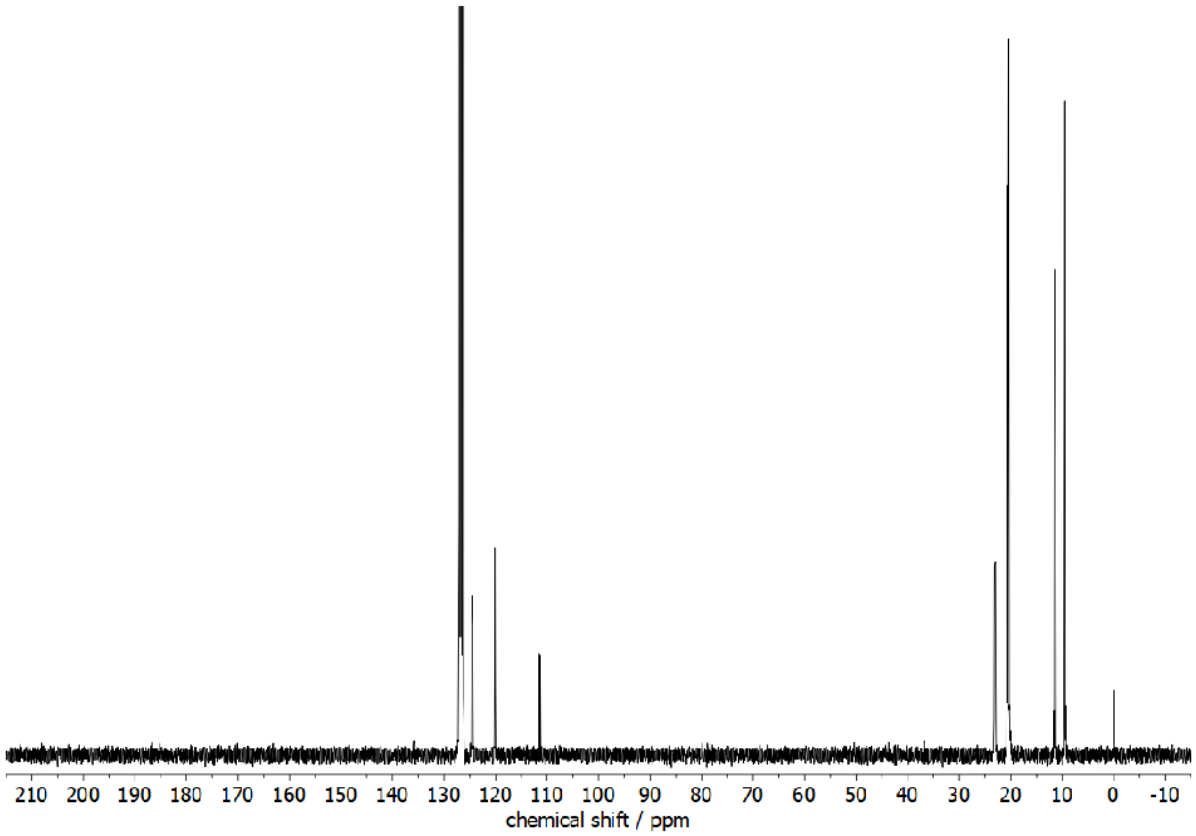

Figure S25: $^{13}C\{^{1}H\}$ NMR spectrum (C_6D_6) of **3a**.

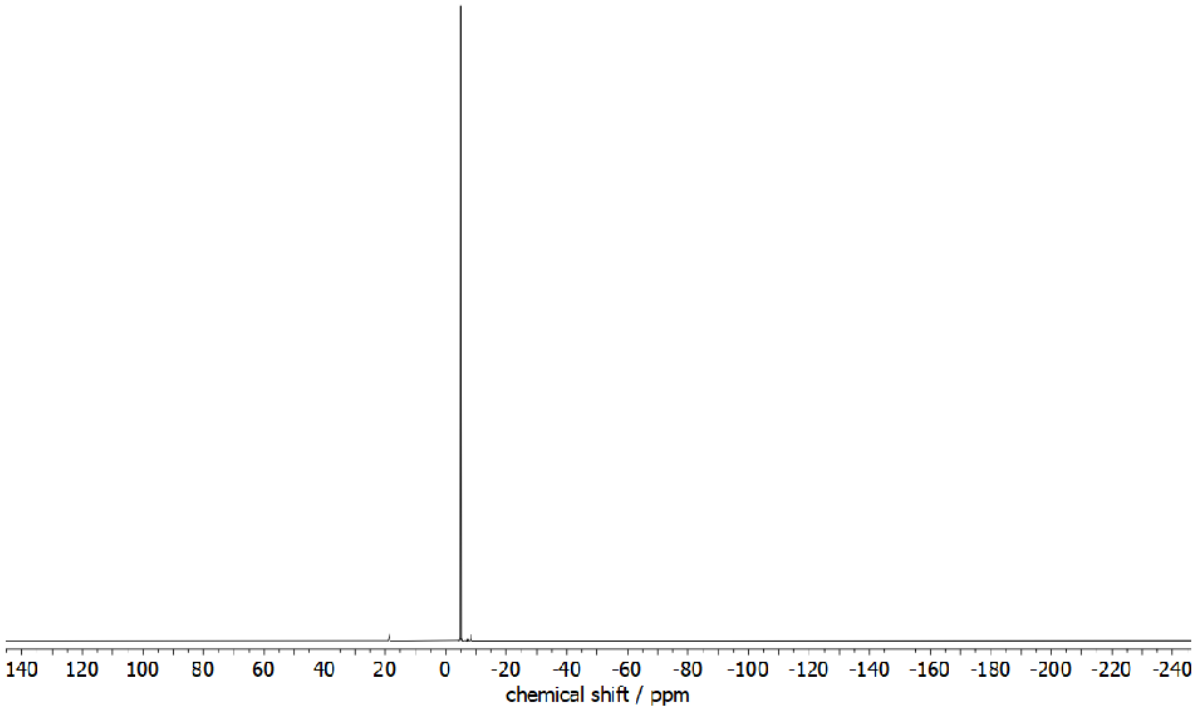

Figure S26: $^{31}P\{^{1}H\}$ NMR spectrum (C_6D_6) of **3a**.

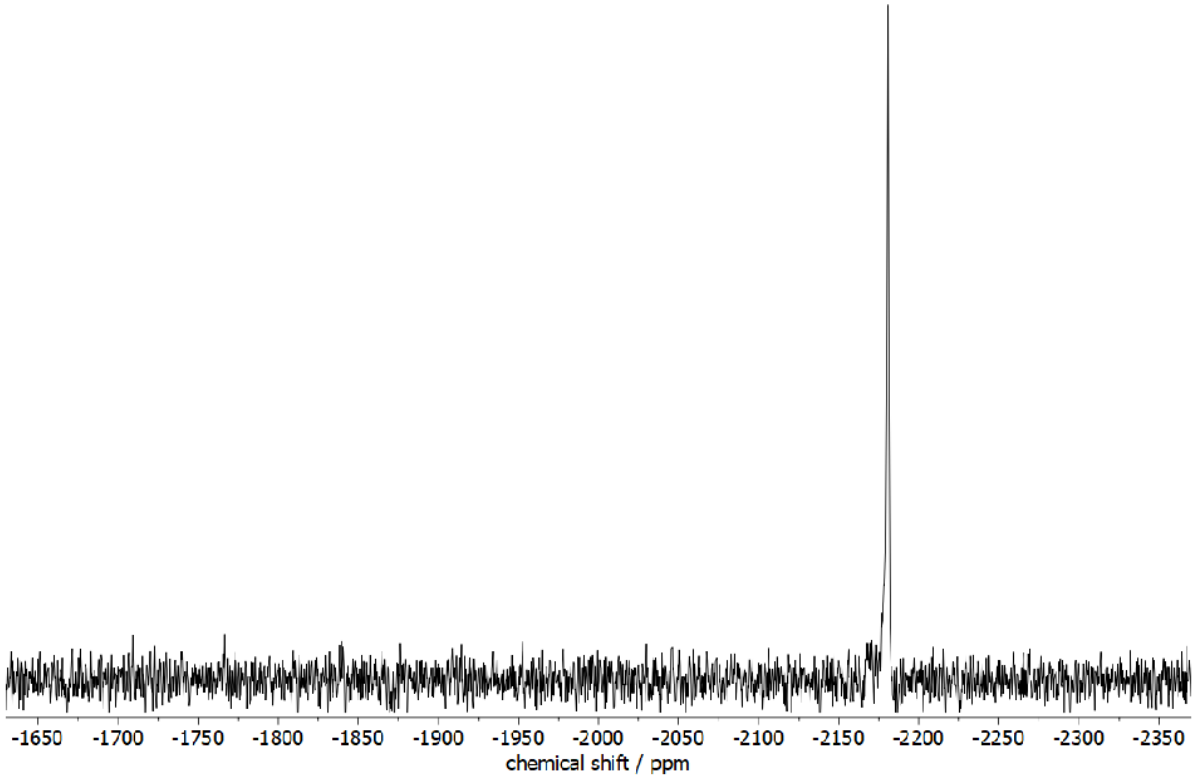

Figure S27: $^{119}Sn\{^{1}H\}$ NMR spectrum (C_6D_6) of **3a**.

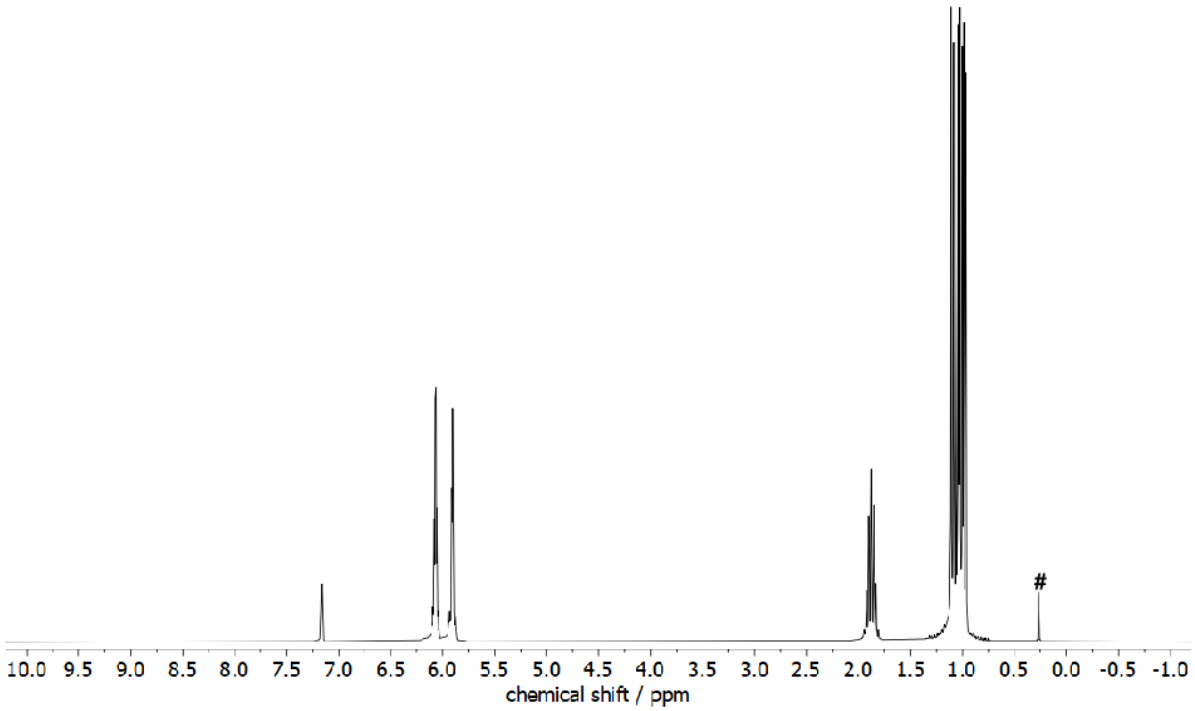

Figure S28: ^{1}H NMR spectrum (C_6D_6) of **3b** (**#** silicon grease).

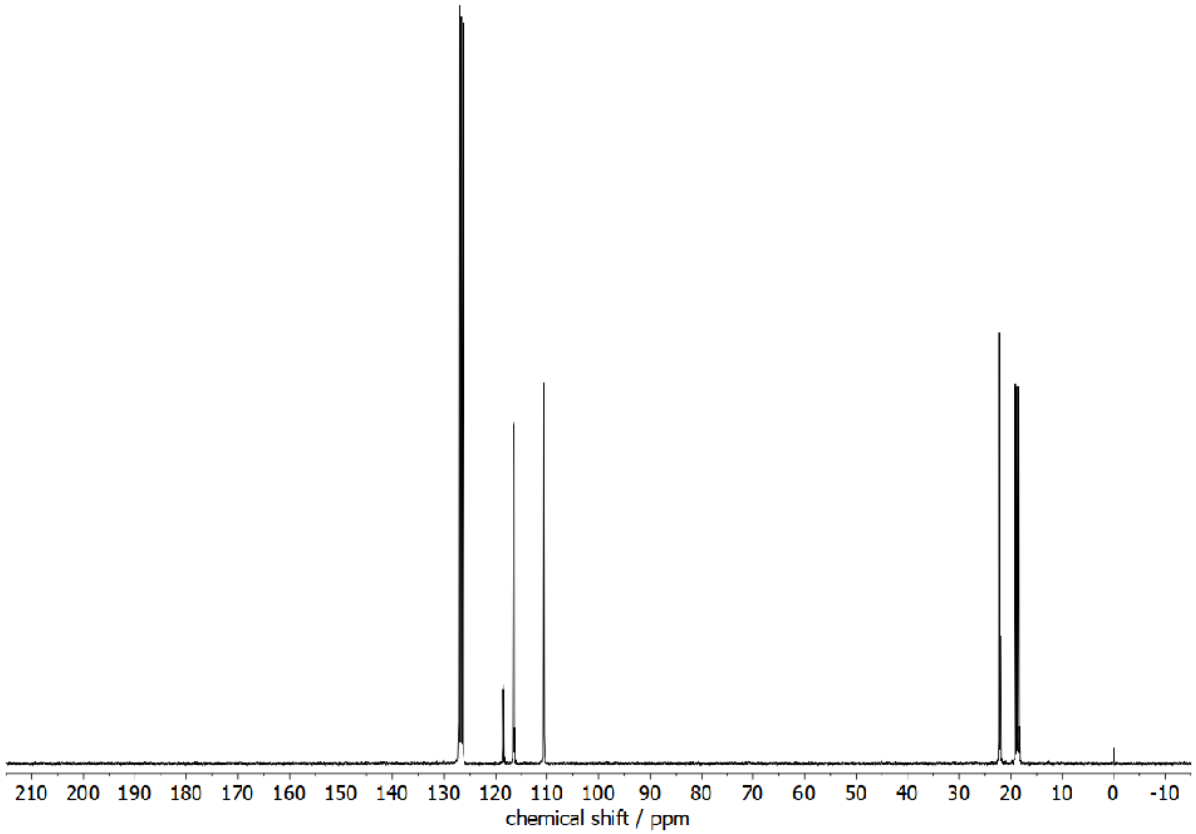

Figure S29: $^{13}C\{^{1}H\}$ NMR spectrum (C_6D_6) of **3b**.

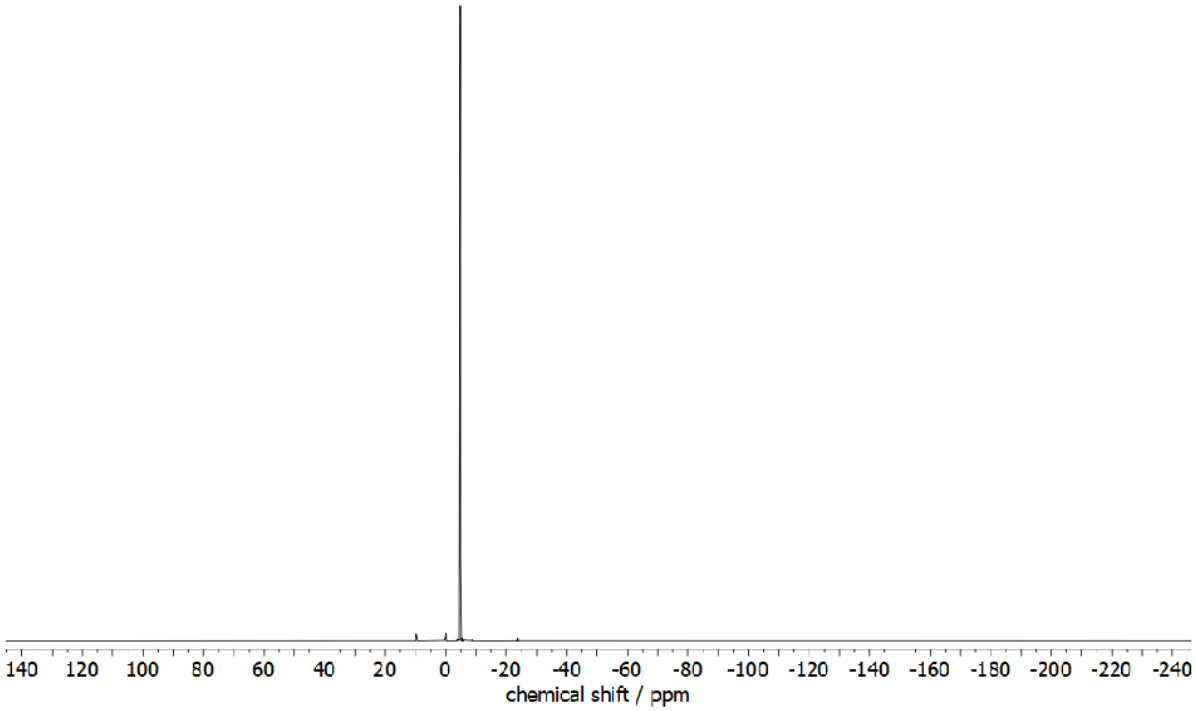

Figure S30: $^{31}P\{^{1}H\}$ NMR spectrum (C_6D_6) of **3b**.

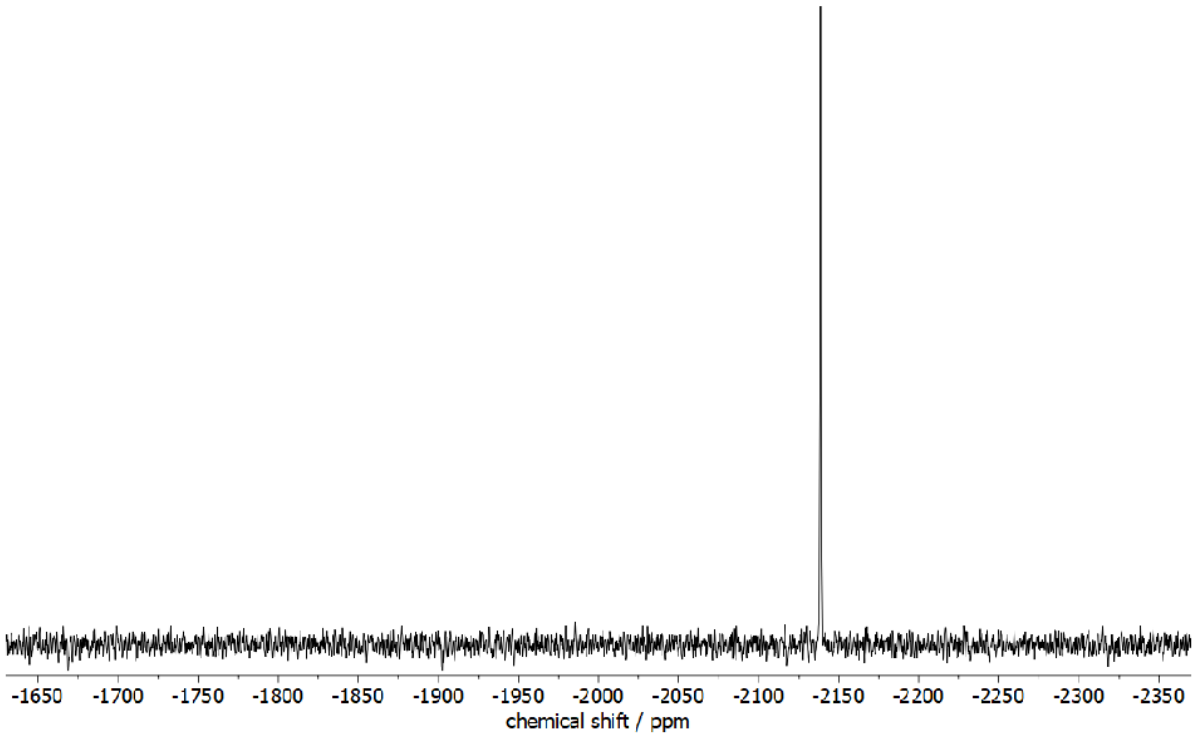

Figure S31: $^{119}Sn\{^{1}H\}$ NMR spectrum (C_6D_6) of **3b**.

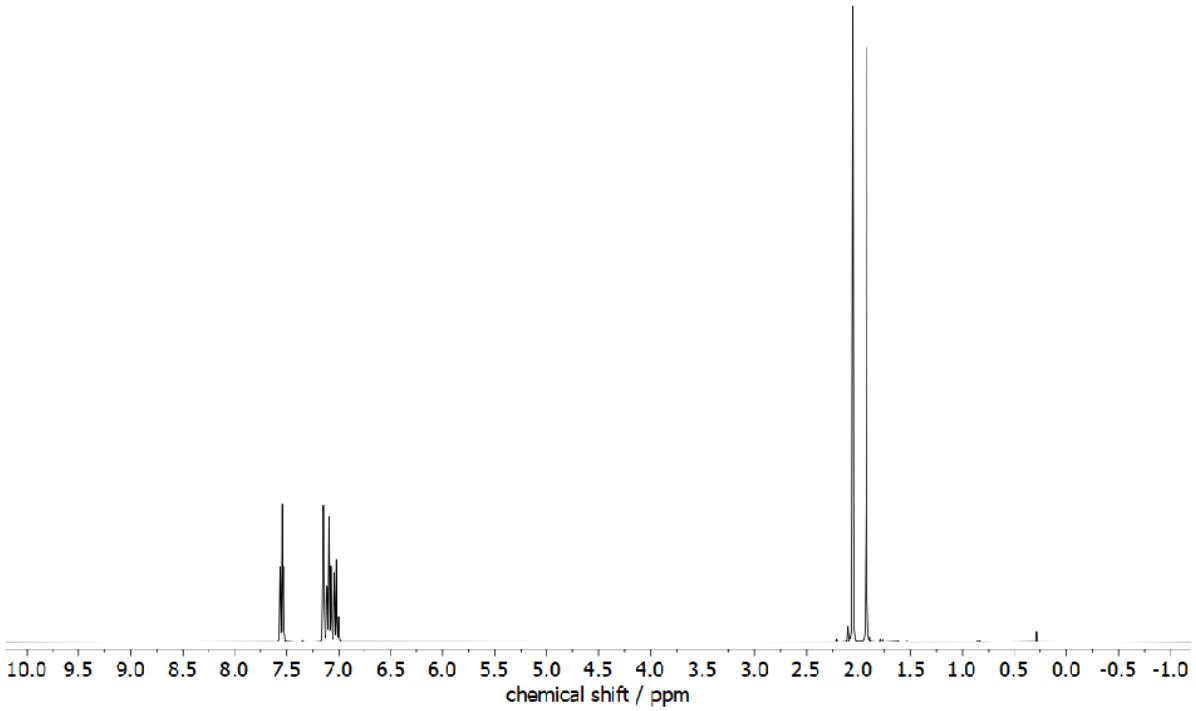

Figure S32: ^{1}H NMR spectrum (C_6D_6) of **3c**.

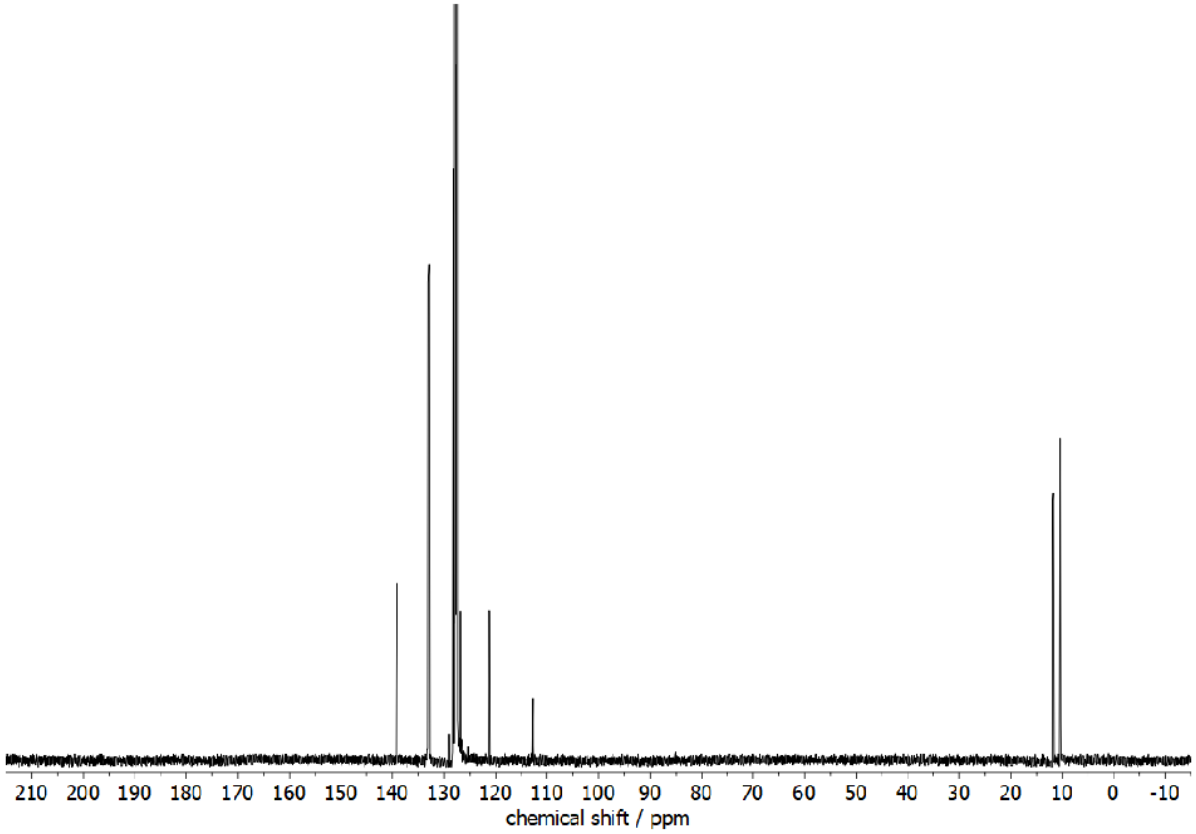

Figure S33: $^{13}C\{^{1}H\}$ NMR spectrum (C_6D_6) of **3c**.

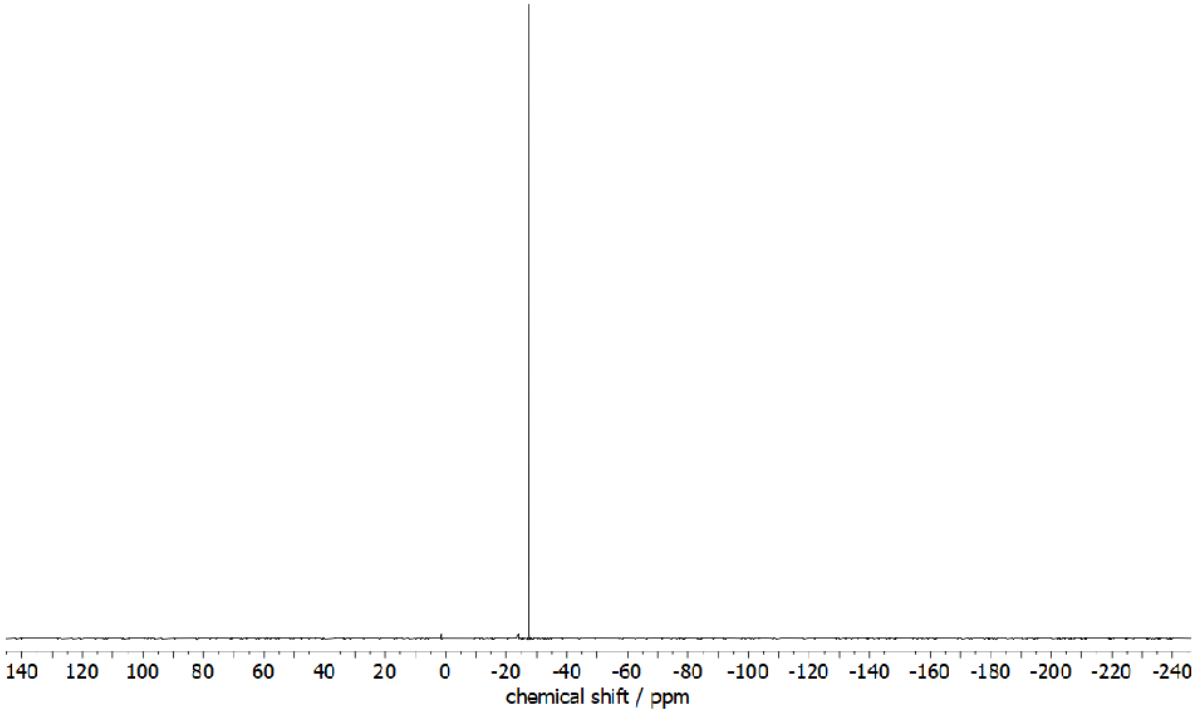

Figure S34: $^{31}P\{^{1}H\}$ NMR spectrum (C_6D_6) of **3c**.

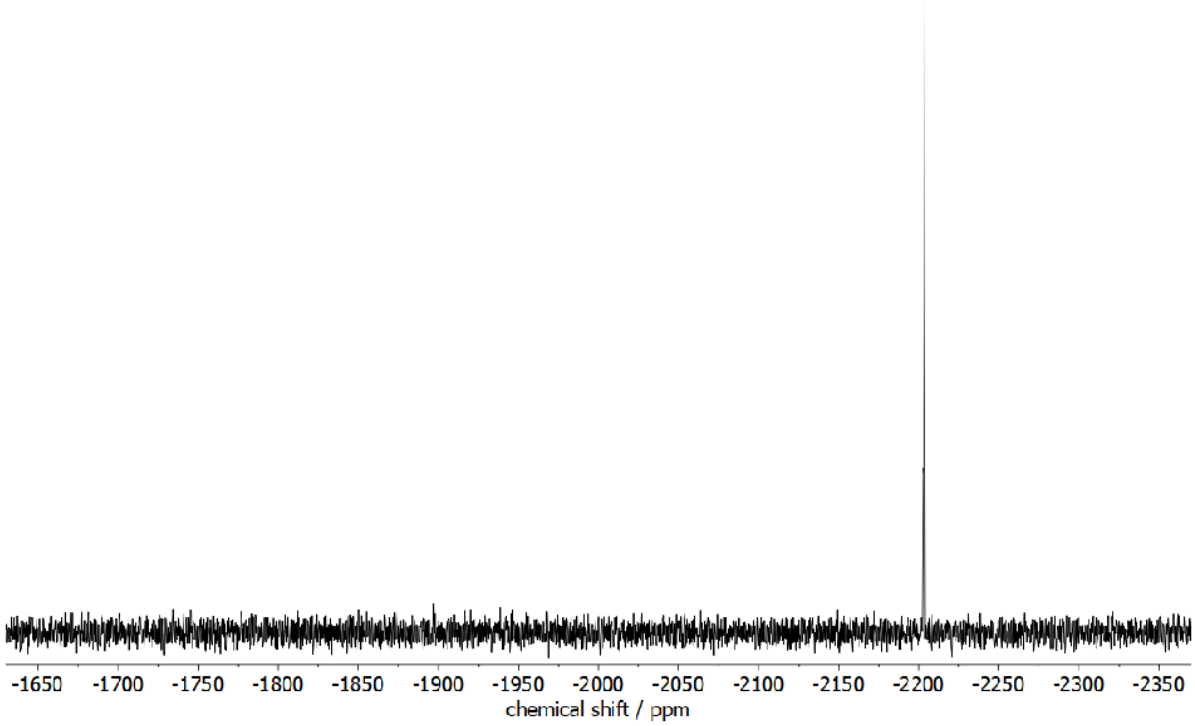

Figure S35: $^{119}Sn\{^{1}H\}$ NMR spectrum (C_6D_6) of **3c**.

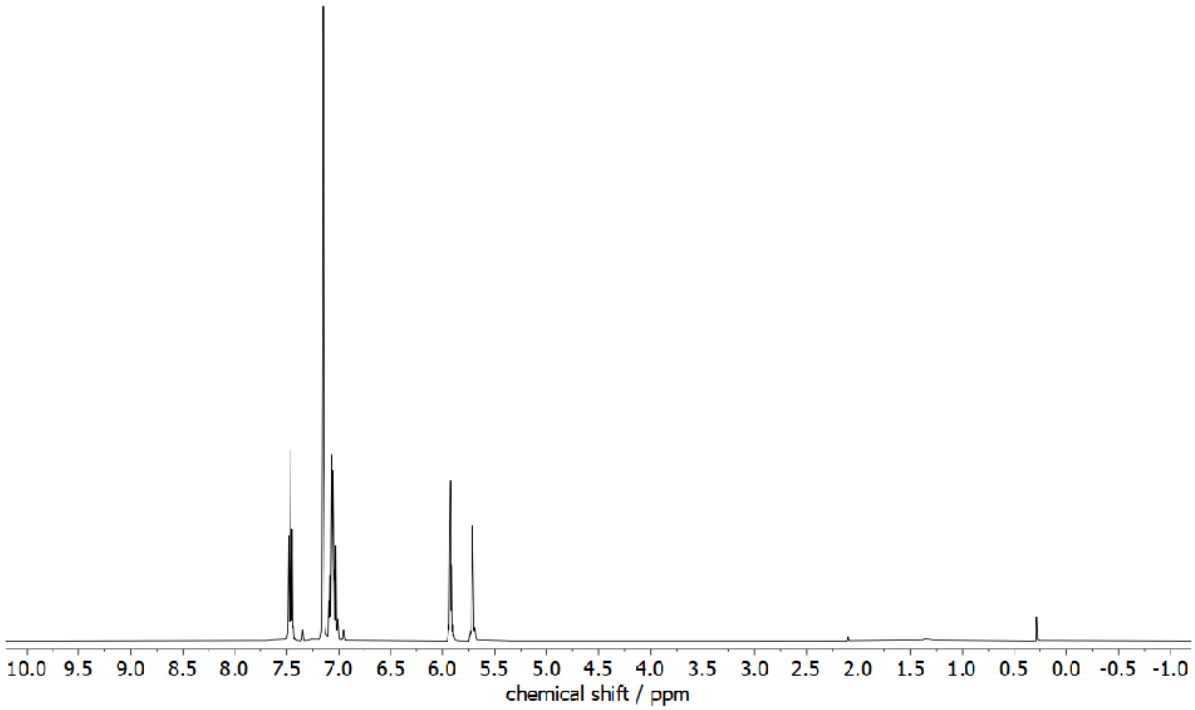

Figure S36: ^{1}H NMR spectrum (C_6D_6) of **3d**.

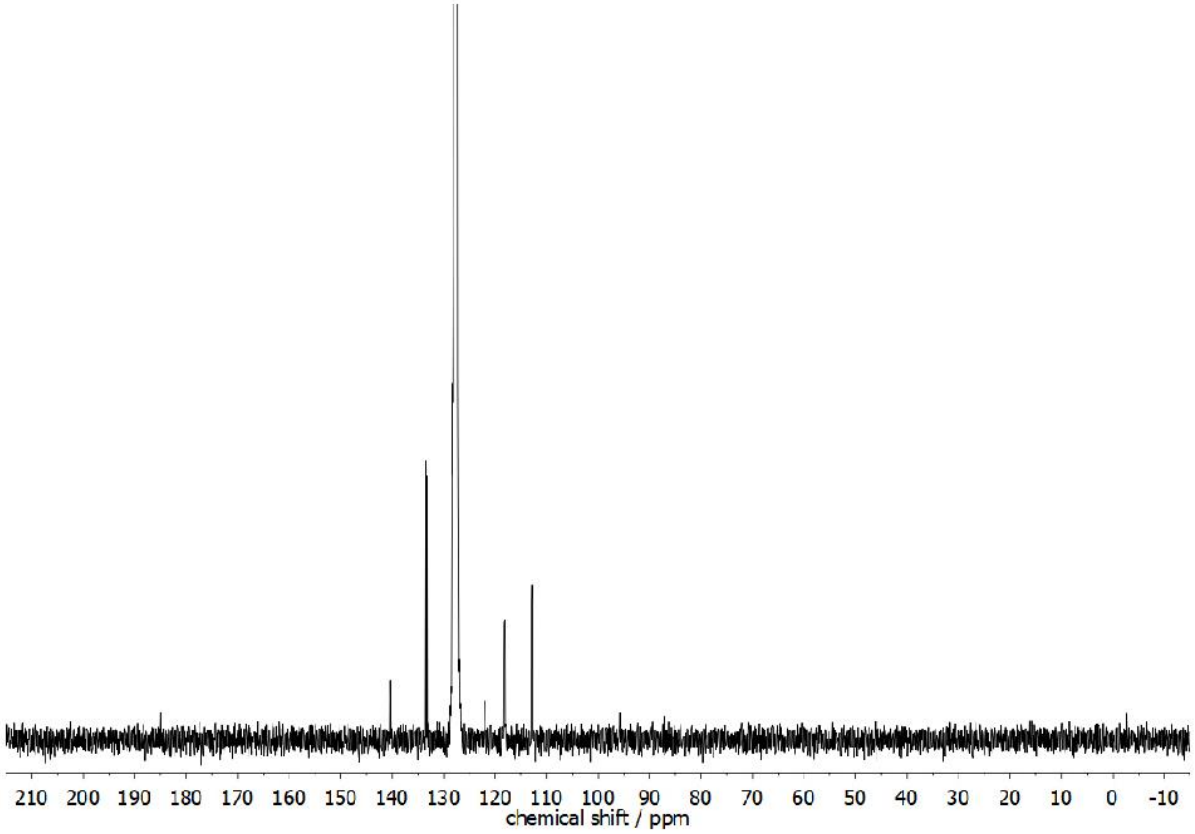

Figure S37: $^{13}C\{^{1}H\}$ NMR spectrum (C_6D_6) of **3d**.

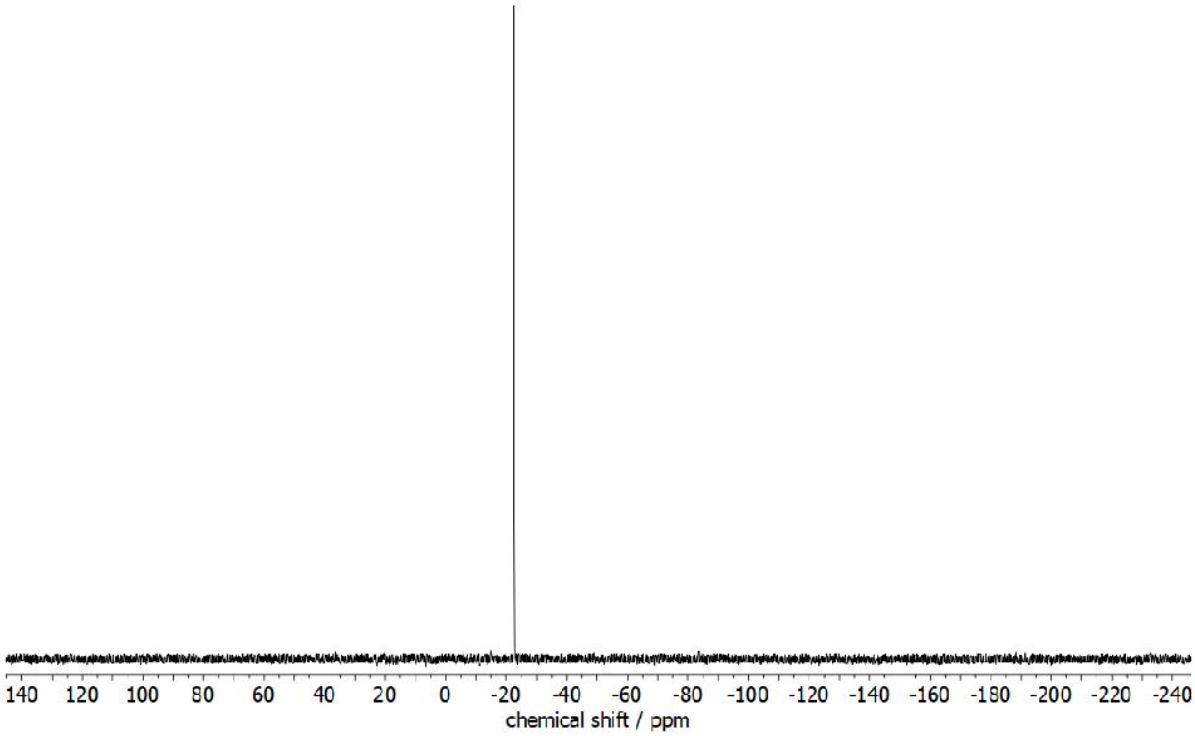

Figure S38: $^{31}P\{^{1}H\}$ NMR spectrum (C_6D_6) of **3d**.

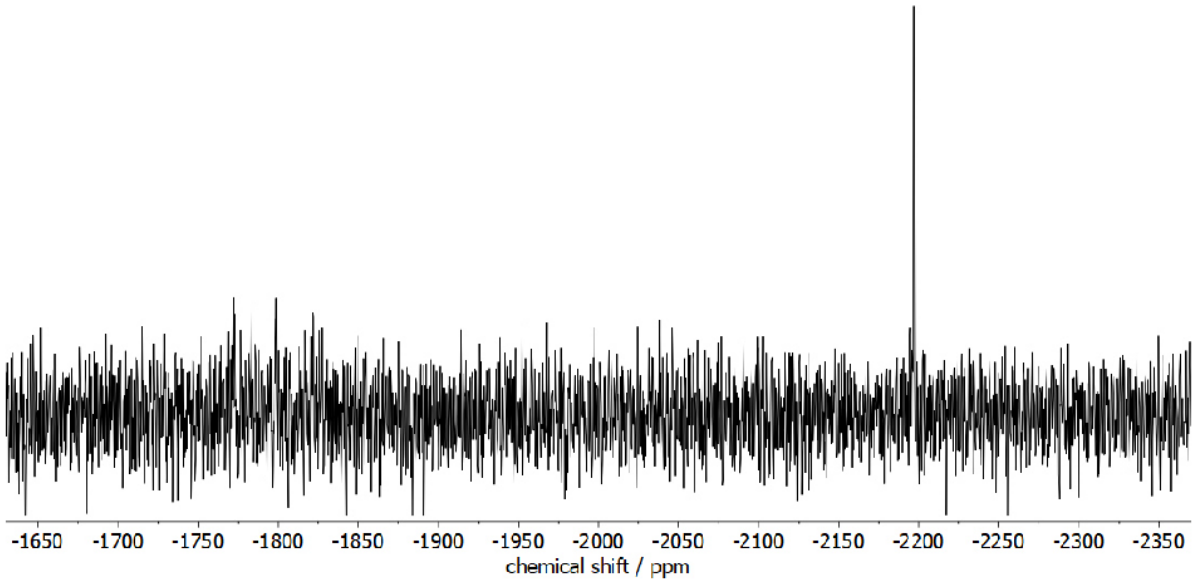

Figure S39: $^{119}Sn\{^{1}H\}$ NMR spectrum (C_6D_6) of **3d**.

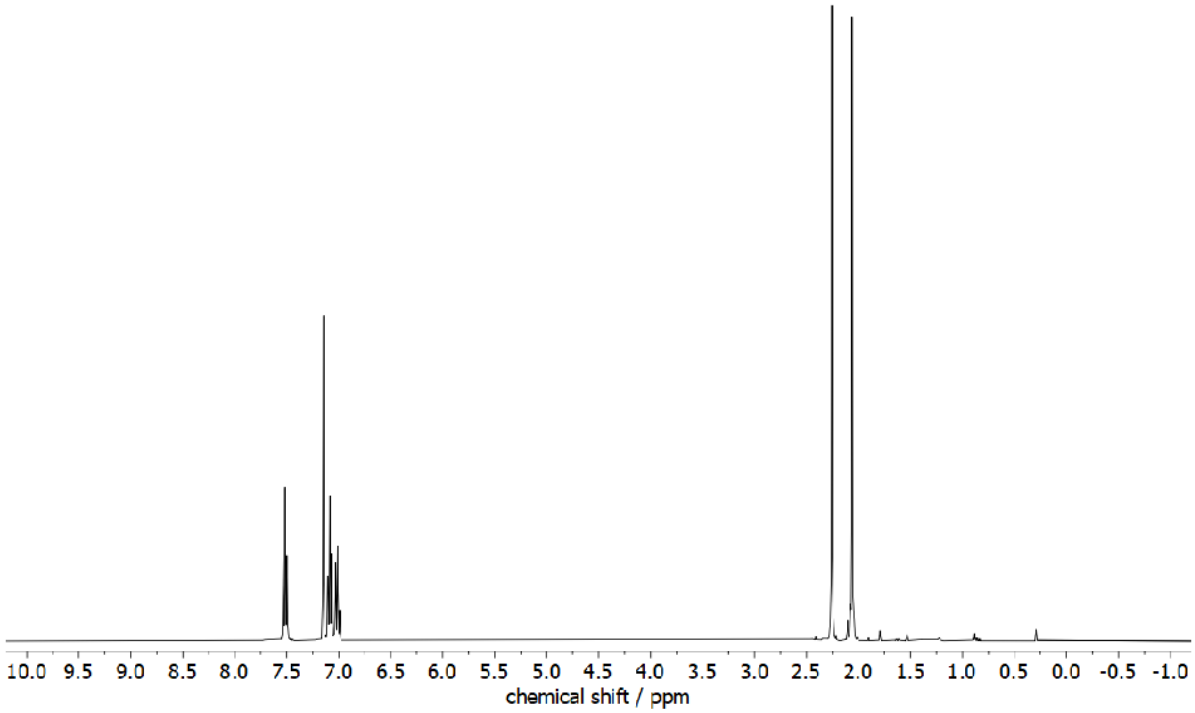

Figure S40: ^{1}H NMR spectrum (C_6D_6) of **4**.

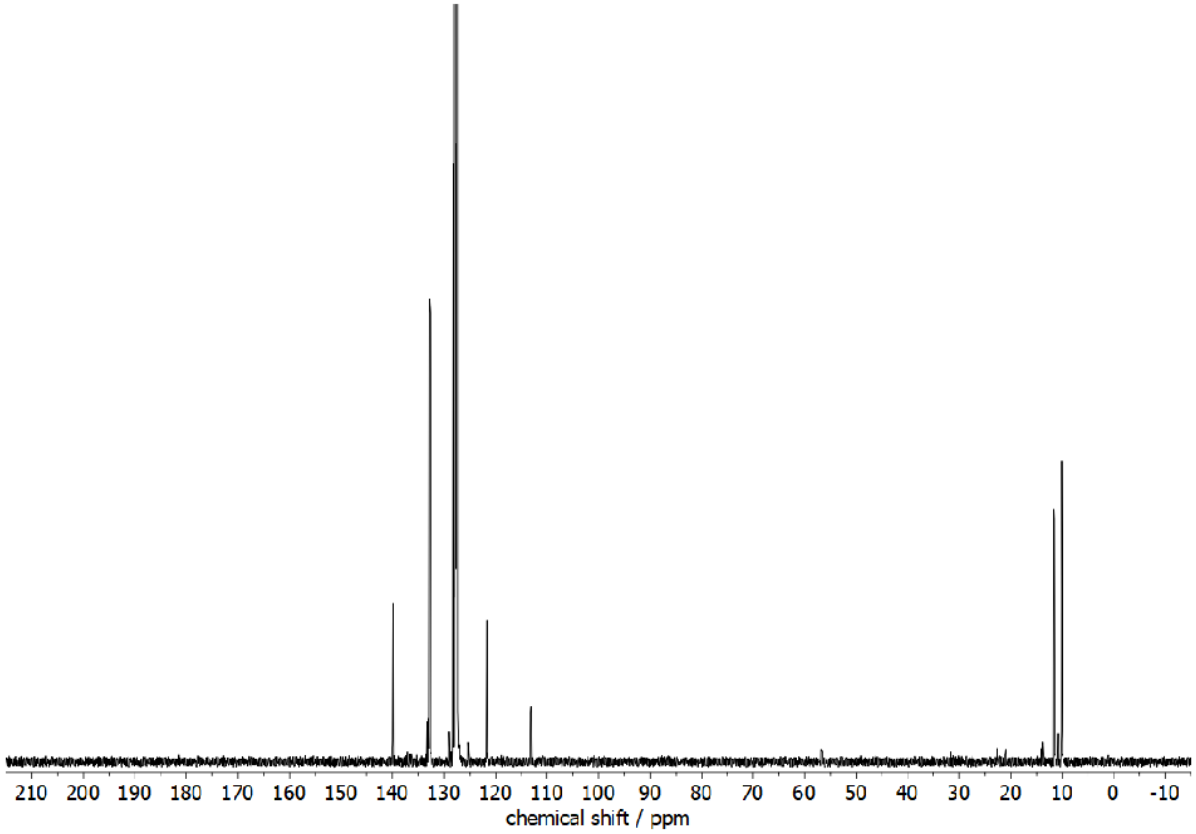

Figure S41: $^{13}C\{^{1}H\}$ NMR spectrum (C_6D_6) of **4**.

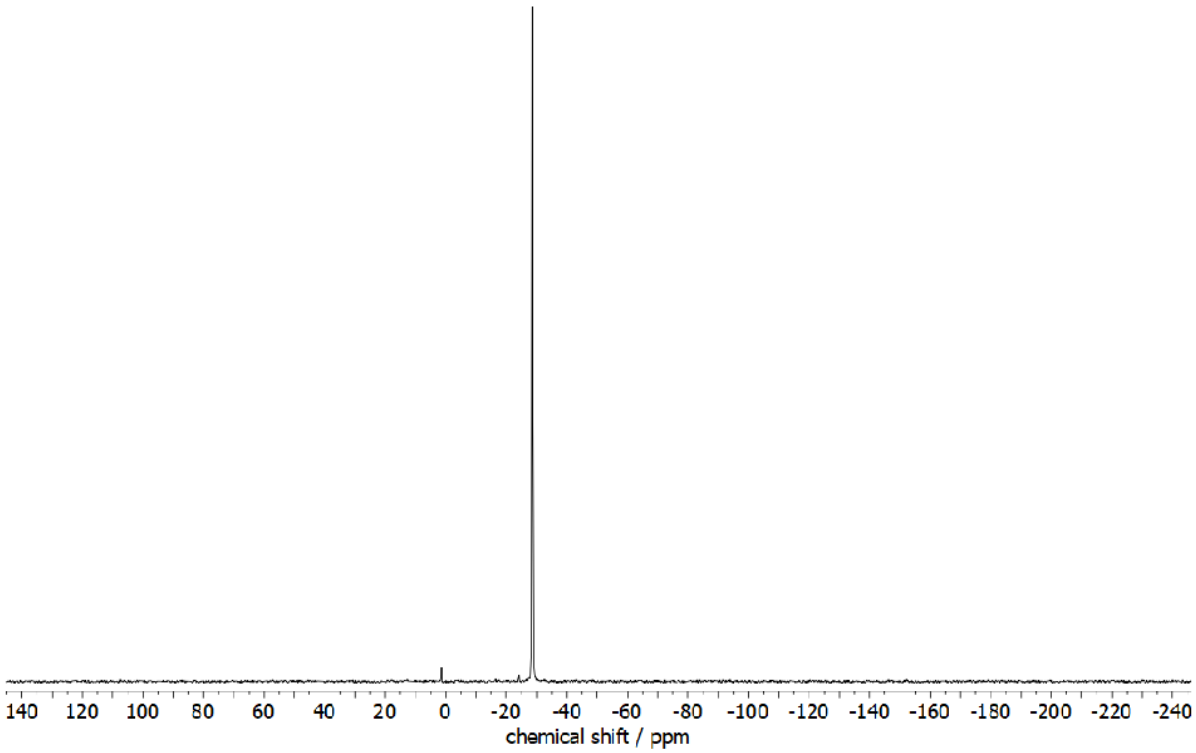

Figure S42: $^{31}P\{^{1}H\}$ NMR spectrum (C_6D_6) of **4**.

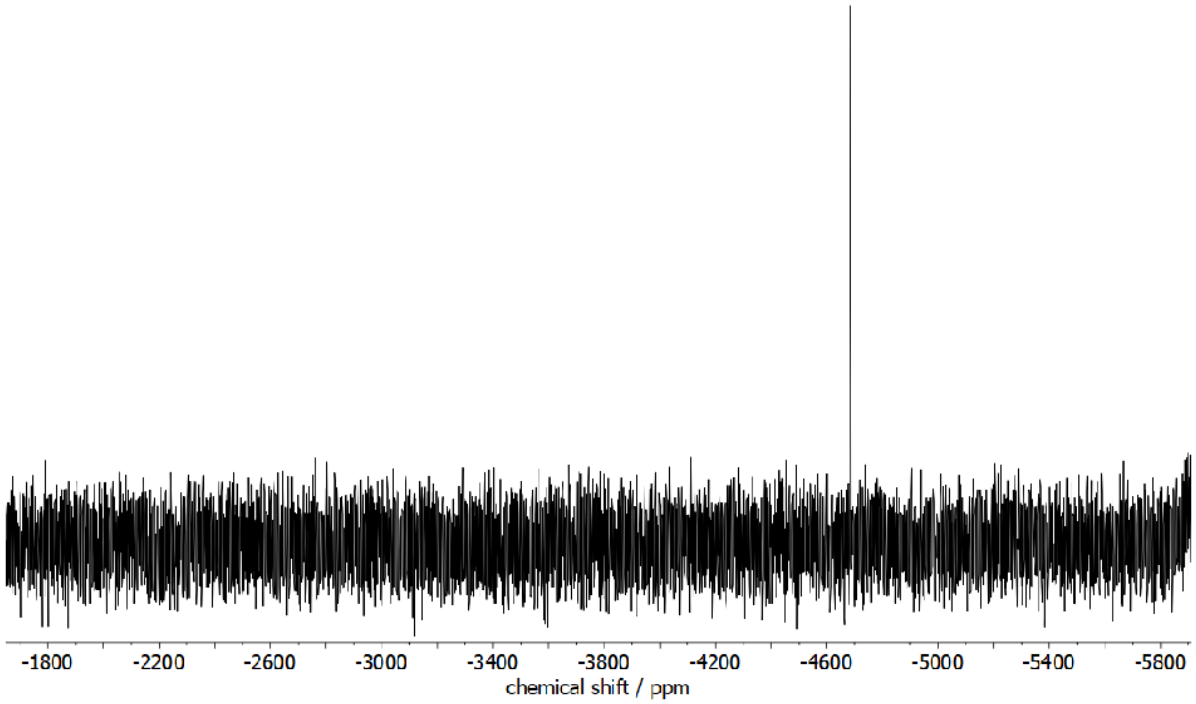

Figure S43: $^{207}Pb\{^{1}H\}$ NMR spectrum (C_6D_6) of **4**.

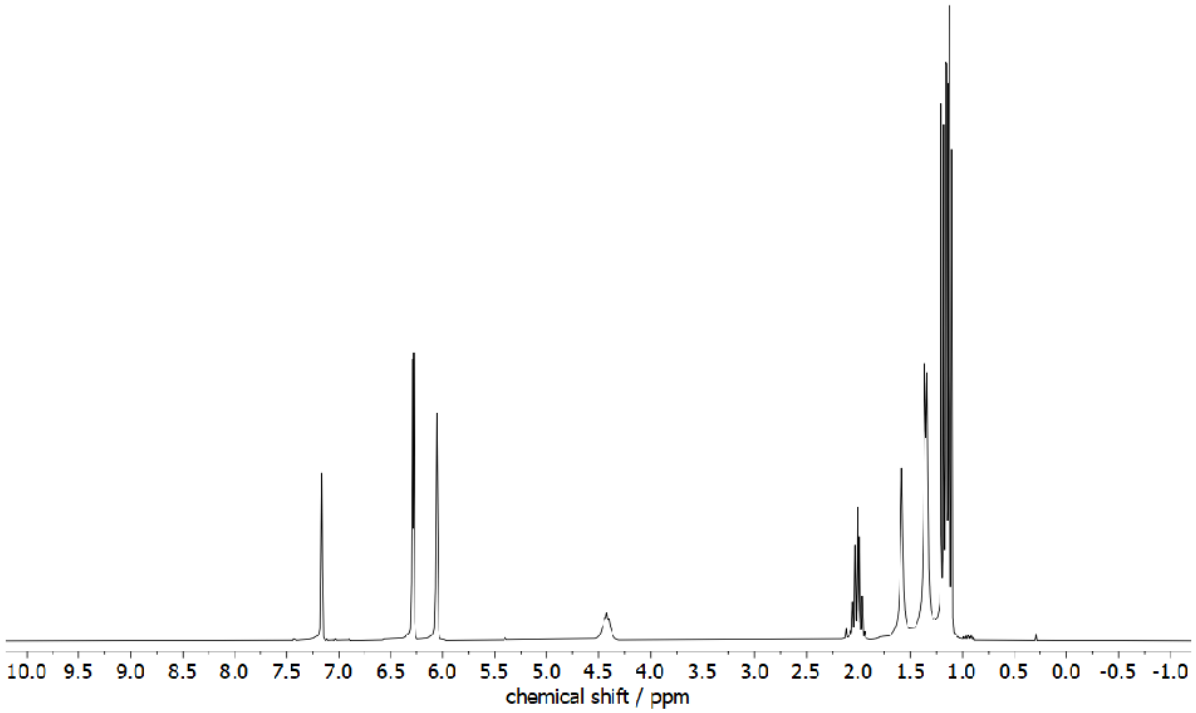

Figure S44: ^{1}H NMR spectrum (C_6D_6) of **3b·NHC**.

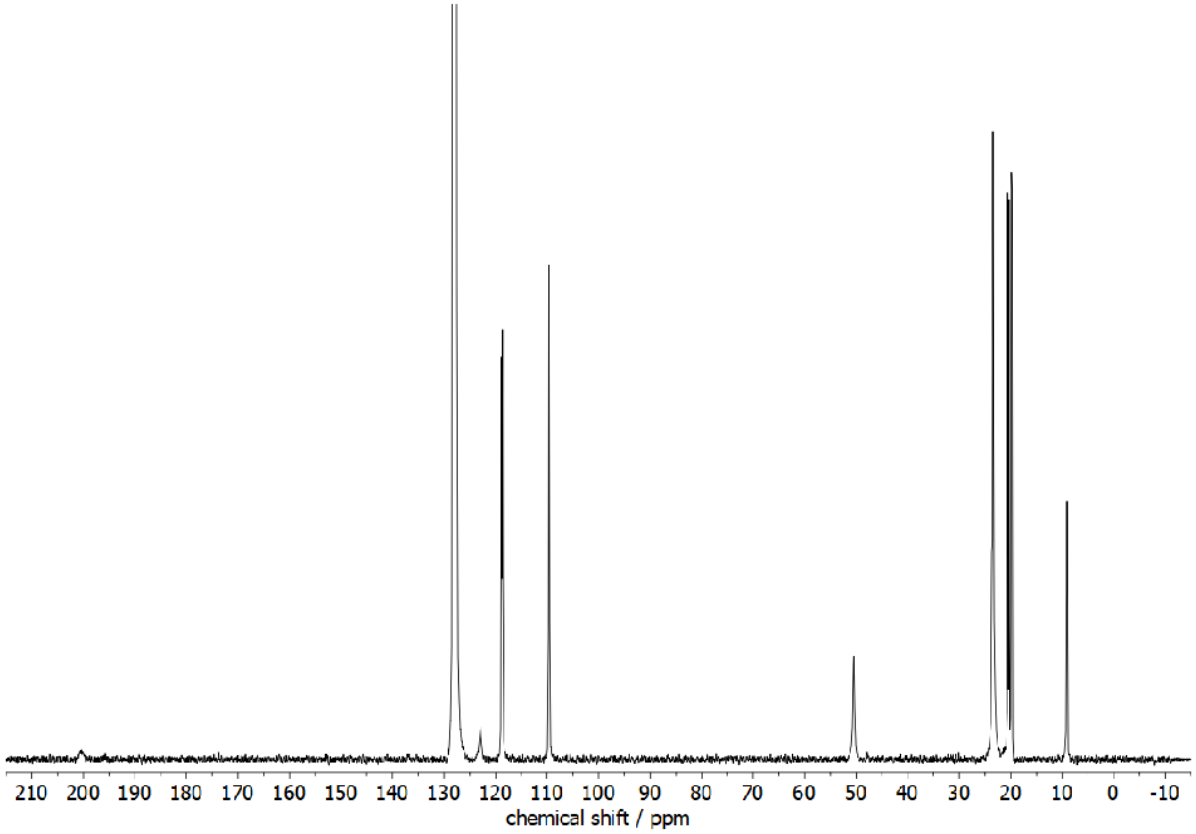

Figure S45: $^{13}C\{^{1}H\}$ NMR spectrum (C_6D_6) of **3b·NHC**.

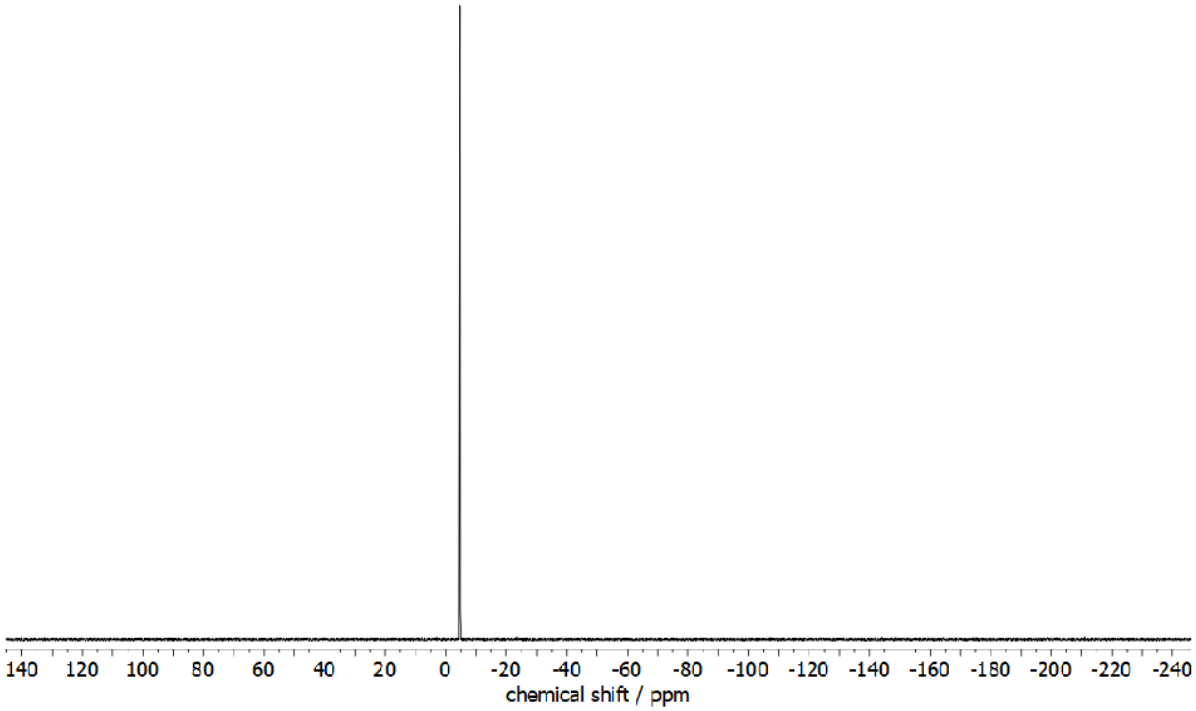

Figure S46: $^{31}P\{^{1}H\}$ NMR spectrum (C_6D_6) of **3b·NHC**.

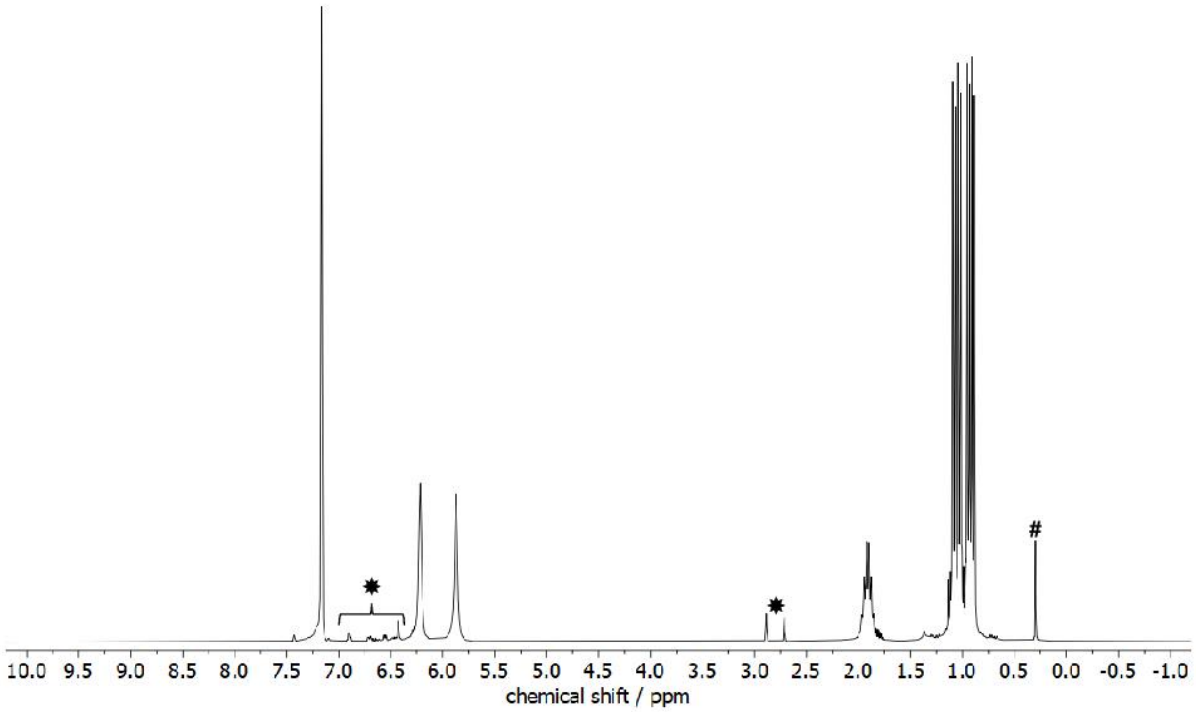

Figure S47: ^{1}H NMR spectrum (C_6D_6) of **3b**·**AlCl$_3$** (# silicon grease; ✱ free ligand).

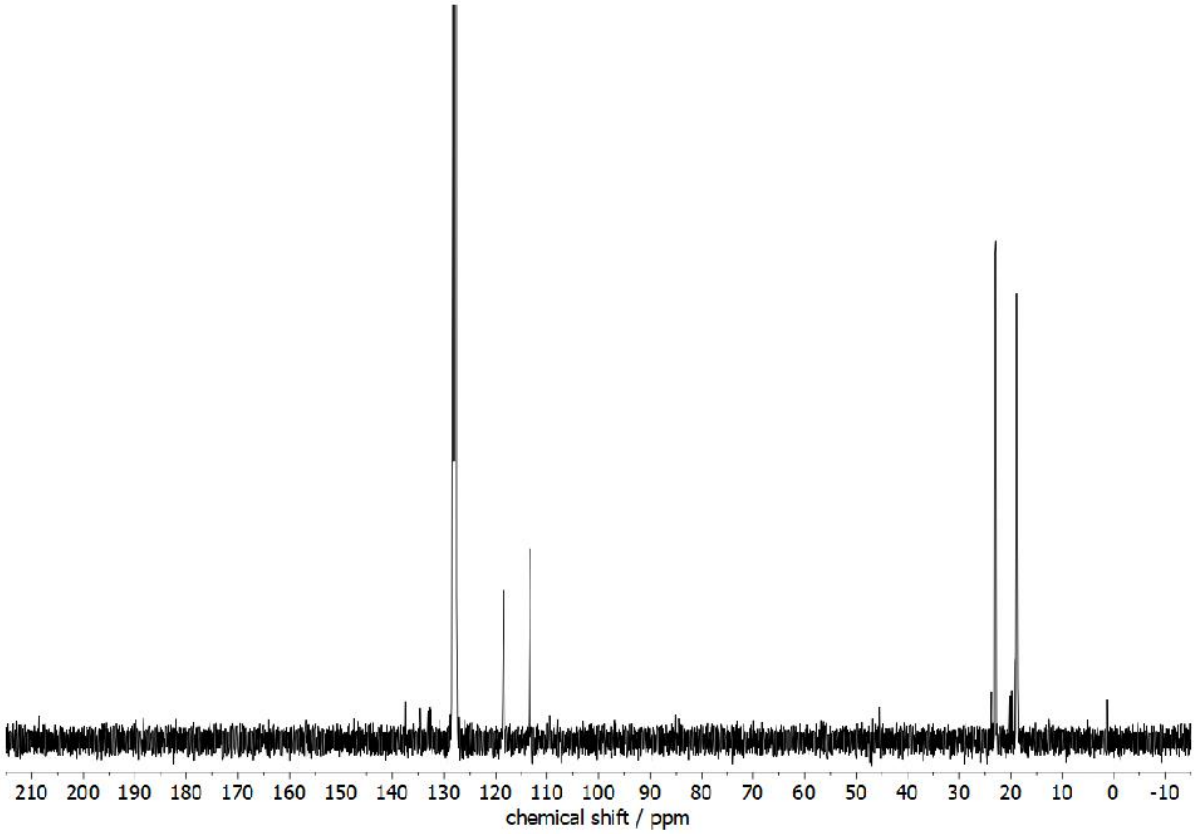

Figure S48: ^{13}C{^{1}H} NMR spectrum (C_6D_6) of **3b**·**AlCl$_3$**.

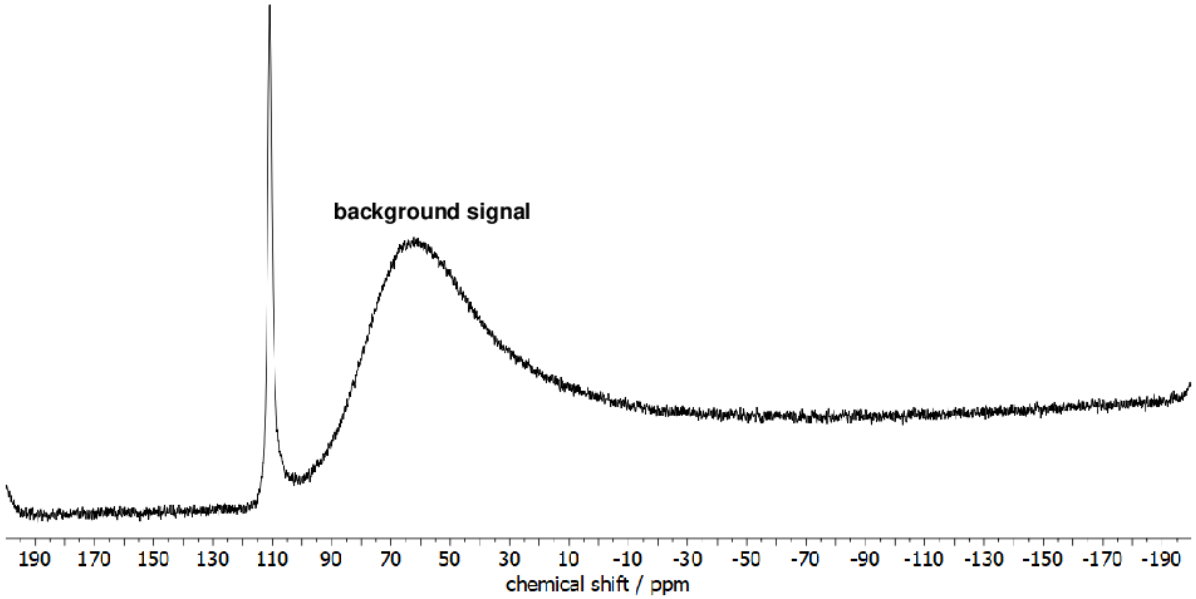

Figure S49: $^{27}Al\{^{1}H\}$ NMR spectrum (C_6D_6) of **3b·AlCl$_3$**.

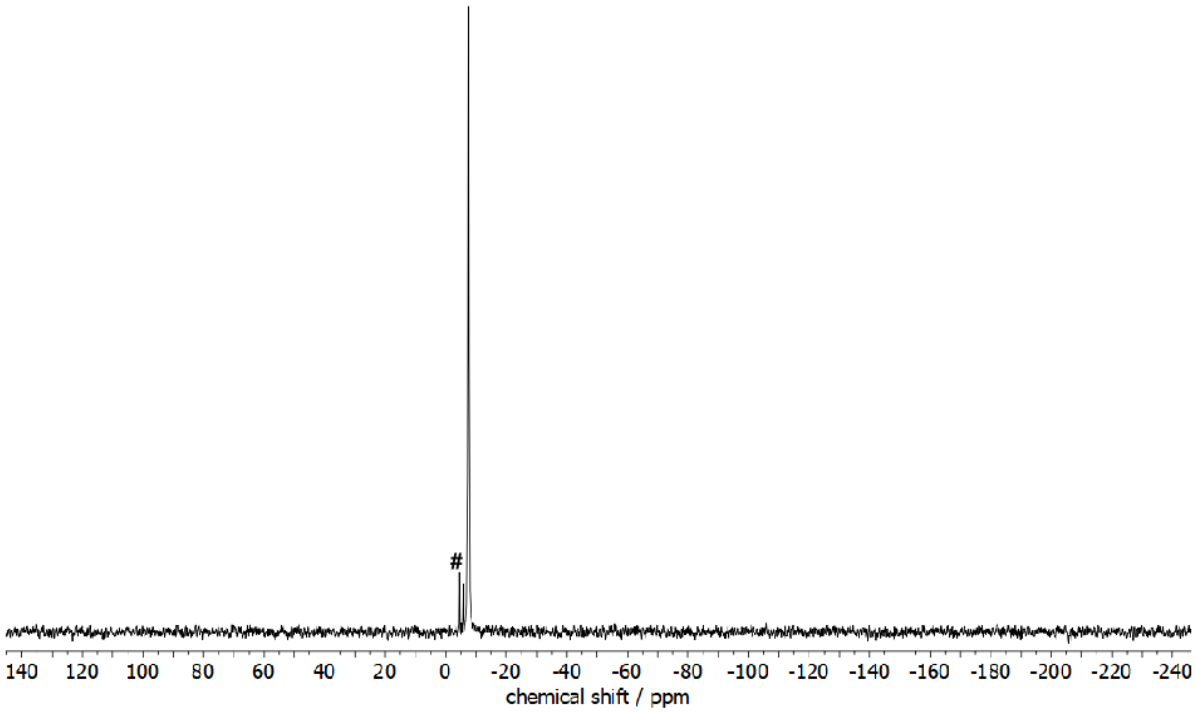

Figure S50: $^{31}P\{^{1}H\}$ NMR spectrum (C_6D_6) of **3b·AlCl$_3$** (**#** free ligand).

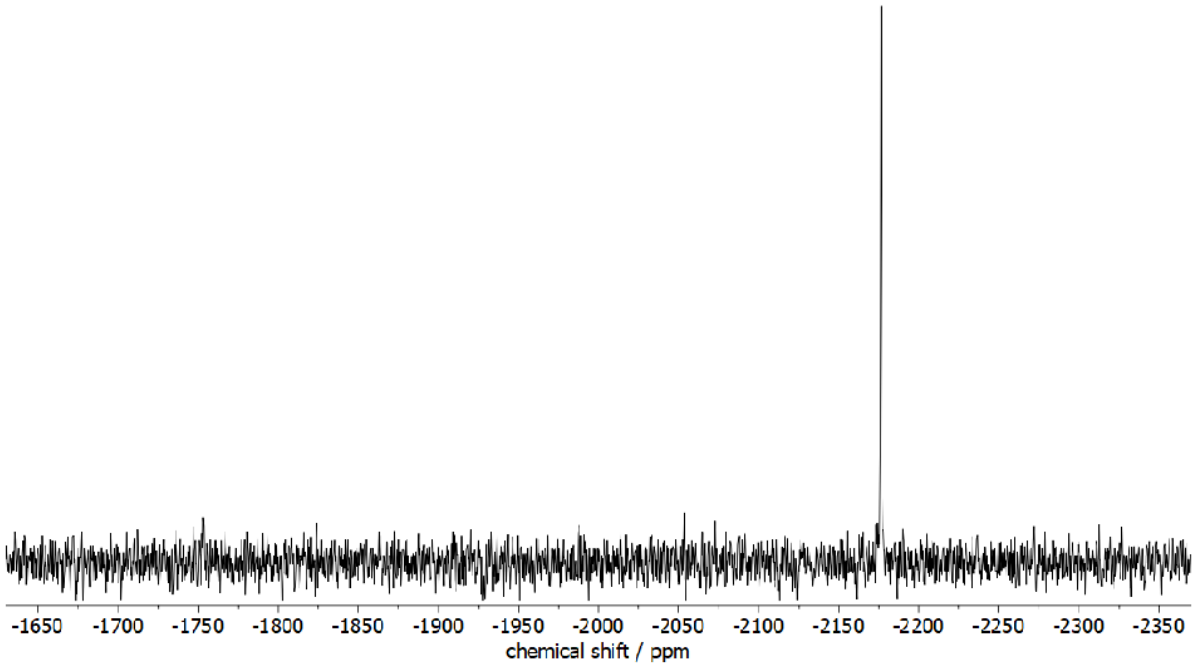

Figure S51: $^{119}Sn\{^{1}H\}$ NMR spectrum (C_6D_6) of **3b**·**AlCl$_3$**.

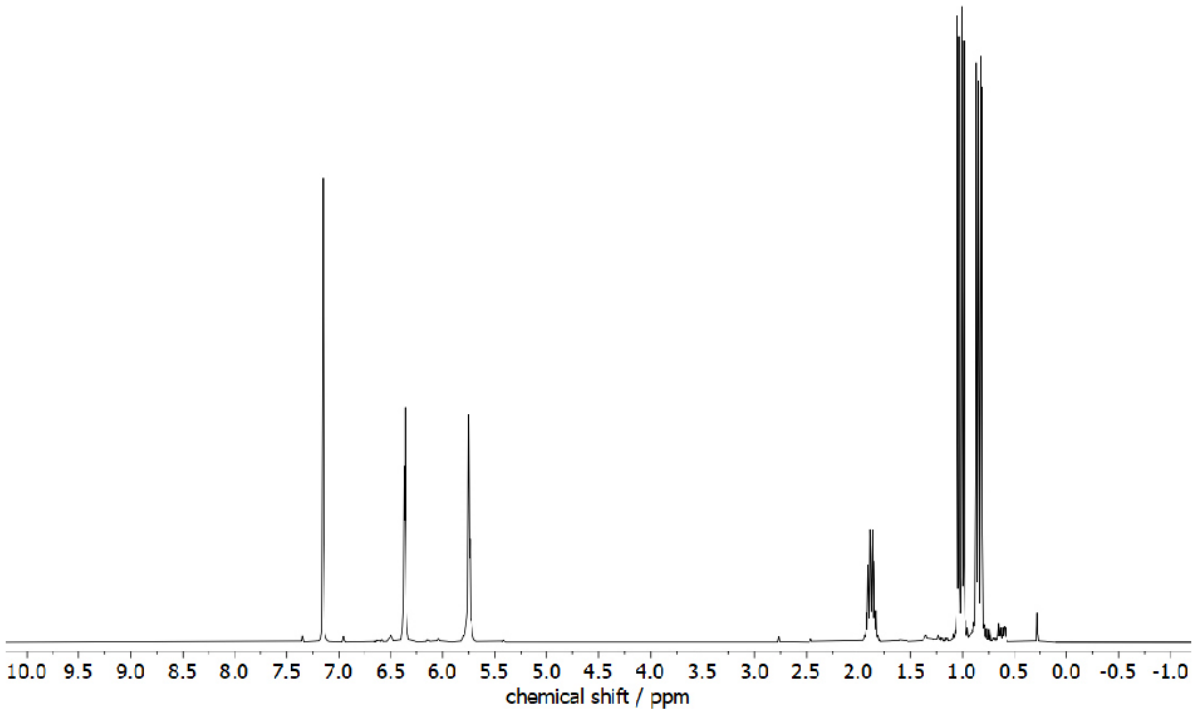

Figure S52: ^{1}H NMR spectrum (C_6D_6) of **3b**·**(AlCl$_3$)$_2$**.

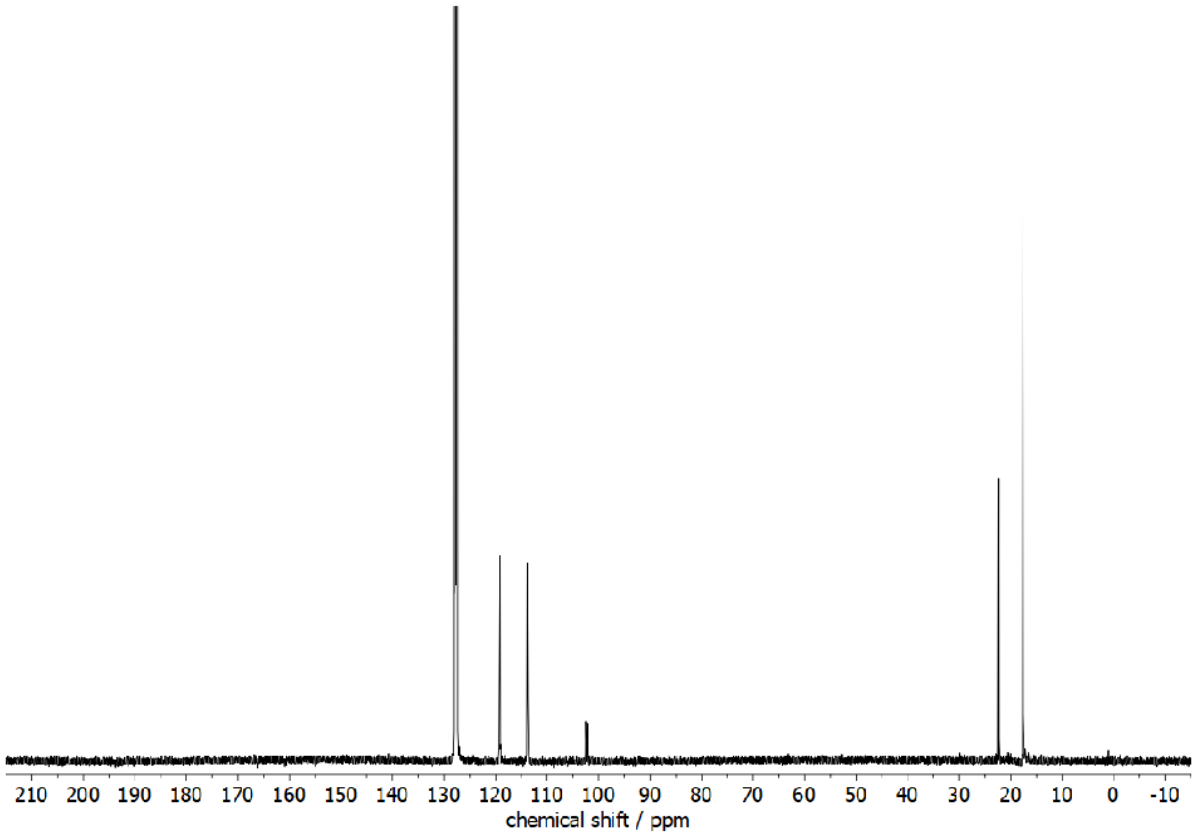

Figure S53: $^{13}C\{^{1}H\}$ NMR spectrum (C_6D_6) of **3b**·$(AlCl_3)_2$.

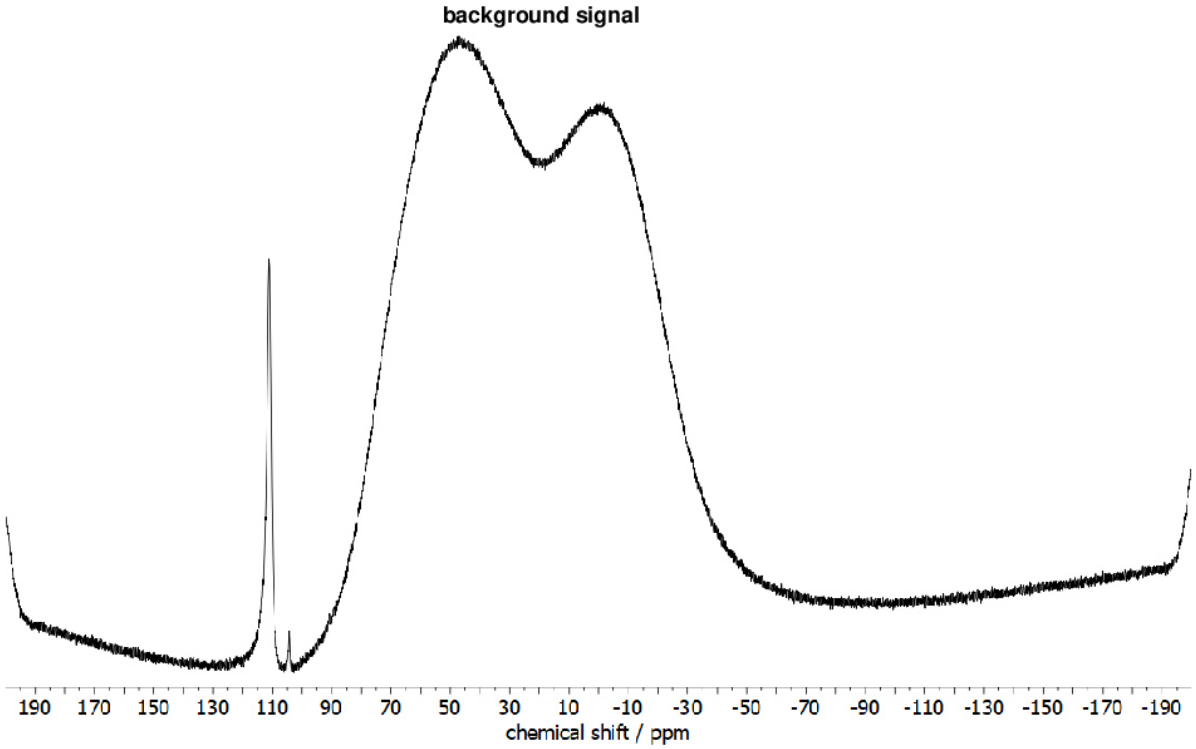

Figure S54: $^{27}Al\{^{1}H\}$ NMR spectrum (C_6D_6) of **3b**·$(AlCl_3)_2$.

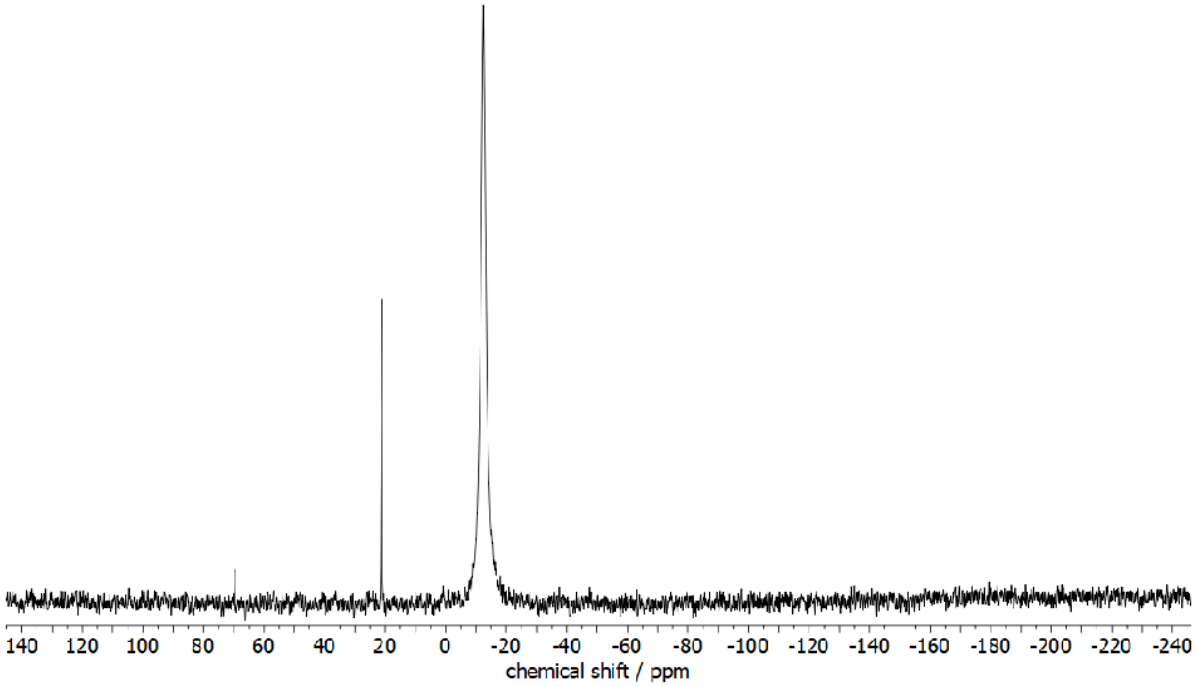

Figure S55: $^{31}P\{^{1}H\}$ NMR spectrum (C_6D_6) of **3b**·$(AlCl_3)_2$.

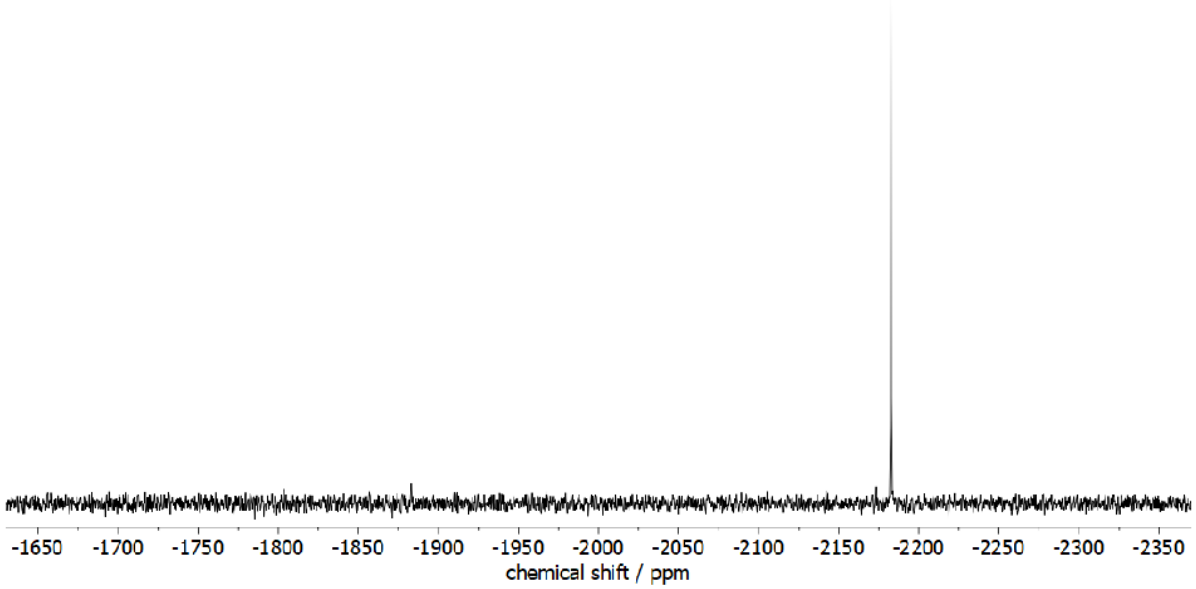

Figure S56: $^{119}Sn\{^{1}H\}$ NMR spectrum (C_6D_6) of **3b**·$(AlCl_3)_2$.

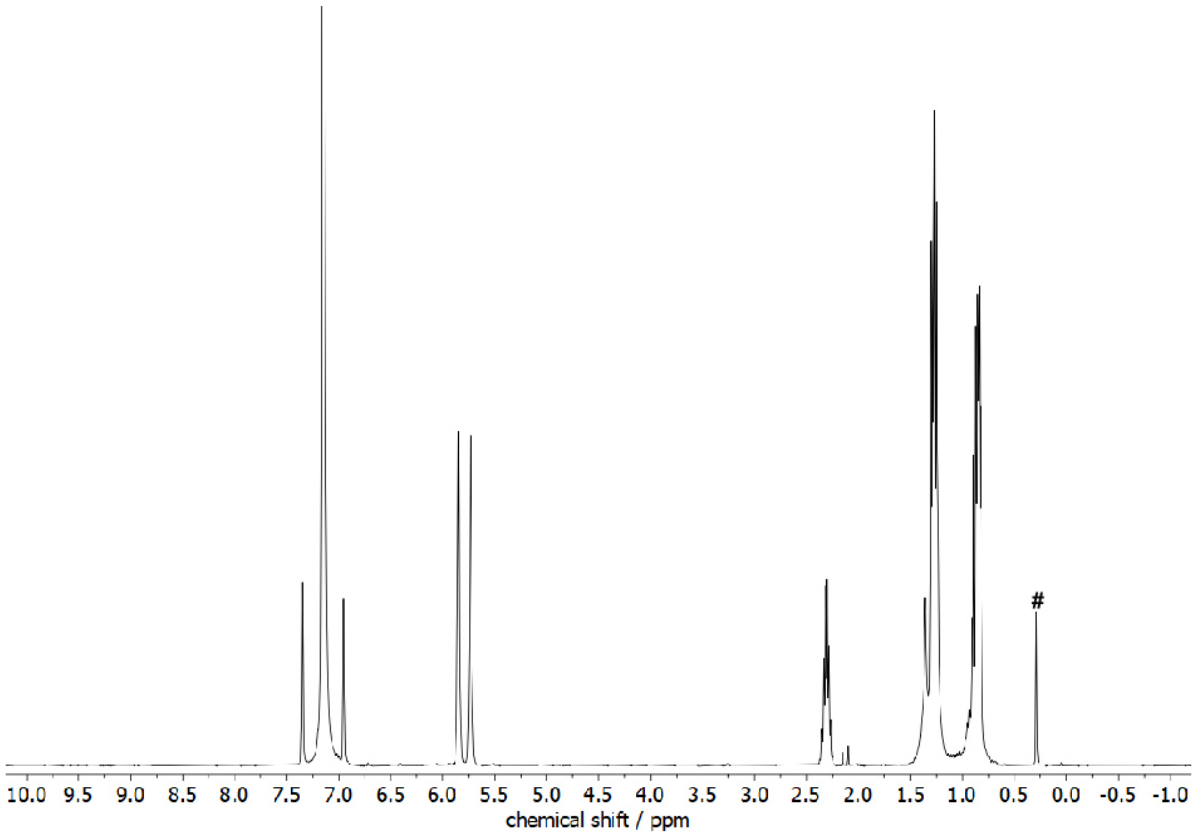

Figure S57: ^{1}H NMR spectrum (C_6D_6) of **3b·W(CO)$_4$** (**#** silicon grease).

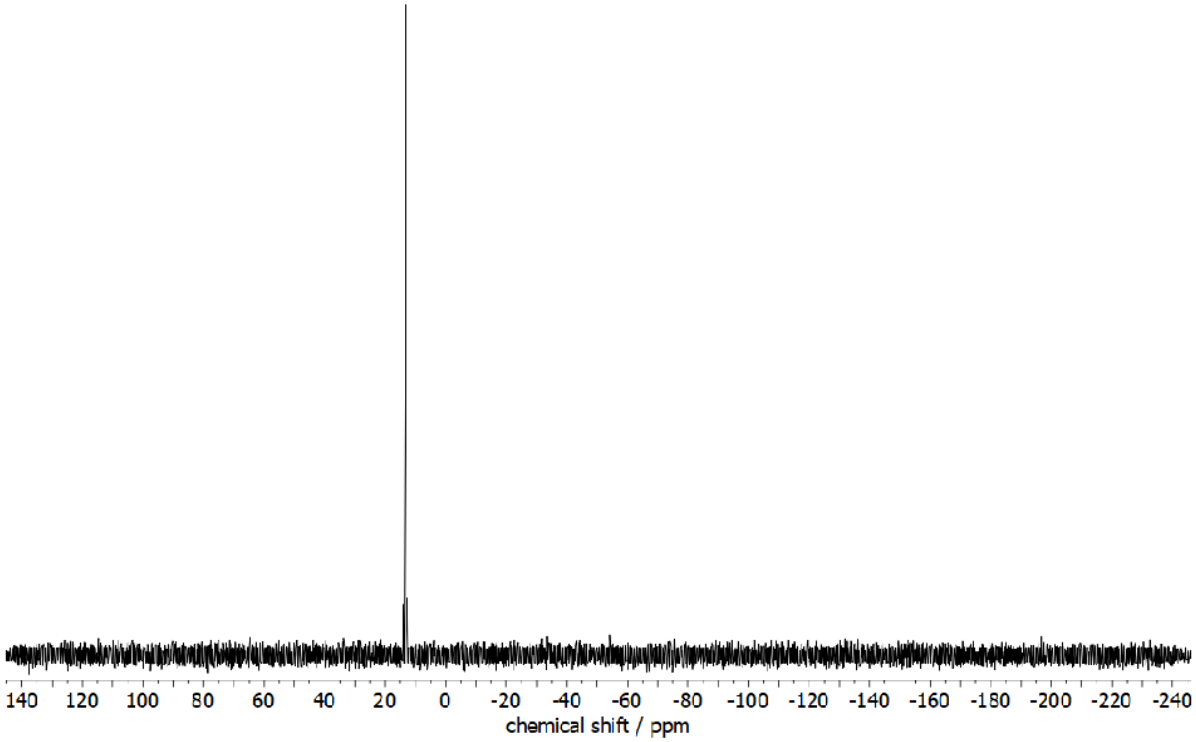

Figure S58: ^{31}P{^{1}H} NMR spectrum (C_6D_6) of **3b·W(CO)$_4$**.

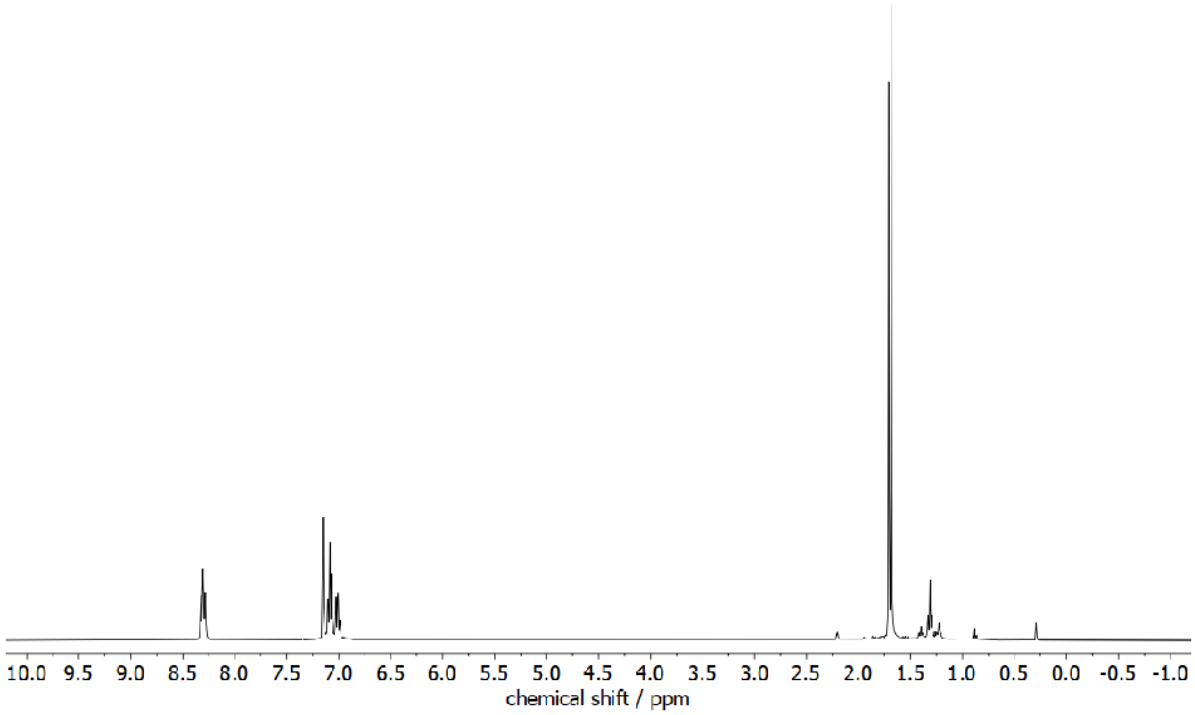

Figure S59: ^{1}H NMR spectrum (C_6D_6) of **2·PtMe$_2$**.

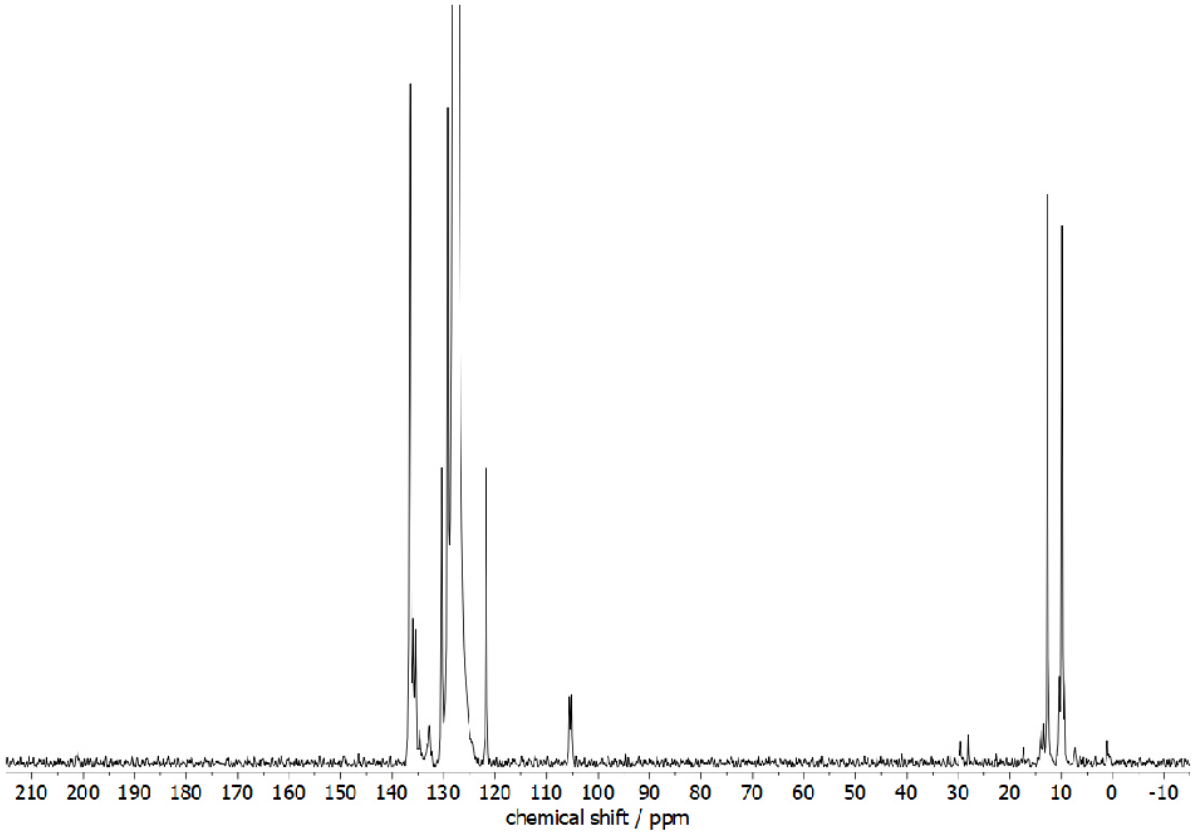

Figure S60: ^{13}C{^{1}H} NMR spectrum (C_6D_6) of **2·PtMe$_2$**.

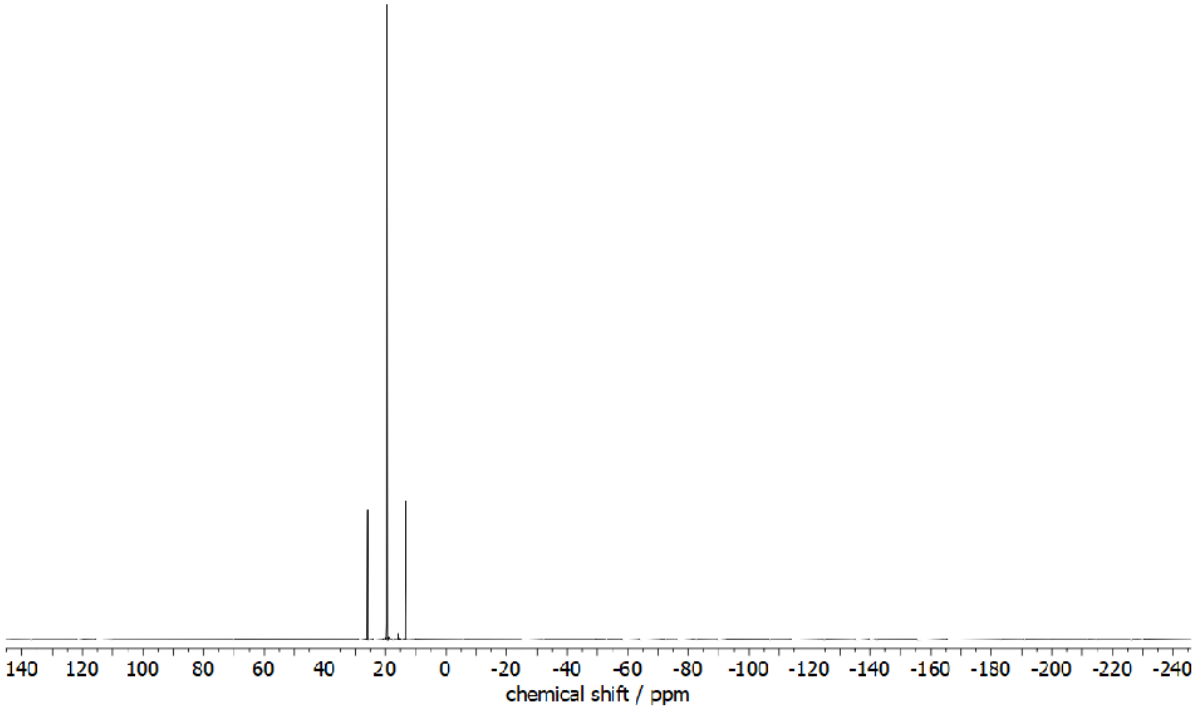

Figure S61: $^{31}P\{^{1}H\}$ NMR spectrum (C_6D_6) of **2·PtMe$_2$**.

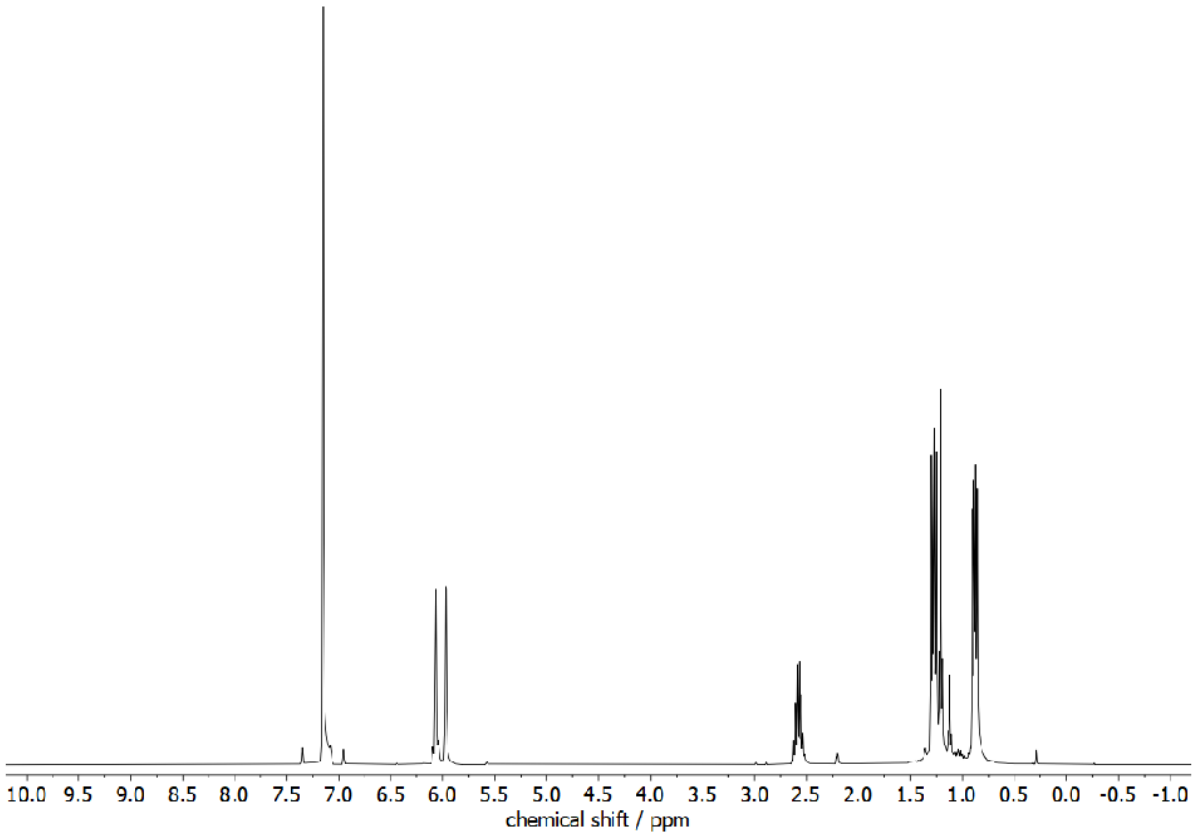

Figure S62: ^{1}H NMR spectrum (C_6D_6) of **3b·PtMe$_2$**.

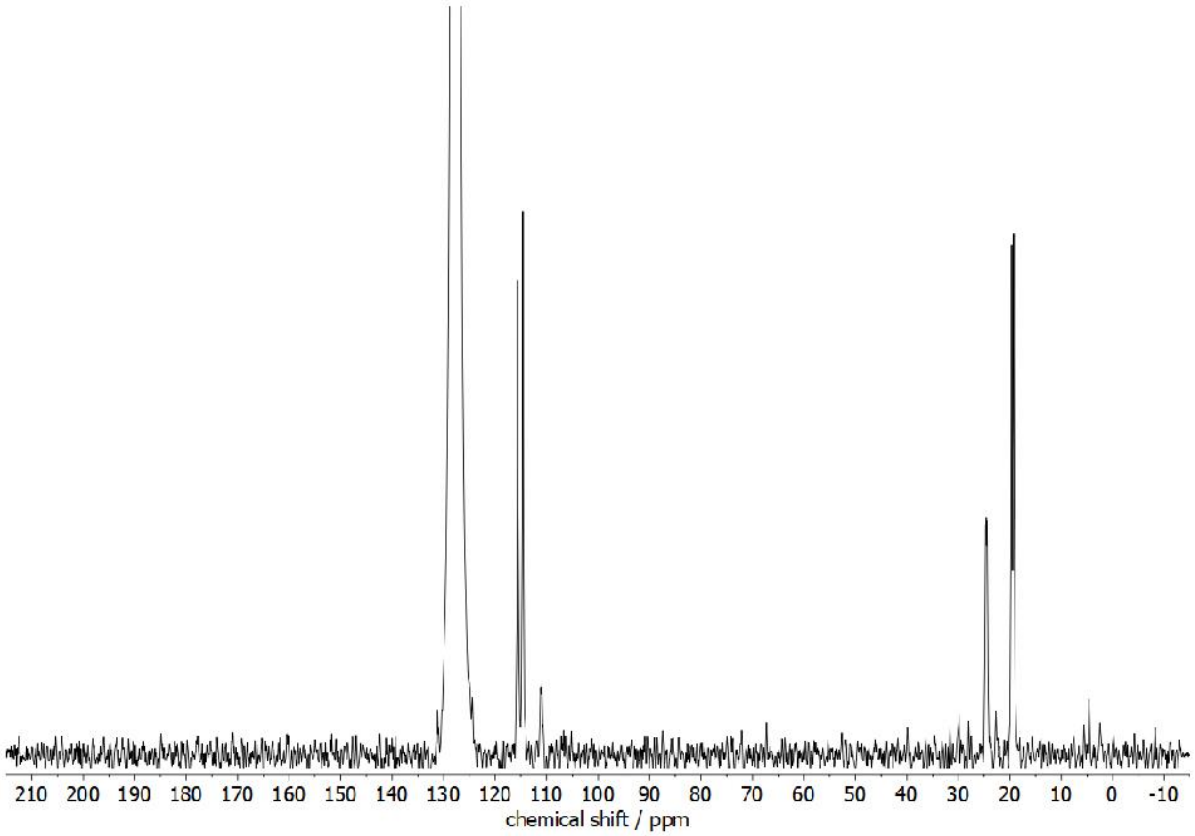

Figure S63: $^{13}C\{^{1}H\}$ NMR spectrum (C_6D_6) of **3b·PtMe$_2$**.

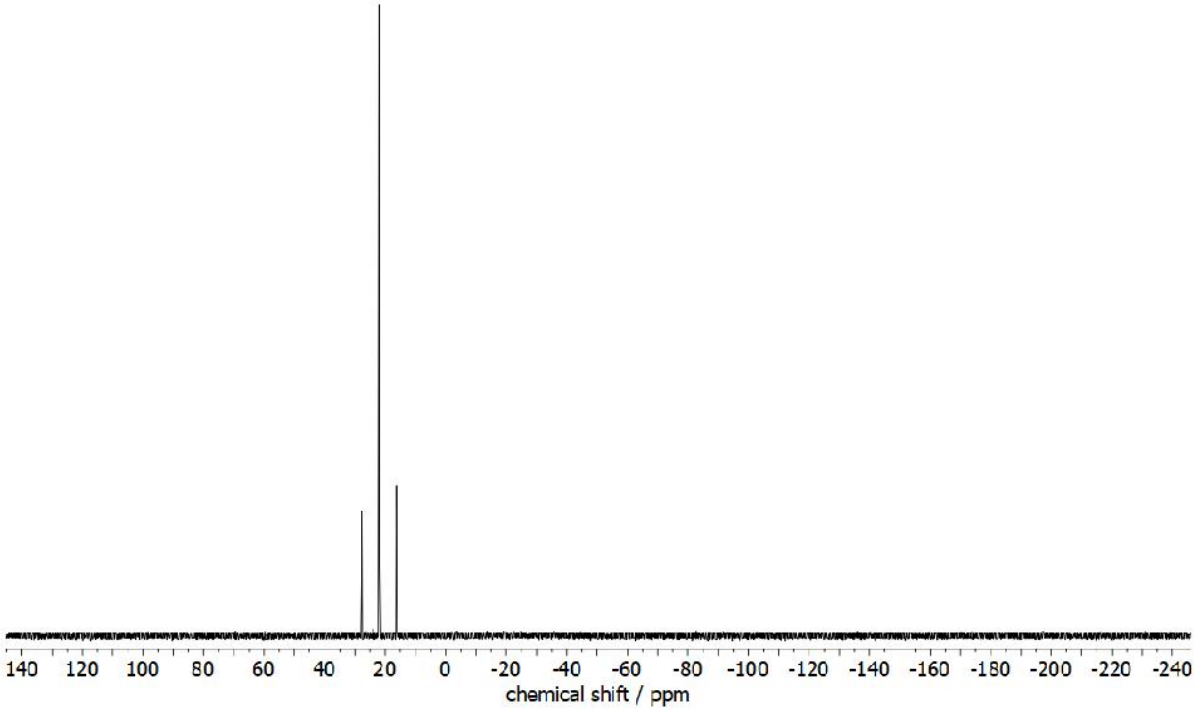

Figure S64: $^{31}P\{^{1}H\}$ NMR spectrum (C_6D_6) of **3b·PtMe$_2$**.

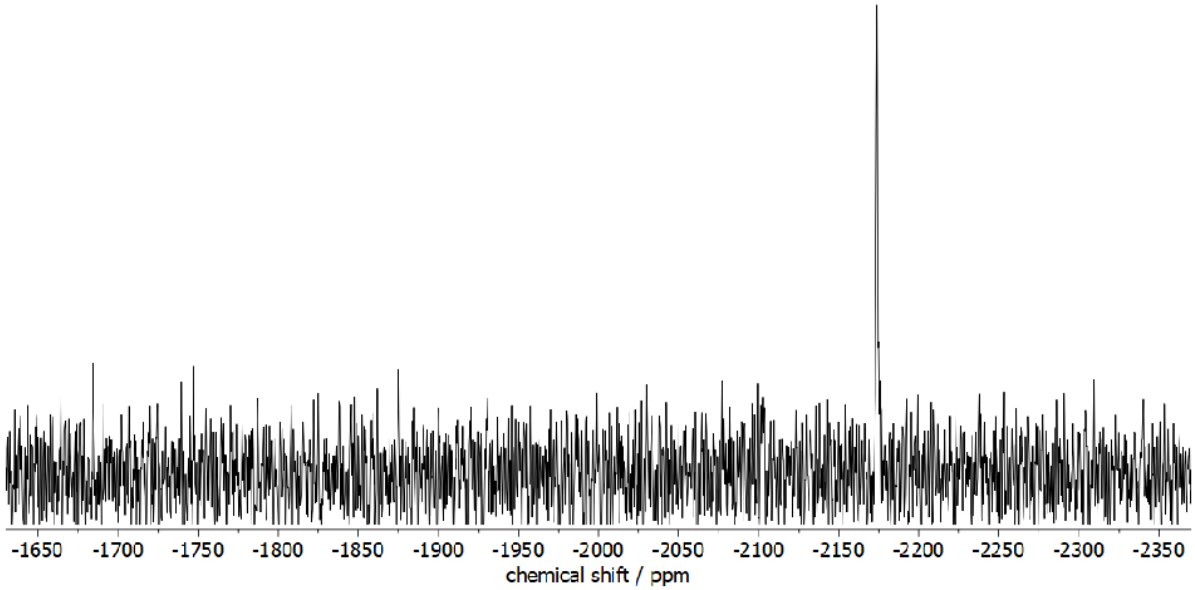

Figure S65: $^{119}Sn\{^{1}H\}$ NMR spectrum (C_6D_6) of **3b**·**PtMe$_2$**.

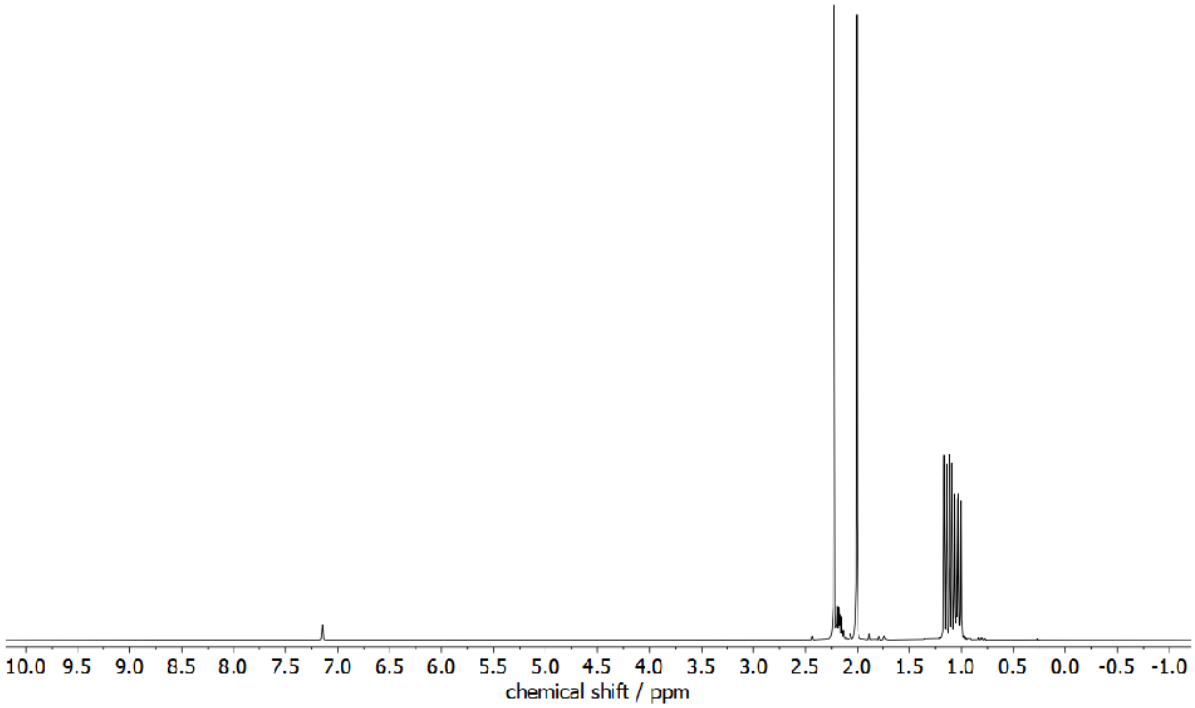

Figure S66: ^{1}H NMR spectrum (C_6D_6) of **5a**.

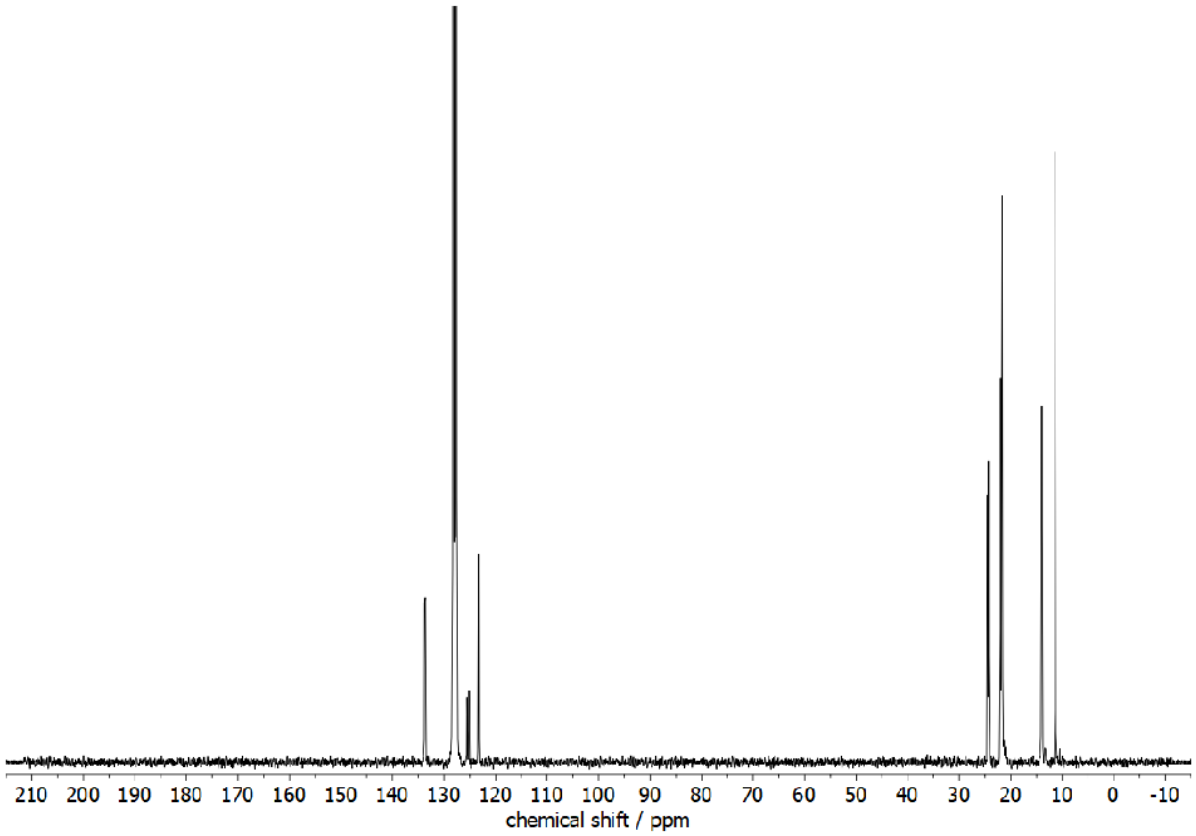

Figure S67: $^{13}C\{^{1}H\}$ NMR spectrum (C_6D_6) of **5a**.

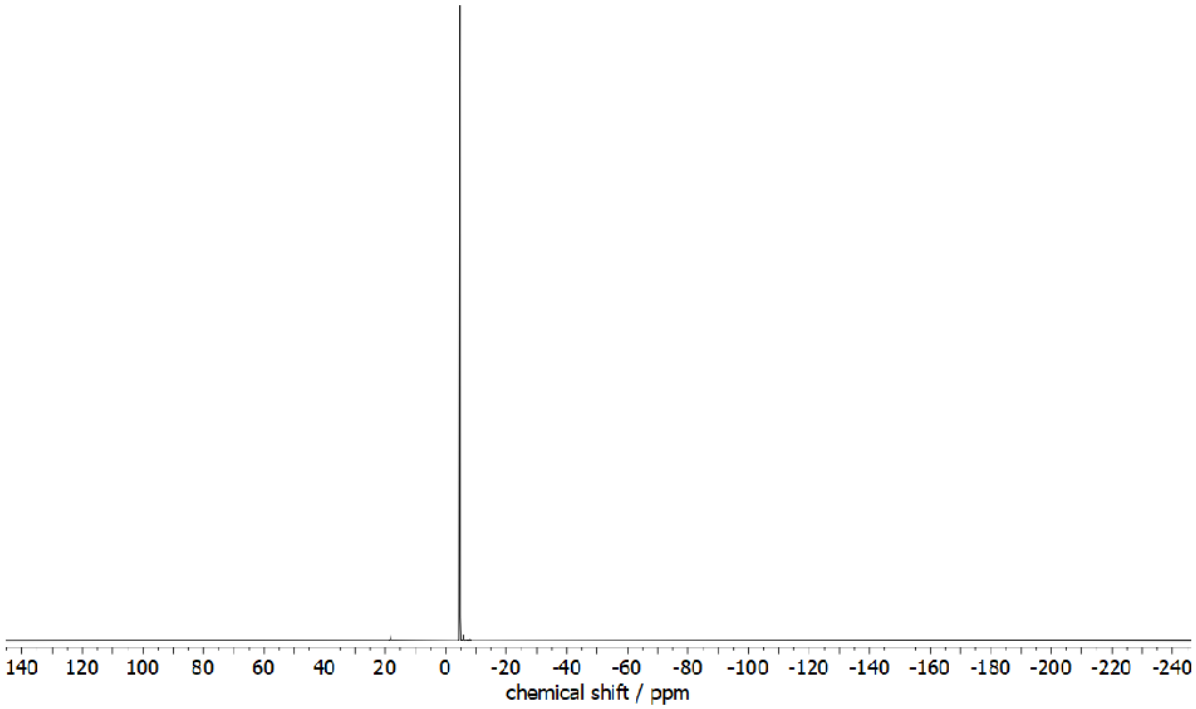

Figure S68: $^{31}P\{^{1}H\}$ NMR spectrum (C_6D_6) of **5a**.

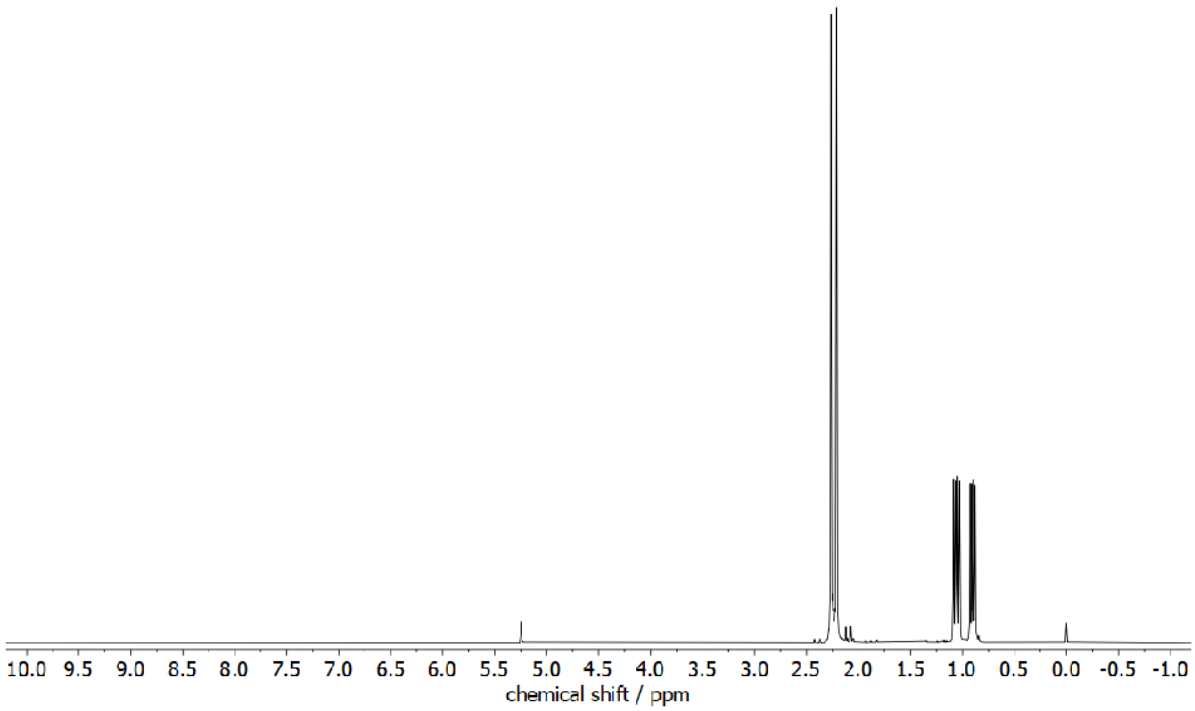

Figure S69: ^{1}H NMR spectrum (CD_2Cl_2) of **5b[$AlCl_4$]**.

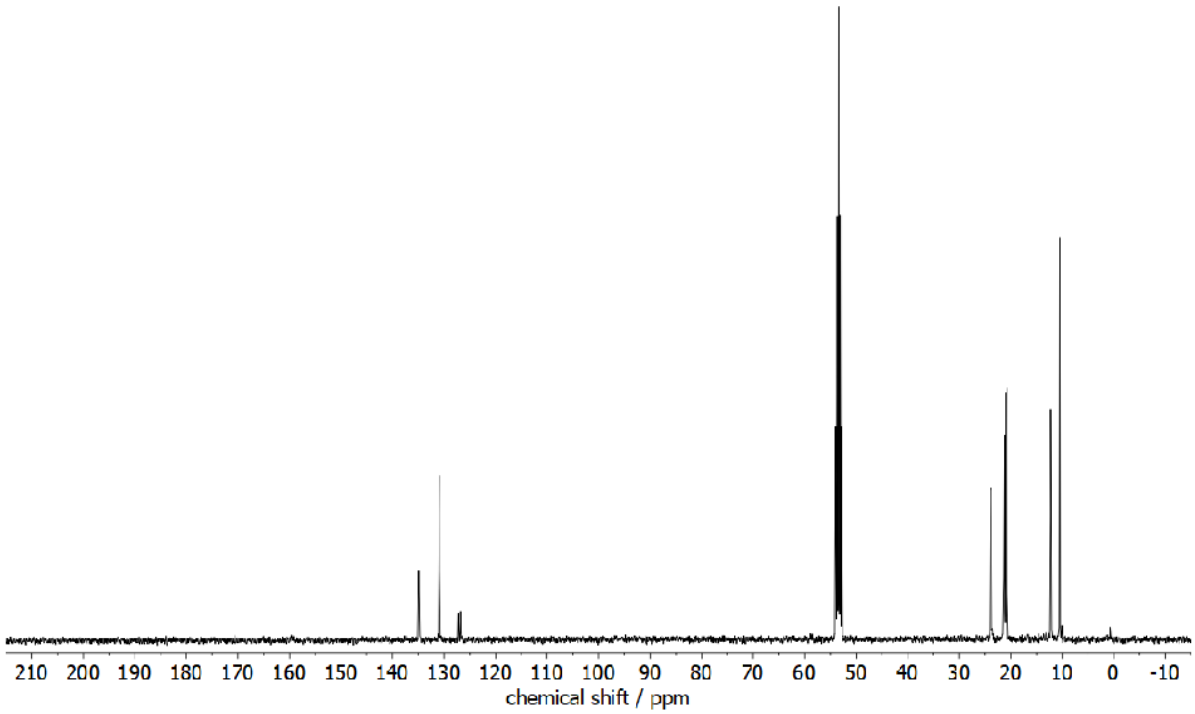

Figure S70: ^{13}C NMR spectrum (CD_2Cl_2) of **5b[$AlCl_4$]**.

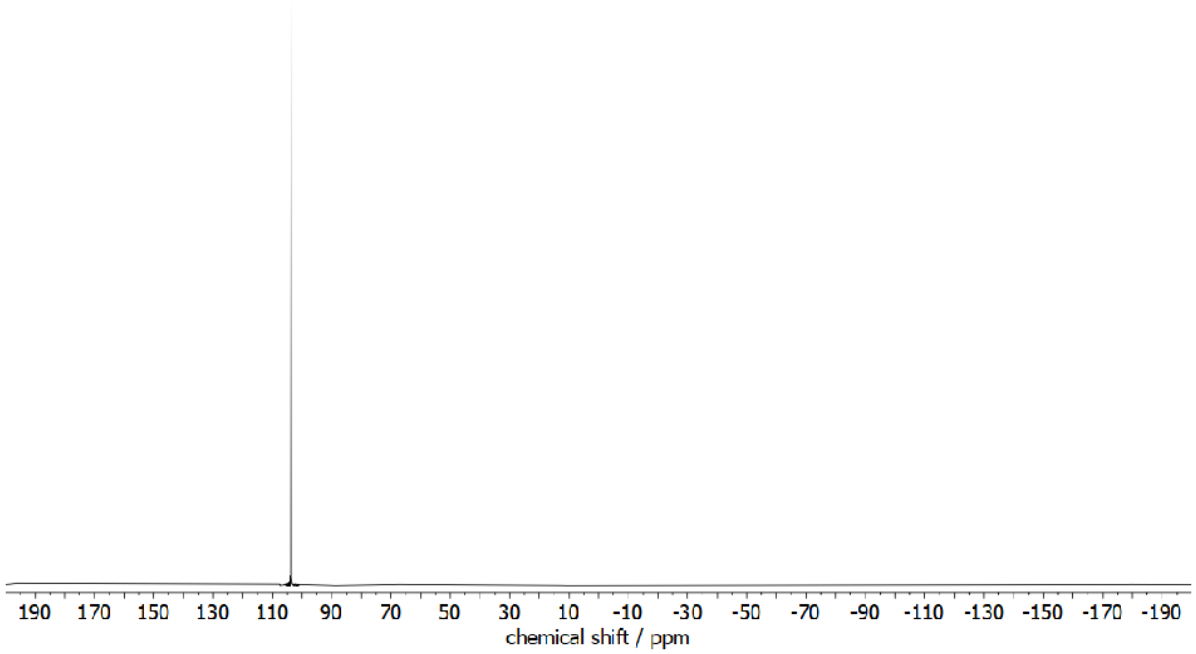

Figure S71: ^{27}Al NMR spectrum (CD_2Cl_2) of **5b[AlCl$_4$]**.

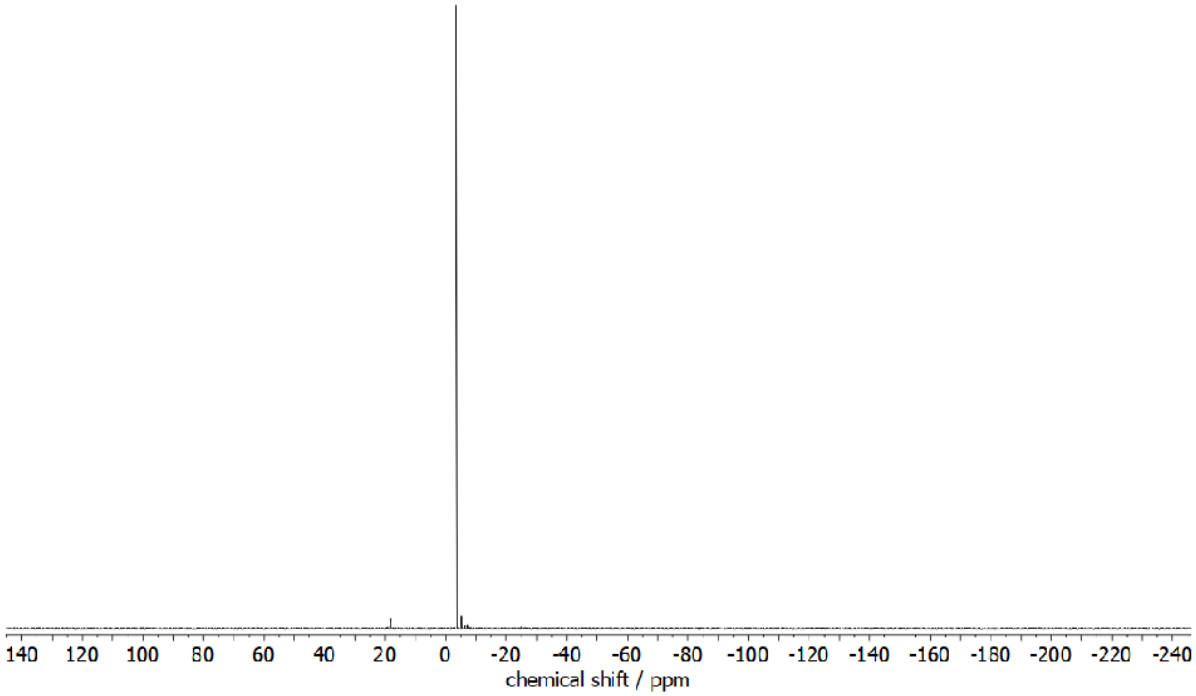

Figure S72: ^{31}P NMR spectrum (CD_2Cl_2) of **5b[AlCl$_4$]**.

IR Spectra

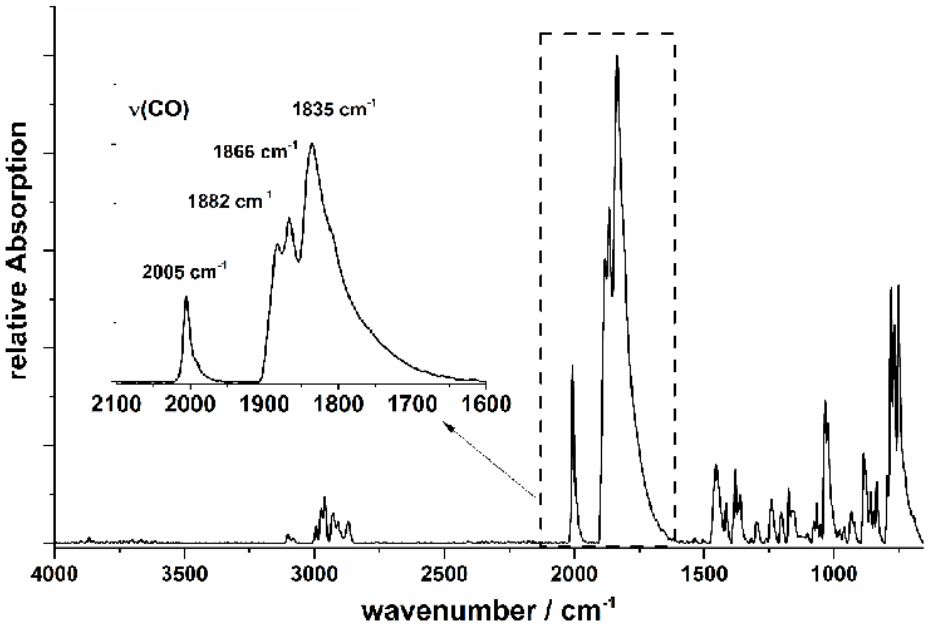

Figure S73: FT-IR spectrum of **3b**·**W(CO)$_4$**.

SUPPORTING INFORMATION

XRD Data

All crystal structure data has been deposited with the Cambridge Crystallographic Data Centre (CCDC) and is available free of charge from the Cambridge Structural Database (see CCDC numbers).

Crystallographic Data for 1a:

CCDC Deposition Number	2038366	
Empirical formula	$C_{30}H_{52}MgP_2$	
Formula weight	498.96	
Temperature	142(2) K	
Wavelength	0.71073 Å	
Crystal system	Monoclinic	
Space group	*C*2/*c*	
Unit cell dimensions	*a* = 21.242(2) Å	α = 90°
	b = 12.0950(10) Å	β = 127.683(4)°
	c = 14.8847(18) Å	γ = 90°
Volume	3026.5(6) $Å^3$	
Z	4	
Density (calculated)	1.095 mg/m^3	
Absorption coefficient	0.180 mm^{-1}	
F(000)	1096	
Crystal size	0.524 x 0.148 x 0.108 mm^3	
Theta range for data collection	2.074 to 35.964°	
Index ranges	-34<=h<=34, -19<=k<=19, -23<=l<=24	
Reflections collected	41938	
Independent reflections	7099 [R(int) = 0.0538]	
Completeness to theta = 25.242°	100.0%	
Absorption correction	Semi-empirical from equivalents	
Max. and min. transmission	0.7470 and 0.7231	
Refinement method	Full-matrix least-squares on F^2	
Data / restraints / parameters	7099 / 0 / 243	
Goodness-of-fit on F^2	1.036	
Final R indices [I>2sigma(I)]	R1 = 0.0407, wR2 = 0.0969	
R indices (all data)	R1 = 0.0703, wR2 = 0.1114	
Extinction coefficient	n/a	
Largest diff. peak and hole	0.448 and -0.243 $e.Å^{-3}$	

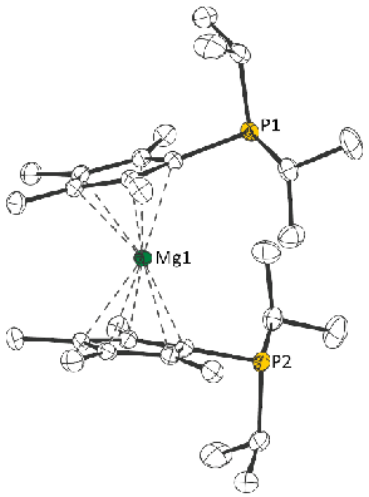

Figure S74: Molecular structure of **1a** in the crystal (displacement ellipsoids at 50% probability level; hydrogen atoms omitted for clarity).

Crystallographic Data for 1b:

CCDC Deposition Number	2038363	
Empirical formula	$C_{22}H_{36}MgP_2$	
Formula weight	386.76	
Temperature	142(2) K	
Wavelength	0.71073 Å	
Crystal system	Monoclinic	
Space group	$P2_1$	
Unit cell dimensions	a = 8.1023(5) Å	α = 90°
	b = 19.2544(11) Å	β = 101.982(3)°
	c = 14.7664(8) Å	γ = 90°
Volume	2253.4(2) $Å^3$	
Z	4	
Density (calculated)	1.140 mg/m^3	
Absorption coefficient	0.224 mm^{-1}	
F(000)	840	
Crystal size	0.328 x 0.189 x 0.126 mm^3	
Theta range for data collection	1.410 to 27.122°	
Index ranges	-10<=h<=10, -24<=k<=19, -17<=l<=18	
Reflections collected	19997	
Independent reflections	9035 [R(int) = 0.0323]	
Completeness to theta = 25.242°	100.0%	
Absorption correction	Semi-empirical from equivalents	
Max. and min. transmission	0.7455 and 0.6581	
Refinement method	Full-matrix least-squares on F^2	
Data / restraints / parameters	9035 / 1 / 467	
Goodness-of-fit on F^2	1.028	
Final R indices [I>2sigma(I)]	R1 = 0.0394, wR2 = 0.0863	
R indices (all data)	R1 = 0.0495, wR2 = 0.0909	
Absolute structure parameter	-0.03(4)	
Extinction coefficient	n/a	
Largest diff. peak and hole	0.317 and -0.206 $e.Å^{-3}$	

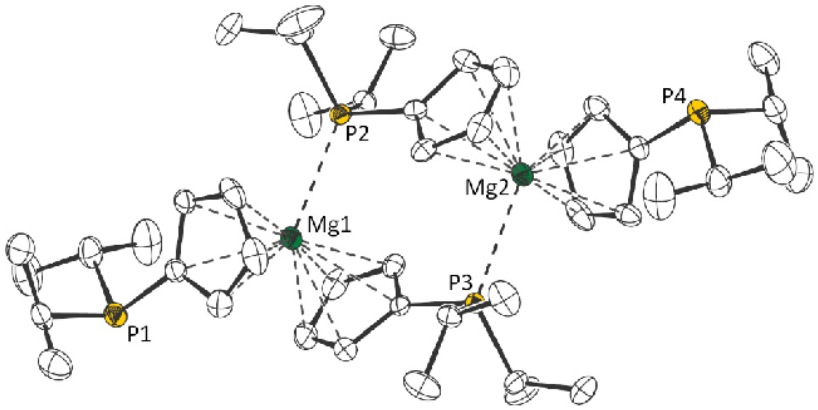

Figure S75: Dimeric structure of **1b** in the crystal (displacement ellipsoids at 50% probability level; hydrogen atoms omitted for clarity).

SUPPORTING INFORMATION

Crystallographic Data for 1c:

CCDC Deposition Number	2038368	
Empirical formula	$C_{42}H_{44}MgP_2$	
Formula weight	635.02	
Temperature	132(2) K	
Wavelength	0.71073 Å	
Crystal system	Monoclinic	
Space group	$P2_1/c$	
Unit cell dimensions	a = 9.440(2) Å	α = 90°
	b = 18.344(3) Å	β = 101.269(6)°
	c = 20.856(4) Å	γ = 90°
Volume	3542.1(12) $Å^3$	
Z	4	
Density (calculated)	1.191 mg/m^3	
Absorption coefficient	0.169 mm^{-1}	
F(000)	1352	
Crystal size	0.300 x 0.169 x 0.052 mm^3	
Theta range for data collection	1.491 to 27.122°	
Index ranges	-11<=h<=12, -20<=k<=23, -26<=l<=23	
Reflections collected	47764	
Independent reflections	7808 [R(int) = 0.0904]	
Completeness to theta = 25.242°	100.0%	
Absorption correction	Semi-empirical from equivalents	
Max. and min. transmission	0.7455 and 0.7153	
Refinement method	Full-matrix least-squares on F^2	
Data / restraints / parameters	7808 / 0 / 570	
Goodness-of-fit on F^2	1.027	
Final R indices [I>2sigma(I)]	R1 = 0.0562, wR2 = 0.1014	
R indices (all data)	R1 = 0.1164, wR2 = 0.1214	
Extinction coefficient	n/a	
Largest diff. peak and hole	0.334 and -0.330 $e.Å^{-3}$	

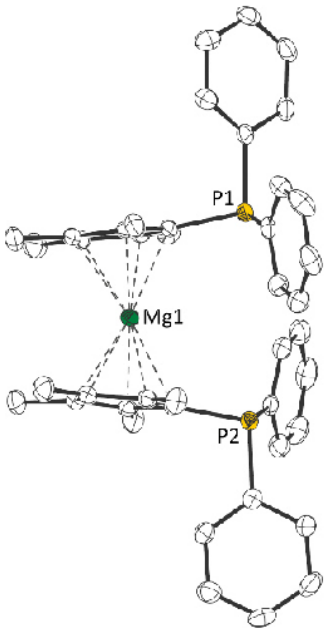

Figure S76: Molecular structure of **1c** in the crystal (displacement ellipsoids at 50% probability level; hydrogen atoms omitted for clarity).

Crystallographic Data for 1b·(thf)$_2$:

CCDC Deposition Number	2038378	
Empirical formula	$C_{30}H_{52}MgO_2P_2$	
Formula weight	530.96	
Temperature	123(2) K	
Wavelength	0.71073 Å	
Crystal system	Triclinic	
Space group	*P*-1	
Unit cell dimensions	*a* = 8.2993(7) Å	α = 73.767(5)°
	b = 13.2758(14) Å	β = 79.572(3)°
	c = 15.5398(14) Å	γ = 71.800(3)°
Volume	1553.4(3) Å^3	
Z	2	
Density (calculated)	1.135 mg/m^3	
Absorption coefficient	0.184 mm^{-1}	
F(000)	580	
Crystal size	0.228 x 0.132 x 0.117 mm^3	
Theta range for data collection	2.395 to 31.689°	
Index ranges	-12<=h<=11, -19<=k<=19, -22<=l<=21	
Reflections collected	36192	
Independent reflections	10352 [R(int) = 0.0459]	
Completeness to theta = 25.242°	99.5%	
Absorption correction	Semi-empirical from equivalents	
Max. and min. transmission	0.7462 and 0.6220	
Refinement method	Full-matrix least-squares on F^2	
Data / restraints / parameters	10352 / 103 / 513	
Goodness-of-fit on F^2	0.961	
Final R indices [I>2sigma(I)]	R1 = 0.0456, wR2 = 0.1130	
R indices (all data)	R1 = 0.0647, wR2 = 0.1262	
Extinction coefficient	n/a	
Largest diff. peak and hole	0.442 and -0.513 e.Å^{-3}	

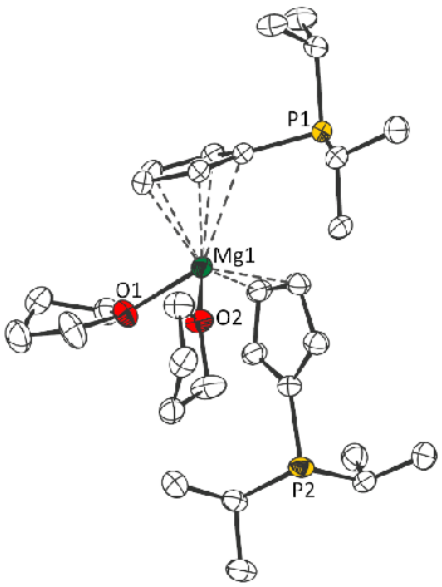

Figure S77: Molecular structure of **1b·(thf)$_2$** in the crystal (displacement ellipsoids at 50% probability level; hydrogen atoms omitted for clarity).

Crystallographic Data for 1b·$(CS_2)_2$:

CCDC Deposition Number	2047150	
Empirical formula	$C_{24}H_{36}MgP_2S_4$	
Formula weight	539.02	
Temperature	133(2) K	
Wavelength	0.71073 Å	
Crystal system	Monoclinic	
Space group	*C*2/*c*	
Unit cell dimensions	*a* = 17.7450(19) Å	α = 90°
	b = 7.1613(6) Å	β = 93.896(6)°
	c = 21.524(2) Å	γ = 90°
Volume	2728.9(5) $Å^3$	
Z	4	
Density (calculated)	1.312 Mg/m^3	
Absorption coefficient	0.500 mm^{-1}	
F(000)	1144	
Crystal size	0.129 x 0.115 x 0.051 mm^3	
Theta range for data collection	2.301 to 26.998°	
Index ranges	-22<=h<=22, -9<=k<=9, -26<=l<=27	
Reflections collected	22873	
Independent reflections	2974 [R(int) = 0.1140]	
Completeness to theta = 25.242°	99.9 %	
Absorption correction	Semi-empirical from equivalents	
Max. and min. transmission	0.7456 and 0.6693	
Refinement method	Full-matrix least-squares on F^2	
Data / restraints / parameters	2974 / 360 / 282	
Goodness-of-fit on F^2	1.073	
Final R indices [I>2sigma(I)]	R1 = 0.0598, wR2 = 0.1249	
R indices (all data)	R1 = 0.1089, wR2 = 0.1532	
Extinction coefficient	0.0022(4)	
Largest diff. peak and hole	0.309 and -0.344 e.$Å^{-3}$	

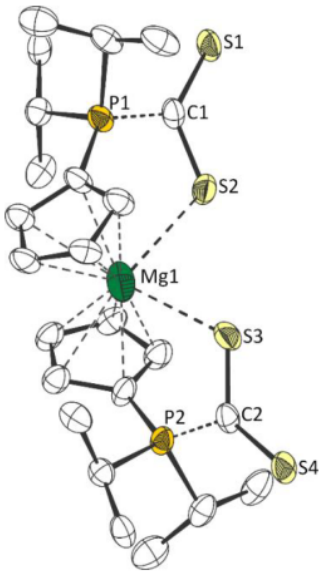

Figure S78: Molecular structure of **1b·$(CS_2)_2$** in the crystal (displacement ellipsoids at 50% probability level; hydrogen atoms omitted for clarity).

Crystallographic Data for 1b·PhNCO:

CCDC Deposition Number	2038377	
Empirical formula	$C_{58}H_{82}Mg_2N_2O_2P_4$; C_7H_8	
Formula weight	1103.88	
Temperature	130(2) K	
Wavelength	0.71073 Å	
Crystal system	Monoclinic	
Space group	$P2_1/c$	
Unit cell dimensions	a = 14.6917(4) Å	α = 90°
	b = 13.3220(4) Å	β = 105.9850(10)°
	c = 16.3497(5) Å	γ = 90°
Volume	3076.28(16) Å^3	
Z	2	
Density (calculated)	1.192 mg/m^3	
Absorption coefficient	0.187 mm^{-1}	
F(000)	1188	
Crystal size	0.487 x 0.077 x 0.039 mm^3	
Theta range for data collection	2.004 to 27.904°	
Index ranges	-19<=h<=19, -17<=k<=17, -21<=l<=21	
Reflections collected	66288	
Independent reflections	7352 [R(int) = 0.0954]	
Completeness to theta = 25.242°	100.0%	
Absorption correction	Semi-empirical from equivalents	
Max. and min. transmission	0.7456 and 0.6925	
Refinement method	Full-matrix least-squares on F^2	
Data / restraints / parameters	7352 / 231 / 449	
Goodness-of-fit on F^2	1.026	
Final R indices [I>2sigma(I)]	R1 = 0.0492, wR2 = 0.1157	
R indices (all data)	R1 = 0.0733, wR2 = 0.1317	
Extinction coefficient	n/a	
Largest diff. peak and hole	0.358 and -0.382 e.Å^{-3}	

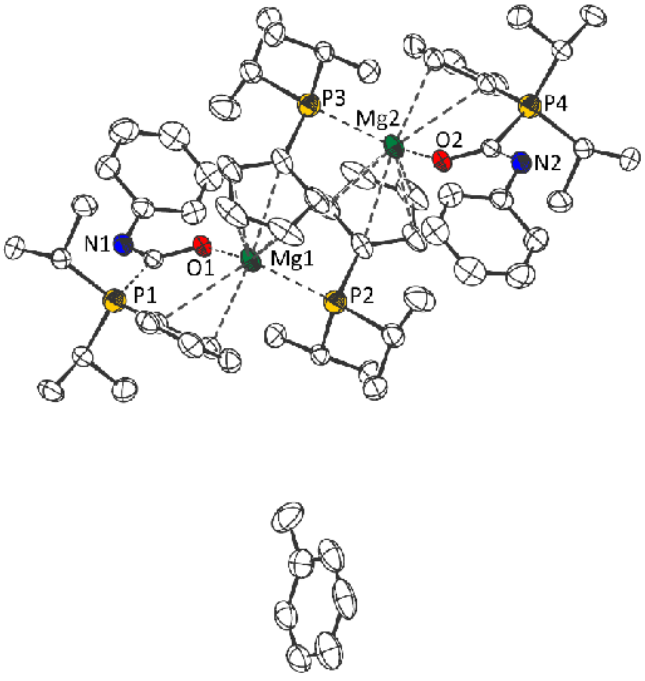

Figure S79: Dimeric structure of **1b·PhNCO** in the crystal (displacement ellipsoids at 50% probability level; hydrogen atoms omitted for clarity).

SUPPORTING INFORMATION

Crystallographic Data for 1b·Pt(Me)$_2$:

CCDC Deposition Number	2038380	
Empirical formula	$C_{24}H_{42}MgP_2Pt$	
Formula weight	611.91	
Temperature	140(2) K	
Wavelength	0.71073 Å	
Crystal system	Triclinic	
Space group	*P*-1	
Unit cell dimensions	*a* = 8.6607(2) Å	α = 85.2200(10)°
	b = 8.7950(2) Å	β = 81.3300(10)°
	c = 18.2563(4) Å	γ = 65.8940(10)°
Volume	1254.46(5) Å^3	
Z	2	
Density (calculated)	1.620 mg/m^3	
Absorption coefficient	5.753 mm^{-1}	
F(000)	612	
Crystal size	0.208 x 0.194 x 0.034 mm^3	
Theta range for data collection	2.598 to 29.658°	
Index ranges	-12<=h<=12, -12<=k<=10, -25<=l<=25	
Reflections collected	41388	
Independent reflections	7054 [R(int) = 0.0285]	
Completeness to theta = 25.242°	99.7%	
Absorption correction	Semi-empirical from equivalents	
Max. and min. transmission	0.7459 and 0.5876	
Refinement method	Full-matrix least-squares on F^2	
Data / restraints / parameters	7054 / 0 / 263	
Goodness-of-fit on F^2	1.061	
Final R indices [I>2sigma(I)]	R1 = 0.0133, wR2 = 0.0321	
R indices (all data)	R1 = 0.0142, wR2 = 0.0325	
Extinction coefficient	n/a	
Largest diff. peak and hole	0.624 and -0.685 e.Å^{-3}	

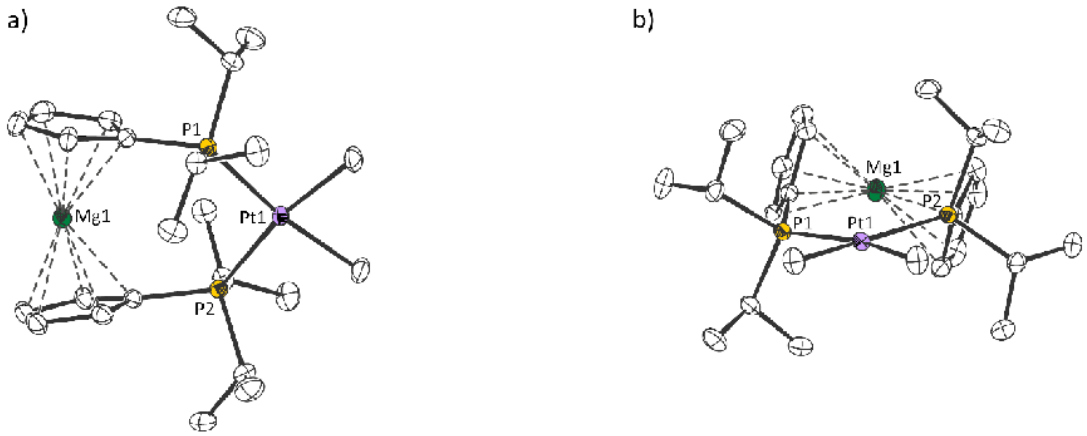

Figure S80: Molecular structure of **1b·Pt(Me)$_2$** in the crystal (a) and b) different viewing angles; displacement ellipsoids at 50% probability level; hydrogen atoms omitted for clarity).

Crystallographic Data for 2:

CCDC Deposition Number	2038372	
Empirical formula	$C_{42}H_{44}GeP_2$	
Formula weight	683.30	
Temperature	152(2) K	
Wavelength	0.71073 Å	
Crystal system	Triclinic	
Space group	*P*-1	
Unit cell dimensions	*a* = 11.7967(8) Å	α = 113.5660(10)°
	b = 13.5338(9) Å	β = 95.109(2)°
	c = 13.9825(9) Å	γ = 114.6170(10)°
Volume	1770.5(2) $Å^3$	
Z	2	
Density (calculated)	1.282 mg/m^3	
Absorption coefficient	0.984 mm^{-1}	
F(000)	716	
Crystal size	0.394 x 0.241 x 0.176 mm^3	
Theta range for data collection	1.669 to 33.267°	
Index ranges	-18<=h<=18, -20<=k<=20, -21<=l<=21	
Reflections collected	107117	
Independent reflections	13604 [R(int) = 0.0461]	
Completeness to theta = 25.242°	100.0%	
Absorption correction	Semi-empirical from equivalents	
Max. and min. transmission	0.7465 and 0.7056	
Refinement method	Full-matrix least-squares on F^2	
Data / restraints / parameters	13604 / 0 / 547	
Goodness-of-fit on F^2	1.047	
Final R indices [I>2sigma(I)]	R1 = 0.0340, wR2 = 0.0815	
R indices (all data)	R1 = 0.0552, wR2 = 0.0922	
Extinction coefficient	n/a	
Largest diff. peak and hole	0.695 and -0.493 e.$Å^{-3}$	

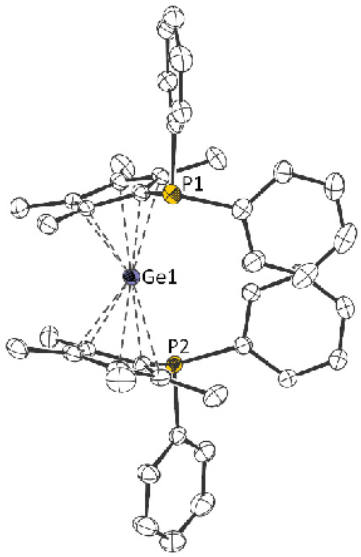

Figure S81: Molecular structure of **2** in the crystal (displacement ellipsoids at 50% probability level; hydrogen atoms omitted for clarity).

SUPPORTING INFORMATION

Crystallographic Data for 3a:

CCDC Deposition Number	2038365	
Empirical formula	$C_{30}H_{52}P_2Sn$	
Formula weight	593.34	
Temperature	132(2) K	
Wavelength	0.71073 Å	
Crystal system	Triclinic	
Space group	*P*-1	
Unit cell dimensions	*a* = 8.5930(5) Å	α = 75.814(2)°
	b = 11.9662(7) Å	β = 78.476(3)°
	c = 15.7849(9) Å	γ = 83.401(3)°
Volume	1538.15(16) $Å^3$	
Z	2	
Density (calculated)	1.281 mg/m^3	
Absorption coefficient	0.950 mm^{-1}	
F(000)	624	
Crystal size	0.526 x 0.326 x 0.168 mm^3	
Theta range for data collection	1.352 to 40.714°	
Index ranges	-15<=h<=14, -21<=k<=21, -28<=l<=25	
Reflections collected	73177	
Independent reflections	19301 [R(int) = 0.0204]	
Completeness to theta = 25.242°	99.7%	
Absorption correction	Semi-empirical from equivalents	
Max. and min. transmission	0.7479 and 0.6792	
Refinement method	Full-matrix least-squares on F^2	
Data / restraints / parameters	19301 / 0 / 498	
Goodness-of-fit on F^2	1.056	
Final R indices [I>2sigma(I)]	R1 = 0.0206, wR2 = 0.0468	
R indices (all data)	R1 = 0.0251, wR2 = 0.0484	
Extinction coefficient	n/a	
Largest diff. peak and hole	0.632 and -0.402 $e.Å^{-3}$	

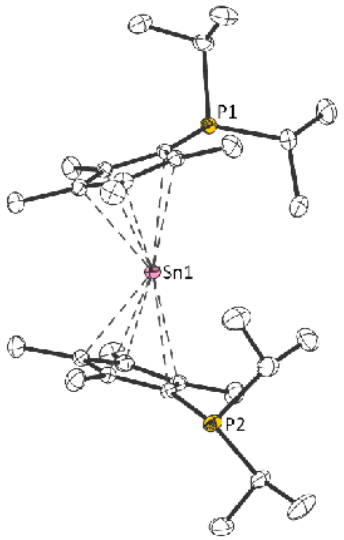

Figure S82: Molecular structure of **3a** in the crystal (displacement ellipsoids at 50% probability level; hydrogen atoms omitted for clarity).

Crystallographic Data for 3b:

CCDC Deposition Number	2038367	
Empirical formula	$C_{22}H_{36}P_2Sn$	
Formula weight	481.14	
Temperature	142(2) K	
Wavelength	0.71073 Å	
Crystal system	Orthorhombic	
Space group	Pbca	
Unit cell dimensions	*a* = 15.5289(9) Å	α = 90°
	b = 10.3010(7) Å	β = 90°
	c = 28.8472(19) Å	γ = 90°
Volume	4614.5(5) $Å^3$	
Z	8	
Density (calculated)	1.385 mg/m^3	
Absorption coefficient	1.249 mm^{-1}	
F(000)	1984	
Crystal size	0.235 x 0.116 x 0.044 mm^3	
Theta range for data collection	1.412 to 27.271°	
Index ranges	-20<=h<=19, -13<=k<=13, -37<=l<=37	
Reflections collected	73167	
Independent reflections	5162 [R(int) = 0.0655]	
Completeness to theta = 25.242°	100.0%	
Absorption correction	Semi-empirical from equivalents	
Max. and min. transmission	0.7455 and 0.6848	
Refinement method	Full-matrix least-squares on F^2	
Data / restraints / parameters	5162 / 0 / 370	
Goodness-of-fit on F^2	1.027	
Final R indices [I>2sigma(I)]	R1 = 0.0259, wR2 = 0.0486	
R indices (all data)	R1 = 0.0454, wR2 = 0.0548	
Extinction coefficient	n/a	
Largest diff. peak and hole	0.359 and -0.377 $e.Å^{-3}$	

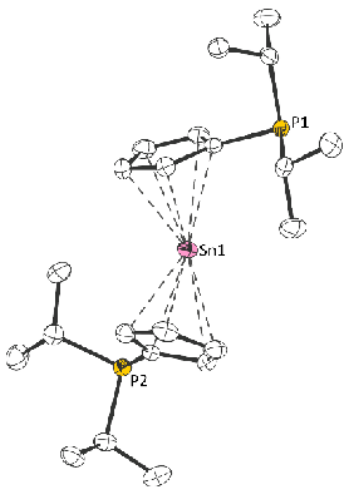

Figure S83: Molecular structure of **3b** in the crystal (displacement ellipsoids at 50% probability level; hydrogen atoms omitted for clarity).

Crystallographic Data for 3c:

CCDC Deposition Number	2038369	
Empirical formula	$C_{42}H_{44}P_2Sn$	
Formula weight	729.40	
Temperature	132(2) K	
Wavelength	0.71073 Å	
Crystal system	Triclinic	
Space group	*P*-1	
Unit cell dimensions	*a* = 9.7258(5) Å	α = 71.643(2)°
	b = 13.4845(5) Å	β = 75.282(2)°
	c = 15.1881(10) Å	γ = 70.2280(10)°
Volume	1754.63(16) $Å^3$	
Z	2	
Density (calculated)	1.381 mg/m^3	
Absorption coefficient	0.848 mm^{-1}	
F(000)	752	
Crystal size	0.150 x 0.078 x 0.033 mm^3	
Theta range for data collection	1.432 to 29.167°	
Index ranges	-13<=h<=12, -18<=k<=18, -20<=l<=20	
Reflections collected	28781	
Independent reflections	9466 [R(int) = 0.0540]	
Completeness to theta = 25.242°	100.0%	
Absorption correction	Semi-empirical from equivalents	
Max. and min. transmission	0.7458 and 0.7025	
Refinement method	Full-matrix least-squares on F^2	
Data / restraints / parameters	9466 / 0 / 521	
Goodness-of-fit on F^2	1.019	
Final R indices [I>2sigma(I)]	R1 = 0.0396, wR2 = 0.0717	
R indices (all data)	R1 = 0.0629, wR2 = 0.0789	
Extinction coefficient	n/a	
Largest diff. peak and hole	0.502 and -0.674 $e.Å^{-3}$	

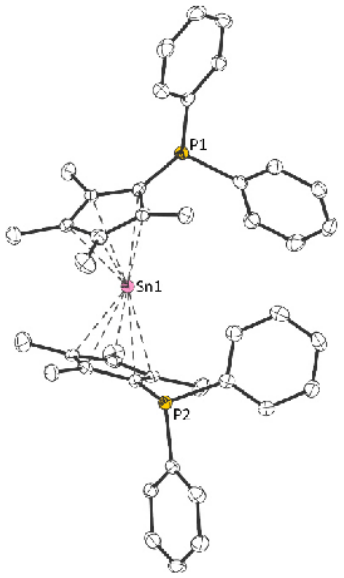

Figure S84: Molecular structure of **3c** in the crystal (displacement ellipsoids at 50% probability level; hydrogen atoms omitted for clarity).

SUPPORTING INFORMATION

Crystallographic Data for 3d:

CCDC Deposition Number	2038370	
Empirical formula	$C_{34}H_{28}P_2Sn$	
Formula weight	617.19	
Temperature	122(2) K	
Wavelength	0.71073 Å	
Crystal system	Triclinic	
Space group	*P*-1	
Unit cell dimensions	*a* = 9.8903(7) Å	α = 109.914(2)°
	b = 11.7254(9) Å	β = 95.6440(10)°
	c = 14.3898(11) Å	γ = 112.5330(10)°
Volume	1397.96(18) $Å^3$	
Z	2	
Density (calculated)	1.466 mg/m^3	
Absorption coefficient	1.050 mm^{-1}	
F(000)	624	
Crystal size	0.419 x 0.344 x 0.050 mm^3	
Theta range for data collection	1.560 to 36.497°	
Index ranges	-16<=h<=16, -19<=k<=19, -24<=l<=23	
Reflections collected	47141	
Independent reflections	13675 [R(int) = 0.0303]	
Completeness to theta = 25.242°	100.0%	
Absorption correction	Semi-empirical from equivalents	
Max. and min. transmission	0.7471 and 0.6731	
Refinement method	Full-matrix least-squares on F^2	
Data / restraints / parameters	13675 / 0 / 446	
Goodness-of-fit on F^2	1.019	
Final R indices [I>2sigma(I)]	R1 = 0.0268, wR2 = 0.0593	
R indices (all data)	R1 = 0.0388, wR2 = 0.0647	
Extinction coefficient	n/a	
Largest diff. peak and hole	0.599 and -0.555 $e.Å^{-3}$	

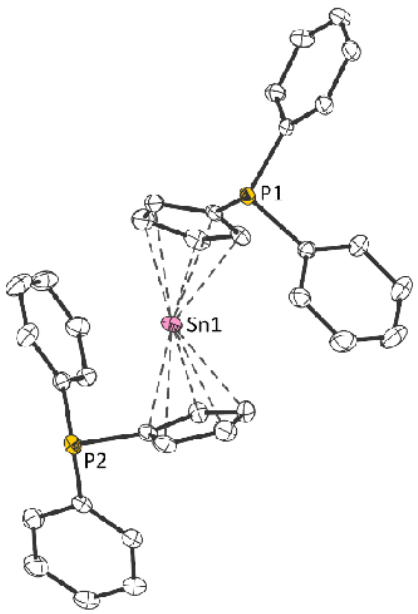

Figure S85: Molecular structure of **3d** in the crystal (displacement ellipsoids at 50% probability level; hydrogen atoms omitted for clarity).

Crystallographic Data for 4:

CCDC Deposition Number	2038371	
Empirical formula	$C_{42}H_{44}P_2Pb$	
Formula weight	817.90	
Temperature	152(2) K	
Wavelength	0.71073 Å	
Crystal system	Triclinic	
Space group	*P*-1	
Unit cell dimensions	*a* = 9.8008(3) Å	α = 71.443(2)°
	b = 13.4303(5) Å	β = 75.198(2)°
	c = 15.1892(5) Å	γ = 70.615(2)°
Volume	1762.64(11) $Å^3$	
Z	2	
Density (calculated)	1.541 mg/m^3	
Absorption coefficient	4.905 mm^{-1}	
F(000)	816	
Crystal size	0.328 x 0.237 x 0.024 mm^3	
Theta range for data collection	1.434 to 35.826°	
Index ranges	-16<=h<=16, -22<=k<=22, -24<=l<=24	
Reflections collected	217523	
Independent reflections	16417 [R(int) = 0.0637]	
Completeness to theta = 25.242°	100.0%	
Absorption correction	Semi-empirical from equivalents	
Max. and min. transmission	0.7470 and 0.5567	
Refinement method	Full-matrix least-squares on F^2	
Data / restraints / parameters	16417 / 0 / 539	
Goodness-of-fit on F^2	1.025	
Final R indices [I>2sigma(I)]	R1 = 0.0239, wR2 = 0.0516	
R indices (all data)	R1 = 0.0321, wR2 = 0.0545	
Extinction coefficient	n/a	
Largest diff. peak and hole	1.572 and -1.236 $e.Å^{-3}$	

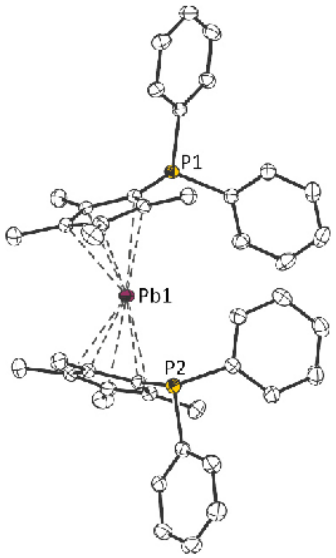

Figure S86: Molecular structure of **4** in the crystal (displacement ellipsoids at 50% probability level; hydrogen atoms omitted for clarity).

Crystallographic Data for 3b·NHC:

CCDC Deposition Number	2038364	
Empirical formula	$C_{33}H_{56}N_2P_2Sn$	
Formula weight	661.42	
Temperature	142(2) K	
Wavelength	0.71073 Å	
Crystal system	Monoclinic	
Space group	$P2_1/c$	
Unit cell dimensions	a = 16.6226(5) Å	α = 90°
	b = 11.9859(3) Å	β = 99.6480(10)°
	c = 17.8355(5) Å	γ = 90°
Volume	3503.23(17) $Å^3$	
Z	4	
Density (calculated)	1.254 mg/m^3	
Absorption coefficient	0.843 mm^{-1}	
F(000)	1392	
Crystal size	0.416 x 0.339 x 0.064 mm^3	
Theta range for data collection	1.243 to 28.312°	
Index ranges	-22<=h<=22, -15<=k<=11, -23<=l<=23	
Reflections collected	34154	
Independent reflections	8696 [R(int) = 0.0333]	
Completeness to theta = 25.242°	100.0%	
Absorption correction	Semi-empirical from equivalents	
Max. and min. transmission	0.7457 and 0.6937	
Refinement method	Full-matrix least-squares on F^2	
Data / restraints / parameters	8696 / 9 / 368	
Goodness-of-fit on F^2	1.019	
Final R indices [I>2sigma(I)]	R1 = 0.0286, wR2 = 0.0626	
R indices (all data)	R1 = 0.0393, wR2 = 0.0669	
Extinction coefficient	n/a	
Largest diff. peak and hole	1.067 and -0.617 $e.Å^{-3}$	

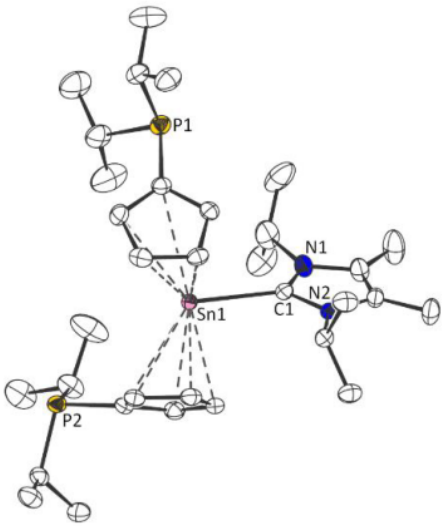

Figure S87: Molecular structure of **3b·NHC** in the crystal (displacement ellipsoids at 50% probability level; hydrogen atoms omitted for clarity).

SUPPORTING INFORMATION

Crystallographic Data for 3b·$AlCl_3$:

CCDC Deposition Number	2038373	
Empirical formula	$C_{44}H_{72}Al_2Cl_6P_4Sn_2$	
Formula weight	1228.93	
Temperature	152(2) K	
Wavelength	0.71073 Å	
Crystal system	Monoclinic	
Space group	$P2_1/n$	
Unit cell dimensions	a = 8.4065(5) Å	α = 90°
	b = 26.2731(17) Å	β = 95.753(3)°
	c = 12.4343(6) Å	γ = 90°
Volume	2732.5(3) $Å^3$	
Z	2	
Density (calculated)	1.494 mg/m^3	
Absorption coefficient	1.386 mm^{-1}	
F(000)	1248	
Crystal size	0.170 x 0.135 x 0.040 mm^3	
Theta range for data collection	1.550 to 27.139°	
Index ranges	-10<=h<=10, -33<=k<=33, -15<=l<=15	
Reflections collected	41778	
Independent reflections	6051 [R(int) = 0.0626]	
Completeness to theta = 25.242°	100.0%	
Absorption correction	Semi-empirical from equivalents	
Max. and min. transmission	0.7455 and 0.6829	
Refinement method	Full-matrix least-squares on F^2	
Data / restraints / parameters	6051 / 0 / 406	
Goodness-of-fit on F^2	1.008	
Final R indices [I>2sigma(I)]	R1 = 0.0317, wR2 = 0.0576	
R indices (all data)	R1 = 0.0520, wR2 = 0.0637	
Extinction coefficient	n/a	
Largest diff. peak and hole	0.414 and -0.729 e.$Å^{-3}$	

Note: A B-level alert was detected, resulting from disorder in the crystal.

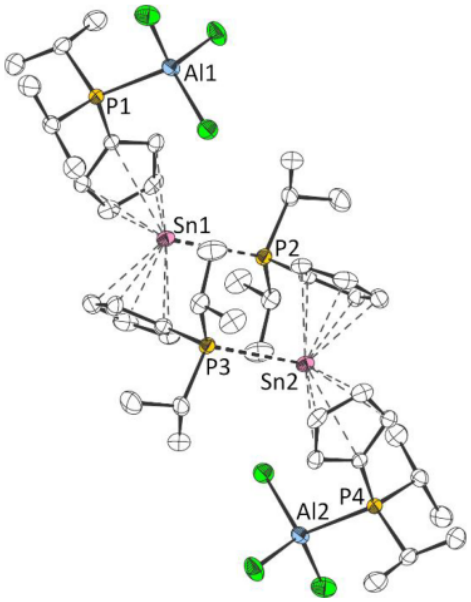

Figure S88: Dimeric structure of **3b·$AlCl_3$** in the crystal (displacement ellipsoids at 50% probability level; hydrogen atoms omitted for clarity).

Crystallographic Data for 3b·$(AlCl_3)_2$:

CCDC Deposition Number	2038379	
Empirical formula	$C_{22}H_{36}Al_2Cl_6P_2Sn$	
Formula weight	747.80	
Temperature	130(2) K	
Wavelength	0.71073 Å	
Crystal system	Monoclinic	
Space group	$P2_1/c$	
Unit cell dimensions	a = 8.4604(2) Å	α = 90°
	b = 12.7411(2) Å	β = 95.7130(10)°
	c = 29.7568(6) Å	γ = 90°
Volume	3191.70(11) $Å^3$	
Z	4	
Density (calculated)	1.556 mg/m^3	
Absorption coefficient	1.470 mm^{-1}	
F(000)	1504	
Crystal size	0.388 x 0.220 x 0.050 mm^3	
Theta range for data collection	2.109 to 30.055°	
Index ranges	-11<=h<=11, -17<=k<=17, -41<=l<=41	
Reflections collected	57702	
Independent reflections	9333 [R(int) = 0.0231]	
Completeness to theta = 25.242°	99.9%	
Absorption correction	Semi-empirical from equivalents	
Max. and min. transmission	0.7460 and 0.6167	
Refinement method	Full-matrix least-squares on F^2	
Data / restraints / parameters	9333 / 0 / 306	
Goodness-of-fit on F^2	1.080	
Final R indices [I>2sigma(I)]	R1 = 0.0224, wR2 = 0.0492	
R indices (all data)	R1 = 0.0256, wR2 = 0.0504	
Extinction coefficient	n/a	
Largest diff. peak and hole	1.007 and -0.704 e.$Å^{-3}$	

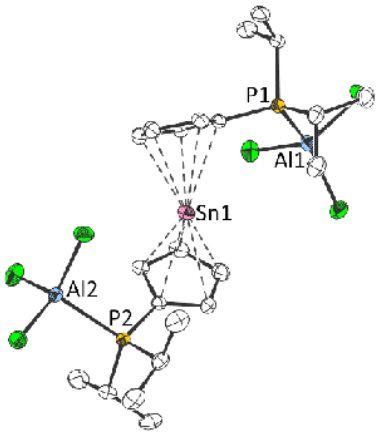

Figure S89: Molecular structure of **3b·$(AlCl_3)_2$** in the crystal (displacement ellipsoids at 50% probability level; hydrogen atoms omitted for clarity).

Crystallographic Data for 3b·W(CO)$_4$:

CCDC Deposition Number	2038374	
Empirical formula	$C_{26}H_{36}O_4P_2SnW$	
Formula weight	777.03	
Temperature	133(2) K	
Wavelength	0.71073 Å	
Crystal system	Triclinic	
Space group	*P*-1	
Unit cell dimensions	*a* = 8.6681(3) Å	α = 86.6000(10)°
	b = 8.8436(3) Å	β = 83.0160(10)°
	c = 19.3662(7) Å	γ = 68.6040(10)°
Volume	1371.81(8) Å^3	
Z	2	
Density (calculated)	1.881 mg/m^3	
Absorption coefficient	5.246 mm^{-1}	
F(000)	756	
Crystal size	0.128 x 0.024 x 0.010 mm^3	
Theta range for data collection	2.474 to 27.110°	
Index ranges	-10<=h<=11, -11<=k<=11, 0<=l<=24	
Reflections collected	5919	
Independent reflections	5919 [R(int) = 0.0631]	
Completeness to theta = 25.242°	98.4%	
Absorption correction	Semi-empirical from equivalents	
Max. and min. transmission	0.7455 and 0.6717	
Refinement method	Full-matrix least-squares on F^2	
Data / restraints / parameters	5919 / 6 / 316	
Goodness-of-fit on F^2	1.076	
Final R indices [I>2sigma(I)]	R1 = 0.0508, wR2 = 0.0809	
R indices (all data)	R1 = 0.0654, wR2 = 0.0857	
Extinction coefficient	n/a	
Largest diff. peak and hole	1.643 and -1.999 e.Å^{-3}	

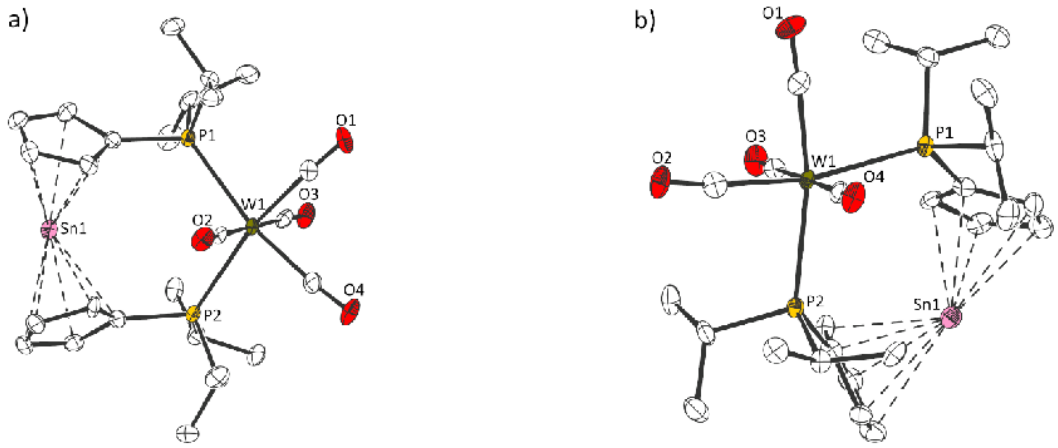

Figure S90: Molecular structure of **3b·W(CO)$_4$** in the crystal (a) and b) different viewing angles; displacement ellipsoids at 50% probability level; hydrogen atoms omitted for clarity).

Crystallographic Data for 2·PtMe$_2$:

CCDC Deposition Number	2038376	
Empirical formula	$C_{44}H_{50}GeP_2Pt$	
Formula weight	908.46	
Temperature	130(2) K	
Wavelength	0.71073 Å	
Crystal system	Triclinic	
Space group	*P*-1	
Unit cell dimensions	*a* = 10.4451(4) Å	α = 79.848(2)°
	b = 10.4724(5) Å	β = 87.208(2)°
	c = 18.4883(8) Å	γ = 82.378(2)°
Volume	1972.43(15) Å^3	
Z	2	
Density (calculated)	1.530 mg/m^3	
Absorption coefficient	4.415 mm^{-1}	
F(000)	908	
Crystal size	0.063 x 0.039 x 0.014 mm^3	
Theta range for data collection	1.968 to 29.640°	
Index ranges	-14<=h<=14, -14<=k<=14, -25<=l<=25	
Reflections collected	54900	
Independent reflections	11072 [R(int) = 0.1628]	
Completeness to theta = 25.242°	100.0%	
Absorption correction	Semi-empirical from equivalents	
Max. and min. transmission	0.7459 and 0.6649	
Refinement method	Full-matrix least-squares on F^2	
Data / restraints / parameters	11072 / 0 / 443	
Goodness-of-fit on F^2	1.033	
Final R indices [I>2sigma(I)]	R1 = 0.0738, wR2 = 0.1532	
R indices (all data)	R1 = 0.1362, wR2 = 0.1817	
Extinction coefficient	n/a	
Largest diff. peak and hole	3.493 and -1.562 e.Å^{-3}	

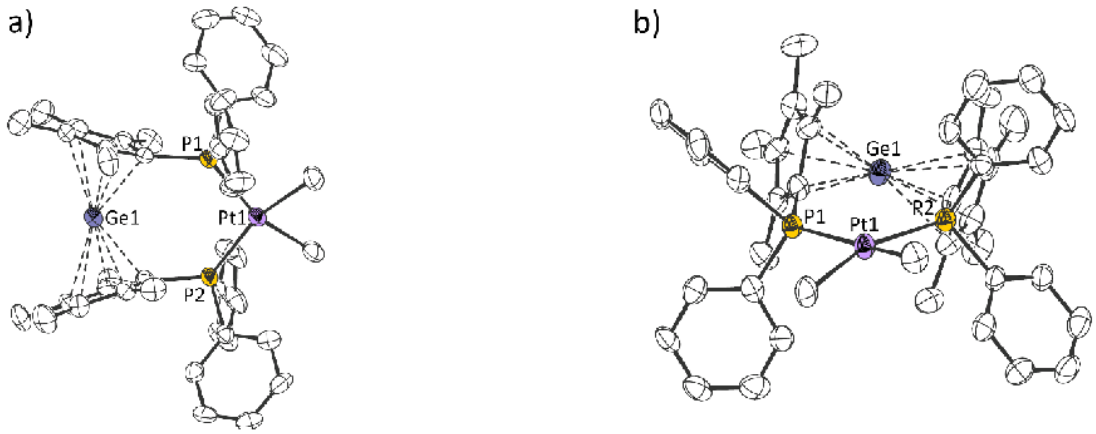

Figure S91: Molecular structure of **2·PtMe$_2$** in the crystal (a) and b) different viewing angles; displacement ellipsoids at 50% probability level; hydrogen atoms omitted for clarity).

SUPPORTING INFORMATION

Crystallographic Data for 3b·PtMe$_2$:

CCDC Deposition Number	2038375	
Empirical formula	$C_{24}H_{42}P_2PtSn$	
Formula weight	706.29	
Temperature	153(2) K	
Wavelength	0.71073 Å	
Crystal system	Triclinic	
Space group	*P*-1	
Unit cell dimensions	*a* = 8.6590(10) Å	α = 83.909(4)°
	b = 8.8532(9) Å	β = 78.528(4)°
	c = 18.8786(19) Å	γ = 64.430(4)°
Volume	1279.1(2) Å^3	
Z	2	
Density (calculated)	1.834 mg/m^3	
Absorption coefficient	6.572 mm^{-1}	
F(000)	688	
Crystal size	0.149 x 0.083 x 0.030 mm^3	
Theta range for data collection	2.551 to 37.165°	
Index ranges	-14<=h<=14, -15<=k<=14, -31<=l<=31	
Reflections collected	25552	
Independent reflections	12911 [R(int) = 0.0288]	
Completeness to theta = 25.242°	99.8%	
Absorption correction	Semi-empirical from equivalents	
Max. and min. transmission	0.7473 and 0.6355	
Refinement method	Full-matrix least-squares on F^2	
Data / restraints / parameters	12911 / 0 / 263	
Goodness-of-fit on F^2	1.028	
Final R indices [I>2sigma(I)]	R1 = 0.0297, wR2 = 0.0610	
R indices (all data)	R1 = 0.0375, wR2 = 0.0638	
Extinction coefficient	n/a	
Largest diff. peak and hole	1.886 and -1.774 e.Å^{-3}	

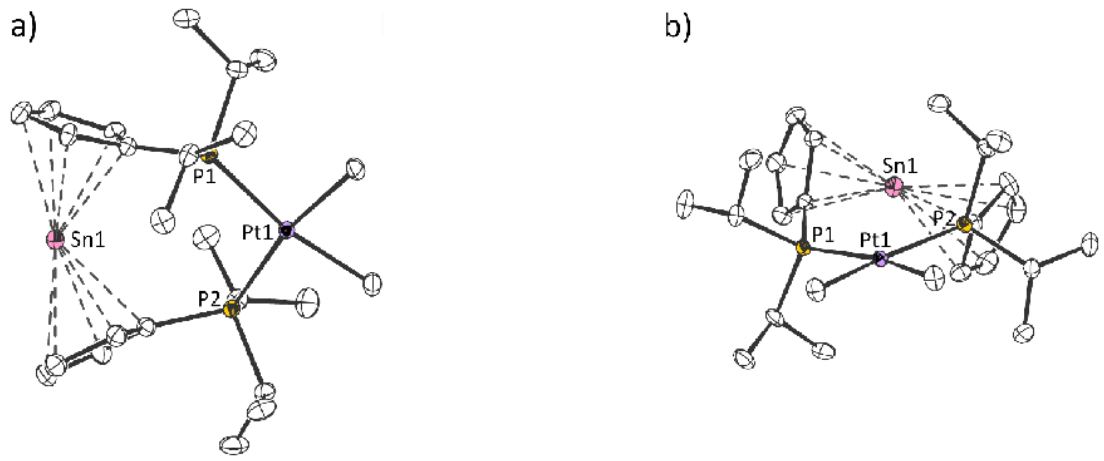

Figure S92: Molecular structure of **3b·PtMe$_2$** in the crystal (a) and b) different viewing angles; displacement ellipsoids at 50% probability level; hydrogen atoms omitted for clarity).

Crystallographic Data for 5a:

CCDC Deposition Number	2038381	
Empirical formula	$C_{30}H_{52}ClP_2Sb$	
Formula weight	631.85	
Temperature	233(2) K	
Wavelength	0.71073 Å	
Crystal system	Monoclinic	
Space group	$P2_1/c$	
Unit cell dimensions	a = 11.5602(9) Å	α = 90°
	b = 10.8014(10) Å	β = 90.014(3)°
	c = 25.375(2) Å	γ = 90°
Volume	3168.5(5) Å^3	
Z	4	
Density (calculated)	1.325 mg/m^3	
Absorption coefficient	1.072 mm^{-1}	
F(000)	1320	
Crystal size	0.223 x 0.174 x 0.132 mm^3	
Theta range for data collection	2.049 to 27.909°	
Index ranges	-15<=h<=15, -14<=k<=14, -33<=l<=33	
Reflections collected	47246	
Independent reflections	7574 [R(int) = 0.0426]	
Completeness to theta = 25.242°	100.0%	
Absorption correction	Semi-empirical from equivalents	
Max. and min. transmission	0.7456 and 0.7138	
Refinement method	Full-matrix least-squares on F^2	
Data / restraints / parameters	7574 / 109 / 349	
Goodness-of-fit on F^2	1.045	
Final R indices [I>2sigma(I)]	R1 = 0.0291, wR2 = 0.0649	
R indices (all data)	R1 = 0.0372, wR2 = 0.0687	
Extinction coefficient	n/a	
Largest diff. peak and hole	0.767 and -0.515 e.Å^{-3}	

Note: An A-level alert was detected, resulting from an unusual bonding situation around antimony (Single Bonded Metal Atom in Structure).

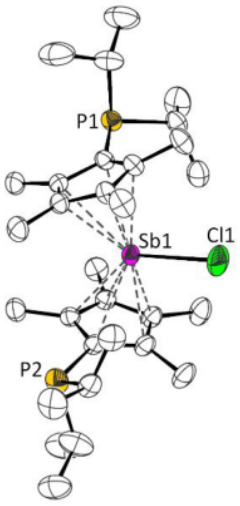

Figure S93: Molecular structure of **5a** in the crystal (displacement ellipsoids at 50% probability level; hydrogen atoms omitted for clarity).

Crystallographic Data for 5b[$AlCl_4$]:

CCDC Deposition Number	2038382	
Empirical formula	$C_{30}H_{52}AlCl_4P_2Sb$	
Formula weight	765.18	
Temperature	132(2) K	
Wavelength	0.71073 Å	
Crystal system	Triclinic	
Space group	*P*-1	
Unit cell dimensions	*a* = 11.1913(5) Å	α = 89.4070(10)°
	b = 12.5275(6) Å	β = 72.8120(10)°
	c = 14.5766(7) Å	γ = 72.1050(10)°
Volume	1850.62(15) $Å^3$	
Z	2	
Density (calculated)	1.373 Mg/m^3	
Absorption coefficient	1.163 mm^{-1}	
F(000)	788	
Crystal size	0.372 x 0.191 x 0.152 mm^3	
Theta range for data collection	1.468 to 30.597°	
Index ranges	-16<=h<=15, -17<=k<=17, -20<=l<=20	
Reflections collected	58486	
Independent reflections	11359 [R(int) = 0.0289]	
Completeness to theta = 25.242°	100.0 %	
Absorption correction	Semi-empirical from equivalents	
Max. and min. transmission	0.7461 and 0.6719	
Refinement method	Full-matrix least-squares on F^2	
Data / restraints / parameters	11359 / 0 / 359	
Goodness-of-fit on F^2	1.029	
Final R indices [I>2sigma(I)]	R1 = 0.0221, wR2 = 0.0504	
R indices (all data)	R1 = 0.0261, wR2 = 0.0525	
Extinction coefficient	n/a	
Largest diff. peak and hole	0.629 and -0.508 $e.Å^{-3}$	

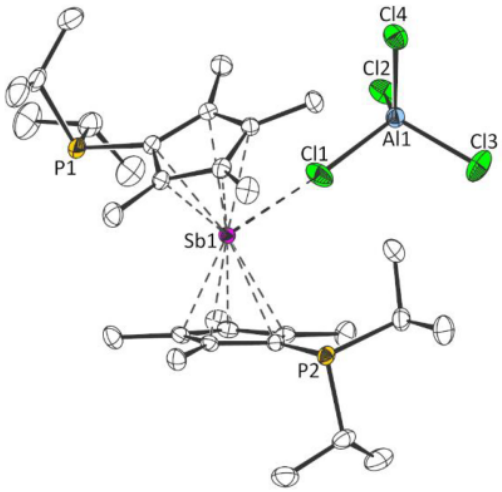

Figure S94: Molecular structure of **5b[$AlCl_4$]** in the crystal (displacement ellipsoids at 50% probability level; hydrogen atoms omitted for clarity).

WILEY-VCH

SUPPORTING INFORMATION

Computational Details

All calculations were performed using the Gaussian 09, Revision D.01 package of programs.[11] All geometry optimizations have been carried out at the B3LYP-D3[12]/def2-tzvp[13] level of theory. Every optimized structure was confirmed to be a minimum on the potential energy surface by a subsequent frequency analysis (all positive eigenvalues).

Total energy and optimized geometry of 1b:

E = -1743.302638 a.u.

Mg	0.00000600	2.24531400	-0.00009900
C	-1.97617500	1.01628500	0.17747300
C	-2.07186600	1.85181700	-0.97397200
C	-1.88717600	1.88754400	1.30485600
C	-2.04956300	3.20615500	-0.55810000
H	-2.14381500	1.51640800	-1.99506500
C	-1.94399500	3.22804100	0.85394000
H	-1.79873900	1.57060200	2.33312500
H	-2.10457700	4.06749500	-1.20569500
H	-1.90670900	4.10913200	1.47548900
C	2.07186900	1.85190200	0.97382600
C	2.04957200	3.20620500	0.55783800
C	1.97618400	1.01627300	-0.17755000
H	2.14380900	1.51657800	1.99494700
C	1.94401500	3.22797100	-0.85420400
H	2.10458300	4.06760000	1.20536000
C	1.88719600	1.88743600	-1.30500700
H	1.90673800	4.10901000	-1.47582800
H	1.79877200	1.57040800	-2.33325100
P	1.95092500	-0.80233000	-0.34047900
P	-1.95093700	-0.80230400	0.34056300
C	1.93829600	-1.36169500	1.45395500
H	1.13657900	-0.73897300	1.86550300
C	3.67252200	-1.11069000	-1.05500100
H	3.51082300	-0.78917100	-2.09071800
C	-1.93827900	-1.36182700	-1.45382200
H	-1.13655000	-0.73914800	-1.86540900
C	-3.67255500	-1.11058300	1.05507400
H	-3.51087400	-0.78898700	2.09076900
C	-4.85161800	-0.30002100	0.51044800
H	-4.61244500	0.76095500	0.43367200
H	-5.16516900	-0.64802800	-0.47254200
H	-5.71033300	-0.40239200	1.18119300
C	-3.98291000	-2.61099300	1.08676200
H	-4.86882300	-2.80281400	1.69788800
H	-4.19017000	-2.99358500	0.08573100
H	-3.15561800	-3.18985900	1.50254600
C	-1.45997100	-2.81694700	-1.55125700
H	-2.16726900	-3.50655200	-1.08607400
H	-1.36002800	-3.10896000	-2.60056000
H	-0.48906800	-2.94681000	-1.07486100
C	-3.19999100	-1.15449200	-2.29790700
H	-3.60877700	-0.14961900	-2.20995900
H	-2.97600800	-1.33700900	-3.35337100
H	-3.98238900	-1.85842300	-2.01060000
C	4.85160900	-0.30010500	-0.51046100
H	4.61245300	0.76088000	-0.43375800
H	5.16517600	-0.64804500	0.47254700
H	5.71030800	-0.40253800	-1.18121700
C	3.98285500	-2.61110700	-1.08658200
H	3.15554000	-3.18999400	-1.50229100
H	4.86874400	-2.80299000	-1.69772100
H	4.19014300	-2.99362300	-0.08552600
C	1.45997700	-2.81680200	1.55152900
H	1.36006800	-3.10872500	2.60086000
H	0.48905700	-2.94669400	1.07517700
H	2.16725300	-3.50645200	1.08638000
C	3.20002500	-1.15429100	2.29799700
H	3.98241400	-1.85825300	2.01074100
H	3.60881500	-0.14942700	2.20995000
H	2.97606100	-1.33671000	3.35348300

Total energy and optimized geometry of 1b·PhNCO:

E = -2143.252674 a.u.

P	-3.65222400	-0.63886700	-0.55220400
H	-4.06752900	2.14401600	-1.41530500
C	-2.30564600	-1.87191500	-0.45398300
C	-2.82556700	0.97582700	-0.05255500
C	-4.64882800	-1.15868700	0.95774200
C	-3.70776900	2.18539900	-0.38559900
Mg	0.04599500	-1.60337600	-0.75915100
C	-1.62837500	-2.41827100	0.67575900
C	-1.89144400	-2.63952300	-1.58218900
H	-1.97287200	1.00487100	-0.73432200
C	-2.26799800	1.06696600	1.36703600
H	-3.97857000	-1.19137800	1.82161300
C	-5.78150100	-0.17243100	1.25694600
C	-5.21073400	-2.56642400	0.72756600
H	-3.13237600	3.10600900	-0.26760400
H	-4.57930100	2.25368000	0.26688200
O	0.31370300	0.32290100	-0.70057200
C	-0.82393100	-3.50141900	0.24785600
H	-0.18692900	-4.10971800	0.87059100
C	-0.98575300	-3.63800400	-1.15302900
H	-0.49359400	-4.36590100	-1.77703800
H	-2.25219000	-2.49868400	-2.58972200
C	2.48808400	-1.65921300	-0.23210900
C	2.25431900	-1.93241300	-1.63934900
H	2.13288900	-1.18794700	-2.41491800
C	2.44818700	-3.30122500	-1.83123600
C	1.30191600	0.97665800	-0.19949500
H	-1.73760700	-2.08898500	1.69650700
H	-1.69212700	1.98982300	1.48390800
H	-3.06254700	1.07407200	2.11670700
H	-1.60287900	0.23311400	1.58704300
H	-6.41975100	-0.56195600	2.05531000
H	-5.40923400	0.79888000	1.58047100
H	-6.41104000	-0.01474200	0.37730600
H	-5.88904300	-2.57906400	-0.12961500
H	-4.42090100	-3.29502300	0.54220600
H	-5.77545700	-2.89605700	1.60442800
P	2.70523900	-0.06005900	0.43238300
C	2.83418200	-2.89976100	0.37692200
H	2.32915100	-3.82048700	-2.77031000
C	2.79335400	-3.89020300	-0.59742900
N	1.48552600	2.23085600	-0.00015600
C	4.28961400	0.73512500	-0.04829700
C	2.60008400	-0.13861600	2.26793200
H	3.04131700	-3.04916300	1.42576800
H	2.95724200	-4.94374700	-0.42726500
C	0.55189200	3.20796500	-0.38655000
H	4.24616800	1.72392800	0.41340400
C	5.48026800	-0.06172500	0.49570400
C	4.36848100	0.90919800	-1.56866100
H	3.31325400	-0.91962300	2.54757400
C	3.00588000	1.18169500	2.93430100
C	1.19257700	-0.57018800	2.69823300
C	0.45051500	4.34937100	0.41681100
C	-0.22378100	3.13533100	-1.55174500
H	6.41054900	0.42699400	0.19978700
H	5.47557000	-0.13010900	1.58443100
H	5.48794200	-1.07577300	0.09134200
H	3.53092600	1.49341300	-1.95029400
H	5.28882500	1.43929800	-1.82137200
H	4.38648400	-0.05660800	-2.07541000
H	2.37210300	1.99987700	2.59190600
H	2.89062300	1.08493100	4.01558000
H	4.04375900	1.44825700	2.73528200
H	0.88268100	-1.50204300	2.22573700
H	1.17258400	-0.71794800	3.77947100
H	0.46129200	0.20091800	2.45377700
H	1.06494000	4.41106700	1.30607800
C	-0.41818300	5.37850400	0.08212500
C	-1.07212400	4.17952900	-1.89335300
H	-0.15913500	2.25939300	-2.17980400
H	-0.49160000	6.24797500	0.72367700
C	-1.18237200	5.30115400	-1.07775700
H	-1.66490400	4.10806200	-2.79686800
H	-1.85625000	6.10535400	-1.34370500

Total energy and optimized geometry of 3b:

E = -1757.531074 a.u.

C	2.28088400	-0.57729300	0.05921300
C	2.84452600	-1.30155200	-1.02977600
C	2.14638600	-1.51203100	1.13663700
C	3.05910000	-2.63189300	-0.63501700
H	3.05763100	-0.90056400	-2.00742700
C	2.63818300	-2.77102800	0.70477400
H	1.81027400	-1.27368100	2.13539100
H	3.45862600	-3.41880000	-1.25678900
H	2.70215800	-3.66457400	1.30740000
C	-1.52967500	-1.27857000	1.30665800
C	-1.73561800	-2.68710700	1.36271300
C	-2.14006400	-0.77614100	0.11768500
H	-1.06918800	-0.68388400	2.07931600
C	-2.46068100	-3.05910400	0.20726600
H	-1.44273200	-3.33509900	2.17507600
C	-2.69142100	-1.90272100	-0.55609300
H	-2.77033800	-4.06075200	-0.04985300
H	-3.21248100	-1.87359600	-1.50086600
P	-2.21069300	0.95975200	-0.46595500
P	1.81759500	1.18030500	0.21675300
C	-2.01310100	1.89588100	1.15093300
H	-1.03507000	1.52068600	1.47001200
C	-4.00957500	1.05221800	-1.02501000
H	-3.97753000	0.39278500	-1.90033800
C	2.11683700	1.81611200	-1.52730700
H	1.64561600	1.03127300	-2.12866700
C	3.19026100	1.81977400	1.34306900
H	2.85700300	1.40814300	2.30327300
C	4.62289800	1.32930900	1.11609300
H	4.66329400	0.24799000	0.98144000
H	5.07994100	1.79589100	0.24496600
H	5.24087700	1.58254300	1.98307900
C	3.12120900	3.34707800	1.45438700
H	3.76506500	3.69904900	2.26465900
H	3.46308100	3.82749200	0.53578500
H	2.10578100	3.69484500	1.65577000
C	1.31259700	3.10163400	-1.76403500
H	1.65945200	3.91778200	-1.12640700
H	1.42065700	3.42821800	-2.80225400
H	0.25220800	2.94133400	-1.56978200
C	3.56215000	1.98017700	-2.00675100
H	4.16922700	1.09660200	-1.81749200
H	3.57731900	2.17710600	-3.08291000
H	4.04366700	2.82851300	-1.51843300
C	-5.10874700	0.53103600	-0.09365600
H	-4.85654800	-0.43736100	0.33700700
H	-5.30058600	1.22626600	0.72230900
H	-6.04365900	0.41721000	-0.65103800
C	-4.34328400	2.45944300	-1.53554700
H	-3.56789500	2.84966700	-2.19742600
H	-5.28671900	2.44763000	-2.08779400
H	-4.46362100	3.16082600	-0.70783300
C	-1.83442300	3.39841400	0.89930900
H	-1.52883200	3.89639500	1.82370800
H	-1.07195300	3.59597600	0.14621300
H	-2.76368900	3.86703900	0.57075900
C	-3.02330600	1.65056000	2.27558900
H	-3.96085900	2.17296900	2.08219700
H	-3.24851500	0.59351400	2.41242200

H	-2.62904400	2.03667600	3.22079700
Sn	0.18246000	-2.19224300	-0.36150100

Total energy and optimized geometry of PhNCO:

E = -399.898483 a.u.

C	1.68067000	1.36630300	-0.00001000
C	0.32514200	1.06991100	-0.00015200
C	-0.09265900	-0.26344000	-0.00015200
C	0.85182900	-1.28868800	-0.00001100
C	2.20572600	-0.97993400	0.00013200
C	2.62627400	0.34543900	0.00013300
H	1.99854300	2.40119900	-0.00001200
H	-0.41238000	1.86262700	-0.00026200
H	0.51322500	-2.31593300	-0.00001700
H	2.93413300	-1.78069900	0.00024400
H	3.68217200	0.58218100	0.00024300
N	-1.44586300	-0.60655900	-0.00032000
C	-2.52694300	-0.08327900	0.00004600
O	-3.62686100	0.31233300	0.00026600

SUPPORTING INFORMATION

References

[1] W. Voskuil and J. F. Arens, *Org. Synth.* **1968**, *48*, 47.

[2] P. Beagley, P. Davies, H. Adams, C. White, *Can. J. Chem.* **2001**, *79*,731-741.

[3] N. Kuhn, T. Kratz, *Synthesis* **1993**, *6*, 561-562.

[4] G. R. Fulmer, A. J. M. Miller, N. H. Sherden, H. E. Gottlieb, A. Nudelman, B. M. Stoltz, J. E. Bercaw, K. I. Goldberg, *Organometallics* **2010**, *29*, 2176-2179.

[5] G. Sheldrick, *Acta Cryst. A* **2008**, *64*, 112-122.

[6] J. Szymoniak, J. Besancon, A. Dormond, C. Moise, *J. Org. Chem.* **1990**, *55*, 1429-1432.

[7] C. Lichtenberg, M. Elfferding, L. Finger, J. Sundermeyer, *J.Organomet. Chem.* **2010**, *695*, 2000-2006.

[8] T. Sixt, M. Sieger, M. J. Krafft, D. Bubrin, J. Fiedler and W. Kaim, *Organometallics* **2010**, *29*, 5511-5516.

[9] A. P. Shaw, J. R. Norton, D. Buccella, L. A. Sites, S. S. Kleinbach, D. A. Jarem, K. M. Bocage and C. Nataro, *Organometallics* **2009**, *28*, 3804-3814.

[10] F. Mathey, J.-P. Lampin, *Tetrahedron* **1975**, *31*, 2685-2690.

[11] Gaussian 09, Revision D.01, M. J. Frisch, G. W. Trucks, H. B. Schlegel, G. E. Scuseria, M. A. Robb, J. R. Cheeseman, G. Scalmani, V. Barone, G. A. Petersson, H. Nakatsuji, X. Li, M. Caricato, A. Marenich, J. Bloino, B. G. Janesko, R. Gomperts, B. Mennucci, H. P. Hratchian, J. V. Ortiz, A. F. Izmaylov, J. L. Sonnenberg, D. Williams-Young, F. Ding, F. Lipparini, F. Egidi, J. Goings, B. Peng, A. Petrone, T. Henderson, D. Ranasinghe, V. G. Zakrzewski, J. Gao, N. Rega, G. Zheng, W. Liang, M. Hada, M. Ehara, K. Toyota, R. Fukuda, J. Hasegawa, M. Ishida, T. Nakajima, Y. Honda, O. Kitao, H. Nakai, T. Vreven, K. Throssell, J. A. Montgomery, Jr., J. E. Peralta, F. Ogliaro, M. Bearpark, J. J. Heyd, E. Brothers, K. N. Kudin, V. N. Staroverov, T. Keith, R. Kobayashi, J. Normand, K. Raghavachari, A. Rendell, J. C. Burant, S. S. Iyengar, J. Tomasi, M. Cossi, J. M. Millam, M. Klene, C. Adamo, R. Cammi, J. W. Ochterski, R. L. Martin, K. Morokuma, O. Farkas, J. B. Foresman, and D. J. Fox, Gaussian, Inc., Wallingford CT, **2016**.

[12] a) A. D. Becke, *J. Chem. Phys.* **1993**, *98*, 5648-5652; b) C. Lee, W. Yang, R. G. Parr, *Phys. Rev. B* **1988**, *37*, 785-789; c) S. H. Vosko, L. Wilk, M. Nusair, *Can. J. Phys.*, **1980**, *58*, 1200-1211; d) P. J. Stephens, F. J. Devlin, C. F. Chabalowski, M. J. Frisch, *J. Phys. Chem.* **1994**, *98*, 11623-11627; e) S. Grimme, J. Antony, S. Ehrlich, H. Krieg, *J. Chem. Phys.* **2010**, *132*, 154104.

[13] a) F. Weigend, R. Ahlrichs, *Phys. Chem. Chem.Phys.* **2005**, *7*, 3297-3305; b) F. Weigend, *Phys. Chem. Chem. Phys.* **2006**, *8*, 1057-1065.